Starch nanocrystals : preparation and application to bio-based flexible packaging

Déborah Le Corre Le Corre

UNIVERSITÉ DE GRENOBLE

THÈSE

Pour obtenir le grade de

DOCTEUR DE L'UNIVERSITÉ DE GRENOBLE

Spécialité : **Matériaux, Mécanique, Génie Civile, Electrochimie**

Arrêté ministériel : 7 août 2006

Présentée par

Déborah LE CORRE

Thèse dirigée par **Alain DUFRESNE**
et codirigée par **Julien BRAS**

préparée au sein du **Laboratoire du Génie des Procédés Papetiers de l'Ecole Internationale du Papier, de la Communication Imprimée et des Biomateriaux, UMR CNRS 5518**

dans **l'École Doctorale Ingénierie – Matériaux, Mécanique, Energétique, Environnement, Procédés de Production**

Starch Nanocrystals:

Preparation and Application to bio-based flexible packaging

Thèse soutenue publiquement le **« 27 Octobre 2011 »**,
devant le jury composé de :

Pr. Eliane ESPUCHE
Professeur de l'Université Lyon 1, Président
Pr. Denis LOURDIN
Directeur de Recherche à l'INRA, Rapporteur
Dr. Patrice DOLE
Directeur Régional du laboratoire CTCPA, Rapporteur
Pr. Alain DUFRESNE
Professeur de Grenoble INP, Membre
Dr. Julien BRAS
Maître de Conférences de Grenoble INP, Membre
Dr. Hélène ANGELLIER-COUSSY
Maître de Conférences de l'Université de Montpellier, Membre
Dr. David GUERIN
Manager d'Unité de Recherche au Centre Technique du Papier, Membre
Dr. Timo MAKARAINEN
Manager projets R&D, Cargill, Membre

« Il vaut mieux savoir tout chercher que chercher à tout savoir… »

P. Mendelson

A ma famille, mes parents et Nicolas,

Pour leur amour,

Leur confiance,

Et leur fierté.

Remerciements

C'est avec une émotion certaine que je voudrais adresser mes sincères remerciements à tous les acteurs plus ou moins directs de cette expérience de thèse.

Tout d'abord, je tiens à remercier les membres du jury, qui m'ont fait l'honneur d'évaluer et de participer à l'issue de ce travail. Professeur Eliane Espuche, en tant qu'experte de la perméabilité, je suis très flattée que vous ayez accepté de présider mon jury de thèse. Je suis également ravie de vous avoir rencontré. Professeur Denis Lourdin, et Docteur Patrice Dole, je suis honorée que vous ayez tout les deux accepté d'évaluer mon manuscrit malgré vos emplois du temps chargés. Merci aussi pour vos remarques avisées sur mes travaux. Docteur Hélène Angellier-Coussy, en tant que prédécesseur et auteure de mon « livre de chevet », votre avis m'importait tout particulièrement. Je vous remercie sincèrement pour votre lecture approfondie de mon manuscrit et vos remarques pertinentes sur mon travail. Merci aussi au Docteur David Guerin d'avoir participé au jury et d'avoir partagé avec moi son réalisme et son pragmatisme. Enfin, je remercie le Docteur Timo Makarainen pour son avis d'expert industriel et son regard particulier sur mon travail.

I would also like to thank all the European project partners whom, on different levels, have all contributed to my scientific and personal growth.
Thank you to Dr. David Guérin (CTP), project coordinator, who allowed me to represent my lab during meetings. Thank you to other CTP members, Dr. Florence Girard and Sylvie Combaz for both their technical support and their kindness. I keep good memories of our travels. Thank you to Frédéric Bébien (ARS) for his full collaboration and friendliness and to Dr Séverine Schott (ARS) for her outspokenness and respect. Merci aussi à Mme Christine Lemasson (ARS) de m'avoir transmis son savoir en couchage et fait découvrir « Jazz à Vienne ». I sincerely thank Drs. Detlef Glittenberg and Timo Makarainen (Cargill) for their passion, full investment and availability all along the project. I also which to express my gratitude to the « Chemical Engineering » department of Karlstad University and to Pr Lars Järnström et Dr Caisa johansson who hosted me for a month as part of their team; and more particularly to Cecilia Land my office partner and to Kristin Sandberg my lab partner. To our English partners from Sheffield University, Pr Chris Breen and Dr Francis Clegg, thank you for your scientific insights, your help and your sense of humor. I learned a lot from you. Thank you to Dr Rikku Talja and Pr Kristina Poppius-Levlin from VTT, for their collaboration, kindness and humility. Thank you also, Catharina Hohental (VTT) for considering to work with me and revise my work. I really enjoyed talking with you. I would also like to acknowledge, those I have not worked directly with, but who nevertheless took the time to share their work, their point of view and show us their facility: Dr Klaus Noller and Dr Markus Schmid from Fraunhofer IVV, Dr Arthur Barthowiak from ZUT, and Dr Daniel Samain from CERMAV.

Je tiens ensuite à remercier Pagora-Grenoble INP (anciennement EFPG) ainsi que le LGP2 pour leur accueil en tant qu'élève ingénieur puis en tant que doctorante. A ce titre, je remercie plus particulièrement les directeurs de laboratoire successifs : Pr Naceur Belgacem et Pr Evelyne Mauret, pour leur considération en tant que collègue, leurs disponibilités, leurs discussions et leur aide lorsque j'en avais besoin.

Je remercie profondément mes encadrants, Pr Alain Dufresne et Dr Julien Bras de m'avoir fait confiance pour mener à bien ce projet. Merci de m'avoir permis de grandir tant professionnellement que personnellement, grâce aux diverses expériences vécues ces trois dernières années. Merci Alain pour tes conseils, ta réactivité, tes encouragements et ton calme olympien qui rassure. Merci Julien pour tes méthodes, ton adaptabilité, ta « positive attitude », tes compliments et ton amitié.

Je teins aussi a remercier toutes les personnes extérieures au laboratoire qui ont gentiment répondu à mes sollicitations. Je pense tout d'abord au CMTC. Un grand merci à Francine Roussel, Stéphane Coindeau, Fréderic Charlot, Alexandre Crisci et tous les autres pour leur chaleureux accueil et leur disponibilité. Vous m'avez souvent sorti des épines du pied ! Merci également à Jean-Luc Putaux et Pierre Sailler du CERMAV d'avoir pris le temps de me former sur certaines manips ; et à Luc Choisnard de l'UJF Pharmacie, de m'avoir accordé du temps et des conseils avisés sur les plans d'expériences.

Je pense maintenant aux personnels scientifiques, techniques, administratifs et informatiques du LGP2 que j'ai souvent sollicité et qui se sont toujours rendus disponibles pour m'aider. Merci à Charlotte, Chu, Olivier, Momo, Phillipe L., Phillipe S., Xavier, Jean-Marc. Merci encore à Cécile B., Stéphane D., Martine R., Sylvie, Isabelle, Stéphane V., Frank, Jean-Luc , Lydia , Zouhir, Mazen… Merci à Névin que j'ai souvent dérangé en dehors des horaires autorisées et qui m'a dégoté un joli petit pull pour ma soutenance. Un chaleureux merci à Tata Anne-Marie ! Grâce à toi, j'ai non seulement eu l'occasion de dormir dans un avion-hôtel mais également dans un aéroport… Merci pour ton réconfort et ton soutien dans la dernière ligne droite ! Je souhaite aussi ajouter un merci particulier à Bertine ! Au delà de tes qualités de microscopiste, je retiendrais nos discussions « hors sujet » et qui détendent, et surtout ta bonne humeur. Merci d'avoir partagé tes débuts au FEG avec moi et pour tous ces rires qui ont littéralement « marqués » les micrographes.

Merci également à Laura, Ophélie, Mathieu et Elina que j'ai eu la chance d'encadrer et grâce à qui j'ai beaucoup appris sur les qualités humaines nécessaires à la transmission et à l'encadrement. Merci pour votre travail. Je vous souhaite bon courage dans vos carrières respectives.

Enfin, la vie du laboratoire ne serait pas ce qu'elle est sans ses thésards et ses post-docs. Je tiens donc à remercier tous ceux que j'ai croisés et/ou avec qui j'ai travaillés pendant ces 3 ans. Merci d'abord aux anciens. Ceux qui nous rappelaient que le thésard est avant tout étudiant et prend donc l'apéro le jeudi : Les Jérém* et les Pierres. Ceux qui prônaient la discussion et la transmission : Abdelkader, David V., Ramzi et j'en oubli surement… Mais également à Jacq, Felipe, Mishra, Styajit, Martha, Claudia et Magalie. Ainsi qu'à mes anciens collègues de promo : BaZile et Fifou!! Un grand merci aussi à Gigi « la bonne humeur » : « Bom Dia Flor de Dia ». J'espère que l'on se recroisera ! Merci aussi à mes contemporains les Oliviers, Cyril « le tranquil », Rrrita Fadouuul, Lucie « Crrrr », Marion « le marmitton », Sousou, Tangi & Fabrice « quand la Bretagne viens à Grenoble » ; et à mes collègues de Bureau : Prince Ali et son successeur Bertrand « Super Geek », Signorina Lara et Nathalie. Merci autant pour les délires que pour nos discussions scientifiques… Merci aussi aux plus « jeunes », que j'ai eu le plaisir de découvrir : Céline (ma co-encadrée), Elsa et Fred (qui m'ont rappelé que Britney ce n'était plus de mon âge…), Aurélie (qui ne peut pas me faire les mêmes remarques) et tout les autres. Enfin … un merci tout particulier (et très gros) à Aurore « les bons conseils » et Karim « Anti-déprime » pour leur amitié. Aurore, collègue de promo, collègue de bureau et coach de rédaction de thèse… 7 ans ca commence à faire (et ce n'est pas fini j'espère) : Merci pour tout ! Karim, merci d'avoir partagé avec moi ton franc (pour certain trop…) parlé, ton dynamisme et ton amour du travail bien fait ! Un gramme de Karim dans ce monde de politiquement correcte… ca rafraichit aussi !

Je souhaite également remercier mes amis extérieurs au labo qui m'ont apporté un certain équilibre : les grenoblois Basile et Romain ; les « lyonnais » Jéjé, Juju, Francis, Alex, et Molik ; Alex le bordelais ; les Parisien(ne)s ; les Toulousains et les itinérants Fab', Jer' et Marion ; et bien sur Delphine ! Merci aussi à ma Clinou qui garde le contact malgré nos vies très différentes.

Je remercie aussi mes « Belles-Familles » pour les bons moments qu'elles me permettent de partager ; mais aussi pour avoir fait le déplacement à ma soutenance : Merci JP & Christiane, Merci à mon beauf : Clem et à mes belles-sœurs (et c'est vrai que vous êtes jolies) : Marie et Cécile.

Je remercie de tout mon cœur ma famille : mes grands-parents qui malgré leur perplexité sont toujours présents; mes parents qui s'extasient toujours des « pas » que leur « Boba » peut faire ; et mon fréro et ma sœurette qui m'encouragent toujours. Merci pour votre soutien et votre amour ! Je vous aime.

Je termine légitimement par celui qui partage désormais ma vie et mon quotidien depuis presque 7 ans : Mon Nico… Merci pour ta contribution inestimable tant logistique que morale ! Merci pour tes encouragements, ta confiance en moi, tes petits plats (et que de progrès!), et tous les week-ends et moments organisés… Merci aussi pour ton écoute !
Tu es mon équilibre et mon bonheur quotidien… Je t'aime.

Merci à tous !!

Table of Contents

Scientific Publications (2008-2011)

Scientific Journals

1. Déborah Le Corre, Julien Bras, Alain Dufresne. Starch Nanoparticles : A Review. *Biomacromolecules,* 2010, 11, (5), 1139-1153.

2. Déborah LeCorre, Julien Bras, Alain Dufresne. Evidence of Micro and Nano-scaled particles during starch nanocrystals preparation and their isolation. *Biomacromolecules, 2011, 12,(8), 3039-3046.*

3. Déborah LeCorre, Julien Bras, Alain Dufresne. Ceramic membrane filtration for isolating starch nanocrystals. *Carbohydrate Polymers, 2011, 86, (4), 1565*-1572.

4. Déborah LeCorre, Julien Bras, Alain Dufresne. Influence of native starch's properties on starch nanocrystals' thermal properties. *Carbohydrate Polymers, 87 (2012) 658-666*

5. Déborah LeCorre, Julien Bras, Alain Dufresne. Influence of botanic origin and amylose content on starch nanocrystals' properties. *Accepted in Journal of Nanoparticle Research, 2011.*

6. Déborah LeCorre, Julien Bras, Alain Dufresne. Influence of starch nanocrystals' botanic origin on morphological and mechanical properties of natural rubber nanocomposites. ***Submitted*** *to Macromolecular Material Engineering, 2011.*

7. Déborah LeCorre, Elina Vahanian, Alain Dufresne, Julien Bras. Enzymatic pre-treatment for preparing starch nanocrystals. ***Submitted*** *to Biomacromolecules* 2011.

8. Déborah LeCorre, Alain Dufresne, Bertine Khelifi, Julien Bras. All starch nanocomposite coating for barrier material. ***Submitted*** *to Progress in Organic coatings*, 2011.

9. Déborah LeCorre, Julien Bras, Catharina Hohenthal, Alain Dufresne. Sustainability assessment of starch nanocrystals. ***Submitted*** *to Starke/Starch*, 2011.

Oral presentations in Scientific Meetings

1. Déborah Le Corre, Julien Bras, Alain Dufresne. Starch nanoparticles for eco-efficient packaging: influence of botanic origin. *2nd International conference on Biodegradable Polymers and sustainable composites*: *Biopol 2009*, *Alicante, Spain*

2. Déborah Le Corre, Julien Bras, Alain Dufresne. Starch Nanocrystals: The New Bionanoparticles? *FlexPakRenew Workshop*, May 2011, Lyon Airport , France

Communications in Scientific meeting

1. Déborah Le Corre, Julien Bras, Alain Dufresne. Starch nanocrystals for eco-efficient barrier coating: Influence of formulation and process parameters. *11th Advanced Coating Fundamentals Symposium TAPPI Conference 2010*, Munich, Germany.

2. Karim Missoum, Déborah Le Corre, Alain Dufresne, Naceur Belgacem, Celine Martin, Julien Bras. Rheological behavior of different bio-based nanoparticles suspensions (Starch nanocrystals, whiskers, microfibrillated cellulose), *TAPPI Intl Conf on Nano for the Forest Product Industry, 2010*, Espoo, Finland

3. Julien Bras, Tangi Sénéchal, Deborah Le Corre, Céline Martin, Alain Dufresne. Cellulose and Starch nanocrystals: Influence of the source on rheological, mechanical and barrier properties. *239th ACS Conference CELL division 2010,* San Francisco, CA, USA.

4. Déborah Le Corre, Miriam Gallur, Julien Bras, S. Ancejo, Alain Dufresne. Potential of pea starch nanocrystals: A comparison with other common sources . *TAPPI Intl Conference on Nano for Renewable Materials, 2011***,** Arlington, VA USA.

5. Déborah Le Corre, Julien Bras, Alain Dufresne. Innovative strategies for isolating starch nanocrystals, *TAPPI Intl Conference on Nano for Renewable Materials 2011***,** Arlington, VA USA

Others

1. Julien Bras, Déborah Le Corre. Chapitre 10: Introduction aux Biopolymères et Polymères biodégradables. In : « De la fibre à l'imprimée » Tome 3.

2. Deborah Le Corre, Julien Bras, Alain Dufresne. Chapter 8 – Preparation of starch nanoparticles. In: *Biopolymer Nanocomposite,* Wiley. *In preparation.*

3. Déborah Le Corre, Julien Bras, Alain Dufresne. Starch nanocrystals for eco-efficient barrier packaging. *PhD candidates' day 2009 (I-MEP2)*, Grenoble, France. Best poster award.

4. Déborah Le Corre, Julien Bras, Alain Dufresne. Starch nanocrystals for eco-efficient barrier packaging. *International Workshop on the future of fibre based biomaterials for packaging: Pagora Days 2009,* Grenoble, France

5. Other Attendance

    a. EPF 4th Summer school on « Bioplastic and Related Materials », Gargnano, Lake Garda, Italy, 24-29 May 2009

6. Exhibitions

    a. Salon de l'emballage, Paris Villepinte, Novembre 2008

    b. Salon de l'emballage, Paris Villepinte, Novembre 2010

Abbreviations

AFM	Atomic Force Microscopy
D.O.E	Design of Experiments
DP	Degree of Polymerization
DS	Degree of substitution
IR	Infrared
LCA	Life Cycle Assessment
NCC	NanoCrystalline Cellulose
NR	Natural Rubber
OMMT	Organically Modified MontMorillonite
OTR	Oxygen transmission Rate
PE	PolyEthylene
PEG	PolyEthylene Glycol
PLA	PolyLactic Acid
PVOH	PolyVinyl Alcohol
SEM	Scanning Electron Microscope
SEM-FEG	Scanning Electron Microscope equipped with a Field Emission Gun
SNC	Starch NanoCrystals
SNP	Starch NanoParticles
WVTR	Water Vapor transmission Rate
WVP	Water Vapor Permeability
XRD	X-Ray Diffraction

General Introduction

General Introduction

Increasing food shelf life duration thanks to packaging is an international concern to limit food waste. This is why global demand for barrier flexible packaging continuously increases, especially in Europe. It is the largest market for these packaging grades. It exceeds that of the US and Canada combined. However, it currently relies on oil-based multi-material packages which will face in coming years both fossil energy depletion and growing concerns for sustainability. The packaging industry will have no choice than find an alternative as soon as possible.

Moreover, consumers demand for bio-based, recyclable and/or biodegradable products is increasing strongly, especially when packaging is concerned. This is why even if bio-based polyolefins are being developed; waste management and end of life will still be selective parameters. Indeed the idea is to limit packaging waste either by developing more effective packaging or by facilitating their end of life (e.g. home compost).

Thus the ambition of the European FlexPakRenew project is to develop a paper-based innovative eco-efficient low-substrate flexible packaging from renewable resources. The idea is to develop a sustainable packaging and thus reduce the industry's reliance on barrier films derived from petroleum. The choice of a paper substrate was motivated both by communication (printable media) and environmental concerns. Indeed, it has been calculated that the production of plastic materials generates approximately $1.6 t_{eq}C$/ton whereas paper and board production generates only $0.50\ t_{eq}C$/ton.

In the framework of the project, a multi-layer strategy was implemented and several biopolymers were considered. Our task, based on an innovative idea, consisted in adding new bio-nanofillers within a bio-based matrix to improve its mechanical and barrier properties. Two matrices were selected: xylan and starch. Xylan is a relatively new biopolymer extracted from hemicellulose in bio-refineries. As such, it is potentially widely available. Starch, on the other hand, is currently widely available all over the world as it is produced by a wide variety of plant's roots and seed; and extracted for commercial use by several companies. Its industry is mature as such and explains why it is a relatively cheap material in comparison to other bio-based polymers.

Most interesting properties of starch lay in its semi-crystallinity and its ability to gelatinize. The latter is exploited to produce plasticized starch that can be used to make bio-based films (e.g. such as developed for biodegradable garbage or shopping bags). The semi-crystallinity of starch is much less exploited whereas that of cellulose, another abundant semi-crystalline polysaccharide, has been under investigation for several decades. It has led

to the development and use of bio-based crystalline rod-shaped nano-fillers called nanocrystalline cellulose or cellulose whiskers. Applications are too numerous to be detailed here but have contributed to the recent development of a production plant in Canada. It led us to wonder “why not do the same with starch nanocrystals, a much more recently developed product (2000’s)?”.

Indeed Starch NanoCrystals (SNCs) have first been investigated as an extension of the work on cellulose nanocrystals. They are prepared by the acid hydrolysis of the amorphous parts of the polymer. However, cellulose occurs as fibers made of an assembly of micro-fibrillated cellulose (MFC), and MFC are themselves nanofibers made of rod-shaped amorphous and crystalline cellulose. Starch, on the other hand, presents a semi-crystalline onion-like granular structure made of alternating amorphous and crystalline growth rings. So the accessibility of their nanocrystals is totally different and thus SNCs morphology differs greatly from cellulose nanocrystals. Contrary to the rod-shaped cellulose crystals, SNCs present platelet morphology.

As such, they have recently been considered as a potential substitute for clay-based platelet nano-fillers and for this reason have been proposed as an alternative in our flexible packaging project. Indeed, as part of this EU project, our intent was to investigate the potential of SNC as bio-nano-fillers for mechanical and barrier reinforcement of starch-based coating.

However and as suggested, such a material (SNC) has been discovered very recently and before the beginning of the project (2007), only 13 papers had been published on the topic.

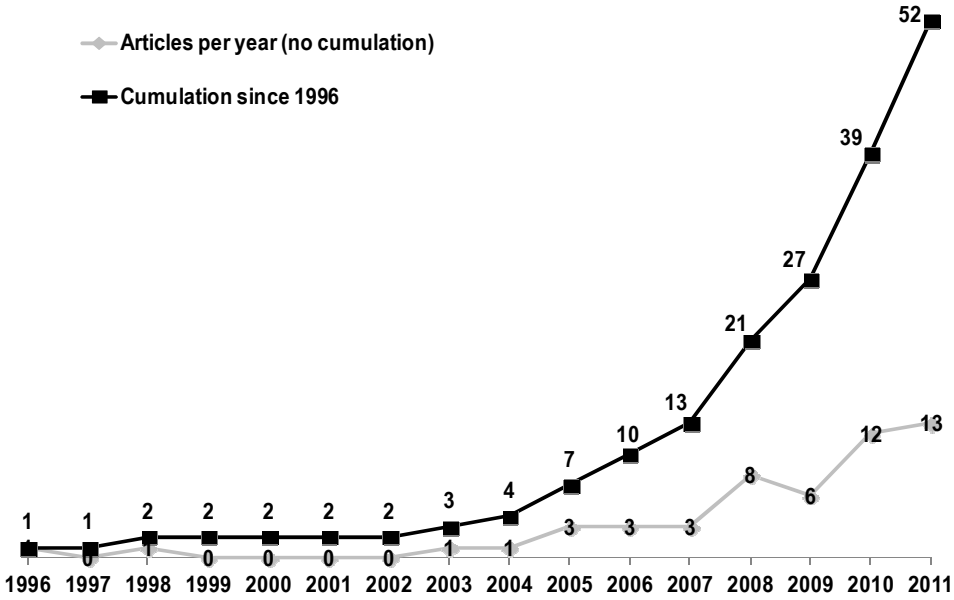

Figure 1. Evolution of the number of articles dealing with SNC (updated September 1st 2011)

As shown in Figure 1, an exponential interest for SNCs, starting more or less at same time as this project, can be evidenced and adds pertinence to our choice.

Obviously, with so few articles at the start of the project, several questions and challenges could be identified. For example, to achieve the goal of using SNCs in flexible packaging, a focus had to be brought on the SNCs potential for scale-up.

After reviewing SNC characterization, preparation and properties, it seemed relevant at the starting point of the project to:

(i) assess the influence of the botanic origin of native starch used to prepare SNC's on the resulting SNCs' properties

(ii) quantify the yields and kinetics of the preparation process

(iii) propose solutions for optimizing and scaling-up the production process

(iv) investigate the compatibility of SNCs with existing processes and applications

Thus, the manuscript was organized in four chapters as presented in Figure 2.

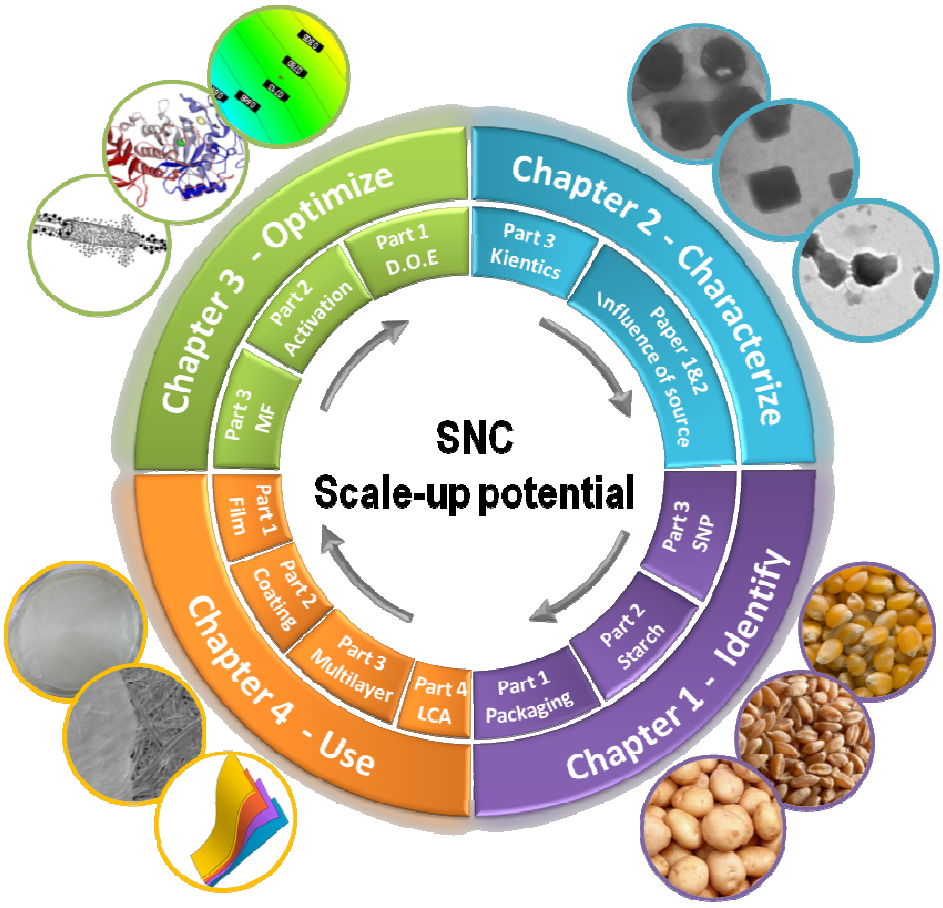

Figure 2. Manuscript organization

Chapter 1 allows **identifying** the remaining challenges to be overcame before being able to scale-up the production process.

Chapter 2 aims at **characterizing** the influence of using different native starches on the final structural (Part 1- *Paper 2*) and thermal (Part 2- *Paper 3*) properties of SNCs. Characterization of the current production process was as well of importance for enhancing know how (Part 3- *Paper 4*).

Chapter 3 considers three different strategies to **optimize** the production process: a design of experiments (D.O.E) to find optimal conditions for preparing SNCs in less than 24 hours (Part 1), a pre-treatment to shorten the current production process (Part 2), and a pilot-scale available technique to continuously extract SNCs as they are produced (Part 3 – *Paper 5*).

Eventually, **Chapter 4** assesses the potential **use** of SNCs in industrial packaging applications such as nanocomposite film (Part 1- Paper 6), in paper coating (Part 2 – Paper 7), and in multilayer packaging (Part 3). The environmental impact of SNCs used in such applications is also assessed (Part 4 – Paper 8).

Chapters are mainly based on scientific papers or on parts following structured as such in order to present a homogeneous manuscript. To specify or complete the original publications, comments, illustrations or complementary results might have been added, and are indicated by *a grey italic font*.

All chapters are tightly linked to each other, so that we hope the complete study brings a global understanding of SNCs preparation and properties, together with new perspectives. Results never achieved with SNC were obtained and new generation SNC has also been defined.

So, before any considerations, we should start with an extensive literature review of these newly studied bio-based nanoparticles, and a presentation of this project's context.

CHAPTER 1. Literature Review

CHAPTER 1. LITERATURE REVIEW

CHAPTER 1. Literature Review

As presented in general introduction, the aim of the present study was to develop industrially producible and processable starch nanocrystals (SNC) for eco-efficient flexible barrier packaging applications. More precisely, most of the research has been focus on assessing if SNC could (i) be produced at an industrial scale; (ii) resist current industrial converting processes such as paper coating; and (iii) provide increase properties to the final product.

Indeed, such material has been discovered very recently and a need for (i) reviewing and classifying the different starch nano-elements and (ii) their know properties reported in literature was identified. Thus giving the aimed applications, this chapter will, in a first part, give an overview of the flexible bio-based packaging materials, processes and market; and will detail basics on barrier properties. Then, focus will be brought on starch and its properties. Finally, the last sub-chapter will aim at clarifying the categories of starch nanoparticles and described the current production process and uses of SNC.

To this end, this chapter 1 is inspired from: D. Le Corre, J. Bras, A. Dufresne, Starch Nanoparticles: A Review, Biomacromolecules 2010, 11, 1139-1153. Also, some comments are added for better understanding of our project's context. They are identified by a grey italic font.

I. Flexible Barrier Bio-based Packaging

I.1. Paper & Flexible packaging

In 2003, the packaging industry was worth an estimated €293 billion globally (Europe €90 billion, North America €81 billion, Japan €57 billion) — representing a significant percentage of global gross domestic product. According to a recent report from Pike Research, worldwide packaging industry revenues will increase from $429 billion in 2009 to $530 billion by 2014, representing a growth rate greater than that of the global economy itself[4]. In 2008, the French Packaging Industry employed 110000 people with a turnover of €19.6 billion (which makes for 3% of the Manufacturing Industry). The packaging industry in Europe consists of four segments classified by material type: paper and board, plastics, glass and metal. The largest segments of the industry are paper and board; and plastics, which account for 35% and 30% , respectively, of the national packaging market's turnover[5]. The consumer market segments are mainly the Food (65%) and the Health and Care (12%) industries[5]. Similar trends are observed in the US. Moreover, paper is a renewable material and thus more and more considered as an alternative to petroleum based-materials.

I.1.1. Paper

Indeed, paper is considered to be the most abundant and the most environmentally friendly biomaterial as:

1. it is based on the most abundant renewable resource (cellulose),
2. the industry widely uses cogeneration and is surely turning to energies extracted from by-products
3. paper can be recycled and are mostly biodegradable.

It is produced from fibrous raw materials such as wood and/or annual non-wood plants by a process resumed in Figure 1.2. Fibers are isolated either by mean of mechanical or chemical processes. The most used process is the "kraft cooking" (about 80% of paper production[6]) as it dissolves the other components of wood and does not cut the fibers, rendering more resistant fibers. Fibers are then bleached to obtain white paper. The pulp is usually shipped to paper mill as thick paper sheet (agglomerated dry fibers). Next steps consist in "re-pulping" the fibers, ie. separating the fibers to obtain an homogenous suspension. The fibers are then refined, ie. made more flexible and more fibrillated to allow for stronger mechanical (entanglement) and chemical (hydrogen

bonds) bonds between fibers. Fibers are then sent to the paper machine's flow box before paper sheet formation. Then by elimination of free water using filtration processes, most of the paper making process consists in pressing and drying the fibers (solid content is increased from 5% to 95%) to favour bonds and mechanical resistance.

Some final processing steps such as (i) sizing or coating, ie. impregnating the paper with a given latex/solution to fill in the pores; and (ii) calendaring to obtain a smoother and glossier surface can be added.

A process similar to that presented in Figure 1.2 was used in our project for coating applications detailed in Chapter 4. Figure 1.1 clearly shows the influence of coating on paper surface. Such a coating step can be done on-line or off-line and is added mainly to obtain better printing or barrier properties. The latter was the target of our project and will be detailed later.

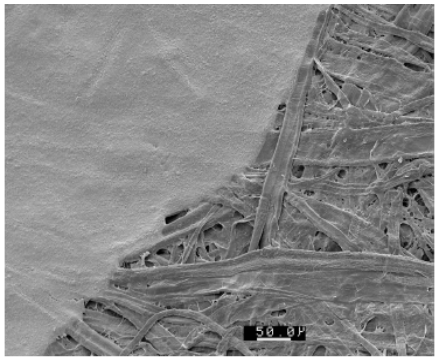

Figure 1.1. Partially coated paper

Contrary to what was announced at the end of last century, the numerical era did not cause the end of the paper industry. Nowadays, printing and packaging papers represent 88.7% of total consumption as shown in Figure 1.3.

Giving its sustainability, cost-effectiveness, strong mechanical properties (stiffness), and printability by all main printing processes, paper is an interesting substrate / base for flexible and bio-based packaging.

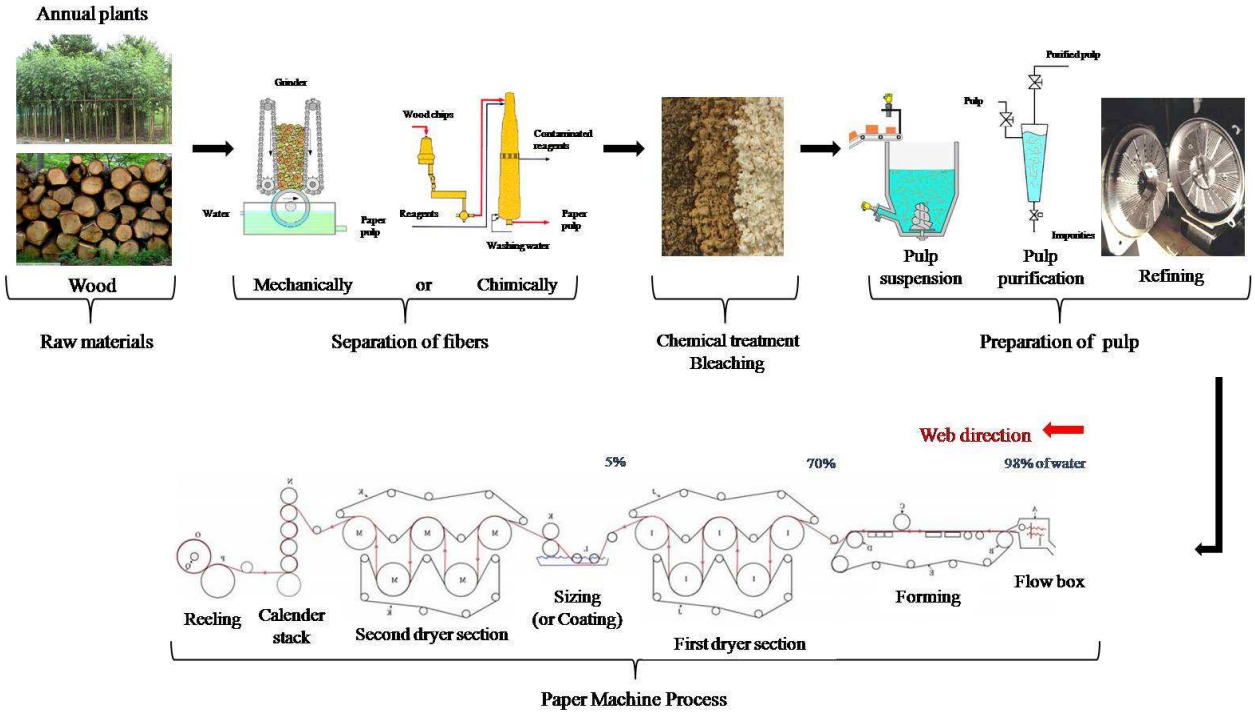

Figure 1.2. Schematization of papermaking process.[7]

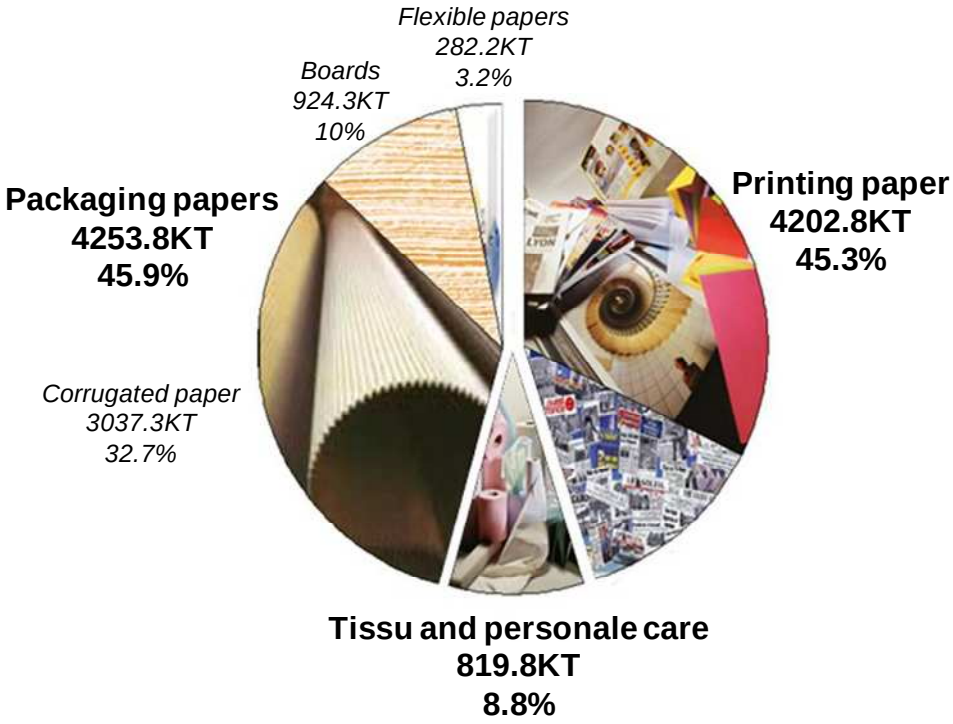

Figure 1.3. Paper consumption according to market segments.[8]

I.1.2. Flexible Packaging

According to the US Federal Regulations definition, Flexible packagings are “any package or part of a package, the shape of which can be readily changed. Flexible packaging includes, but is not limited to, bags, pouches, labels, liners and wraps utilizing paper, plastic, film, aluminum foil, metalized or coated paper or film, or any combination of these materials.” It can also be defined as the manufacture, supply and conversion of plastic and cellulose films, aluminum foils and papers that are used separately or in combination for primary food packaging or non food applications.

According to the Flexible Packaging Association Statistics of 2010[9], the flexible packaging is the second largest packaging segment in the U.S., garnering 18 percent of the U.S. $143 billion packaging market (ie. $26.4 billion) as forecasted in 2006. In Europe, the flexible packaging market represents 3.5 million tons of which 73% are dedicated to the food industry, as shown in Figure 1.4. In Western Europe, consumption of flexible packaging is estimated above 5kg per capita, whereas in Eastern Europe it is still below 2 kg.

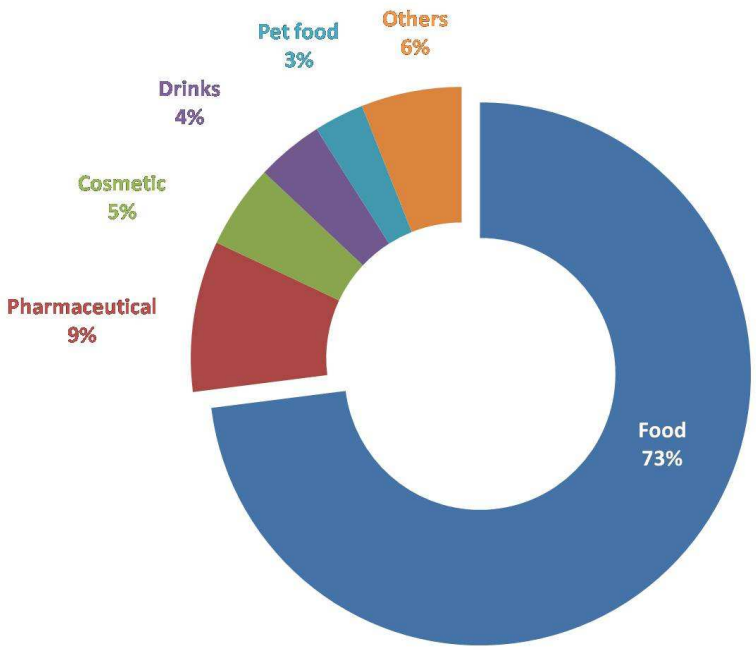

Figure 1.4. European Flexible Packaging Market (Adapted from [10]).

Flexible packaging based on paper combines the properties of the paper with those of other materials such as plastics, aluminium, wax and other materials by coating, lamination or impregnation. They are sometimes referred to as “specialty papers” or multilayers. Depending on the combination of material used, they can provide mechanical resistance, sealability, and barrier properties to gases, greases and light. Barrier properties are the most important requirement and will be discussed later. The

well-know TetraPak® application for liquid packaging is the most famous example of such material.

Our European project (FlexPakRenew, European Community's Seventh Framework Program (FP7/2007-2013) under grant agreement n°207810) focuses on the elaboration of a similar multi-layer, but based on bio-polymers, to compete with paper/PE for snack application as shown on Figure 1.5. It is important to keep in mind that such multi-layers are not symmetrical and comprise (i) one side in contact with the food product and (ii) another side for printing commercial messages.

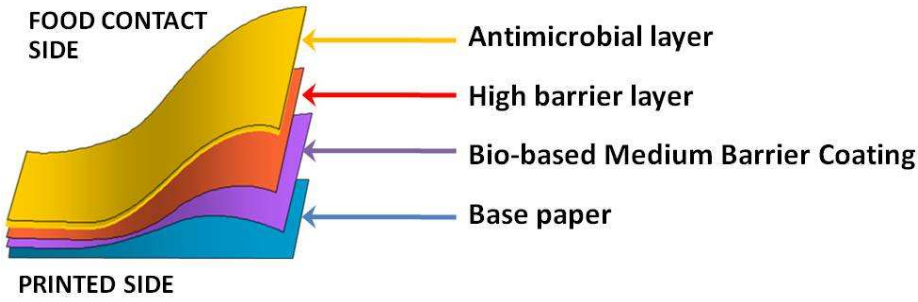

Figure 1.5. Multi-layer elaborated in the FlexPakRenew Project.

To combine paper with other materials, it undergoes a series of converting processes which can be described as follow.

- **Printing and varnishing**. The main processes in packaging are flexography and gravure printing. Some printers also use web offset lithography. The print quality depends mainly on the paper surface. Pigments pre-coating are classically used for improving paper surface. *It is the case of the industrial paper used in this project (chapter 4)*.

- **Coating** is the simplest method for adding other functions to papers[11]. The main processes for coating can be gathered in three families:

  - **Liquid-based coatings** are applied by most classic coating processes and use mainly water-based suspensions: A roll applies the coating suspension to the paper, and then the coat weight and smoothness are controlled by either air-knife, blade or rod as represented in Figure 1.6. Other more recent processes, such as film press (inspired from size press) and curtain coating, have been developed for the last 2 decades.

The latter was used in our project for coating SNC, and for pilot scale-up organized by our team during the European project. More details will be given in Chapter 4.

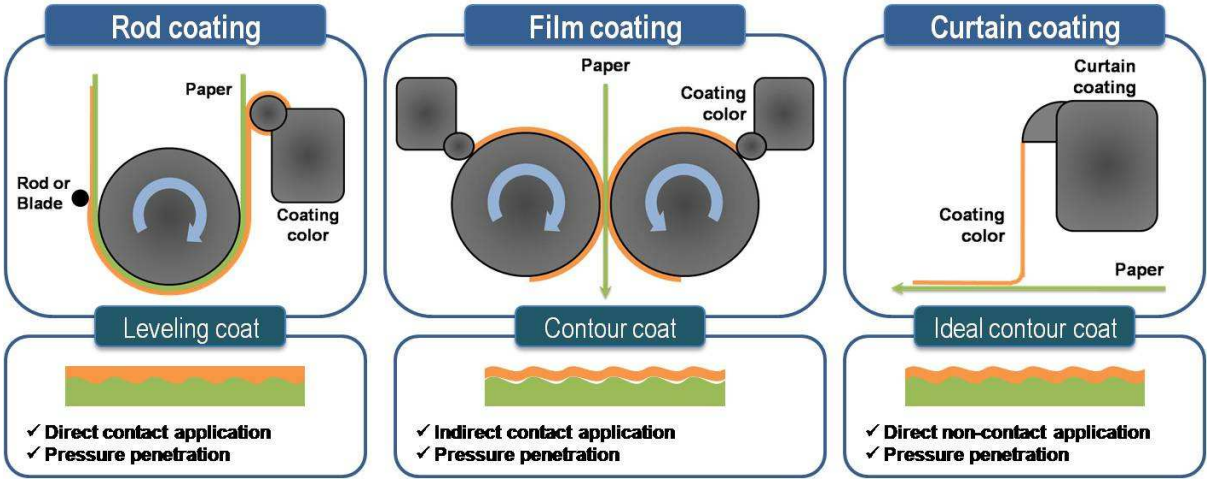

Figure 1.6. Main processes for coating.

Coating suspensions, also called coating colors, can be based on: (a) a polymer in solution such as starch or PVA; (b) a polymer in emulsion like styrene-butadiene latex or (c) a solvent based varnish such as UV cured solutions.

- **Extrusion coating**. Some polymers are not water soluble or do not exist as emulsions thus they are sold at solid state, as pellets. These pellets need to be extruded, ie. thermo-mechanically treated before being coated and immediately cooled down as shown in Figure 1.7. The main drawbacks of this technique are: its energy consumption; and low productivity (off line process at low speed). *Our target and reference paper (polyethylene coated paper for flexible packaging) is obtained with such a process and is one of the most commonly used for barrier packaging application.*

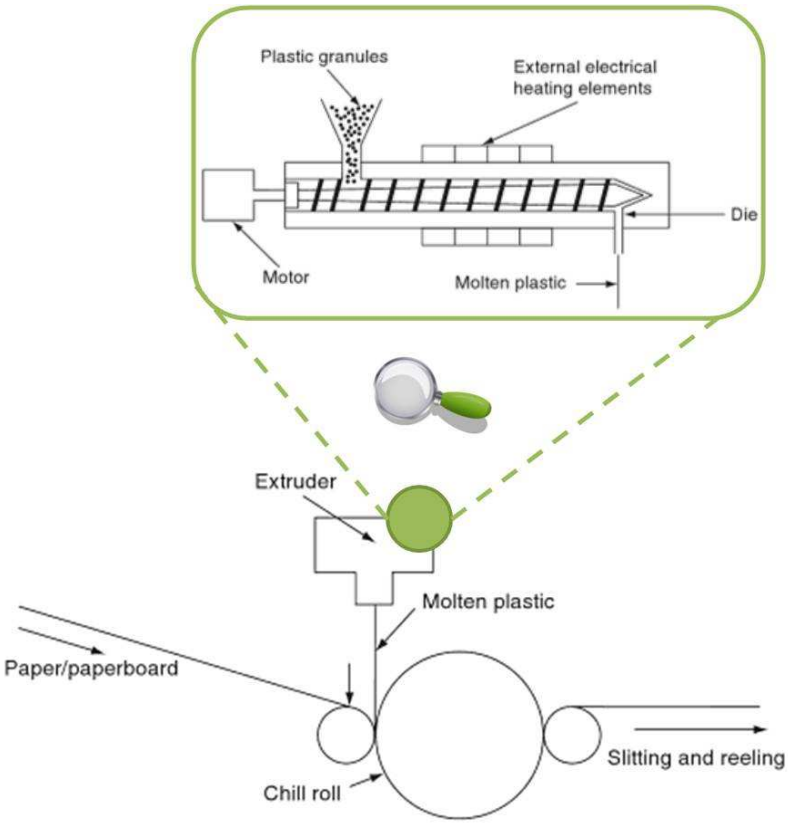

Figure 1.7. Extrusion coating (based on [12])

- **Vacuum coating or Metallization** is a process whereby aluminum is vaporized in vacuum and deposited to form a thin film on the surface of the substrate. This process, described in Figure 1.8, can be applied to paper, but as it requires a very smooth surface it is usually applied on plastic films.

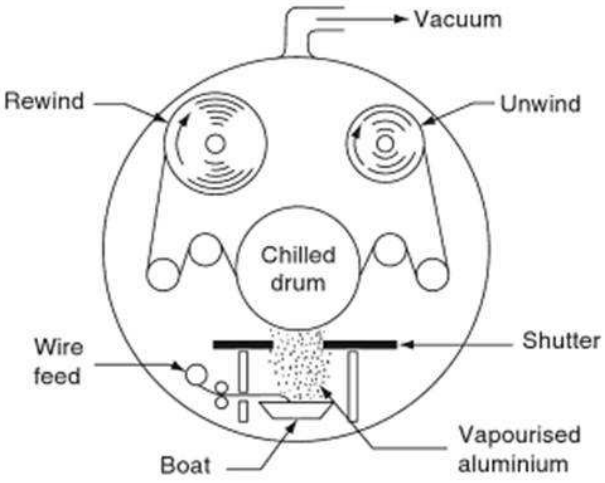

Figure 1.8. Vacuum coating process (based on [12])

- **Lamination** is another well-developed solution for obtaining multilayers. Indeed some materials/layers to be added on the paper surface are already processes films. An adhesive is applied to the surface of one of the materials which is then applied to the other by nip pressure. The adhesives can be water-based, solvent-based, wax (for barrier properties) or solid. For the later, the adhesive is extruded first. It is called extrusion-lamination.

Even if it is an offline process, the film-like materials added with this process bring much more functionality. This is why some innovative nanocomposite films have also been prepared and characterized in Chapter 4.

The packaging ensued from these different processes present numerous advantages and modified properties. However such polymer or metal addition will modify the end-of-life and the environmental impact of the paper-based material. The European Directive 2004/12/EC[13] on packaging and packaging waste, sets new targets (e.g. 60% of material recycled for paper based packaging) that have to be reached between 2008 and 2015 depending on State Members. It aims at harmonizing packaging waste recycling in Europe.

In this context companies were encouraged to adapt their products and optimize their performances, leading to intensive research and innovations. The fast development of bio-packaging is one of the most visible consequences.

I.2. Bio-based packaging

I.2.1. Trends and definitions

The sustainable packaging sector is growing much faster than the overall packaging industry, and the Cleantech market intelligence firm anticipates that eco-friendly packaging will nearly double in revenues between 2009 and 2014, from €61 billion to €118 billion[4]. Pike Research anticipates that plastic-based packaging will be the fastest-growing segment of the sustainable packaging sector between now and 2014. "More eco-friendly plastic packaging will have a huge impact," says Wheelock, "because it represents more than a third of the total global packaging industry, second only to paper packaging".[4]

The association "European Bioplastics"[14] reports the following applications or product segments to exhibit high growth rates: compostable waste bags to collect organic waste and carrier bags, biodegradable mulch film which can be ploughed into the field once it has been used, catering and snack food products, film packaging for foods with short shelf life and rigid packaging such as containers and bottles.

There is no known official definition for "bio-packaging". Most current developments of bio-packaging are bio-plastics (also called bio-polymers). The term "bio" is indifferently used to identify bio-based and biodegradable and/or compostable materials. However, since the end of the 1990's and Pertesen et al.'s definition[15], it seems that the current trend among scientists is to define "*bio-polymers*" as a bio-based , ie. polymer produced from renewable resources, therefore including also some non biodegradable materials.[14]

Figure 1.9. aims at clarifying the fact that bio-based does not imply biodegradable and petroleum based does not imply non degradable.

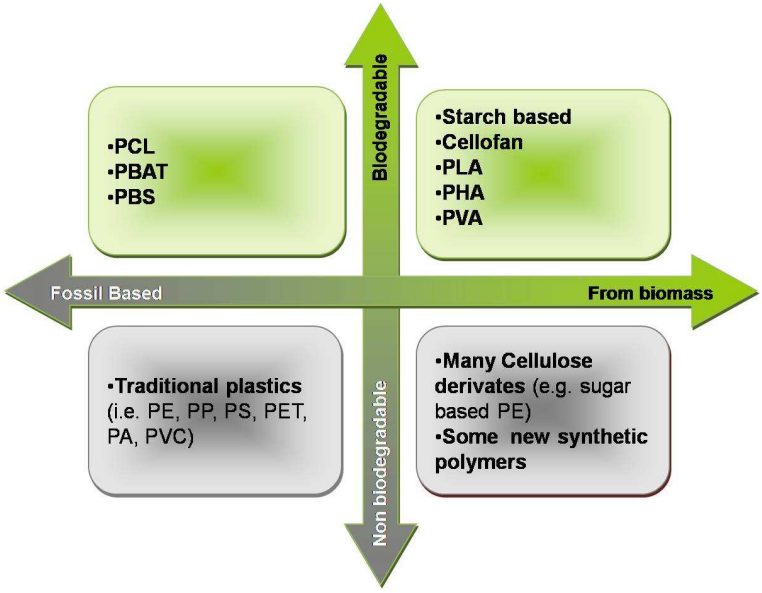

Figure 1.9. Distinction between fossil-based, bio-based, biodegradable and non biodegradable.

Traditional plastics names are: Polyethylene (PE), Polypropylene (PP), Polystyrene (PS), Poly(ethylene terephtalate) (PET), Polyamide (PA), Polyvinyl chloride (PVC). Fossil-based biodegradable polymers are: Poly(caproLactone) (PCL), poly(butylene adipate-co-terephthalate) (PBAT), Poly(butylenes succinate) (PBS). Biodegradable and bio-based polymers are: Poly(lactic acid) (PLA), polyhydroxyalkanoate (PHA), Polyvinyl alcohol (PVA or PVOH).

For consumers the confusion is still great between biodegradable, bio-compostable, bio-based, bio-organic and biocompatible. The term biodegradable implies that the material can be 90% degraded in H_2O, CO_2 or CH_4 by bio-fragmentation and mineralization under a 6 month time. It does not indicate under which specific conditions. This is why the standard used in the field of packaging, the EN13432, is based on the specific conditions of compost (at 40-60% RH, 60℃ for a week and 40℃ for a month). Four requirements have to be achieved for this standard: biodegradability, disintegration, heavy metal and compost quality. Also the term synthetic polymer is sometimes used to name a bio-based polymer that was synthesized. This term relates to the production process rather to the nature or the property of the polymer.

In this study, we will consider biopolymers as bio-based polymers and the main part of our work will focus on starch-based materials (see Figure 1.9).

I.2.2. Biopolymers

Depending on their origin and production, bio-based polymers are commonly divided in three categories[15, 16] as represented in Figure 1.10: ***Category 1.*** Polymers directly extracted from biomass such as polysaccharides and proteins. ***Category 2.*** Polymers produced by classical chemical synthesis using renewable bio-based monomers. Poly(lactic acid) for instance is a bio-polyesters polymerized from lactic acid monomers obtained by fermentation of carbohydrate feedstocks[17]. ***Category 3.*** Polymers produced by micro-organism or genetically modified bacteria.

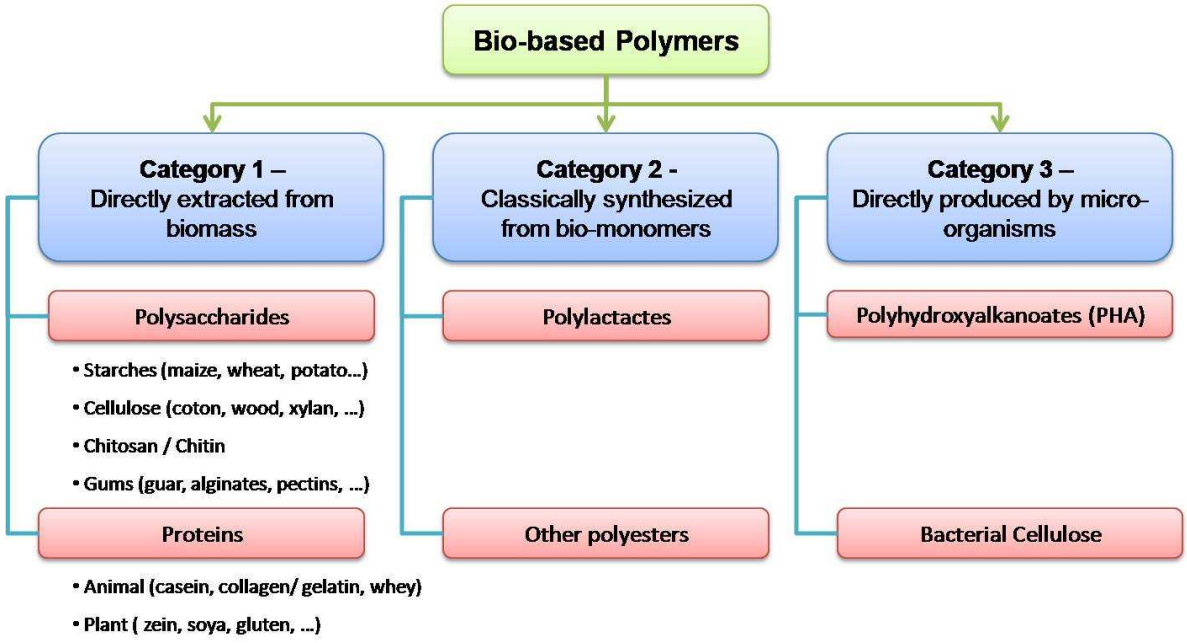

Figure 1.10. Classification of bio-polymers according to their origin and production process. [16]

Biopolymers, despite their enormous potential due to their variety, availability and numerous applications, still have many challenges to overcome. The challenges are of three types: (i) **economical** – with needs to have optimized production processes to reduce both costs and environmental impacts; (ii) **legislative**; and **linked to** (iii) **their properties** – with the need to compete with fossil based plastics in terms of shelf life duration, mechanical and barrier properties.

Our study focused on the last one.

Table 1.1. Commercially available biodegradable plastics (polyssacharides and polyesters) and their main features related to packaging.

Based on available industrial data and [18]

Types	Commercial Name	Company	Certifications					Composition	Properties		
			Ok Compost Ok Compost home Ok biodegradable Compostable ASTM D 6400 (USA) Green Pla (Japan)						Food contact	WV barrier	O2 barrier
Starch -based	Mater-bi	Novamont SPA (IT)	x	x	x	x	x	Maize starch + biodegradable polymer	x	n.d.	x
	PlanticR1	Plantic (AU)	x	x	x	x		Maize starch	x	x	x
	Biomax TPS	Dupont (plantic technology)	x	x	x	x		High amylose starch	x	x	x
	Biostarch's films	Biostarch TM	x					Starch + PLA	n.d.	No	No
	Biograde group's fims	Biograde group (AU/CN)				x	x	TPS, aliphatic polyesters (AP) and natural plasticizers	n.d.	n.d.	n.d.
	Biolice	Limagrain (FR)	x					Cereal starch + biodegradable polymer/PLA/PBS	n.d.	n.d.	n.d.
	Bioplast TPS	Bioplast GF 106/02	x			x		Potatoe starch	x	x	x
	Bioplast GF 106/02	Biotec(DE) / Biosphere (FR)						Potato starch + copolyester	x	n.d.	x
	Bioplast GS 2189							Potato starch + PLA	No	n.d.	No
	Bioceres	Futuramat' (FR)				x		Wheat starch + polyester	n.d.	n.d.	n.d.
	Polyceres	Futuramat' (FR)	"biofragmentable"					Wheat starch + polyoleofine	n.d.	n.d.	n.d.
	Solanyl	Rodenburg (NL)	"biodegradable"					Potatoe starch	No	n.d.	n.d.
	Ecoflex	BASF (DE)				x	x	TPS + biodegradable synthetic polymers	x	x	x
	Ecovio	BASF (DE)				x	x	Blend of Ecoflex® & PLA based on corn	x	x	x
	Biopar MFS	BIOP (DE)						Potato starch + ecoflex	x	x	x
	Cereplast compostable	Cereplast				x		Starch copolymers (PLA, PBS)			
Cellulose	Nature Flex NE 30	Innova Films (GB)	x	x		x	x	Eucalyptus	x	x	x
	Biograde (C7500&C9550)	FKUR (DE)				x	x	Cellulose blends	x		n.d.
PLA	Ingeo Resins - PLA from Puralact (PLA monomer)	Nature Works - Cargill (US) Futurro (Galactic & Total) Purac & SulzerChemTech (NL)	OK bio-based			x *	x	PLA from maize starch	x	n.d.	x
PHAs	Mirel	Telles (US)	*		x		x	PHB copolymer	x	x	x
	Nodax technology	Meridian Inc (US) - stopped in 2006	*					P(3HB-co-3Ho)	n.d.	x	x
	Biomer	Biomer (DE)	*		n.d.			P(3HB)	n.d.	*	*
	Enmat	Tianan (CN)	*		n.d.			PHBV + Ecoflex	n.d.	*	*
	Biocycle	PHB Industrial (BR)	x					P(3HB), P(3HB-co-3HV)	n.d.	*	*
	Biogreen	Mitsubishi Gas Chemical (JP)	*		n.d.			P(3HB)	n.d.	*	*
	TephaFlex	Tepha (US)	absorbable (medical application)						n.d.	*	*
	Biomatera	Biomatera (CA)	*		n.d.			P(3HB-co-3HV)	n.d.	*	*
	PLA	Ecomann (CN)	*		n.d.			PHA (P34HB)	x	*	*
	Green Bio	DSM (CN)	*		n.d.			P(3HB-co-4HB)	n.d.	*	*
Other polyesters	EastarBio (PBST)	Eastman Chemical (US)				x		Copolyester	x	x	x
	Bionolle 1000 (PBS)	Showa (JP)	x					Copolyester	x	n.d.	n.d.
	Bionolle 3000 (PBSA)	Showa (JP)	x					Copolyester	x	n.d.	n.d.

x = existing property
n.d. = non determined
* could apply for certification

PLS = Thermoplastic starch
PLA = Poly Lactic Acid
PHA = Polyhydroxyalkanoate
PHBV = polyhydroxybutyrate-valerate

Most promising biopolymers for packaging are starch, PLA, PHA and cellulose. As shown in Table 1.2, even though biopolymers remain slightly more expensive than traditional plastics, they are competitive in terms of environmental impact: Gross Energy Requirements (GER) and Global Warming Potential (GWP).

Table 1.2. Bio-based polymers' main commercial and environmental features. Data gathered from [17-20].

		To replace	Price (€/kg)	Target (€/kg)	GER (MJ/kg)	GWP (kg CO2 eq/kg)
Bio-based polymers	Starch	HDPE, LDPE, PP, EPS	**1.5-4.5**	**0.7-0.9**	**25 - 54**	**1.14-1.2**
	Cellulose Acetate	LDPE in some cases	3-7	-	-	-
	PLA	HDPE, LDPE, PP, PET, PS	1.8-3	0.6	29.2	3.45
	PHAs	**PP,** PVC, LDPE, HDPE	2.5-10	3.4-3.52	21-90	-
Ref.	*LDPE*		*0,7-2*	-	*80*	*4,84*
	PS		*1-2*	-	*87*	*5,98*

Numerous studies have been undertaken to find the best production process for these materials and/or the best compound of bio-polymers. They can be used following different strategies: (i) alone, after a forming process, (ii) in a compound (ie. mixed with different additives such as pigments or plasticizers) or (iii) as a multi-layers material. Since the 1990's, several commercial products have emerged and are presented Table 1.1. Main strategies for improving bio-plastics performances are the addition of plasticizers and the incorporation of fillers or nanofillers as further discussed in the next chapter.

I.2.3. Plasticizers

The new trend in plasticizers is the use and development of natural-based plasticizers. During last decade, plasticizers worldwide production was 5 million tons per year, and is still increasing and offering numerous choices[21]. It represents a **global market of €7.6 billion** annually. However, 90% is consumed in PVC based formulation.

In 1951, the International Union of Pure and Applied Chemistry (IUPAC) developed a universally accepted **definition of a plasticizer** as a substance or a material incorporated in a material to increase its flexibility, workability or extensibility.

As mentioned earlier, **bio-polymers** often suffer from poor mechanical properties and/ or poor film formation property (brittleness). To avoid this problem, plasticizers are added to improve flexibility and processability by lowering the second order transition

temperature (the glass transition temperature T_g). Nevertheless, the use of plasticizers is being questioned due to their possible migration and toxicity. In response, some countries have developed new and restrictive regulations. Recent trend is, therefore, the use of natural-based plasticizers characterized by low toxicity and low migration (ie. polymeric plasticizers).

Currently, **most commonly used bio-plasticizers** are polyols, mono-, di- and oligosaccharides. Also, as reviewed very recently[22], many studies on edible and/or biodegradable films have focused on the use of **polyols** such as ***glycerol (G)*****,** ethylene glycol (EG), diethylene glycol (DEG), triethylene glycol (TEG) tetraethylene glycol and ***polyethylene glycol (PEG)***, propylene glycol (PG), sorbitol, mannitol and xylitol.

Other studied bioplasticizers are: **monosaccharides** (glucose, mannose, fructose, sucrose), **fatty acids, ethanolamine** (EA), **urea, triethanolamine** (TEA), **vegetable oils, lecithin, waxes** and **amino acids. Water** remains the most powerful "natural" plasticizer of hydrocolloid-based films such as starch based-films.

For starch film applications, the first category is most widely used even if monosaccharides appear to be interesting as well. They have been compared in terms of final mechanical properties, water vapor permeability, final glass transition temperature and transparency[23]. Monosaccharide-plasticized films were comparable to the polyol-plasticized films in terms of tensile strength, elongation, elastic modulus and transparency; but more resistant in terms of moisture permeation. It is assumed that the structural compatibility of monosaccharides with starch might result in denser polymer-plasticizer complex, smaller size of free volume and less segmental motion of starch chains (cf. chapter on barrier properties). Moreover, most recent studies (2009 – 2011) focus on epoxydized vegetable oils (EO) and epoxydized fatty acid esters (E-FAEs)[24, 25] from: soy bean oil (ESO)[26], linseed oil(ELO)[27], castor-oil, sunflower oil, rice oil[22], but mainly for PVC applications.

However, in our project, two polyols have been considered: GLY and PEG. The first one was most readily available for our partners and the second was proved efficient with dispersing nanoclays for barrier application[28] as targeted in this project.

I.3. Barrier Packaging

Barrier properties increases shelf life duration by protecting the inside product from deteriorations such as oxidation, humidity and bacteria. Better understanding of deterioration process has lead to distinguish five different types of barrier properties: gas (mainly oxygen), water vapor, aroma, grease and water and light.

Depending on the packaged product, privileged barriers will be sought.

Barrier properties are characterized by the permeability to the given element. Roughly, it represents the amount of the given element which can go through a given area of the tested material per time unit and per pressure difference across the material. The better the barrier, the higher the resistance opposed by the material to the element's molecules and the lower the permeability.

I.3.1. Mass transfer through packaging materials

Permeation, absorption and diffusion are typical mass transfer phenomena occurring in packaging systems. The equations behind these phenomena have been widely reviewed[29-31] and are presented as follow.

(i) Diffusion

The molecules diffuse, as a result of random molecular motion, through the material to the less concentrated side until equilibrium is reached. The phenomenon is often modeled in three steps, as presented in Figure 1.11. First, the molecules adsorb at the surface of the membrane / material; then they diffuse – ideally linearly - through the membrane; and finally they desorb on the other side.

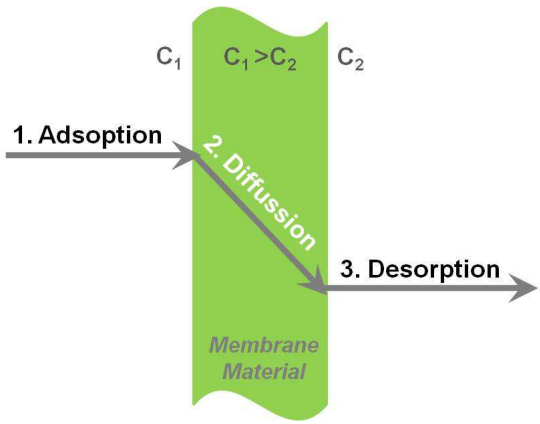

Figure 1.11. Schematic representation of the permeation phenomenon.

The mathematical theory of diffusion *in isotropic* substances is based on the hypothesis that the rate of transfer of diffusing substance through unit area is proportional to the concentration gradient measured normal to the section, ie.

$$F = -D\frac{\partial C}{\partial x}$$ **(Eq. 1. Fick's first law of diffusion)**

where F is the rate of transfer per un it area of section (g/m²/s), C the concentration of the diffusing substance (g/m^3), x the space coordinate measured normal to the section (m) and D is called the diffusion coefficient (m²/s).

The negative sign in Eq.1. arises because diffusion occurs, as mentioned earlier, in the direction opposite to that of increasing concentration[30].

Under the hypothesis of constant diffusion through the material and stationary state, the transfer rate F can be written as follow

$$\boldsymbol{F = \frac{-\mathrm{D}.\Delta C}{\Delta x} = \frac{\Delta m}{\mathrm{A}.\mathrm{t}}} \qquad \textbf{(Eq. 2. simplified equation of diffusion)}$$

Where Δm is the amount of permeate which diffuses through the material (g), A is the area of material / film through which the permeate diffuses (m²); and t the duration of diffusion phenomenon. From equation 2, we can write:

$$\boldsymbol{D = -\frac{\Delta m.\Delta x}{\Delta C.A.t}} \qquad \textbf{(Eq.3. Expression of diffusivity)}$$

Diffusivity (D) is a measure of how well the compound diffuses in the material[31].

(ii) Solubiltity

Adsorption and ***desorption*** measure the affinity of a given substance for two media with which it comes into contact[31]**.**

So, before gas can diffuse through the material, it must first dissolve into the material. Henry's law is applied to relate surface concentration of a gas component with the partial pressure in the atmosphere in which the material is in contact:

$$\boldsymbol{C = S.p} \qquad \textbf{(Eq. 4. Henry's law)}$$

where C is the concentration of the solute (mol/m^3), S is Henry's solubility (mol/m^3/Pa) and p is the partial pressure of the solute (Pa). From Henry's law, we deduce that solubility can be expressed as follow:

$$\boldsymbol{S = \frac{\Delta \mathrm{C}}{\Delta \mathrm{p}}} \qquad \textbf{(Eq. 5.)}$$

(iii) Permeation

Permeation is the ability of permeates to penetrate and pass right through an entire material in response to a difference in partial pressure.

Permeability includes both kinetic (diffusion) and thermodynamic (solubility) properties of the permeate system. Diffusivity (D), solubility (S) and permeability (P) have therefore the following relationship:

$$\boldsymbol{P = D.S} \qquad \textbf{(Eq. 6.)}$$

From equations (3), (5) and (6), for a system at equilibrium, permeability is:

$$\boldsymbol{P = D.S = \left(-\frac{\Delta m.\Delta x}{\Delta C.A.t}\right).\left(\frac{\Delta C}{\Delta p}\right) = -\frac{\Delta m.\Delta x}{\mathrm{A.t.\Delta p}}}$$

(Eq. 7. Expression of permeability)

Permeability is usually expressed in [g/m/s/Pa]. Most common permeability is measured to oxygen (PO_2) and water vapor (WVP).

One should note that in the Industry (paper for instance), the measurement of the **Permeance** – also called **Transmission Rate (TR)** - is preferred. It measures the flow of permeate without taking into account the thickness of the sample. Ensuing properties such as oxygen transmission rate (OTR) and water vapor permeability (WVTR) are expressed in [$g.m^{-2}.s^{-1}$] or more practically in [$g.m^{-2}.day^{-1}$].

The permeation mechanisms are specific to given polymers. It depends on the chemical nature of the polymer. It also depends on the polymer's grafting, blending with other polymers or the addition of a plasticizing agent. Finally, it depends on the permeate characteristics such as solubility (as seen above), the size and shape of the molecules, polarity and its interaction with the polymer, explaining why barrier properties are classified according to the type of permeate.[32] These parameters are reviewed in the next section.

Most important external parameters are temperature and humidity. They both greatly affect the behavior and the structure of both the polymer and the permeate. This is why it is very important to know in which conditions tests have been carried out. Unfortunately, this information is often forgotten in the literature.

I.3.2. Oxygen Barrier Property

Under ambient temperature and humidity, oxygen is most responsible for both oxidative and non-oxidative deterioration (appearance, mouth feel, change of flavor, microbial growth) of the packaged foods[33]. This explains why a large segment of commercial manufacturing deals with the production of packaging that extends shelf-life of food by controlling oxygen transport.

(i) Influencing parameters

The **chemical structure** of the polymer material will have a tremendous effect on its gas permeability by influencing two main factors: how tightly the polymer chains are bounded together (cohesive energy density) and how much free volume exists between chains.[34]

In general, the higher the **polymer's cohesive energy density**, the more difficult it is for the polymer chains to open and allow the permeate to pass. Highly polar permeates such as water are an exception to this rule as it can force the polymer chains open to engage in hydrogen bonding. This is why PO_2 is often measured at low **relative humidity**.

Free volume is a measure of the degree of interstitial space between the molecules in a polymer.[35] Diffusion and ensuing permeability both increases with increasing free volume. The addition of a **plasticizer** to a polymer film or an increase in **temperature** decreases its permeability as it increases the free volume and macromolecular mobility.

Orientation refers to the alignment of the polymer chains of the polymer's backbone**.** It will result in a diminution of the fractional free volume of the amorphous region, and/or an increase in tortuosity of the penetrant's path, reducing the permeability (in the case of semi-crystalline polymers).

Tacticity, which refers to the stereochemical arrangement of the substituted groups in relation to the plane of the polymer backbone, has also been identified as influencing the packing configuration of the polymer.

Crystallinity is a measure of the degree of order of the molecule in a polymer. The mass transfer of a gas in a semi-crystalline polymer is primarily a function of the amorphous phase, because the crystalline phase is usually assumed to be impermeable. Therefore, the higher the crystallinity of a polymer, the lower the permeability.

(ii) Test method

The oxygen transmission of a film is generally measured using a Mocon Ox-Tran (Modern Controls Inc., Minneapolis, USA) in accordance with ASTM method D 3985-95 "Standard test method for oxygen transmission rate through plastic film and sheeting using a coulometric sensor"[36].

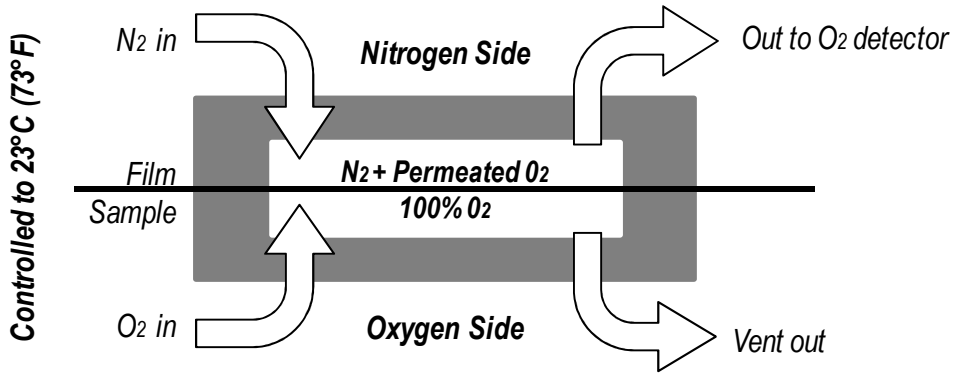

Figure 1.12. Measurement principle for oxygen permeability

As presented in Figure 1.12, the sample is placed as to separate the measuring cell in two. On one side, the air is continuously, purged with nitrogen whereas controls flow of oxygen is injected on the other side. The oxygen crossing over the sample is detected with a coulometric sensor. The measurement is usually made at low relative humidity (0%RH) and is calculated once steady state is reached. Some apparatus, dedicated to high barrier films, allow for the measurement and variation of relative humidity and temperature.

Other lab-made systems have been developed and follow the same principle.[37]

(iii) Oxygen barrier materials

Several polymers, such as PET, EVOH, and PVDC are well known for their oxygen barrier properties. Figure 1.14 gives an overview of different barrier polymers used in packaging. PVDC (Polyvinylidene chloride) is commercialized as Saran® for oxygen barrier. PET (PolyEthylene Terephthalate) can be crystallized (with loss of transparency) to increase its barrier properties. EVOH (Ethylene Vinyl Alcohol) is sensitive to water vapor and therefore, commonly used in between two layers of another water vapor barrier film.

Concerning biopolymers, more details will be given in the following section. However, it is important to already have in mind that polysaccharides and/or proteins

(category 1) have often been considered for protecting various food products through gas transfer control.[38, 39] They exhibit good oxygen barrier properties.

Polysaccharide films such as alginate and carrageenan films have been investigated[40-42] for such purposes, mostly mixed with other polysaccharides such as chitosan or pectin. Their polymer chains form ionic and hydrogen bonds which strongly decrease the permeability.

More recently, cellulose and hemicellulose derivates films have attracted some attention. For example, the oxygen barrier permeability of the AcGGM (acetylated galactoglucomannan hemicelluloses) films was found to be similar to, or lower than, the values reported on oxygen barrier films made from glucuronoxylan (hard wood xylan)[43]. Hartman reported oxygen permeability of 2.0 $cm^3 \cdot \mu m/m^2 \cdot d \cdot kPa$ for GGM-sorbitol film.[44] Most recent studies[45-47] now investigate xylan – polysaccharide nanocrystals composites.

In our project, main raw material is starch which films present rather good barrier properties at low hydration levels and plasticizer content compared to conventional membranes such as EVOH[48]. Early investigations on starch film properties were focused on amylose and amylomaize starches. Amylose film was observed to have a very low oxygen permeability under dry conditions at 25℃.[49] More recently amylopectin films have also been studied revealing comparable[50] or slightly higher permeability.[51] Structures of the starch polymers did not affect the oxygen transport indicating the very similar chemical nature of the two starchy polymers, and perhaps their similar interactions with water.

However, such results are obtained at dry state, and water vapor barrier usually also required in a multi-layer strategy, to protect starch films for instance, as *developed in our project FlexPakRenew.*

I.3.3. Water Vapor Barrier Property

(i) Influencing parameters

Parameters influencing water vapor permeability are similar to those of other gaseous molecules such as oxygen. The same mechanisms apply.

However, water molecules exhibit high polarity and high capacity to form hydrogen bonds which increases its permeability through some polymers.[32] Obviously, non-hydrophilic polymers should be preferred for water vapor barrier. Nevertheless, contrary to water, water vapor can go through a hydrophobic polymer.

(ii) Test method

As for oxygen permeability, a **dynamic** measurement of water vapor permeability is possible using a **Mocon Permatran** (Modern Controls Inc., Minneapolis, USA). Principle is the same as for Oxtran except that nitrogen is replaced by O%RH air flow and oxygen is replaced by 100%RH air flow. Moisture passing through the sample is detected.

However, the most widely used method for measuring water vapor permeability is **static** and in accordance with ASTM E96-95 "Standard test methods for water vapor transmission of materials". It is called the **"Cup method"** as it consists in using the sample material to close a cup filled with a desiccant (silica gel or calcium chloride typically) to maintain partial pressure to zero inside the cup as described in Figure 1.13. The cup is placed in a controlled atmosphere room (typically 23-25℃ and 50-60 HR %). The water vapor transmission across the material is assessed thanks to the mass gain of the cell at specific time.

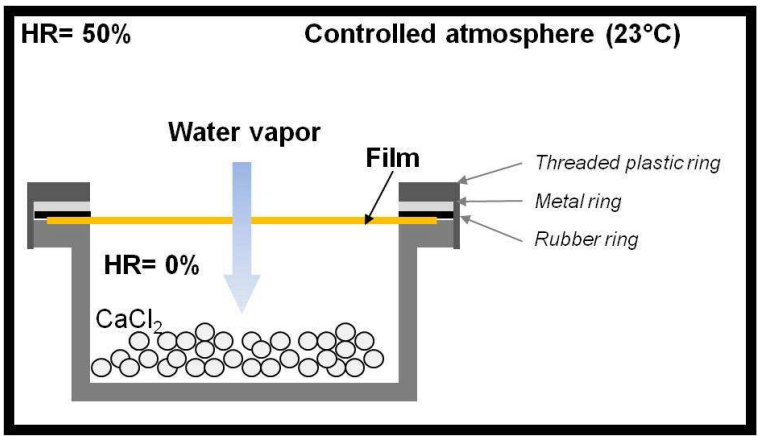

Figure 1.13. Cup Method for water vapor permeability

(iii) Water Vapor barrier materials

As shown in Figure 1.14, one given material rarely answered to all sough properties. We can see that oxygen and water vapor permeability are often contradictory. Therefore, other polymers such as PP and PE are sought for water vapor barrier. However, one polymer stands out: PVDC, as it provides a good barrier to both oxygen and water vapor.

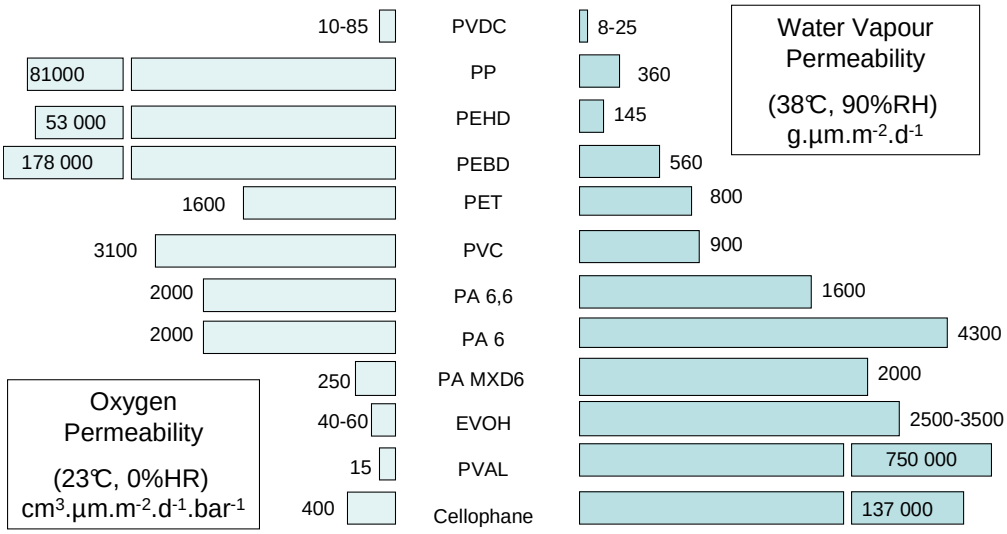

Figure 1.14. Water Vapour and Oxygen permeability of polymers commonly used in the packaging industry[32].

To combine both water and oxygen barrier properties in packaging, multi-layer and polymer mixtures are developed as an alternative, offering the possibility of using biopolymers as barrier materials.

I.3.4. Barrier properties of biopolymers

Giving the current interest is towards bio-polymers, water vapor and oxygen permeability of the most common ones are shown in Table 1.3. Even though results from different research teams are difficult to compare due to the differences in methods and measuring conditions, the data (sometimes recalculated from original data) show the tendency for most common bio-polymers. As for non bio-based polymers, oxygen and water vapor barrier properties are often contradictory.

Not all bio-based polymers can be used in coating for flexible packaging (e.g. PLA). It is also obvious that there is still an important gap between bio-based and petroleum-based polymers. So, over the last few years, there has been a lot of development in the area of new barrier technologies such as thin vaccum coating, new barrier polymers or nanocomposite materials[52].

Table 1.3. Water Vapor and Oxygen permeability of bio-based polymers and standard references.

Material (film thickness)	T (°C)	RH (%)	WVP [10^{11} g/m.s.Pa]	PO_2 [(cm^3.µm)/($day.m^2$.kPa)]	Ref.
Amylose + 40% glycerol	23	50	119	7	51
Amylopectin + 40% glycerol	23	50	144	14	51
Chitosan +40% glycerol	20	75		0.1-04	53
Pure Chitosan (15.2µm/ 2µm)	20 / 23 [b]	75 / 0 [b]	4,5	0.5203 cm^3/m^2.d	53, 54,55
Corn Starch (63.1µm)	25	75	17.7		54
Wheat starch (500µm)	20	n.a.		1.2096 [a]	56
Cassava (300-4000µm)	25	58	45[a]		57
Cassava + 20% glycerol (100µm)	23	50	240		58
Waxy Maize (300-4000µm)	25	58	38 [a]		57
Pea starch + 6.5% sorbitol	22	10	99.4 [a]		23
Pea starch + 10.87%% sorbitol	22	10	186.1 [a]		23
High Amylose	25	50	34		59
Zein coated High Amylose	25	50	1170		60
Natural Rubber (NR)	23	50	0.0107 [a]	1.67 [a]	61
PLA	23	50	1.34	160	62, 16
PHA	23	50		150	16
PHB (61µm)	25	50	0.245		63
Ecovio	ASTM F1249		0.92 [a]	1426 [a]	64
Ecoflex	ASTM F1249		1.7 [a]	3329 [a]	64
LDPE	ASTM D1434		0.01	1. 6897 [a]	65
PET	23	0/95[b]	0.28	153.2	62

[a] recalculated from original paper

n.a. Data non available in original paper

[b] differing conditions for O2 permeability

A widely exploited solution for improving barrier properties of bio-polymers is the incorporation of nano-fillers in the polymer to render bio-nano-composites. Indeed, tortuosity is an important parameter which increases molecules migration pathways and consequently limits permeability. Table 1.4 detailed later gathers main results from this research.

I.4. Nanocomposites

Composites are materials made of two types of components: (i) the matrix whose role is to support and protect the filler material and transmit and distribute the applied load to them; and (ii) the mentioned fillers, which are the stronger and stiffer components reinforcing the matrix.

Now, in the era of nanotechnologies, the reinforcing materials are often nanoscaled. Pioneer-work on nanocomposites was initiated by researchers at Toyota in the early 1990's that created nanoclay reinforced polymers, opening new research path on composites. Shortly after, researchers started working on bionanoparticles such as cellulose whiskers reinforced polymers.[66-70]

Indeed, for decades, studies had been conducted with non renewable inorganic fillers and petroleum based matrix. Increasing environmental concerns have led to developing new flexible barrier bio-based packaging and investigating the potential uses of renewable resources as matrix as well as nano-fillers.

Polysaccharides are good candidates for renewable nanofillers because they have partly crystalline structures conferring interesting properties. Recent reviews have been published on cellulose nanocrystals,[71-74] which is by far the most studied polysaccharide for nanoparticles. However, as far as we know, nothing similar had been done before 2010 for SNC except for mentioning in book chapters[75, 76]. Since then, two simultaneous reviews have been published. The first one[77] deals with starch nanoparticles and give an overview of structure, preparation, characterization and applications, whilst the second one[78] focuses on modification methods and ensuing properties as filler material.

Nanoparticles (fillers) not only enhance mechanical properties but also physical properties such as permeability. Their properties depend on the quantity, the nature and effectiveness of interactions at the interfacial region, i.e. on both the surface area and the dispersion of the particles. The surface area depends on the dimensions of the dispersed particles[76] from 0.5g/m² to 250g/m² for natural fibers and up to 1000g/m² for cellulose nanofibrils, exfoliated clays and carbon nanotubes.

One of the most wide sprayed classifications of nanoparticles is made according to particle shape. (i) Particulate, such as metallic nanoparticles or carbon black, are generally iso-dimentionnal and show moderate reinforcement due to their low aspect ratio. They are used to enhance resistance to flammability and decrease costs. (ii) Elongated particles which show better mechanical properties thanks to their high aspect

ratio. Such particles include, for example, cellulose nanocrystals and carbon nanotubes. (iii) Layered particles, like nanoclays, used to make what is referred to as LPN: Layered polymer nanocomposites. This latter family is the most used industrially and can show different degrees of dispersion as shown in Figure 1.15 viz. intercalated nanocomposites (intercalated polymer chains between layered nanocomposites), exfoliated nanocomposites (separation of individual layers) and flocculated or phase separated nanocomposites which are also called micro-composites and consequently show the poorer physical properties. Exfoliation is sought for by nanocomposite producers as it gives, by far, the best results. In light of reviewed classifications for fillers, starch nanocrystal fit the last category, "layered particles".

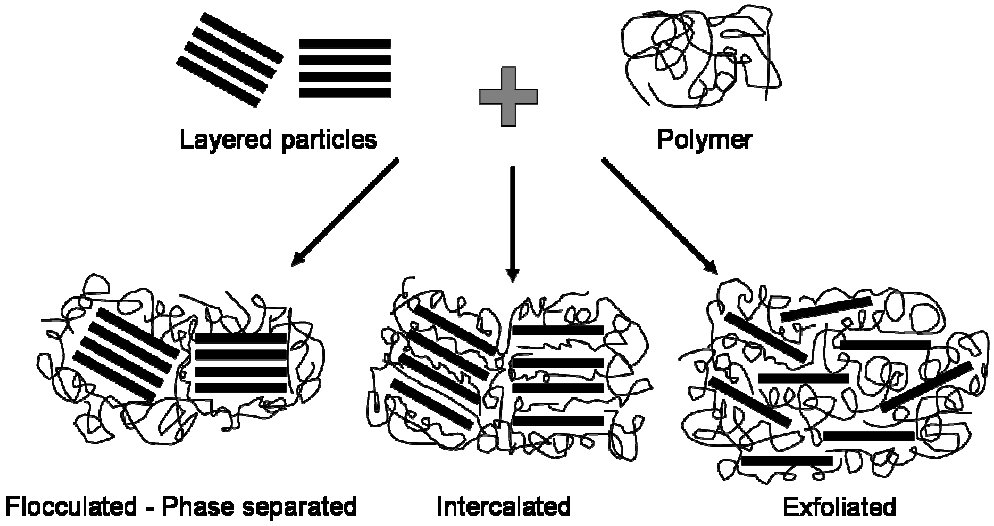

Figure 1.15. Possible dispersion of layered particles in a polymeric matrix.

Reproduced with permission from Alexandre and Dubois.[79] – Copyrigth 2000 Elsevier

There are several techniques for preparing such nanocomposites. For all techniques there are two steps: mixing and processing which often occur at the same time. Processing methods are usually the same as for pure polymers: extrusion, injection moulding, casting or compression moulding. Special attention must be brought to the processing temperature when working with organic nanofillers.

The choice of the matrix depends on several parameters such as the application, the compatibility between components, the process and costs. However, the current tendency is to use eco-friendly polymers such as PLA or starch blends. For food packaging applications and together with mechanical properties, barrier properties are of the most importance. Therefore, platelet shaped particles are preferred since they are thought to alter the diffusion path of penetrant molecules and improve the barrier

properties of the material. Clays and SNC could therefore both be fitted for flexible food packaging applications *as selected in our project (FlexPakRenew).*

Polymer matrix/clay-based nanocomposites have largely dominated the polymer literature,[80-85] since their first applications as reinforcement in the automotive industry. Packaging industry has focused its attention mainly on layered inorganic solids like clays and silicates, due to their availability, low cost, significant enhancement and relative simple processability.[86] Several studies have reported the effectiveness of nanoclay to decrease water vapor[87-90] and oxygen permeabilities[81, 82, 91] and improve mechanical properties.[80, 92] Most widely studied type of clay is montmorillonite (MMT).

Concerning renewable nano-fillers, an exponentially increasing number of studies have been undertaken since the first announcement of using cellulose whiskers as a reinforcing phase by Favier et al. in 1995[68]. New nanocomposite materials with original properties were obtained using cellulose whiskers and micro fibrillated cellulose; and leading to the development of studies on chitin whiskers[93-95] and SNC[61, 66, 96-100] by analogy. In comparison to nanoclay, literature on these bio-nanofillers is scarce. However, most studies report improved mechanical properties and water vapor barrier [21, 35, 36], although a few reported a negative impact on oxygen permeability despite improved mechanical properties.[101]

Water Vapor Permeability (WVP) values of polymeric matrices filled with mineral fillers compared to organic fillers are summarized in Table 1.4. Values are in the same order of magnitude. However, for the same polymeric matrix more microcrystalline cellulose is needed to reach values comparable to nanoZnO.[102]

Table 1.4. Water Vapor Permeability (WVP) of polymeric matrix filled either mineral fillers or organic fillers. Relative WVP refers to WVP values divided by the value obtained for the unfilled matrix.

	Matrix	Filler Content %	T (°C)	RH (%)	WVP [10^{11}g/m.s.Pa]	Relative WVP	Ref.
Mineral fillers	Glycerol Plasticized Pea Starch						
		Nano ZnO					
		0%	25	75	47.6	1.00	102
		0.5%	25	75	37.5 [a]	0.79	
		1%	25	75	27.5 [a]	0.58	
		2%	25	75	25 [a]	0.53	
		3%	25	75	22.1	0.46	
		4%	25	75	21.8	0.46	
	Glycerol Plasticized Chitosan						
		Unfilled	27.1	76.2	131	1.00	87
		Na-MMT 5%	26.4	78.8	98	0.75	
		Cloisite 30B 5%	24.3	78.2	92	0.70	
		Nano-Silver 5%	24.5	78.1	95	0.73	
		Ag-Ion 5%	22.3	77.3	96	0.73	
	PLA						
		Unfilled	25	50	1.8	1.00	88
		Cloisite Na+ 5%	25	50	2.08	1.16	
		Cloisite 30B 5%	25	50	1.7	0.94	
		Cloisite 20A 5%	25	50	1.15	0.64	
Organic fillers	Glycerol Plasticized Pea Starch						
		Microcrystalline Cellulose					
		0%	25	75	50.1	1.00	103
		2.5%	25	75	33 [a]	0.66	
		6%	25	75	27.5 [a]	0.55	
		8.5%	25	75	25.5	0.51	
		12%	25	75	30 [a]	0.60	
	Xylan						
		Sulfonated Cellulose Whiskers			gmil/hm² (WVTR*film thickness)		90
		0%	25	75	304	1.00	
		10%	25	75	174	0.57	
	Natural Rubber						
		Waxy Maize SNC					
		0%	25	50	34.1	1.00	61
		5%	25	50	24.1 [b]	0.71	
		10%	25	50	23.6 [b]	0.69	
		20%	25	50	18.8 [b]	0.55	

[a] recalculated from figure

[b] *recalculated from original paper's data*

As previously stated, starch is the second most studied organic materials for producing nanocrystals. To understand how these nanocrystals are extracted, it is first necessary to give more details on starch and its structure.

II. Starch

II.1. A widely used biopolymer

Starch is a natural, renewable, biodegradable polymer produced by many plants as a source of storage energy. It is one of the most abundant biomass materials in nature. It is found in plant roots, stalks, crop seeds and staple crops such as rice, corn, wheat, tapioca and potato.[104] Worldwide the main sources of starch are maize (82%), wheat (8%), potatoes (5%) and cassava (5%) from which tapioca starch is derived.[100] In 2010, the world starch market was estimated to be 68 million tons[105]. The value of the output is worth €48.8 billion per year, explaining the industrialists & researchers seeking for new properties or high value application.

Humans and their ancestors have always eaten starchy foods[106]. Starch grains have recently (2010) been identified from grinding stones in Europe (Italy, Czech Republic and Russia) dating back to 30,000 years ago.[107] The practical use of starch products (ie. non-food application) developed when Egyptians, in the pre-dynastic period, cemented strips of papyrus together with starch adhesive made from wheat.[106] Later, from 700 AD, rice starch was used as surface treatment of Chinese papers. A high fluidity starch was coated onto the paper to provide resistance to ink penetration, and then it was covered with powered starch to provide weight and thickness. Romans also used it in cosmetic creams, to powder the hair and to thicken sauces[108].

Nowadays, main uses of starch have not changed much, with around 60% being used for food and 40% for industrial applications (as described in Figure 1.16).[109]

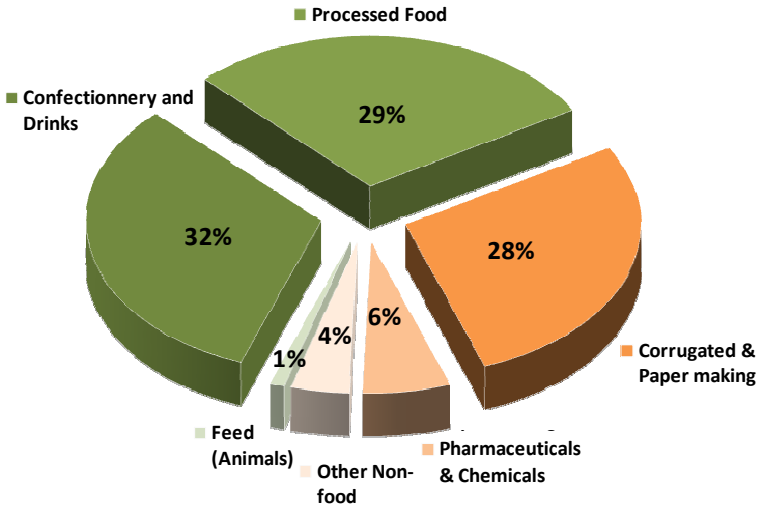

Figure 1.16. Sector of application of starch products (value %)
Green: food application – Orange: Industrial application.

The starch industry extracts and refines starches by wet grinding, sieving and drying. It is either used as extracted from the plant and is called “native starch”, or it undergoes one or more chemical modifications to reach specific properties and is called “modified starch”. However, most starches in the native form present limitations. For this reason, most granular starch used in Food or Industrial applications is first modified[110]. Starches are chemically and/or physically modified to accentuate their positive characteristics, diminish their undesirable qualities (such as high viscosisty, susceptibility to retrogradation, lack of process tolerance), or add new attributes (retention, film formation, digestibility, solubility etc…). Main properties and applications of modified starches are gathered in Table 1.5.

Table 1.5. Properties and use of physically and chemically modified starch.[111]

Type	Distinguishing properties	Common commercial non-food use
Acid-modified	Decreased hot-paste viscosity compared to unmodified starches	Textile sizing agent; binding material in cardboard-making
Cross-linked	Reduced peak viscosity, increased paste stability	Ingredients in antiperspirants and textile printing paste; oil-well drilling mud, printing ink, charcoal briquette binders, fiberglass sizing and textile sizing.
Acetylated (ester)	Excellent paste clarity and stability, good freeze-thraw stability; hydrophobic for high DS	Low DS: wrap sizing in textiles, forming sizes, and surface sizing in papermaking. High DS: thermoplastic molding and plasticizer.
Phosphate monoesters (ester)	Reduced gelatinization temperature, reduced retrogradation	Wet-end additives in paper-making; sizes in textile (polyester) and thickeners in textile printing inks.
Hydroxy-propylated (ether)	Increased paste clarity, reduced retrogradation, good freeze-thraw stability	Surface sizing and wet-ends in papermaking; Low DS : as wrap sizing in textiles.

However, for the last couple of decades, the increasing social and governmental demand for bio-based materials and energy has changed the way we consider starch and its industry. It is now faced with the dramatic rise in raw material costs as well as the controversial biofuel and biomaterial boom and other industry challenges. Frost & Sullivan reported that Europe's food starch market was characterized by further consolidation in 2007. The five leading players respectively Cargill, Roquette, Syral, Avebe and national starch announced either acquisitions (Cargill bough Cerestar and Syral bough Tate&Lyle production sites) or alliances (Avebe the belgian company and the US national starch).[112]

In our project, modified starch was used for coatings and composites applications (to obtain better film formation properties) and native starches have been used for the production of SNC. Indeed, several sources were investigated to assess the influence of botanic origin and chemical composition (Chapter 2).

For the corn starch used in our project, the detailed production process can be pictured as in Figure 1.17. Main steps include:

- **Cleaning** to remove batch contaminants such as broken corn, stones, dusts, and foreign grains.
- **Steeping** at 50℃, for 40-50h and at acid pH by addition of sulphuric acid or hydrochloric acid and treated with sulphur dioxide in order to achieve the loosening of the protein matrix and the consequence release of soluble, swelling of the kernels by water absorption (water content increases from 15-45%), controlled fermentation by lactic acid bateriae. The growth of lactic acid bateriae also prevents the development of unwanted micro-organisms.
- **Milling** and germ separation (degermination)
- **Gluten separation** from starch milk by successive continuous centrifugal separators.
- **Starch refining** with hydro-cyclone.
- **Dehydration and Drying** with flash dryers. For optimal shelf life residual moisture must not exceed 14 %.

Such a process is that of our starch manufacturer project partner with whom we had close collaboration. Several discussions and visits led to (i) the understanding of the starch production process, to (ii) considering the possible introduction of an SNC production process in their process, and to (iii) assess environmental impacts (as explained in Chapters 3 & 4).

Steps are roughly similar for other starches although some might slightly differ by name or to fit the given product. For Potato starch, for example, steeping is replaced by “Rasping” (mashing of potatoes); and gluten separation by fruit water extraction (which has a high content of proteins).

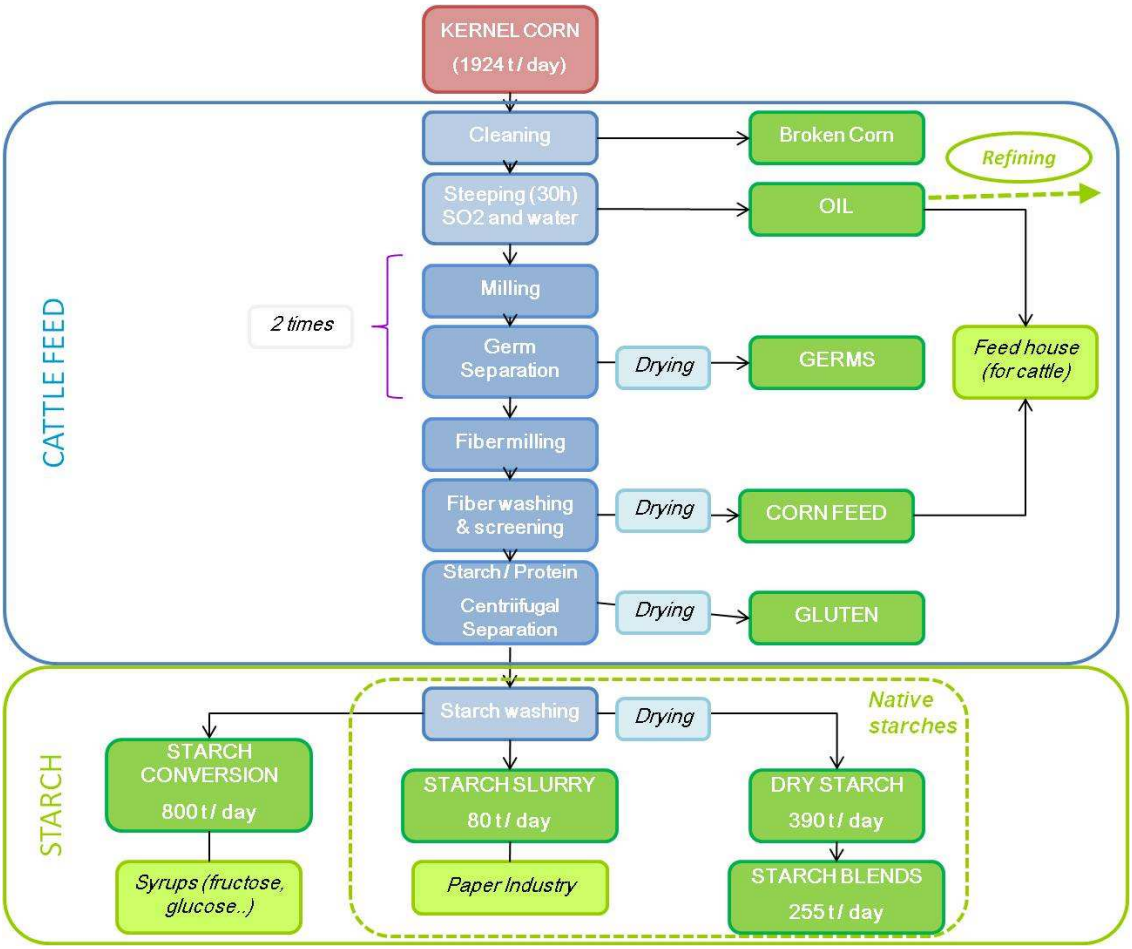

Figure 1.17. Maize starch extraction process.

Figure 1.18. Maize starch production site.

II.2. Starch structural features

II.2.1. Composition

After its extraction from plants, starch occurs as a flour-like white powder insoluble in cold water. This powder consists of microscopic granules with diameters ranging from 2 to 100µm depending on the botanic origin and with density 1.5.[113]

The basic formula of this polymer is $(C_6H_{10}O_5)_n$ and the glucose monomer is called α-D-glycopyranose (or α-D-glucose) when in cycle. Depending on conformation of the covalent bond between each anhydroglucose unit (AGU), different polysaccharides can be obtained such as cellulose and starch. In the case of starch, the AGU are α(1,4) and α(1,6) linked.

Detailed reviews[113-115] and articles[1, 116, 117] on starch structure have been published and we recommend referring to them for more details. Starch's composition was first determined by studying the residue of its total acid hydrolysis. It consists of mainly two glucosidic macromolecules: amylose and amylopectin as shown on Figure 1.19.

(a) Amylose

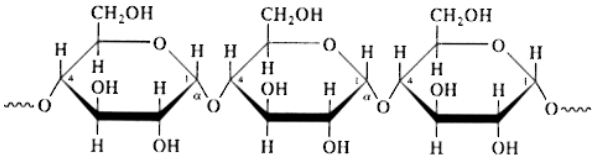

(b) Amylopectin

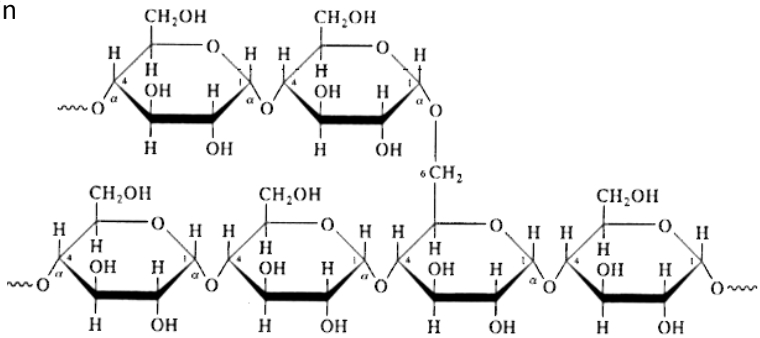

Figure 1.19. Chemical structure of (a) amylose and (b) amylopectin

In most common types of starch the weight percentages of amylose ranges between 72% and 82%, and the amylopectin's ranges from 18 to 28%. However, some mutant types of starch have very high amylose content (up to 70% and more for amylomaize) and some very low amylose content (1% for waxy maize).

Depending on their botanic origin, starch raw materials have different chemical content and thus size, shape and conversion factors (amount of starch in initial product) as described in Table 1.6.

Table 1.6. Conversion factor and characteristics of starches from different botanic origin.

Botanic Source	Maize	Wheat	Rice	Waxy	High	Cassava	Potato	Sweet	Smooth	Wrinkled
Ref.	113, 118, 119	113, 118, 119	114	113, 118	113, 118, 119	57, 119, 120	118, 119	119, 121, 122	123	123
Conversion factor	0.65	0.65	0.65	n.r.	n.r.	0.3	0.2	0.2	n.r.	n.r.
Granular size (µm)	30	30	2-7	15	5-25	3-30	40-100	3-27	2-40	17-30
Amylose (%)	25-28	25-29	20-25	0.5	60-73	28	20-25	19-22	33-48	60-80
Crystallinity (%)	39	36	38-51	39	19	n.r	25	n.r	18-36	n.r.
Crystalline Type	A	A	A	A	B	B	B	C	C	B

n.r. = non reported

Amylose is defined as a linear molecule of glucose units linked by α-(1-4)-D-glycoside bonds, slightly branched by α-(1-6) linkages. Amylopectin is a highly branched polymer consisting of relatively short branches of α-D-(1-4) glycopyranose that are interlinked by α-D-(1-6) –glucosidic linkages approximately every 22 glucose units.[124] Main characteristic of amylose and amylopectin are summarized in Table 1.7.

Table 1.7. Some characteristic of amylose and amylopectin

Property	Amylose	Amylopectin
Structure	Mostly linear	Branched
Av. chain length (units)	100-550	18-25
DP	700-6000	10^3-10^6
Av. Mw ($g.mol^{-1}$)	10^5-10^6	10^7-10^9
lamba max (nm)	640-660 (blue)	530-550 (red-brown)

The multiplicity in branching lead Peat et al.[125] to describe the basic organization of the chains in terms of A, B and C chains. This classification has nothing to do with crystalline types. The single C chain per molecule, with a mean degree of polymerization (DP) above 60, carries other chains as branches and contains the terminal reducing end of the amylopectin macromolecule. The A chains are glycosidically linked to the rest of the molecule by their reducing group trough C6 of a glucose residue. The B chains are defined as bearing other chains as branches. They are linked to the rest of the molecule by their reducing group on one side and by an α-(1-6) linkage on the other, thus being the backbone of the grape-like macromolecule. From then, several models have been proposed, all referring to the cluster model presented in Figure 1.20.

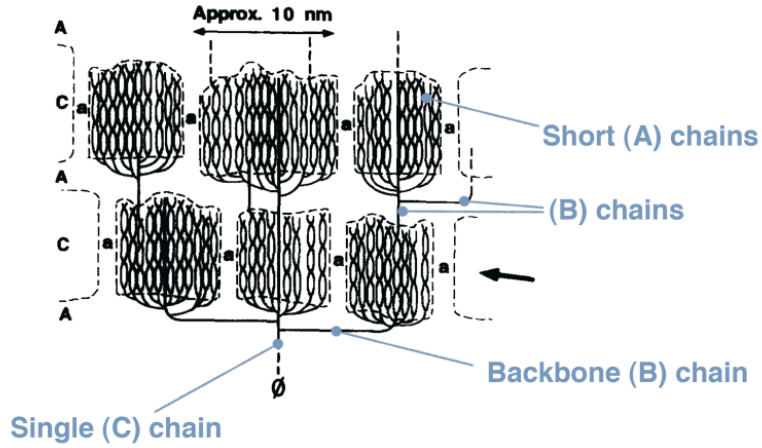

Figure 1.20. Amylopectin cluster model.
Reproduced with permission from Gallant et al.[1] – Copyrigth 1997 Elsevier

The structural differences in amylopectin macromolecule, related to the botanical species, are linked to the linkage rate. Aside from the C chain, amylopectin is made of two types of chains: Short chains (S) consisting in (A) chains and (B) chains with a mean DP ranging from 14 to 18; and (B) long chains (L), of DP 45-55 and sometimes above 60. The L/S ratio, expressed as molar basis was estimated at 5 for B-crystalline type (potato) starch and at 8-10 for normal cereal from A-crystalline type. These crystalline types are discussed later.

Investigation of the branch-chain length distribution of amylopectin was made possible using high-performance anion-exchange chromatography. Results from debranched amylopectin showed a polymodal distribution of chains[116] with five populations (A, B1,B2, B3 and B4). The A fraction was proposed to contain the A-chains, while the B1, B2, B3 and B4 represent the B- chains that stretch across 1, 2, 3 and 4 clusters, respectively. Hanashiro et al.[126] further assigned the chain-length distributions as A-chains, DP 6-12; B1-chains DP13-24; B2-chains DP 25-36; and B3-chains DP > 37.

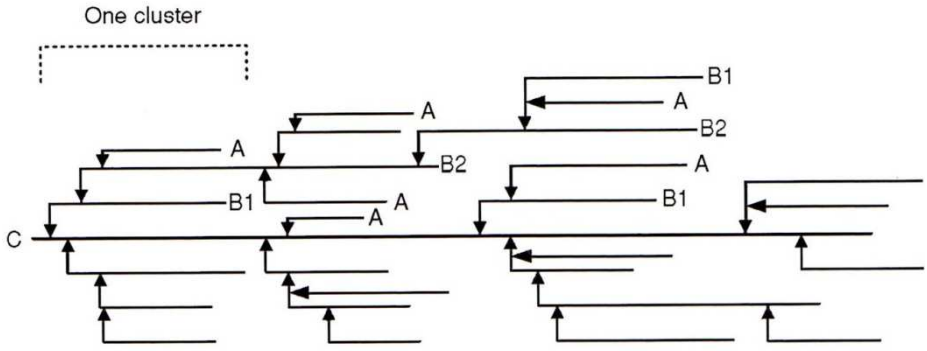

Figure 1.21. Illustration of amylopectin chain fractions[127]

Recent studies tend to demonstrate that granular size and shape are linked to chain length distribution. A comparative study on the molecular structures of the large (A) and the small (B) granules of wheat, barley and triticale starches shows that the amylopectin of the large, disk-shaped A granules consists of substantially more B2-chains and lesser A and B1-cahins than that of the small spherical B granules.[128] The authors suggest that amylopectin molecules consisting of more B2- and fewer A and B1-chains have cylindrical shapes, are easily aligned in parallel and lead to disk shaped granules. In contrast, amylopectin molecules consisting of more A- and B1-chains display cone shape, which tends to develop into spherical granules.

Minor components associated with starch granules are of three types: (i) cell-wall fragments, (ii) surface components, and (iii) internal components. The main constituents of surface components are proteins, enzymes, amino acid and nucleic acid, whereas internal components are composed mainly of lipids. Thus minor components of starch are often described as proteins, lipids and minerals.[113, 129] The proportion of these components depends on the botanical origin of starch (species and varieties). However, typical well washed cereal starch contain ~0.3% protein and up to 1.0% lipid, while typical root and tuber starch may contain ~0.05% protein and 0.05-0.1% lipids.[130] Starch contains several different minerals in small amounts, but the most important mineral is phosphorus.[113]

II.2.2. Starch structure

Starch structure has been under research for years and because of its complexity, a universally accepted model is still lacking.[113] However, this last decade a model seems predominant. It is a multi-scale structure shown in Figure 1.22. consisting in the (a) granule (2-100µm), into which we find (b) growth rings (120-500nm) composed of (d) blocklets (20-50nm) made of (c) amorphous and crystalline lamellae (9 nm)[1] containing (g) amylopectin and (h) amylose chains (0.1-1nm).

The shape and particle size of granules depends strongly on its botanic origin. On the surface, pores can be observed as can be seen in Figure 1.22.a. They are thought to be going through the growth rings to the hilum (centre of the granule). Observed under a microscope and polarized light, starch shows birefringence. The refracted “Maltese cross” corresponding to the crystalline region is characteristic of a radial orientation of the macromolecules.[113] X-ray diffraction study showed that starch is a semi-crystalline polymer.[131] Starch granules consist of concentric alternating amorphous and semi-crystalline growth rings. They grow by apposition from the hilum of the granule.

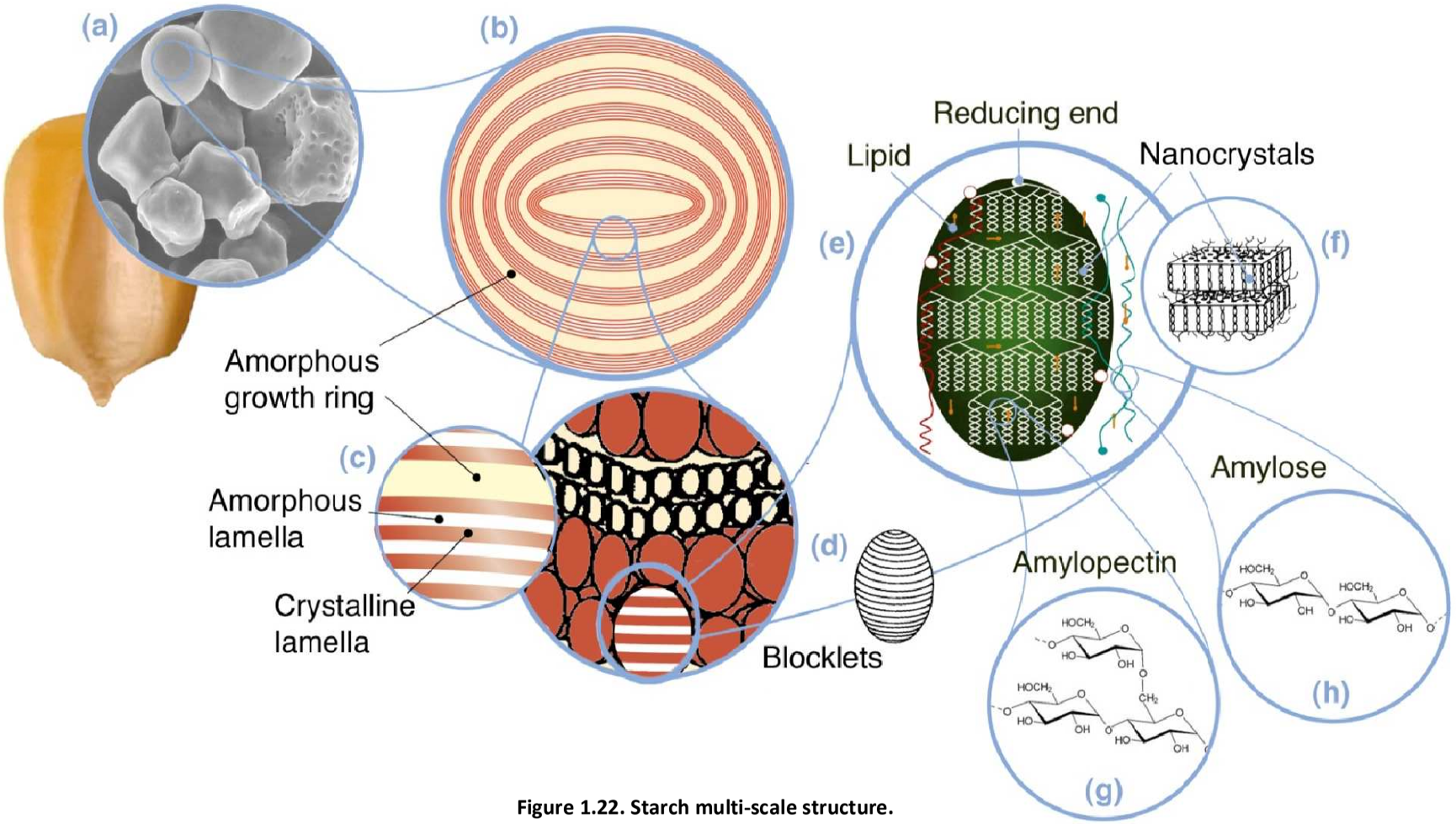

Figure 1.22. Starch multi-scale structure.

(a) Starch granules from normal maize (30µm), (b) Amorphous and Semi-crystalline growth rings (120-500nm), (c) Amorphous and Crystalline lamellae (9nm): magnified details of the semi crystalline growth ring:, (d) Blocklets (20-50nm): constituting unit of the growth rings, (e) Amylopectin double helices forming the crystalline lamellae of the blocklets:, (f) Nanocrystals: other representation of the crystalline lamellae called SNC when separated by acid hydrolysis, (g) Amylopectin's molecular structure, (h) Amylose's molecular structure (0,1-1nm). Reproduced with permissions from Gallant et al.,1 – Copyrigth 1997 Elsevier; Donald et al.,2 – Copyrigth Science and Technology Facilities Council 1997 ; and Tang et al.3 – Copyrigth 2006 Elsevier

The number and thickness of these layers depend on the botanical origin of starch. They are thought to be 120-400nm thick.[132] Details on the structure of amorphous growth ring are not found in literature.

The blocklet concept was developed in the 1930's by Hanson and Katz[131] but quickly opposed to the fibrillar concept developed by Sterling[48] and the following cluster organization model developed by Nikuni et al.,[133] one reducing group at the hilum and thus, one macromolecule of amylopectin for the whole granule. It was later corrected by French[132] and Lineback[134] representing starch layers as clusters of short chains. More recently SEM observations have enabled the observation of blocklets structure.[135-137] Although the blocklet concept is not commonly mentioned in the literature, it was heavily supported and brought back to discussion by Gallant et al.[1] They suggested that both semi-crystalline and amorphous growth rings are subdivided into respectively large (diameter 20-500nm for wheat) and small (25nm) spherical blocklets. More recently, Tang et al.[3] supposed the blocklets of the amorphous region and the surface pores (as mentioned earlier) to be defective blocklets, with lower branching molecules. On average two end-to-end blocklets would constitute a single semi-crystalline growth ring. These blocklets have an average size of 100 nm in diameter and are proposed to contain 280 amylopectin side chain clusters.[114]

Schematically, the semi-crystalline growth rings consist of a stack of repeated crystalline and amorphous lamellae (Figure 1.22). The thickness of the combined layers is 9 nm regardless the botanic origin. In reality it is believed that the crystalline region is created by the interwining of chains with a linear length above 10 glucose units to form double helices[115] which are packed and form the crystallites; and the amorphous region corresponds to branching points.

Until now, the location and state of amylose within granules is one of the most important questions remaining to be answered. Depending on the botanic origin of starch, amylose has been found in the amorphous region[138] (e.g. wheat starch), in bundles between amylopectin clusters,[138] or interspersed among amylopectin clusters in both the amorphous and crystalline regions (e.g. normal maize starch).[138] However, it has been demonstrated via cross-linking experiments using corn starch, that amylose molecules do not crosslink to one another, but do crosslink to amylopectin chains.[139, 140] Thus, it invalidates the hypothesis of amylose chains forming bundles. The currently accepted model of amylose location in starch granule is therefore, as individual, radially-oriented chains randomly distributed among amylopectin chains.[141] Also, there is, now, evidence of an enrichment of amylose towards the periphery of the granule and that

amylose molecules found towards the surface of the granules have shorter chain length than those located in the center.[142]

II.3. Organization of the crystalline structure

Crystallization or double helices formation can occur either in the same amylopectin branch cluster or between adjacent clusters, in three dimensions and is called the superhelical structure as proposed by Oostergetel et al. and described in Figure 1.23.a. Bertoft suggested the super-helical structure not necessarily be based on the cluster model (Figure 1.23.b) but could also be based on a two-directional backbone formed by a single amylopectin molecule (Figure 1.23.c).

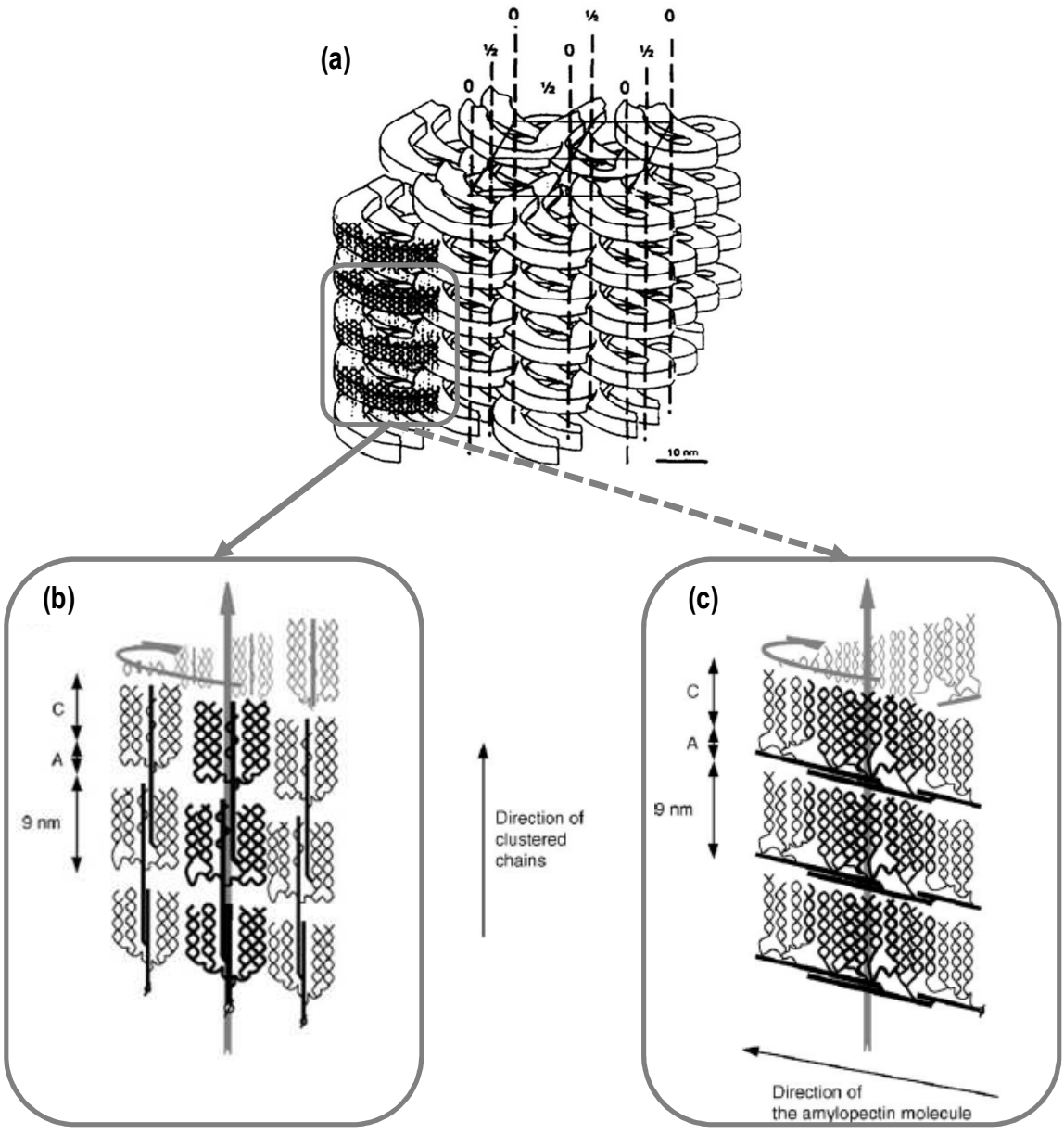

Figure 1.23. Schematic model for the arrangement of amylopectin in potato starch showing the 'super-helical' structure and the amorphous areas inside the crystalline organization. From Oostergetel and van Bruggen[143] and Bertoft[144]

Although this model follows the fibrillar concept, Gallant et al.[1] supported the helical lamellar model because studies showed that amylopectin lamella were also observed within blocklets (about 10). The super-helix has a diameter of 18nm and a central cavity with a diameter ~8nm. They calculated that assuming that an amylopectin side chain cluster is 10 nm, a small blocklet (20-50 nm) is composed of about 2 to 5 side chain clusters.

Tang et al.[3] illustrated the blocklet model as shown in Figure 1.22(d) making amylopectin the backbone of the blocklet structure. Amylose molecules are thought to occur in the granule as individual molecules, randomly interspersed among amylopectin molecules and in close proximity with one another, in both the crystalline and amorphous regions.[115]

Native starches contain between 15% and 45% of crystalline material. Depending on their X-ray diffraction pattern, starches are categorized in three crystalline types called A, B and C. Hizukuri et al.[116, 145] postulated that amylopectin chain length was a determining factor for crystalline polymorphism. Imberty et al.[146, 147] proposed a model for the double helices packing configuration to explain difference between A and B type starches. A-type structures are closely packed with water molecules between each double helical structure, whereas B-types are more open and water molecules are located in the central cavity formed by 6 double helices as shown in Figure 1.24.

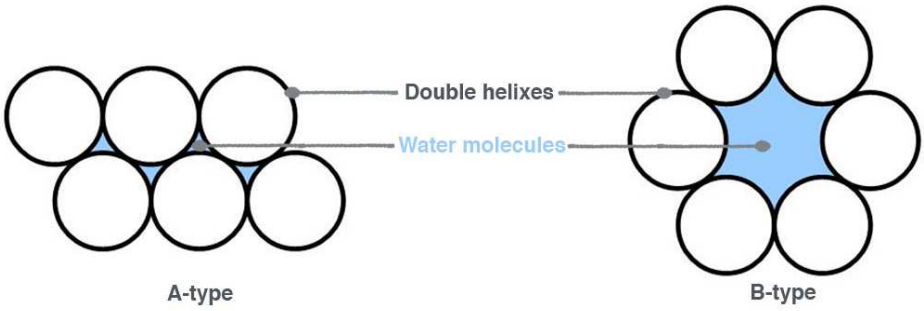

Figure 1.24. Double helices packing configuration according to crystalline type.

It was later envisaged that branching patterns of the different types of starch may also differ.[148] It was suggested that the B-type amylopectin branching points are clustered forming a smaller amorphous lamella whereas A-type amylopectin branching points are scattered in both the amorphous and the crystalline regions, giving more flexibility to double helices to pack closely. Gerard et al.[149] recently confirmed that the distance between two α(1-6) linkages and the branching density inside each cluster are determining factors for the development of crystallinity in starch granules. Clusters with numerous short chains and short linkage distance produce densely packed structures which crystallizes into the A allomorphic type. Longer chains and distances lead to a B-type.

C-type starch pattern has been considered to be a mixture of both A and B-types *(*presented in Figure 1.25*)* since its X-ray diffraction pattern can be resolved as a combination of the previous two. It has been suggested by Bogracheva et al.[150] that C-type starch granules contain both types of polymorph: the B-type at the centre of the granule and the A-type at the surrounding.

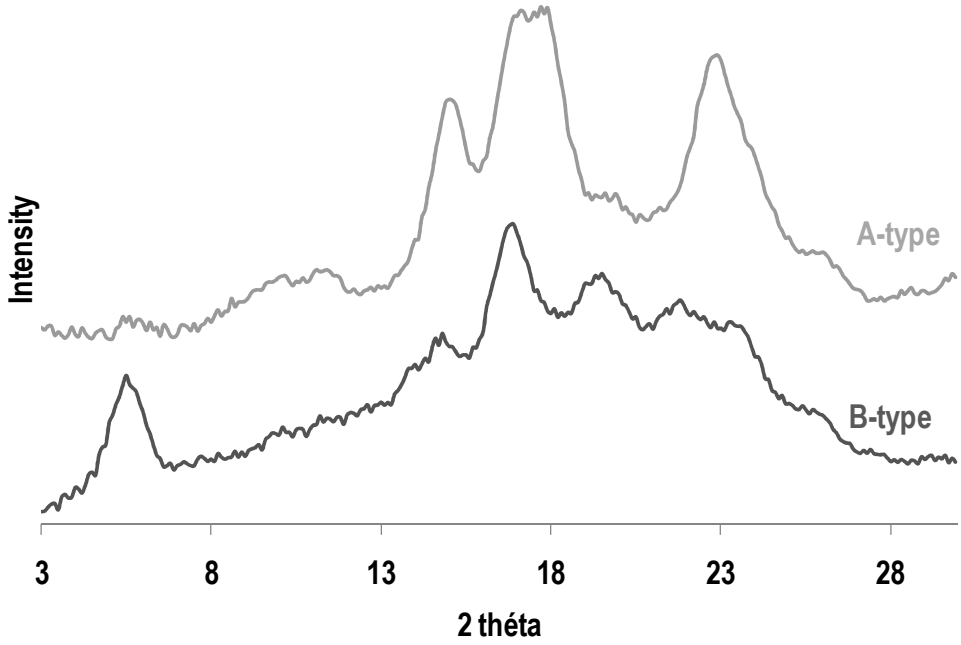

Figure 1.25. Typical X-Ray diffraction pattern for (a) A-type starch and (b) B-type starch.

Several attempts of structural characterization of C-type starch were conducted using acid hydrolysis by Wang et al.[151, 152] They revealed that the core part of C-type starch was preferably hydrolyzed and that hydrolyzed starch showed A-type diffraction pattern, suggesting that B-type polymorphs constitute mainly the amorphous regions and are more readily hydrolyzed than A-types constituting mainly the crystalline region. This is in agreement with the previous conclusions of Jane et al.,[148] that B-type starches are more acid-resistant than A-types. These conclusions are of importance for SNC preparation (detailed in Chapter 2).

Another V-type was also identified as the result of amylose being complexed with other substances such as iodine, fatty acid, emulsifiers or butanol. This crystalline form is characterized by a simple left helix with six glucose units per turn.[153] *This complex-formation property allows its separation from amylopectin. It lead to the development of qualitative and quantitative methods to detect amylose presence or content in starch. Details on the iodine test are proposed in Chapter 2.*

Cheetman et al.[154] established a correlation between the maize starch amylose content (0-84%) and both the average chain length of amylopectin and the ratio of short chains to long chains (S/L). Higher amylose content granules display a higher average chain length and a lower ratio than lower amylose granules. The results showed a transition of crystalline type from A through C to B, accompanying a decrease in the degree of crystallinity from 41.8 to 17.2% across a range of apparent amylose content from 0% to 84%. These findings are summarized in Table 1.8 together with Imberty et al.'s[146, 147] and Gerard et al.'s[149] conclusions mentioned earlier.

Jenkins & Donalds,[117] concluded that an increase in amylose content has the effect of increasing the size of the crystalline lamella and acts to disrupt their packing. Two mechanisms to explain this disrupting have been introduced: firstly co-crystallization between amylose and amylopectin chains, and secondly, the penetration of amylose into amorphous regions.

Table 1.8. Correlation between crystalline type and nanostructure of maize starch.

Crystalline type	A	C	B	Ref.
Amylose content (%)	Low (0-30%)	40%	High (50-90%)	154
Amylopectin CL	Short		Long	145
L/S amylopectin chains	High (10 mole %)		Low (4 mole %)	154
Crystallinity	High (30-40%)		Low (17-20%)	154
Double helices structure	Closed packed arrangement with water molecules between each double helical structure		More open arrangement with water molecules are located in the central cavity formed by 6 double helices	147
Branching density & distance between α(1-6) linkages	High density and short distance		Low density and long distance	149
Crystalline lamellae	Thin		Large	

Thus starch crystalline type most likely has an influence on the granule's and the crystallites' (i) thermal and (ii) hygrothermal stability.

Thermal stability of crystallites has been further studied in chapter 2. Starch's hygro-thermal propery, though, is an important particularity of starch which explains why it is used in industrial applications such as coating.

II.4. Hygrothermal property of starch

II.4.1. Starch cooking

At ambient temperature, starch is insoluble in water. However, in excess water and at temperature higher than 60°C, starch undergo es an irreversible change of state leading to solubilisation called **gelatinization**.

First, the granules absorb and swell with water. Then, further swelling leads to hydrogen bonds breakage and subsequent diffusion of low molecular mass material (amylose, intermediate material) from granule to water. The suspension loses its white color and turns translucent.

Upon cooling down, phase separation occurs and the polymer chains rearrange to form a network (re-crystallization) – it is called **gelification or retrogradation**. The suspension displays a gel-like appearance and loses its translucent aspect in favour of an opaque aspect.

These steps are represented in Figure 1.26.

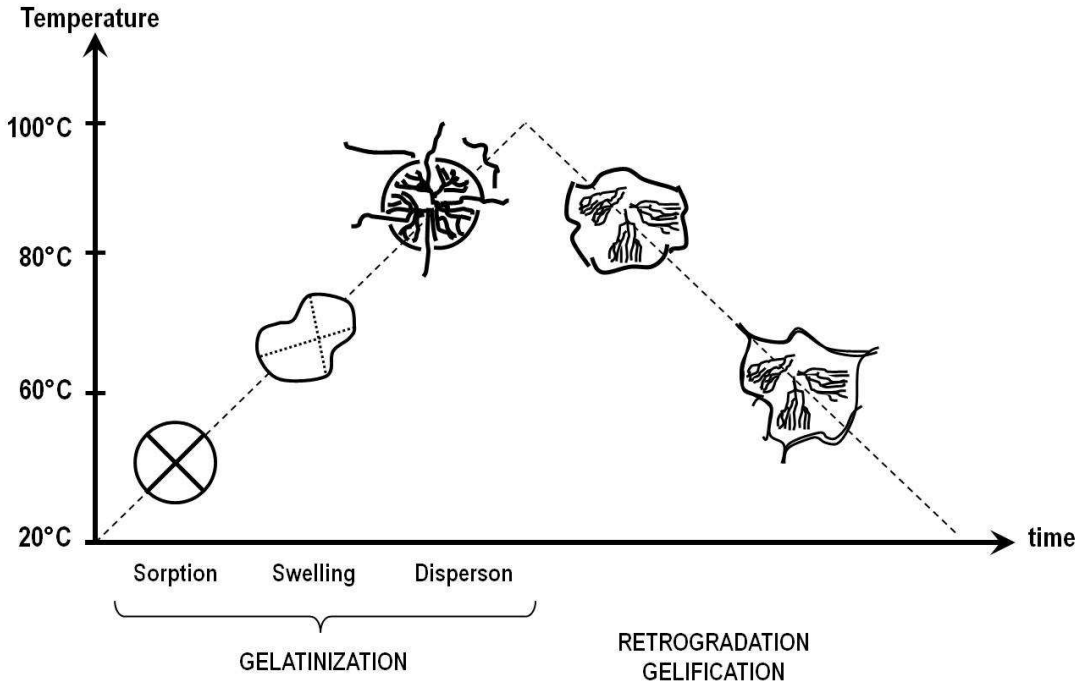

Figure 1.26. Starch transformation upon heating in excess water (Adapted from [155]).

II.4.2. Granular starch thermal transitions

Starch granules thermal properties have been widely investigated[156-162] and have been shown to be strongly dependent on water content. Most common technique for studying the thermal behavior of polymers is Differential Scanning Calorimetry (DSC). It detects changes in heat flow associated with first-order transitions (melting) and second-order transitions (glass transition) of polymers[163]. In excess water, an increase in temperature leads to the apparition of an endothermic peak (about 50℃-70℃) linked to the gelatinization of starch. At intermediate water content (30-60%), several models have been developed to explain the two peaks generally observed: the first peak is shifted up in temperature, and a higher temperature second peak is observed. At very low water content (>20%), only the second peak is observed.

Several explanations have been developed. First, it was suggested[164] that in excess water, the amorphous growth ring is believed to suck in water and expand. As they are cross-linked by the amorphous backbone, the semi-crystalline lamellae are disrupted causing a loss of order and crystallinity. When the amount of water becomes insufficient to fully swell the granule, the remaining crystallites melt at higher temperature (second peak). An alternative explanation for the two peaks was provided by Evans and Haisman[165]. They attributed the first peak to the melting of least stable crystallites which upon melting absorb all remaining water. Thus second peak reflects the melting at higher temperatures of remaining crystallites. However this hypothesis did not take into account possible reorganization of polymer chains in the amorphous phase and the remaining crystallites during DSC heating.[163] Biliaderis et al.[166] suggested that the multiple melting transition profile was due to partial melting followed by recrystallization and final melting. Barron[156] suggested it is rather linked to the heterogeneous repartition of water in starch. Zong et al.[158] attributed them to respectively the melting of crystallites and the melting of amylose lipid complexes

Another approach to the understanding of starch thermal behavior consists in considering it from a polymeric point of view, as a semi-crystalline polymer whose specific heat-temperature curves exhibit the characteristics of both glassy and crystalline polymers[163]. The most important property of an amorphous polymer is the glass transition which reflects the gradual phase transition from glassy to rubbery state. For crystalline polymers, the phase transition from crystalline to amorphous is sharp and is called melting. The temperatures associated with the phases transitions are respectively T_g the glass transition temperature and T_m the melting temperature.

As for more classic polymers, Biliaderis et al.[163] revealed that regardless of the amount of water, melting (T_m) is T_g dependent in that a previous softening (relaxation) of the amorphous parts is required before crystallites can melt. As such, the melting temperature of starch crystallites is also affected by plasticizers such as water. However, despite good correlation between experimental data and the two-phase Flory Huggins model at intermediate and low water content, a tree-phase model was proposed. It consisted in (i) a bulk amorphous region responsible for T_g, (ii) a non-ordered intercrystalline phase which mobility is restricted by crystallinity induced cross-linking and (iii) a fully ordered crystalline phase. In 1990, Tester and Morisson[167] proposed that the swelling property of starch granules is the results of the property of amylopectin with amylose acting as a dilutants.

More recently others[162, 168] proposed a liquid-crystal approach to explain the gelatinization of starch. Side-chain liquid-crystalline polymers (SCLCP) consist of three separate components: backbones, spacers and mesogens[168] as described in Figure 1.27. **Mesogen** is the fundamental unit of a liquid crystal that induces structural order in the crystals.

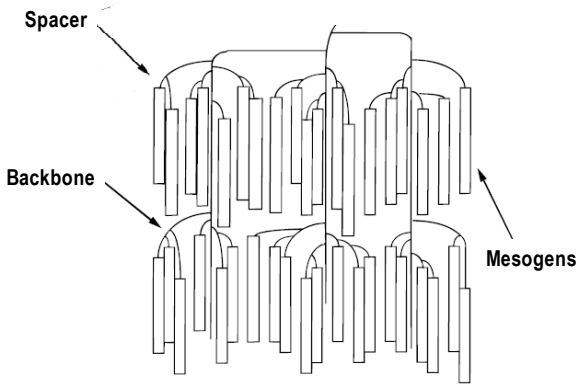

Figure 1.27. Illustration of the SCLCP potential of amylopectin side chain clusters. (Adapted from [169])

The double helices of the amylopectin side chains correspond to mesogens, which are attached to the backbones by short spacer units (connecting points). Considering the SCLCP nature of amylopectin, Waigh et al.[162] and Atichokudomchai et al., 2002[161], described, as presented in Figure 1.28, a first thermal transition corresponding to a smectic (lamellar order)/ nematic (orientationally ordered) transition for B-type starches, and to a nematic / isotropic phase transition for A-type starches (ie. helix-helix dissociation). They also attributed the second transition to an helix-coil transition (ie. unwinding of double helices to a gel phase). In excess water (>60%) (Figure 1.28 a), the difference between the two endotherms is immeasurably small and are thought to occur almost simultaneously. At intermediate water content (30-60%)

(Figure 1.28 b), the two endotherms can be evidence one after the other. In low water content (<30%) (Figure 1.28 c), a direct glassy-nematic (or crystalline) to gel transition occurs as the helices unwind for B and A-type crystallinity respectively (one peak).

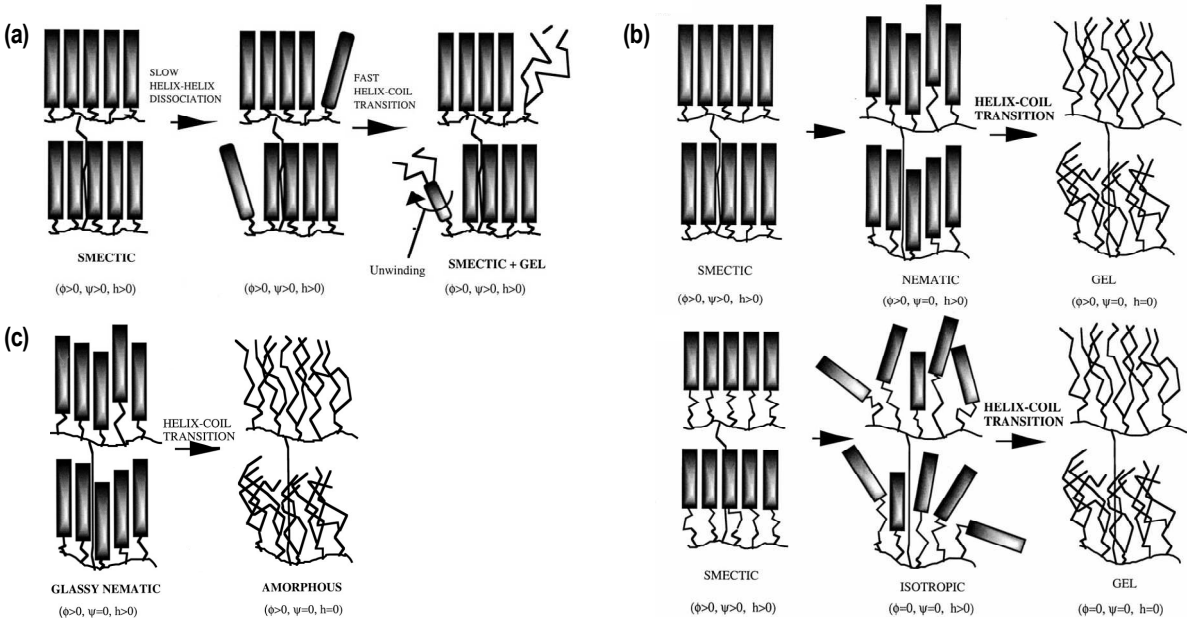

Figure 1.28. Processes involved in the gelatinisation of starch in (a) excess water, (b) limiting water Two different processes are shown for A and B type starches: in B-type starch the intermediate phase is nematic in character, and in A-type starch the intermediate phase is isotropic in character ; and (c) in very low water content. It is proposed that the intermediate phase is determined by the length of the amylopectin helices. Relative values of the orientational (ϕ), lamellar (ψ), and helical order parameter (*h*) are included. Adapted from Waigh et al.[162])

This hygrothermal property is very important in the framework of our project and had to be managed all along the different production steps, such as:

- *The SNC production: The acid hydrolysis is a water-based process. To avoid the gelatinization of granular starch, and keep its semi-crystalline structure, the temperature has to be kept below 50℃.*
- *The waterborne starch coating: In this project, starch is also used as a thermoplastic polymeric matrix (or coating color) that should contain the coating fillers. As such, it has to be thoroughly "cooked" (i.e. gelatinized) before use to ensure homogeneity.*
- *The SNC used as fillers should either be used in dry processed to avoid gelatinization; or the processing temperature of water-based processes should be carefully monitored to avoid gelatinization. Gelatinized SNC would otherwise "loose" their structural nano-impact.*

Now that starch structure and properties have been detailed, SNC's structure, preparation and properties can be described with references to its native structure.

III. Starch nanocrystals (SNC)

This part of the chapter is inspired from: D. Le Corre, J. Bras, A. Dufresne, Starch Nanoparticles: A Review, Biomacromolecules 2010, 11, 1139-1153. As the literature review was submitted in December 2009, studies published since then or at the same time have been added to update the review. Also, some general comments are added for better understanding of our project's context. They are both identified by a grey italic font.

First of all, it is important to clarify the terms commonly used. Starch crystallite, starch nanocrystal, microcrystalline starch and hydrolyzed starch all refer to the crystalline part of starch obtained by hydrolysis but at different extent (from the most to the least). It has to be distinguished from starch nanoparticles, presented later, which can be amorphous.

First interest in SNC has been studied by analogy with cellulose whiskers to be used as reinforcing fillers in a matrix. In 1996, Dufresne et al.[66] reported a method for preparing what they called at the time "microcrystalline starch" and which they reported to be agglomerated particles of a few tens of nanometers in diameters. The procedure consisted in hydrolyzing starch (5 wt%) in a 2.2N HCl suspension for 15 days. Since it was shown that classical models for polymers containing spherical particles could not explain the reinforcing effect of microcrystals, further studies on the morphology of these microcrystals were conducted by Dufresne and Cavaillé[170] in light of aggregate formation and percolation concept.

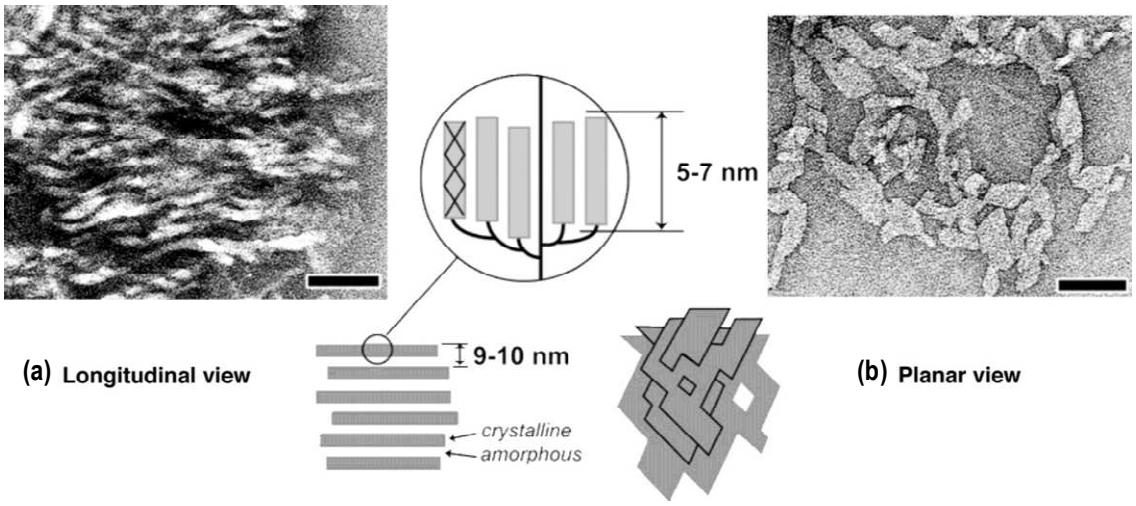

Figure 1.29. First TEM observations of SNC: (a) longitudinal view & (b) planar view. Reproduced with permission from Putaux et al.[99] Copyright 2003 American Chemical Society.

In 2003, Putaux et al.[99] revealed the morphology of "nanocrystals resulting from the disruption of waxy maize starch granules by acid hydrolysis". After 6 weeks of hydrolysis, TEM observations (Figure 1.29) showed: (a) a longitudinal view of lamellar fragments consisting of stack of elongated elements, with a width of 5-7 nm and (b) a planar view of individualized platelet after hydrolysis. Shapes and lateral dimensions were derived from observation of individual platelets in planar view: a marked 60-65° acute angles for parallelepipedal blocks with a length of 20-40 nm and a width of 15-30 nm.

However, more recent publications report bigger SNC (40-70nm for potato SNC[171]; 30-80nm[172] and 60-150nm[173, 174] for pea SNC; and 50nm[175] and 70-100nm[176] for waxy SNC), with round edges[177] and found as grape-like aggregates of 1-5µm. The heterogeneity in particle size could be explained by the differences in starch types but also by the difficulty to obtain well define pictures of non-aggregated nanocrystals.

Contrary to cellulose nanocrystals SNC are not almost 100% crystalline but rather 45% crystalline with variations depending on the botanic origin as recently presented by Le Corre et al.[178]

III.1. SNC preparation

III.1.1. Acid hydrolysis kinetic

Acid hydrolysis has been used for a long time to modify starch and its properties. Nageli [179] reported the obtaining of a low molecular weight acid resistant fraction after the hydrolysis of potato starch, at room temperature during 30 days in a 15% H_2SO_4 suspension. The fraction would be known as Nageli amylodextrin. Lintner[180] also gave his name to a hydrolysis process consisting of a 7.5% (w/v) HCl suspension of potato starch at 30-40°C to produce a high molecular weigh t starch suspension called "lintnerized starch". Most recent publications use either one of these two acidic conditions.

In the industry, starch slurry is treated with dilute HCl or H_2SO_4 at 25-55°C for various periods of time, to produce "acid-thinned" starch used as sizing agents, in gum candies production, in paper and paper board production.

Nowadays, most existing acid-modifications aim at producing "soluble" starch or glucose syrup for biotechnologies with production of PLA or biofuels for examples. Only few studies have reported the use of acid hydrolysis to produce microcrystalline starch[66,

[181] and SNC.[100] Figure 1.30 reports the hydrolysis kinetics for different starches and from different research groups.

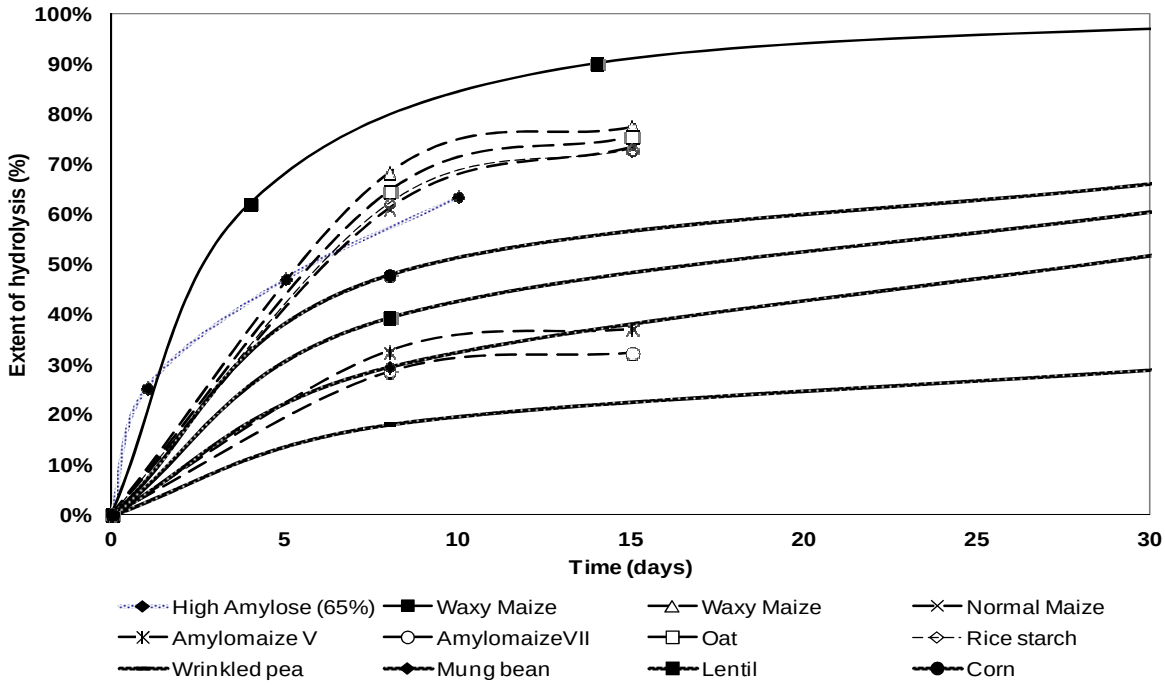

Figure 1.30. Hydrolysis kinetic of different starches.

High amylose (65%) from Li et al.[181] (dotted line); Waxy maize (■) from Angellier et al.[182] (plan line); Waxy maize, normal maize, amylomaize V, amylomaize VII, oat and rice starch from Jayakody et al.[183] (dash line--); Wrinkled pea, mung bean, lentil and corn from Robin et al.[184] (dot filled line).

For all starches a two-stage hydrolysis profile can be evidenced, viz. (i) an initial fast hydrolysis step -presumably due to the hydrolysis of the amorphous regions of starch granules – and (ii) a second slower step presumably due to the hydrolysis of the crystalline regions.[183, 185] Some authors distinguish three steps of hydrolysis: a rapid one, a slow one and a very slow one,[155] presumably corresponding to the hydrolysis of amorphous layers, semi-crystalline layers and crystalline ones, respectively. There are two common hypotheses to account for the slower hydrolysis rate of the crystalline domain. The first one is that the dense packing of starch in the crystalline regions does not allow readily the penetration of H_3O^+. [181] The second one is that the hydrolysis of the glucosidic bonds requires a change in conformation from chair to half-chair.[132] Putaux et al.[16] concluded from TEM observations that, even though slow, crystalline growth rings and amorphous areas degradations are concomitant.[99]

The obvious factors influencing hydrolysis kinetic are: time, acid type, acid concentration and temperature. The influence of acid and starch type has been studied extensively by Singh & Ali.[186-189] They showed, through different characterization

techniques such as alkali fluidity number (AFN), number average molecular weight, and intrinsic viscosity, that for the same equal normality, HCl and HNO_3 gave the highest thinning effect followed respectively by H_2SO_4 and H_3PO_4. Angellier et al.[100] also obtained a lower yield of hydrolysis with H_2SO_4 compared to HCl for the production of nanocrystals but showed that final suspensions were more stable with H_2SO_4 due to the presence of sulfate groups at the surface (Figure 1.31).

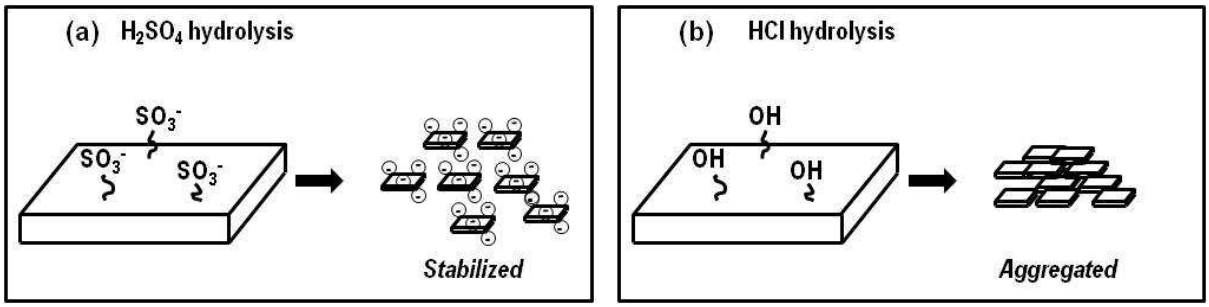

Figure 1.31. Comparison between SNC prepared with (a) H_2SO_4 and (b) HCl.

The difference in the rate and yield of hydrolysis among starch types was attributed to the difference in granules size and number of pores on the granule surface.[188] However, Biliaderis & Grant[185] thought that the granular organization had probably more influence. Jayakody & Hoover[183] studied further the susceptibility of different cereal starches to hydrolysis. Roughly, the extent of hydrolysis was more pronounced for waxy maize than for oat, rice, normal maize, amylomaize V (50-60% amylose) and amylomaize VII (70% amylose) starches.

They concluded that:

(i) the first stage of hydrolysis (amorphous regions) is influenced by the granule size, pores on the surface, amylose content and the amount of lipid-complexed amylose chains

(ii) the second step of hydrolysis (crystalline region) is influenced by the amylopectin content, mode of distribution of α(1-6) branches between the amorphous and the crystalline regions; and degree of packing of the double helices within the crystallites (i.e. the parameters also influencing crystallinity).

Wang et al.[190] observed as expected that the rate of hydrolysis increased when increasing the concentration of acid while the temperature was kept at 50℃. Angellier et al.[100] in the intent of producing SNC studied the influence of these parameters using a surface response methodology. They concluded that both the acid concentration and temperature should not be too high: acid concentration was kept at 3.16M and

temperature at 40°C. Hydrolysis conditions do not change much among researchers, as reported in Table 1.9 and Table 1.10.

However, techniques for following the extent of hydrolysis are numerous. The most common one consists in following the total solubilized carbohydrates content.[181] It is sometimes expressed as a percentage of initial starch[183] or analyzed as molecular weight fractions.[186] To produce acid-thinned starch, Wang et al.[190] evaluated the extent of hydrolysis with viscosity of the resulting slurry, measured by Brabender Viscograph-E.

For the production of SNC, Angellier et al.[100] followed the dry weight of non solubilized particles as a percentage of initial starch. Following the same purpose, it would also be interesting to establish a correlation between characterization techniques such as those used by Singh et al.[189] – mainly rheological (AFN, intrinsic viscosity) - and the extent of hydrolysis.

III.1.2. SNC's preparation protocols

Only a limited number of articles concerning SNC preparation have been published during the past decade. They are gathered in Table 1.9 when nanocrystals were produced for characterization, and in Table 1.10 when prepared to be used for composite applications. Most of them relate the use of acid hydrolysis and even though a variety of starch sources has been used, they all refer to the same two processes:

- Dufresne et al.'s process using HCl as previously discussed. [66]
- Angellier et al.'s optimize the process using H_2SO_4 which was as follow.[100] A given amount of starch granules (14.69 wt%/acid) was mixed with a given volume of 3.16M H_2O_2 in an Erlenmeyer and stirred constantly at 100 rpm while maintained at 40°C. After 5 days, the suspension was washed by successive centrifugations with distilled water until neutrality using centrifuge SIGMA 6K15, for 10 min at 10,000 rpm. The suspension was then submitted to a mechanical treatment with homogenizer Ultra Turrax for 2 min at 13,000 rpm to disperse aggregates and obtain a "stable" suspension. To avoid bacterial development during storage a few drops of chloroform were added to the suspension that was kept in a 4°C cell.

Most recently, the use of pea starch for the preparation of SNC by acid hydrolysis has also been investigated.[191]

Paper 1

To our knowledge, no work on a purely enzymatic hydrolysis method for producing SNC has been reported. However, an attempt has been reported by Kim and Lim[192] rendering 500nm particles believed to be blocklets. Very recent publication reports the use of enzymes for the characterization of SNC and the assessment of the DPs of polymer chains[193] with SEC of the ensuing solution.

Also, Kümmerer et al.[194] studied the biodegradability of organic nanoparticles in the aqueous environment via the OECD's standardized procedure of the close bottle test (CBT). SNC showed significantly faster degradation in the first 7 days than was recorded for macroscopic starch and cellulose whiskers. After 28 days, SNC reached a degradation percentage of 60% which is the excluded limit defined by the OECD for biodegradability. For comparison cellulose whiskers reached 53% and carbon nanotubes (CNT) and fullerene did not degrade at all. Furthermore, none of the particles were found to be toxic to micro-organisms necessary for oxygen take-up.

Table 1.9. Preparation conditions of SNC and their characterization (features,[66, 99] optimization,[100] kinetic,[181] molecular structure[193]) – Adapted from original paper[77] for update.

Starch		Acid		Duration	T	Year	Ref
Type	C%	Type	Conc	(days)	°C		
Potato	5.0%	HCl	2.2N	15	35	1996	66
Waxy maize	5.0%	HCl	2.2N	15	36	2003	99
Waxy maize	14.1%	H_2SO_4	2,87M	7	40	2004	100
Waxy maize	14.7%	H_2SO_4	3,16M	5	40	2004, 2009 and 2011	100, 193, 194
Waxy maize	n.a	HCl	mild	42		2005	195
Hi-maize / Hylon VII	10.0%	HCl	2.2N	8	40	2007	181
Rhizoma Dioscorea	12.5%	HCl	2.2N	16/32/40	35	2008	151
High Amylose corn	Enzymatic hydrolysis					2008	192
High Amylose corn	Complex formation + enzymatic hydrolysis					2009	196
Pea starch	14.7%	H_2SO_4	3,16M	5	40	2011	197

n.a. Non available

III.2. Use of SNC

III.2.1. Nanocomposites and applications

As presented in Table 1.9 and Table 1.10, before 2006, polymer matrices were poly(styrene-co-butyl acrylate)[170] and natural rubber[96]. Since then, most work has been oriented towards the use of new environment-friendly polymers such as waterborne polyurethane[171] (WPU also called organic solvent-free polyurethane), starch (waxy maize[97, 198], cassava[175]), pullulan[199] (obtained by starch fermentation), PLA[173] , polyvinyl alcohol (PVA)[172] and most recently soy protein isolate (SPI)[200] and PBS[201]. Main targeted applications were in nano-composites films for general purposes and for packaging. The impact of SNC on mechanical and barrier properties is detailed latter.

Data should be carefully compared since filler contents were not similarly calculated, depending on authors. Some reported filler contents were expressed in percentages, as the ratio of the amount of starch nanoparticles to the total solid content (matrix and starch nanoparticles)[175] whereas others calculate it as the ratio of the amount of starch nanoparticles to the amount of unfilled matrix before[200] and after[199] the addition of plasticizer. Finally others report filler contents as part per hundred (pph).[172] These differences make it harder to compare results since they introduce differences in the process (more drying might be necessary if more water is introduced) and in the final composition of the composite (different solid contents).

Most recent studies (2010-2011), bring to light new opportunities for using SNC in non-film application.

***Biomedical** applications have been considered: SNC have been investigated as potential stabilizers, rheology modifier and **drug release** regulator for drug delivery[202, 203]. Zhang et al.[203] studied the potential of cellulose whiskers (CW), chitin whiskers (CHW) and SNC (SNC) for improving the mechanical strength of a supramolecular hydrogel based on cyclodextrin inclusion (which serve to encapsulate cell or drugs) and regulating the release behavior. As only 0,5% of SNC were added, they had little effect on viscosity and gelation contrary to CW which aspect ratio is higher. However, it was verified that SNC did not produce additional cytotoxicity to the hydrogel. Lin et al.[202] aimed at developing a sodium alginate microsphere as controlled release system for drug delivery. The polymer was cross-linked around polysaccharide nanocrystals which rendered stable microspheres with improved mechanical properties due to improved crystallization thanks to nanocrystals. Microspheres swellability was also increased but the integrity was maintained. Finally, the encapsulation efficiency was greatly improved*

from 33% to 55% due to restricted motion of alginate polymer chains, inhibiting diffusion of drug and slow dissolution and collapse of the microsphere.

Another specific application is the use of isocyanate cross-linked reactive ***SNC for thermo-responsive applications*** *by Valodkar et al.[204]. SNC are used as cross-linkers in the synthesis of PPG-based polyurethanes (PU). First the PPG (polypropylene glycol) reacts with HMDI (1,4-hexamethylene diisocyanate) to give NCO-terminated prepolymer; then hydroxyl groups of SNC react with the prepolymer to form a 3D network, that is cross-link PU. Compared to neat SNC, modified SNC have higher hydrophobicity and thermal stability. Final conductivity reached 10^{-4} to 10^{-2} S/cm, which is in the same range as semi-conductors. Also, reaction with toxic HMDI does not destroy the basic virtue of biodegradability of starch; however, it lowers its biodegradability.*

III.2.2. Processing

Currently, there are two different processing strategies existing at lab-scale to prepare nano-fillers reinforced polymer materials: (i) dry hot processes such as molding, extrusion and thermoprocessing and (ii) solvent and water-based suspension processes such as casting evaporation and coating.

Up to our knowledge, there is no reported study dealing with SNC reinforced coating on flexible substrate. The present study investigated for the first time this processing strategy, thus arising several questions, linked to SNC orientation or the influence of drying (Chapter 4).

As Dufresne and Cavaillé,[170] Angellier at al.[87] reported composite preparation by hot pressing. The SNC – poly(styrene-co-butyl acrylate) mixtures were previously freeze dried, heated at 90°C for 10 min and then hot-pressed during 1 min under 2 MPa (300 psi) pressure to obtain films about 1mm thick.[182] *Since then, only one study[201] reported the use of compression molding (120°C, 20MPa for 5 min) for the preparation and comparison of polysaccharide nanocrystals filled PBS. Polysaccharide nanocrystals induced nucleation and the formation of a percolation network which lead to enhanced tensile properties, crystallinity and thermal stability of the nanocomposite. However, questions about possible SNC gelatinization should be answered.*

From 2006 on, authors have opted for a simpler casting-evaporation method at 40°C for 24h. It was necessary to decrease the temperature of gelatinized starch before adding waxy maize SNC to avoid SNC gelatinizing.[97]

Table 1.10. Use of SNC in composites and the measured properties.

Adapted from original paper[77] for update.

Starch		Acid		Duration	Temperature	Matrix	Measured Properties								Year	Ref.
Type	C%	Type	Conc	(days)	°C		X Ray	FTIR	DMA	DSC	DMA	Tensile	WU	WVP		
PS	5.0	HCl	2.2N	15	30	Poly(S-co-BuA)							*		1998	170
WM	5.0	HCl /H_2SO_4			35/40	Poly(S-co-BuA)			*						2005	182
WM	14.7	H_2SO_4	3.16M	5	40	Grafted SNC	*	*							2005	98
WM	14.7	H_2SO_4	3.16M	5	40	Natural Rubber							*	*	2005	61
WM	14.7	H_2SO_4	3.16M	5	40	Natural Rubber			*						2005	96
WM	14.7	H_2SO_4	3.16M	5	40	Grafted SNC	*	*							2006	205
WM	14.7	H_2SO_4	3.16M	5	40	Natural Rubber					*				2006	206
WM	14.7	H_2SO_4	3.16M	5	40	TPS (glycerol)			*			*			2006	97
WM	5.0	HCl	2.2N	15	35	Pullulan (sorbitol)	*		*			*	*	*	2007	199
WM	14.7	H_2SO_4	3.16M	5	40	TPS (sorbitol)			*	*	*	*			2007	198
WM	14.7	H_2SO_4	3.16M	5	40	Grafted SNC	*	*							2007	207
NM	14.7	H_2SO_4	3.16M	5	40	Grafted SNC	*	*							2007	208
PS	14.7	H_2SO_4	3.16M	5	40	WPU (waterborne polyurethane)					*				2008	171
Pea	14.7	H_2SO_4	3.16M	5	40	PCL Grafted SNC PLA matrix	*	*	*	*		*			2008	173
Pea	14.7	H_2SO_4	3.16M	5	40	PCL Grafted SNC WPU matrix	*	*	*	*		*			2008	209
PS	5.0	HCl	2.2N	15	30	PCL Grafted SNC	*	*		*					2008	210
WM	14.7	H_2SO_4	3.16M	5	40	Cassava and waxy with glycerol	*	*	*				*	*	20092010	175, 211
Pea	14.7	H_2SO_4	3.16M	5	40	Soy Protein Isolate (SPI)	*		*	*		*	*		2009	174
WM	*14.7*	*H_2SO_4*	*3.16M*	*5*	*40*	*Isociyanate cross-linked SNC PPG-based PU*	*			*TGA*					*2010*	*204*
Pea	*14.7*	*H_2SO_4*	*3.16M*	*5*	*40*	*Cyclodextrin based hydrogel*	*				*				*2010*	*203*
Pea	*14.7*	*H_2SO_4*	*3.16M*	*5*	*40*	*Sodium alginate (SA)*	*	*					*		*2011*	*212*
Pea	*14.7*	*H_2SO_4*	*3.16M*	*5*	*40*	*PBS*	*	*	*	*	*	*			*2011*	*201*
						SA	*	*		*					*2011*	*212*

PS: Potato; WM: Waxy maize; NM: Normal maize; PU: polyurethane

However, Ma et al.[213] proceeded by casting-evaporation at 50℃ for 6-8 hours in a Petri dish after constant stirring of the nanoparticles in thermoplastic pea starch at 90℃ for half an hour. Garcia et al. [175] also report casting-evaporation at 50℃ but for 24 hours and taking care of degassing thermoplastic cassava starch solution before and after the introduction of starch nanoparticles. Chen et al.[171] tested the incorporation of potato SNC at three different stages of the synthesis of WPU (waterborne polyurethane), viz. post emulsification (method 1), midst of emulsification (method 2) and chain-extending of polyurethane pre-polymer (method 3). Nanocomposites were prepared by casting-evaporation of the mixture. Number of active -NCO groups, and subsequently number of chemical grafting increased depending on the method leading to a decrease in tensile strength and elongation at break. However, method 3 resulted in a much higher Young's modulus.

Most recently, compression molding was used to prepare glycerol-plasticized starch nanocrystals composites at 120℃ from a freeze-dried powder.[200] One could assume that the fillers are amorphous after this processing.

Two recent (2010) review articles[214, 215] have focused their attention on the processing of such nanocomposites. Dufresne[214] extended his review to polysaccharides nanocrystals and focused on nanocomposites' transformation into a co-continuous material; whereas Lin et al.[215] overview the starch nanocrystal's reinforced polymers with emphasis on methods and strategies for chemical modifications. Indeed, when nanofillers can agglomerate in the dry state (e.g. nano-polysaccharides), modification of nanofillers' surface is an interesting option for dry processes[216] or for improving compatibility[217, 218].

The influence of chemical grafting on the reinforcing effect of SNC was also proved to be positive. Indeed, Angellier et al.[96] reported a decrease in the reinforcing effect of SNC in NR above 20%. This was attributed to hydrophilic nature of starch which decreases the compatibility between SNC and the hydrophobic matrix.

There are three strategies for chemical modification of SNC: (i) modification by chemical reaction with small molecules, (ii) grafting onto polymer chains with coupling agents, and (iii) grafting from polymer chains with polymerization of a monomer.[215]

Angellier et al. [98] first reported the study of functionalization, *by* ***chemical reaction*** *of SNC* to broaden the number of possible polymeric matrices by allowing the processing of composite materials from an organic solvent (instead of aqueous suspensions). The chemical modification consisted in transforming the polar hydroxyl

group sitting at the surface of SNC into moieties capable of enhancing interactions with non polar polymers. Studied reactions were: esterification with an anhydride function and urethane formation using isocyanate. *In a recent study by Xu et al.[219], acetylated SNC were prepared to improve their solubility in organic solvents such as acetone, chloroform and ethyl acetate. Solubility and turbidity were assessed visually. Peculiar observation of change of crystalline type from A to V was reported with increasing DS values.*

Thielemans et al.[205] studied *the "**grafting onto**" approach* with longer-chain surface modification for forming directly a polymer matrix phase at nanocrystals surface or at least for achieving near-perfect stress transfer between matrix and reinforcement thanks to strong covalent linkages. Two modifications were studied: stearate grafting and polyethylene glycol methyl ether (PEGME) modification via TDI. In continuation of that work, Labet et al.[207] reported the grafting of PTHF, PPGBE and PCL. Partial grafting of SNC with conservation of both morphological and crystalline properties was reported for both studies.

Following studies considered *a "**grafting from**" approach*. Song et al.[208] prepared amphiphilic SNC by free radical polymerization (FRP) to allow the substitution of carbon black by SNC as a green filler of natural rubber at high filler content. In this study, styrene graft copolymerization was undertaken to introduce hydrophobic groups or polymer chains onto the polysaccharide backbone.

Namazi and Dadkhah focused their work on methods for surface modification of SNC. They first studied the SNC grafting with PCL via classic ring opening polymerization (ROP)[210] and more recently (2010) reported a method for preparing hydrophobically modified SNC using fatty acid[176]. In contrast with work using heterogeneous reaction conditions[98, 205, 207, 210], their interest was focused on homogeneous reactions by taking advantage of SNC specific area. Others[220] developed also this ROP treatment for an extrusion process application.

*Most recent study dealing with modified SNC[221] continued the work initiated by Thielemans et al.[205] to find a very interesting **application: water treatment**. SNC were modified with hydrophobic shell consisting of stearic acid chains and then tested as ad/absorbent for organic in an aqueous phase. Results indicate that efficient uptake of dissolved organic compounds can be achieved using a fixed bed column with adequate operating parameters.*

Paper 1

III.3. SNC reinforced polymers properties

III.3.1. Mechanical properties

The potential use of SNC as a reinforcing phase in a polymeric matrix has been evaluated from a mechanical point of view both in the non linear range (tensile test) and linear range (DMA). In their early work on SNC, Dufresne and Cavaillé[66] found that SNC brought great reinforcing effect especially in the rubbery plateau region, i.e. for temperatures higher than T_g of the matrix. This observation was confirmed by most authors. Angellier et al. reported on several occasions[61, 96, 182, 206] an increase in the relaxed storage modulus at 50°C of 10%, 75% and 200 % for respectively, 10 wt%, 20 wt% and 30 wt% filler content in a natural rubber matrix as presented in Figure 1.32. They also reported an increase in the glassy modulus up to 3GPa at 30 wt% filler content. The effect of moisture content was investigated. The higher it is, the lower the rubbery modulus.

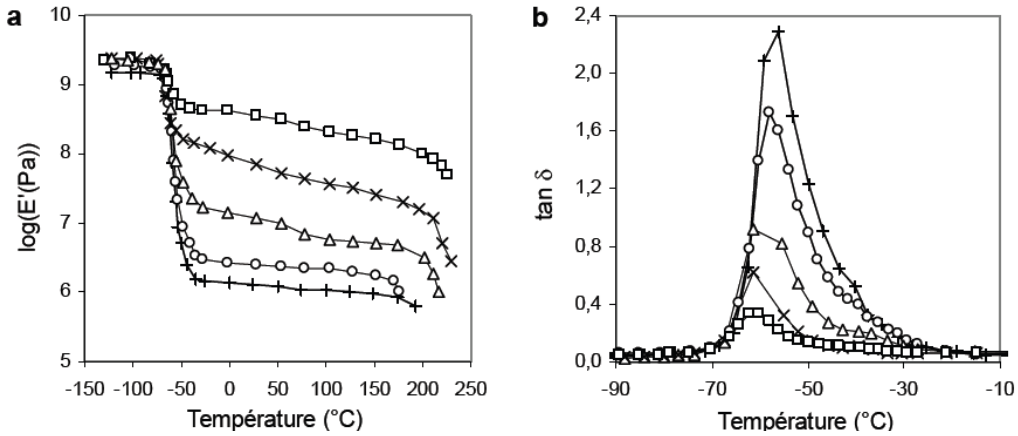

Figure 1.32. Evolution of (a) storage modulus and (b) tanδ with increasing filler content: (+) 0%, (○) 5%, (Δ) 10%, (x) 20% and (□) 30%.

Other authors reported the same reinforcing effect in a pullulan matrix[199] and sorbitol plasticized starch matrix[175, 198, 211] with an increase in the relaxed storage modulus at 100°C by 2 and 9 times, respectively, fo r 5 wt% and 30 wt% SNC in pullulan and an increase by more than 2 times at 15 wt% in a sorbitol plasticized matrix. The reinforcing effect was lower in pullulan than in thermoplastic starch[97] but comparable to the one reported for natural rubber.[96] Authors also reported an increase of Tg when increasing the filler content attributed to the existence of an interphase of immobilized matrix in contact with particle surface that probably displays a higher Tg value.[96, 198, 199] Similar properties were shown for amorphous starch nanoparticles[213] as detailed later.

The reinforcing effect of SNC was also evidence from tensile tests. Relative values of Young's modulus, strength and elongation at break reported by different authors are collected in Table 1.11 for comparison.

Table 1.11. Relative tensile test data (Young's modulus -E-, strength -σ_b-, and strain at break -ε_b) for SNC filled nanocomposites.

Samples are marked as follow: Matrix – Plasticizer content (%) – Filler content (%) with the following abbreviations: NR = Natural Rubber; TPS = Thermoplastic Starch; PVA = Poly(vinyl alcohol); SPI = Soy Protein Isolate; G = Glycerol; S = Sorbitol.

Samples	Starch	RH (%)	E_R (MPa)	$\sigma_{b,R}$ (MPa)	$\varepsilon_{b,R}$ (%)	Ref
NR - 5%	Waxy	0	1.6	1.95	0.91	
NR - 10%	Waxy	0	2.5	2.97	0.9	96
NR - 20%	Waxy	0	5	3.89	0.76	
NR - 5%	Waxy	43	2.5	2	0.9	
NR - 10%	Waxy	43	7.5	3	0.9	
NR - 20%	Waxy	43	19.2	3.1	0.8	97
TPS- G25 - 5%	Waxy	43	7.3	3.6	0.3	
TPS- G25 - 10%	Waxy	43	7.5	4.2	0.2	
TPS -G25 - 20%	Waxy	43	22	9.8	0.007	
TPS- S25 - 6%	Waxy	11	1.08	0.96	0.73	
TPS- S25 - 20%	Waxy	11	1.08	0.58	0.34	
TPS -S25 - 40%	Waxy	11	0.98	0.42	0.24	
TPS- S25 - 6%	Waxy	43	1.3	1.11	0.94	
TPS- S25 - 20%	Waxy	43	2.18	1.75	0.66	
TPS -S25 - 40%	Waxy	43	2.99	1.65	0.04	199
TPS- S25 - 6%	Waxy	53	2.51	1.68	0.5	
TPS- S25 - 20%	Waxy	53	8.58	2.9	0.21	
TPS -S25 - 40%	Waxy	53	15.52	5.1	0.06	
TPS- S25 - 20%	Waxy	75	7.74	2.12	0.56	
TPS -S25 - 40%	Waxy	75	35.46	4.01	0.26	
TPS- S25 - 5%	Waxy	43	2.13 [a]	2.61 [a]	0.90 [a]	
TPS- S25 - 10%	Waxy	43	2.23 [a]	3.61 [a]	0.92 [a]	
TPS -S25 - 15%	Waxy	43	2.69 [a]	4.18 [a]	0.65 [a]	198
TPS- S35 - 5%	Waxy	43	1.65 [a]	2.61 [a]	0.86 [a]	
TPS- S35 - 10%	Waxy	43	3.12 [a]	6.06 [a]	0.60 [a]	
TPS -S35 - 15%	Waxy	43	7.06 [a]	12.33 [a]	0.42 [a]	
PVA - G2 - 5%	Pea	43	n.a	1.11 [b]	1.04 [b]	
PVA - G2 - 10%	Pea	43	n.a	1.08 [b]	1.03 [b]	172
PVA - G2 - 15%	Pea	43	n.a	0.97 [b]	1.00 [b]	
SPI - G30 - 1%	Pea	RT	2.36 [b]	1.37 [a]	0.38 [a]	174
SPI - G30 - 2%	Pea	RT	2.91 [b]	1.52 [a]	n.a	
PBS - 0 - 5%	*Pea*	*35*	*580* [b]	*27* [b]	*9* [b]	*201*

[a] *recalculated from original data*

[b] *recalculated from figure*

For most authors,[96, 97, 171, 172, 199, 222] the introduction of nanofillers resulted in an increase in both the elastic modulus and tensile strength of the composite together with a decrease in the strain at break. Reported modulus values are lower in tensile tests than with DMA since the adhesion between the filler and the matrix is more involved during high strain experiments. The reinforcement rate was higher above 10 wt% filler content. The tensile modulus increased exponentially with SNC content and maximum nominal stress was obtained for 20 wt% SNC.[96, 199] As expected, increasing relative humidity was shown to have a strong negative impact on the reinforcing effect

The use of more recent and popular matrix such as PLA, PVA or soy proteins together with pea SNC lead to slightly more unpredictable behaviors. Using PVA as a matrix, Chen et al.[172] reported even a lower reinforcing effect with a slight improvement of properties when the SNC content was lower than 10 wt% and a decrease in both the elongation at break and strength when the nanocrystal content was higher than 10 wt%. Zheng et al.[200] reported an increase in strength and Young's modulus, together with a decrease in the elongation at break, at low pea SNC loading level (lower than 2 wt%) in a soy protein isolate (SPI) matrix, attributed to a uniform dispersion. For higher content, the authors believe that nanocrystals self-aggregate which decreases the surface for interactions with the SPI matrix and destroys the ordered structure. This leads to a decrease of strength and modulus at 40 wt% filler content to values close to those obtained for the unfilled matrix.

Another interesting reported phenomenon is the observation, for some composite, of a constant elongation at break with increasing filler contents. Indeed, Wang and Zhang[177] reported the preparation of a high strength WPU-based elastomer reinforced with 1% to 5% waxy maize SNC. Low filler content allowed better dispersion of the SNC in the WPU matrix allowing stronger interactions. Maximum tensile properties were reported for 1% with an increase in tensile strength from 10.4 to 24.1MPa and in Young's modulus from 0.6 to 3.2MPa, while elongations at break remain stable (from 1148% +/- 11% to 1136% +/- 27%) as for all other filler contents. The same observations have been made on NR / SNC composites, by different authors, and for 5% and 30% SNC from different botanic origin.[178]

The reinforcing effect of SNC is more significant in thermoplastic starch than in natural rubber. The higher reinforcing effect observed with the former matrix was assumed to result from strong interactions between the filler and amylopectin chains and a possible crystallization at the filler/matrix interface.[97] Also, the reinforcing effect of SNC

within a thermoplastic starch matrix was higher than with tunicin[223] or sugar cane bagasse cellulose whiskers.

An interesting and innovative approach to use nanocrystals as fillers is the investigation of a synergistic reinforcement of waterborne polyurethane by both SNC and cellulose whiskers.[203] Authors reported that the system (WPU/ 1% SNC/ 0.4% cellulose whiskers) exhibits a much better reinforcing effect than all other tested WPU/SNC and WPU/ cellulose whiskers composites. The tensile strength and Young's modulus were enhanced by 135% (from 5.5 to 12.7 MPa) and 252% (from 0.5 to 1.8 MPa) respectively. As reported earlier, elongation at break remains basically unchanged. Results are attributed to the formation of a new type of network allowed by strong hydrogen bondings interactions both between the nanofillers, and between the nanofillers and the WPU matrix. An increase of the density of the network was demonstrated by measurements and calculation.

From 2008 and on, grafted SNC were used in biodegradable matrices, in particular PCL grafted SNC through microwave assisted ROP[173, 209]. Yu et al.[173] reported that the addition of PCL-grafted pea SNC to a PLA matrix resulted in the enhancement of the elongation at break (up to 25%) together with a decrease of the Young's modulus – which can however contribute to the practical applications of PLA-based products. As explained earlier, this is attributed to the introduction of the PCL component which provided flexibility to the nanocomposites, as well as the formation of an interfacial layer which facilitated the stress transfer to rigid starch nanocrytals. In continuation with previous work, Chang et al.[209], prepared PCL grafted pea SNC/WPU nanocomposites for assessing structural and mechanical properties. Elongation at break remained rather stable as reported by other authors, while for filler content higher than 5%, tensile strength gradually decreased and Young's modulus increased strongly upon addition of grafted SNC indicating increased rigidity of the nanocomposite materials. With both matrices, PLA and WPU, optimal filler content was reported around 5 wt%. The respective tensile strength was 57.2 MPa and 40.2 MPa, for neat matrices and 43.4MPa and 31.1MPa for composites.

The literature is significantly lacking in comprehensive explanation of the reinforcing mechanism of SNC, contrarily to cellulose nanocrystals for instance. Similarly to the latter, the reinforcing effect of SNC is generally ascribed to the formation of a hydrogen bonded percolating filler network above a given starch content corresponding to the percolation threshold. However, this assumption is difficult to evidence because the connecting particles should be starch clusters or aggregates with ill-defined size and

geometry. This percolation phenomenon was evidenced from swelling experiments (water uptake discussed later), for which changing behavior was reported above certain filler concentration depending on starch type.[31] This phenomenon should most probably affect the mechanical properties of the composites in the linear range. This percolation mechanism should depend among other parameters on the dimensions of primary starch nanoparticles, isolation process, processing method of nanocomposite films and interactions with the polymeric matrix. Attempts to model the mechanical behavior of SNC reinforced poly(styrene-co-butyl acrylate)[61, 170] and natural rubber[61] have been reported in the literature using simple models such as the generalized Kerner or Guth equations modified for non-spherical particles. The main drawback of these phenomenological approaches lies in the use of an adjustable parameter, which value was found to vary at the percolation threshold of starch aggregates.

III.3.2. Water uptake

To consider potential applications for nanocrystals filled nanocomposites, several authors assessed the water uptake of their composites. Early on, Dufresne and Cavaillé[170] reported that the higher the starch microcrystal content in the poly(styrene-co-butyl acrylate) matrix, the greater the water uptake (WU). The rapid increase of the diffusion coefficient after 20 wt% of starch content was attributed to the creation of a geometrical percolation effect leading to the creation of a diffusion pathway.

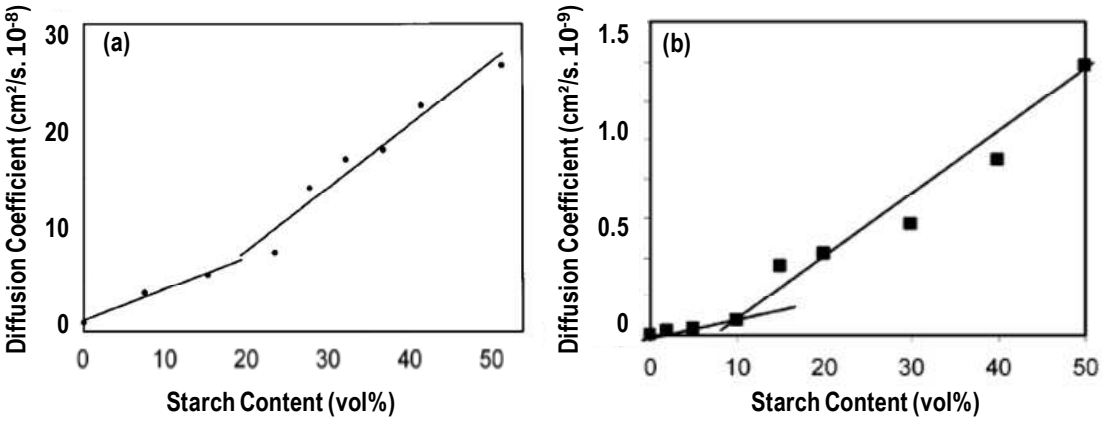

Figure 1.33. Evolution of water uptake with (a) potato SNC[170] and (b) waxy SNC[61] content.

Immersing films in distilled water, Angellier et al.[61] confirmed the previous findings. The unfilled natural rubber matrix displayed the lowest water uptake (WU) value, and the addition of SNC induced an increase in water diffusivity. Up to 10 wt% filler content the WU remained roughly constant at 6%, and then increased more or less linearly to 33% for 50 wt% filled films (Figure 1.33 b). The critical volume fraction of SNC

at the percolation is difficult to determine due to their heterogeneity and ill-defined geometry. However, contrary to previous findings estimating the percolation at 20 vol% for potato SNC, they estimated it around 6.7 vol% (i.e. 10 wt%) for waxy maize SNC (Figure 1.33.a). This difference was explained by the potentially higher surface area of waxy maize SNC.

Other authors preferred a conditioning technique, at different relative humidity, to assess the water sensitivity of films. Garcia et al.[175] using a cassava plasticized matrix, reported the same observation as Dufresne et al.[170] and Angellier et al.[61] Zheng et al.[200], observed no obvious changes in WU between the unfilled soy protein matrix (SPI) and the pea SNC filled nanocomposites attributed to a strong interfacial interaction between the filler and the SPI matrix.

On the other hand, Kristo et al.[199] reported a decrease of WU at equilibrium from 69.7% for the unfilled pullulan matrix to 50.6% when increasing the SNC content up to 40 wt%. Using a PVA matrix, Chen et al.[172] reported also a decrease in WU from 78% to 62% for the unfilled matrix and 40 wt% SNC reinforced composites, respectively. Similar tendencies were reported for cellulose microfibrils[224, 225] and tunicin whiskers[223] reinforced thermoplastic starch. *Then, it is difficult, from literature, to clearly conclude on the influence of SNC on water diffusion.*

III.3.3. Barrier properties

Giving their platelet morphology, SNC were suspected, as nanoclays do, to create a tortuous diffusion pathway for water vapor and oxygen molecules to pass through. *This assumption was the starting point for the launching of our project to use SNC for barrier packaging, as developed in Chapter 4.*

However, very few researchers investigated barrier properties to oxygen and water vapor, presumably because of the hydrophilic nature of SNC. Contrary to what could have been expected from WU – the creation of a continuous starch pathway that would allow the diffusion of water - all authors reported a decrease in water vapour permeability (WVP) when increasing the maize SNC content. Values, matrices and testing methods are reported in Table 1.12.

Angellier et al.[61] observed a continuous decrease in permeability upon starch nanocrystal addition whereas Kristo et al.[199] observed no significant differences in WVP between the unfilled film and those containing up to 20 wt% nanocrystals. Adding 30 wt% and 40 wt% leads to a significant decrease in WVP. This observation was explained

by the presence of a minimum concentration necessary to create an actual tortuous pathway. However, Garcia et al.[175] reported a decrease of WVP of 40% for a cassava starch plasticized matrix reinforced with only 2.5 wt% starch nanoparticles.

Table 1.12. Water Vapour Permeability (WVP) values for maize SNC filled nanocomposites.

	Matrix	Filler %	T (°C)	RH (%)	Thickness (*μm*)	Testing method	WVP [10^{10}g/(m.s.Pa)]	Ref.
	Natural Rubber	0	25	50	600	ISO 2528-1974F	3.41[a]	61
		5	25	50	600		2.41[a]	
		10	25	50	600		2.36[a]	
		20	25	50	600		1.88[a]	
	Pullulan + 30% sorbitol	0	25		70	ASTM E96-63T	12	61
		3	25		75		12.4	
		6	25		70		12.5	
		10	25		75		12.5	
		15	25		72		12.8	
		20	25		69		12.6	
		30	25		73		9.6	
		40	25		73		9.3	
	Cassava + 50% glycerol	0	25	0/58		ASTM E96-00	4.5	175
		3	25	0/58			2.7	
NM SNC	*Waxy maize + 33% glycerol*	*0*	*25*	*0/58*	*200-300*	*ASTM E96-00*	*3,8*	*211*
		2,5	*25*	*0/58*	*200-300*	*ASTM*	*6,8*	
NM SNP	Pea Starch + 30% glycerol	0	25	75	500	ASTM E96 (1996)	4.75	213
		1	25	75	500		3.2	
		2	25	75	500		3.1	
		3	25	75	500		2.9	
		4	25	75	500		2.75	

[a] *recalculated from original data*

NM: normal maize; SNP: starch nanoparticles

An explanation for this disparity could also be found in the way SNC are dispersed *as mentioned more recently by same authors. Recent study[211] using glycerol plasticizer waxy maize starch filled with 2,5% SNC reported contradictory results. It was attributed to SNC being glue-glycerol bonded, forming threads with high concentration of OH and thus, forming a preferential path for water vapour diffusion through the nanothreads, which clearly increases the permeability of the film.*

SNC were also reported to reduce oxygen diffusion and permeability through the nanocomposite films upon increasing the filler content by Angellier et al.[61] The phenomenon was attributed to the platelet-like low permeable structure of starch standing in the way of oxygen molecules. Permeability values in barrier were converted in cm^3.µm/day.m².Pa and collected in Table 1.13.

Table 1.13. Oxygen Permeability values for waxy maize SNC filled nanocomposites.

Matrix	Filler %	T (°C)	O2 permeability (cm^3*µm/day.m².Pa)	O2 permeability (barrer) *0%RH*	Ref.
Natural Rubber	0	25	29.53 [a]	25.7	
	5	25	24.2 [a]	21.1	61
	10	25	19.3 [a]	16.8	
	20	25	10.22 [a]	8.9	

[a] recalculated from original data

Up to our knowledge, only four papers deal with barrier properties of SNC; and only for cast-evaporated nanocomposites. It seems that, such properties have never been measured when SNC filled polymers are coated. This is why such a promising and innovative process for this material was selected as the focus of this study.

III.4. Starch nanoparticles & commercial products

As detailed before, SNC are obtained mainly by acid hydrolysis, a process which seems very challenging for up-scaling. This is why most recent studies, new processes have been tried out to produce starch nanoparticles by (i) precipitation of amorphous starch by Ma et al.[213] and Tan et al.[226]; by (ii) combining complex formation and enzymatic hydrolysis by Kim and Lim[196] yielding in V-type nanocrystals (ie. complexed with lipids as described in Figure 1.34) and by (iii.) microfluidization by Liu et al.[227]

It is worth noting that such starch nanoparticles are following totally different strategies than SNC as described in Figure 1.34. Consequently, ensuing nanoparticles have different properties, crystallinity and shape.

Indeed, Ma et al.[213] prepared starch nanoparticles by precipitating a starch solution within ethanol as the precipitant. Native starch was mixed with water and completely gelatinized (90°C, 1h). Then ethanol was added drop wise to the solution at room temperature and stirred for 50 min. The suspension was then centrifuged with ethanol to remove water and the settled material was dried at 50°C to remove ethanol. The resulting nanoparticles were used to prepare a bio-nanocomposite. However, this process for producing starch nanoparticles does not allow producing nanocrystals. Kim

and Lim[228] studied alternative ways to obtain starch nanoparticles. They proposed a process for preparing nanoscale starch particles by complex formation with other components. Experiments were conducted with n-butanol. Starch was dissolved in an aqueous DMSO solution heated for 1h and stirred for 24h. The aliquot was passed through a PTFE 10 µm pore size membrane filter into n-butanol (3 days at 70°C). Maximum starch precipitation was 6.78% of the initial amount. Complex formation involved mainly amylose rather than amylopectin. The precipitate (starch – butanol complex) was collected by centrifugation and washed 3 times in n-butanol. However, the complex contained a large portion of amorphous matrix, so that its selective removal by enzymatic hydrolysis was needed. Since most of the starch was hydrolyzed (85-90%), the resulting yield of the nanoparticles was extremely low. Starch nanoparticles display spherical or oval shape with diameters in the range 10-20 nm. Liu et al.[227] transferred the method for producing microfibrillated cellulose (MFC) to the production of starch colloids. Indeed, a 5% slurry of high amylose corn starch was ran through a Microfluidizer for several passes (up to 30). The particles size of samples obtained from more than 10 passes was below 100 nm, and the gel-like suspension remained stable for more than a month. The thermal stability was not affected and since no chemical nor thermal degradation occurred during the treatment reported yield was almost 100%. However, the resultant starch colloids were obtained from breaking down both amorphous and crystalline domains rendering an amorphous diffraction pattern after 10 passes.

To the best of our knowledge, there are no commercial SNC available on the market. In fact, only two patents - in Chinese and from the same authors - dealing with SNC have been found. They both deal with the preparation of polyurethanes from starch nanocrystal-grafted polyester[229, 230]

All other patents and commercial products deal with starch nanoparticles. Most popular commercial products are Mater-Bi™ from Novamont and Eco-Sphere™ from Ecosynthetix. They both fit the “Regenerated starch” nanoparticles category presented Figure 1.34.

Mater-Bi™ (Novamont) is a destructurized and modified starch with variable quantities of complexing agents. Mixing that complexed starch with at least one hydrophobic polymer incompatible with starch such as Ecoflex™ (BASF)[231-233]. As described previously, such complexed starches are also called starch nanoparticles. However, it is commercialized as pellets. Most famous application for Mater-bi is BioTRED™, a bio-tire, developed in collaboration with Goodyear. Mater-bi was used to replace part of the lampblack and silica usually contained in the tire mixture.[232] Instead of

adding nanoscaled material to the tire, the biopolymer itself was nanosized and used as a bio-nano-filler.

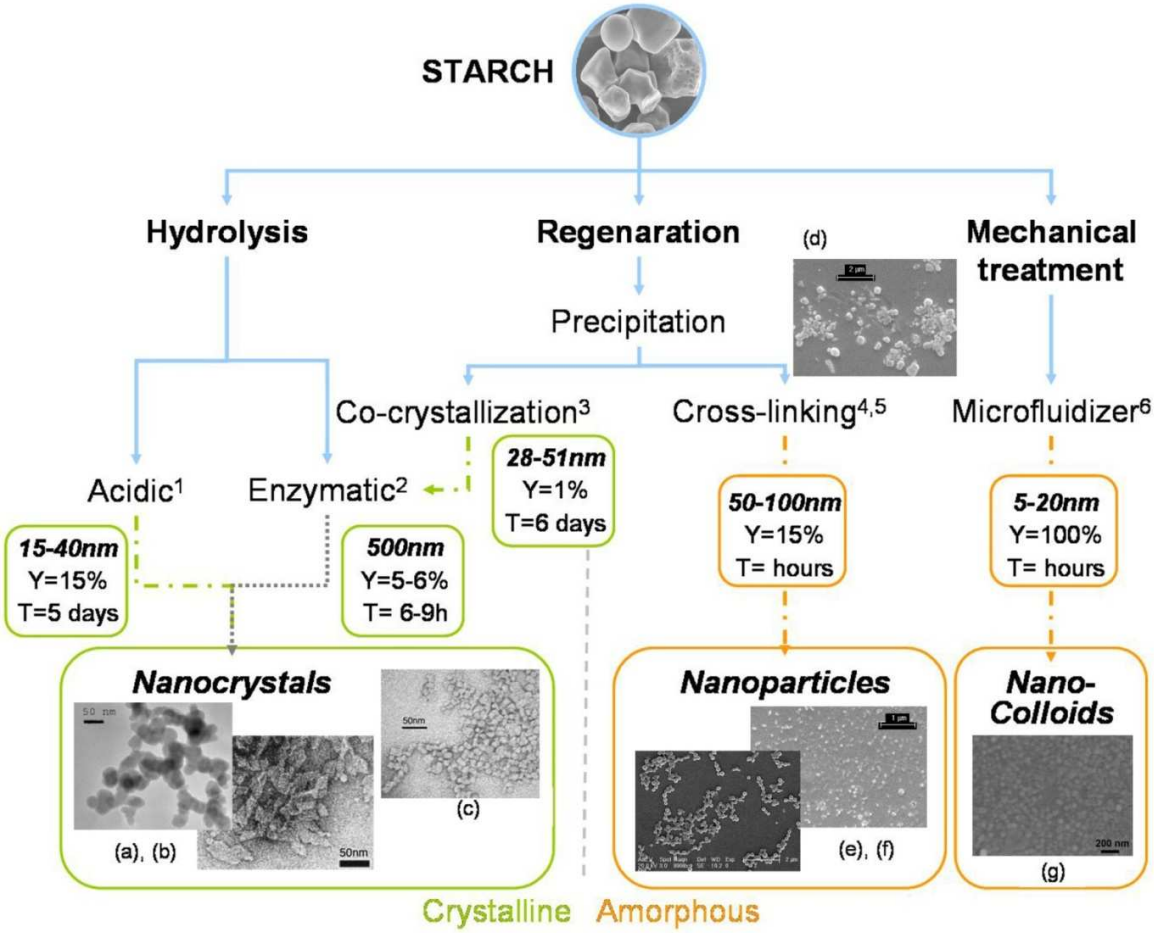

Figure 1.34. Different ways of producing crystalline and amorphous starch nanoparticles, hydrolysis leads to nanocrystals, whereas regeneration and mechanical treatment lead to both amorphous and crystalline particles in final batch.[77]

1) References to SNC production by acid hydrolysis are gathered in Tables 6&7 as it is reviewed in this paper – (a) TEM micrograph of SNC from Garcia et al.[175]– (b) TEM micrograph of SNC from Putaux et al.[99]
2) Intent to produce SNC by enzymatic hydrolysis as reported by Kim et al.[192] It is believe that the process leads to blocklets rather than nanoparticles.
3) Kim and Lim[196] report the preparation of nanocrystals by complex formation between amylose and n-butanol. Enzymatic hydrolysis is used to selectively keep crystalline particles. (c) TEM micrograph of SNC after co-crytallisation and enzymatic hydrolysis.
4) Tan et al.,[226] and 5) Ma et al.[213] report the production of starch nanoparticles by precipitation of gelatinized starch in non solvent followed by cross-linking reaction.– (e) starch nanoparticles from Tan et al.[226] – (d) precipitated starch nanoparticles before cross-linking from Ma et al.[213] (f) Citric acid cross-linked starch nanoparticles from Ma et al.[213]
6) By analogy with microfibrillated cellulose (MFC), Liu et al.[227] intended producing starch nanoparticles by fluidization. It leads to crystalline microparticles turning into amorphous nanoparticles with an increasing number of run. (g) TEM micrograph of starch nano-colloid from Liu et al.[227]
Photos reproduced with permission from: Ref. 99,211, 225 – Copyright (2003, 2008, 2009) American Chemical Society; Ref. 175 – Copyright 2009 Wiley-VCH Verlag GmbH & Co. KGaA.; Ref. 196– Copyright 2008 Elsevier; Ref. 227– Copyright 2009 Elsevier.

Eco-sphere™ is a starch-based bio-latex substituting for oil-based latexes providing adhesive applications such as paper coating, tissue complexing or even as a replacement of polyvinyl acetate. Starch granules are extruded and cross-linked simultaneously (reactive extrusion process). The process converts starch into a thermoplastic melt that is transformed into an agglomerate of dry crosslinked nanoparticles. The product is commercialized dry and has to be re-dispersed to form the latex.[234]

Five other patents dealing with starch nanoparticles have been identified. Two are in Chinese and relate to the production of starch nanoparticles for respectively water treatment and medical application. The first one describes crosslinked starch nanoparticles grafted with lignin quaternary ammonium salt to be used as antichlor.[235] The second claims polylysine-starch nanoparticles with cationic starch as a core and polylysine as a shell.[236] WO Patent "Process for producing biopolymer nanoparticles",[237] written in English, describes the reactive extrusion process used by EcoSynthetix. Last two patents were Korean and from same authors Lim and Kim.[238, 239] The first one claims starch /alcohol complex nanoparticles as in article from Kim and Lim[196] and the second, enzymatically hydrolyzed nanoparticles as reported in article from Kim and Lim[192] and both represented in Figure 1.34. The aim of producing such nanocrystals or nanoparticles is to use them as fillers in polymeric matrices to improve their mechanical and/or barrier properties.

IV. Discussion & perspectives

In light of this review, there is no doubt that our society is expecting efficient biopackaging, such as bio-based materials with barrier properties. For this purpose, and especially when flexibility is expected, bio-based nano-composites are an interesting solution both as standing films and as a paper-based coating.

Among renewable nano-fillers, SNC are promising fillers. This field is, at the moment, much less reported in the literature than that of the fast growing nanocelluloses field. However, increasing works start to be done and will be done in the near future on starch nanoparticles*. This is supported by industrialists interest, such as Ecosynthetix, and the fact that our review[77] has been the most read scientific paper published in Biomacromolecules during the last 12 months.* It is worth noting that the main interest of starch in addition to a low cost is that the raw material is relatively pure and does not need as an intensive purification procedure as with lignocellulosic materials.

Obviously, the reinforcing properties of SNC are limited compared to cellulose nanocrystals and a higher amount of the formers is necessary to reach similar reinforcing effects. However, other interesting properties can be obtained from their platelet-like morphology such as barrier properties. *For this reason, this property has been investigated in Chapter 4, with a focus on SNC applications.*

There is also a lack of knowledge of the reinforcing mechanism induced by SNC, although this point as recently been investigated for waxy maize SNC in a natural rubber matrix.[240] An important feature of SNC nanocomposite is that their processing by extrusion and injection molding should be easier in comparison with cellulose or chitin rod-like nanocrystals because no orientation phenomena are expected to occur.

Another limitation of SNC is the duration of the hydrolysis process, much longer than for cellulose, which is performed at lower temperature owing to the higher sensitivity of starch to the acid attack. Optimization of the disintegration process of starch granules and transition from the micro to the nanoscale should be investigated in more details to facilitate the isolation of crystalline regions, in the form of nanocrystals. Weakening of the native starch granules by different means to facilitate the release of crystalline domains should probably be investigated *as presented in Chapter 3*.

Also, most of the reported work was done using waxy maize, *whereas our literature review on starch properties indicate we might expect different behavior from structurally and chemically different starches.* Other sources of starch should be tested *and compared for SNC preparation as in Chapter 2 of this study*.

As a result of this review, significant scientific and technological challenges to take up have been clearly identified as presented in Figure 1.35.

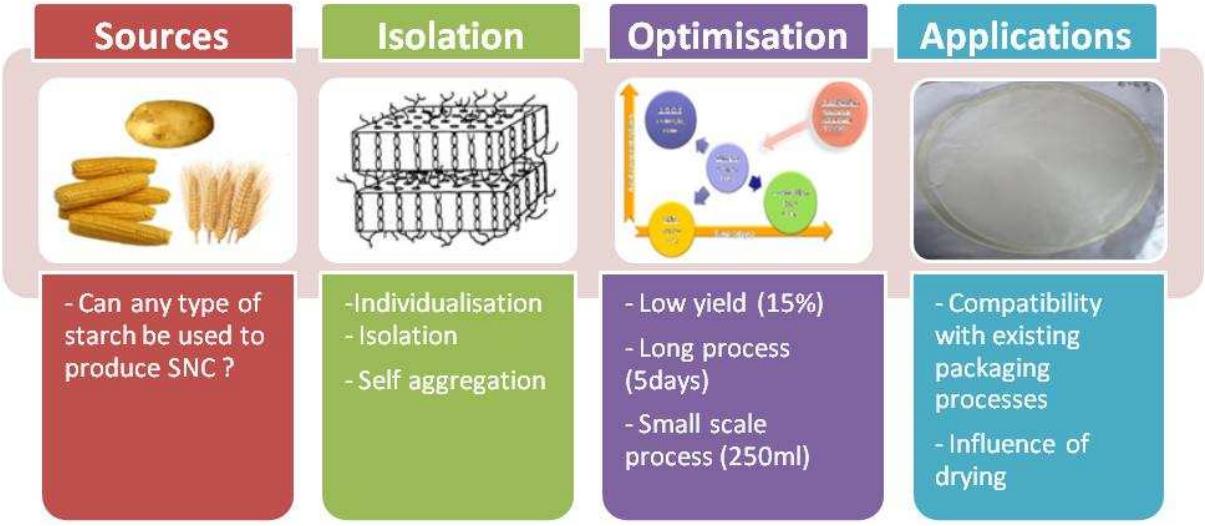

Figure 1.35. Representation of the different classes of challenges to overcome before reaching industrial production of SNC.

Next chapters will try to overcome these issues and give leads and answers to these challenges.

V. References – Chapter 1

1. Gallant, D. J.; Bouchet, B.; Baldwin, P. M., Microscopy of starch: evidence of a new level of granule organization. *Carbohydrate Polymers* **1997,** 32, (3-4), 177-191.

2. Donald, A.; Jenkins, P.; Waigh, T. *Cooking corn on LOQ*; RAL-TR-97-050; Council for the Central Laboratory of the Research Councils: **1997**; p 54.

3. Tang, H.; Mitsunaga, T.; Kawamura, Y., Molecular arrangement in blocklets and starch granule architecture. *Carbohydrate Polymers* **2006,** 63, (4), 555-560.

4. Research, P., http://www.pikeresearch.com/newsroom/sustainable-packaging-market-to-reach-170-billion-worldwide-by-2014. In *Pike Research news room*, **2010**.

5. SESSI *L'industrie de l'emballage*; **2008**.

6. Understanding the Kraft Process in Paper Production. http://www.paperindustry.com/kraft-process.asp, **2011,** Access (July 7th 2011).

7. Denneulin, A.; Bras, J.; Blayo, A.; Khelifi, B.; Roussel-Dherbey, F.; Neuman, C., The influence of carbon nanotubes in inkjet printing of conductive polymer suspensions. *Nanotechnology* **2009,** 20, (38), 385701.

8. COPACEL - Confédération Française de l'Industrie des Papiers Cartons & Celluloses, Consommation apparente de papiers et cartons par sortes http://www.lepapier.fr/cestlavie.htm, **2009,** Access (June 2011).

9. Flexible Packaging Association, Flexible Packaging Facts & Figures. http://www.flexpack.org/INDUST/industry_facts_figures.asp, **2010,** Access (June 2011).

10. Saudemont, T. *The lastest flexible packaging grades - PackScope N°30* ; **2007**.

11. Kirwan, M. J., Paper-based flexible packaging. In *Paper and paperboard packaging technology*, Kirwan, M. J., Ed. Blackwell Publishing Ltd: London, UK, **2005**; p 92.

12. Selke, S. E.; Hernandez, R. J.; Buschow, K. H. J.; Robert, W. C.; Merton, C. F.; Bernard, I.; Edward, J. K.; Subhash, M.; Patrick, V., Packaging: Polymers in Flexible Packaging. In *Encyclopedia of Materials: Science and Technology*, Elsevier: Oxford, **2001**; p 6652-6656.

13. Directive 2004/12/EC of the European Parliament and of the Council of 11 February 2004 amending Directive 94/62/EC on packaging and packaging waste - Statement by the Council - 18/02/2004. In *Official Journal L 047*, **2004**; p P. 0026 - 0032.

14. *European Bioplastics; Plastics Additives & Compounding*, In EFPS Summer School 2009, May/June 2008.

15. Petersen, K.; Væggemose Nielsen, P.; Bertelsen, G.; Lawther, M.; Olsen, M. B.; Nilsson, N. H.; Mortensen, G., Potential of biobased materials for food packaging. *Trends in Food Science & Technology* **1999,** 10, (2), 52-68.

16. Van Tuil, R.; Fowler, P.; Lawther, M.; Weber, C. J., Properties of biobased packaging materials. In *Biobased packaging materials for the food industry: Status and perspectives*, Weber, C. J., Ed. KVL, Department of Dairy and Food Science: Frederiksberg C, Denmark, **2000**; p 13- 44.

17. Weber, C. J., *Biobased Packaging Materials for the Food Industry: Status and Perspectives*. **2000**; p.

18. Shen, L.; Haufe, J.; Patel, M. K. *Product overviw and market projection of emerging bio-based plastics. PRO-BIP 2009*; Copernic Institute for Sustainable Development and Innovation - Utrecht University: **2009**; p 245.

19. Drachman, P. *Carbon Neutrality and Life Cycle: Analysis for Biodegradable Plastics*; Surrey, UK, **2009**.

20. Roes, A. L.; Marsili, E.; Nieuwlaar, E.; Patel, M. K., Environmental and Cost Assessment of a Polypropylene Nanocomposite. *J. Polym. Environ.* **2007,** 15, 212-226.

21. Rahman, M.; Brazel, C. S., The plasticizer market: an assessment of traditional plasticizers and research trends to meet new challenges. *Progress in Polymer Science* **2004,** 29, (12), 1223-1248.

22. Altenhofen da Silva, M.; Adeodato Vieira, M. G.; Gomes Maçumoto, A. C.; Beppu, M. M., Polyvinylchloride (PVC) and natural rubber films plasticized with a natural polymeric plasticizer obtained through polyesterification of rice fatty acid. *Polymer Testing* **2011,** 30, (5), 478-484.

23. Zhang, Y.; Han, J. H., Plasticization of Pea Starch Films with Monosaccharides and Polyols. *Journal of Food Science* **2006,** 71, (6), E253-E261.

24. Fenollar, O.; Sanchez-Nacher, L.; Garcia-Sanoguera, D.; López, J.; Balart, R., The effect of the curing time and temperature on final properties of flexible PVC with an epoxidized fatty acid ester as natural-based plasticizer. *Journal of Materials Science* **2009,** 44, (14), 3702-3711.

25. Fenollar, O.; García, D.; Sánchez, L.; López, J.; Balart, R., Optimization of the curing conditions of PVC plastisols based on the use of an epoxidized fatty acid ester plasticizer. *European Polymer Journal* **2009,** 45, (9), 2674-2684.

26. Baltacioğlu, H.; Balköse, D. m., Effect of zinc stearate and/or epoxidized soybean oil on gelation and thermal stability of PVC-DOP plastigels. *Journal of Applied Polymer Science* **1999,** 74, (10), 2488-2498.

27. Fenollar, O.; Balart, R.; Sanchez-Nacher, L.; Garcia-Sanoguera, D.; Boronat, T., Mechanical and morphological characterization of novel vinyl plastisols with

epoxidized linseed oil as natural-based plasticizer. *AIP Conference Proceedings* 1255, (1), 326-328.

28. SUSTAINPACK, *EU Framework 6 Integrated Project on New Packaging Materials.* , **June 2004 to May 2009**.

29. Jacques, C. H. M.; Hopfenberg, H. B.; Stannett, V. T., *The permeability of plastic films and coatings to gas, vapors, and liquids*. Plenum Publishing Corp: New York and London, **1974**; Vol. 6, 73 p.

30. Crank, J., *The mathematics of diffusion*. 2nd ed.; Clarendon Press: Oxford, **1975**

31. Han, J. H.; Scanlon, M. G., Chapter 2 - Mass transfer of gas and solute through packaging materials. In *Innovation in Food Packaging*, Han, J. H., Ed. Elsevier **2005**.

32. Bras, J. Etude de Proprietes Barrires de Derives Cellulosique. Application au gel de cellulose du papier sulfurisé. *PhD thesis* INP Toulouse, Toulouse, France, **2004**.

33. Brody, A. L.; Strupinsky, E. R.; Kline, L. R., *Active packaging for food applications*. CRC Press: New York, **2001**; p.

34. Robertson, G. L., Permability of Thermoplastic Polymers. In *Food Packaging: Principles and Practice*, Dekker, M., Ed. **1993**; p 73-110.

35. Miller, K. S.; Krochta, J. M., Oxygen and aroma barrier properties of edible films: A review. *Trends in Food Science & Technology* **1997,** 8, (7), 228-237.

36. ASTM Standard test method for oxygen transmission rate through plastic film and sheeting using a coulometric sensor designation D 3985-9. In *Annual Book of ASTM Standards*, American Society for Testing and Materials: **1995**.

37. Desobry, S.; Hardy, J., The increase of CO2 permeability of paper packaging with increasing hydration. *International Journal of Food Science & Technology* **1997,** 32, (5), 407-410.

38. Gontard, N.; Thibault, R.; Cuq, B.; Guilbert, S., Influence of Relative Humidity and Film Composition on Oxygen and Carbon Dioxide Permeabilities of Edible Films. *J. Agric. Food Chem.* **1996,** 44, (4), 1064-1069.

39. Kester, J. J.; Fennema, O., Edible Films and Coatings: a review. *Food Technol.* **1986,** 40, 47-59.

40. Karbowiak, T.; Hervet, H.; LÃ©ger, L.; Champion, D.; Debeaufort, F. d. r.; Voilley, A. e., Effect of Plasticizers (Water and Glycerol) on the Diffusion of a Small Molecule in Iota-Carrageenan Biopolymer Films for Edible Coating Application. *Biomacromolecules* **2006,** 7, (6), 2011-2019.

41. Almeida, M.; Alves, R.; Nascimbem, L.; Stephani, R.; Poppi, R.; de Oliveira, L., Determination of amylose content in starch using Raman spectroscopy and multivariate calibration analysis. *Analytical and Bioanalytical Chemistry* **2010,** 397, (7), 2693-2701.

42. Park, S. Y.; Lee, B. I.; Jung, S. T.; Park, H. J., Biopolymer composite films based on [kappa]-carrageenan and chitosan. *Materials Research Bulletin* **2011,** 36, (3-4), 511-519.

43. Grandahl, M.; Eriksson, L.; Gatenholm, P., Material Properties of Plasticized Hardwood Xylans for Potential Application as Oxygen Barrier Films. *Biomacromolecules* **2004,** 5, (4), 1528-1535.

44. Hartman, J.; Albertsson, A.-C.; Lindblad, M. S.; Sjöberg, J., Oxygen barrier materials from renewable sources: Material properties of softwood hemicellulose-based films. *Journal of Applied Polymer Science* **2006,** 100, (4), 2985-2991.

45. Saxena, A.; Elder, T. J.; Kenvin, J.; Ragauskas, A. J., High oxygen nanocomposite barrier films based on xylan and nanocrystalline cellulose. *Nano-Micro Lett.* **2010,** 2, 235-241.

46. FlexPakRenew Consortium In *Innovative bio-based materials for water-based barrier coating* FlexPakRenew Workshop, Lyon Airport, May 10th 2011, **2011**.

47. Talja, R.; Poppius-Levlin, K. In *Xylan from wood biorefinery - A novel approach*, FlexPakRenew Workshop - Innovating in fibre based flexible packaging through water based barrier coatings, anti microbial coatings, nanotechnologies and life cylce analysis., Lyon Airport, May 10th 2011, **2011**; CTP, Ed.

48. Dole, P.; Joly, C.; Espuche, E.; Alric, I.; Gontard, N., Gas transport properties of starch based films. *Carbohydrate Polymers* **2004,** 58, (3), 335-343.

49. Rankin, J.; Wolff, I.; Davis, H.; Rist, C., Permeability of Amylose Film to Moisture Vapor, Selected Organic Vapors, and the Common Gases. *Industrial & Engineering Chemistry Chemical & Engineering Data Series* **1958,** 3, (1), 120-123.

50. Forssell, P.; Lahtinen, R.; Lahelin, M.; Myllärinen, P., Oxygen permeability of amylose and amylopectin films. *Carbohydrate Polymers* **2002,** 47, (2), 125-129.

51. Rindlav-Westling, A.; Stading, M.; Hermansson, A.-M.; Gatenholm, P., Structure, mechanical and barrier properties of amylose and amylopectin films. *Carbohydrate Polymers* **1998,** 36, (2-3), 217-224.

52. Lange, J.; Wyser, Y., Recent innovations in barrier technologies for plastic packaging—a review. *Packaging Technology and Science* **2003,** 16, (4), 149-158.

53. Butler, B. L.; Vergano, P. L.; Testin, R. F.; Bunn, J. M.; Wiles, J. L., Mechanical and barrier properties of edible chitosan film as affected by composition and storage. *Journal of Food Science* **1996,** 61 953-961.

54. Garcia, M. A.; Pinotti, A.; Zaritzky, N. E., Physicochemical, Water Vapor Barrier and Mechanical Properties of Corn Starch and Chitosan Composite Films. *Starch - Stärke* **2006,** 58, (9), 453-463.

55. Salleh, E.; Muhamad, I.; Khairuddin, N., Preparation, characterization and antimicrobial analysis of antimicrobial starch-based film incorporated with chitosan and lauric acid. *Asian Chitin Journal* **2007,** 3, 55-68.

56. Gaudin, S.; Lourdin, D.; Forssell, P. M.; Colonna, P., Antiplasticisation and oxygen permeability of starch-sorbitol films. *Carbohydrate Polymers* **2000,** 43, (1), 33-37.

57. García, N. L.; Famá, L.; Dufresne, A.; Aranguren, M.; Goyanes, S., A comparison between the physico-chemical properties of tuber and cereal starches. *Food Research International* **2009,** 42, (8), 976-982.

58. Alves, V. D.; Mali, S.; Beléia, A.; Grossmann, M. V. E., Effect of glycerol and amylose enrichment on cassava starch film properties. *Journal of Food Engineering* **2007,** 78, (3), 941-946.

59. Bertuzzi, M. A.; Castro Vidaurre, E. F.; Armada, M.; Gottifredi, J. C., Water vapor permeability of edible starch based films. *Journal of Food Engineering* **2007,** 80, (3), 972-978.

60. Ryu, S. Y.; Rhim, J. W.; Roh, H. J.; Kim, S. S., Preparation and Physical Properties of Zein-Coated High-Amylose Corn Starch Film. *Lebensmittel-Wissenschaft und-Technologie* **2002,** 35, (8), 680-686.

61. Angellier, H.; Molina-Boisseau, S.; Lebrun, L.; Dufresne, A., Processing and Structural Properties of Waxy Maize Starch Nanocrystals Reinforced Natural Rubber. *Macromolecules* **2005,** 38, (9), 3783-3792.

62. Auras, R. A.; Harte, B.; Selke, S.; Hernandez, R., Mechanical, Physical, and Barrier Properties of Poly(Lactide) Films. *Journal of Plastic Film and Sheeting* **2003,** 19, (2), 123-135.

63. Erkskea, D.; Viskerea, I.; Dzenea, A.; Tupureinaa, V.; Savenkovab, L., Biobased polymer composites for films and coatings. *Proc. Estonian Acad. Sci. Chem.* **2006,** 55, (2), 70-77.

64. Plastics, B., Biodegradable Polymers – Inspired by Nature Ecoflex®, Ecovio®. **October 2008**, p, http://www.packaging.basf.com/p02/Packaging/en_GB/function:pi:/wa/plasticsEU~en_GB/portal/show/content/literature/ecoflex.

65. Arvanitoyannis, I.; Biliaderis, C. G.; Ogawa, H.; Kawasaki, N., Biodegradable films made from low-density polyethylene (LDPE), rice starch and potato starch for food packaging applications: Part 1. *Carbohydrate Polymers* **1998,** 36, (2-3), 89-104.

66. Dufresne, A.; Cavaille, J. Y.; Helbert, W., New nanocomposite materials: Microcrystalline starch reinforced thermoplastic. *Macromolecules* **1996,** 29, (23), 7624-7626.

67. Dufresne, A.; Cavaille, J. Y.; Helbert, W., Thermoplastic nanocomposites filled with wheat straw cellulose whiskers .2. Effect of processing and modeling. *Polymer Composites* **1997,** 18, (2), 198-210.

68. Favier, V.; Canova, G. R.; Cavaillé, J. Y.; Chanzy, H.; Dufresne, A.; Gauthier, C., Nanocomposite materials from latex and cellulose whiskers. *Polymers for Advanced Technologies* **1995,** 6, (5), 351-355.

69. Favier, V.; Cavaille, J. Y.; Chanzy, H.; Dufresne, A., CELLULOSE WHISKERS IN POLYMERIC MATRIX FORMING NANOCOMPOSITES. *Abstracts of Papers of the American Chemical Society* **1995,** 209, 29-MACR.

70. Helbert, W.; Cavaille, J. Y.; Dufresne, A., Thermoplastic nanocomposites filled with wheat straw cellulose whiskers .1. Processing and mechanical behavior. *Polymer Composites* **1996,** 17, (4), 604-611.

71. Azizi Samir, M. A. S.; Alloin, F.; Dufresne, A., Review of Recent Research into Cellulosic Whiskers, Their Properties and Their Application in Nanocomposite Field. *Biomacromolecules* **2005,** 6, (2), 612-626.

72. Siqueira, G.; Bras, J.; Dufresne, A., Cellulose Whiskers versus Microfibrils: Influence of the Nature of the Nanoparticle and its Surface Functionalization on the Thermal and Mechanical Properties of Nanocomposites. *Biomacromolecules* **2008,** 10, (2), 425-432.

73. Dubief, D.; Samain, E.; Dufresne, A., Polysaccharide Microcrystals Reinforced Amorphous Poly(Î²-hydroxyoctanoate) Nanocomposite Materials. *Macromolecules* **1999,** 32, (18), 5765-5771.

74. Habibi, Y.; Lucia, L.; Rojas, O., Cellulose nanocrystals: chemistry, self-assembly, and applications. *Chemical Reviews* **2010,** 110, ((6)).

75. Dufresne, A., Biopolymers on Biocomposites. In *Biopolymers Technology*, Bertolini, A. C., Ed. Sao Paulo, **2007**; Vol. Cultura Academica.

76. Dufresne, A.; Meideiros, E. S.; Orts, W. J., Chapter 9. Starch-based nanocomposites. In *Starch: Characterization, Properties and Applications*, Bertolini, A., Ed. CRC Press, Taylor & Francis Group: **2010**; p 205-251.

77. Le Corre, D.; Bras, J.; Dufresne, A., Starch nanoparticles: A review. *Biomacromolecules* **2010,** 11, (5), 1139-1153.

78. Lin, N.; Huang, J.; Chang, P. R.; Anderson, D. P.; Yu, J., Preparation, modification and application of starch nanocrystals in nanomaterials: A review. *J. Nanomater.* **2011,** 2011, 13.

79. Alexandre, M.; Dubois, P., Polymer-layered silicate nanocomposites: preparation, properties and uses of a new class of materials. *Materials Science and Engineering: R: Reports* **2000,** 28, (1-2), 1-63.

80. Sengupta, R.; Chakraborty, S.; Bandyopadhyay, S.; Dasgupta, S.; Mukhopadhyay, R.; Auddy, K.; Deuri, A. S., A short review on rubber/clay nanocomposites with emphasis on mechanical properties. *Polymer Engineering & Science* **2007,** 47, (11), 1956-1974.

81. Choudalakis, G.; Gotsis, A. D., Permeability of polymer/clay nanocomposites: A review. *European Polymer Journal* **2009,** 45, (4), 967-984.

82. Lu, C.; Mai, Y.-W., Influence of Aspect Ratio on Barrier Properties of Polymer-Clay Nanocomposites. *Physical Review Letters* **2005,** 95, (8), 088303.

83. Peiyao, L.; Li, W.; Guojun, S.; Lanlan, Y.; Feng, Q.; Liangdong, S., Characterization of high-performance exfoliated natural rubber/organoclay nanocomposites. *Journal of Applied Polymer Science* **2008,** 109, (6), 3831-3838.

84. Wilhelm, H. M.; Sierakowski, M. R.; Souza, G. P.; Wypych, F., Starch films reinforced with mineral clay. *Carbohydrate Polymers* **2003,** 52, (2), 101-110.

85. Bordes, P.; Pollet, E.; Avérous, L., Nano-biocomposites: Biodegradable polyester/nanoclay systems. *Progress in Polymer Science* **2009,** 34, (2), 125-155.

86. Azeredo, H. M. C. d., Nanocomposites for food packaging applications. *Food Research International* **2009,** 42, (9), 1240-1253.

87. Rhim, J.-W.; Ng, P. K. W., Natural Biopolymer-Based Nanocomposite Films for Packaging Applications. *Critical Reviews in Food Science and Nutrition* **2007,** 47, (4), 411 - 433.

88. Rhim, J.-W.; Hong, S.-I.; Ha, C.-S., Tensile, water vapor barrier and antimicrobial properties of PLA/nanoclay composite films. *LWT - Food Science and Technology* **2009,** 42, (2), 612-617.

89. Döppers, L.-M.; Breen, C.; Sammon, C., Diffusion of water and acetone into poly(vinyl alcohol)-clay nanocomposites using ATR-FTIR. *Vibrational Spectroscopy* **2004,** 35, (1-2), 27-32.

90. Saxena, A.; Ragauskas, A. J., Water transmission barrier properties of biodegradable films based on cellulosic whiskers and xylan. *Carbohydrate Polymers* **2009,** 78, (2), 357-360.

91. Lu, C.; Mai, Y.-W., Permeability modelling of polymer-layered silicate nanocomposites. *Composites Science and Technology* **2007,** 67, (14), 2895-2902.

92. Tjong, S. C., Structural and mechanical properties of polymer nanocomposites. *Materials Science and Engineering: R: Reports* **2006,** 53, (3-4), 73-197.

93. Paillet, M.; Dufresne, A., Chitin Whisker Reinforced Thermoplastic Nanocomposites. *Macromolecules* **2001,** 34, (19), 6527-6530.

94. Gopalan Nair, K.; Dufresne, A., Crab Shell Chitin Whisker Reinforced Natural Rubber Nanocomposites. 2. Mechanical Behavior. *Biomacromolecules* **2003,** 4, (3), 666-674.

95. Morin, A.; Dufresne, A., Nanocomposites of Chitin Whiskers from Riftia Tubes and Poly(caprolactone). *Macromolecules* **2002,** 35, (6), 2190-2199.

96. Angellier, H.; Molina-Boisseau, S.; Dufresne, A., Mechanical Properties of Waxy Maize Starch Nanocrystal Reinforced Natural Rubber. *Macromolecules* **2005,** 38, (22), 9161-9170.

97. Angellier, H.; Molina-Boisseau, S.; Dole, P.; Dufresne, A., Thermoplastic Starch-Waxy Maize Starch Nanocrystals Nanocomposites. *Biomacromolecules* **2006,** 7, (2), 531-539.

98. Angellier, H.; Molina-Boisseau, S.; Belgacem, M. N.; Dufresne, A., Surface Chemical Modification of Waxy Maize Starch Nanocrystals. *Langmuir* **2005,** 21, (6), 2425-2433.

99. Putaux, J. L.; Molina-Boisseau, S.; Momaur, T.; Dufresne, A., Platelet Nanocrystals Resulting from the Disruption of Waxy Maize Starch Granules by Acid Hydrolysis. *Biomacromolecules* **2003,** 4, (5), 1198-1202.

100. Angellier, H.; Choisnard, L.; Molina-Boisseau, S.; Ozil, P.; Dufresne, A., Optimization of the preparation of aqueous suspensions of waxy maize starch nanocrystals using a response surface methodology. *Biomacromolecules* **2004,** 5, 1545-1551.

101. Petersson, L.; Oksman, K., Biopolymer based nanocomposites: Comparing layered silicates and microcrystalline cellulose as nanoreinforcement. *Composites Science and Technology* **2006,** 66, (13), 2187-2196.

102. Ma, X.; Chang, P. R.; Yang, J.; Yu, J., Preparation and properties of glycerol plasticized-pea starch/zinc oxide-starch bionanocomposites. *Carbohydrate Polymers* **2009,** 75, (3), 472-478.

103. Ma, X.; Chang, P. R.; Yu, J., Properties of biodegradable thermoplastic pea starch/carboxymethyl cellulose and pea starch/microcrystalline cellulose composites. *Carbohydrate Polymers* **2008,** 72, (3), 369-375.

104. Whistler, R. L.; Paschall, E. F., *Starch: Chemistry and Technology*. New York, **1965**; p.

105. Wood, L., Marketing Brief of Starch, Modified Starch and other Derivatives Industry Reports http://www.businesswire.com/news/home/20110207006369/en/Research-Markets-Marketing-Starch-Modified-Starch-Derivatives, **2009 & 2010** Access (July 8th 2011).

106. Whistler, R. L.; BeMiller, J., *Starch: Chemistry and Technology*. Third ed.; Elsevier: New York, **2009**; 879 p.

107. Revedin, A.; Aranguren, B.; Becattini, R.; Longo, L.; Marconi, E.; Lippi, M. M.; Skakun, N.; Sinitsyn, A.; Spiridonova, E.; Svobodahi, J., Thirty thousand-year-old evidence of plant food processing. *Proceedings of the National Academy of Sciences of the United States of America* **2010,** 107, (44), 18815-18819.

108. Pliny the Elder, Book XIII (Chapter 17 and 26). In *The Natural History*, Pliny, Ed. **AD 77-79**.

109. Association des Amidonniers et Féculiers, The markets: Sectors of application of starch products. http://www.aaf-eu.org/html/markets.php, **2009,** Access (July 9th 2011).

110. Huber, K. C.; BeMiller, J. N., Modified starch: Chemistry and Properties. In *Starches: Characterization, Properties and Applications*, Bertolini, A. C., Ed. CRC Press: Boca Raton, **2010**; p 145-203.

111. Daniel, J. R.; Whistler, R. L.; Röper, H., Starch. In *Ullmann's Encyclopedia of Industrial Chemistry 2007*, Wiley, Ed. VCH Verlag GmbH & Co: **2000**.

112. Flexnews, Starch – An 'Indispensable' Food Ingredient Faced With Market Challenges. http://www.flex-news-food.com/console/PageViewer.aspx?page=13882&str=China%20MSG, **2008,** Access (July 9th 2011).

113. Buléon, A.; Colonna, P.; Planchot, V.; Ball, S., Starch granules: structure and biosynthesis. *International Journal of Biological Macromolecules* **1998,** 23, (2), 85-112.

114. Vandeputte, G. E.; Delcour, J. A., From sucrose to starch granule to starch physical behaviour: a focus on rice starch. *Carbohydrate Polymers* **2004,** 58, (3), 245-266.

115. Oates, C. G., Towards an understanding of starch granule structure and hydrolysis. *Trends in Food Science & Technology* **1997,** 8, (11), 375-382.

116. Hizukuri, S., Polymodal distribution of the chain lengths of amylopectins, and its significance. *Carbohydrate Research* **1986,** 147, (2), 342-347.

117. Jenkins, P. J.; Donald, A. M., The influence of amylose on starch granule structure. *International Journal of Biological Macromolecules* **1995,** 17, (6), 315-321.

118. Avérous, L.; Halley, P. J., Biocomposites based on plasticized starch. *Biofuels, Bioproducts and Biorefining* **2009,** 3, (3), 329-343.

119. Fuglie, K. O., Raw Materials for Starch in Asia: Some Economic Considerations. *UPWARD [Users' Perspective With Agricultural Research and Development Network] Fieldnotes* **1999,** 7(2), 5-7.

120. Sanguanpong, V.; Chotineeranat, S.; Piyachomkwan, K.; Oates, C. G.; Chinachoti, P.; Sriroth, K., Preparation of small-particle cassava starch. *Journal of the Science of Food and Agriculture* **2003,** 83, 760-768.

121. Chen, Z.; Schols, H. A.; Voragen, A. G. J., Physicochemical Properties of Starches Obtained from Three Varieties of Chinese Sweet Potatoes. *Journal of Food Science* **2003,** 68, (2), 431-437.

122. McPherson, A. E.; Jane, J., Comparison of waxy potato with other root and tuber starches. *Carbohydrate Polymers* **1999,** 40, (1), 57-70.

123. Wajira, S. R.; Ratnajothi, H.; Tom, W., Pea Starch: Composition, Structure and Properties - A Review. *Starch - Stärke* **2002,** 54, (6), 217-234.

124. Dufresne, A., Polymer Nanocomposites from Biological Sources. In *Biopolymers Technology*, Bertolini, A. C., Ed. Sao Paulo, Brazil, **2007**; Vol. Cultura Academica, p 59-83.

125. Peat, S.; Whelan, W. J.; Thomas, G. J., Evidence of multiple branching in waxy maize starch. *Journal of the Chemical Society* **1952**, 4546-4548.

126. Hanashiro, I.; Abe, J.-i.; Hizukuri, S., A periodic distribution of the chain length of amylopectin as revealed by high-performance anion-exchange chromatography. *Carbohydrate Research* **1996,** 283, (22), 151-159.

127. Bergthaller, W.; Hollmann, J.; Johannis, P. K., Starch. In *Comprehensive Glycoscience*, Elsevier: Oxford, **2007**; p 579-612.

128. Ao, Z.; Jane, J.-l., Characterization and modeling of the A- and B-granule starches of wheat, triticale, and barley. *Carbohydrate Polymers* **2007,** 67, (1), 46-55.

129. Hizukuri, S., Starch: analytical aspects. In *Carbohydrates in food*, Eliasson, A.-C., Ed. Marcel Dekker: New York, **1996**; p 347–429.

130. Swinkels, J. J. M., Composition and Properties of Commercial Native Starches. *Starch - Stärke* **1985,** 37, (1), 1-5.

131. Katz, J. R., Abhandlungen zur physikalischen Chemie der Stärke und der Brotbereitung. *Zeitschrift für Physikalische Chemie* **1930,** 150, 37-59.

132. French, D., Organization of starch granules. In *Starch: Chemistry and Technology*, Whistler, R. L.; BeMiller, J. N.; Paschall, E. F., Eds. New York, USA, **1984**; p 183-247.

133. Nikuni, Z., Proposed model of a starch granule or a starch molecule. *Chori Kagaku (Japan)* **1969** 2 (1969), 6.

134. Lineback, D. R., The Starch Granule: Organisation and Properties. *Bakers Dig* **1984,** 58, (1984), 16-21.

135. Gallant, D. J. Contribution à l'étude de la structure et de l'ultrastructure du grain d'amidon. *PhD thesis* University of Paris VI, Paris, France, **1974**.

136. Gallant, D. J.; Bouchet, B.; Buleon, A.; S. Perez, Physical Characteristics of Starch Granules and Susceptibility to Enzymatic Degradation. *European Journal of Clinical Nutrition* **1992,** 46, S3–S16.

137. Duprat, F.; Gallant, D. J.; Guilbot, A.; Mercier, C.; Robin, J. P., L'amidon. In *Les Polymères Végétaux. Polymères pariétaux et alimentaires non azotés*, Monties, B., Ed. Gauthier Villars: Paris **1980**; p 176–231.

138. Blanshard, J. M. V., Starch granule structure and function: a physicochemical approach. In *Starch: Properties and Potentials*, Galliard, T., Ed. Society of Chemical Industry: London , U.K. , **1987**; Vol. 13, p 16-54.

139. Jane, J.-l.; Shen, J. J., Internal structure of the potato starch granule revealed by chemical gelatinization. *Carbohydrate Research* **1993,** 247, 279-290.

140. Kasemsuwan, T.; Jane, J., Location of amylose in normal starch granules. II. Locations of phosphodiesterase cross-linking revealed by phosphorus-31 nuclear magnetic resonance. *Cereal Chemistry* **1994** 71 282-287.

141. Pérez S; Baldwin P; DJ, G., Structural Features of Starch Granules I In *Starch: Chemistry and Technology*, Third ed.; Whistler, R. L.; BeMiller, J., Eds. Elsevier: New York, **2009**.

142. Shannon, J. C.; Garwood, D. L.; Boyer, C. D., Genetic and physiology of Starch Development. In *Starch: Chemistry and Technology - Third Edition*, BeMiller, J.; Whistler, R., Eds. Academic Press - Elsevier: **2009**; p 28.

143. Oostergetel, G. T.; van Bruggen, E. F. J., The crystalline domains in potato starch granules are arranged in a helical fashion. *Carbohydrate Polymers* **1993,** 21, (1), 7-12.

144. Bertoft, E., On the nature of categories of chains in amylopectin and their connection to the super helix model. *Carbohydrate Polymers* **2004,** 57, (2), 211-224.

145. Hizukuri, S.; Kaneko, T.; Takeda, Y., Measurement of the chain length of amylopectin and its relevance to the origin of crystalline polymorphism of starch granules. *Biochimica et Biophysica Acta (BBA) - General Subjects* **1983,** 760, (1), 188-191.

146. Imberty, A.; Chanzy, H.; Perez, S.; Buleon, A.; Tran, V., New three-dimensional structure for A-type starch. *Macromolecules* **1987,** 20, (10), 2634-2636.

147. Imberty, A.; Perez, S., A revisit to the three-dimensional structure of B-type starch. *Biopolymers* **1988,** 27, (8), 1205-1221.

148. Jane, J.-l.; Wong, K.-s.; McPherson, A. E., Branch-structure difference in starches of A- and B-type X-ray patterns revealed by their Naegeli dextrins. *Carbohydrate Research* **1997,** 300, (3), 219-227.

149. Gérard, C.; Planchot, V.; Colonna, P.; Bertoft, E., Relationship between branching density and crystalline structure of A- and B-type maize mutant starches. *Carbohydrate Research* **2000,** 326, (2), 130-144.

150. Bogracheva, T. Y.; Morris, V. J.; Ring, S. G.; Hedley, C. L., The granular structure of C-type pea starch and its role in gelatinization. *Biopolymers* **1998,** 45, (4), 323-332.

151. Wang, S.; Yu, J.; Jin, F.; Yu, J., The new insight on ultrastructure of C-type starch granules revealed by acid hydrolysis. *International Journal of Biological Macromolecules* **2008,** 43, (2), 216-220.

152. Wang, S.; Yu, J.; Yu, J., The semi-crystalline growth rings of C-type pea starch granule revealed by SEM and HR-TEM during acid hydrolysis. *Carbohydrate Polymers* **2008,** 74, (3), 731-739.

153. Luc, A.; Peter, J. H., Biocomposites based on plasticized starch. *Biofuels, Bioproducts and Biorefining* **2009,** 3, (3), 329-343.

154. Cheetham, N. W. H.; Tao, L., Variation in crystalline type with amylose content in maize starch granules: an X-ray powder diffraction study. *Carbohydrate Polymers* **1998,** 36, (4), 277-284.

155. Angellier, H. Nanocristaux d'amidon de maïs cireux pour applications composites. *Ph.D thesis* University Joseph Fourier, Grenoble, France, **2005**.

156. Barron, C. Destructuration d'amidons peu hydratés sous cisaillement. , Université de Nantes, Nantes, **1999**.

157. Cooke, D.; Gidley, M. J., Loss of crystalline and molecular order during starch gelatinisation: origin of the enthalpic transition. *Carbohydrate Research* **1992,** 227, 103-112.

158. Zhong, Z.; Sun, X. S., Thermal characterization and phase behavior of cornstarch studied by differential scanning calorimetry. *Journal of Food Engineering* **2005,** 69, (4), 453-459.

159. Randzio, S. a. L.; Flis-Kabulska, I.; Grolier, J.-P. E., Reexamination of Phase Transformations in the Starchâ"Water System. *Macromolecules* **2002,** 35, (23), 8852-8859.

160. Colonna, P.; Buleon, A., Thermal transitions of starches. In *Starches: characterization, properties, and applications*, Bertolini, A. C., Ed. CRC Press: NW, **2010**; p 71-102.

161. Atichokudomchai, N.; Varavinit, S.; Chinachoti, P., Gelatinization Transitions of Acid-modified Tapioca Starches by Differential Scanning Calorimetry (DSC). *Starch - Stärke* **2002,** 54, (7), 296-302.

162. Waigh, T. A.; Gidley, M. J.; Komanshek, B. U.; Donald, A. M., The phase transformations in starch during gelatinisation: a liquid crystalline approach. *Carbohydrate Research* **2000,** 328, (2), 165-176.

163. Biliaderis, C. G.; Page, C. M.; Maurice, T. J.; Juliano, B. O., Thermal characterization of rice starches: a polymeric approach to phase transitions of granular starch. *Journal of Agricultural and Food Chemistry* **1986,** 34, (1), 6-14.

164. Donovan, J. W., Phase transitions of the starch–water system. *Biopolymers* **1979,** 18, 263-275.

165. Evans, I. D.; Haisman, D. R., The effect of solutes on gelatinization temperature range of potato starches. *Stärke* **1982,** 34 (7).

166. Biliaderis, C. G.; Page, C. M.; Slade, L.; Sirett, R. R., Thermal behavior of amylose-lipid complexes. *Carbohydrate Polymers* **1985,** 5, (5), 367-389.

167. Tester, R. F.; Morrison, W. R., Swelling and gelatinization of cereal starches. I. Effects of amylopectin, amylose, and lipids. *Cereal Chemistry* **1990,** 67, 551-557.

168. Waigh, T. A.; Kato, K. L.; Donald, A. M.; Gidley, M. J.; Clarke, C. J.; Riekel, C., Side-chain liquid-crystalline model for starch. *Starch - Stärke* **2000,** 52, ((12)), 450-460.

169. Waigh, T. A.; Perry, P.; Riekel, C.; Gidley, M. J.; Donald, A. M., Chiral Side-Chain Liquid-Crystalline Polymeric Properties of Starch. *Macromolecules* **1998,** 31, (22), 7980-7984.

170. Dufresne, A.; Cavaillé, J.-Y., Clustering and percolation effects in microcrystalline starch-reinforced thermoplastic. *Journal of Polymer Science Part B: Polymer Physics* **1998,** 36, (12), 2211-2224.

171. Chen, G.; Wei, M.; Chen, J.; Huang, J.; Dufresne, A.; Chang, P. R., Simultaneous reinforcing and toughening: New nanocomposites of waterborne polyurethane filled with low loading level of starch nanocrystals. *Polymer* **2008,** 49, (7), 1860-1870.

172. Chen, Y.; Cao, X.; Chang, P. R.; Huneault, M. A., Comparative study on the films of poly(vinyl alcohol)/pea starch nanocrystals and poly(vinyl alcohol)/native pea starch. *Carbohydrate Polymers* **2008,** 73, (1), 8-17.

173. Yu, J.; Ai, F.; Dufresne, A.; Gao, S.; Huang, J.; Chang, P. R., Structure and mechanical properties of poly(lactic acid) filled with (starch nanocrystal)-graft-poly(e-caprolactone). *Macromolecular Materials and Engineering* **2008,** 293, (9), 763-770.

174. Zheng Hua; Ai Fujin; Chang Peter, R.; Huang Jin; Dufresne Alain, Structure and properties of starch nanocrystal-reinforced soy protein plastics. *Polymer Composites* **2009,** 30, (4), 474-480.

175. García, N. L.; Ribba, L.; Dufresne, A.; Aranguren, M. I.; Goyanes, S., Physico-Mechanical Properties of Biodegradable Starch Nanocomposites. *Macromolecular Materials and Engineering* **2009,** 294, (3), 169-177.

176. Namazi, H.; Dadkhah, A., Convenient method for preparation of hydrophobically modified starch nanocrystals with using fatty acids. *Carbohydrate Polymers* **2010,** 79, (3), 731-737.

177. Wang, Y.; Zhang, L., High-strength waterborne polyurethane reinforced with waxy maize starch nanocrystals. *J. Nanosci. Nanotechnol.* **2008,** 8, (11), 5831-5838.

178. Le Corre, D.; Bras, J.; Dufresne, A., Starch Nanoparticles for eco-efficient packaging: influence of botanic origin. In *2nd International Conference on Biodegradable Polymers and Sustainable Composites (BIOPOL 2009)*, Jimenez, A., Ed. Alicante, Spain, **2009**.

179. Nägeli, W., Beiträge zur näheren Kenntnifs der Stärkegruppe. *Justus Liebigs Annalen der Chemie* **1874,** 173, 218-227.

180. Lintner, C. J., Studien über Diastase. *Journal für Praktische Chemie* **1886,** 34, 378-394.

181. Li, W.; Corke, H.; Beta, T., Kinetics of hydrolysis and changes in amylose content during preparation of microcrystalline starch from high-amylose maize starches. *Carbohydrate Polymers* **2007,** 69, (2), 398-405.

182. Angellier, H.; Putaux, J.-L.; Molina-Boisseau, S.; Dupeyre, D.; Dufresne, A., Starch nanocrystal fillers in an acrylic polymer matrix. *Macromolecular Symposia* **2005,** 221, (1), 95-104.

183. Jayakody, L.; Hoover, R., The effect of lintnerization on cereal starch granules. *Food Research International* **2002,** 35, (7), 665-680.

184. Robin, J. P.; Mercier, C.; Charbonniere, R.; Guilbot, A., Gel filtration and enzymatic studies of insoluble residues from prolonged acid treatment of potato starch. *Cereal Chemistry* **1974,** 51 389-406.

185. Biliaderis, C. G.; Grant, D. R.; Vose, J. R., Structural characterization of legume starches I. Studies on amylose, amylopectin, and beta-limit dextrins. *Cereal Chem.* **1981,** 58, 496-502.

186. Singh, V.; Ali, S. Z., Comparative Acid Modification of Various Starches. *Starch - Stärke* **1987,** 39, (11), 402-405.

187. Singh, V.; Ali, S. Z., Divakar, S. 13C CP/MAS NMR Spectroscopy of Native and Acid Modified Starches. *Starch/Staerke* **1993,** 45 59-62.

188. Singh, V.; Ali, S. Z., Acid degradation of starch. The effect of acid and starch type. *Carbohydrate Polymers* **2000,** 41, 191-195.

189. Singh, V.; Ali, S. Z., Properties of Starches Modified by Different Acids. *International Journal of Food Properties* **2008,** 11, (3), 495 - 507.

190. Wang, Y.-J.; Truong, V.-D.; Wang, L., Structures and rheological properties of corn starch as affected by acid hydrolysis. *Carbohydrate Polymers* **2003,** 52, (3), 327-333.

191. LeCorre, D.; Gallur, M.; Bras, J.; Ancejo, S.; Dufresne, A., Potential of pea starch nanocrystals: A comparison with other common sources In *TAPPI Intl Conference on Nano for Renewable Materials*, Arlington, VA USA, **2011**.

192. Kim, J.-Y.; Park, D.-J.; Lim, S.-T., Fragmentation of Waxy Rice Starch Granules by Enzymatic Hydrolysis. *Cereal Chemistry* **2008,** 85, (2), 182-187.

193. Angellier-Coussy, H.; Putaux, J.-L.; Molina-Boisseau, S.; Dufresne, A.; Bertoft, E.; Perez, S., The molecular structure of waxy maize starch nanocrystals. *Carbohydrate Research* **2009,** 344, (12), 1558-1566.

194. Kuemmerer, K.; Menz, J.; Schubert, T.; Thielemans, W., Biodegradability of organic nanoparticles in the aqueous environment. *Chemosphere* **2011,** 82, (10), 1387-1392.

195. Putaux, J.-L., Morphology and Structure of Crystalline Polysaccharides: Some Recent Studies. *Macromolecular Symposia* **2005,** 229, (1), 66-71.

196. Kim, J.-Y.; Lim, S.-T., Preparation of nano-sized starch particles by complex formation with n-butanol. *Carbohydrate Polymers* **2009,** 76, (1), 110-116.

197. Le Corre, D.; Gallur, M.; Bras, J.; Ancejo, S.; Dufresne, A., Potential of pea starch nanocrystals: A comparison with other common sources In *2011 TAPPI Intl Conference on Nano for Renewable Materials*, Washington, USA, **2011**.

198. Viguié, J.; Molina-Boisseau, S.; Dufresne, A., Processing and Characterization of Waxy Maize Starch Films Plasticized by Sorbitol and Reinforced with Starch Nanocrystals. *Macromolecular Bioscience* **2007,** 7, (11), 1206-1216.

199. Kristo, E.; Biliaderis, C. G., Physical properties of starch nanocrystal-reinforced pullulan films. *Carbohydrate Polymers* **2007,** 68, (1), 146-158.

200. Zheng, H.; Ai, F.; Chang, P. R.; Huang, J.; Dufresne, A., Structure and properties of starch nanocrystal-reinforced soy protein plastics. *Polymer Composites* **2009,** 30, (4), 474-480.

201. Lin, N.; Yu, J.; Chang, P. R.; Li, J.; Huang, J., Poly(butylene succinate)-based biocomposites filled with polysaccharide nanocrystals: Structure and properties. *Polymer Composites* **2011,** 32, (3), 472-482.

202. Lin, N.; Huang, J.; Chang, P. R.; Feng, L.; Yu, J., Effect of polysaccharide nanocrystals on structure, properties, and drug release kinetics of alginate-based microspheres. *Colloids and Surfaces B: Biointerfaces* **2011,** 85, (2), 270-279.

203. Zhang, X.; Huang, J.; Chang, P. R.; Li, J.; Chen, Y.; Wang, D.; Yu, J.; Chen, J., Structure and properties of polysaccharide nanocrystal-doped supramolecular hydrogels based on Cyclodextrin inclusion. *Polymer* **2010,** 51, (19), 4398-4407.

204. Valodkar, M.; Thakore, S., Isocyanate crosslinked reactive starch nanoparticles for thermo-responsive conducting applications. *Carbohydrate Research* **2011,** 345, (16), 2354-2360.

205. Thielemans, W.; Belgacem, M. N.; Dufresne, A., Starch nanocrystals with large chain surface modifications. *Langmuir* **2006,** 22, (10), 4804-4810.

206. Angellier, H.; Molina-Boisseau, S.; Dufresne, A., Waxy maize starch nanocrystals as filler in natural rubber. *Macromolecular Symposia* **2006,** 233, (1), 132-136.

207. Labet, M.; Thielemans, W.; Dufresne, A., Polymer Grafting onto Starch Nanocrystals. *Biomacromolecules* **2007,** 8, (9), 2916-2927.

208. Song, S.; Wang, C.; Pan, Z.; Wang, X., Preparation and characterization of amphiphilic starch nanocrystals. *Journal of Applied Polymer Science* **2008,** 107, (1), 418-422.

209. Chang, P. R.; Ai, F.; Chen, Y.; Dufresne, A.; Huang, J., Effects of starch nanocrystal-graft-polycaprolactone on mechanical properties of waterborne polyurethane-based nanocomposites. *Journal of Applied Polymer Science* **2009,** 111, (2), 619-627.

210. Namazi, H.; Dadkhah, A., Surface modification of starch nanocrystals through ring-opening polymerization of ϵ-caprolactone and investigation of their microstructures. *Journal of Applied Polymer Science* **2008,** 110, (4), 2405-2412.

211. García, N. L.; Ribba, L.; Dufresne, A.; Aranguren, M.; Goyanes, S., Effect of glycerol on the morphology of nanocomposites made from thermoplastic starch and starch nanocrystals. *Carbohydrate Polymers* **2011,** 84, (1), 203-210.

212. Lin, N.; Huang, J.; Chang, P. R.; Feng, L.; Yu, J., Effect of polysaccharide nanocrystals on structure, properties, and drug release kinetics of alginate-based microspheres. *Colloids and Surfaces B: Biointerfaces* **2011,** In Press, Accepted Manuscript.

213. Ma, X.; Jian, R.; Chang, P. R.; Yu, J., Fabrication and Characterization of Citric Acid-Modified Starch Nanoparticles/Plasticized-Starch Composites. *Biomacromolecules* **2008,** 9, (11), 3314-3320.

214. Dufresne, A., Processing of polymer nanocomposites reinforced with polysaccharide nanocrystals. *Molecules* **2010,** 15, 4111-4128.

215. Rooj, S.; Das, A.; Thakur, V.; Mahaling, R. N.; Bhowmick, A. K.; Heinrich, G., Preparation and properties of natural nanocomposites based on natural rubber and naturally occurring halloysite nanotubes. *Materials & Design* **2010,** 31, (4), 2151-2156.

216. Junior De Menezes, A.; Siqueira, G.; Curvelo, A. A. S.; Dufresne, A., Extrusion and characterization of functionalized cellulose whiskers reinforced polyethylene nanocomposites. *Polymer* **2009,** 50, (19), 4552-4563.

217. Habibi, Y.; Dufresne, A., Highly Filled Bionanocomposites from Functionalized Polysaccharide Nanocrystals. *Biomacromolecules* **2008,** 9, (7), 1974-1980.

218. Siqueira, G.; Bras, J.; Dufresne, A., New process of chemical grafting of cellulose nanoparticles with a long chain isocyanate. *Langmuir* **2010,** 26, 402-411.

219. Xu, Y.; Ding, W.; Liu, J.; Li, Y.; Kennedy, J. F.; Gu, Q.; Shao, S., Preparation and characterization of organic-soluble acetylated starch nanocrystals. *Carbohydrate Polymers* **2010,** 80, (4), 1078-1084.

220. Goffin, A.-L. Polymer bionanocomposites reinforced by functionalized nanoparticles: impact of nanofiller size, nature and composition. *PhD Thesis*, Mons University, Mons, Belgium, **2010**.

221. Alila, S.; Aloulou, F.; Thielemans, W.; Boufi, S., Sorption potential of modified nanocrystals for the removal of aromatic organic pollutant from aqueous solution. *Industrial Crops and Products* **2011,** 33, (2), 350-357.

222. Jiahui Yu; Ai, F.; Dufresne, A.; Gao, S.; Huang, J.; Chang, P. R., Structure and Mechanical Properties of Poly(lactic acid) Filled with (Starch nanocrystal)-graft-poly(e-caprolactone). *Macromolecular Materials and Engineering* **2008,** 293, (9), 763-770.

223. Angles, M. N.; Dufresne, A., Plasticized Starch/Tunicin Whiskers Nanocomposites. 1. Structural Analysis. *Macromolecules* **2000,** 33, (22), 8344-8353.

224. Dufresne, A.; Vignon, M. R., Improvement of Starch Film Performances Using Cellulose Microfibrils. *Macromolecules* **1998,** 31, (8), 2693-2696.

225. Dufresne, A.; Dupeyre, D.; Vignon, M. R., Cellulose microfibrils from potato tuber cells: Processing and characterization of starch-cellulose microfibril composites. *Journal of Applied Polymer Science* **2000,** 76, (14), 2080-2092.

226. Tan, Y.; Xu, K.; Li, L.; Liu, C.; Song, C.; Wang, P., Fabrication of Size-Controlled Starch-Based Nanospheres by Nanoprecipitation. *ACS Applied Materials & Interfaces* **2009,** 1, (4), 956-959.

227. Liu, D.; Wu, Q.; Chen, H.; Chang, P. R., Transitional properties of starch colloid with particle size reduction from micro- to nanometer. *Journal of Colloid and Interface Science* **2009,** 339, (1), 117-124.

228. Kim, J.-Y.; Lim, S.-T., Preparation of nano-sized starch particles by complex formation with n-butanol. *Carbohydrate Polymers* **2009,** In Press, Corrected Proof.

229. Huang, J.; Chen, G.; Dufresne, A.; Wei, M.; Cui, G. Method for preparing starch nano-crystal-modified aqueous polyurethane. CN 101020739 A, 20070822, **2007**.

230. Huang, J.; Yi, F.; Zhang, R.; Xia, W.; Wei, M. Preparation of polyurethanes from polysaccharide nanocrystal-grafted polyesters. CN 101230189 A, 20080730, **2008**.

231. Bastioli, C.; Floridi, G.; Tredici, G. D. Biodegradable compositions based on nanoparticulate starch WO2008037749 (A2) **2008**.

232. Novamont, MaterBi Company Brochure. http://www.materbi.com/ing/html/PDF/company_brochure.pdf, Access (June 2009).

233. Bastioli, C.; Floridi, G.; Tredici, G. D. Biodegradable compositions based on nanoparticulate starch. US 2009/03114455 A1, **2009**.

234. Ecosynthetix, Ecosphere. http://www.ecosynthetix.com/ecosphere.html, **2010,** Access (June 2009).

235. Ma, B.; Zhu, X. Method for preparing polysaccharide nanoparticles as antichlor used in industrial water purification. CN 101597387, 20091209, **2009**.

236. Liu, X.; Xiao, S.; Liu, B.; Liu, J.; Tang, D. Polylysine / starch nanoparticle, its preparation and application as gene carrier. CN 1462763 A, 20031224, **2003**.

237. EugeniusGiezen, F.; Jongboom, R. O. J.; Feil, H.; Gotlieb, K. F.; Boersma, A. Process for producing biopolymer nanoparticles. WO 2000069916 A1, 20001123, **2000**.

238. Lim, S. T.; Kim, J. Y. Method for preparing starch nanopaticles. KR 873015 B1, 20081209, **2008**.

239. Lim, S. T.; Kim, J. Y. Crystalline nanoscale starch-alcohols complex, and method for manufacturing starch nanoparticles with this complex. KR 2009054547, 20090601, **2009**.

240. Mélé, P.; Angellier, H.; Molina-Boisseau, S.; Dufresne, A., Reinforcing mechanisms of starch nanocrystals in a nonvulcanized natural rubber matrix. *Biomacromolecules* **2011,** 12, 1487-1493.

FIGURES

TABLES

CHAPTER 2.

SNC Production & Characterization

CHAPTER 2. SHORT SUMMARY

RÉSUMÉ FRANCAIS– FRENCH ABSTRACT

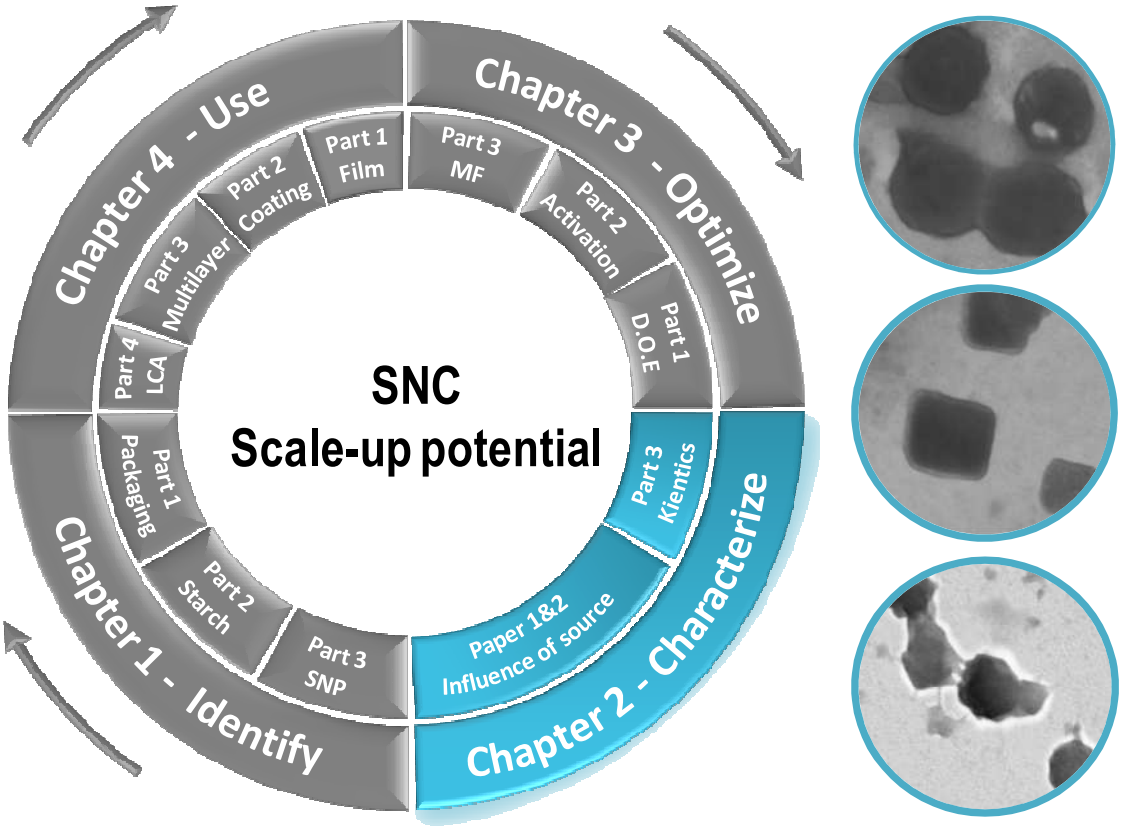

Figure Chapitre 2. Représentation schématique de l'organisation du projet de thèse

Comme nous venons de le voir dans le chapitre précédant, les nanocristaux d'amidon sont des nanoparticles très prometteuses de part leurs propriétés mécaniques et barrières, ainsi que leur caractère renouvelable. Toutefois, de nombreuses questions (présentées en Conclusion du Chapitre 1) restent à résoudre avant de pouvoir envisager un procédé de production à l'échelle pilote et industrielle.

Dans ce Chapitre 2, il s'agit d'une part, d'évaluer l'influence de l'origine botanique et du taux d'amylose de l'amidon utilisé pour produire les nanocristaux d'amidon (SNCs) sur les propriétés structurale et thermique des SNCs ; et d'autre part de caractériser la suspension de nanocristaux obtenue par le procédé actuel.

En effet, comme évoqué dans le Chapitre 1, le matériau organique le plus utilisé pour produire des bio-nano-cristaux est la cellulose. Pour ces nanocristaux de cellulose (appelés « whiskers » en raison de leur forme en bâtonnets), d'importantes différences de composition, de taille, de facteur de forme et donc de propriétés sont observées pour

des origines botaniques différentes. Il semble donc pertinent d'évaluer s'il en est de même pour les nanocristaux produits à partir d'amidon puisque la quasi totalité des SNCs produits avant le début de ce projet, l'était à partir d'une seule source : le maïs cireux.

Dans la **première partie** (Papier 2 – Soumis à *Journal of Nanoparticle Research* – Juillet 2011), nous avons donc sélectionné 5 amidons différents couvrant 3 origines botaniques différentes pour un taux d'amylose semblable, et 3 taux d'amylose différents pour une même origine botanique ; ainsi que 2 types cristallins différents (A et B). A partir de ces amidons, des SNCs ont été préparés en suivant le procédé actuel (décrit dans le Chapitre 1), puis comparés en termes de morphologie (largeur, hauteur et forme), de cristallinité et de viscosité de la suspension.
L'étude a révélé que, contrairement aux nanocristaux de cellulose, l'origine botanique de l'amidon à peu d'effet sur les propriétés finales des nanocristaux d'amidon (SNCs). Toutefois, les effets du taux d'amylose de l'amidon natif (c'est à dire non transformé) et du type cristallin semblent observables. Plus le taux d'amylose de l'amidon est élevé, plus la taille moyenne et le taux d'amylose des SNCs obtenus seront élevés et la cristallinité faible. Il semble également que les SNCs produits à partir d'amidon de type cristallin A soient plus carrés que leurs homologues de type B qui présentent une forme arrondie. Les résultats obtenus montrent que différentes sources d'amidon peuvent être utilisées pour produire des SNCs. Selon, l'utilisation visée, certains critères de sélections peuvent être envisagés pour sélectionner un amidon en particulier. Notamment certains SNCs présentent une forme rectangulaire, ce qui, combiné à une forme plaquettaire, offre des perspectives d'applications en tant que matériau barrière. La viscosité des suspensions de SNCs offre un critère supplémentaire de sélection.

Les SNCs étant destinés à être utilisés dans des procédés industriels, c'est à dire sous des contraintes thermiques et hydriques particulières, la ***deuxième partie*** (Papier 3 – Accepté dans *Carbohydrate Polymer* - 2011) prolonge l'étude précédente par la caractérisation des propriétés hygrothermiques des SNCs de 5 sources différentes. Le but est d'évaluer: (i) la stabilité thermique des SNCs à l'état sec et à l'état humide, afin de pouvoir envisager avec quel(s) procédé(s) industriel(s) les SNCs seraient compatibles ; et (ii) l'influence de l'origine botanique sur cette stabilité thermique.
L'étude révèle que, tout comme l'amidon natif, les SNCs présentent des transitions thermiques différentes à l'état sec et à l'état humide. Cependant, et comme attendu pour des nanocristaux, ces transitions interviennent à des températures supérieures à celles des amidons natifs. Les SNC peuvent donc être utilisées dans des procédés dont la température ne dépasse pas les 100°C à l'état humide et 150-200°C à l'état sec : une

information précieuse en vue des applications des SNCs (développées au Chapitre 4). Une revue des propriétés thermiques de l'amidon natif nous permet également de postuler quant au mécanisme de transition thermique des SNCs. Enfin, aucune corrélation n'est observée entre l'origine de l'amidon et la stabilité thermique des SNCs.

A l'issue de ces deux études, l'intérêt des SNCs pour des applications industrielles a été confirmé. Nous avons donc sélectionné deux types d'amidon pour poursuivre notre étude : les deux amidons permettant d'obtenir les SNCs les plus carrés (Papier 2), c'est à dire l'amidon de mais cireux (« waxy ») et de blé.

Dans la Revue sur les SNCs du Chapitre 1, ainsi que lors des deux études précédentes, la question de l'évaluation du rendement en SNCs du procédé de production actuel s'est posée. En effet, au delà des différences entre les techniques utilisées pour calculer ce rendement, il est apparu que les rendements annoncés étaient : (i) faibles (~15%) comparés à la cristallinité théorique de l'amidon (~40%) et (ii) calculés, soit à partir de la quantité d'amidon hydrolysé, soit à partir de la masse d'amidon restante après le traitement acide. Dans tous les cas, cela suppose que la suspension finale obtenue soit composée uniquement de SNCs. Les études précédentes ont permis de mettre en doute cette hypothèse.

La **troisième partie** (Papier 4 – publié dans Biomacromolecules – 2011), a donc été entreprise dans l'optique d'éclaircir les questions liées au rendement en SNCs du procédé de production. Pour expliquer la différence entre le rendement expérimental et théorique en SNCs, il a été suggéré que certains SNCs disparaissaient suite à une trop longue exposition au traitement acide. En effet, la structure stratifiée de l'amidon (décrite au Chapitre 1), laissait à penser que, contrairement à l'idée reçue selon laquelle les SNCs seraient tous obtenus au bout de 5 jours, ils pourraient commencer à apparaître plus tôt. Une cinétique d'hydrolyse a donc été mise en évidence et a révélée que: (i) des SNCs apparaissent dès le premier jour de traitement et (ii) à tout moment, il coexiste en suspension des micro et des nanoparticles d'amidon. Une solution pour, à la fois, déterminer et augmenter le rendement réel en SNC, serait de pouvoir isoler les SNC du reste de la suspension à n'importe quel moment pendant le procédé. Pour cela, une technique de séparation par centrifugation a été mise en place. Cette technique s'est révélée peu efficace en raison : de l'agglomération de SNC sur les grains d'amidon non-hydrolysés (par liaisons hydrogènes), d'une grande disparité de densité au sein d'un même grain d'amidon et d'une force de centrifugation limitée. Toutefois, cette étude se révèle très importante puisqu'elle remet en question la vision communément acceptée des SNCs produits en 5 jours et résistants au traitement acide. Elle permet de suggérer

que tous les rendements en SNCs proposés jusque là sont donc faussés. Elle souligne également la nécessité de trouver un procédé d'extraction des SNC au court de leur production (envisagé au Chapitre 3 – Papier 5).

Etant donnée les avantages (utilisation de différentes sources possible, résistance thermique) et les limites d'un point de vue industriel (faible rendement, durée) du procédé de préparation actuel des SNC, des pistes d'optimisation semblent indispensables et seront proposées au Chapitre 3 suivant.

Ce Chapitre 2, propose des résultats importants sur la caractérisation et les propriétés des SNC issues de différentes sources en vue de leurs applications ; ainsi que sur le procédé de production en lui-même. Il constitue donc la base de toute étude ultérieure.

ENGLISH ABSTRACT – RESUME ANGLAIS

In Chapter 1, starch nanocrystals (SNCs) have been identified as potential candidates in industrial applications where mechanical and barrier properties are sought. However, as seen in the previous chapter, several challenges still have to be overcome before reaching pilot or industrial scale production and use.

Chapter 2 investigates in detail the influence of starch source (botanic origin, amylose content and crystalline type) on the final properties of SNCs; and characterizes the SNC preparation process and final suspensions.

Indeed, cellulose nanocrystals (also called whiskers because of their shape) produced from different sources exhibit very different sizes and properties. Thus, in papers 2 and 3, five different kinds of starches, covering three different botanic origins, three different amylose contents and two different crystalline types, are used to prepare SNCs and characterized to assess potential differences.

In the **first part** (Paper 2 submitted to *Journal of Nanoparticles Research*, July 2011), SNC are compared in terms of size, shape, crystallinity and viscosity. Contrary to cellulose whiskers, little difference was found between the different SNCs. Yet, most influencing parameters were initial amylose content and crystalline type. They reflected mainly on the morphology of SNCs and somewhat on their size. Starch botanic origin showed only moderate influence on size distribution, thickness and viscosity, due to differences in amylose distribution and blocklet sizes among starches. The study shows that, depending on the application, some criteria can be found for selecting one type of native starch over another. For example, some SNCs show rather square platelet-like morphology compared to other disk-like ones, which could be favorable for barrier applications. Viscosity of the suspension could be another criterion for selection.

SNC are designed to be used in industrial processes, i.e. used under hydro and thermal constraints, thus the **second part** (Paper 3 accepted in *Carbohydrate Polymer*, 2011) completes the previous paper with the study of the thermal properties of the same 5 types of SNC. A review of starch's thermal properties allowed us postulating for the mechanism involved in the thermal transitions of SNCs. Conclusion reveals that SNCs can be used in industrial processes with temperatures below 100℃ in excess water and below 150-200℃ in the dry state.

Giving the industrial potential of SNCs, 2 starches were selected for further studies: the most square-like SNCs, namely waxy maize and wheat. Also, Chapter 1 revealed that the question of the evaluation of SNC yield was important to discuss. Indeed, besides being measured with different techniques, reported yields are (i) low (15%) compared to the crystallinity of starch (~40%), and (ii) calculated in reference to the amount of hydrolyzed starch or to the remaining starch, implying the final suspension contains only SNC. However, previous studies allowed questioning that assumption.

Thus, the **third part** if this chapter (Paper 4 published in *Biomacromolecules*, 2011) investigates these questions by (i) following the kinetics of hydrolysis, and (ii) assessing the possibility of classifying the resulting suspension for better assessment of SNCs yield. Results proved that contrary to common belief, SNC do not appear all at once on the fifth day. Rather, at any time during the hydrolysis (from the first day on at least) both micro and nanoparticles are present in the suspension. The study suggests that (i) all previously reported yields overestimated the amount of SNCs, (ii) that SNCs "released" on the first day might not resist prolonged exposure to catalysts, explaining for low yields; and (iii) the necessity to develop a continuous extraction process for SNC's isolation to limit exposure to catalysts and possibly reach higher non-overestimated yields (a process is proposed in Chapter 3). Differential centrifugation, used in this paper, is revealed not as efficient as expected. Therefore and giving the pros (possible use of different starches, thermal resistance) and cons (low yield, duration) of SNCs from an industrial point of view, other leads for optimization are developed in the next chapter (Chapter 3).

This chapter (Chapter 2) focuses on the characterization of SNCs from different starch sources and their preparation process to assess important and useful bases for their future application.

CHAPTER 2. SNC PRODUCTION & CHARACTERIZATION

Chapter 2-I. Influence of botanic origin and amylose content on the morphology of starch nanocrystals

Déborah LeCorre, Julien Bras, Alain Dufresne

The International School of Paper, Print Media and Biomaterials (Pagora), Grenoble Institute of Technology, BP 65 - F-38402 Saint Martin d'Hères Cedex, France

Abstract

Starch nanocrystals (SNC) are crystalline platelets resulting from the disruption of the semi-crystalline structure of starch granules by the acid hydrolysis of amorphous parts. The aim of the present study was to assess the influence of botanic origin and amylose content of native starches on the morphology and properties of resulting nanoparticles. SNC were prepared from five different starches: normal maize, high amylose maize, waxy maize, potato and wheat; covering 3 botanic origins, 2 crystalline types and 3 ranges of amylose content (0, 25 and 70%) for maize starch. Different types of nanocrystals were obtained with a thickness ranging between 4 and 8 nm and diameter from about 50 to 120 nm depending on the source. The comparison of their morphology, crystallinity and rheological properties is proposed for the first time. For the same amylose content, maize, potato and wheat resulted in rather similar size and crystallinity of SNC proving the limited influence of the botanic origin. For the same botanic origin (maize), differences in size were more important indicating the influence of the amylopectin content. Also, particles tended to show square shapes with increasing native starch's amylopectin content and A-type crystallinity. So only high-amylose content starches should be avoided to prepare SNC.

Keywords

Starch; Nanocrystals; Botanic origin; Amylose ; Hydrolysis

Inspired from: *D. LeCorre, J. Bras, A. Dufresne, Journal of Nanoparticle Research (**2011**), Accepted*

I.1. Introduction

Polymers reinforced with nanosized particles, or nanocomposites are increasingly present in our society thanks to their unique properties at low filler content compared to conventional composites. Moreover, increasing environmental concerns have led to investigate the potential use of renewable resources to replace their non-renewable or fossil-based counterparts. Renewable resources, such as polysaccharides, present the added advantage to be available world-wide and from different plant sources limiting geopolitical conflicts.

In the early 1990's, shortly after pioneer-work on nanoclay reinforced polymer nanocomposites by researchers at Toyota, work on cellulose nanofillers (such as whiskers) reinforced polymers started. Even if studies on nanofibrillated cellulose have strongly increased last decade [1], most studies were carried out with cellulose nanocrystals (whiskers). They are obtained by acidic elimination of the amorphous phase of cellulose; and a wide variety of plant source has been investigated showing a strong influence of botanic origin on their morphological properties [2]. It was soon followed by works on chitin and starch, mainly potato [3, 4] and waxy maize [5, 6] by extension. Most of the work consisted in determining the best hydrolysis conditions for a given polysaccharide and in checking reinforcement or barrier properties improvement of ensued nanocomposites.

Starch is one of the most abundant biomass materials in nature and has already found numerous industrial applications. Carbohydrate chemists have developed numerous products that have greatly expanded starch use and utility [7]. Indeed, acid hydrolysis has been used for a long time to modify starch and its properties. In industry, starch slurries are treated with dilute HCl or H_2SO_4 at 25-55℃ for various periods of time, to produce "acid-modified" starch used as sizing agents, in gum candies production, and in paper and paper board production. Most recent publications use either of these two acids for preparing SNC but conditions have been optimized over the years. In 1975, Battista reported the production of highly crystalline insoluble residues using HCl for 40 days [8]. In 1996, Dufresne et al., prepared so-called microcrystalline starch in only 15 days still using HCl [9].

More recently [10], the process for obtaining SNC was optimized, taking it down to 5 days using H_2SO_4. It was shown that the formation of sulfate-ester groups on the surface of the nanocrystals during H_2SO_4 hydrolysis limits the flocculation of the nanoparticles and leads to the production of more stable suspension [5]. Even if the

framework of this work is focused on SNC obtained by acid hydrolysis, it is possible using other processes, to produce SNC as well as amorphous starch nanoparticles as recently described in a review on starch nanoparticles [11]. Their use in polymeric matrices has also been recently detailed [11, 12] and showed some important improvement of mechanical and barrier properties.

Nowadays, the use of SNC is also being investigated for industrial packaging in a European research project (FlexPakRenew FP7 EU project). However, despite this increase of interest for the past 2 years, up to our knowledge, no studies have: compared the influence of starch sources, considered what source can be used, and which will potentially give the best nanocrystals with respect to their shape, size and yield.

Depending on the botanic origin of starch, it is well known that native granules present a wide variety of size (2-100 µm), size distribution, shape, extraction from plant conversion factors and chemical contents [13]. Starch granules consist of mainly two glucosidic macromolecules: amylose and amylopectin. Amylose is defined as a linear molecule of glucose units linked by (1-4) α-D-glycoside bonds, slightly branched by (1-6) α-linkages. Amylopectin is a highly branched polymer consisting of relatively short branches of α-D-(1-4) glycopyranose that are interlinked by α-D-(1-6) –glycosidic linkages approximately every 22 glucose units [14].

The predominant model for starch structure is multi-scaled and consists in the granule (2-100 µm), into which are found growth rings (120-500 nm) composed of blocklets (20-50 nm) made of amorphous and crystalline lamellae (9 nm [15]) containing amylopectin and amylose chains (0.1-1 nm) as represented in Figure 2-I.1.

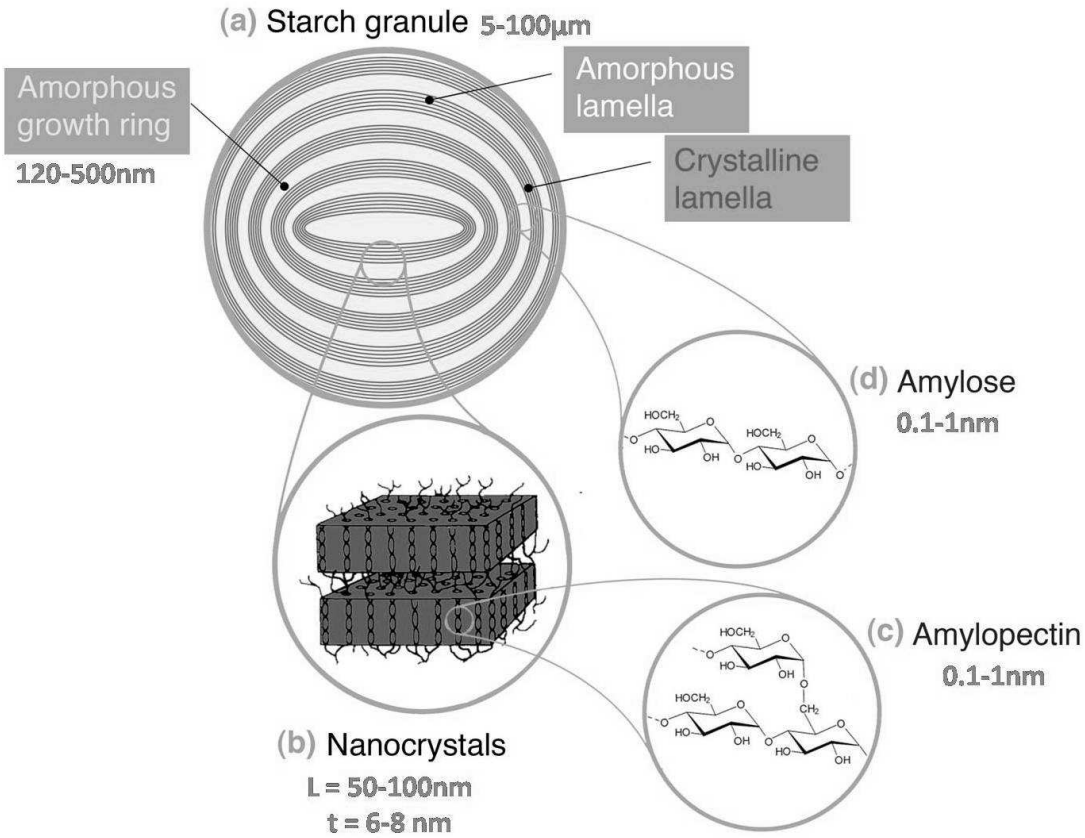

Figure 2-I.1. Representation of the starch granule multi-scale structure adapted from [11].

Native starches contain between 15% and 45% of crystalline material. It is believed that the crystalline region is created by the intertwining of chains with a linear length above 10 glucose units to form double helices [16] which are packed and form the crystallites; and the amorphous region corresponds to branching points. Amylose molecules are thought to occur in the granule as individual molecules, randomly interspersed among amylopectin molecules and in close proximity with one another, in both the crystalline and amorphous regions [16]. Depending on the botanic origin of starch, amylose is preferably found in the amorphous region (e.g. wheat starch), interspersed among amylopectin clusters in both the amorphous and crystalline regions (e.g. normal maize starch), in bundles between amylopectin clusters, or co-crystallized with amylopectin (e.g. potato starch). Amylose content and botanic origin should therefore considerably influence the crystalline organization.

Depending on their X-ray diffraction pattern, starches are categorized in three crystalline types called A, B and C. Imberty et al. [17, 18] proposed a model for the double helices packing configuration to explain difference between A- and B-type starches. A-type structures are closely packed with water molecules between each double helical structure, whereas B-types are more open and water molecules are located in the central cavity formed by 6 double helices as shown in Figure 2-I.2.

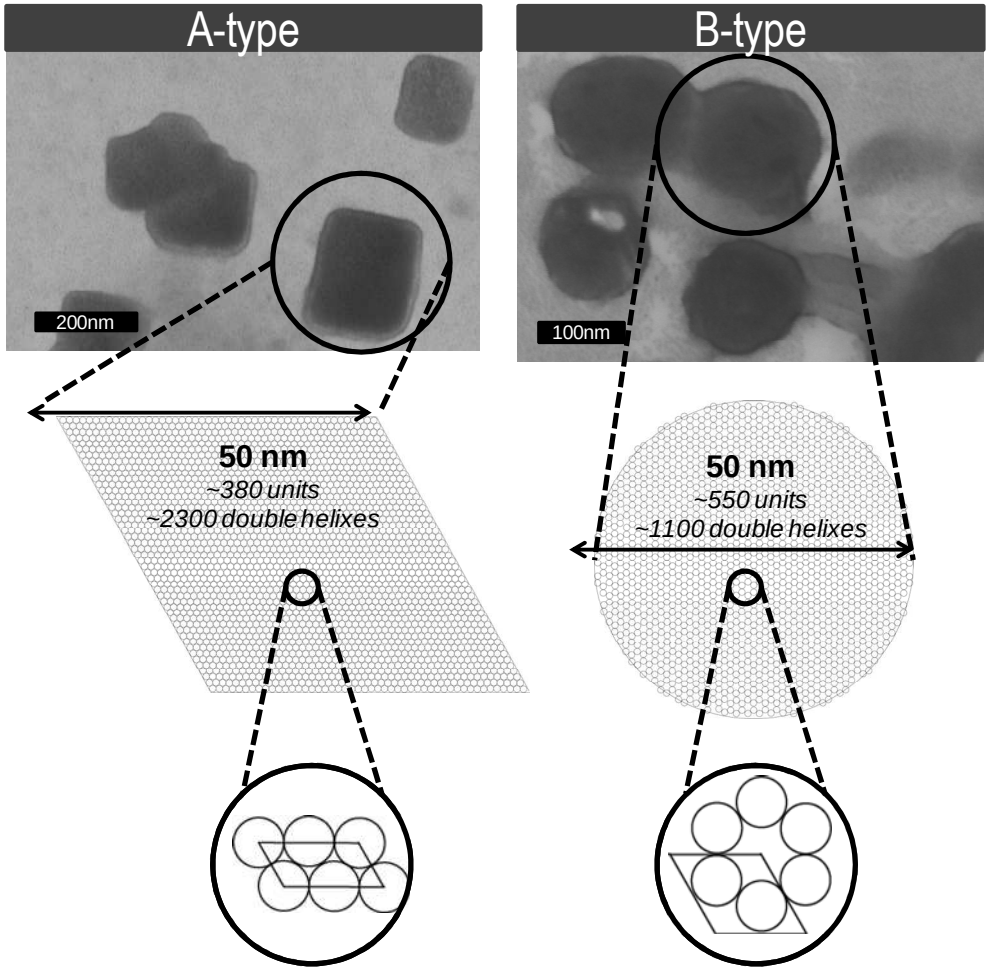

Figure 2-I.2. Double helixes packing configuration depending on crystalline type and corresponding picture of starch nanocrystals from wheat starch (A-type) and high amylose starch (B-type).

This difference in crystalline types could render different nanocrystals morphology. However, this point has never been investigated. The aim of the present study is to assess the influence of some botanic origin, amylose content and crystalline type of native starches on the features and properties of resulting SNC.

I.2. Materials & Methods

I.2.1. Materials

Starches were kindly provided by Cargill (Krefeld, Germany) according to requirements: waxy maize starch (C☆Gel 04201, 98% amylopectin), normal maize starch (Cerestar RG 03453), amylomaize (Amylogel 03003, 65-75% amylose), potato starch (C☆Gel 30002) and wheat starch (Cerestar PT 20002). Sulfuric acid (96%-99%, Sigma Aldrich) was used after dilution at 3.16M with distilled water. Pure amylose from potatoes (10130, Fluka) and pure amylopectin from potato starch (10118, Sigma) were used as references in the iodine binding test.

I.2.2. Preparation of starch nanocrystals

The optimized hydrolysis process developed by Angellier et al. [10] was adapted to 1L to prepare nanocrystals from the five different starches. Briefly, 147g of native starch was mixed with 1L of previously prepared diluted sulfuric acid (3.16M). The suspension was kept under 100 rpm mechanical stirring at 40℃, using a silicon bath, for 5 days. The final suspensions were washed by successive centrifugation with distilled water until reaching neutral pH and redispersed using Ultra Turrax for 5 min at 13,000 rpm to break aggregates. The obtained suspensions were filtered on a filter tissue (40 µm, ref. 03-41/31 Buisine, France). Sodium azide was added to the suspensions before storage at 4℃ to avoid microbial growth.

I.2.3. Starch nanocrystals characterization

Microscopies

An environmental scanning electron microscope (ESEM) on a Quanta 200 FEI device (Everhart-Thornley Detector) was used at high voltage (10 kV) to confirm the morphology of native starches. Native starches were simply deposited onto carbon tape before observation.

The morphology and average dimensions of SNC were studied using a Zeiss Ultra 55 Field Emission Gun Scanning Electron Microscope (SEMFEG) equipped with a STEM detector. All samples were prepared by depositing 2.5µL of SNC suspension (with concentration 0.01wt %) on a TEM grid. A thin Au-Pd conductive coating (ab.1nm) was deposited on top of the sample to reduce charge effect. The best compromise in terms of SNC contrast and residual charge was obtained at 10 kV accelerating voltage and working distance of about 6 mm. In order to obtain the best possible resolution, the

secondary electron imaging mode with the In-lens detector was preferred (reflective mode). However, some samples were better observed in the transmission mode using the STEM detector. The average dimensions were determined using digital image analyses. Starch nanoparticles were assimilated to spherical particles. Between 70 and 500 measurements were performed depending on the source to determine the average diameter and standard deviation.

Atomic Force Microscopy measurements were performed on a Multimodal AFM (DI, Veeco, Instrumentation Group) with both tapping and conductive mode (C-AFM). The tips were Multi130 for tapping and MESP for C-AFM. A drop a SNC suspension was deposited on a mica substrate (split with adhesive tape) and dried for a few minutes at 40℃. Between 30 and 110 measurements were performe d depending on the source to determine the average thickness and standard deviation.

Determination of amylose/amylopectin ratio by iodine-binding capacity

This procedure consists in staining a dilute suspension of starch with potassium iodine/iodine solution ($KI:I_2$) and analyzing the absorbency of the suspension. To determine the amylose content, a solution of potassium iodine and iodine with $KI:I_2$ 10:1 was prepared according to Williams et al. [19] and added to the diluted starch suspension. The absorbencies of the iodine stained solutions were measured using a UV-VIS spectrophotometer (Unicam UV5 Serie, Thermo Spectronic, Cambridge UK) at 650 nm for amylose and at 540 nm for amylopectin, their respective absorbance maxima [20]. A correlation between absorbance at 600 nm and amylose content according to a rapid single-wave colorimetric method [21] was assessed. The equation modeling this relationship allows us to determine the amylose content of some SNC.

X-Ray Diffraction

Wide angle X-ray diffraction analysis was performed on powder obtained from both native starch and air-dried SNC suspensions kept at ambient temperature (23℃) and relative humidity (28.8%). The samples were placed in a 2.5 mm deep cell and measurements were performed with a PANanalytical, X'Pert PRO MPD diffractometer equipped with a X'celerator detector. The operating conditions for the refractometer were: Copper Kα radiation, 2θ between 4 and 44°, step size 0.067°, counting time 90 s.

The degree of crystallinity of the samples was quantitatively estimated following the method of Nara and Komiya [22] adapted, also called the "two-phase" method. A curve connecting the peaks baseline was plotted on the diffractogram. The area above the

curve was assumed to correspond to the crystalline domains, and the lower area to the amorphous part. The ratio of upper area to total area was taken as the degree of crystallinity.

However, Lopez-Rubio et al. reported that this “two-phase” method may underestimate the crystalline content of starches as it does not take into account the diffuse scattering from non-perfect crystalline structures [23]. Therefore, a second set of measurements, using more complete statistical method of analysis, was performed. Samples were conditioned at 90% RH as higher water content increases the definition of crystalline peaks. Indeed, the chiral side-chain liquid–crystalline model for starch proposed by Waigh et al. considers that an amylopectin molecule consists of three sections: the chiral double helices, the amorphous spacers and the amorphous backbone [24]. It is postulated that the crystalline smectic lamellar periodicity is due to the antagonistic effect of the entropy of the backbone and the ordering of the helices. The entropy gain of the side-chains and the backbone upon plasticization by the water molecules pushes the helices into a lamellar structure due to the reduced free energy of this configuration [25].

Rheological measurements

Rheological measurements were carried out using a controlled stress rheometer (MCR 301, Anton Paar Physica, Austria) calibrated and certificated, with a cone-plate fixture at 25.0℃ controlled via a Peltier system, and a solvent trap was used to prevent solvent evaporation.

I.3. Results & Discussions

I.3.1. Preparation of starch nanocrystals

In order to investigate a wide range of structural differences, the following criteria were chosen to select starches: amylose content, crystalline type, size of the native granules and botanic origin. Some criteria like amylose content and crystalline types can be linked for maize starch [26]. It also seems obvious when analyzing starch and SNC' structure as detailed in Figure 2-I.1.

Therefore, three types of maize starches covering a wide range of amylose content were selected (Table 2-I.1): waxy maize, normal maize and high amylose maize starches. Potato starch presenting B-type crystallinity, a bimodal granular size distribution and particularly large granules was also selected. We also used wheat starch that presents a multi-modal granular size distribution with larger A-type granules and possibly smaller B-type ones.

Table 2-I.1. Main features of selected starches.

Botanic origin	Granular size	Amylose (%)*	Non glucosic material			Crystalline type	Referred to as
			Lipids**	Proteins**	Ash**		
High Amylose	5-20 µm	65-75%	1,11%	0,50%	0,20%	B	**M70**
Normal Maize	5-20 µm	27%	0,61-0,65%	0,30%	0,10%	A	**M27**
Waxy Maize	5-20 µm	1%	0,23%	0,10%	0,10%	A	**M1**
Wheat	2-30 µm	28%	0,24%	0,33%	0,30%	A	**W28**
Potato	5-80 µm	21%	0,09%	0,05%	0,30%	B	**P21**

* Supplier data
**[27]. % of dry starch

The crystalline type could indeed have its importance. Imberty et al. proposed a model for the double helices packing configuration to explain the difference between A- and B-types starches [17, 18]. A-type structure is closely packed with water molecules between each double helical structure, whereas B-type is more open with water molecules being located in the central cavity formed by 6 double helices as shown in Figure 2-I.2. It was later envisaged that branching patterns of the different types of starch may also differ [28]. C-type starch pattern has been considered to be a mixture of both A- and B-types since its X-ray diffraction pattern can be resolved as a combination of the previous two.

The five selected starches were treated following the five-day optimized acid hydrolysis process [10] in order to obtain SNC. Ensuing nanoparticles were labeled according to their botanic source (M for maize, W for wheat and P for potato) and amylose content. For instance sample M27 refers to maize starch with 27% amylose. All preparations were successful and their features are gathered in Table 2-I.2.

Table 2-I.2. SNC features and influence of hydrolysis on crystallinity

Starch type	Crystallinity			Amylose	Diameter		Thickness			Percolation		
	Native (%)	SNC (%)	ΔC (%)	(%)	(nm)	Counts	(nm)		Counts	Celzard et al, 1996 inf	sup	Lu et Mai, 2005
M70	23%	35%	12%	11%	118 +/- 53	190	7,6 +/- 1,6	*	76	7,1%	10,8%	13,9%
M27	28%	42%	14%	1%	58 +/- 36	576	6,1 +/- 1,9	*	112	11,4%	17,1%	22,7%
M1	34%	48%	14%	0%	47 +/- 42	71	5 +/- 1,6	**	14	11,5%	17,3%	22,9%
W28	25%	35%	10%	NA	100 +/- 50	71	8,3 +/- 3,1	***	30	9,1%	13,8%	17,9%
P21	28%	43%	15%	0%	52 + /-4	951	3,7 +/- 0,6	*	31	7,8%	11,9%	15,3%

*Personnal measurements using Gwyddon
** Conducted at SMPC, Mons, Belgium
*** Personnal measurements on AFM software
NA. Non Available

I.3.2. Influence of botanic source on crystallinity

This part of the investigation aimed at checking if the acid hydrolysis treatment effectively led to the removal of amorphous domains of starch granules while leaving the crystalline part intact regardless the botanic source and amylose content. The degree of crystallinity of starch samples before and after hydrolysis was calculated following two methods as explained in the Experimental Section. The first method ("two-phase" method) performed at ambient temperature and relative humidity is based on the ratio of the area of crystalline peaks to the total area of the diffractograms. Results are reported in Table 2-I.2 for native starch granules and SNC from the five different sources. The second method performed at 90% RH took into account diffuse scattering from non-perfect crystalline structures. This second set of measurements uses a more complete statistical method of analysis (not presented here). For all samples, it was observed that the degree of crystallinity was underestimated by 10% in average when using the "two-phase" method. As expected, the acid hydrolysis treatment induces an increase of the degree of crystallinity of the material (Table 2-I.2).

Figure 2-I.3 shows the diffraction patterns obtained for A-type maize starch (M27) (panels a and b) and B-type high amylose starch (M70) (panels c and d). The diffractograms obtained for both the native granules (panels a and c) and hydrolyzed granules (panels b and d) are reported. The relative area of crystalline peaks (e.g. 28%

and 23% for native M27 and M70, respectively) is clearly increased after acid hydrolysis (42% and 35% for SNC obtained from M27 and M70, respectively) proving an increase in crystallinity. Values obtained for native starches are somewhat comparable to that found in the literature [23, 26] and no significant difference between A- and B-type was observed. The extent of the increase of the degree of crystallinity upon acid hydrolysis (ΔC) is reported in Table 2-I.2. SNC features and influence of hydrolysis on crystallinity and similar values were observed for both sources of starch. However, the degree of crystallinity remains low even after acid hydrolysis showing that an important amount of non-organized materials remains in the SNC suspension.

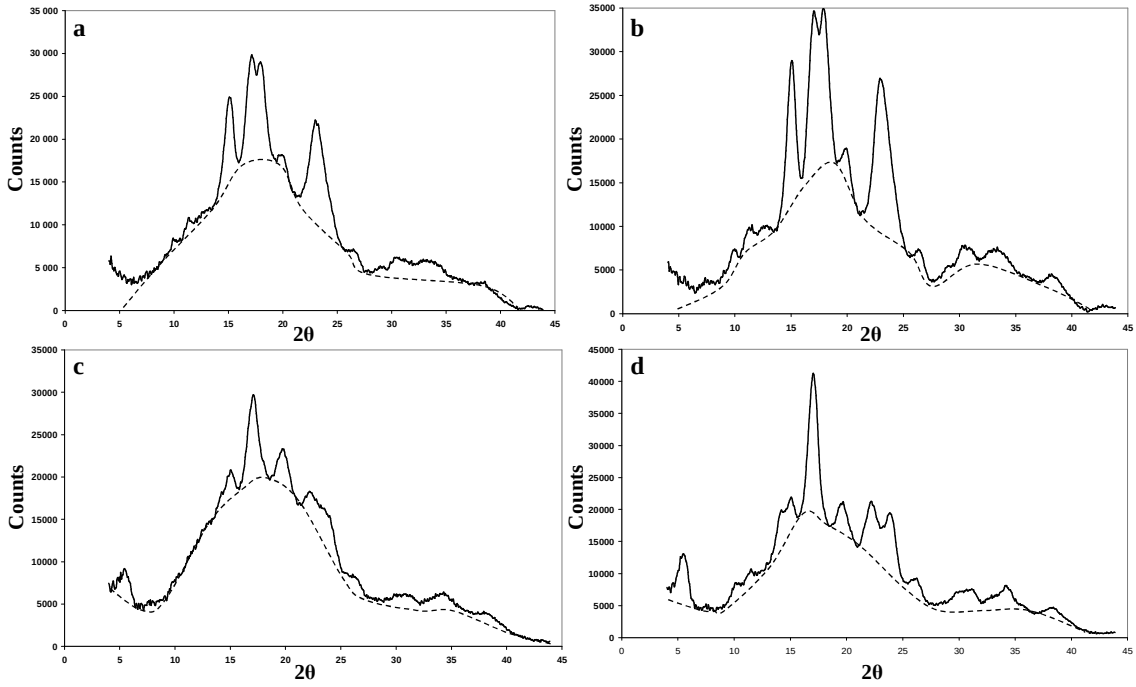

Figure 2-I.3. A-type maize starch X-ray diffraction patterns for a) native starch and b) starch nanocrystals and B-type high amylose maize starch X-ray diffraction patterns for c) native starch and d) starch nanocrystals. The dashed line is a schematic representation of the limit between crystalline peaks and the amorphous part.

As described earlier, the crystallinity of starch is attributed to the packing of double helixes formed by amylopectin side chains (Figure 2-I.1). Therefore, amylopectin-rich starches are more crystalline than amylose-rich ones (e.g. M1 vs. M70,Table 2-I.2)[26]. It can be seen when plotting the evolution of the degree of crystallinity as a function of amylose content for native starch granule from the same botanic origin (Figure 2-I.4.a). However, the increase in crystallinity remains quite low compared to the increase in amylopectin content. An important amount of amylopectin chains remains in a non-organized state.

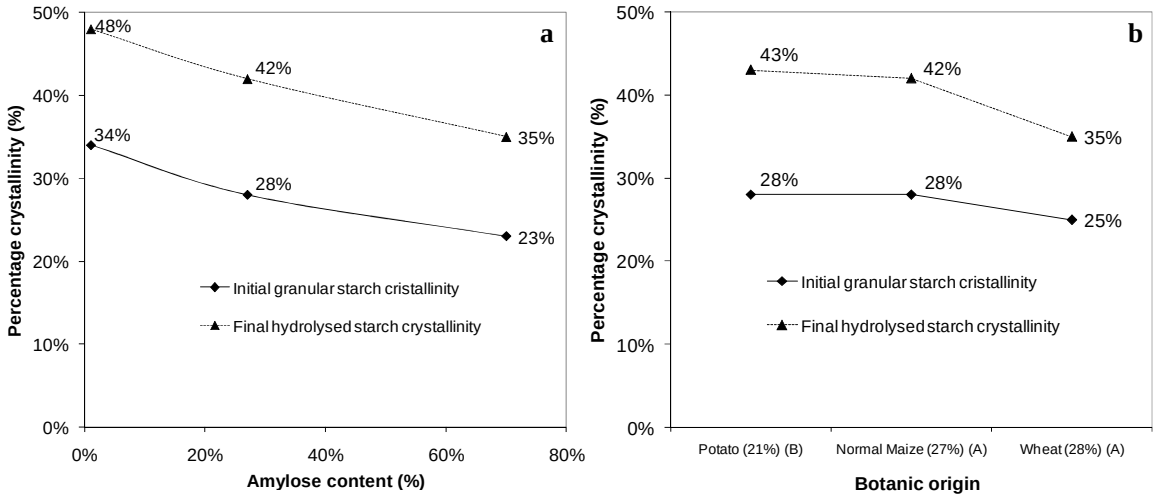

Figure 2-I.4. Original crystallinity (plain ♦) and final crystallinity (dot ▲) for starches with same amylose content and different botanic origin (a) and for starches with same botanic origin and different amylose content (b).

Higher crystallinity was expected for hydrolyzed amylopectin-rich (waxy) starch since there is less amorphous starch to hydrolyze. Indeed, when looking to the evolution of the degree of crystallinity of SNC as a function of increasing amylose content of native starch (Figure 2-I.4.a), a decrease is observed. Therefore, it seems that the higher the crystallinity of native starch, the higher the crystallinity of the ensuing SNC. The two curves corresponding to native starch granules and SNC are simply vertically shifted even if increased differences were expected for high amylopectin contents. Indeed, for starches with already relatively high crystallinity, the relative gain in crystallinity was limited.

However, two important parameters should be taken into account when interpreting the data. The first one is related to acid hydrolysis conditions we used, as they were optimized for waxy maize starch. It is probable that optimized conditions should be different for other botanic sources. The second parameter which is interconnected with the first one is that more crystalline domains in amylopectin-rich starch should be more easily accessible for acid hydrolysis. It might, with this long process, hydrolyze defective crystallites and induces solubilization of part of the crystalline structure.

For starches with similar amylose content but from different botanic origin, no significant differences were observed for the degree of crystallinity of both native granules and SNC (Figure 2-I.4.b). The crystalline type doesn't seem to play an important role (comparing potato and normal maize), nor only the botanic origin

(comparing normal maize and wheat). Consequently, the most important parameter determining the degree of crystallinity of SNC seems to be the amylopectin content.

I.3.3. Influence of botanic source on amylose content of starch nanocrystals

As already explained and described in Figure 2-I.1, SNC are thought to consist in amylopectin side chains [29]. To verify the accuracy of this assumption, the amylose/amylopectin ratio needs to be assessed for all starches before and after hydrolysis. There are a lot of different techniques for determining the amylose content in starches. The most readily used is iodine binding. It exploits the ability of iodine to stain amylose and amylopectin helixes by forming amylose-iodine complexes. Although potentiometric titration offers the most definitive measurement of the iodine binding capacity of a sample, spectrophotometric determinations are more widely used because of convenience and simplicity of use [30].

The use of this method for native starches confirmed differences in initial amylose content. However, suspensions made of freeze-dried starch re-dispersed in water colored very slightly in excess iodine but did not stain.

Bailey and Whelan reported that when hydrolyzed (i.e. decreasing chain length) in random fashion by acid or alpha-amylase both polysaccharides gradually lose the capacity to stain with iodine [31]. The blue amylose color becomes purple, then red, brown and finally disappears. The blue color for the stain is due to the amylose component of starch. The amylopectin gives a red-purple color which is less intense than the amylose stain. Indeed, for amylose–iodine helical inclusion complex to form, the chains have to be at least 18 unit longs. The amylopectin double helical structure has been reported to consist of about 15 glycosyl units (DP = 15 close to 5.3 nm in length for potato [29], DP = 14.2 close to 5 nm in length for waxy maize [32]) and the amylose is quickly depolymerized during hydrolysis, which could explain why no lasting coloration was observed for SNC samples. This consideration rules out all techniques consisting in complexing amylose with another reagent for determining its content in SNC.

However, this non-coloration could also reveal that freeze-drying affects the complexing properties of hydrolyzed starch. It might, for instance, favor double helixes formation stabilized by hydrogen bonding during the slow drying, and prevent solubilization and complex inclusion with iodine.

As the same reagent for dissolving starch was used to prepare the native starch and SNC suspension before testing, tests were duplicated without the treatment. This treatment was suspected to further de-polymerize residual chains. However, results were similar than without pre-treatment.

Further tests were carried out for never-freeze-dried maize SNC suspensions. They exhibited different colorations ranging from light brown to yellow for high amylose content starch to waxy maize, respectively. Indeed, UV-VIS absorption spectra for SNC suspensions clearly differed from that of their native counter parts whereas they were closer to the pure amylopectin reference as presented in Figure 2-I.5.

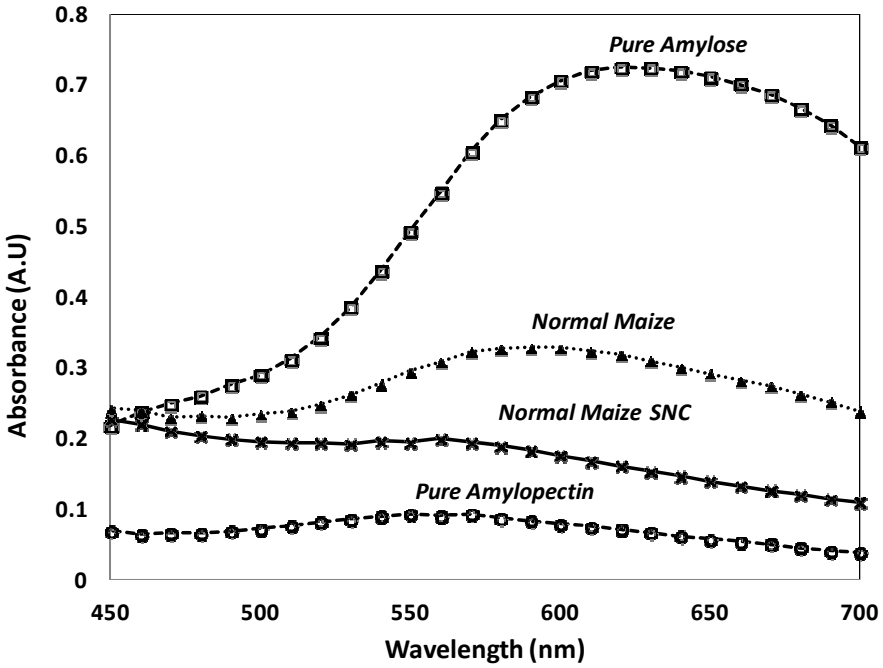

Figure 2-I.5. Absorption spectra of normal maize starch nanocrystals with native, amylose and amylopectin references.

Maximum absorption for amylose-iodine complex is around 630 nm. Native starches exhibit a peak around 600 nm. All SNC suspensions showed maximum absorption around 400 nm (magenta) which reflects the yellowish color of the samples due to iodine. For clarity, this wavelength is not presented in Figure 2-I.5. High amylose and normal maize SNC suspension also exhibit a large peak around 560 nm (green) representative of their brownish-purplish color. This wavelength is supposed to be the maximum absorption for amylopectin-iodine complex. Waxy maize nanocrystals suspension did not stain. No peak was observed at higher amylose-iodine complex absorption wavelength for SNC.

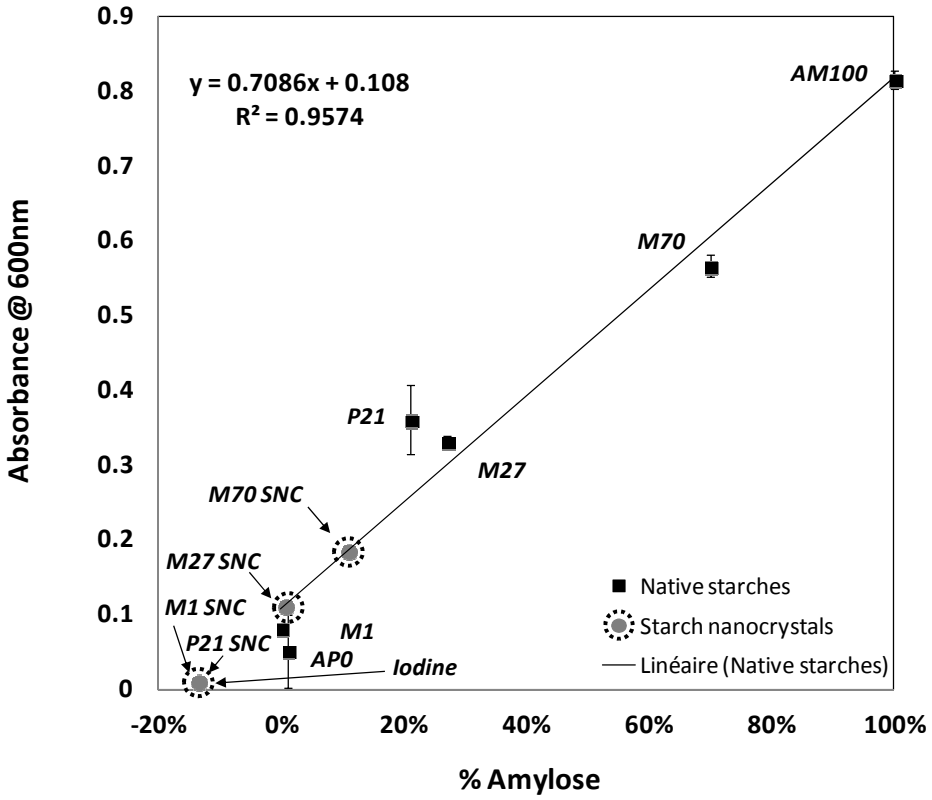

Figure 2-I.6. Calibration graph of absorbance at 600nm against percentage amylose for native starche [21].

Figure 2-I.6 shows the correlation between absorbance at 600 nm and amylose content according to a rapid single-wave colorimetric method [21]. The equation modeling this relationship allows us to determine that the amylose content of P21, M1, M27 and M70 is respectively 0%, 0% (or too low a DP to be measured), 1% +/- *1.8%* and 11% +/- *2.1%* (as reported in Table 2-I.2 and Figure 2-I.6). Results suggest that SNC suspensions are made of low DP amylopectin.

Given the uniqueness of the samples, authors will dedicate another study to the assessment of quantitative amylose/amylopectin content in SNC.

I.3.4. Influence of botanic source on starch nanocrystal morphology

Figure 2-I.7 to Figure 2-I.9 show SEM images obtained for native starch granules and their corresponding SNC with different botanic origins (Figure 2-I.7), amylose contents (Figure 2-I.8) and crystalline typse (Figure 2-I.9). As for native granules, SNC display very different shapes, size and size distribution.

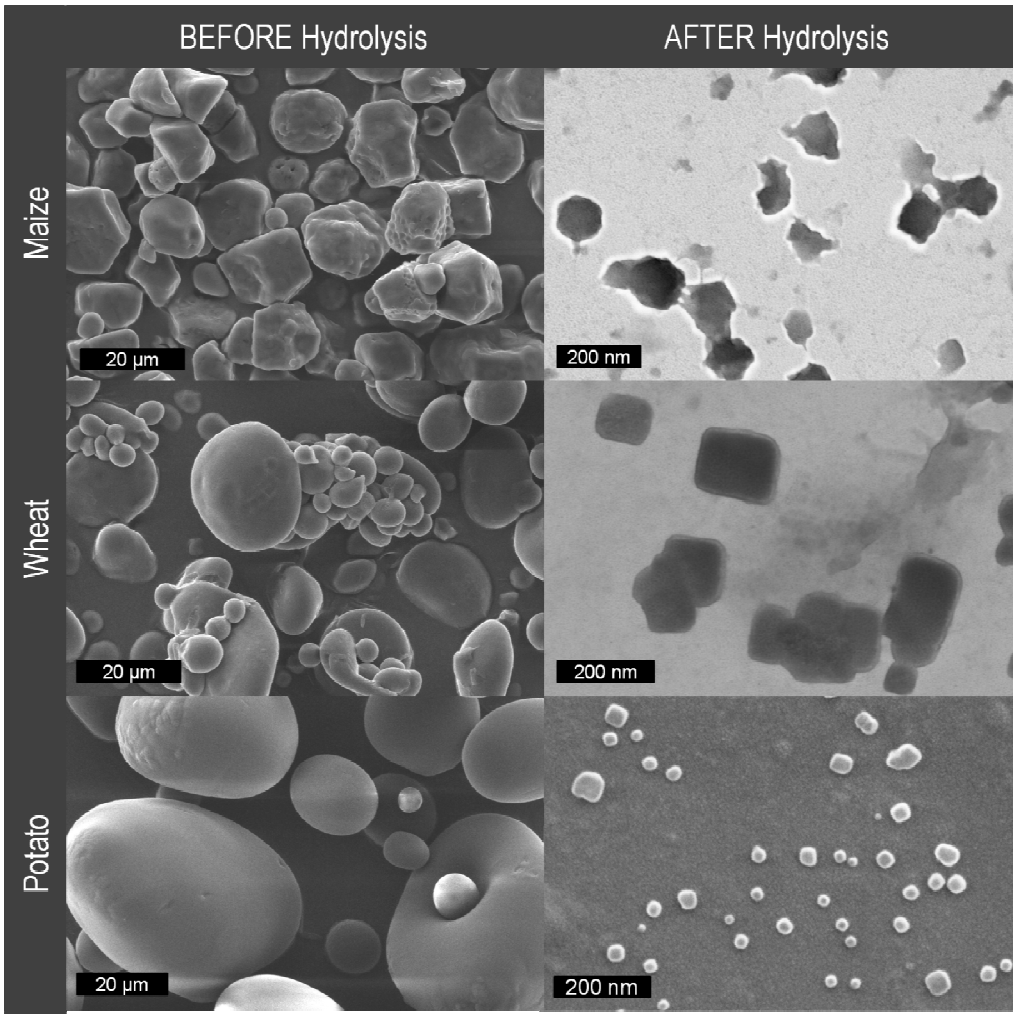

Figure 2-I.7. Scanning Electron Microscopy micrograph of starches before (First column) and after (Second column) hydrolysis for different botanic source.

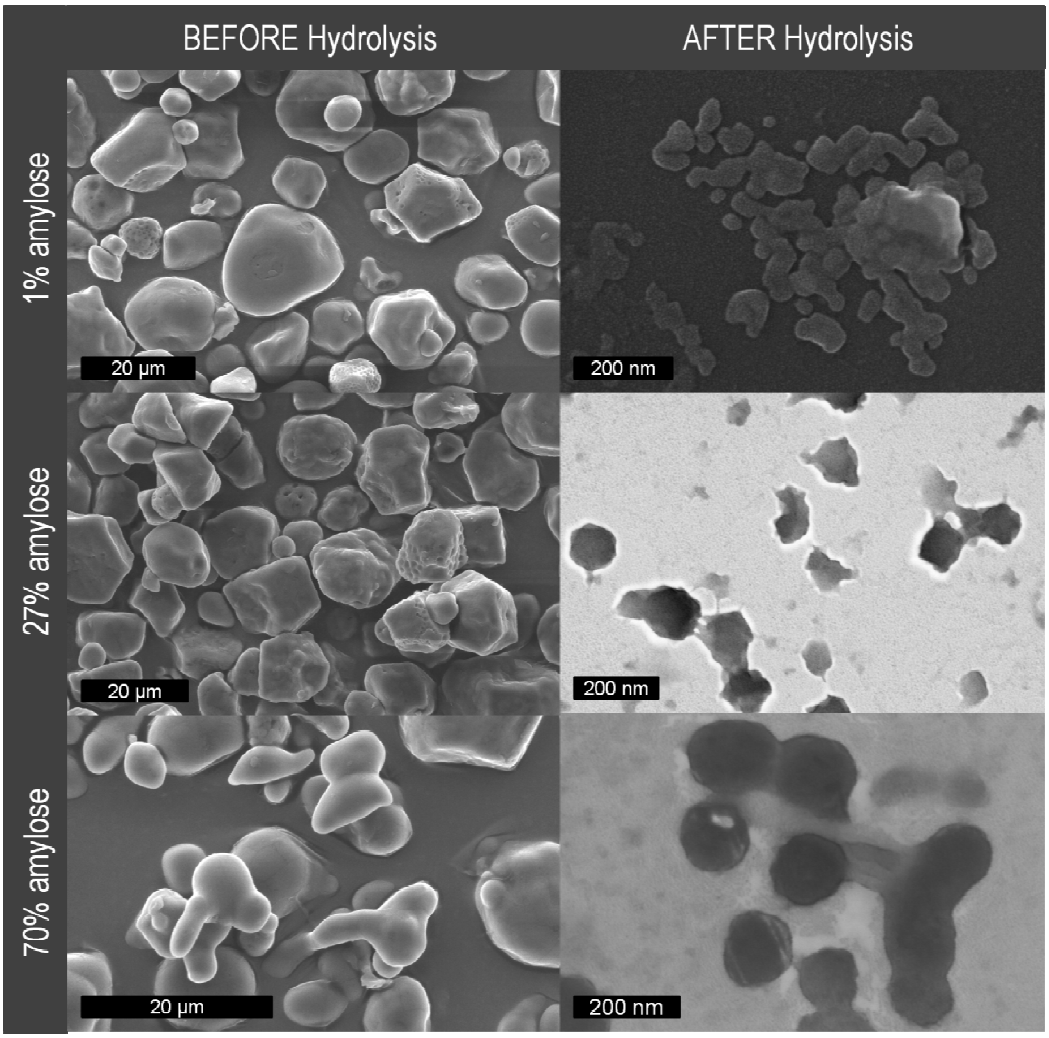

Figure 2-I.8. Scanning Electron Microscopy micrograph of Maize starch before (First column) and after (Second column) hydrolysis for increasing amylose contents. The lower the amylose content, the squarer the final particles.

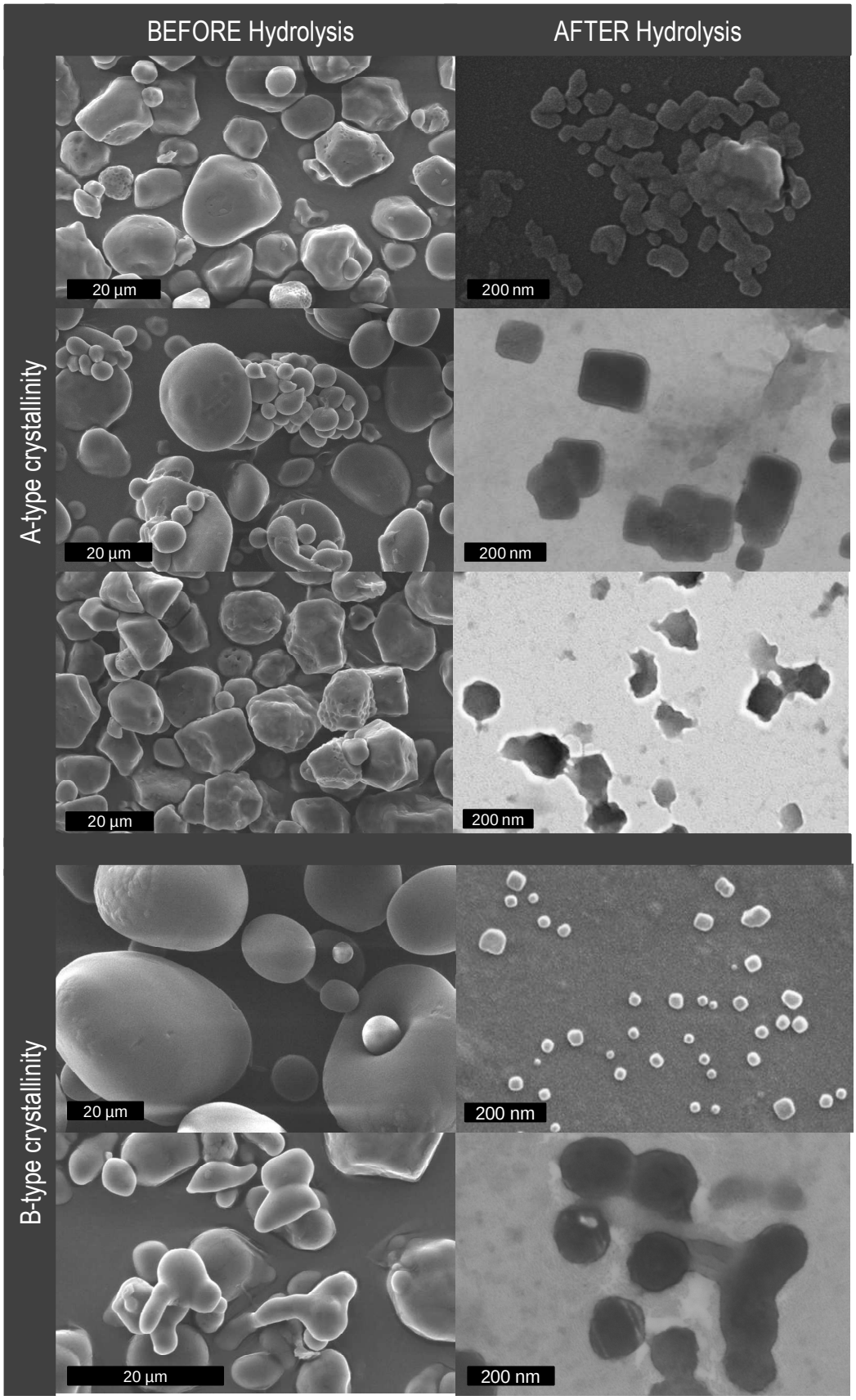

Figure 2-I.9. Scanning Electron Microscopy micrograph of starches before (First column) and after (Second column) hydrolysis for different crystalline types.

Regarding the shape of the nanoparticles, no correlation with botanic origin (Figure 2-I.7) or amylose content (Figure 2-I.8) was observed. Their morphology seems to be mainly linked to the crystalline type (Figure 2-I.9). Indeed, waxy maize and wheat starch (A-type) rendered respectively parallelepipedic and square-like nanocrystals. Nanocrystals obtained from normal maize starch were more difficult to characterize since no precise shapes were recognized. High amylose maize SNC (B-type) were rather round and potato SNC (B-type) seemed to be made of both round and rounded-corner-square particles depending on size. So schematically, nanocrystals produced from A-type starches rendered square-like particles whereas nanocrystals produced from B-type starches rendered round-like particles. This could be explained by the different packing configurations of amylopectin chains for A and B-type starches, as shown in Figure 2-I.2. The A-type closely packed configuration displays a parallelepipedic pattern whereas the B-type cavity-like configuration displays a circular one. The packing of these patterns might render respectively square-like and disk-like particles. These results prove for the first time the importance of starch crystallinity type on nanocrystals shape. It should also be considered that the SNC observed might correspond to the crystalline part of the blocklets reported by some authors thus explaining the size distribution among SNC.

SNC' size and size distributions were assessed by SEMFEG image analysis. Results are reported in Figure 2-I.10. For a given botanic origin (i.e. maize starch, Figure 2-I.10.a), a sliding of size distribution's main peak is observed with increasing the amylose content. This result is not surprising since amylose is believed to jam the pathways for hydrolysis. It makes it slower, harder and renders, for a given time, bigger particles (or aggregates) when amylose content is high.

Differences in size and size distribution were also observed for starches from different botanic origin with similar amylose content as shown in Figure 2-I.10.b. No tendency linked neither to the degree of crystallinity nor to the crystalline type was observed for nanocrystals sizes since:

(i) for the same amylose content wheat starch nanoparticles (W28) are almost twice as big as normal maize starch nanocrystals (M27), and

(ii) for the two different crystalline types (A and B) corresponding to normal maize starch (M27) and potato starch (P21), respectively, SNC have almost the same size .

However, as mentioned before, it has been reported that depending on the botanic origin of starch, amylose is preferably found in the amorphous region [33] (e.g. wheat starch), or interspersed among amylopectin clusters in both the amorphous and

crystalline regions (e.g. normal maize starch) [34], or in bundles between amylopectin clusters, or co-crystallized with amylopectin (e.g. potato starch) [33]. It most likely influences the hydrolysis patterns of starches. Also, some authors reported different size of blocklets depending on the botanic origin of starch. Long axial diameters of the blocklets are 10-30 nm for maize starches [35], 20-50 nm for potato starches [36] and 25-100nm for wheat starches [37] thus giving a possible explanation for bigger wheat SNC.

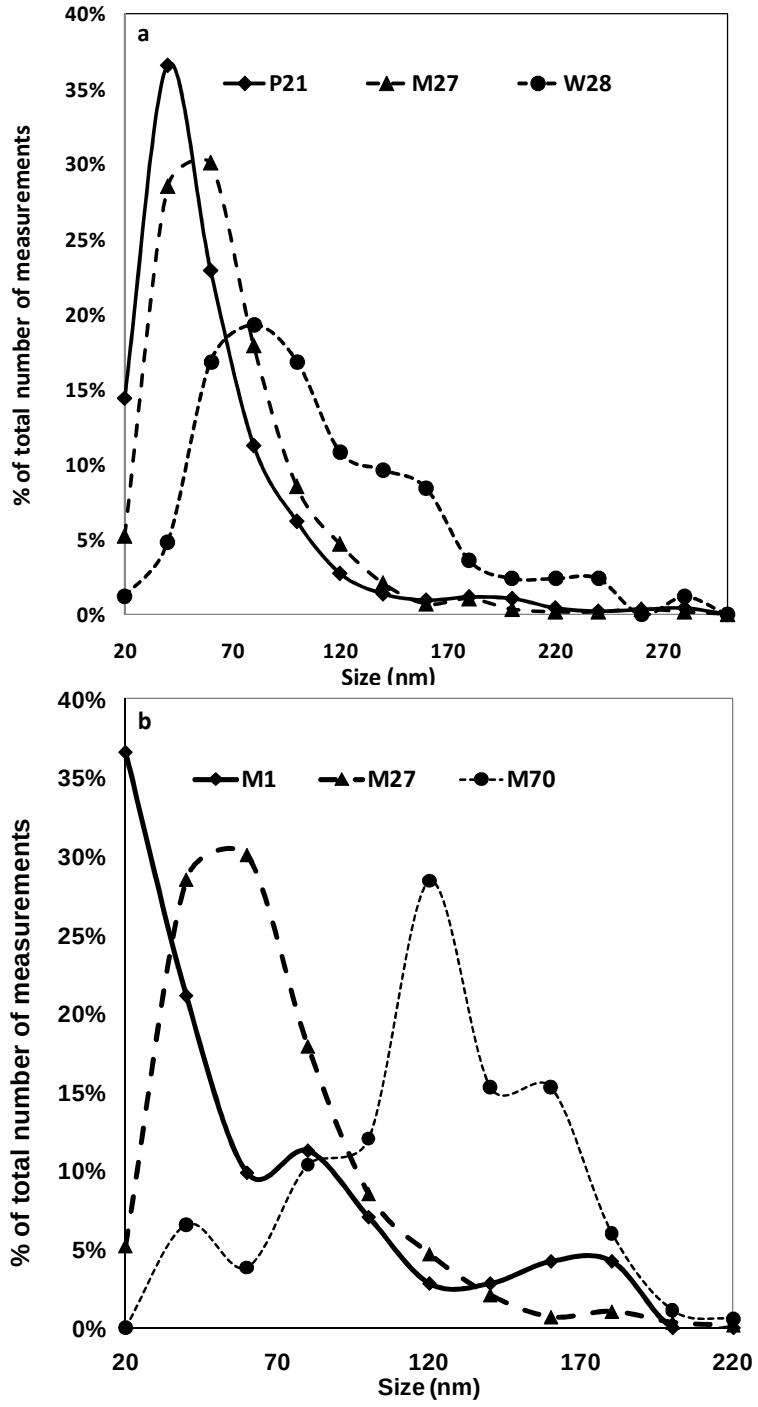

Figure 2-I.10. Size distribution for (a) the same botanic origin, (b) the same amylose content

I.3.5. Influence of botanic source on starch nanocrystal thickness

As mentioned earlier, SNC are described as platelets resulting from the hydrolysis of branching point (amorphous lamellae) of the alternating crystalline lamellae associated with crystallites made of packed amylopectin double helices. To confirm and assess the thickness of those platelets, atomic force microscopy (AFM) measurements were carried out on the different SNC.

Measured thicknesses were between 4 and 8 nm and values are reported in Table 2. Our results seem to be in accordance with current models [15, 29, 32] which report the crystalline lamellae to be 5-7 nm and the cumulated size of crystalline and amorphous lamella to be 9-10 nm for all starches [15]. Thus, this confirms that SNC are individualized crystallites. Also, it is suggested in literature [28, 38] that the B-type amylopectin branching points are clustered in an ensued smaller amorphous lamella (i.e. thicker crystalline lamellae) whereas A-type amylopectin branching points are scattered in both the amorphous and the crystalline regions, giving more flexibility (lower entropy barrier) to double helixes for packing closely (i.e. thinner crystalline lamellae). Unfortunately, the use of different software for the measurements analysis makes it difficult to compare the values and their accuracy. Nevertheless, as expected, high amylose (B-type) SNC were thicker than normal maize SNC, itself thicker than waxy maize SNC. However, no relationship to amylose content (%) can be postulated. Indeed, for the same amylose content, wheat SNC were much thicker than others, and surprisingly potato SNC were significantly thinner and better individualized than any other nanocrystals. This last phenomenon might be explained by the use of ultrasonic treatment but also by the different locations of amylose inside the granules. Thus it seems that the thickness of SNC is rather linked to the botanic origin of starch via its internal organization (i.e. where the amylose is located inside the granule) as explained in previous section 3.3.

I.3.6. Viscosity of starch nanocrystal suspensions

The ultimate objective of the project (FlexPakRenew FP7 EU project) within which this study was undertaken aims at using SNC for the development of complex flexible packaging. The rheological behavior of SNC aqueous suspensions is therefore important for the processing of such materials. The type of information sought for was twofold:

1. get useful information for the processing of such suspensions, and

2. determine experimentally the percolation threshold of the suspensions.

First, waxy maize SNC suspensions were prepared at different concentrations. All suspensions display a shear-thinning behavior as presented in Figure 2-I.11 and fit a power-law distribution. Indeed, a fitting with Heschel-Buckley's model rendered a yield stress (τ_0) equal to zero. The flow behavior index, n, varies only moderately with increasing the SNC content suggesting that we remain far from the percolation threshold.

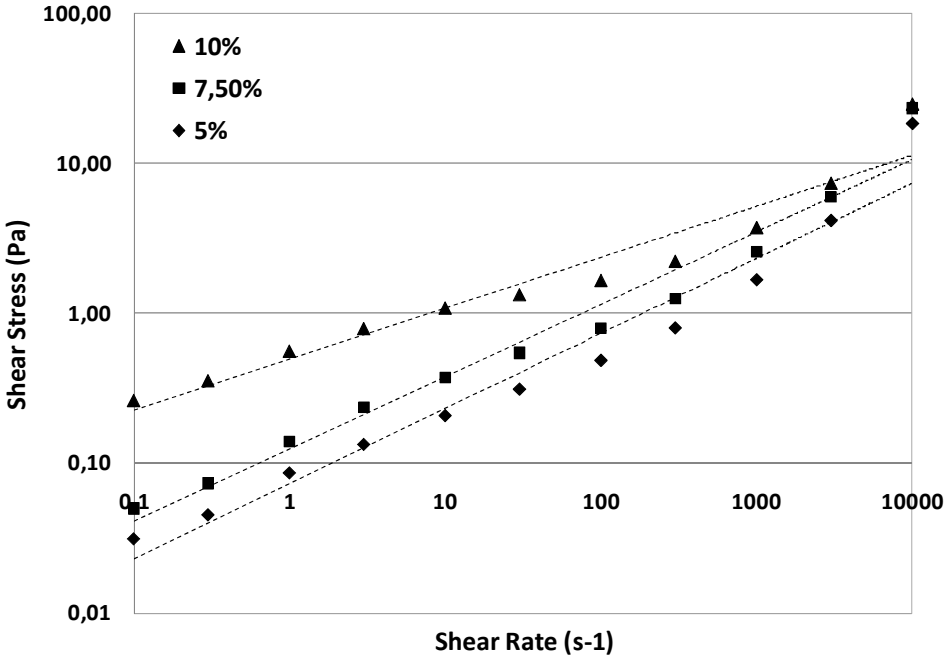

Figure 2-I.11. Waxy maize starch nanocrystals suspension power-law fitting and corresponding Heschel-Buckley's coefficients.

Previous work [39] has shown the influence of surface charge on cellulose nanocrystals and demonstrated that nanocrystals produced by sulfuric acid hydrolysis presented surface charges which limited time dependency. As their cellulosic counter-parts, SNC suspensions showed little time dependence at low shear rate (stable

measurements, results not presented) and measurements were reproducible as the error bars in Figure 2-I.11 are smaller than the size of symbols.

The suspensions' viscosity displayed moderate power law concentration dependence which increased with decreasing shear rate. On industrial machines, a SNC suspension will undergo very high shear during very little time. For example, on a coating machine shear rate will be about 10^5 s^{-1} for a couple of milliseconds. At such shear rate, the suspension will be damaged and particles might artificially aggregate. Therefore, there is no point in studying its behavior with a time ramp at high shear rate. On the contrary, to work with stable SNC suspensions, studies at relatively low shear rate and longer time will be preferred. This is why the different SNC suspensions have been studied at 10 s^{-1} after 60 s stabilization. Suspensions with different SNC concentrations have been prepared for each source of starch and results are shown in Figure 2-I.12.

No particular relationship was found between viscosity and SNC size, thickness, surface area or specific surface. However, suspensions with lowest viscosity were M70 and P21 which corresponds to suspensions with respectively disc-like morphology and ill-defined morphology (mix of square and disc) nanoparticles. Highest viscosity was achieved with wheat starch (W28) which presents square-like platelets SNC.

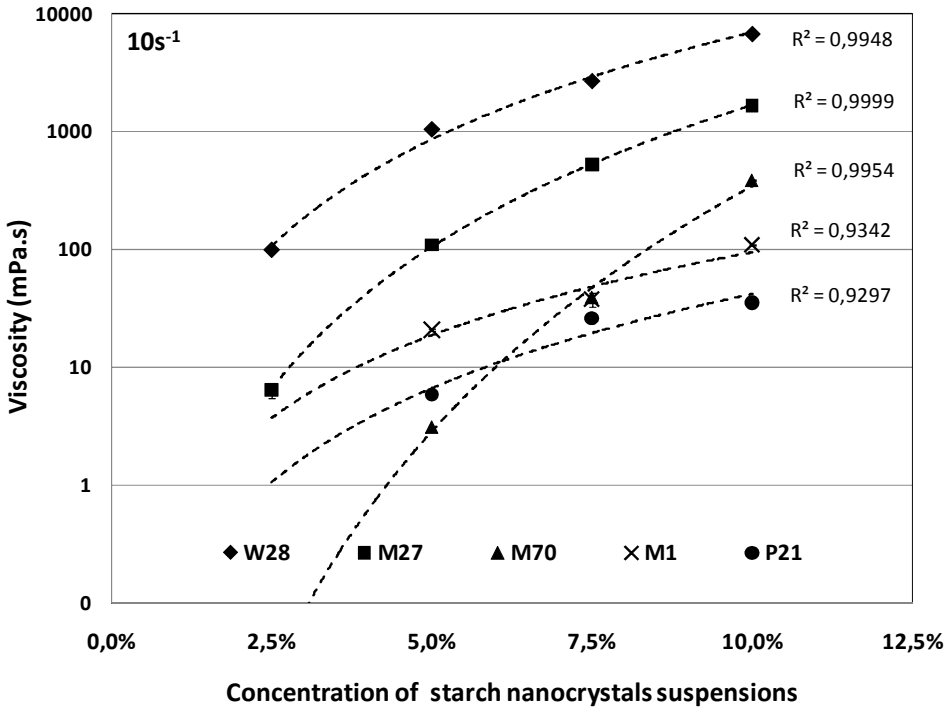

Figure 2-I.12. Evolution of viscosity of starch nanocrystal suspensions with increasing concentration at $10s^{-1}$. Dash lines are power-law fittings.

Flow properties of SNC suspensions have been studied for different concentration seeking the rheological percolation concentration. Unfortunately, above 15 wt.% SNC suspensions formed “cakes” in the gap of the cone-plane rheometer preventing from measuring the sought data. In previous papers [4, 40], the percolation threshold for SNC in a polymeric matrix were determine using water uptake measurements. They were reported to be 20 vol% (31 wt.%) and 6.7 vol% (10 wt.%), respectively, for potato SNC [4] and waxy maize SNC [41] thus explaining why no percolation threshold was observed during our rheological measurements (limited to 10 wt.%).

Models for calculating the percolation threshold of clay nanoparticles can be found in the literature. Celzard et al., proposed the “excluded volume model”, from which was extracted Equation (1), to assess the percolation threshold of high aspect ratio nanoclay [40]. Lu and Mai determined recently Equation (2) using a re-normalization group approach for characterizing the barrier properties of nanoclay [42].

$$1-\exp\left(-\frac{3{,}6t}{\Pi d}\right) \le \phi_c \le 1-\exp\left(-\frac{5{,}6t}{\Pi d}\right) \quad (1)$$

$$\phi_c = \frac{2{,}154t}{d} \quad (2)$$

within both equations: d the diameter and t the thickness of the particles. According to Li et al., these two models underestimate the percolation threshold [43]. Table 2 presents the theoretical percolation threshold for each botanic source according to each model.

Differences are observed for the different botanic sources regardless the model. Indeed, both high amylose maize (M70) and potato (P21) SNC display the lowest percolation thresholds. Unfortunately, such differences are not observed in our viscosity measurements and do not seem to be related to amylose content. This might either be due to the fact that our viscosity measurements are at too high a shear rate, or to the polydispersity of SNC in suspensions. Nevertheless, one could notice that these two types of SNC were prepared from B-type starches, and both render more or less disc-like nanoparticles. However, the data from the models are in contradiction with previously reported values according to which potato SNC’s percolation threshold (31wt%) is higher than that of waxy maize SNC (10wt%), as mentioned earlier.

Therefore, concerning coating applications, no starch source is preferred even though waxy maize SNC seems to be the best compromise with rather low viscosity and small square-like shaped nanocrystals.

I.4. Conclusion

It has always been suspected that the type of starch use for producing starch nanocrystals (SNC) was an important parameter. This study shows for the first time that the botanic origin of starch shows only a moderate influence (through the distribution of amylose inside the granule and blocklet size) on final properties of ensuing SNC (such as size, size distribution, thickness and viscosity), whereas amylose content and crystalline type would be more of influence (on respectively size and shape). Differences in size are rather moderate whereas differences are more pronounced when comparing shapes and crystallinity. In the intent to use starch nanocrystals as filler in polymeric matrices, more attention should be brought to selecting the native starch. Indeed, when seeking for barrier properties, one should favor particles rendering square-like platelets as waxy and wheat starches. Normal maize starch nanocrystals seem to contain both round and square-like particles. Potato and high-amylose starch nanocrystals on the contrary presented disk-like platelets. Rheological properties of SNC suspensions from different starches have also been compared for the first time. The differences in viscosity can be quite important and will strongly help the selection of the best source depending on application.

I.5. References

1. Siró, I.; Plackett, D., Microfibrillated cellulose and new nanocomposite materials: a review. *Cellulose* **2010,** 17, (3), 459-494.

2. Bras, J.; Viet, D.; Bruzzese, C.; Dufresne, A., Correlation between stiffness of sheets prepared from cellulose whiskers and nanoparticles dimensions. *Carbohydrate Polymers* **2011,** 84, (1), 211-215.

3. Chen, G.; Wei, M.; Chen, J.; Huang, J.; Dufresne, A.; Chang, P. R., Simultaneous reinforcing and toughening: New nanocomposites of waterborne polyurethane filled with low loading level of starch nanocrystals. *Polymer* **2008,** 49, (7), 1860-1870.

4. Dufresne, A.; Cavaillé, J.-Y., Clustering and percolation effects in microcrystalline starch-reinforced thermoplastic. *Journal of Polymer Science Part B: Polymer Physics* **1998,** 36, (12), 2211-2224.

5. Angellier, H. Nanocristaux d'amidon de maïs cireux pour applications composites. *Ph.D thesis* University Joseph Fourier, Grenoble, France, **2005**.

6. Putaux, J. L.; Molina-Boisseau, S.; Momaur, T.; Dufresne, A., Platelet Nanocrystals Resulting from the Disruption of Waxy Maize Starch Granules by Acid Hydrolysis. *Biomacromolecules* **2003,** 4, (5), 1198-1202.

7. Whistler, R. L.; BeMiller, J., *Starch: Chemistry and Technology*. Third ed.; Elsevier: New York, **2009**; p.

8. Battista, O. A., Microcrystal Polymer Science. In McGraw-Hill Book Company: New York, **1975**; p 138.

9. Dufresne, A.; Cavaille, J. Y.; Helbert, W., New nanocomposite materials: Microcrystalline starch reinforced thermoplastic. *Macromolecules* **1996,** 29, (23), 7624-7626.

10. Angellier, H.; Choisnard, L.; Molina-Boisseau, S.; Ozil, P.; Dufresne, A., Optimization of the preparation of aqueous suspensions of waxy maize starch nanocrystals using a response surface methodology. *Biomacromolecules* **2004,** 5, 1545-1551.

11. Le Corre, D.; Bras, J.; Dufresne, A., Starch nanoparticles: A review. *Biomacromolecules* **2010,** 11, (5), 1139-1153.

12. Lin, N.; Huang, J.; Chang, P. R.; Anderson, D. P.; Yu, J., Preparation, modification and application of starch nanocrystals in nanomaterials: A review. *Journal of Nanomaterials* **2011,** doi:10.1155/2011/573687, 1-13.

13. Whistler, R. L.; BeMiller, J. N.; Paschall, E. F., *Starch: Chemistry and technology, 2nd edition* New Yorl and London, **1967**; 733 p.

14. Dufresne, A., Polymer Nanocomposites from Biological Sources. In *Biopolymers Technology*, Bertolini, A. C., Ed. Sao Paulo, Brazil, **2007**; Vol. Cultura Academica, p 59-83.

15. Gallant, D. J.; Bouchet, B.; Baldwin, P. M., Microscopy of starch: evidence of a new level of granule organization. *Carbohydrate Polymers* **1997,** 32, (3-4), 177-191.

16. Oates, C. G., Towards an understanding of starch granule structure and hydrolysis. *Trends in Food Science & Technology* **1997,** 8, (11), 375-382.

17. Imberty, A.; Chanzy, H.; Perez, S.; Buleon, A.; Tran, V., New three-dimensional structure for A-type starch. *Macromolecules* **1987,** 20, (10), 2634-2636.

18. Imberty, A.; Perez, S., A revisit to the three-dimensional structure of B-type starch. *Biopolymers* **1988,** 27, (8), 1205-1221.

19. Williams, P. C.; Kuzina, F. D.; Hlynka, I., A Rapid Colorimetric Procedure for Estimating the Amylose Content of Starches and Flours. *Cereal Chemistry* **1970,** 47, 411-421.

20. Shannon, J. C.; Garwood, D. L.; Boyer, C. D., Genetic and physiology of Starch Development. In *Starch: Chemistry and Technology - Third Edition*, BeMiller, J.; Whistler, R., Eds. Academic Press - Elsevier: **2009**; p 28.

21. McGrance, S. J.; Cornell, H. J.; Rix, C. J., A Simple and Rapid Colorimetric Method for the Determination of Amylose in Starch Products. *Starch - Stärke* **1998,** 50, (4), 158-163.

22. Nara, S.; Komiya, T., Studies on the Relationship Between Water-satured State and Crystallinity by the Diffraction Method for Moistened Potato Starch. *Starch - Stärke* **1983,** 35, (12), 407-410.

23. Lopez-Rubio, A.; Flanagan, B. M.; Gilbert, E. P.; Gidley, M. J., A novel approach for calculating starch crystallinity and its correlation with double helix content: A combined XRD and NMR study. *Biopolymers* **2008,** 89, ((9)), 761-768.

24. Waigh, T. A.; Gidley, M. J.; Komanshek, B. U.; Donald, A. M., The phase transformations in starch during gelatinisation: a liquid crystalline approach. *Carbohydrate Research* **2000,** 328, (2), 165-176.

25. Waigh, T. A.; Kato, K. L.; Donald, A. M.; Gidley, M. J.; Clarke, C. J.; Riekel, C., Side-chain liquid-crystalline model for starch. *Starch - Stärke* **2000,** 52, (12), 450-460.

26. Cheetham, N. W. H.; Tao, L., Variation in crystalline type with amylose content in maize starch granules: an X-ray powder diffraction study. *Carbohydrate Polymers* **1998,** 36, (4), 277-284.

27. Duprat, F.; Gallant, D. J.; Guilbot, A.; Mercier, C.; Robin, J. P., L'amidon. In *Les Polymères Végétaux. Polymères pariétaux et alimentaires non azotés*, Monties, B., Ed. Gauthier Villars: Paris **1980**; p 176–231.

28. Jane, J.-l.; Wong, K.-s.; McPherson, A. E., Branch-structure difference in starches of A- and B-type X-ray patterns revealed by their Naegeli dextrins. *Carbohydrate Research* **1997,** 300, (3), 219-227.

29. Robin, J.-P. Comportement du grain d'amidon à l'hydrolyse acide ménagée. Etude Physico-Chimique et Enzymatique de la fraction insoluble. Contribution a la connaissance de la structure de l'amylopectine. , Université Pierre et Marie Curie de Paris, Nancy, **1976**.

30. Knutson, C. A., Evaluation of variations in amylose-iodine absorbance spectra. *Carbohydrate Polymers* **2000,** 42, (1), 65-72.

31. Bailey, J. M.; Whelan, W. J., Physical properties of starch. I. Relationship between iodine stain and chain length. *The Journal of biological chemistry* **1961,** 236, (4), 969-973.

32. Angellier-Coussy, H.; Putaux, J.-L.; Molina-Boisseau, S.; Dufresne, A.; Bertoft, E.; Perez, S., The molecular structure of waxy maize starch nanocrystals. *Carbohydrate Research* **2009,** 344, (12), 1558-1566.

33. Blanshard, J. M. V., Starch granule structure and function: a physicochemical approach. In *Starch: Properties and Potentials*, Galliard, T., Ed. Society of Chemical Industry: London , U.K. , **1987**; Vol. 13, p 16-54.

34. Kasemsuwan, T.; Jane, J., Location of amylose in normal starch granules. II. Locations of phosphodiesterase cross-linking revealed by phosphorus-31 nuclear magnetic resonance. *Cereal Chemistry* **1994** 71 282-287.

35. Baker, A. A.; Miles, M. J.; Helbert, W., Internal structure of the starch granule revealed by AFM. *Carbohydrate Research* **2001,** 330, (2), 249-256.

36. Szymonska, J.; Krok, F., Potato starch granule nanostructure studied by high resolution non-contact AFM. *International Journal of Biological Macromolecules* **2003,** 33, (1-3), 1-7.

37. Perez, S.; Baldwin, P. M.; Gallant, D. J., Structural Features of Starch Granules I. In *Starch: Chemistry and Technology - Third Edition*, BeMiller, J.; Whistler, R., Eds. **2009**; p 176.

38. Gérard, C.; Planchot, V.; Colonna, P.; Bertoft, E., Relationship between branching density and crystalline structure of A- and B-type maize mutant starches. *Carbohydrate Research* **2000,** 326, (2), 130-144.

39. Araki, J.; Wada, M.; Kuga, S.; Okano, T., Influence of surface charge on viscosity behavior of cellulose microcrystal suspension. *Journal of Wood Science* **1999,** 45, (3), 258-261.

40. Celzard, A.; McRae, E.; Deleuze, C.; Dufort, M.; Furdin, G.; Marêché, J. F., Critical concentration in percolating systems containing a high-aspect-ratio filler. *Physical Review B* **1996,** 53, (10), 6209.

41. Angellier, H.; Molina-Boisseau, S.; Lebrun, L.; Dufresne, A., Processing and structural properties of waxy maize starch nanocrystals reinforced natural rubber. *Macromolecules* **2005,** 38, (9), 3783-3792.

42. Lu, C.; Mai, Y.-W., Influence of Aspect Ratio on Barrier Properties of Polymer-Clay Nanocomposites. *Physical Review Letters* **2005,** 95, (8), 088303.

43. Li, J.; Kim, J.-K., Percolation threshold of conducting polymer composites containing 3D randomly distributed graphite nanoplatelets. *Composites Science and Technology* **2007,** 67, (10), 2114-2120.

Chapter 2-II. Influence of native starch's properties on starch nanocrystals thermal properties

Déborah Le Corre, Julien Bras, Alain Dufresne

The International School of Paper, Print Media and Biomaterials (Pagora), Grenoble Institute of Technology, BP 65 - F-38402 Saint Martin d'Hères Cedex, France

Abstract

Starch nanocrystals (SNC) are crystalline square-like platelet about 10 nm thick and 50-100 nm equivalent diameters. Depending on the botanic origin of starch these platelets show different features. The aim of the present study was (i) to assess the thermal stability of SNC in different processing conditions (i.e. excess water and dry) and (ii) to investigate the potential influence of botanic origin on thermal stability. The thermal properties of five types of starches (waxy maize, normal maize, high amylose maize, potato and wheat) and their corresponding SNC were characterized by differential scanning calorimetry (DSC) and thermogravimetric analysis (TGA). SNC revealed two endothermic transitions. No correlation between melting temperature and botanic origin was found. However, a review of starch thermal properties allowed to postulate for the mechanism involved in SNC thermal transitions. It was also found that SNC can be used in wet processes below 100℃ and in dry processes below 150-200℃ to avoid melting.

Keywords

Starch; Nanocrystals; Botanic origin; Amylose; thermal properties.

1. ***Inspired from:*** *D. LeCorre, J. Bras, A. Dufresne, Carbohydrate Polymer 87 (2012) 658-666*

II.1. Introduction

In material science, researchers are looking for more and more efficient renewable materials in order to face petroleum shortage and environmental concerns. Starch is one of the most abundant materials produced by nature and this polysaccharide has already found numerous industrial applications.

It is a multi-scale structure consisting of concentric alternating amorphous and crystalline lamellae. It is made of mainly two structurally distinct α-D-glucan components: amylose which is linear and amylopectin which is highly branched. Each polymer constitutes a family with differences in size, fine structure and function [1]. It is believed that the crystalline region is created by the interwining of amylopectin side-chains [2]. Amylose molecules are thought to occur in the granule as individual molecules, randomly interspersed among amylopectin molecules. Depending on the botanic origin of starch, amylose is preferably found in the amorphous region (e.g. wheat starch) [3], interspersed among amylopectin clusters in both the amorphous and crystalline regions (e.g. normal maize starch) [4], in bundles between amylopectin clusters [3], or co-crystallized with amylopectin chains (e.g. potato starch) [3]. Amylose content should therefore considerably influence the crystalline organization. Depending on their X-ray diffraction pattern, reflecting long-range ordering in the granule, starches are categorized in three crystalline types (polymorphs) called A, B and C.

However, a property common to most starches is gelatinization. It refers to the collapse (disruption) of molecular order (breaking of H-bonds) within the granule, along with all concomitant and irreversible changes in properties such as water uptake, granular swelling, crystallite melting, birefringence loss, starch solubilization and viscosity development. [1] It is now widely accepted that it can be view as a melting process which can be evidenced as an endothermic thermal transition in DSC measurements. Depending on the application, this property is sought for or not.

Carbohydrate chemists have developed products that have greatly expanded starch use and utility [5]. Most recent developed products from starch chemistry include starch derivatives [6, 7] and starch nanocrystals (SNC). SNC are crystalline platelets obtained by the acid hydrolysis of amorphous parts of starch. They are believed to correspond the starch granule's crystallites. The aim of a previous study [8] was to assess if starch from any source could indifferently be used to prepare SNC, and if amylose content and/or botanic origin's influence on SNC's final properties. Results showed that for the same amylose content maize, potato and wheat starches resulted in rather similar size and crystallinity of SNC proving the limited impact of the botanic origin. For the same botanic origin (maize),

differences in size were more important indicating the strong influence of the amylopectin content and molecular structure. Particles tended to show square-like morphology with increasing initial amylopectin content and A-type crystallinity (and thus shorter chain length). Also, it was shown by x-ray diffraction measurement that although SNC's crystallinity was higher than that of their corresponding native starches, SNC were not fully crystalline.

Current potential application for SNC is bio-nano-composites. They are added as nano-fillers in a polymeric matrix to improve its mechanical and/or barrier properties as described elsewhere [9, 10]. Most work has been oriented towards the use of new environmentally friendly polymers such as non vulcanized natural rubber [11, 12], waterborne polyurethane (WPU also called organic solvent free polyurethane) [13], waxy maize starch [14, 15], cassava starch [16], pullulan (obtained by starch fermentation) [17], PLA [18] , polyvinyl alcohol (PVA) [19] and soy protein isolate (SPI) [20]. Although early work [21, 22] reported composite preparation by hot pressing, since 2006 authors have opted for a simpler casting-evaporation method at 40°C for 24h. The hot-pressing process co nsisted in first mixing freeze-dried SNC with a copolymer of styrene and butyl acrylate in latex form and heating the mixture at 90°C for 10 min. It was then hot-pressed during 1 min under 2 MPa (300 psi) pressure to obtain films about 1 mm thick [22].

However, this process raises the question of the potential melting of SNC. Similar issue should be considered if classical polymer processing methods, e.g. extrusion or injection molding is used. With the casting process, it was necessary to decrease the temperature of the polymer matrix before adding waxy maize SNC to avoid melting [14]. However, other authors [16] report casting-evaporation at 50°C after constant stirring of SNC in thermoplastic starch at 90°C for half an hour. Most recently, compression molding was used to prepare glycerol-plasticized starch nanocrystals composites at 120°C from a freeze-dried powder [20]. One could wonder if starchy nanoparticles are still crystalline after this treatment.

The aim of the present study is two-fold. First, it aims at assessing the maximum processing temperature for SNC in the dry state and in excess water. Second, it intends to assess the influence of using different native starches, with different botanic origin, amylose content and crystalline type, on the thermal properties of resulting SNC.

II.2. Materials & Methods

II.2.1. Materials

Native starch granules were kindly provided by Cargill (Krefeld, Germany) according to requirements: waxy maize starch (C☆Gel 04201, 98% amylopectin), normal maize starch (Cerestar RG 03453), amylomaize (Amylogel 03003, 65-75% amylose), potato starch (C☆Gel 30002) and wheat starch (Cerestar PT 20002). Sulfuric acid (96%-99%, Sigma Aldrich) was used after dilution at 3.16M with distilled water.

II.2.2. Preparation of starch nanocrystals

The same optimized hydrolysis process developed by Angellier et al.[23] was modified and used for preparing SNC from the five different starches. Briefly, 147g of native starch was mixed with 1L of previously prepared diluted sulfuric acid (3M). The suspension was kept under 400 rpm mechanical stirring at 40℃, usi ng a silicon oil bath, for 5 days. The final suspensions were washed by successive centrifugations in distilled water until reaching neutral pH and redispersed using Ultra Turrax for 5 min at 13,000 rpm to avoid aggregates. The obtained suspensions were filtered on a filter tissue (40 µm, ref. 03-41/31 Buisine, France). Sodium azide was added to the suspensions before storage at 4℃ to avoid microbial growth.

II.2.3. Microscopies

An environmental scanning electron microscope (ESEM) on a Quanta 200 FEI device (Everhart-Thornley Detector) was used at high voltage (10 kV) to confirm the morphology of native starches. Native starches were simply deposited onto carbon tape before observation.

SNC' mean size and morphology were studied using a Zeiss Ultra 55 Field Emission Gun Scanning Electron Microscope (FEGSEM). A thin Au-Pd conductive coating (~1 nm) was deposited to reduce charge effect. The samples were observed and imaged at a 6-mm working distance and 10-kV accelerating voltage. These conditions illustrate the best compromise in terms of SNC contrast and residual charge effect. In order to obtain the best possible resolution, the secondary electron imaging mode with the In-lens detector was used. The average diameter was determined using digital image analyses (ImageJ). Image analysis allows measuring the surface area of SNC. From this area, an equivalent diameter was calculated with the approximation that SNC are disc-like particles. Between 70 and 500 measurements were carried out depending on the source to determine the average diameter and standard deviation.

Atomic Force Microscopy measurements were performed on a Multimodal AFM (DI, Veeco, Instrumentation Group) with both tapping and conductive mode (C-AFM). The tips were Multi130 for tapping and MESP for C-AFM. A drop of SNC suspension was deposited on a mica substrate (split with adhesive tape) and dried for a few minutes at 40℃. Between 30 and 110 measurements were used depending on the source to determine the average thickness and standard deviation.

II.2.4. Differential Scanning Calorimetry (DSC)

Differential scanning calorimetry measurements were done with DSC Q100 (TA Instruments, NewCastle) filled with a manual liquid nitrogen cooling system. Freeze-dried SNC powder, conditioned at 50% relative humidity (RH), was placed in a hermetically sealed pan. For samples in excess water (water content – WC = 70 wt%), the amount of water necessary to reach a 30:70 starch/H_20 ratio was directly added to the pan using a micropipette, to avoid inhomogeneous withdrawals. The sealed pans were set aside for 1 day to equilibrate. Each sample was heated from 20℃ to 120℃ when in excess water and to 260℃ when dried with a heating rate of 10℃.min $^{-1}$. Measurements were done in triplicate to ensure repeatability. The sample weight was between 6 and 10 mg.

II.2.5. Thermogravimetric Analysis (TGA)

Thermogravimetric analysis (STA 6000, Perkin Elmer Instruments model, USA) was carried out to determine the thermal stability of samples under oxygen flow of 20mL.min^{-1}. The samples were heated from 30℃ to 600℃ with a h eating rate of 10℃.min $^{-1}$. The sample weight was plotted as a function of temperature for all samples.

Paper 3

II.3. Results & Discussions

II.3.1. Starch nanocrystals features

The influence of botanic origin, amylose content and crystalline type on the morphology of SNC has been very recently studied by our group [8]. The main conclusion was that the botanic origin of starch shows only a moderate influence on final properties whereas amylose content and crystalline type would be more of influence. Differences in size were rather moderate whereas differences were more pronounced when comparing shapes and crystallinity. Figure 2-II.1 shows SEM and FEG-SEM micrographs obtained for the native starches used in this study and their corresponding SNC.

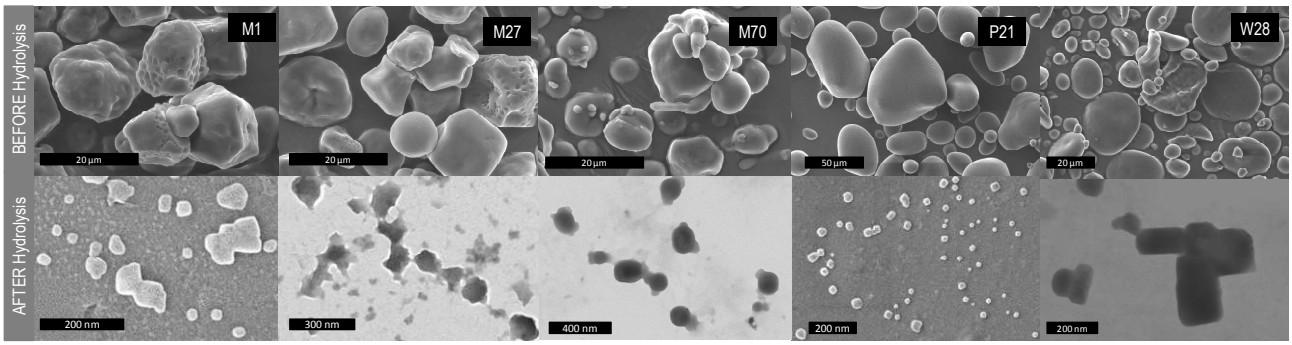

Figure 2-II.1. Micrograph of native starches and corresponding SNC.

Features of native starches and ensuing SNC used in this study are presented inTable 2-I.1. All SNC exhibit a platelet-like morphology with thickness 5-8 nm (Table 2-I.1). Therefore, although platelet with square-like shape should be preferred for barrier properties, all SNC can be considered as potential fillers in nanocomposites.

Table 2-II.1. Main features of native starches, and diameter and thickness of corresponding SNC.

Botanic Origin	Referred to as	Granular Size (µm)	Amylose (%) #	Crystalline Type	SNC Diameter		SNC Thickness	
					(nm)	Count	(nm)	Count
High Amylose Maize	**M70**	5-20	65-75	B	118+/-*53*	190	5+/- *1.6**	76
Normal Maize	**M27**	5-20	27	A	58 +/- *36*	576	8.3+/-*3.1**	112
Waxy Maize	**M1**	5-20	1	A	47 +/- *42*	71	6.1+/- *1. 9***	14
Wheat	**W28**	2-30	28	A	100+/-50	71	3.7+/- *0. 6****	30
Potato	**P21**	5-80	21	B	52 +/-*4*	951	7.6+/- *1. 6**	31

Supplier's data
**Personnal measurements using software Gwyddon for image analysis*
*** Conducted at « Service des Matériaux Polymères et Composites » (SMPC), Mons, Belgium*
**** Personnal measurements on AFM software*

II.3.2. Thermal behavior of starches and their corresponding SNC

SNC and corresponding native starches' thermal behavior were studied both in excess water (70% WC), to simulate use in aqueous suspension such as coating or water-based composite processing, and freeze-dried (0% WC) to assess processability in "dry processes" such as extrusion. Typical responses are presented in Figure 2-II.2.a. in excess water and Figure 2-II.2.b in dry state. SNC and starch granules show completely different thermograms with different number, intensity and temperature of thermal transitions. Before comparing them, it is important to understand the thermal behavior of each kind of particles i.e. starch granules and SNC.

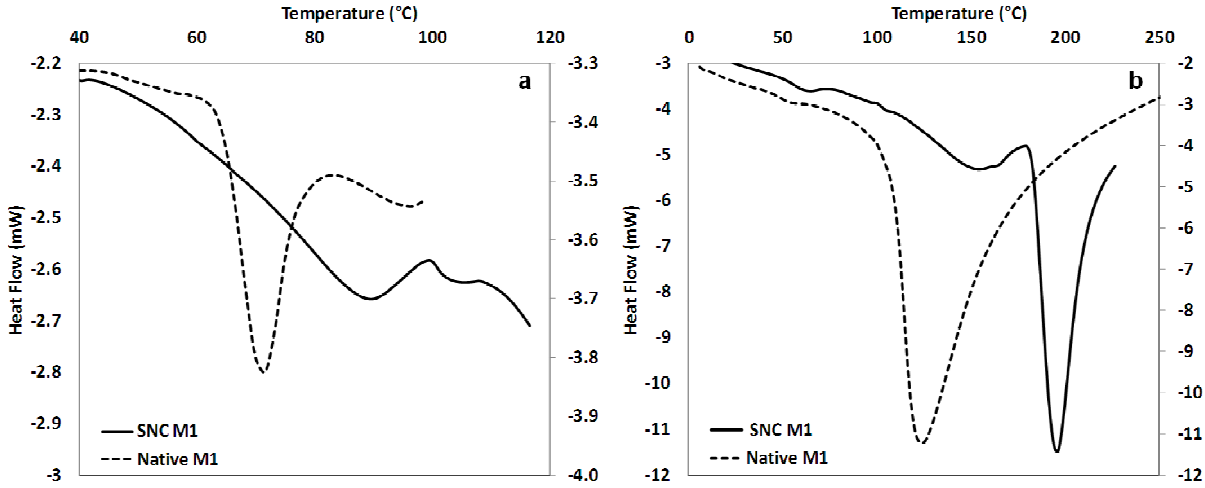

Figure 2-II.2. DSC thermograms for native and SNC from M1 (a) in excess water and (b) in the dry state (0%WC, 50%RH conditioning)

Thermal behavior of native starches

The characteristic temperatures observed for the endothermic transitions of the 5 native starches in excess water (70%) are reported in Table 2-II.2. As expected, only one endothermic peak was observed.

Data for dried samples conditioned at 50% RH are reported in Table 2-II.3. Our measurements seem to be in agreement with the latter described models as for all dry native starches only one endothermic peak was observed. For dry native starches (0% WC), the maximum of the endothermic peak ranged between 120 and 150℃ (Table 2-II.3).

This temperature range is below expectations as the theoretical melting point of perfect crystallites without water is estimated at 160-210℃ [24]. This might be due to the presence of residual moisture in our samples. Several authors also reported anhydrous melting point of starches by linear extrapolation of experimental data [25]. For a given botanic origin, the temperature can also differ by up to 50℃ [25]. In our study, no influence of the source, amylose content or crystalline type alone was observed. Indeed, starch's heat-moisture induced structural transformations (gelatinization) seem to depend rather on the interconnected factors that are its botanic source, its component molecules (amylose, amylopectin, intermediate material and minor components) content, its components molecular structure and organization, and its crystalline type". The thermal properties of starch granules have been widely investigated [24-31] and have been shown to be strongly dependent on the water content. In excess water, an increase in temperature leads to the appearance of an endothermic peak (around 50℃-80℃) linked to the gelatinization of starch. At intermediate water content (30-60%), the first peak is shifted up in temperature, and a higher temperature second peak is observed. At very low water content (<20%), only the higher temperature peak is observed.

Several explanations have been developed to explain the two peaks generally observed (and referred to as M1 and M2).

First, it was suggested [32] that in excess water, the amorphous growth ring absorbs water and expands. As they are cross-linked by the amorphous backbone, the semi-crystalline lamellae are disrupted causing a loss of order and crystallinity (first peak M1). When the amount of water becomes insufficient to fully swell the granule, the remaining crystallites melt at higher temperature (leading to the second peak M2). An alternative explanation [33] attributes the first peak (M1) to the melting of least stable crystallites which upon melting absorb all remaining water. Thus the second peak (M2) reflects the melting at higher temperatures of remaining crystallites. However, this hypothesis did not take into account possible reorganization of polymer chains in the amorphous phase and the remaining crystallites during DSC heating[31]. Biliaderis et al. suggested that the multiple melting transition profile was due to partial melting (M1) followed by recrystallization and final melting (M2) [34]. Barron suggested that it was rather linked to the heterogeneous repartition of water in starch [25]. Zong et al. attributed them to the melting of crystallites and amylose lipid complexes, respectively [27].

Table 2-II.2. Characteristic temperatures observed for the endothermic transitions of starches and corresponding SNC in excess water (starch: H20 30:70).

			NATIVE				NANOCRYSTALS							Comparison
Starch type	**WC (%)**		**Ti (°C)**	**Tmax (°C)**	**Tf (°C)**	**Range Δ(°C)**	**Ti (°C)**	**+/-**	**Tmax (°C)**	**+/-**	**Tf (°C)**	**+/-**	**Range Δ(°C)**	**Shift of peak (°C)**
M70	70	P1	69.1	72.5	78.3	9.2	84.5	12.5	93.0	2.1	99.9	1.0	15.4	20.5
		P2					106.7	6.3	103.1	3.5	112.9	5.2	6.2	
M27	70	P1	63.9	69.4	81.9	18.1	67.6	2.2	85.5	1.3	99.7	0.5	32.1	16.1
		P2					100.2	0.1	106.6	2.1	112.9	3.2	12.8	
M1	70	P1	65.0	71.4	83.4	18.4	54.5	14.9	79.7	11.6	99.2	0.3	44.7	8.3
		P2					99.9	0.5	104.0	1.6	108.6	0.8	8.6	
W28	70	P1	53.3	59.1	76.4	23.1	59.0	9.1	77.7	11.8	100.7	1.7	41.8	18.6
		P2					101.7	1.1	105.5	0.3	111.3	2.2	9.6	
P21	70	P1	59.6	64.0	82.5	22.9	82.1	10.2	91.3	4.3	100.3	0.5	18.2	27.3
		P2					101.6	0.4	105.5	0.1	110.0	1.6	8.4	

Ti: Onset temperature Tmax: Maximum peak temperature ; Tf: Final temperature

P1: First Endothermic peak P2: Second endothermic peak

Table 2-II.3. Characteristic temperatures observed for the endothermic transitions of starches and corresponding SNC in the dry state (50% RH conditioning).

			NATIVE				NANOCRYSTALS							Comparison
Starch type	**WC (%)**		**Ti (°C)**	**Tmax (°C)**	**Tf (°C)**	**Range Δ(°C)**	**Ti (°C)**	**+/-**	**Tmax (°C)**	**+/-**	**Tf (°C)**	**+/-**	**Range Δ(°C)**	**Shift of peak (°C)**
M70	0	P1	94.6	122.6	231.1	136.5	116.0	2.2	148.3	2.8	178.2	2.5	62.1	25.7
		P2					193.3	3.3	205.4	3.8	246.0	0.5	52.6	
M27	0	P1	109.6	148.7	255.0	145.4	105.0	7.8	126.1	6.3	161.0	0.2	56.0	-22.6
		P2					247.2	1.4	253.5	1.0	256.9	0.0	9.7	
M1	0	P1	107.6	124.7	223.5	115.9	123.4	11.2	154.0	2.2	180.3	10.2	56.9	29.3
		P2					188.0	9.1	200.0	10.2	234.0	7.4	46.0	
W28	0	P1	104.8	130.7	241.4	136.6	186.6	2.5	199.0	9.3	212.8	12.0	26.2	68.3
		P2					215.9	13.2	218.9	12.6	248.3	6.4	32.4	
P21	0	P1	111.6	147.6	204.8	93.2	178.9	3.0	191.4	9.2	205.4	23.1	26.4	43.8
		P2					207.0	21.7	215.3	9.7	245.5	5.6	38.4	

Ti: Onset temperature Tmax: Maximum peak temperature ; Tf: Final temperature

P1: First Endothermic peak P2: Second endothermic peak

Another approach to the understanding of starch thermal behavior consists in considering it from a classic polymeric point of view, as a semi-crystalline polymer whose specific heat-temperature curves exhibit the characteristics of both amorphous and crystalline polymers [31]. As for more classic polymers, Biliaderis et al. revealed that regardless of the water content, the melting point (T_m) is T_g-dependent in that a previous softening (relaxation) of the amorphous parts is required before crystallites can melt [31]. As such, the melting temperature of starch crystallites is also affected by plasticizers such as water. However, despite good correlation between experimental data and the two-phase Flory Huggins model at intermediate and low water content, a three-phase model was proposed. It consisted in (i) a bulk amorphous region responsible for T_g, (ii) a non-ordered intercrystalline phase which mobility is restricted by crystallinity-induced cross-linking, and (iii) a fully ordered crystalline phase with T_g(mobile amorphous) < T_g (rigid amorphous)< T_m(rigid crystalline).

More recently, other authors [30, 35] proposed a liquid-crystal approach to explain the gelatinization of starch. Considering the side chain liquid crystal polymer (SCLCP) nature of amylopectin, they described a first thermal transition corresponding to a smectic (lamellar order)/nematic (orientationally ordered) transition for B-type starches, and to a nematic/isotropic phase transition for A-type starches (i.e. helix-helix dissociation) [29, 30]. They also postulated a second transition attributed to an helix-coil transition (i.e. unwinding of double helices to a gel phase). In excess water (>60%), the difference between the two endotherms is immeasurably small for natives starches and are thought to occur almost simultaneously. At intermediate water content (30-60%), the two endotherms can be evidenced one after the other. At low water content (<30%), a direct crystalline-to-gel transition occurs as the helices unwind and only one peak is observed.

Thermal behavior of SNC

Based on starch analysis and proposed models, the thermal behavior of SNCs has been characterized and deeply analyzed to postulate mechanisms. The characteristic temperatures of the thermal transitions of SNC immersed in water and in the dry state are reported in Table 2-II.2 and Table 2-II.3, respectively. Two observations can be made: (i) two endothermic peaks can be observed in excess water content as well as in the dry state, and (ii) a clear shift up in temperatures is observed compared to native starch granules.

Reports on the thermal behavior of SNC is scarce in literature with, up to our knowledge, only two studies [36, 37]. Thermal behavior data for freeze-dried waxy maize SNC was reported by Angellier to observe the plasticizing influence of water [36], and by Thielemans et al. to compare with grafted SNC [37]. The first author [36] reported the existence of two endothermal peaks in excess water with a broad temperature range, and the disappearance of the first peak in the dry state. The other authors [37] presented a DSC thermogram for waxy maize SNC in dry conditions for comparison and evidencing of grafting. The thermogram for freeze-dried SNC also showed two endothermic peaks. The first maximum peak is located around 150°C and the second one around 200°C. No explanation for these two peaks in the dry state could be found in the literature. Also, no data was found concerning SNC from other sources. The peak temperatures for the first peak in excess water are much higher than that reported by Angellier for waxy maize SNC [36]. This could be attributed to an inhomogeneous water repartition [25] among SNC in the DSC pan. However, in the dry state, data are comparable to that of Thielmans et al.[37]. Angellier attributed this first peak to the "gelatinization" of the nanocrystals and the shift up in temperature to the crystalline nature of SNC [36]. The broadening of the peak was attributed to the heterogeneity of waxy SNC. At 20% WC, the disappearance of this peak was reported.

Considering a classic polymeric approach (and the fact that melting temperature (T_m) is T_g-dependent), several factors could increase the melting temperature of the semi-crystalline polymer, such as (i) an increase in crystallinity, (ii) a more perfect crystals or (iii) a decrease in plasticizer content. In the case of SNC, all explanations are equally possible to explain the shift up in temperature for the first peak. Indeed, it has been demonstrated that SNC are more crystalline than their native counterparts [8]. Also, due to freeze-drying, it is possible that SNC, or at least the crystalline parts of SNC, are more tightly packed and bonded via hydrogen bonds forming more perfect crystals. Finally, it has been suggested that amylose acts as a plasticizer (dilutant [38]) in the starch granule. After hydrolysis, most of the amorphous starch has been hydrolyzed limiting its effect as plasticizer. Indeed, very recently, the increase in amylopectin content when hydrolyzing starch into SNC, and thus the decrease in amylose "plasticizer" content, has been confirmed [8]. If no amorphous starch is left then no more T_g can be evidenced and T_m should be high. However, it is most likely that some amorphous starch is still present leading to increased T_g and thus T_m. In excess water, the water can penetrate SNC and lower their thermal transitions compared to dry SNC.

Under the SCLCP approach, the first peak could be attributed to the smectic-nematic transition. However, with the hydrolysis of the backbone and possibly the flexible spacers of amylopectin, it takes more energy to disassociate and displace the double helixes from their lamellar organization (smectic) to nematic or isotropic state. Water facilitates this transition, explaining the lower temperatures observed in excess water.

In excess water, the second peak maximum temperatures are smaller (103-107℃) (Table 2-II.2) than that reported by Angelli er (140-160℃) [36]. Angellier demonstrated with mass spectroscopy, that SNC heated up in excess water (80%) and above 110℃ had reduced DP [36]. They concluded that the second peak reflected a heat-induced depolymerization rather than melting. However, no TGA data was available to confirm. Literature for cellulose nanocrystals [39-41] reported similar lower decomposition temperature for nanocrystals compared to micro-crystalline cellulose. It was attributed to the small size of the particles, the high specific surface area and thus to the outer surface structure including the presence of sulfate groups [40], also found on SNC ([36]and confirmed by elemental analysis not presented here). The neutralization of these sulfate groups shifted the degradation to higher temperatures.

However, under the SCLCP approach, the second peak should rather be attributed to further melting (i.e. to the helix-coil transition). This is why the thermal degradation process is detailed latter in this study.

In dry conditions, data for waxy maize SNC was in agreement with those reported by Thielmans et al. with a very high second peak maximum temperature of about 200℃ [37]. The presence of two endothermic peak could be attributed, as it is the case for granular starch according to Evans and Haisman [33], to the presence of weak crystallites (least stable) that melt first (M1 peak) and of more stable crystallites that melt at higher temperature (M2 peak).

Combining the polymeric approach and the SCLCP model, the observed melting transitions could be explained as such. On the one hand, when the experiment starts in excess water, the first peak should be attributed to the helix-helix dissociation (smectic/nematic or isotropic transition) and the second one, which happens right after (only 20℃ later), to the unwinding of the helixes (helix-coil transition), which agrees with the interpretation given by Tester and Morisson and Biliaderis et al.[42, 43] to the melting transitions M1 and M2 observed for granular starch.

On the other hand, when the experiment starts from the dry state, the two peaks could be attributed to the direct transition from smectic to coil (gel state), as reported by Waigh et al. for starch at low water content [30] of two types of crystallites. Thus, the first peak (corresponding to the M1 peak of native starches according to Evans and Haisman[33]) could be attributed to the melting of least stable crystallites, and the second one (corresponding to M2) to the more stable remaining crystallites. Especially since the temperature range observed for SNC peaks corresponds to the theoretical melting temperature of crystallites (168-257°C) [25] as mentioned earlier. To confirm this postulated mechanisms, it was important to prove that no degradation or depolymerization occurred in these conditions.

II.3.3. Thermal degradation of starches and ensuing SNC

To assess the possibility that the second endothermal peak in dry conditions corresponds to the melting of the crystallites, TGA measurements were carried out for the five different starch sources and freeze-dried SNC used for DSC measurements. Typical superimposed DSC and TGA curves for native starch and SNC are presented in Figure 2-II.3.

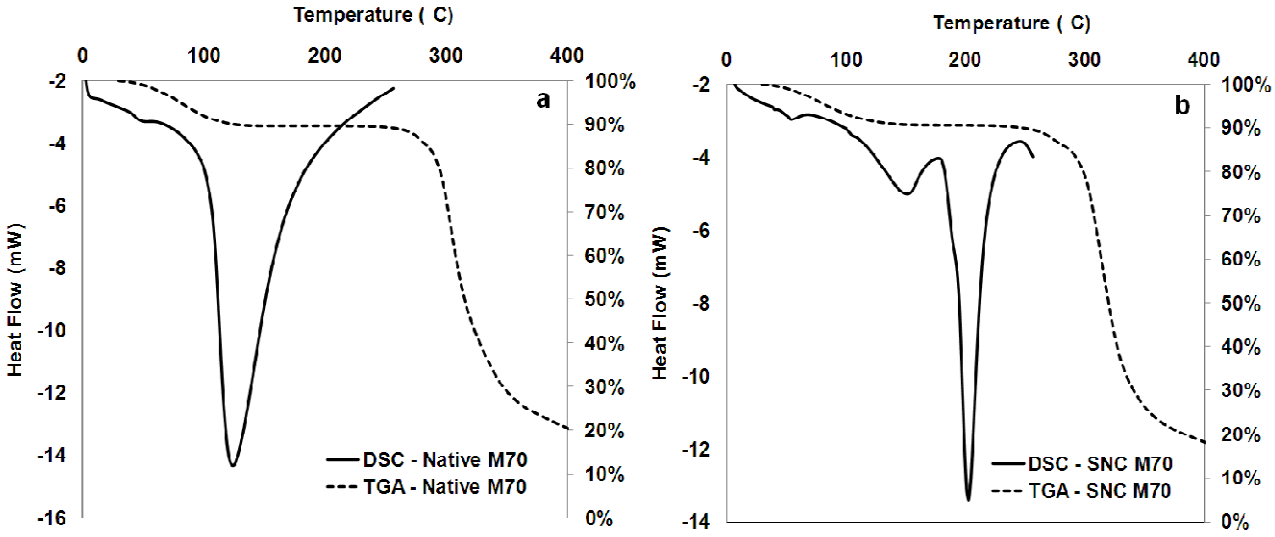

Figure 2-II.3. DSC and TGA curves for dry (0%WC, 50%RH) (a) native M70 and (b) M70SNC

For native starches, the mechanism is confirmed with degradation at temperatures much higher (about 300°C) than the end othermic peaks (about 120-150°C). Similar results were obtained whatever the starch source. Concerning SNC, it seems that the two endothermic transitions observed in DSC measurements occur before the thermal degradation observed in TGA. Even if initial water evaporation is observed with TGA for freeze-dried SNC, no early stage depolymerization is observed.

The degradation temperature of SNC is higher than the temperature of the second DSC peak, whatever the source of starch. This confirms that (i) the second endotherm reflects the melting of the crystallites (as extrapolated from calculations)[25] and that (ii) SNC correspond to starch crystallites described in literature.

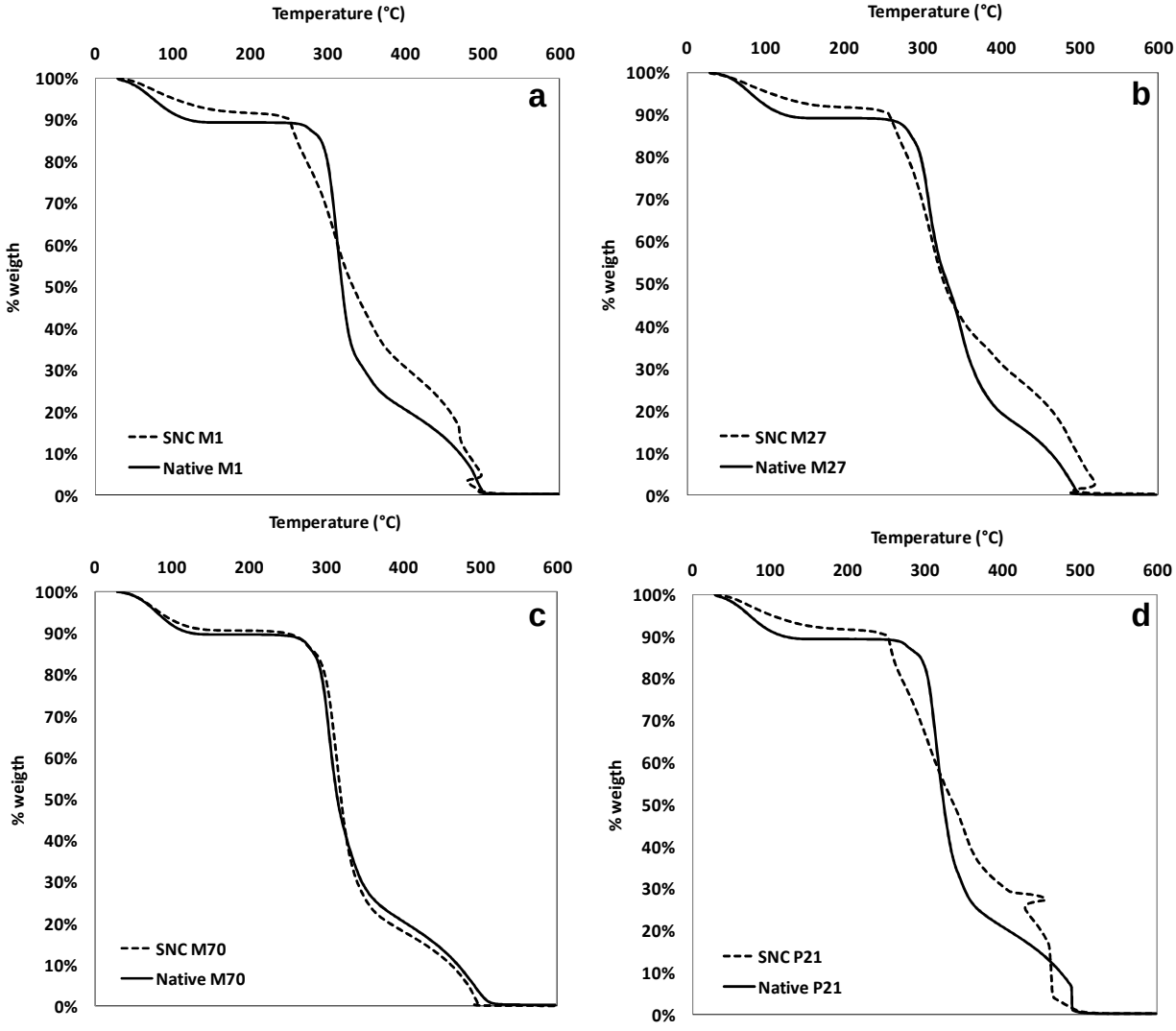

Figure 2-II.4. Comparison between TGA curves of native starch and SNC for (a) M1, (b) M27, (c) M70 and (d) PS28

It should also be noted, from TGA results presented in Figure 2-II.4, that slight differences between native starches and SNC can be observed. Indeed, SNC depolymerization starts earlier than for native starch. This is attributed to the presence of sulfate groups at the surface of SNC [36] which catalyze the reaction as explained earlier. At 200-300℃, the sulfonic acid groups are thermally decompose [44] and thus the depolymerization rate slows down. The final weigh is found to be identical. This phenomenon was also observed when comparing cellulose nanocrystals and MCC (Microcrystalline cellulose) with comparable acid sulfate content [40].

This difference is not observed for M70 SNC as particles are bigger (Table 2-II.1), and thus the specific surface area is smaller and less sulfate groups can catalyze the reaction. The higher the initial amylose content, the bigger the SNC and the higher the degradation temperature and the more similar to the initial starch's thermal behavior (as less sulfate groups can catalyze the degradation) as reported in Figure 2-II.5.c. Indeed, considering the proposed mechanisms and models (described earlier), amylose might play a role not only during hydrolysis but also in apparent particles size and plasticization. This is why a comparison of the different sources is proposed.

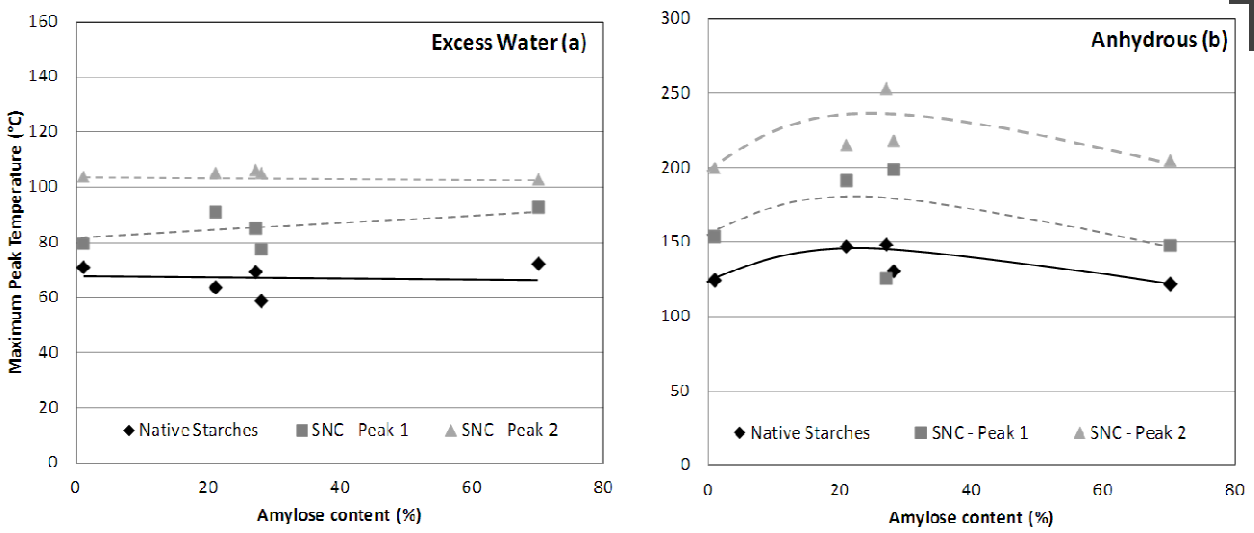

Figure 2-II.5. Evolution of the endothermic peaks for native starch and freeze-dried SNC as a function of the initial amylose content in native starch (a) in excess water (70% water content) and (b) in the dry state (50%RH).

II.3.4. Influence of starch type

Differences between starches used for preparing SNC are: amylose/amylopectin ratio, intermediate material content, lipid content, amylose and amylopectin structure and interchain organization and crystalline types.

In excess water, differences among the first endothermic peak temperature (corresponding to the unpacking of double helices) of SNC from different crystalline types are observed. The results are presented in Table 2-II.2. In its native state, the B-type crystalline packing is described as less dense than A-type and hence more mobile and more prone to disruption [45]. Our results show opposite tendency. Indeed, for B-type starches SNC (M70 and P21) the first endothermic peak was shifted up to higher temperatures by 20 to 30℃, whereas for A -type starches SNC the shift was below 20℃ (Table 2-II.2).

Speculated explanation could be that (i) the amorphous backbone has been hydrolyzed and thus cannot exert pressure on the "less-densely organized" B-crystallites, and (ii) since B-type starches have longer amylopectin helixes, it induces a "rigidity effect"[30] which translates in the nematic state (i.e. out of lamellar order but still oriented) as opposed to an isotropic state. In the dry state on the contrary, the shift to higher temperatures is more important (up to 70℃) as seen in Table 2-II.3. However, the second endothermic peak temperature (corresponding to the unwinding of helices) is the same for all SNC. No direct correlation between thermal transitions' temperature and initial amylose content was found as shown in Figure 2-II.5.a. Although, it seems for maize starch that the higher the amylose content, the higher the first endothermic peak temperature. This could be attributed to the fact that for maize starch , amylose content correlates with branch chain length; and thus the longer, the more rigid (as previously described) and the more stable.

In any case, the results also prove that SNC in excess water should not be processed at temperatures higher than 80℃ for wheat (W28) and waxy maize (M1) starches, 85℃ for normal maize starch (M27) and 90 ℃ for potato (P21) and high amylose (M70) starches. Indeed, if the integrity of the crystal is altered (by the opening up of the double helixes packing) then there is no point in using it as barrier material for example.

In dry conditions, no apparent correlation between thermal transitions' temperature and crystalline type or amylose content could be evidenced as seen in Figure 2-II.5.b. However, for maize starches, the two peaks were further apart than for wheat and potato starches, indicating that crystallites were less homogeneous.

Concerning degradation temperature, no influence of the starch source is observed for native starches as presented in Figure 2-II.6.a. For SNC, it could seem (Figure 2-II.6.b) that the higher the initial (and possibly residual) amylose content, the latter the onset for degradation. However, these data correlate better with SNC's diameter (Table 2-II.1) and thus with potential amount of sulfate groups at the surface as suggested before. These results show that, to a certain extent, SNC could be used in dry processing methods where temperature does not exceed 180℃ such as "cold" extrusion.

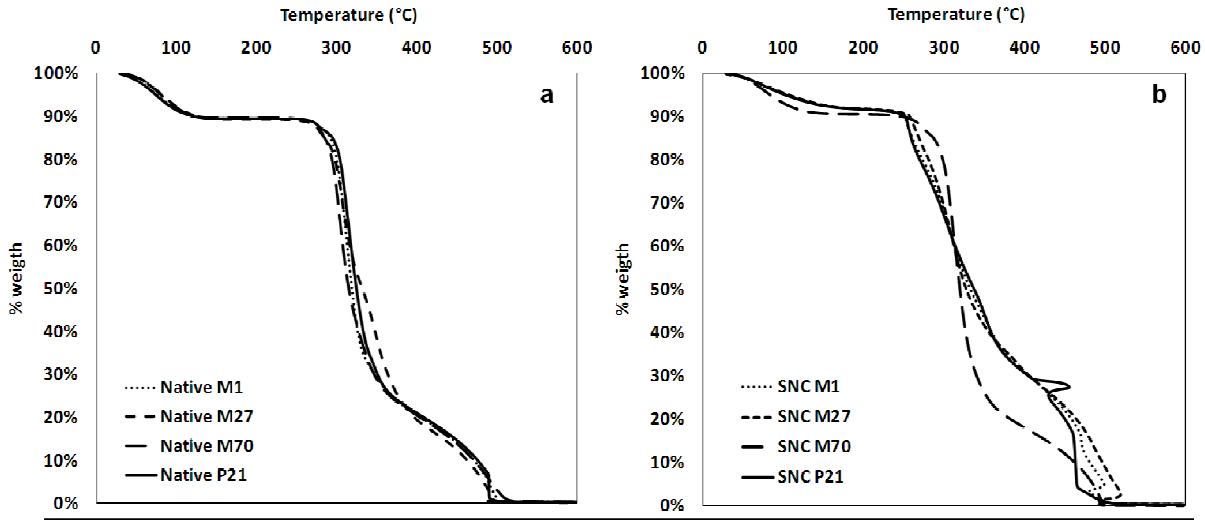

c

Temperature @ 15% weight loss			
	Native	SNC	Δ
M1	292	261	**31**
M27	286	268	**18**
M70	288	287	**1**
P21	286	262	**24**
W28	N.A.	N.A.	-

Figure 2-II.6. TGA thermograms for (a) native starches and (b) corresponding SNC.

II.4. Conclusion

Investigation of the thermal properties of SNC from different sources by DSC revealed two thermal transitions, contrary to native starches which show only one transition. In excess water, the first peak was attributed to the first stage of crystallites melting (unpacking of the double helixes) and the second transition to the second stage of crystallites melting (unwinding of the helixes). B-type crystallinity SNC "gained" more stability than A-type SNC as they consist of more rigid crystallites. In the dry state, the peaks were attributed to crystallites melting, with a direct transition from packed helixes to unwinded helixes; and the presence of two peaks was attributed to heterogeneity in crystallites quality. It was demonstrated by TGA measurements that the second peak occurred before depolymerization and corresponded to the theoretical values of perfect crystallites melting. It confirms that SNC are individualized crystallites with small polymer chain length and high melting temperature. It has always been suspected that the type of starch used for preparing SNC was an important parameter. This study shows that the amylose content of starch shows little influence on final thermal properties of SNC. On the contrary, differences between starches observed in the native state are somewhat compensated when in SNC. However, it seems that in excess water B-type crystallites (with longer chain length) are more stable and that in dry conditions, maize SNC showed least homogeneous crystallites. Finally, it was proved that SNC can be used in wet

processes, such as coating, if temperature remains lower than 80-100℃, and in dry processes at temperatures below 150-200℃.

II.5. References

1. Biliaderis, C. G., Structural transitions and related physical properties of starch. In *Starch chemistry and technology*, Miller, J. B.; Whistler, R., Eds. Elsevier - Academic Press: **2009**; p 293-372.

2. Oates, C. G., Towards an understanding of starch granule structure and hydrolysis. *Trends in Food Science & Technology* **1997,** 8, (11), 375-382.

3. Blanshard, J. M. V., Starch granule structure and function: a physicochemical approach. In *Starch: Properties and Potentials*, Galliard, T., Ed. Society of Chemical Industry: London , U.K. , **1987**; Vol. 13, p 16-54.

4. Kasemsuwan, T.; Jane, J., Location of amylose in normal starch granules. II. Locations of phosphodiesterase cross-linking revealed by phosphorus-31 nuclear magnetic resonance. *Cereal Chemistry* **1994** 71 282-287.

5. Whistler, R. L.; BeMiller, J., *Starch: Chemistry and Technology*. Third ed.; Elsevier: New York, **2009**; p.

6. Ma, X.; Chang, P. R.; Yu, J.; Stumborg, M., Properties of biodegradable citric acid-modified granular starch/thermoplastic pea starch composites. *Carbohydrate Polymers* **2009,** 75, (1), 1-8.

7. Salam, A.; Pawlak, J. J.; Venditti, R. A.; El-tahlawy, K., Synthesis and Characterization of Starch Citrateâˆ'Chitosan Foam with Superior Water and Saline Absorbance Properties. *Biomacromolecules* **2010,** 11, (6), 1453-1459.

8. LeCorre, D.; Bras, J.; Dufresne, A., Influence of botanic origin and amylose content on the morphology of starch nanocrystals. *Journal of Nanoparticle Research* **Unpublished results**, (2011).

9. Le Corre, D.; Bras, J.; Dufresne, A., Starch nanoparticles: A review. *Biomacromolecules* **2010,** 11, (5), 1139-1153.

10. Lin, N.; Huang, J.; Chang, P. R.; Anderson, D. P.; Yu, J., Preparation, modification and application of starch nanocrystals in nanomaterials: A review. *Journal of Nanomaterials* **2011,** 2011, (2011), 1-13.

11. Angellier, H.; Molina-Boisseau, S.; Dufresne, A., Mechanical properties of waxy maize starch nanocrystal reinforced natural rubber. *Macromolecules* **2005,** 38, (22), 9161-9170.

12. Angellier, H.; Molina-Boisseau, S.; Lebrun, L.; Dufresne, A., Processing and structural properties of waxy maize starch nanocrystals reinforced natural rubber. *Macromolecules* **2005,** 38, (9), 3783-3792.

13. Chen, G.; Wei, M.; Chen, J.; Huang, J.; Dufresne, A.; Chang, P. R., Simultaneous reinforcing and toughening: New nanocomposites of waterborne polyurethane filled with low loading level of starch nanocrystals. *Polymer* **2008,** 49, (7), 1860-1870.

14. Angellier, H.; Molina-Boisseau, S.; Dole, P.; Dufresne, A., Thermoplastic Starch-Waxy Maize Starch Nanocrystals Nanocomposites. *Biomacromolecules* **2006,** 7, (2), 531-539.

15. Viguié, J.; Molina-Boisseau, S.; Dufresne, A., Processing and Characterization of Waxy Maize Starch Films Plasticized by Sorbitol and Reinforced with Starch Nanocrystals. *Macromolecular Bioscience* **2007,** 7, (11), 1206-1216.

16. Garcia, N. L.; Ribba, L.; Dufresne, A.; Aranguren, M. I.; Goyanes, S., Physico-mechanical properties of biodegradable starch nanocomposites. *Macromolar Materials and Engineering* **2009,** 294, (3), 169-177.

17. Kristo, E.; Biliaderis, C. G., Physical properties of starch nanocrystal-reinforced pullulan films. *Carbohydrate Polymers* **2007,** 68, (1), 146-158.

18. Yu, J.; Ai, F.; Dufresne, A.; Gao, S.; Huang, J.; Chang, P. R., Structure and mechanical properties of poly(lactic acid) filled with (starch nanocrystal)-graft-poly(e-caprolactone). *Macromolecular Materials and Engineering* **2008,** 293, (9), 763-770.

19. Chen, Y.; Cao, X.; Chang, P. R.; Huneault, M. A., Comparative study on the films of poly(vinyl alcohol)/pea starch nanocrystals and poly(vinyl alcohol)/native pea starch. *Carbohydrate Polymers* **2008,** 73, (1), 8-17.

20. Zheng, H.; Ai, F.; Chang, P. R.; Huang, J.; Dufresne, A., Structure and properties of starch nanocrystal-reinforced soy protein plastics. *Polymer Composites* **2009,** 30, (4), 474-480.

21. Dufresne, A.; Cavaillé, J.-Y., Clustering and percolation effects in microcrystalline starch-reinforced thermoplastic. *Journal of Polymer Science Part B: Polymer Physics* **1998,** 36, (12), 2211-2224.

22. Angellier, H.; Putaux, J.-L.; Molina-Boisseau, S.; Dupeyre, D.; Dufresne, A., Starch nanocrystal fillers in an acrylic polymer matrix. *Macromolecular Symposia* **2005,** 221, (1), 95-104.

23. Angellier, H.; Choisnard, L.; Molina-Boisseau, S.; Ozil, P.; Dufresne, A., Optimization of the preparation of aqueous suspensions of waxy maize starch nanocrystals using a response surface methodology. *Biomacromolecules* **2004,** 5, 1545-1551.

24. Colonna, P.; Buleon, A., Thermal transitions of starches. In *Starches: characterization, properties, and applications*, Bertolini, A. C., Ed. CRC Press: NW, **2010**; p 71-102.

25. Barron, C. Destructuration d'amidons peu hydratés sous cisaillement. , Université de Nantes, Nantes, **1999**.

26. Cooke, D.; Gidley, M. J., Loss of crystalline and molecular order during starch gelatinisation: origin of the enthalpic transition. *Carbohydrate Research* **1992,** 227, 103-112.

27. Zhong, Z.; Sun, X. S., Thermal characterization and phase behavior of cornstarch studied by differential scanning calorimetry. *Journal of Food Engineering* **2005,** 69, (4), 453-459.

28. Randzio, S. a. L.; Flis-Kabulska, I.; Grolier, J.-P. E., Reexamination of Phase Transformations in the Starch/Water System. *Macromolecules* **2002,** 35, (23), 8852-8859.

29. Atichokudomchai, N.; Varavinit, S.; Chinachoti, P., Gelatinization Transitions of Acid-modified Tapioca Starches by Differential Scanning Calorimetry (DSC). *Starch/Stärke* **2002,** 54, (7), 296-302.

30. Waigh, T. A.; Gidley, M. J.; Komanshek, B. U.; Donald, A. M., The phase transformations in starch during gelatinisation: a liquid crystalline approach. *Carbohydrate Research* **2000,** 328, (2), 165-176.

31. Biliaderis, C. G.; Page, C. M.; Maurice, T. J.; Juliano, B. O., Thermal characterization of rice starches: a polymeric approach to phase transitions of granular starch. *Journal of Agricultural and Food Chemistry* **1986,** 34, (1), 6-14.

32. Donovan, J. W., Phase transitions of the starch–water system. *Biopolymers* **1979,** 18, 263-275.

33. Evans, I. D.; Haisman, D. R., The effect of solutes on gelatinization temperature range of potato starches. *Starch/Stärke* **1982,** 34 (7).

34. Biliaderis, C. G.; Page, C. M.; Slade, L.; Sirett, R. R., Thermal behavior of amylose-lipid complexes. *Carbohydrate Polymers* **1985,** 5, (5), 367-389.

35. Waigh, T. A.; Kato, K. L.; Donald, A. M.; Gidley, M. J.; Clarke, C. J.; Riekel, C., Side-chain liquid-crystalline model for starch. *Starch/Stärke* **2000,** 52, (12), 450-460.

36. Angellier, H. Nanocristaux d'amidon de maïs cireux pour applications composites. *Ph.D thesis* University Joseph Fourier, Grenoble, France, **2005**.

37. Thielemans, W.; Belgacem, M. N.; Dufresne, A., Starch nanocrystals with large chain surface modifications. *Langmuir* **2006,** 22, (10), 4804-4810.

38. Tester, R. F.; Morrison, W. R., Swelling and gelatinization of cereal starches. I. Effects of amylopectin, amylose, and lipids. *Cereal Chemistry* **1990,** 67, 551-557.

39. Roman, M.; Winter, W. T., Effect of sulfate groups from sulfuric acid hydrolysis on the thermal degradation behavior of bacterial cellulose. *Biomacromolecules* **2004,** 5, (5), 1671-1677.

40. Wang, N.; Ding, E.; Cheng, R., Thermal degradation behaviors of spherical cellulose nanocrystals with sulfate groups. *Polymer* **2007,** 48, (12), 3486-3493.

41. George, J.; Ramana, K. V.; Bawa, A. S.; Siddaramaiah, Bacterial cellulose nanocrystals exhibiting high thermal stability and their polymer nanocomposites. *International Journal of Biological Macromolecules* **2011,** 48, (1), 50-57.

42. Biliaderis, C. G.; Mazza, G.; Przybylski, R., Composition and physio-chemical properties of starch from cow cockle (Saponaria vaccaria L.) seeds. *Starch/Starke* **1993,** 45, 121-127.

43. Tester, R. F.; Morrison, W. R., Swelling and gelatinization of cereal starches. III. Some properties of waxy and normal nonwaxy barley starches. *Cereal Chemistry* **1992,** 69, (6), 654-658.

44. Jiang, D. D.; Yao, Q.; McKinney, M. A.; Wilkie, C. A., TGA/FTIR Studies on the Thermal Degradation of Some Polymeric Sulfonic and Phosphonic Acids and their Sodium Salts. *Polym. Degrad. Stab.* **1999,** 63, 423-434.

45. Luo, Z.-g.; Fu, X.; Gao, Q.-y.; Yu, S.-J., Effect of acid hydrolysis in th epresence of anhydrous alcohols on the strucutre, thermal and pasting properties of normal, waxy and high amylose maize starches. *International Journal of Food Science & Technology* **2011,** 46, 429-435.

Chapter 2-III. Evidence of micro and nano-scaled particles during starch nanocrystals preparation and their isolation

Déborah Le Corre, Julien Bras, Alain Dufresne

The International School of Paper, Print Media and Biomaterials (Pagora), Grenoble Institute of Technology, BP 65 - F-38402 Saint Martin d'Hères Cedex, France

Abstract

Great work has been done to reduce the batch production time of starch nanocrystals (SNC) and improve their compatibilization with different matrices. However, only one study was reported on SNC' production kinetics, and none on size distributions and isolation techniques. This study was designed to assess if non-solubilized particles in the hydrolyzed starch suspension reflect the actual amount of SNC. It was observed that SNC are produced from a very early stage. It suggests, for the first time, that (i) nanocrystals are mixed together with other microparticles and that (ii) some nanocrystals might turn to sugar by the end of the batch production process explaining the low yields. An isolation process has been proposed but limits of differential centrifugations as washing step and isolation technique were also evidenced. This study clearly shows the need for a continuous production and extraction process of SNC.

Keywords

Starch; Nanocrystals; Isolation Technique; Bionanocomposites

Inspired from: *D. LeCorre, J. Bras, A. Dufresne, Biomacromolecules (**2011**), 12, (8), 3039-3046*

III.1. Introduction

Over the last decades, two concepts have strongly emerged in the scientific literature: (i) on the one side, nanotechnologies with the development of innovative and efficient materials, and (ii) on the other side, sustainable products with the use of renewable raw materials for the development of future application. Current work on renewable bio-based nanomaterials gathers these two important fields. As recently reviewed by Le Corre et al.[1], starch nanocrystals (SNC) are candidates of growing interest. They are crystalline platelets resulting from the disruption of the semi-crystalline structure of starch granules by the hydrolysis of amorphous parts. In 2003, the morphology of SNC extracted from waxy maize was revealed.[2] Transmission electron microscopy (TEM) observations showed: (a) a longitudinal view of lamellar fragments consisting of stack of elongated elements, with a thickness of 5-7 nm and (b) a planar view of individualized platelets after hydrolysis. Shapes and lateral dimensions were derived from observation of individual platelets in planar view and marked 60-65° acute angles for parallelepiped blocks with a length of 20-40 nm and a width of 15-30 nm were reported. However, more recent publications reported bigger SNC[3-7], with round edges[8] and found as grape-like aggregates of 1-5 µm. The heterogeneity in particle size could be explained by the differences in starch botanic origin as recently presented[9] but also by the difficulty to obtain well define pictures of non-aggregated nanocrystals.

Until now, work on SNC has been focusing either on their use in a polymeric matrix or on the kinetics of acid hydrolysis (mainly using HCl). The first issue led to work on chemical grafting; and the latter on kinetics was scarcely addressed by a few teams working (i) on starch granule structure[10, 11], (ii) lintnerized starch[12] or (iii) starch nanocrystals[13] in an attempt to optimize the hydrolysis process.

Despite differences in hydrolysis mechanisms both enzymatic and acidic hydrolysis studies showed evidence of concentric “soft” layers which are more readily hydrolyzed. Hydrolysis has been described at different scales. At an atomic scale, it was found that α-1,6 bonds (found in amylopectin) are thought to be more resistant to hydrolysis than α-1,4.[14] When observed at the microscopic scale, with an optical or scanning electron microscope, acid hydrolysis is decomposed in 3 steps:[15] (i) erosion of the surface, (ii) collapse of the granule’s wall due to radial diffusion of the acid, and (iii) fragmentation of the growth rings. Indeed, between the second and third step, hollow shells suggesting that the outer-layer is more acid-resistant can be observed. At the macroscopic scale, techniques for following the extent of hydrolysis are numerous. The most common one consists in following the total solubilized carbohydrates content.[10] It is

sometimes expressed as a percentage of initial starch[11] or analyzed as molecular weight fractions.[16] To produce acid-thinned starch, Wang et al.[17] evaluated the extent of hydrolysis with viscosity of the resulting slurry, measured by Brabender Viscograph-E. For the preparation of SNC, Angellier et al.[18] followed the dry weight of non solubilized particles as a percentage of initial dry starch.

However, one can wonder if the extent of hydrolysis really reflects the amount of SNC in the final suspension. Indeed, no studies checked: (1) if the hydrolysis render only nano-scaled particles; (2) if it is not the case, if one can isolate the nano-scaled particles from the other ones; and (3) how long it takes for first starch nanocrystals to "appear" in the suspension.

Considering the stratified structure of starch, one can imagine that SNC could be released continuously during the hydrolysis process, and that at a given time both micro and nano-scaled particles could coexist in the hydrolyzed suspension. This is why an isolation process, such as differential centrifugation, should be proposed. It was recently reported to be a successful mean to classify cellulose nanocrystals precipitates in narrow size distribution[19]. Another technique, which could be investigated, is micro-filtration as it is already used in water treatment and starch syrup production.

To answer these important pending questions, we have analyzed in this work the current SNC preparation process and the hydrolyzed suspension of starch at different stage of hydrolysis. We also investigated means to isolate nanoparticles in order to optimize the production process of such nanoparticles.

III.2. Materials & Methods

III.2.1. Materials & Chemicals

Starch used to prepare nanocrystals was native waxy maize starch, kindly provided by Cargill (Krefeld, Germany). Sulfuric Acid (96-98%) was purchased from Chimie Plus (Denice, France). Sodium Azide was purchase from Sigma-Aldrich. All water was deionized water.

III.2.2. Preparation of Starch Nanocrystals

Waxy maize starch (147g) was mixed with 1L of previously prepared diluted sulfuric acid (3M). The suspension was kept under 400 rpm mechanical stirring at 40°C, using a silicon oil bath. The experiments were carried out during 1 day, 3 days and 5 days. The final suspensions were washed by successive centrifugations *(Centrifuge 6K-15C, Sigma)* at 10,000 rpm (relative centrifugal force (RCF) = 16,211g) in deionized water until reaching neutral pH. In between centrifugations, starch suspensions were re-dispersed using Ultra-Turrax for 1 min at 14,000 rpm to ensure better homogeneity. The obtained suspensions were filtered on a coarse filter tissue (40 µm, ref. 03-41/31 Buisine, France) to remove granules' ghosts. Sodium azide was added to the suspensions before storage at 4°C to avoid microbial growth.

III.2.3. Extent of Hydrolysis

In this paper, the yield, Y, refers to the dry weight of non solubilized particles, after coarse filtration (40 µm), as a percentage of initial starch's dry weight :

$$Y\,(\%) = \frac{Weight\ of\ \ starch\ at\ a\ given\ time\ (g)}{Weight\ of\ \ initial\ native\ starch\ (g)} \qquad (1)$$

The extent of hydrolysis thus refers to 1-Y(%), e.g. at t = 0, the extent of hydrolysis is 1-100% = 0%.

III.2.4. Hydrolysis Kinetics

To assess the kinetics of hydrolysis, the 5 days optimized protocol[20] was followed to prepare SNC. The hydrolysis was stopped after 1 day, 3 days and 5 days and for each the yield was assessed in triplicate (Figure 2-III.1.Route 1).

III.2.5. Starch Nanocrystals Characterization

Dynamic Light Scattering (DLS)

Particle size measurements were performed at 25℃ w ith a commercial Zetasizer (Zetasizer NanoZS, Malvern, France). The particle radii were controlled by light scattering. For each measurement, a given volume of the suspension was injected in the Zetasizer cell right after 1 min homogenization with ultrasonic bath. Ultrasonic probe was not used to avoid possible gelatinization of SNC close to the tip. Measurements were performed after reaching stable values. Size distribution graphs were drawn from the most representative measurement for a given time and rotational speed.

Scanning Electron Microscopy

An environmental scanning electron microscope (ESEM) on a Quanta 200 FEI device (Everhart-Thornley Detector) was used at high voltage (10 kV) to access the morphology of native starches. Native starches were simply deposited onto carbon tape before observation.

SNCs' mean size and morphology were studied using a Zeiss Ultra 55 Field Emission Gun Scanning Electron Microscope (FEG-SEM). A thin Au-Pd conductive coating (ab.1 nm) was deposited to reduce charge effect. The images obtained at 10 kV accelerating voltage illustrate the best compromise in terms of SNC contrast and residual charge effect. In order to obtain the best possible resolution, the secondary electron imaging mode with the In-lens detector was used.

The average diameter and length were determined using digital image analyses (ImageJ). Between 70 and 500 measurements were used to determine the diameter. The average diameter and length compared with Zetasizer measurements.

III.2.6. Successive Centrifugations

As mentioned in the protocol for preparing SNC, suspensions are washed using centrifugation as described in Figure 2-III.1. However, no classification was intended at that stage. For successive centrifugations (Figure 2-III.1.Route 2), the suspension was first centrifuged at first set rotational speed. Precipitate (fraction) was kept aside for analysis and supernatant was centrifuged at second higher rotational speed setting. This operation was repeated until all desired rotational speeds were investigated, viz. 1,000, 2,000, 4,000, 6,000, 8,000, and 10,000 rpm.

III.2.7. One-step Centrifugation

Fractionation protocol (Figure 2-III.1. Route 3) was designed to identify a rotational speed at which SNC could be separated from non-fully hydrolyzed particles after a batch production. For all experiments, hydrolysate was equally distributed in 6 centrifuge bottles. Two were centrifuged at 2,000 rpm (RCF = 648g), two at 3,000 rpm (RCF = 1,459g) and two at 4,000 rpm (RCF = 2,594g). The supernatant for each fraction was kept aside for analysis using nanosizer. Indeed, the idea behind fractionation was to obtain a mono-dispersed size distribution in each fraction allowing the measurement of particle size using dynamic light scattering (DLS).

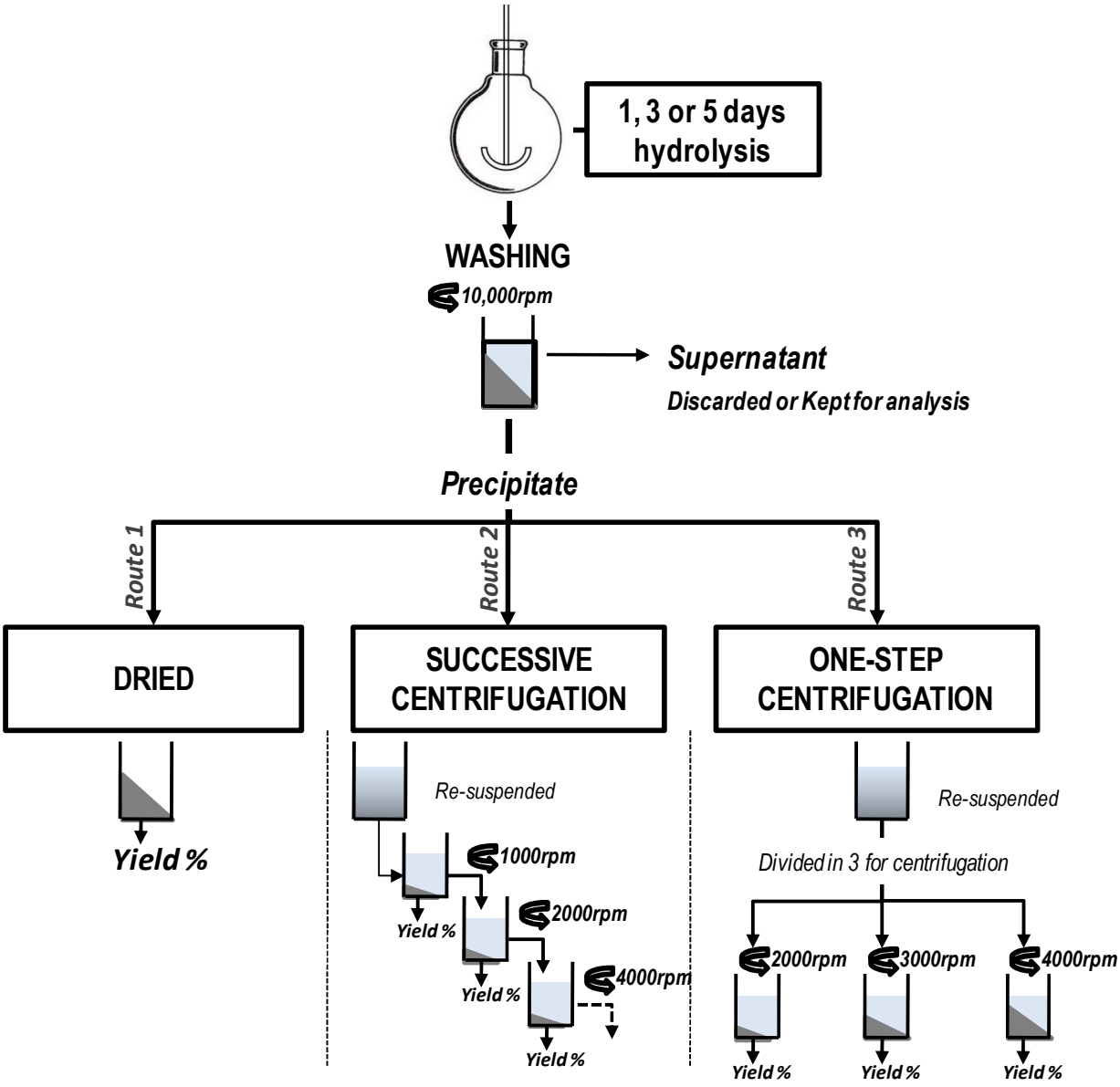

Figure 2-III.1. Schematic representation of the 3 different routes chosen for analysis of starch nanocrystals obtained from the 1, 3 or 5 days hydrolysis.

III.3. Results & Discussions

III.3.1. Starch Nanocrystals Preparation Kinetics - "First Appearance" of Nanocrystals

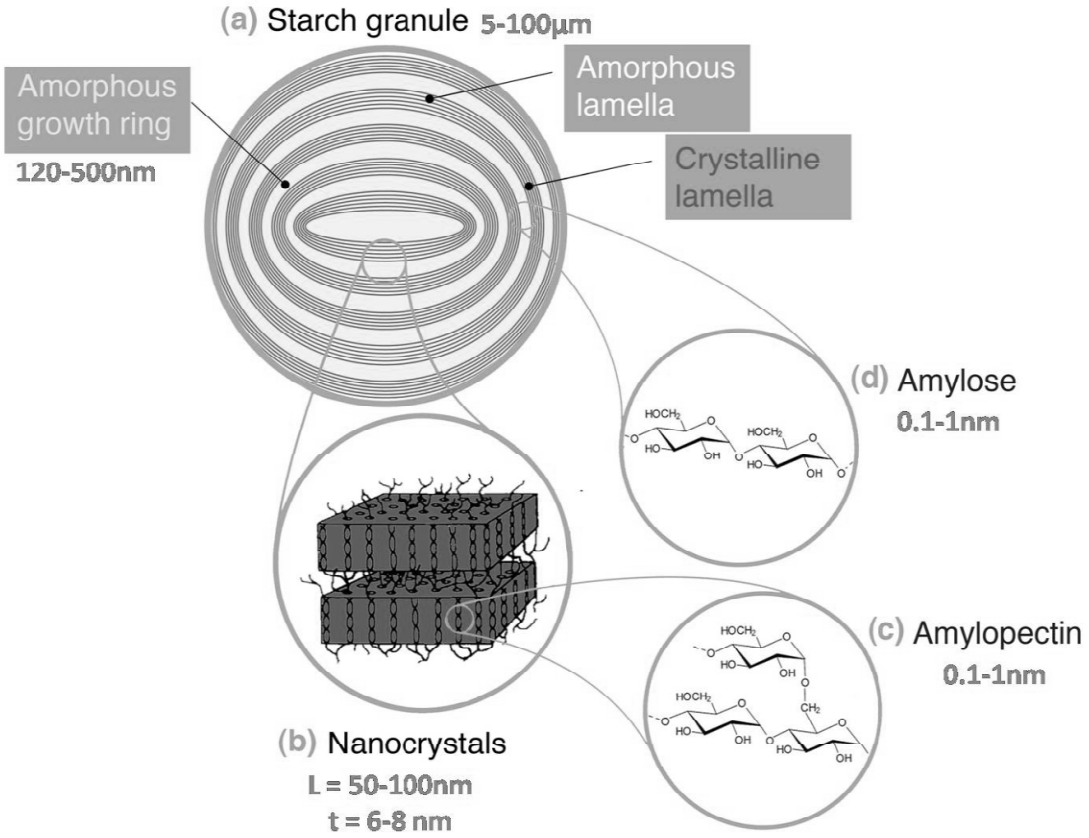

Figure 2-III.2. Starch granule structure (inspired from Le Corre et al.[1]).

As presented in Figure 2-III.2, the commonly accepted model for starch granule structure is a concentric semi-crystalline (i.e. alternating amorphous and crystalline regions) multi-scale structure. Keeping that in mind, the hydrolysis of starch could be schematically described as a "peeling process" of nanomaterials from microparticles. Thus, the kinetics of such a process will evolve with granule hydrolysis. This is why the extent of hydrolysis was followed by assessing the mass yield. Results are shown in Figure 2-III.3. As reported elsewhere[11, 20, 21] a two-stage hydrolysis profile was observed: (i) an initial fast hydrolysis step presumably due to the hydrolysis of the amorphous regions of starch granules, and (ii) a second slower step presumably due to the hydrolysis of the crystalline regions[11, 20] or the concomitant hydrolysis of amorphous and crystalline areas.[21] Some authors distinguished three steps during hydrolysis: a rapid one, a slow one and a very slow one,[15] presumably corresponding to the hydrolysis of amorphous layers, semi-crystalline layers and crystalline ones, respectively. There are

two common hypotheses to account for the slower hydrolysis rate of crystalline domains. The first one is that the dense packing of starch double helixes in the crystalline regions does not allow readily the penetration of H3O+ ions.[10] The second one is that the hydrolysis of the glucosidic bonds requires a change in conformation from chair to half-chair.[21] However, there are no mention and no distinction concerning the size of starch particles during the different stages in literature. Indeed, most papers focus their analysis on the final suspension.

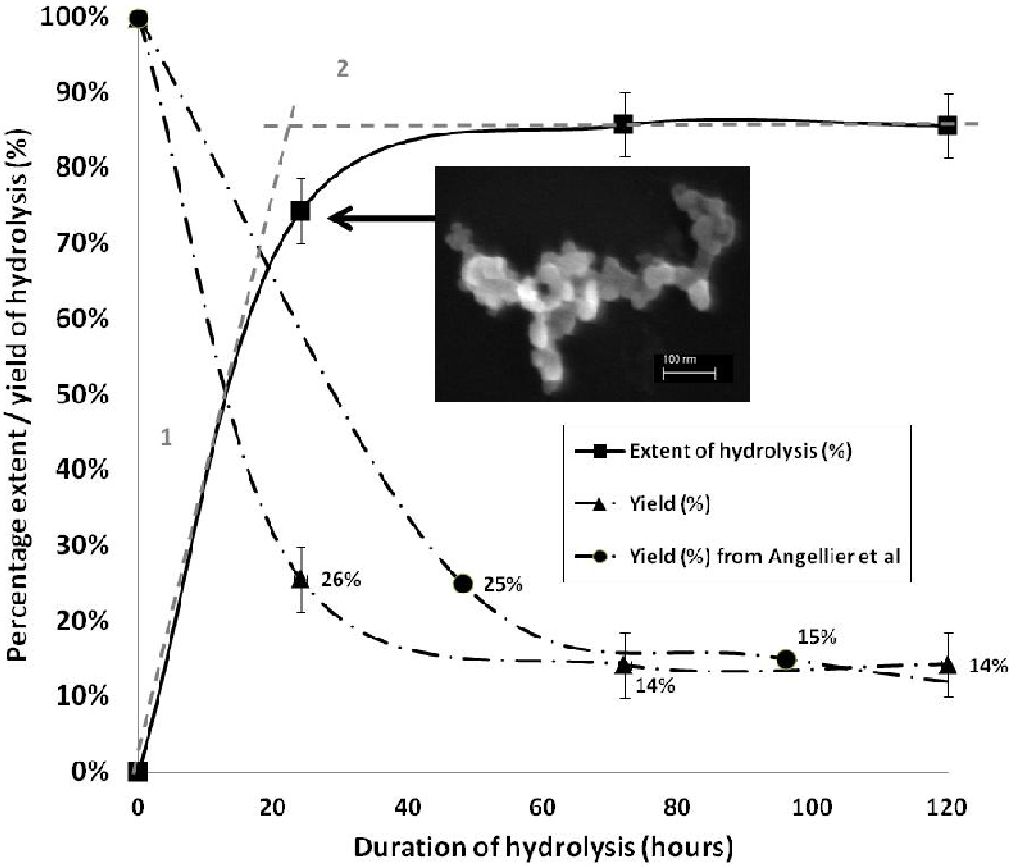

Figure 2-III.3. Kinetics of hydrolysis of (▪) waxy maize starch using sulfuric acid 3M, 40°C and 15% starch and (▲)corresponding yield (%). (●)Yield of hydrolysis of waxy maize in the same conditions reported by Angellier et al.[13] has been added. The SEM-FEG micrograph taken at day 1 clearly shows the existence of SNC.

This explains the motivation to analyze samples produced after one day hydrolysis using FEG-SEM to determine the possible existence of SNC at an early stage.

Microscopic observations revealed, as presented in Figure 2-III.4, that SNC could be found already from the first day on. We suspect these nanocrystals to be fully hydrolyzed after 5 days of hydrolysis which should strongly limit the SNC production yield. Indeed, the size of such nanoparticles obtained after one day is 25-70 nm, with an average length of 50 nm and an average width of 35 nm. These values correspond to the dimensions reported in the literature for SNC obtained after five days hydrolysis.[3-7, 22]

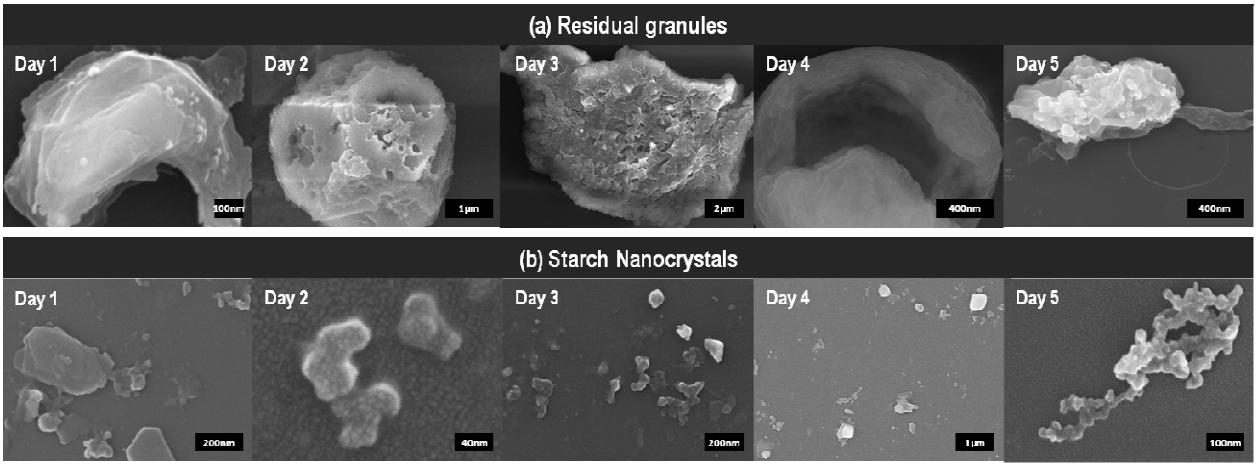

Figure 2-III.4. FEG-SEM micrographs of residual granules and starch nanocrystals, at different stage of hydrolysis (no separation process).

For the first time, an important drawback in the current preparation process of SNC has been raised. Contrary to common belief, SNC are not "released" all at once upon the fragmentation of the "core-hydrolyzed" granule, nor pealed-off from the onion-like structure. We do not question the acid hydrolysis mechanism (described in the introduction) but would like to underline the following: this mechanism applies for a given granule in acid. However, all granules do not have the same size or the same pore distribution leading to certain heterogeneity in the hydrolyzed granules. Also the use of intense stirring during the preparation process favors the fragmentation of weakened granules. First works studying the acid hydrolysis treatment of starch used moderate conditions (HCl 1N to 3.6N) and no stirring[23] to allow keeping the granular structure of starch while studying the influence of temperature, time and acid concentration. Angellier et al.[18] added stirring speed and starch concentration as parameters for optimization of the hydrolysis process. They concluded that the stirring speed and the overall starch concentration do not have any significant influence on the yield and the median size of SNC. However, current protocols mention the continuous stirring of the suspension during hydrolysis.

Therefore, from day 1, we observe granule fragments with hollow center (Figure 2-III.4.a) as well as starch nanoparticles (Figure 2-III.4.b). The latest can originate either from the surface erosion, accentuated with stirring, or from hydrolyzed fragments. These experimental results open new ways of thinking SNC suspensions and lead to consider separation processes such as centrifugation in order to increase the final yield.

As mentioned in the introduction, nanoparticles of any kind show unique properties which originate mainly from their size and even small amounts of coarse particles can impair the properties of the final product. These results prove that an isolation and fractionation of SNC suspensions could strongly improve their homogeneity and thus their properties.

III.3.2. Successive fractionation with differential centrifugation

Differential centrifugation is a separation technique based on size and density with larger and/or denser particles precipitating at lower centrifugal forces. For a single material suspension, the mechanism can be described as followed. The uniformly dispersed particles travel to the bottom of the bottle with a velocity (v), when the centrifugal force (F_c), the frictional force (F_f) and the buoyant force (F_b) (equal to the weight of displaced fluid) are balanced, with:

$$F_c = m\omega^2 r \qquad (2)$$

$$F_f = fv \qquad (3)$$

$$F_b = m_o\omega^2 r \qquad (4)$$

and

$$m = \rho_p V_p \qquad (5)$$

$$m_o = \rho_w V_p \qquad (6)$$

where ω is the angular velocity (rpm), f the frictional coefficient, m_0 the mass of displaced water, ρ_w the density of water (solvent), and r, m, v, V_p and ρ_p, the radius, mass, velocity, volume and density, respectively, of the particle.

The force balance leads to equation (7) which combines equations (2) to (6):

$$V_p(\rho_p - \rho_w) = \frac{fv}{\omega^2 r} \qquad (7)$$

The relationship between the angular velocity (in rpm) and the relative centrifugal force (RCF, in g) being given by equation (8):[24]

$$RCF = 1.118 \times 10^{-6} \omega^2 r \qquad (8) \qquad \text{with} \qquad \rho_w = 1\,g.cm^{-3}$$

Equation (7) becomes:

$$V_p\left(\rho_p - 1\right) = \frac{1.118 \times 10^{-6} fv}{RCF} \qquad (9)$$

At fixed RCF and if the starch density is considered uniform and the charge density similar for each particle then the volume of a particle is proportional to the velocity. That is, bigger particles (in volume) will precipitate much faster than smaller ones. For a given time, RCF will have to be increased for smaller particles to settle. That is the basic idea behind separating SNC with this centrifugation technique.

The centrifugation apparatus used in this study can operate up to RCF = 16,211g (10,000 rpm). As previously mentioned in the Introduction Section, differential centrifugation processes have been already applied for cellulose nanocrystals.[19] The frictional force applied to these cellulose nanocrystals was re-calculated backward, from the results. Values ranging from 9.15×10^{-9} N to 6.26×10^{-8} N were reported. Despite obvious differences in shape between cellulose whiskers (rod-like) and SNC (square platelets), whiskers 400 nm long and 10 nm wide, represent the same volume than SNC with thickness 6 nm and length 70 nm.Under these considerations, we can assume that SNC are submitted to a similar frictional force than cellulose nanocrystals. Thus, considering density is 1.1 $g.cm^{-3}$,[25] and SNC of 6x70x70 nm^3 particles should precipitate at RCF ranging between 3,291g (ie. 4,500 rpm) and 22,518g (i.e. 11,790 rpm). If considering the lower value of the frictional force (2.7×10^{-8} N), particles of all sizes should be able to precipitate. However, if we consider the higher value of the frictional force (1.8×10^{-7} N), particles smaller than 80 nm will not be able to precipitate at highest operating RCF = 16,211g (10,000 rpm). On the contrary, native starch granules placed in water, will settle naturally and therefore even with minimal RCF. Moreover, sulfuric acid hydrolysis of polysaccharides renders anionic sulfate groups ($-SO_3^-$) at the surface which favor hydrocolloid stability of the SNC suspension.[18] This explains why screening tests have been carried out on final (5 days) hydrolyzed suspension. The idea was to check at which rotational speed no more particles precipitated.

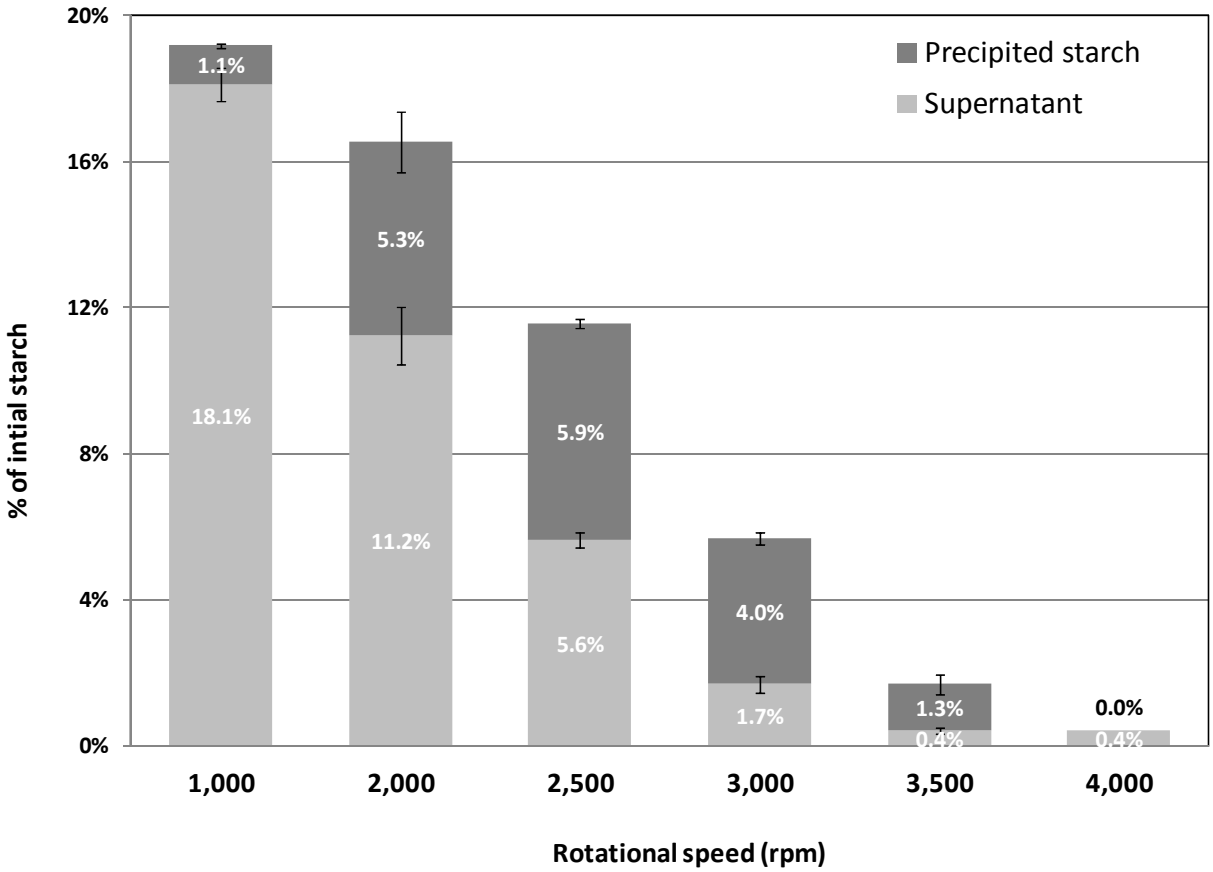

Figure 2-III.5. Weight percentage of initial starch obtained from successive fractionation with differential centrifugation for the 5 days hydrolysate from waxy maize.

Results showed that particles were collected in both the precipitate and the supernatant for each fraction from 1,000 rpm to 3,500 rpm after which no more sedimentation was observed, as presented in Figure 2-III.5. Only a very small amount of SNC (~0.4%) remained in the supernatant contrary to what was expected. Several explanations will be proposed later on in this study. However, it already gives a proof of the heterogeneity and the relatively high dimensions (~100 nm) of the SNC after 5 days hydrolysis. As such little material was collected at intermediate rotational speed, we decided to set rotational speed at 2,000, 3,000 and 4,000 rpm for 10 min for the following experiments.

III.3.3. One-Step Separation Process with Differential Centrifugation

The one-step separation protocol was designed as to identify a ("cut-off") rotational speed at which SNC could be separated by precipitation from non-fully hydrolyzed particles (see Figure 2-III.1. Route 3). For a given extent of hydrolysis (i.e. 1 day, 3 days or 5 days), the mass yield of hydrolyzed particles in precipitate and supernatant was evaluated at 2,000, 3,000 and 4,000 rpm. Results are gathered in Figure 2-III.6.

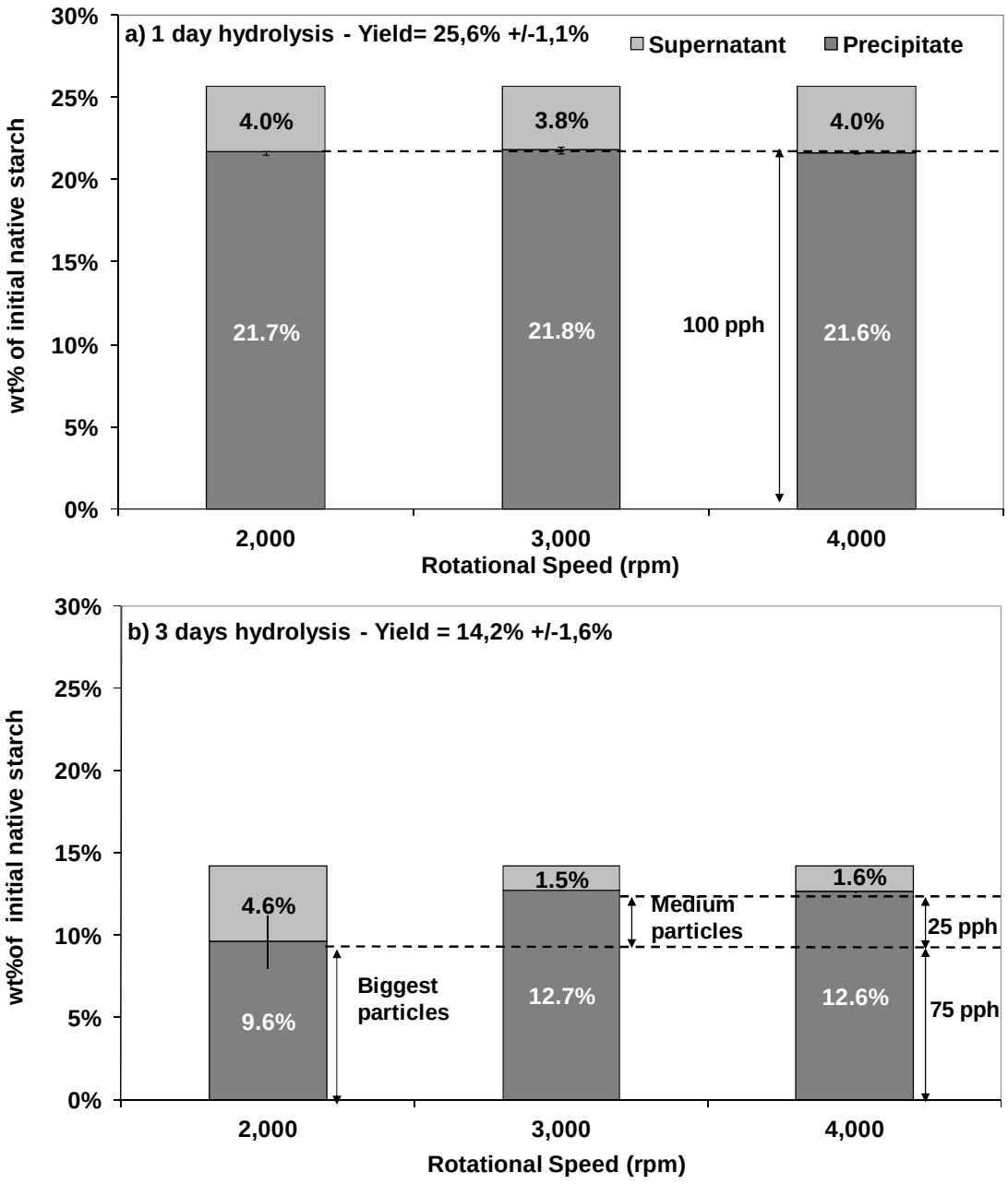

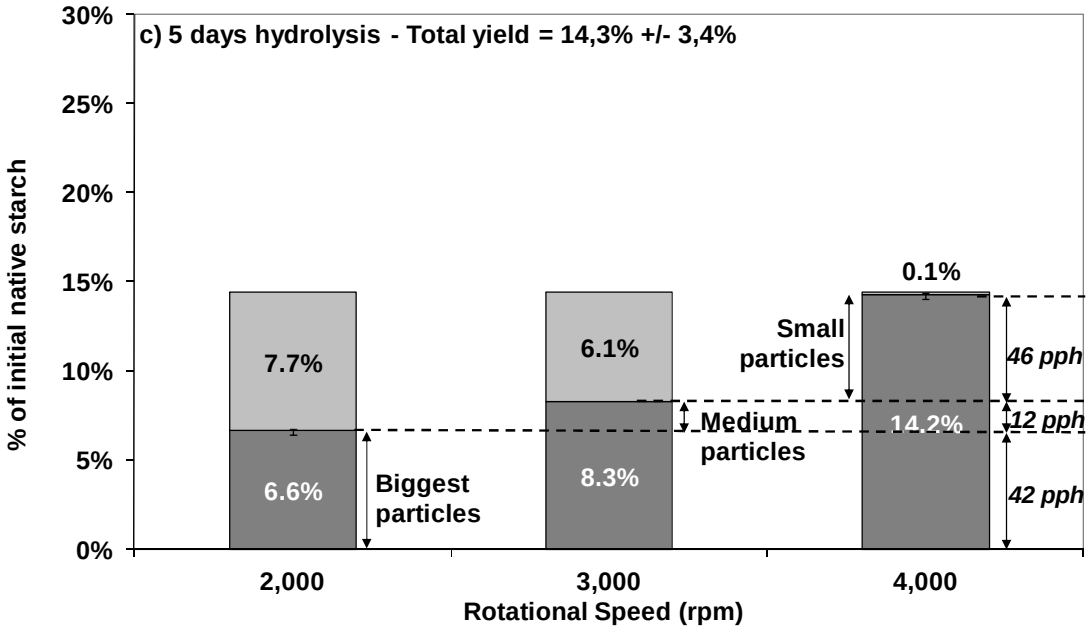

Figure 2-III.6. Mass yield compared to initial amount of native starch for a) 1 day, b) 3 days and c) 5 days hydrolysis.

For starch hydrolyzed for 1 day (Figure 2-III.6.a), almost all particles already precipitate at 2,000 rpm. It suggests that most particles are rather big in size. Consequently, they precipitate at lower and higher rotational speed as well. About 4% of particles stayed in the supernatant suggesting that already 4% SNC were obtained after 1 day hydrolysis.

For starch hydrolyzed for 3 days (Figure 2-III.6.b), differences were observed for centrifugation at 2,000 rpm and above. At 2,000rpm, 9.6% of the initial amount of starch precipitates whereas it reaches 12.7% at 3,000 rpm and above. That suggests that biggest particles precipitate at 2,000rpm and medium size particles precipitate at higher speed with a 75:25 big/medium size repartition as illustrated in Figure 2-III.6.b. This is coherent with a 3 days-hydrolysis. As in day 1, granules have started to "release" starch nanoparticles. However, after 3 days, they start fragmenting (as described in introduction) thus leading to the presence of medium size particles in the suspension. The amount of starch collected in supernatant is only 1.6%. An increase in material collected in supernatant was expected. Indeed, more SNC should be produced and thus remain in the supernatant. It suggests that (i) SNC already produced after day 1 might have been hydrolyzed or (ii) medium-size particles precipitated some SNC by aggregation or hydrogen bonding or (iii) produced SNC aggregated.

Finally, after 5 days hydrolysis (Figure 2-III.6.c), the amount of particles which precipitate increases with increasing rotational speed 2,000 rpm/3,000 rpm/4,000 rpm suggesting multimodal size dispersion inside the suspension with distribution 42/12/46 pph for big/medium/small particles as illustrated in Figure 2-III.6. Very few particles are left in the supernatant at that stage but were collected for DLS analysis.

Observations made at day 3 and 5 seem to confirm our suspicion that SNC produced early on are further hydrolyzed after 3 days and that nanocrystals might aggregate with medium non-fully hydrolyzed particles widely present in the suspension.

First results confirmed the hydrolysis kinetics and showed promising results for classification of particles at different stages of hydrolysis. It seemed that centrifugation at 3,000 rpm would allow to collect larger particles and keep in the supernatant smaller particles and/or SNC.

As mentioned previously, the supernatant of each fraction was kept aside for analysis using nanosizer. Indeed, the idea behind fractionation was to obtain a mono-dispersed size distribution in each fraction allowing the measurement of particle size using Dynamic Light Scattering (DLS).

Measurements presented in Table 2-III.1 show a decrease in precipitated mean hydrodynamic diameter with increasing rotational speed regardless the hydrolysis duration in accordance with differential centrifugation techniques.

Table 2-III.1. Z-average mean size for 1, 3 and 5 days precipitated hydrolyzed fractions isolated by differential centrifugation at fixed time (10 min) (averaged on 5 samples).

Rotational speed	**RCF**	**Z-average mean size (d.nm)**		
rpm	*g*	*1 day*	*3 days*	*5days*
2000	648	1041 ± 332	1169 ± 301	953 ± 231
3000	1459	875 ± 321	684 ± 250	391 ± 36
4000	2594	882 ± 217	647 ± 135	285 ± 59

Indeed, small particles which remained in the supernatant at 2,000 rpm, are most likely to precipitate at 3,000rpm and/or 4,000 rpm lowering the mean diameter size of higher rotational speed precipitates.

Figure 2-III.7 shows experimental DLS data obtained for precipitated particles after different hydrolysis durations and using different rotational speeds. It is observed that with increasing hydrolysis time, peaks are more distinct. After 5 days hydrolysis, differential centrifugation allows to better discriminate particles as also evidenced by decreasing the standard deviation (Table 2-III.1).

It is important to note that the hydrodynamic size measured by DLS is defined as "the size of a hypothetical hard sphere that diffuses similarly to the particle being measured".[26] Because of this, the diameter calculated from the diffusion properties of the particle are only indicative of the apparent size of the dynamic hydrated/solvated particle. Hence the terminology, "Hydrodynamic diameter". It does not reflect the actual particle size for non spherical and non mono-dispersed samples. Indeed, despite fractionation, measurements remained complicate. The polydispersity of a sample corresponds to its the relative standard deviation. It reflects the width of the detected peak. For all samples, the Polydispersity Index was high (>0.5 at day 1 and 3; and ranging from 0.2 to 0.5 for day 5), implicating that samples are polydisperse and that Z-average cannot reflect the particle size. Sometimes two peaks were detected (the second one being ignored because of its very small size <10 nm).

Therefore, reported hydrodynamic diameters cannot be used as an approximation of size but rather for comparison purposes. FEG-SEM micrographs of the different precipitated fractions presented in Figure 2-III.8 were taken to assess visually the size distribution in each fraction and confirm DLS measurements. It was observed that SNC do not remain in the supernatant contrary to the theory of isolation of nanoparticles by differential centrifugation.

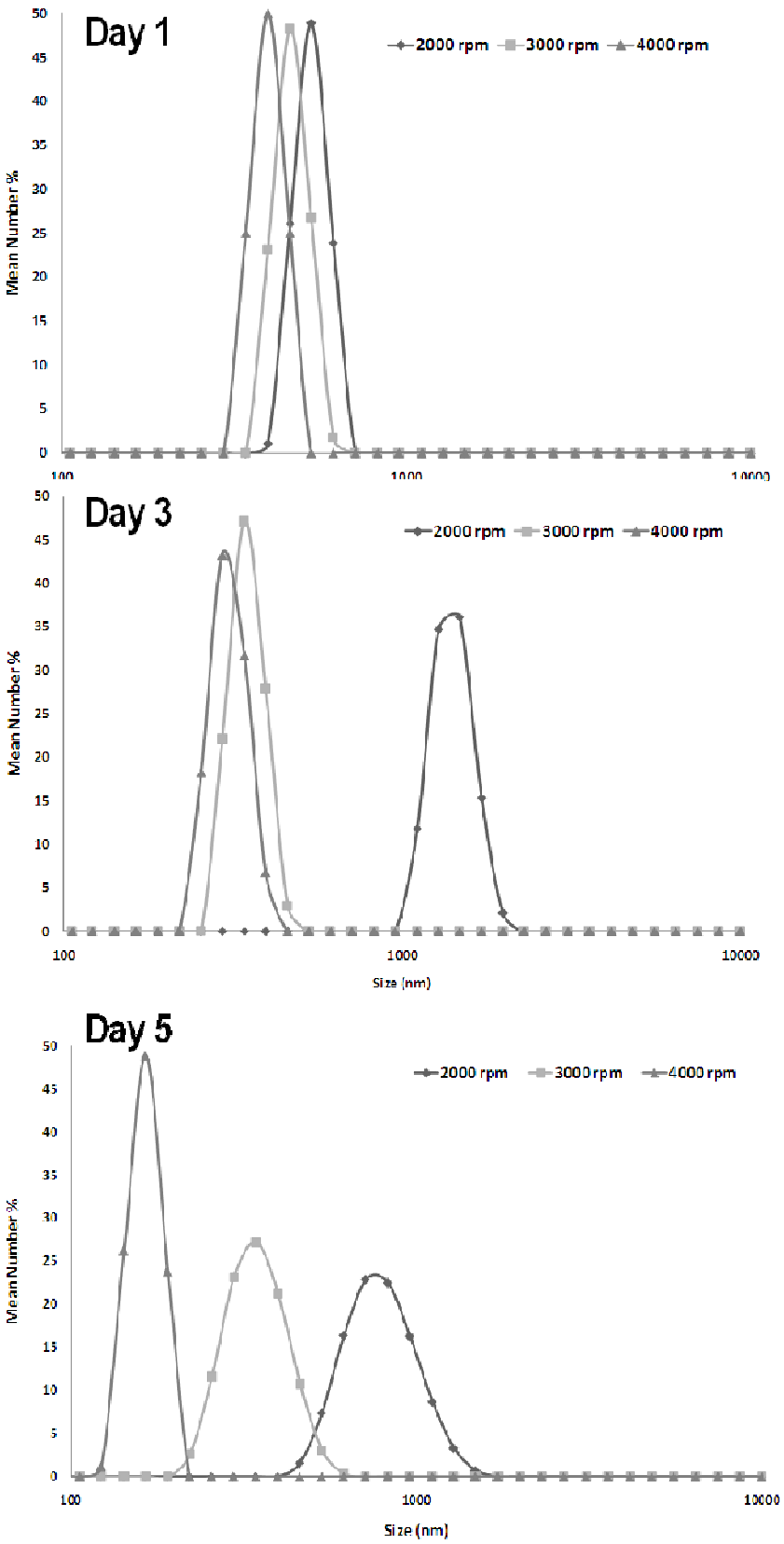

Figure 2-III.7. Precipitated particles hydrodynamic diameter size distribution at 2,000 rpm, 3,000rpm and 4,000 rpm after respectively 1 day, 3 days and 5 days hydrolysis. (Non averaged).

An explanation could be that smaller particles, although isolated by hydrolysis, remain attracted by non-fully hydrolyzed particles due to hydrogen bonding or aggregate. Therefore, during centrifugation small crystalline particles precipitate together with bigger particles or as clusters.

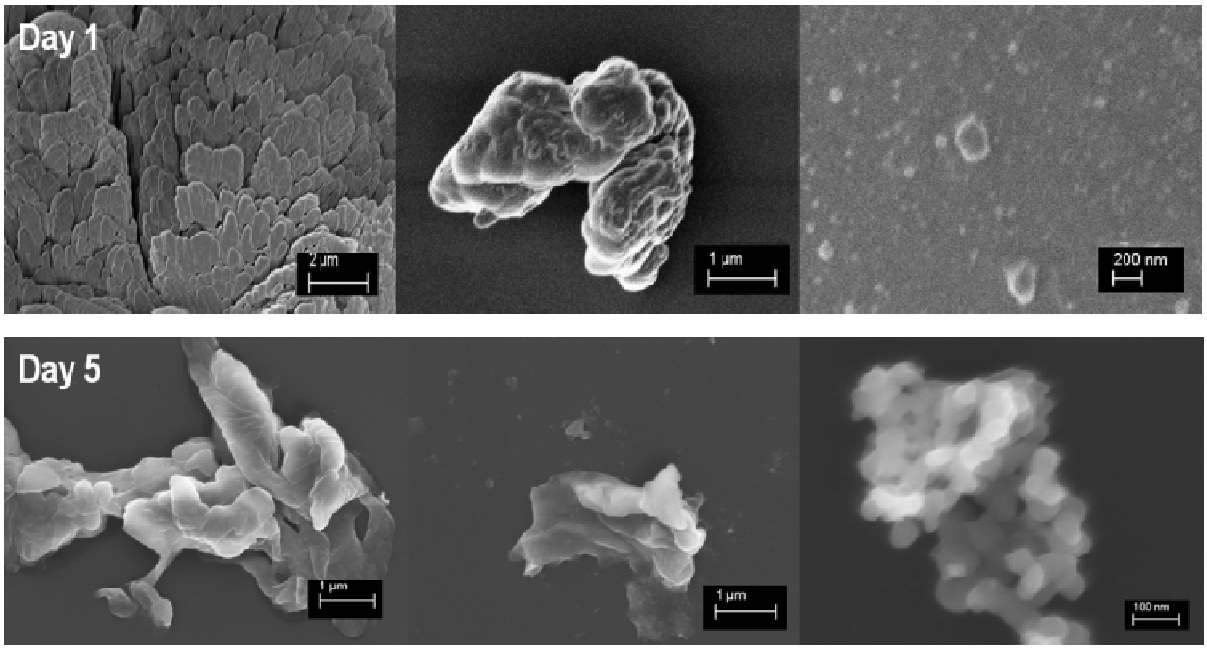

Figure 2-III.8. FEG-SEM micrographs obtained for respectively 1day and 5 days hydrolyzed starch precipitates at 4,000 rpm, showing multi-modal size distribution.

Another explanation could be a difference in molecular density in the initial material due to the heterogeneity of starch granule. Indeed, the hydrolysis of starch for the production of SNC is based on its semi-crystalline feature identified by X-ray diffraction in the 1930's.[27]

In reality, starch is much more complex than cellulose. Indeed, as widely reported, the generally accepted model for starch granule is a multi-scale structure (Figure 2-III.2) consisting in the (a) granule (2-100 µm), into which we find (b) growth rings (120-500 nm) composed of (d) blocklets (20-50 nm) made of (c) amorphous and crystalline lamellae (9 nm)[28] containing (g) amylopectin and (h) amylose chains (0.1-1 nm).[1]

At the mesoscopic scale, at least 3 phases can be identified: the amorphous background (also called amorphous growth rings), the alternating crystalline lamella and the amorphous lamella (the combination of which is called semi-crystalline growth ring). Although the amorphous growth ring's existence and non periodicity has been revealed by different techniques, its composition remains unknown. The blocklet concept,

developed in the 1930's by Hanson and Katz,[27] and supported by more recent SEM observations[29, 30] offers a possible explanation. They suggested that both semi-crystalline and amorphous growth rings are subdivided into respectively large (50 to 500 nm depending on species) and smaller spherical blocklets.

Contemporaneous study[31] using small angle neutron scattering (SANS) has evidenced variations in the local molecular density of the different regions of starch granules for different starch species. For all species except potato, the molecular density of the amorphous growth ring region differed, not only with crystalline lamellae as expected but also with amorphous lamellae. For waxy maize, molecular densities found in literature are reported Table 2-III.2.

The starch molecular density of amorphous growth ring is about 50% higher than that of amorphous lamella. This could be evidence for defective blocklets as reported by Tang et al.[32] In any case, results indicate that amorphous lamellae appear to have a more "open" structure, which will therefore be more easily penetrated by water than the amorphous background. Such considerations could also explain for the presence of bigger and probably less dense particles (small blocklets) in supernatant, whereas smaller and denser crystallites precipitate.

Table 2-III.2. Starch and water molecular density in the three different regions of a granule.[31]

(g/m^3)	Waxy Maize		Potato	
	Starch	Water	Starch	Water
Amorphous background	0.7	0.7	0.5	0.8
Crystalline lamella	1.2	0.3	1.1	0.4
Amorphous lamella	0.5	0.8	0.5	0.7

III.3.4. Centrifugation Used in Starch Nanocrystals Preparation Protocol

Despite previous results indicating that some SNC precipitate even at low rotational speed, a concern was the potential discarding of SNC during the washing step of final hydrolyzed starch suspension at 10,000 rpm (see Figure 2-III.1. Route 1). According to the described protocol, the supernatant from the first centrifugation/washing at 10,000 rpm is discarded and replaced by water to reduce the pH of the suspension. SNC washing via centrifugation, as described in the protocol, cannot be avoided. Indeed, without such a washing "post-treatment", acid would not be removed, hydrolysis would carry on and SNC would turn to glucose or oligomers.

For analysis, the acidic supernatant from 1 day and 3 days hydrolysis were kept and both diluted and dialyzed for a week to reduce the pH. SEM-FEG micrographs, displayed in Figure 2-III.9 revealed that not only SNC were thrown away during the first washing. It also contained aggregates and starch granules shell ghosts. It is the first time that such results are presented. They present another limitation of SNC preparation by batch with "unavoidable" loss of material.

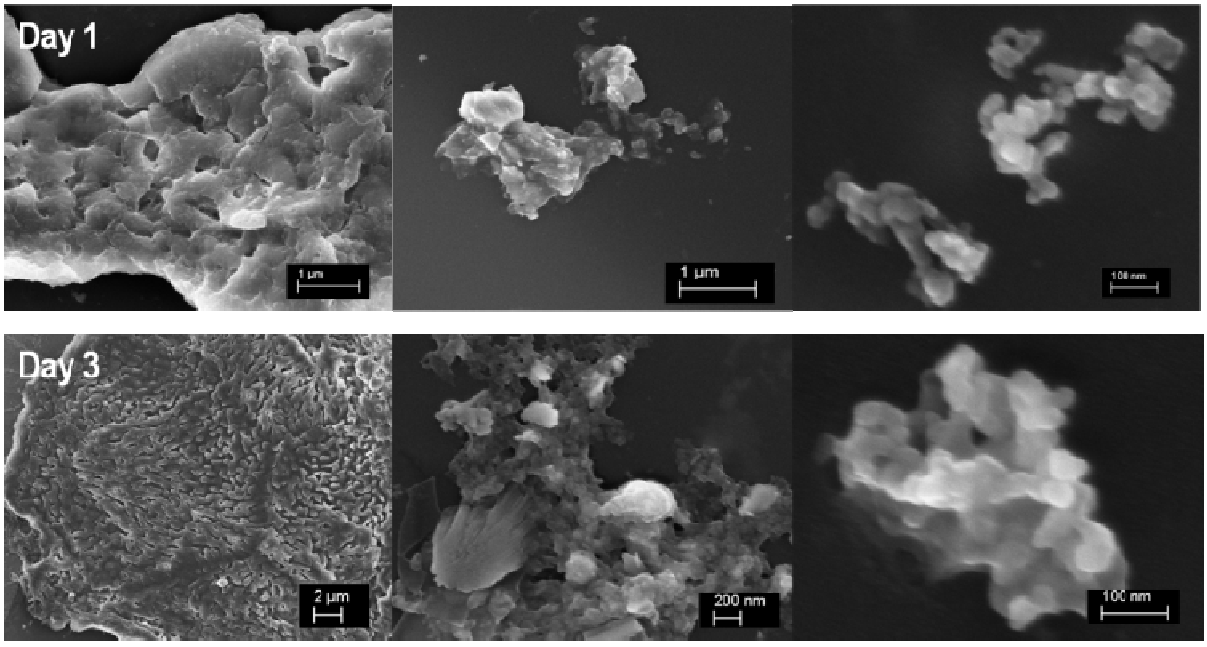

Figure 2-III.9. FEG-SEM micrographs of discarded supernatant from washing hydrolyzed starch after 1 day and 3 days hydrolysis.

Differential centrifugation as a tool for washing or fractionating SNC is therefore not the best solution. Other techniques should be proposed. Nevertheless, this technique allows showing the presence of multi-sized nanoparticles in not only the one-day-hydrolysis suspensions but also in the discarded supernatant of the well established 5

days process. Therefore, this study proves that, up to date, all scientific papers describing the yield of SNC as either the dry weight of non-solubilized particles, or the total solubilized carbohydrates content, measured in reality SNC and other microparticles.

III.4. Conclusion

Experiments carried out in this study provided important information not found in the literature concerning the preparation of relatively new bio-based nanoparticles, namely starch nanocrystals (SNC). Indeed, it was evidenced for the first time that (1) first SNC "appear", at least, after only 24h of sulfuric acid hydrolysis; (2) consequently, at any time including final suspension, both micro-scaled and nano-scaled particles can be found and coexist. Differential centrifugation has been tested as an isolation process for separating these two kinds of particles, but does not seem fitted for fractionation due to hydrogen bonding and different densities within starch granules. Moreover, the study proves that the suspension post-centrifugation (for washing) should be carried out at higher rotational speed to avoid loss of material. Actually, this study completely modifies the way of thinking SNC suspensions and shows with emphasis the need for a continuous extraction process of SNC. We believe that such a system would allow assessing the actual nanocrystals yield - as opposed to the gross yield reflecting the hydrolysis extent- and would strongly increase that yield.

III.5. References

1. Le Corre, D.; Bras, J.; Dufresne, A., Starch nanoparticles: A review. Biomacromolecules **2010**, 11, (5), 1139-1153.

2. Putaux, J. L.; Molina-Boisseau, S.; Momaur, T.; Dufresne, A., Platelet Nanocrystals Resulting from the Disruption of Waxy Maize Starch Granules by Acid Hydrolysis. Biomacromolecules **2003**, 4, (5), 1198-1202.

3. Chen, G.; Wei, M.; Chen, J.; Huang, J.; Dufresne, A.; Chang, P. R., Simultaneous reinforcing and toughening: New nanocomposites of waterborne polyurethane filled with low loading level of starch nanocrystals. Polymer **2008**, 49, (7), 1860-1870.

4. Chen, Y.; Cao, X.; Chang, P. R.; Huneault, M. A., Comparative study on the films of poly(vinyl alcohol)/pea starch nanocrystals and poly(vinyl alcohol)/native pea starch. Carbohydrate Polymer **2008**, 73, (1), 8-17.

5. Yu, J.; Ai, F.; Dufresne, A.; Gao, S.; Huang, J.; Chang, P. R., Structure and mechanical properties of poly(lactic acid) filled with (starch nanocrystal)-graft-poly(e-caprolactone). Macromolecular Materials and Engineering **2008**, 293, (9), 763-770.

6. García, N. L.; Famá, L.; Dufresne, A.; Aranguren, M.; Goyanes, S., A comparison between the physico-chemical properties of tuber and cereal starches. Food Research International **2009**, 42, (8), 976-982.

7. Namazi, H.; Dadkhah, A., Convenient method for preparation of hydrophobically modified starch nanocrystals with using fatty acids. Carbohydrate Polymers **2010**, 79, (3), 731-737.

8. Wang, Y.; Zhang, L., High-Strength Waterborne Polyurethane Reinforced with Waxy Maize Starch Nanocrystals. Journal of Nanoscience and Nanotechnology **2008**, 8, (11), 5831-5838.

9. Le Corre, D.; Bras, J.; Dufresne, A., Starch Nanoparticles for eco-efficient packaging: influence of botanic origin. In 2nd International Conference on Biodegradable Polymers and Sustainable Composites (BIOPOL 2009), Jimenez, A., Ed. Alicante, Spain, **2009**.

10. Li, W.; Corke, H.; Beta, T., Kinetics of hydrolysis and changes in amylose content during preparation of microcrystalline starch from high-amylose maize starches. Carbohydrate Polymers **2007**, 69, (2), 398-405.

11. Jayakody, L.; Hoover, R., The effect of lintnerization on cereal starch granules. Food Research International **2002**, 35, (7), 665-680.

12. Robin, J. P.; Mercier, C.; Charbonniere, R.; Guilbot, A., Gel filtration and enzymatic studies of insoluble residues from prolonged acid treatment of potato starch. Cereal Chemistry **1974**, 51, 389-406.

13. Angellier, H.; Putaux, J.-L.; Molina-Boisseau, S.; Dupeyre, D.; Dufresne, A., Starch nanocrystal fillers in an acrylic polymer matrix. Macromolecular Symposia **2005**, 221, (1), 95-104.

14. Wolfrom, M. L.; Thompson, A.; Timberlake, C. E., Comparative hydrolysis rates of the reducing disaccharides of D-glucopyranose. Cereal Chemistry **1963**, 40, (1), 82-86.

15. Angellier, H. Nanocristaux d'amidon de maïs cireux pour applications composites. Ph.D thesis University Joseph Fourier, Grenoble, France, **2005**.

16. Singh, V.; Ali, S. Z., Comparative Acid Modification of Various Starches. Starch/ Stärke **1987**, 39, (11), 402-405.

17. Wang, Y.-J.; Truong, V.-D.; Wang, L., Structures and rheological properties of corn starch as affected by acid hydrolysis. Carbohydrate Polymers **2003**, 52, (3), 327-333.

18. Angellier, H.; Choisnard, L.; Molina-Boisseau, S.; Ozil, P.; Dufresne, A., Optimization of the preparation of aqueous suspensions of waxy maize starch nanocrystals using a response surface methodology. Biomacromolecules **2004**, 5, 1545-1551.

19. Bai, W.; Holbery, J.; Li, K., A technique for production of nanocrystalline cellulose with a narrow size distribution. Cellulose **2009**, 16, (3), 455-465.

20. Biliaderis, C. G.; Grant, D. R.; Vose, J. R., Structural characterization of legume starches I. Studies on amylose, amylopectin, and beta-limit dextrins. Cereal Chem. 1981, 58, 496-502.

21. Robin, J.-P. Comportement du grain d'amidon à l'hydrolyse acide ménagée. Etude Physico-Chimique et Enzymatique de la fraction insoluble. Contribution a la connaissance de la structure de l'amylopectine. , Université Pierre et Marie Curie de Paris, Nancy, **1976**.

22. French, D., Organization of starch granules. In *Starch: Chemistry and Technology*, Whistler, R. L.; BeMiller, J. N.; Paschall, E. F., Eds. New York, USA, **1984**; p 183-247.

23. Zheng, H.; Ai, F.; Chang, P. R.; Huang, J.; Dufresne, A., Structure and properties of starch nanocrystal-reinforced soy protein plastics. Polymer Composites **2009**, 30, (4), 474-480.

24. Boyer, R. F., Modern Experimental Biochemistry. Benjamin Cummings: Redwood City, CA, **1993**.

25. Cheetham, N. W. H.; Tao, L., Variation in crystalline type with amylose content in maize starch granules: an X-ray powder diffraction study. Carbohydrate Polymers **1998**, 36, (4), 277-284.

26. Zetasizer nano Series User Manual. In Malvern Instruments Ltd: March **2005**; Vol. MANO317 Issue 2.2.

27. Katz, J. R., Abhandlungen zur physikalischen Chemie der Stärke und der Brotbereitung. Z. Phys. Chem. **1930**, 150, 37-59.

28. Gallant, D. J.; Bouchet, B.; Baldwin, P. M., Microscopy of starch: evidence of a new level of granule organization. Carbohydrate Polymers **1997**, 32, (3-4), 177-191.

29. Gallant, D. J.; Bouchet, B.; Buleon, A.; S. Perez, Physical Characteristics of Starch Granules and Susceptibility to Enzymatic Degradation. European Journal of Clinical Nutrition. **1992**, 46, S3–S16.

30. Gallant, D. J. Contribution à l'étude de la structure et de l'ultrastructure du grain d'amidon. PhD thesis University of Paris VI, Paris, France, **1974**.

31. Perry, P. A.; Donald, A. M., SANS study of the distribution of water within starch granules. International Journal of Biological Macromolecules **2000**, 28, (1), 31-39.

32. Tang, H.; Mitsunaga, T.; Kawamura, Y., Molecular arrangement in blocklets and starch granule architecture. Carbohydrate Polymers **2006**, 63, (4), 555-560.

Chapter 2-IV. Conclusions

In the present chapter, significant results concerning the impact of native starch source on final properties of ensuing SNCs were presented. The current production process was further characterized and conditions for using SNCs in industrial processes were clearly identified.

It was found that SNCs can be prepared from different starch sources without rendering substantial differences in morphology, rheological and thermal properties (contrary to cellulose nanocrystals). Yet, some moderate differences among SNCs were observed and their high amylopectin content was verified. This allows for potential discrimination (based on morphology, rheology and/or thermal stability) among sources depending on the given application, such as coating for barrier packaging (investigated in Chapter 4).

From a more fundamental point of view, the thermal properties of SNC have been extensively investigated and a mechanism has been postulated. It was confirmed from their melting temperature that SNCs correspond to native starches' crystallites and that they can be used at high temperature when dry. However, results also indicated heterogeneity in SNC's quality.

Thus, the SNCs suspension obtained with the current 5 days preparation process was characterized in terms of kinetics, yields and homogeneity. It was found that, indeed, SNC suspensions were made, at any time during the five-day preparation, of both micro and nano-particles. It was deduced that (i) the preparation process duration could possibly be further decreased to 1 day and/or that (ii) an isolation process, other than differential centrifugation, should be developed to obtain a new generation of SNCs. These two points will be investigated in Chapter 3.

Before using SNCs in nanocomposites or coating application (Chapter 4), next step (Chapter 3) will consist in developing several strategies for optimizing the SNC preparation process.

FIGURES

TABLES

CHAPTER 3.

SNC preparation process optimization

CHAPTER 3. SHORT SUMMARY

RESUME FRANÇAIS – FRENCH ABSTRACT

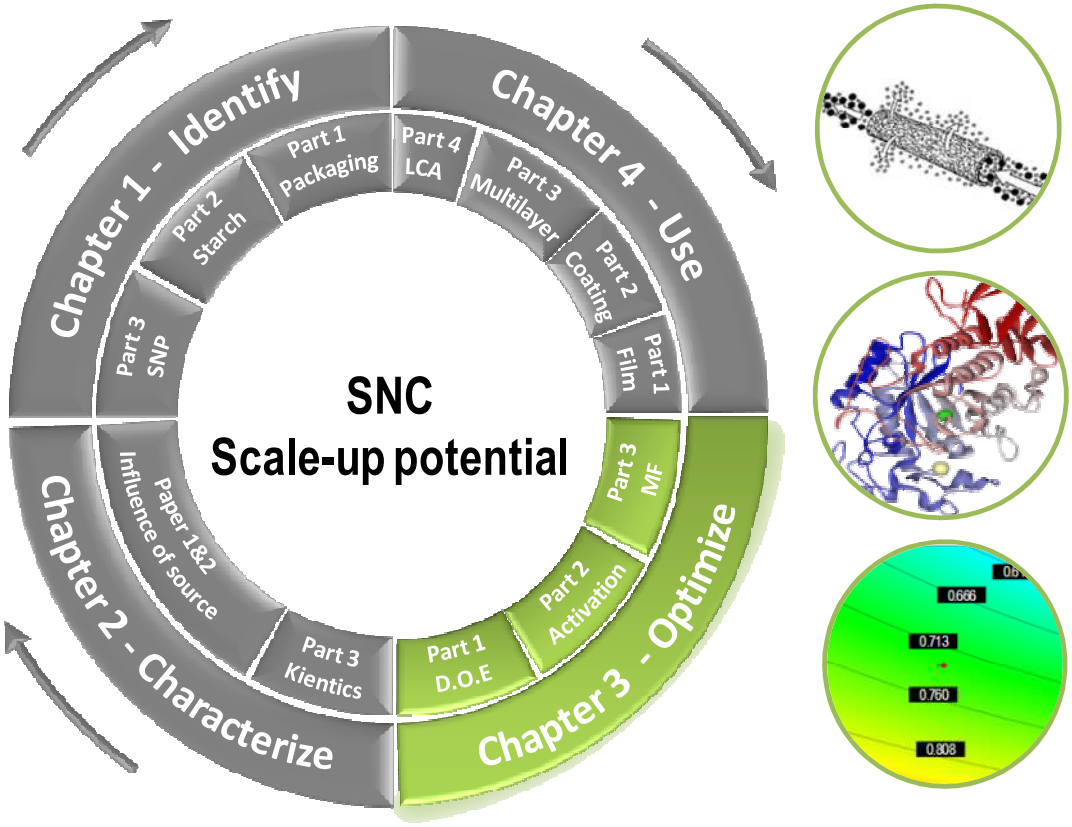

Figure 1. Représentation schématique de l'organisation du projet de thèse

Comme nous venons de le voir dans le chapitre précédant, les nanocristaux d'amidon peuvent être produit à partir de différentes sources d'amidon, sans observer de différences majeures de morphologie et de propriétés. Toutefois, de fines différences sont observées et peuvent permettre de choisir une source d'amidon plutôt qu'une autre pour une application donnée.

Par ailleurs, il a été mis en évidence que les suspensions de nanocristaux d'amidon obtenues classiquement par le procédé actuel de préparation par « batch » présentent une hétérogénéité conséquente. De plus, et malgré l'optimisation remarquable réalisée par Angellier et al. en 2004 (réduisant le temps de préparation de 40 à 5 jours), des limites pour une plus grande utilisation des nanocristaux d'amidon (SNCs) demeurent, comme notamment : (i) la durée de préparation, (ii) un faible rendement et (iii) l'hétérogénéité de la suspension ; d'où la nécessité de continuer à optimiser le procédé de préparation.

Dans ce Chapitre 3, **trois stratégies d'optimisation** du procédé de préparation des SNCs ont été développées en faisant varier à la fois les concentrations en acide, le temps de réaction et le procédé, comme présenté sur la Figure 2. Les deux premières visent essentiellement à diminuer le temps de préparation. A contrario, la troisième privilégie le rendement et l'homogénéité de la suspension.

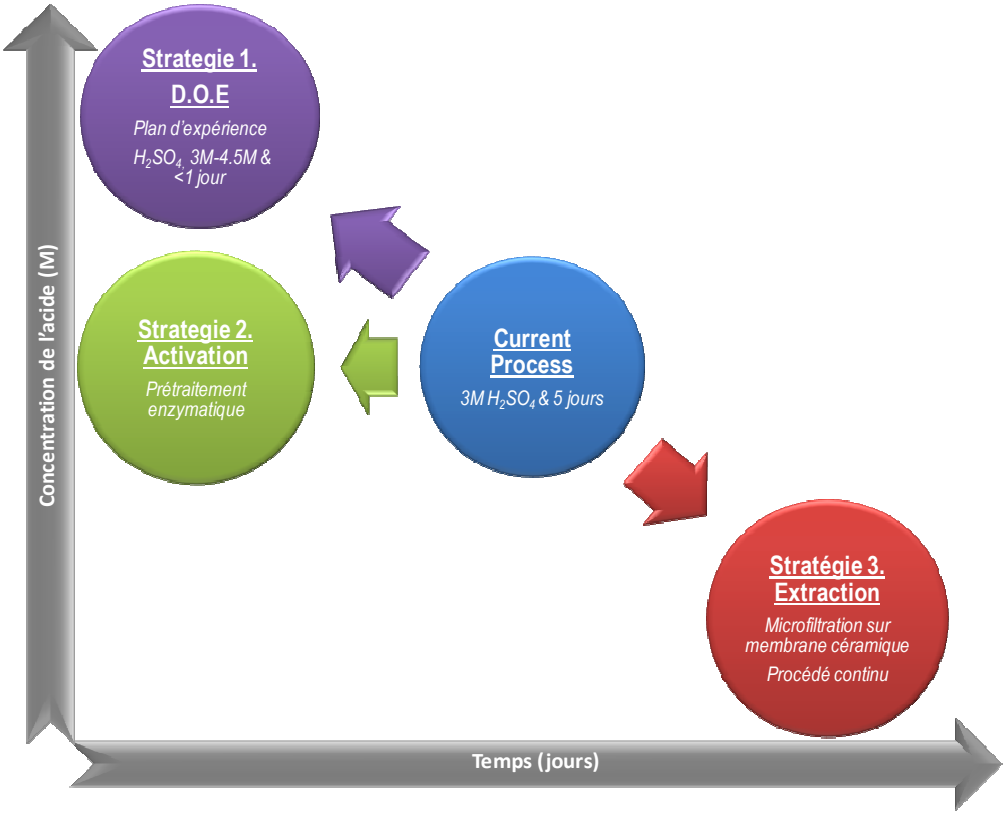

Figure 2. Représentation schématique des stratégies d'optimisation développées dans ce chapitre

La première stratégie, développée dans la première partie de ce chapitre, consiste à mettre en œuvre un plan d'expérience (Design of Experiment, D.O.E) pour un temps de préparation inférieur à 24h et des conditions expérimentales plus extrêmes, afin d'observer l'évolution des propriétés des suspensions obtenues.

La deuxième stratégie (Activation) consiste à évaluer l'intérêt d'un prétraitement enzymatique en vue de diminuer le temps d'hydrolyse acide avec les conditions expérimentales actuelles de préparation des nanocristaux d'amidon. Elle constitue la deuxième partie de ce chapitre.

La troisième stratégie (Extraction), exposée dans la dernière partie de ce chapitre, consiste à étudier la possibilité d'extraire en continu (et non en « batch »), par microfiltration, les nanocristaux d'amidon.

Dans chacune de ces parties, les nanocristaux de deuxième génération (plus petits et plus homogènes), qui ont été observés dans le chapitre précédent, sont étudiés plus en détail et constituent une cible pour l'optimisation. Ce sont les tout premiers travaux sur ce type de nanocristaux d'amidon.

Dans la **première partie**, nous avons donc mis en place un plan de 20 expériences permettant d'évaluer l'influence des quatre principaux paramètres expérimentaux (température, concentration de l'acide, durée d'hydrolyse et concentration en amidon) sur les propriétés finales des suspensions. Le domaine expérimental est délimité par une gamme de température limitée (25℃-40℃) ; une gamme de concentration en acide élevée (3M-4.5M) ; une gamme de temps très limitée (1h-15h) et une gamme de concentration en amidon allant des conditions actuelles à des conditions plus industrielles (15%-40%). Pour prendre en compte l'hétérogénéité constatée des suspensions de SNCs, les propriétés finales des suspensions (rendement et taille) ont été évaluées pour les suspensions hétérogènes obtenues classiquement (après une filtration très grossière, désignée F_1), ainsi que pour ces mêmes suspensions une fois filtrées sur une toile de maille 1µm, et donc plus homogènes (désignées F_2 ou SNCs de deuxième génération).

Avec plus d'une centaine d'analyses, l'étude donne des certitudes sur la présence des SNCs de seconde génération, leur taille, leur rendement mais traite aussi de la présence de groupements sulfate à leur surface influençant leur agrégation à l'état sec.

Toutefois, l'étude n'a pas permis de modéliser l'évolution de la taille des particules sur notre domaine expérimental. En effet, la taille des SNCs produits est plus ou moins la même quelles que soient les conditions expérimentales. Les filtrations influencent donc fortement la taille finale des particules, rendant le paramètre « taille » non pertinent.

L'étude a permis, en revanche, d'établir un modèle linéaire du premier ordre représentatif du rendement en SNC de 1ère génération ; mais aussi, pour la première fois, de celui des SNC de 2nde génération (F_2). Ce dernier est (i) plus prédictif que celui établit pour les suspensions de SNCs (F_1) et (ii) conduit à des résultats opposés. En effet, plus les conditions expérimentales sont extrêmes, plus le rendement F_1 diminue (car l'amidon est hydrolysé) mais plus le rendement F_2 augmente (les SNCs sont « libérés »). Dans notre domaine expérimental, les meilleurs rendements (autour de 6-7%) semblent être obtenus pour la plus haute température (40℃), la plus haute concentration en acide (4.5M), la durée la plus importante (15h) et la plus grande concentration en amidon (40%). L'étude confirme (i) que des SNCs peuvent être produits en moins de 15h et (ii) qu'il est nécessaire d'isoler les SNCs produits du reste de la suspension.

Par ailleurs, des recommandations sont faites pour le développement d'un modèle quadratique permettant de détecter l'optimum expérimental et d'en prédire le rendement.

L'étude précédente révèle notamment que l'utilisation d'acide plus concentré (c'est-à-dire d'une plus grande quantité d'acide) pourrait permettre de diminuer le temps de préparation des SNCs. Toutefois, l'utilisation d'acide concentré peut être plus problématique au niveau industriel et de plus, le temps de préparation reste élevé pour des rendements faibles. La **deuxième partie** de ce chapitre étudie donc la possibilité d'utiliser un prétraitement des amidons natifs moins néfaste pour l'environnement et largement disponible dans l'industrie de l'amidon : les enzymes. L'idée est de soumettre, avant l'hydrolyse classique, les grains d'amidon natifs à un prétraitement enzymatique qui les fragiliserait en les fragmentant ou en créant des chemins de diffusion plus rapides pour l'acide.
Pour cela, l'effet de trois type d'enzymes l'α-, la β- et la gluco-amylase, sur la porosité, la cristallinité et le taux d'hydrolyse des grains d'amidon a été étudié et optimisé. La cristallinité des grains prétraités reste la même que pour l'amidon natif, signifiant la non sélectivité des enzymes sélectionnées dans les conditions fixées. La gluco-amylase, qui permet d'obtenir les grains les plus microporeux, à été sélectionnée comme enzyme de prétraitement. Elle a permis de réduire de manière significative le temps d'hydrolyse des grains. Le rendement en suspension de SNCs, de 15% généralement obtenu en 5 jours (120h) est obtenu en 40-45h et celui de 30% correspondant à 24h d'hydrolyse est obtenu entre 2 et 6h. Ceci confirme la présence de chemins de diffusion préférentielle créés par le prétraitement enzymatique et l'analyse cristallographique prouve qu'il n'y a pas eu de « pré-gélatinisation » (modification de cristallinité) via ce prétraitement. Toutefois, même si le temps est plus court, le faible rendement reste un défaut péremptoire avant toute industrialisation.

C'est pourquoi la **troisième partie** de ce chapitre (Papier 5 – publié dans *Carbohydrate Polymers* – 2011), est basée sur des considérations plus industrielles. En effet, beaucoup de procédés industriels ne s'effectuent pas par « batch » mais plutôt en continu. La notion de durée d'hydrolyse devient donc moins contraignante si tant est que l'on puisse extraire au fur et à mesure de leur production les SNCs. Par ailleurs, nous disposons, à cette échelle, de procédés plus efficaces énergiquement. Après une étude en amidonnerie du procédé de production de l'amidon (détaillée au Chapitre 1), nous avons identifié (i) la possibilité de préparer des SNCs en l'intégrant au procédé actuel de production d'amidon et (ii) d'extraire des SNCs potentiellement produits lors de la

fabrication d'amidon modifié. Nous avons voulu tester la possibilité d'extraire par microfiltration les SNCs d'une suspension d'amidon après seulement 24h d'hydrolyse.
Pour cela une suspension de SNCs a été filtrée sur un pilote de microfiltration permettant (i) de tester 4 tailles de pores de membranes de filtration différentes (de 0.1µm à 0.8µm) et (ii) le potentiel de recirculation des SNCs. L'étude révèle que (i) peu de différences sont observées entre les différentes membranes de filtration et (ii) les particules isolées sont plus petites et plus cristallines que le reste de la suspension, quelque soit la taille des pores de la membrane.
Par conséquent, la microfiltration est un moyen efficace de séparer les SNCs de seconde génération des autres particules, puisqu'elle n'affecte pas (par contrainte mécanique) la cristallinité des SNCs. L'intérêt est que tout ceci peut se faire en continu, et que la partie non nano-cristalline peut continuer à produire des SNCs, ou peut être utilisée par ailleurs. Ces derniers points sont très importants car ils mettent au second plan la problématique de rendement et permettent d'envisager une industrialisation.

Etant donnée les perspectives de production à l'échelle pilote ou industrielle des SNCs en moins de 24h, des applications possibles de ces derniers dans des procédés industriels (tels que préparation de composites, couchage de papier, ou emballage multicouches) seront étudiés au Chapitre 4 suivant. Leur impact environnemental et leur potentielle toxicité seront également abordés.

Ce chapitre 3, propose des résultats importants sur les possibilités d'optimisation du procédé de préparation des SNCs de seconde génération. Il précise le mécanisme de « libération » des SNCs et confirme la possibilité des produire des SNCs en moins de 24h. Par ailleurs, il propose des solutions pour un passage à l'échelle semi-industrielle de la préparation des SNCs.

ENGLISH ABSTRACT – RÉSUMÉ ANGLAIS

In Chapter 2, it was demonstrated that different starch sources can be used for preparing SNCs without rendering substantial difference; and that they can be used in processes with temperature below 100℃-200℃ depend ing on hygrothermal conditions. Also, it proved that SNC suspensions contain both micro and nano-scaled particles, and that first SNCs appear at least after 24h. First results will be of importance when considering applications (in Chapter 4). The latter gives leads for the development of new preparation processes. Indeed, despite the great optimization already performed by Angellier et al., 2004 (which took the preparation time from 40 down to 5 days), the limited use of SNCs is partially explained by (i) the preparation duration, (ii) the low yield and (iii) the heterogeneity of the suspension.

Thus, in this Chapter 3, three strategies have been developed for the optimization of the preparation process. The first one consists in studying the evolution of the final SNC suspension properties when varying the process parameters over an experimental domain with more drastic conditions (i.e. more concentrated acid and shorter time) than the current process. The second strategy investigates the potential of enzymes to be used as pretreatment to reduce the current process's hydrolysis duration. The last one considers a continuous filtration process that would allow staying free from the duration constraint.

In the **first part**, we designed a set of 20 experiments to model the evolution of the SNCs suspensions' properties when varying main process parameters of a less-than-24h hydrolysis to take into account the heterogeneity of the suspension. The properties of the SNCs obtained from the SNC suspensions were also assessed. The modeling of the evolution of particle sizes was not possible. However, the evolution of the yield of the suspension (F_1) and that of the SNCs (F_2) were fitted with a linear model; and evolved in opposite direction. The intuitive assumption from previous studies was verified: the lower the yield of the suspension (i.e. the more hydrolyzed the suspension), the higher the yield of SNC (i.e. SNCs are "released). In our experimental domain (Acid concentration from 3M to 4.5M; temperature from 25°C to 40℃; duration of 1h to 15h and starch concentration from 15% to 40%), the highest yield for SNCs (about 6-7%) seemed to be obtained for the highest setting of parameters. Recommendations are made to assess more precisely (i.e. using a quadratic model) the optimum and its corresponding yield. The study brought out (i) an important result: SNCs can be

produced in less than 15h, and (ii) the necessity to extract SNCs from the bulk suspension.

The **second part** of this Chapter was dedicated to the study of three different enzymes as potential starch pretreatment for reducing the current preparation process duration. The effect of α-, β-, and gluco amylase on the porosity and crystallinity of the granular starch was assessed. Glucoamylase was selected as it rendered more porous granules and did not deteriorate starch crystallinity. Compared to non-treated starch, enzymatically-treated starches were hydrolyzed about 3 times faster. However, as for the first strategy, yields remained rather low.

Thus, the **third part** of this Chapter (Paper 5 – published in Carbohydrate Polymers – 2011) was based on more industrial considerations. Many industrial processes are continuous and not “batch-based” limiting the notion of preparation duration. After a quick study of the industrial processes developed in starch plants (presented in Chapter 1), we identified possible locations for the integration of a scaled-up continuous preparation process. As a result we studied the potential of microfiltration (using four different ceramic membranes from 0.1µm to 0.8µm) to isolate the SNCs already produced after 24h of hydrolysis from the bulk suspension. Microfiltration was proved efficient to isolate most crystalline particles (as proved by X-ray diffraction), no matter the membrane pore size; and recirculation was possible.

Giving the perspective to be able to prepare more homogeneous SNCs, at larger scale, potential industrial applications have been investigated in the next Chapter 4. Their environmental impact will also be assessed.

CHAPTER 3. SNC PREPARATION PROCESS OPTIMIZATION

Chapter 3-I Optimization of the batch preparation of starch nanocrystals to reach daily time-scale

Déborah Le Corre[1], Julien Bras[1], Luc Choisnard[2], Alain Dufresne[1]

[1]*The International School of Paper, Print Media and Biomaterials (Pagora), Grenoble Institute of Technology, BP 65 - F-38402 Saint Martin d'Hères Cedex, France*

[2]*Département de Pharmacologie Moléculaire, Université Joseph Fourier (DPM-UJF), 38240 Saint Martin d'Hères, France.*

Abstract

Current environmental concerns have turned starch nanocrystals (SNC) into candidates of growing interest as bio-nano-fillers for nanocomposite applications. However, despite previous drastic optimization, the main drawbacks for the more extensive use of SNC remain (i) the preparation duration (5 days) and (ii) their relatively low yield (15%). Also, the final suspension of SNC actually contains both nanocrystals and microparticles. Thus, previous study optimized the SNC suspension yield, rather than the SNC yield. As an attempt to (i) further limit preparation time to 1 day and (ii) increase the yield of SNC assessed after filtration (as opposed to that of the SNC suspension), a response surface methodology (RSM) analysis has been undertaken. The modeling of size and sulfate content was not possible. On the contrary, a linear model with first order interactions was postulated and allowed the modeling for SNC mass yields. The model used to fit the SNC yield of the filtered suspension (1µm) was more descriptive and predictive than that of the current poorly filtered suspension. Opposite effects for the same parameters have been evidenced. This confirmed the need to better isolate SNC, not only before use, but also for better modeling and optimization.

Keywords

Starch; Nanocrystals; Design of Experiment; Filtration; Yield

I.1. Introduction

Current environmental concerns have brought up together two important fields: (i) nanotechnologies with the development of innovative and efficient materials, and (ii) sustainable products with the use of renewable raw materials. In this perspective, starch nanocrystals (SNC) are candidates of growing interests[1, 2].

They are produced from starch, one of the most abundant, cheapest, renewable and biodegradable natural polymers available on earth. Granules (2-100µm) exhibit a semi-crystalline, multi-scale structure based on two structurally different polymers, namely amylopectin and amylose chains. [1, 3] It is believed that the crystalline regions are created by the intertwining of amylopectin side chains with a linear length above 10 glucose units to form double helixes[4] which are packed and form the crystallites. Thus SNC are crystalline nano-platelets obtained from the acid hydrolysis of amorphous starch and connecting points of amylopectin.

For the last decades, they have often been used as nano-fillers of polymeric materials to develop bio-nano-composites.[2, 5] Over the years, the preparation process has strongly evolved. Lintner[6] reported a 40 days hydrolysis process consisting of a 7.5% (w/v) HCl suspension of potato starch at 30-40°C to produce a high molecular weight starch suspension called “lintnerized starch”. In 1996, by analogy with cellulose whiskers, Dufresne et al.[7] reported a method for producing what they called at the time “microcrystalline starch” and which they reported to be agglomerated particles of a few tens of nanometers in diameters. The procedure consisted in hydrolyzing starch (5 wt%) in a 2.2N HCl suspension for 15 days.

Much more recently and with the objective of taking the preparation process down to 5 days, Angellier et al [8] developed an optimized process using response surface methodology. They showed it was possible to produce SNC with a yield of 15wt% after only 5 days of hydrolysis by using H_2SO_4 at 3.16M. Despite this outstanding time reduction, the main drawbacks for more extensive use of SNC remain (i) the preparation duration and (ii) the low yield. Further optimization is expected from the industries.

Furthermore, a recent study[9] shows that with current preparation process, the final suspension of SNC contains both nanocrystals and microparticles consisting of aggregates and non-fully hydrolyzed granules. Thus the current reported yields of SNC suspensions (measured by following the total solubilized carbohydrates content[10]; the viscosity of the resulting slurry with a Brabender Viscograph-E[11]or the percentage of dry weight of non solubilized particles as a percentage of initial dry starch[8]) are over estimated. It was suggested[9] that a filtration process could allow calculating a yield which would really reflect the amount of SNC (i.e. nano-scaled particles) in the final suspension.

The aim of the present study was to determine SNC's preparation parameters which would allow to: (i) limit preparation time to 1 day and (ii) increase the yield of SNC assessed after filtrations (as opposed to that of the SNC suspension).

Response surface methodology (RSM) was selected to reach this target. Indeed, RSM is largely used and well adapted to process optimization. It is a collection of statistical and mathematical tools used in the empirical study of relationships between one or more responses, or product characteristics, with a group of input variables. The main idea of RSM is to use a sequence of designed experiments (D.O.E) to (i) understand how the response changes in a given direction by adjusting the design variables (in general, the response-surface can be visualized graphically) and (ii) determine an optimal response.

In the present study, the main differences with previous work[8] are: (i) the investigated experimental domain (i.e. the higher setting of the process parameters) and (ii) the type of answers/results investigated (i.e. the yield of 1µm-filtered SNC and the sulfate percentage). This new process optimization should give clear answers to researchers and industrials for the optimization and scaling-up of the production of such innovative bionanoparticles.

I.2. Materials & Methods

I.2.1. Materials

Waxy maize starch (C☆Gel 04201, 98% amylopectin) was kindly provided by Cargill (Krefeld, Germany). Sulfuric acid (96%-99%, Sigma Aldrich) was used after dilution at 3.16M with distilled water. Deionized water was used all along the process.

I.2.2. Acid hydrolysis

A given weight of waxy maize native starch granules was mixed to 1L of previously prepared diluted sulfuric acid. The suspension was kept at constant temperature under 400 rpm mechanical stirring in a three-necked balloon twice the volume of the suspension, using a silicon oil bath. Different temperatures, acid concentrations, times and starch concentrations were used according to the matrix of experiment detailed later. The final suspensions were washed by successive centrifugation with distilled water until reaching neutral pH and redispersed using Ultra Turrax for 5 min at 13,000 rpm to break aggregates. The obtained suspensions were filtered on a filter tissue (40 µm, ref. 03-41/31 Buisine, France). Sodium azide was added to the suspensions before storage at 4℃ to avoid m icrobial growth.

I.2.3. Characterization

The **hydrolysis yields** were calculated as the dry weight of non solubilized particles as a percentage of initial starch's dry weight. The yield was calculated before any filtration and named "gross yield", after a coarse filtration (40µm) referred to as "**yield F1**", and after a fine filtration (1µm) referred to as "**yield F2**" in an attempt to distinguish respectively, unhydrolyzed starch shells, aggregates and micrometric particles, and nanometric particles.

$$Y\,(\%) = \frac{Weight\ of\ starch\ at\ a\ given\ time\ (g)}{Weight\ of\ initial\ native\ starch\ (g)}$$

Particle size measurements were performed at 25℃ with a commerc ial Zetasizer (Zetasizer NanoZS, Malvern, France). The particle radii were controlled by light scattering (DLS). For each measurement, a given volume of the suspension was injected in the Zetasizer cell right after 1 min homogenization with ultrasonic bath. Ultrasonic probe was not used to avoid possible gelatinization of SNC close to the tip. Size was measured after reaching stable values. The suspensions were characterized by the

mean particle size of a size distribution. All measurements were performed in, at least, triplicates.

The average dimensions of SNC after fine filtration (at 1µm) were studied using a Zeiss Ultra 55 Field Emission Gun Scanning Electron Microscope (**SEM-FEG**). A thin Au-Pd conductive coating (ab.1nm) was used to reduce charge effect. The best compromise in terms of starch nanocrystals contrast and residual charge was obtained at 10kV accelerating voltage and working distance of about 6mm. In order to obtain the best possible resolution, the secondary electron imaging mode with the In-lens detector was used. The average dimensions were determined using digital image analyses. Starch nanoparticles were assimilated to spherical particles. Between 70 and 500 measurements were performed depending on the source to determine the average diameter and standard deviation.

The **surface charge** of SNC particles was determined by conductimetric measurement. An aqueous NaOH solution (0.01 M) was added drop wise from a microburette with continuous stirring to five hundred milliliters of the suspensions (diluted to 0.1wt %). The change in conductivity was recorded by a conductimeter after each step. At equivalency, Eq.1 is verified:

$$V_{eq}.C_{NaOH} = n_{starch}.DS = \frac{m_{starch}}{M_{starch}}.DS \qquad \textbf{Eq.1}$$

with V_{eq} the known volume of dosed NaOH, C_{NaOH} the known concentration of NaOH (0.01M), n_{starch} the number of moles of glucose residues, m_{starch} the mass of SNC, M_{starch} the mean molecular weight of substituted glucose residues and DS the substitution degree.

The mean molar mass of substituted glucose can also be expressed as in Eq.2:

$$M_{starch} = (1 - DS).162 + 242\,DS \qquad \textbf{Eq.2}$$

The combining of Eq.1 and Eq.2 renders Eq.3 which allows the calculation of the mean molecular weight of substituted glucose and the ensuing DS:

$$M_{starch} = \frac{162}{\left(1 - 80.\left(\frac{V_{eq}C_{NaOH}}{m_{starch}}\right)\right)} \qquad \textbf{Eq.3}$$

The degree of substitution is then expressed as a "**sulfate percentage**" according to Eq.4 with $M_{sulfate}$=32g.mol^{-1}

$$\tau_S = \frac{32.DS}{M_{starch}} \qquad \textbf{Eq.4}$$

I.2.4. Modeling of the experiments

Parameters' setting are summarized in Table 3-I.1. They are the minimal, midrange and maximal values for each parameters which correspond to, respectively, the -1, 0 and +1 levels in terms of orthogonal variable x_i defined as Eq.5 and used to define the matrix of experiments:

$$x_i = \frac{2(p_i - p_{i,min})}{p_{i,max} - p_{i,min}} \qquad \textbf{Eq 5}$$

Table 3-I.1. Setting levels of Parameters p_1 to p_4

Parameters	Units	Low level x_i = -1	Mid. level x_i = 0	High level x_i = 1
p_1, temperature	°C	25.0	32.5	40.0
p_2, acid concentration	M	3.00	3.75	4.50
p_3, time	hours	1	8	15
p_4, starch concentration	g/100ml	15.0	27.5	40.0

A **model** taking into account the linear effects as well as the first order interactions was postulated. This model may be expressed in Eq.6 and requires estimating the coefficients b_i and b_{ij}:

$$R_k = b_0 + \sum_1^4 b_i x_i + \sum_1^4 b_{ij} x_{ij} \qquad \textbf{Eq 6.}$$

Experiments were conducted adopting a fractional factorial design 2^{4-1} (trials 1 to 8) and 2 replicates at the central point (trials 9 and 10, all coordinated equal to zero) as represented in the first part of Table 3-I.2. This model was later completed with face centers trials (trials 11 to 18, all coordinates equal to zero except one equal to +1 or -1) and two more replicates to form a central composite face design (CCFD). The CCFD allows to model quadratic interactions which will be discussed later.

Once the experiments were conducted, and the characterizations performed, the data were computed into the Design Expert 7.1.3 software for analysis.

I.2.5. Model Analysis

An ANalysis Of Variance (**ANOVA**) of the coefficients was performed. It is based on the breaking down of its total deviation (from the mean value), as presented in Figure 3-I.2, into: (i) a deviation due to the model's coefficient deviation (Regression deviation) and (ii) a deviation that cannot be modeled (Residual deviation). The latter represents the difference between the response measured experimentally and the response obtained from the model. The Residual deviation can further be decomposed into an Experimental deviation (lack of repeatability of the experiments) and an Adjustment deviation (lack of fit of the model), as represented in Figure 3-I.1.

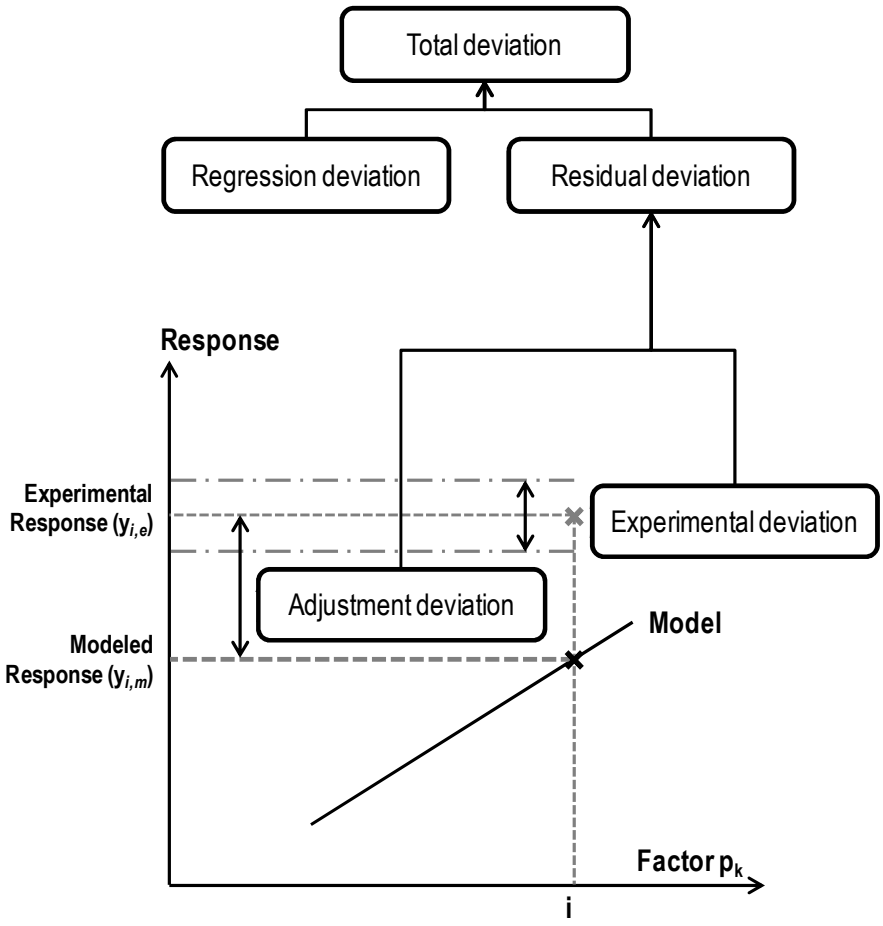

Figure 3-I.1. Deviation decomposition

For the model to be satisfactory, two conditions have to be verified: Condition 1 deals with the **model significance** and Condition 2 deals with **the lack of fit**. The regression deviation has to been significantly larger than the residual deviation: Regression deviation >> Residual deviation (Cond.1); and the lack of adjustment has to be negligible before the experimental deviation (pure error): Experimental deviation >> Adjustment deviation (Cond.2). To compare these deviations, their corresponding variances are assessed as described in Table 3-I.2.

Table 3-I.2. ANOVA parameters for the refining of model parameters

	Sum of squares	Degrees of liberty	Variance	Test
Total Deviation	$SS_{tot} = \sum_{i=1}^{n}(\eta_i - \bar{Y}_i)^2$	v_{tot} = n+n_0-1	$V_{Tot} = \frac{SS_{Tot}}{\upsilon_{Tot}}$	
Residual Deviation	$SS_{Res} = \sum_{i=1}^{n}(\eta_i - y_i)^2 = \sum_{i=1}^{n} e_i$	v_{Res} = n+n_0-r	$V_{Res} = \frac{SS_{Res}}{\upsilon_{Res}}$	F_1
Regression Deviation	$SS_{Reg} = SS_{tot} - SS_{Res}$	$v_{Reg} = v_{Tot} - v_{Res}$= r-1	$V_{Reg} = \frac{SS_{Reg}}{\upsilon_{Reg}}$	
Experimental Deviation	$SS_{Exp} = \sum_{i=1}^{n}\left(y_i^0 - \overline{y^0}\right)^2$	v_{Exp} = n_0-1	$V_{Exp} = \frac{SS_{Exp}}{\upsilon_{Exp}}$	
Adjustment deviation	$SS_{Adj} = SS_{Res} - SS_{Exp}$	$v_{Adj} = v_{Res} - v_{Exp}$ = n-r+1	$V_{Adj} = \frac{SS_{Adj}}{\upsilon_{Adj}}$	F_2

η_i: model predicted response; Y_i: experiments' mean response; e_i: error; y_0: response for replicate experiments
n: Total number of experiments, n_0: number of replicate, r: number of coefficient in the model

Comparison is done by postulating that measured deviations are distributed following a Laplace-Gauss distribution and using a Fisher test (F_k).

The first condition on the model's significance (Cond.1) is:

$$F_1 = \frac{V_{Reg}}{V_{Res}} \qquad \textbf{Eq.7}$$

A critical rejection threshold F_α determined by a Fischer-Snedecor table and considering a given probability α and the respective degree of freedom υ_{Reg} and υ_{Res}: $F_\alpha(\alpha, \upsilon_{Reg}, \upsilon_{Res})$.

If $F_1 \leq F_\alpha$: the model cannot explain for the total variance with a probability α.

If $F_1 > F_\alpha$: the model can effectively explain for the total variance with a probability α. The model is considered significant.

The second condition (Cond.2) assessing a possible "lack of fit" is tested with F_2:

$$F_2 = \frac{V_{Adj}}{V_{Exp}} \quad \textbf{Eq.8}$$

On the same principle, the lack of fit of the model (adjustment deviation) is negligible before the experimental error if $F_2 > F_\alpha$. In this study, α was set to 0.05 (i.e. 5%). The F_α-values, the model's and the lack of fit's significance were extracted from the software.

Combined to the ANOVA analysis, the **regression coefficient** R^2, the coefficient of determination R^2_{adj} and the **coefficient of prediction** Q^2 of the model are indicators (model's statistics) of the quality of the model and can be calculated as follow:

- $R^2 = \frac{SS_{Reg}}{SS_{Tot}} = \frac{SS_{Tot} - SS_{Res}}{SS_{Tot}}$ **Eq. 9**

- $R^2_{adj} = \frac{V_{Reg}}{V_{Tot}}$ **Eq. 10**

R^2 reflects the descriptive quality of the model i.e. how well the model fits the experimental data. R^2_{adj} is derived from R^2 and allows freeing this statistics from the influence of the number experiment undertaken and the number of variables used. A R^2>0.9 value indicates an excellent descriptive power: 90% of the response's variance is due to the choice of the linear model itself. For R^2<0.7, models have to be rejected.

- $Q^2 = \frac{SS_{Tot} - PRESS}{SS_{Tot}}$ **Eq. 11**

with PRESS, the Predicted Residual Error Sum of Squares

$PRESS = \sum_{i=1}^{n} (\eta'_i - y_i)^2$ and η'_i the model predicted response for yi obtained from the model taking into consideration all the responses except y_i and $\bar{Y}$, the model's mean response.

Q^2 reflects the predictive quality of the model i.e. how well the model will predict new data. A Q^2>0.7 value indicates an excellent predictive power. Ideally the difference between R^2 and Q^2 should be less than 0.2.

Once the model quality was assessed by ANOVA, the **significance of each parameter** was tested. A coefficient is deemed not significant when its absolute value is smaller than its confidence interval I_c determined as in Eq.12:

Eq.12

with t_α extracted from the Student table, giving a confidence interval of 95% (i.e. α=0.05) and s_i^2 the standard deviation of its residues as in Eq.13.

Eq.13

Once the model's quality and parameter's significance has been verified, the **curvature** of the model has to be assessed. Indeed, a curvature of the model is observed when a linear model cannot accurately predict the response of the experiment at the center of the tested domain (Figure 3-I.2). When postulating a linear model, the experiments used for modeling are conducted at the lower (-1) and higher (+1) settings of parameters (in this study, experiments 1 to 8). The center experiments (when all parameters are set to 0), are conducted to assess the experimental error but do not take part in the modeling. Thus, even though the model's quality can be high, the curvature of the model (i.e. the difference between the center experiments and the computed responses when all parameters are set to zero as presented in Figure 3-I.2) can be high.

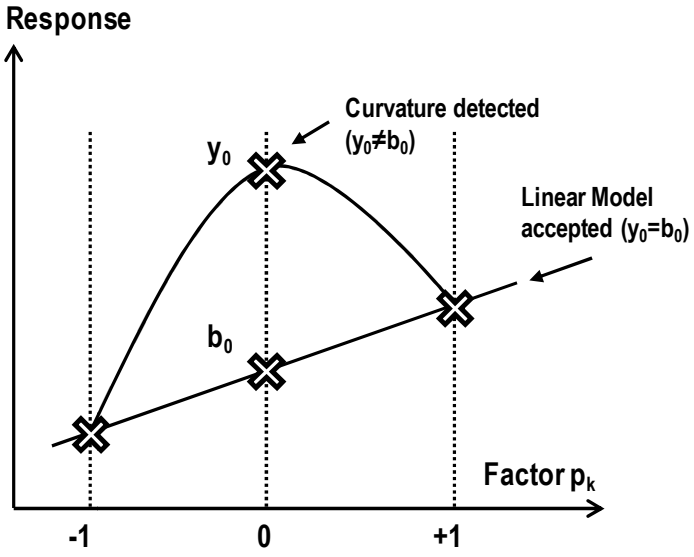

Figure 3-I.2. Schematic representation of the curvature of a modeled response.

The significance of this deviation (b_0-y_0) is calculated with the software and compared to the significance of the model. A high contribution of the curvature to the model indicates that the experiments would be better modeled by a quadratic model.

I.3. Results & Discussions

I.3.1. Process parameters' selection and corresponding results

Before setting up the parameters of our experiments, conclusions from Angellier et al.[8] were taken into account. The previous work identified the following process parameters as variables: hydrolysis duration, temperature, acid concentration, starch concentration and stirring speed. The results revealed that speed and starch concentration had no significant influence on final suspensions. Thus, in the present study, stirring speed was not selected as a process parameter and set to 400rpm. Starch concentration was kept as a parameter with the intent of setting higher concentrations closer to industrial one (i.e. 40wt%).

Moreover Angellier et al.'s[8] optimum conditions were close or identical to the higher setting level of parameters, the investigated hydrolysis conditions were, for the most, set to even more drastic conditions. Hydrolysis temperature was kept low to avoid starch melting and decomposition (giving the high acid concentrations used). Also, as only one interaction (of insignificant parameters) and one quadratic interaction were previously detected, a linear model was postulated.

Thus, four parameters were taken into account in the present study: the hydrolysis temperature p_1, the acid concentration p_2, the hydrolysis duration p_3 and the starch concentration p_4. The setting of these parameters followed an intuitive rule: if selecting a too narrow range, the optimal conditions have a lot of chance to be outside the studied region; and if choosing a too wide range, the model risks being poor. Table 3-I.1 summarizes the setting of each parameter.

Very recent study has shown that more homogeneous SNC could be obtained from the classically used SNC suspension.[9] Thus the present design of experiment was oriented towards the study of this "2nd generation" SNC.

This is why, the responses under study were of two kinds: (i) those representatives of the classic SNC suspension, such as (1) "yield $_{F1}$" and (2) the mean particle size d_{F1}; and (ii) those representatives of the nano-scaled particles: (3) "yield $_{F2}$", (4) the mean particle size d_{F2} and (5) the previously detailed sulfate percentage "$SO^{3-}{}_{F2}$".

The performed experiments (about 20) and corresponding measured responses (about 100 in triplicates) are gathered in Table 3-I.3.

Table 3-I.3. Matrix of experiment and results for the complete set of experimental points

		Trials #	p_1	p_2	p_3	p_4	Yield $_{F1}$ (%)	Size $_{F1}$ (nm)	Yield $_{F2}$ (%)	Size $_{F2}$ (nm)	Sulfate$_{F2}$ (%)
Block 1	Fractional factorial design	1	-1	-1	-1	-1	47,6	350	3,3	56	0,54
		2	+1	-1	-1	+1	43,7	357	3,8	92	0,48
		3	-1	+1	-1	+1	30,3	354	1,4	75	0,53
		4	+1	+1	-1	-1	76,3	330	5,0	81	0,18
		5	-1	-1	+1	+1	49,8	298	2,2	65	0,34
		6	+1	-1	+1	-1	63,0	300	2,4	57	0,22
		7	-1	+1	+1	-1	58,7	277	5,5	73	0,16
		8	+1	+1	+1	+1	51,1	172	7,6	64	0,14
	Rep.	9	0	0	0	0	86,7	550	1,9	147	2,28
		10	0	0	0	0	86,9	537	1,7	227	2,5
Block 2	Face centers	11	-1	0	0	0	87,8	390	1,3	-	0,92
		12	+1	0	0	0	68,0	439	7,4	-	0,33
		13	0	-1	0	0	81,6	225	3,7	-	5,12
		14	0	+1	0	0	70,7	378	4,4	-	2,44
		15	0	0	-1	0	91,4	395	0,4	-	4,64
		16	0	0	+1	0	75,6	249	4,5	-	0,45
		17	0	0	0	-1	68,0	260	3,8	-	1,63
		18	0	0	0	+1	77,2	261	5,2	-	7,3
	Rep.	19	0	0	0	0	87,5	236	2,0	-	3,43
		20	0	0	0	0	84,6	248	4,0	-	1,84

Important differences in size and yield are observed between SNC obtained after filtration F_1 at 40µm and SNC obtained after filtration F_2 at 1µm. These observations confirm, as recently published,[9] the presence of both micro and nano-scaled particles in classic SNC suspensions. Indeed, particles go from 500nm before filtration F_2 to under 100nm for the 2nd generation of SNC. Also, compared to previous study by Angellier et al.,[8] "yield$_{F1}$" responses are higher (from 30.3% to 91.4% instead of 2.1% to 76.3%) and "size$_{F1}$" are smaller (from 172 to 550nm instead of 6.45 to 13.4µm). The increase in mass yield is explained by the fact that the hydrolysis duration has been divided by 5. Thus more non-fully hydrolyzed amorphous starch is present in the final suspension. One could have expected measured particles size to be bigger as a consequence, but they are smaller. This could be explained by (i) the difference in measurement techniques which, in our study, involves sonication before measurements (i.e. breakage of aggregates), and (ii) because contrary to common belief, SNC are not produced "all at once" but seem to be rather "peeled off" continuously. Also, it is possible that micro-scaled particles settled during the measurement leading to underestimated sizes.

Also, sulfate content of SNC obtained after F_2 have been measured (as never reported). Results show that measured sulfate content are much higher than that reported[12] for a 3M sulfuric acid hydrolyzed suspension (0.03%), and correspond rather to values reported for non-filtered cellulose nanocrystals (NCC) (0.3%-0.7%).[12] Thus filtered individualized SNC should, as NCC do, be less susceptible to aggregation. Indeed, as observed in Figure 3-I.3, there is a clear difference in the aspect of the suspension filtered at 40µm (F_1) and the one filtered at 1µm (F_2). The latter has more of a cotton-like appearance after freeze-drying suggesting that particles are homogeneously smaller and better individualized.

Figure 3-I.3. Photographs of freeze-dried suspension from run #18 with filtration at 40µm (F_1) and filtration 1µm (F_2).

However, it seems that although some sulfate groups at the surface of SNC prevent aggregation, too many have an opposite effect (Figure 3-I.4). It seems that there is an optimum sulfate content (supposedly towards 0.14%) for which particles are better individualized. Indeed, when the acid concentration (used for the hydrolysis) is too low, few sulfate groups are created at the surface of SNC, and particles aggregate via H-bonds. On the contrary, when the acid concentration is too high, SNC might be partially oxidized or degraded (explaining the brownish color) and less H-bonds can be formed and create a cotton-like structure upon freeze-drying. Thus it seems that there is an "optimal" acid concentration for which SNC present enough surface sulfate groups to prevent aggregation, but not so much that they are degraded (dextrin).

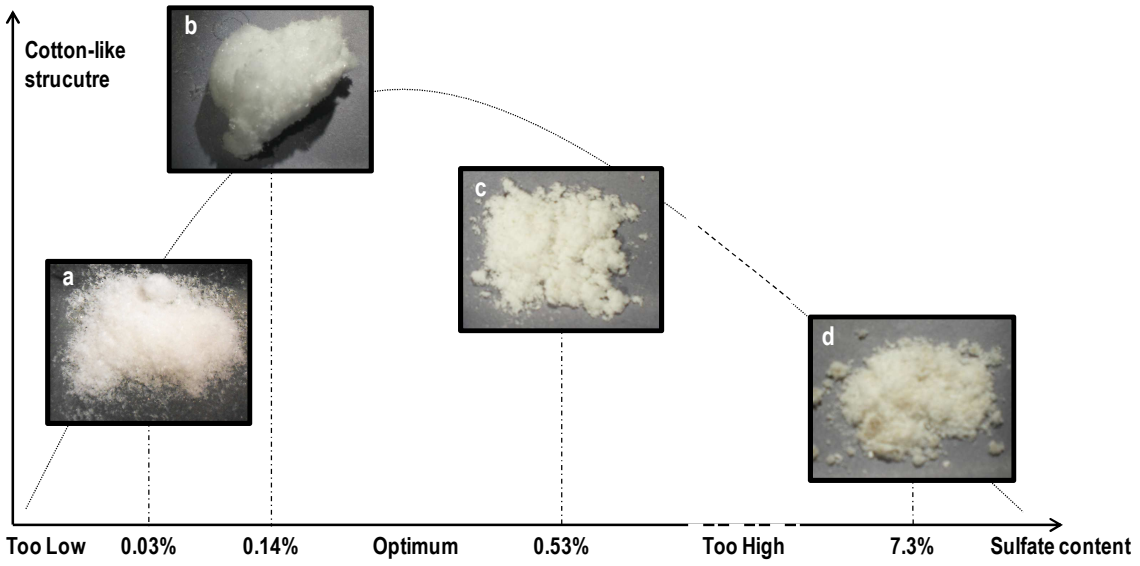

Figure 3-I.4. Photographs of freeze-dried suspension of F2 SNC with increasing sulfate content: (a) classic 5-days acid hydrolysis with 3.16M H2SO4 with sulfate content 0.03%[12] (b) run #8, (c) run #3 and (d) run #18.

I.3.2. Linear Model and Analysis

The responses were fitted with a multi-linear regression method (MLR) according to the linear model already presented (Eq.6). The analysis of raw data through the Box-Cox transformation showed that no response transformation was useful to improve the previously described model, considering a 0.95 confidence interval.

When a model comprises many factors (as it is the case here), a refining of the model is necessary as not all the coefficient are significant.[13] The most common refining method consists in excluding “step by step” the insignificant coefficients from the model as described in Figure 3-I.5.

A classical ANOVA of the coefficients was performed, and the model was refined using a backward step by step technique based on a 0.95 confidence level. Irrelevant parameters were excluded from the model to lower the risks of lack of fit.

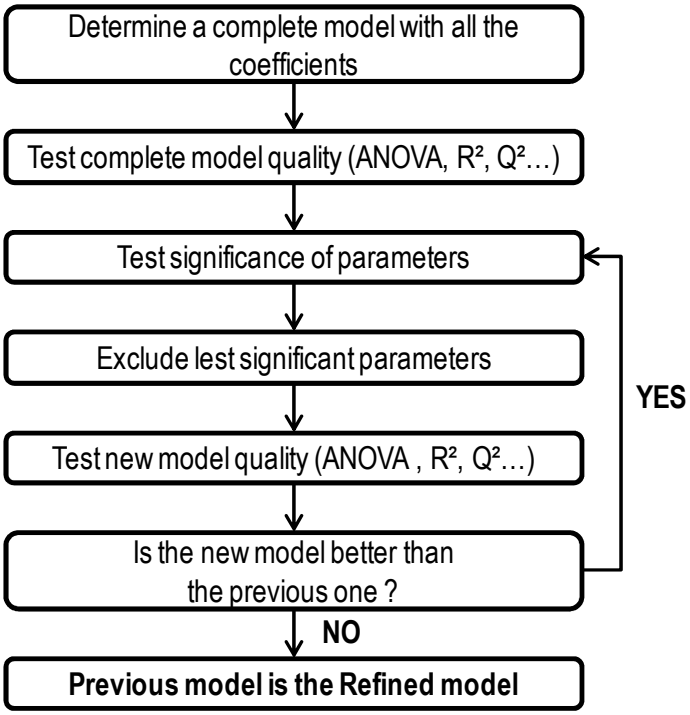

Figure 3-I.5. Model refining method with ANOVA: Analysis Of Variance; R^2 : regression coefficient and Q^2 : prediction coefficient.

The final refined models and their corresponding statistics (R^2, Q^2) are described below with x_1, x_2, x_3 and x_4 corresponding respectively to the temperature, acid concentration, time and starch concentration's orthogonal variables.

Response 1 – yield $_{F1}$

$$Y = 0.7305 - 0.0398x_1 - 0.0698x_2 - 0.1023x_3 + 0.0168x_1.x_2 - 0.0170\ x_1.x_3$$

R^2=0.995, R^2_{adj}=0.988, Q^2=0.929

As could be predicted from the previous study[8], the starch concentration parameter was excluded from the model as it did not have a significant influence. A slight influence of the curvature of the model was detected but contributed to less than 18% of the model. No lack of fit was detected. The probability of significance (p-value) of the model was superior to the critical value of 0.05 supporting its significance. However, parameters p_2 (acid concentration) and p_3 (time) were lower than 0.0008. These parameters were kept in the model according to the hierarchy principle. Indeed, their interaction coefficients with p_1 (temperature) were significant. The corresponding response surfaces have been drawn (Figure 3-I.6). They allow the impact of the two selected parameters to be illustrated by keeping the others at constant values.

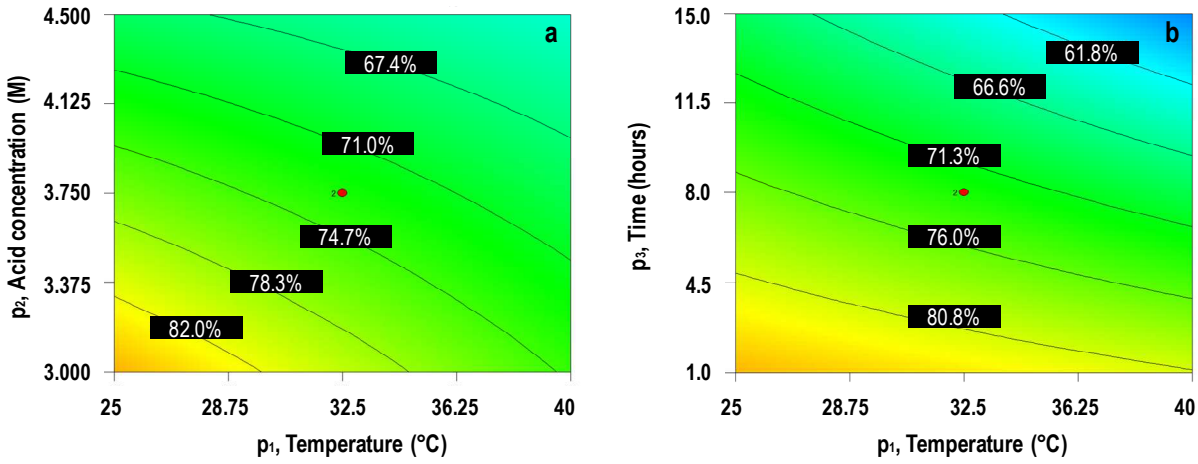

Figure 3-I.6. Response-surface plot and its contour plot of Yield F1: Temperature versus (a) Acid concentration at constant level of time (t=8h) and starch concentration (C=27.5g/100ml); and (b) versus time at constant acid concentration (C=3.75M) and starch concentration (C=27.5g/100ml).

It was fully expected that the interaction of temperature and acid concentration was an important parameter. This is why temperature was not set higher. As seen in Figure 3-I.6.a, the higher the temperature and the acid concentration, the lower the yield. However, the interaction of temperature with time was as important, as evidenced with the equation's coefficients: (x_1x_2) Vs. (x_1x_3). These interactions were not detected in the previous quadratic model[8]. The only first order interaction kept then was between starch concentration and stirring which were the least significant parameters.

Nevertheless, the response-surface plot and its contour plot of $yield_{F1}$ (at fixed acid concentration and starch content – Figure 6b) are comparable in tendency to that reported by Angellier et al.[8] The higher the temperature and time are, the lower the yield is. However, as already mentioned, yields are higher than for the previous study as time has been divided by a factor 5.

To summarize, results for $Yield_{F1}$ are very intuitive: the higher the temperature, the acid concentration and the time, the lower the yield. This is, as true on a 1-day scale as it was for a 9-days scale.[8]

Response 2 – Size $_{F1}$

$$Y = 304.75 - 15.00x_1 - 21.50x_2 - 43.00x_3$$

R^2=0.769, R^2_{adj}=0.630, Q^2=0.075

As could be expected, the starch concentration parameter p_4 was also excluded from the model as it was not significant. The R^2>0.7 indicates a good descriptive quality of the model, but Q^2 indicates that this model will not allow any prediction. Although, the modeling of the response showed no lack of fit, the contribution of curvature was very high (~78%) and thus significant. This indicates that a quadratic model would be better suited for concluding on the effects of direct factors. This is why no model and its corresponding surface-response are proposed here.

Response 3 – Yield $_{F2}$

$$Y = 0.0528 + 0.0108x_1 + 0.0196x_2 + 0.0125x_3 - 3.4875.10^{-3}x_4 + 5.7375.10^{-3}x_1.x_2 - 0.0149\ x_1.x_4$$

R^2=0.999, R^2_{adj}=0.997, Q^2=0.966

The linear model comprising all parameters was found to be very descriptive (R^2=0.999) and very predictive (Q^2=0.966), even more so than for $Yield_{F1}$. It indicates that the second filtration (1µm) allows to better isolate the SNC and thus has a more representative evolution of SNC production with parameters. The most significant parameter was p_4 (starch concentration) but most contribution came from p_2 (acid concentration), the interaction of p_1 and p_4 (temperature*starch concentration), p_3 (time) and p_1 (temperature) respectively. The corresponding response surfaces have been drawn in Figure 3-I.7.

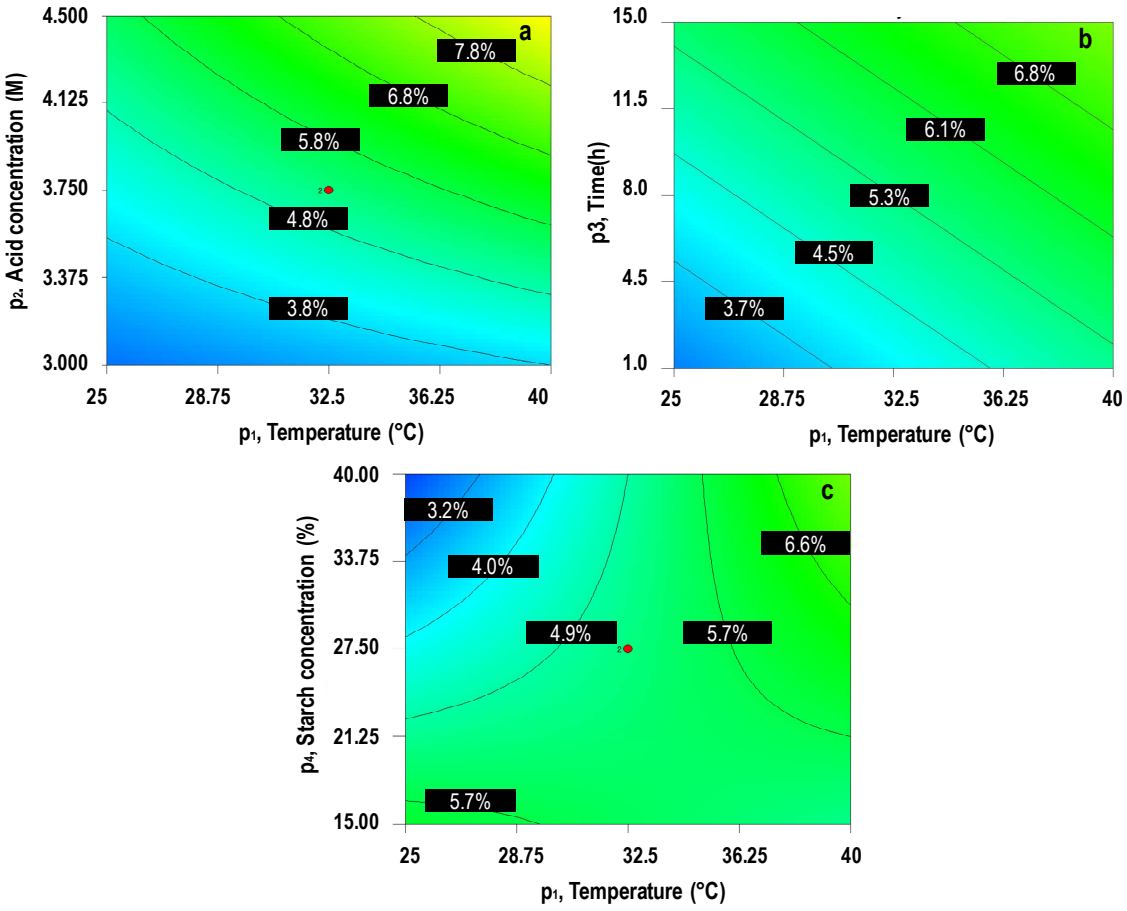

Figure 3-I.7. Response-surface plot and its contour plot of $Yield_{F2}$: Temperature versus (a) Acid concentration at constant starch concentration (C=27.5g/100ml) and time (8h), (b) Time at constant starch concentration (C=27.5g/100ml) and constant acid concentration (C=3.75M) and (c) starch concentration at constant acid concentration (C=3.75M) and time (8h).

The response-surface plots for "$yield_{F2}$" shows opposite trend compared to "$yield_{F1}$". It seems that the higer the temperature and the acid concentration, the higher the yield in nano-scaled SNC (Figure 3-I.7.a). Also, the higher the temperature and the time, the higher the yield (Figure 3-I.7.b). This is easily understandable. It seems that the more drastic the hydrolysis conditions, the more starch is hydrolyzed (i.e. "$yield_{F1}$" decreases) and the more SNC are "released" (i.e. "$yield_{F2}$" increases). However, when conditions are too drastic (e.g. 60°C and 4.5M), some SNC might be melted (as witnessed in unpublished preliminary study). Even if yields F_2 are quite low, these results are very promising. They show that 2^{nd} generation SNC can be produced in less than 15h, with a yield of about 6%. This correspond to the current amount of 2^{nd} generation SNC that can isolated from a classic five days hydrolysis, as reported elsewhere[9].

Finally, the weak influence of starch concentration is observed in Figure 3-I.7.c. It shows that at lower temperatures (below 30°C), an increase in starch concentration decreases the "yield$_{F2}$", whereas it has no influence at higher temperatures. This can be attributed to the fact that at ambiant temperature the hydrolysis reaction is not catalyzed and low amount of nano-scaled SNC are produced; whereas at higher temperatures where the hydrolysis is catalyzed, the starch concentration has little influence but the acid is still in excess.

No lack of fit was evidenced. However, the contribution of the curvature was still high (~20%) and indicates that a quadratic model could allow reaching better modeling. Indeed, the center experiments (when all parameters are set to 0), are conducted to assess the experimental error but do not take part in the modeling. Thus, even though the model's quality can be high (from boundaries), the curvature of the model (i.e. the difference between the experimental response from center experiments and the computed responses when all parameters are set to zero) can be high.

Response 4 – Size $_{F2}$

$$Y = 70.3750 + 3.1256x_1 + 2.8750x_2 - 5.6250x_3 + 3.6250x_4 - 3.8750x_1.x_2 - 7.3750\ x_1.x_3 + 0.8750\ x_1.x_4$$

R^2=0.000, R^2_{adj}=0.000, Q^2=-2.327

As evidenced by the nil values of R^2 and Q^2, the linear model was rejected for modeling response 4 (Size$_{F2}$). Indeed, with the postulated model, the curvature contributes to about 84% of the model. A quadratic model would be necessary to model this response and conclude on direct factors' effects.

Response 5 – Sulfate Content $_{F2}$

$$Y = 0.3237 - 0.1087x_3$$

R^2=0.411, R^2_{adj}=0.326, Q^2=-0.280

As for the previous response, the model's values of R^2 and Q^2 are very poor. The linear model comprising only one significant parameter (p_3, time) was rejected (not significant) for modeling response 5 (sulfate content$_{F2}$). With the postulated model, the curvature contributes to about 97% of the model. A quadratic model would be necessary to model this response and conclude on direct factors' effects.

I.3.3. Discussion of Responses

SNC's sizes and sulfate contents cannot be modeled by a simple linear model. This is not surprising as previous model from Angellier et al.,[8] showed some lack of fit for the particles size response. This could be attributed to the fact that, postulating a continuous release of SNC, starch granules render similar SNCs no matter the experimental conditions. Moreover, aggregates are most likely present and create ill-estimated results. Another artifact comes from the measurement techniques themselves. Indeed, DLS is a technique which can easily be disturbed by, sedimentation, aggregation of the particles and by their ill-defined shapes. FEG-SEM micrographs analysis suffers similar problems, as image analysis does not recognize aggregated particles and requires a high number of pictures to obtain a mean value.

Also, despite much higher setting of the starch concentration, the parameter was still not significant (except for the response $yield_{F2}$ for which it had a very little contribution at low temperatures), indicating that it does not impact the catalyst's action and thus that acid is still in large excess in the reactor.

On the contrary, it seems that SNC yields can be somewhat modeled by a linear model with even higher descriptive and predictive quality than with a quadratic model. Tendencies for classic multi-scale SNC (F_1) are similar to that of the previous study[8], whereas opposite trends are observed for nano-scaled 2nd generation SNC (F_2). The higher the acid concentration and the temperature, the higher the yield of F_2 SNC. This is explained as such: the more drastic the conditions, the more hydrolyzed is the granule (decrease of "$yield_{F1}$") and the more nano-scaled SNC are released (increase in "$yield_{F2}$"). However, for both models, the contribution of curvature for a linear model was quite high (~20%).

Thus it is most likely that a quadratic model would allow (i) better modeling of the reaction and (ii) finding optimum conditions, for obtaining the highest yields of F_2 SNC in the shortest time.

From the present experiments, it could be deduced that best parameters for producing 2nd generation SNC in less than a day would be: 40°C; 4.5M; 15h and 40% for respectively temperature, acid concentration, time and starch concentration.

I.3.4. Quadratic Model and Analysis.

For most responses, a quadratic model was recommended. Thus, the model should take into account the quadratic effects as well as the linear and first order interactions. The model was expressed as in Eq. (7) and requires estimating the coefficients b_i, b_{ij} and b_{ii}:

$$R_k = b_0 + \sum_1^4 b_i x_i + \sum_1^4 b_{ij} x_{ij} + \sum_1^4 b_{ii} x_{ii}^2 \qquad \text{Eq (7)}$$

To estimate these coefficients, the matrix of experiment was completed, with a second block, to design a CCFD as reported in Table 3.

The modeling of responses by the newly postulated model was very poor. As an example, Response 2's modeling ($Size_{F1}$) including all parameters, had a much lower p-value (not significant) and a lack of fit was evidenced. This was attributed to a strong experimental error comparable to variations induced by parameter setting (Cond. 1 not verified).

Indeed, when comparing responses for trials 9-10 and 19-20 which are all experiments at the center (replicates), large differences awere observed. The fact that center trials are replicable within one block of experiments but differ from one block to another indicates a "block effect". To confirm this point, the block effect was tested. The first set of experiment was tagged "block1" and the second set "block2". For Response 2, the block parameter showed very high variance superior to most parameters, confirming a block effect. Similar results were observed for other responses.

This block effect is generally attributed to either (i) non-controlled parameters during experiments or (ii) non-controlled parameters during analysis.

(i) In this study, all process parameters (such as stirring rotational speed, temperature, duration, acid concentration and starch concentration) were controlled. Thus, differences between the two blocks can only be attributed to external parameters such as: the season during which the experiments were conducted (summer vs. winter), the experimenters' touch (mostly during the critical step of filtration), the filter tissue quality, or the storage time before analysis (a mean of 3 months vs. 1 month).

(ii) As the block effect is evidenced with all answers (except $yield_{F1}$), it is tempting to reject the possibility of non-controlled parameter during analysis. However, several non-controlled parameters could explain for artefacts in all measurements. For example, one could argue that the previous study[8] was performed on a 5-day-stabilized system whereas it might not be the case after only 15h. Also, it has been demonstrated that results are better with 1µm-filtered (F_2) suspensions than with 40µm-filtered (F_1) ones, indicating a problem of heterogeneity or aggregation of the particles.

To conclude on the quadratic modeling of the batch preparation of SNC by acid hydrolysis, several more precautions should be undertaken to ensure that no block effect will lower the quality of the model.

I.4. Conclusion

As an attempt to establish a predictive model for the optimal parameters setting for preparing SNC in 1 day, a statistical experimental design and a multi-linear regression analysis were performed. A linear model with first order interactions was postulated and allowed the modeling of yields. The model used to fit the yield of the 1µm-filtered homogeneous suspension was more descriptive and predictive than that of the poorly 40µm-filtered one, and lead to opposite results. Thus it is most likely that an optimum can be found, at high parameter setting (such as 40℃ temperature;4.5M acid concentration; 15h duration and 40% starch concentration), for 2nd generation SNC's preparation in one day. This also confirms the need to better isolate SNC, not only before use, but also for modeling.

However, for all studied answers a strong contribution of the curvature indicated that a second order model would be better suited. Further experiments, performed to that intent, could not allow that modeling as they were performed as a second set, and thus induced a block effect. Before undertaking new trials, special attention should be brought to the study of identified external parameters. The effect of ambient temperature, storage time and order of introduction of the chemicals should be assessed. Also, all experiments should be performed as one set and in random fashion.

Nevertheless, this study brings clear information concerning the actual yield in SNC (F_2) as opposed to the suspension yield (F_1). For future trial, if the suspension is filtered (1µm), the (poorly modeled) particle size response could be left out of the model. Also the model could be simplified to concentrate on relevant parameters that are temperature, acid concentration and temperature, and relevant response that is the yield in F_2 SNC. Other interesting parameters to be tested could be the acid type and storage time, and an interesting response could be the suspension stability.

I.5. References

1. Le Corre, D.; Bras, J.; Dufresne, A., Starch nanoparticles: A review. *Biomacromolecules* **2010,** 11, (5), 1139-1153.

2. Lin, N.; Huang, J.; Chang, P. R.; Anderson, D. P.; Yu, J., Preparation, modification and application of starch nanocrystals in nanomaterials: A review. *J. Nanomater.* **2011,** 2011, 13.

3. Gallant, D. J.; Bouchet, B.; Baldwin, P. M., Microscopy of starch: evidence of a new level of granule organization. *Carbohydrate Polymers* **1997,** 32, (3-4), 177-191.

4. Oates, C. G., Towards an understanding of starch granule structure and hydrolysis. *Trends in Food Science & Technology* **1997,** 8, (11), 375-382.

5. Dufresne, A., Polysaccharide nano crystal reinforced nanocomposites. *Canadian Journal of Chemistry* **2008,** 86, 484-494.

6. Lintner, C. J., Studien über Diastase. *Journal für Praktische Chemie* **1886,** 34, 378-394.

7. Dufresne, A.; Cavaille, J.-Y.; Helbert, W., New Nanocomposite Materials:Microcrystalline Starch Reinforced Thermoplastic. *Macromolecules* **1996,** 29, (23), 7624-7626.

8. Angellier, H.; Choisnard, L.; Molina-Boisseau, S.; Ozil, P.; Dufresne, A., Optimization of the preparation of aqueous suspensions of waxy maize starch nanocrystals using a response surface methodology. *Biomacromolecules* **2004,** 5, 1545-1551.

9. LeCorre, D.; Bras, J.; Dufresne, A., Evidence of Micro- and Nanoscaled Particles during Starch Nanocrystals Preparation and Their Isolation. *Biomacromolecules* **2011,** 12, (8), 3039-3046.

10. Li, W.; Corke, H.; Beta, T., Kinetics of hydrolysis and changes in amylose content during preparation of microcrystalline starch from high-amylose maize starches. *Carbohydrate Polymers* **2007,** 69, (2), 398-405.

11. Wang, Y.-J.; Truong, V.-D.; Wang, L., Structures and rheological properties of corn starch as affected by acid hydrolysis. *Carbohydrate Polymers* **2003,** 52, (3), 327-333.

12. Angellier, H. Nanocristaux d'amidon de maïs cireux pour applications composites. *Ph.D thesis* University Joseph Fourier, Grenoble, France, **2005**.

13. Goupy, J., *Plans d'expériences pour surfaces de réponse*. Dunod ed.; **1999**; 409 p.

Chapter 3-II Enzymatic pre-treatment for preparing starch nanocrystals

Déborah LeCorre, Elina Vahanian, Alain Dufresne, Julien Bras

LGP2 – Laboratory of Pulp and Paper Sciences – 461, Rue de la Papeterie – BP 65 – 38402 Saint Martin d'Hères Cedex – France

Abstract

Starch nanocrystals (SNC) are crystalline platelet resulting from the acid hydrolysis of starch. A limiting factor for their more wide sprayed use is their preparation duration. Therefore, this study investigates the possibility of developing an enzymatic pre-treatment of starch to reduce the acid hydrolysis duration. A screening of three types of enzymes, namely α-amylase, β-amylase and gluco-amylase, is proposed and the latter was selected for a pre-treatment. Compared to the regular kinetics of hydrolysis for preparing SNC, that of pre-treated starch was much faster. The extent of hydrolysis normally reached in 24h was obtained after only 6h, and the regular final yield (15% after 5 days) was reached in 36h. AFM and X-ray diffraction measurements confirmed that the obtained nanoparticles were indeed SNC.

Keywords

Starch; nanocrystals; enzymes; hydrolysis;

Inspired from: *D. LeCorre, J. Bras, A. Dufresne, Biomacromolecules (**2011**), Submitted*

Paper 5

II.1. Introduction

For the last decade, starch nanocrystals (SNC) have attracted growing interest[1], due to their nano-scaled size but also to their renewable and biodegradable nature. SNC result from the hydrolysis of the amorphous parts of starch mainly by sulfuric acid. However, up to date, the optimized process for producing such SNC is still 5 day-long.[2] Thus it is needed to work on pre-treatments that could reduce the hydrolysis time. An ideal pre-treatment would break the granule or create holes through the granule; and allow, by that mean, for better acid diffusion through the granule.

The use of enzymes could be an answer as they are widely used and available industrially. The starch processing industry is in fact one of the largest segments of the industrial enzyme market. Applications include sweeteners production, bakery and anti-stalling, brewing and beverages, digestive aids, cyclodextrin for food and drug encapsulation [3]. Basically, starch transforming enzymes can be divided into two categories: the ones that hydrolyze glucosidic bonds, called amylases, and the ones that transfer them, called -transferases. Obviously, the first category (amylases) will be used in this study.

Amylases are often divided into 3 groups: *endo*-amylases, that cleave internal α(1,4) bond resulting in α-anomeric products; *exo*-amylases which cleave α(1,4) and α(1,6) from the non-reducing end resulting in α- or β- anomeric products; and *debranching* enzymes which include isoamylase and pullulanase which hydrolyze exclusively α(1,6) bonds leaving long linear polysaccharides.[3]

Enzymatic hydrolysis (using amylases) is mainly used to modify soluble starch properties such as viscosity and degree of depolymerization (DP). It is often though that they cannot hydrolyze insoluble native granules. However, as nature seldom offers animals and plants the luxury of cooked or molecularly dispersed food, they have developed enzymes that can digest uncooked granular starch.[4]

α-amylases, produced by many animals, are usually described as *endo* enzymes and can attack at any point (randomly) in the interior of a linear chain to completely reduce starch chain length. Kim and Lim (2008) reported[5] the fragmentation of waxy rice starch granules using α-amylases in 3 to 6h. The resulting fragments were assumed to be blocklets of the crystalline regions; and that the erosion of the amorphous region induced the fragmentation of the granules. Also, Valetudie et al.[6] studied the action of porcine pancreatic α-amylase on starch granules and found that the majority of the

digestion occurred in the amorphous regions whereas crystalline parts of the granules were only slightly digested.

Some plants and bacteria produced enzymes qualified as *exo* that remove sugar units from the non reducing end of a polymer. Some are more specific for a linkage type, such as β-amylase which hydrolyzes only one out of two α(1,4) and therefore is often used for starch analysis. [7] Others, such as glucoamylase from Aspergillus niger, can hydrolyze both α(1,4) and α(1,6). Using this last enzyme combined with ultrasound, Wu et al. prepared very recently[8] (2011) microporous starch from corn starch. Also, the amylase treatment did not seem to impact the granule's crystallinity.

Finally, as starch is the storage energy of many plants, many plants and bacteria contain *debranching* enzymes which break the α-1,6 bond in the amylopectin.[4] However, they mainly found intensive use in the determination of the fine structure of amylopectin, such as reported by Angellier-Coussy et al.(2010)[7] for the study of the molecular structure of SNC.

To our knowledge, no work on enzymatic hydrolysis pre-tratment for producing SNC has been reported. However, an attempt of using purely enzymatic hydrolysis has been reported by Kim and Lim.[5] It rendered 500nm-particles believed to be blocklets with a yield of 5-6%, as described in recent review on SNCs.[1] In our study, the strategy was different from the previous two.

The aim was to assess (i) if the pre-treatment of granular starch with enzymatic hydrolysis could reduce the current acidic preparation time of SNC; and ii) if one type of enzyme should be favored over another to create pathways without fully damaging the crystalline structure of starch. To this end, three amylases have been selected for this study, namely α-amylase, β-amylase and glucoamylase, which correspond to three different action mechanisms. Their kinetics of hydrolysis and ability to create pit holes at the surface of native granules has been assessed over a 2-hours period, before selecting one for a complete acid-hydrolysis of enzymatically pre-treated starch.

II.2. Materials & Methods

II.2.1. Materials

Waxy maize starch was kindly provided by Cargill (C☆Gel 04201, 98% amylopectin, Krefeld, Germany). α-amylase EC3.2.1.1 from porcine pancreas, β-amylase EC3.2.1.2 from barley and glucoamylase EC3.2.1.3 from Aspergillus Niger were purchased from Sigma Aldrich France. Sodium phosphate (Na_3PO_4) and sodium acetate (CH_3COONa at 0.2M) were purchased respectively from Rectapur, France and from Chimie Plus Laboratoires, France. Acetic acid ($C_2H_4O_2$ at 0.2M from Acros Organics France) and citric acid ($C_6H_8O_7$ at 0.5M, from Sigma Aldrich, France) were used diluted to adjust pH. Sodium hydroxide (from Roth France) and ethanol (>99% Chimie Plus Laboratoires, France) were used to stop the enzymatic hydrolysis. Sulfuric acid (96%-99%, Sigma Aldrich France) was used after dilution at 3.16M with distilled water.

II.2.2. Preparation of starch nanocrystals with acid

The optimized hydrolysis process developed by Angellier et al. [2] was adapted to 1L to prepare nanocrystals from the five different starches. Briefly, 147g of native starch was mixed with 1L of previously prepared diluted sulfuric acid (3.16M). The suspension was kept under 100 rpm mechanical stirring at 40℃, using a silicon bath, for 5 days. The final suspensions were washed by successive centrifugation with distilled water until reaching neutral pH and redispersed using Ultra Turrax for 5 min at 13,000 rpm to break aggregates. The obtained suspensions were filtered on a filter tissue (40 µm, ref. 03-41/31 Buisine, France). Sodium azide was added to the suspensions before storage at 4℃ to avoid microbial growth.

II.2.3. Starch pre-treatment with enzymes

Alpha amylases

α-amylase hydrolysis was adapted from Kim et al.[5] with modifications. The enzyme activity of the α-amylase form porcine pancreas was 21.6U/mg (ie. superior to that of Kim et al. 2008). Thus the amount of material used was adapted to keep the same activity/starch ratio (804U/g of starch) as described in Table 3-II.1.

The reference for the α-amylase pre-treatment is performed in the exact same conditions as for the pre-treatment (i.e. all the chemical are used), except that the enzymes are not added. All experiments were performed in triplicates.

Beta amylases

β-amylases hydrolysis was done according to Qian et al. [9] with modifications. The enzyme activity of the fungal β-amylase was 55.7 U/mg. Thus the amount of material used was adapted to keep the same activity/starch ratio as in Qian et al. (500U/g of starch) as described in Table 3-II.1.

The reference for the β-amylase pre-treatment is performed in the exact same conditions as for the pre-treatment (i.e. all the chemical are used), except that the enzymes are not added.

Glucoamylases

Glucoamylase hydrolysis was done according to Wu et al.[8] . First, the hydrolysis was performed without modifications, with activity/starch ratio of 125U/g, as presented in Table 3-II.1.Then, three other hydrolysis were performed with the same protocol but with changing starch concentration and thus enzyme activity per grams of starch. Changes can be summarized in Table 3-II.1. First, starch concentration was divided by two, which increased enzyme activity per gram of starch to 249U/g, then enzyme content was decreased to intermediate level with brought enzyme activity per gram of starch down to 70U/g, and finally to a low level of 15U/g.

The reference for the glucoamylase pre-treatment is performed in the exact same conditions as for the pre-treatment (i.e. all the chemical are used), except that the enzymes are not added.

II.2.4. Starch nanocrystals characterization

Filtration / Fractionnation

As described in a previous study[10], SNC suspensions contain starch particles of different sizes (micro- and nano-scaled). Thus filtrations have been performed on all tested suspension with a filtering fabric, and three types of suspensions can be distinguished: the non-filtered (referred to as G), the 40µm filtered ones (referred to as F_1), and the 1µm-filtered ones (referred to as F_2). They theorically correspond to a suspension containing respectively: (SNC, starch fragments and starch shell ghosts); (SNC and starch fragments), and (SNC).

Extent of Hydrolysis

In this paper, the yield (Y) refers to the dry weight of non solubilized particles as a percentage of initial starch's dry weight:

$$Y\,(\%) = \frac{Weight\ of\ starch\ at\ a\ given\ time\ (g)}{Weight\ of\ initial\ native\ starch\ (g)} \qquad (1)$$

The extent of hydrolysis thus refers to 1-Y(%), e.g. at t = 0, the extent of hydrolysis is 1-100% = 0%.

To assess the kinetics of each hydrolysis (acid, enzymatic, acid with enzymatic pre-treatment): samples were taken out at 2h, 4h, 6h, 22h and 24h; and for each sample the yield was assessed in triplicate.

Also, the yield calculated before any filtration was referred to as "Gross yield, Y_G", after the first filtration as "Yield, Y_{F1}", and after the second filtration as "Yield Y_{F2}".

Particle Size Measurements

For 40µm-filtered suspensions, particle size measurements were performed at 25℃ with a Cilas 1190 microsizer using the Fraunho fer measurement method. For 1µm-filtered suspensions, particle size measurements were performed at 25℃ and suspension concentration at 0.01wt%, with a commercial Zeta-sizer (Zetasizer NanoZS, Malvern, France). The particle radii were controlled by light scattering. A given volume of the tested suspension was injected in the cell after 30 s homogenization with ultrasonic bath. The size was measured after reaching stable values.

Degree of oil absorption[11]

DOA of microporous starch was determined using sunflower oil: 2.5mL of oil and 0.5g of dry microporous starch, designated W, were stirred by vortex (2000rpm) in a centrifuge tube for 5 min, settled for 20 min and then filtered. After the dripping of the oil has ceased, the amount of oil impregnated into the microporous starch, designated W_1, was weighted. The Degree of Oil Absorption was calculated as flow:

DOA (%) = $(W_1-W)/W*100$

Scanning Electron Microscopy

An environmental scanning electron microscope (ESEM) on a Quanta 200 FEI device (Everhart-Thornley Detector) was used at high voltage (10 kV) to confirm the morphology of native starches. Native starches were simply deposited onto carbon tape before observation.

X-Ray Diffraction

Wide angle X-ray diffraction analysis was performed on powder obtained from both native starch and air-dried SNC suspensions kept at ambient temperature (23℃) and relative humidity (28.8%). The samples were placed in a 2.5 mm deep cell and measurements were performed with a PANanalytical, X'Pert PRO MPD diffractometer equipped with a X'celerator detector. The operating conditions for the refractometer were: Copper Kα radiation, 2θ between 4 and 44°, step size 0.067°, counting time 90 s.

The degree of crystallinity of the samples was quantitatively estimated following the method adapted from Nara and Komiya[12], also called the "two-phase" method. A curve connecting the peaks baseline was plotted on the diffractogram. The area above the curve was assumed to correspond to the crystalline domains, and the lower area to the amorphous part. The ratio of upper area to total area was taken as the degree of crystallinity.

AFM

Atomic Force Microscopy measurements were performed on a Multimodal AFM (DI, Veeco, Instrumentation Group) with both tapping and conductive mode (C-AFM). The tips were Multi130 for tapping and MESP for C-AFM. A drop a SNC suspension was deposited on a mica substrate (split with adhesive tape) and dried for a few minutes at 40℃.

II.3. Results & Discussions

II.3.1. Enzymatic hydrolysis pre-treatment

Each enzyme was used for a 2h-enzymatic hydrolysis of waxy maize starch according to the following conditions (Table 3-II.1).

Table 3-II.1. Material used for enzymatic hydrolysis.

	α-amylase	β-amylase	γ-amylase 1	γ-amylase 2	γ-amylase 3	γ-amylase 4
Enzyme activity	21.6U/mg	55.7U/mg	300U/ml	300U/ml	300U/ml	300U/ml
pH	6.9	5.1	4	4	4	4.2
Temperature(°C)	37	55	40	40	40	40
Starch (%)	33.3g/L (1.7g/50ml)	333.33g/L (15g/45ml)	400g/L (20g/50ml)	200g/L (10g/50ml)	200g/L (10g/50ml)	200g/L (10g/50ml)
Buffer (ml)	50ml	45ml	50ml	50ml	50ml	50ml
Qté enzyme (mg)	61.8	134.6	8.3	8.3	2.3	0.5
U	1335	7500	2500	2490	700	150
U/g of starch	804	500	125	249	70	15

As the activity per grams of starch and the resulting extent of hydrolysis seemed quite low for glucoamylase[8] as compared to the protocol for the other enzymes, other conditions were developed and tested, as justified by the following results.

Extent of hydrolysis

Table 3-II.2 reports the yields before and after each filtration for the performed pretreatments.

Table 3-II.2. Calculated yields for 2h pre-treatments.

	Filtration	$Yield_G$ (%)	$Yield_{F1}$ (%)	$Yield_{F2}$ (%)
Ref.	γ-amylase	96 +/- 2	77 +/- 1	0.91 +/- 0.13
	α-amylase	126 +/- 27	68 +/- 21	0.13 +/- 0.05
	β-amylase	98 +/- 1	69 +/- 2	0.30 +/- 0.06
Enzymatic pretreatment	γ-amylase 1	84.2 +/- 6.5	59.5 +/- 5.7	0.51 +/- 0.13
	γ-amylase 2	80.3 +/- 1.9	61.7 +/- 1.1	0.37 +/- 0.54
	γ-amylase 3	71.1 +/- 0.2	51.8 +/- 1.2	0.45 +/- 0.32
	γ-amylase 4	58.6 +/- 0.9	41.8 +/- 0.4	0.56 +/- 0.05
	α-amylase	59 +/- 3	38 +/- 1	0.47 +/- 0.49
	β-amylase	65 +/- 1	40 +/- 1	0.04 +/- 0.03

Although enzymatic hydrolysis are performed in slightly acidic conditions, references (which include all acidic chemicals but the enzymes) show yields around 100%, indicating that no or very little acid hydrolysis occurs. Thus the 40% yield reductions after filtration at 40µm (F_1) of the reference samples indicate that granules readily swell (or aggregate) when immersed in the buffer suspension. Finally, yields after filtration at 1µm (F_2), indicated that some nanoparticles are produced by the process itself (possibly during stirring or by an "acidic" polishing of the granules' surface).

As mentioned earlier, for the glucoamylase hydrolysis, the activity per gram of starch seemed rather low and its corresponding yields (i.e. amount of non-hydrolyzed starch) higher than for α- and β-amylases. Therefore, another protocol was tested by divided the starch concentration by two and thus multiplying the activity per gram of starch. The yield of the resulting suspension (G) was slightly lower, but that of the suspension F_1 was slightly higher or equivalent, as reported in Figure 3-II.1. Also, scanning electron micrograph, presented in Figure 3-II.2, showed that the resulting granules were less porous. As a result, the opposite strategy was investigated. The enzyme concentration was drastically decreased, first to 70U/g and then to 15U/g. Results showed significantly lower yields and much more porous resulting granules. The final set of conditions (glucomylase 4) was selected for comparison with α- and β-amylases.

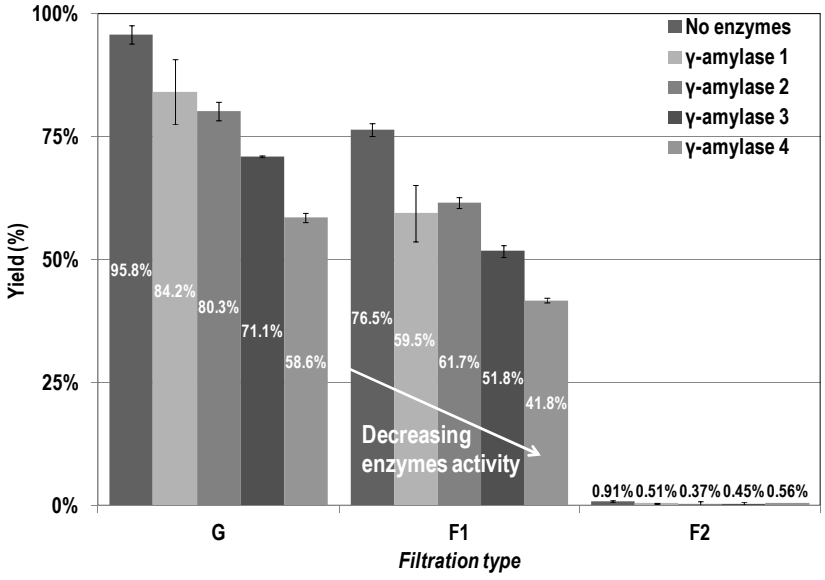

Figure 3-II.1. Yields of waxy maize starch after a 2h-glucoamylase-hydrolysis at different enzyme activity per gram of starch.

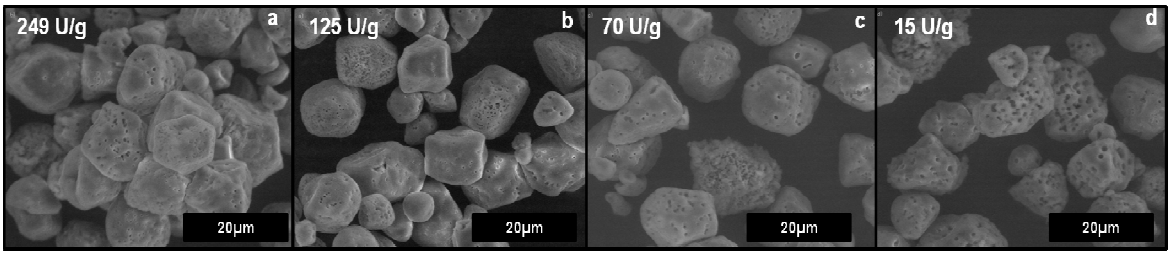

Figure 3-II.2. Scanning electron micrographs of waxy maize starch granules after a 2h-enzymatic hydrolysis pretreatment with glucoamylase with decreasing enzymes activity.

The yield of each 2h-enzymatically pretreated starch suspension was compared, as presented in Figure 3-II.3. For a given filtration, differences among yields were not significant. Also, it can be observed from the yield obtained after F_2 (Figure 3-II.3) that, as for their reference, the enzymatic hydrolysis do not seem to "produce" starch nanoparticles. Furthermore, the yields (G and F_1) indicates if the enzymes are active, but does not guaranty that the granules are made porous or are fragmented. Thus, a visual and porosity evaluation of the granules is necessary to discriminate the enzymes.

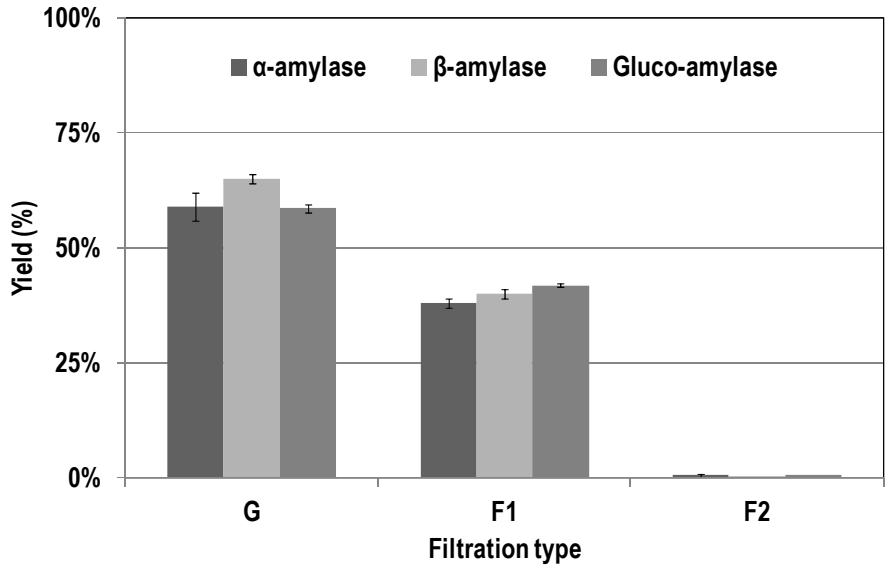

Figure 3-II.3. Comparison of hydrolysis yield(%) obtained by using different amylases, and after different filtrations.

Porosity of starch granules (SEM & DOA)

The pretreated granules were freeze dried for observation with a scanning electron microscope. Resulting micrographs are presented in Figure 3-II.4.

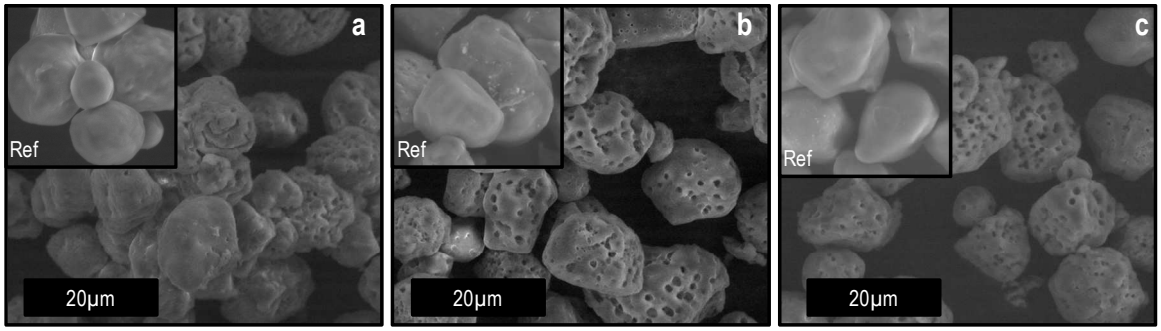

Figure 3-II.4. Scanning electron micrographs of waxy maize starch granules after a 2h-enzymatic hydrolysis pretreatment with (a) α-amylase, (b) β-amylase and (c) glucoamylase in optimal conditions.

Paper 5

It can be observed that α-amylase, despite its effectiveness in hydrolyzing waxy maize starch (as reflected in the lowest yields), renders less porous granules than β- and γ-amylases. β-amylase and γ-amylase seemed to render equally porous granules. The first one presents rather few and large pores, whereas the second presents numerous smaller pores. To discriminate between the two, a porosity test called Degree of Oil Absorption (DOA) test was undertaken as detailed in the experimental section. Results from Table 3-II.3 revealed that the DOA of α-amylase pretreated starches was indeed the lowest, whereas that of β-amylase pre-treated starches was higher and that of gluco-amylase pre-treated starches even higher.

Table 3-II.3. Percentages of porosity of granules hydrolyzed with α-amylase, β-amylase and gluco-amylase compared to a native starch granule as measured via their respective degree of oil absorption (DOA).

	DOA (%)
Native starch	3 ± 1
α-amylase pre-treated starch	43.3 ± 5.8
β-amylase pre-treated starch	48.0 ± 2.0
Gluco-amylase pre-treated starch	60.7 ± 5.8

Particle size analysis (Microsizer)

The mean particle sizes of the granules in suspension are displayed in Figure 3-II.5.

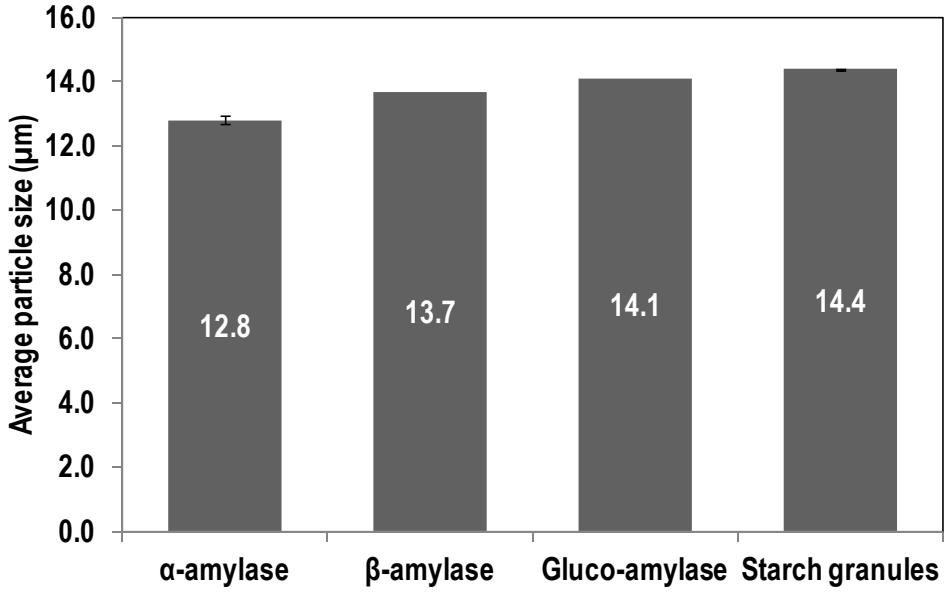

Figure 3-II.5. Average particule size in F1 suspension diluted to 0.01% after, respectively, α-amylase, β-amylase and gluco-amylase 2h-hydrolysis. Non hydrolyzed starch granules in suspension are added for comparison.

This information allows us to postulate the mechanism of each enzyme and the structure of the resulting granules. Indeed, α-amylase hydrolyzed granules are, at the same time, the least porous and the smallest. It suggests, as observed in Figure 3-II.4.a, that α-amylases hydrolyze the granule from the external layers in, thus reducing the size without creating much porosity. β-amylases exhibit intermediate size and porosity (Figure 3-II.4.b and Figure 3-II.5) and gluco-amylase highest size and porosity (Figure 3-II.4.c) and Figure 3-II.5). This suggests that both the selected exo-enzymes, not only attack the outer layers of the granules but also create channels through the granule. Gluco-amylases seem to create more channels than β-amylase, since resulting granules are more porous and remain slightly bigger. This might be due to the fact that gluco-amylase can hydrolyze different types of bonds contrary to β-amylase. However, the fact that gluco-amylase can hydrolyze α(1,6) bonds could be detrimental to the crystallinity of the resulting granule since they are characteristic of amylopectin chains. Thus the crystallinity of the granules after the 2h-hydrolysis with β-amylase and gluco-amylase pretreatment has been assessed.

Crystallinity of pre-treated starch (XRD)

An important property of the starch used for preparing SNC is its semi-crystallinity. Indeed, SNC correspond to the crystalline parts of a native starch granule, as detailed elsewhere [1]. Thus, it has to be verified that after the pre-treatment, the granules are still crystalline.

Figure 3-II.6 shows that the crystallinity of the starches which have been enzymatically hydrolyzed is comparable to that of the crystallinity of the native starch. So, despite the 45-55% gain in porosity, pre-treated granules have not lost their semi-crystalline nature. However, that also means that enzymes hydrolyze indifferently amorphous and crystalline starch. As a consequence, the amount of SNC that will be extracted from these granules will most likely be lower than that of un-treated granules. However, as recently presented[13], the current production process's yield (~15%) is below the theorical crystallinity of starch (~40%). This is partially attributed to the duration of the hydrolysis (5 days) which might lead to the hydrolysis of some SNC.

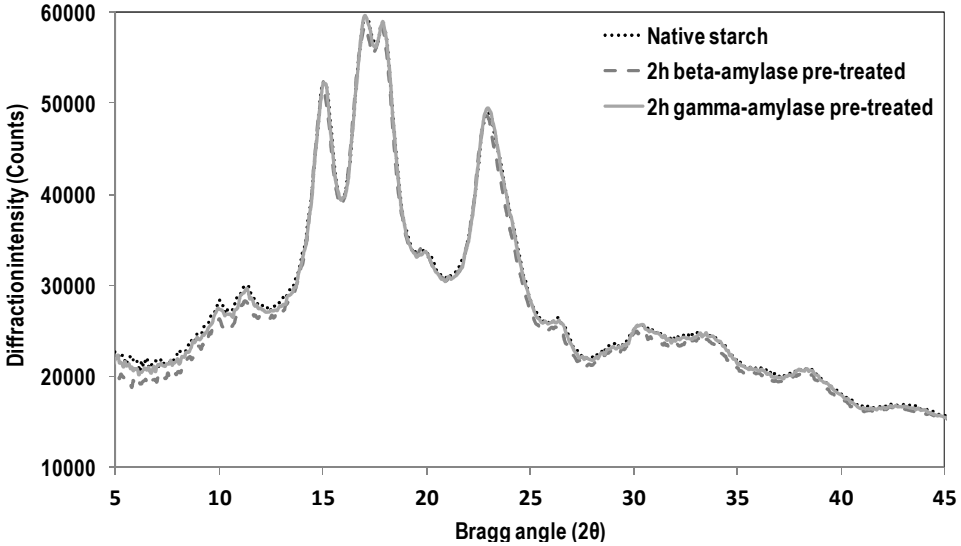

Figure 3-II.6. X-ray diffractogram of (a) native waxy maize starch, (b) starch pretreated with β-amylase and (c) with gluco-amylase.

Giving the previous analysis and corresponding results, summarized in Table 3-II.4, gluco-amylase was selected as an enzyme for pre-treating starch before the acid hydrolysis.

Table 3-II.4. Summary of properties of starch treated with a 2h-enzymatic hydrolysis

	Native starch	α-amylase	β-amylase	Gluco-amylase
Extent of hydrolysis (%)	0%	41% ± 3%	65% ± 1%	58.6% ± 0.9%
Porosity DOA(%)	3% ± 1%	43.3% ± 5.8%	48.0% ± 2.0%	60.7% ± 5.8%
Crystallinity (%)	34%	-	34%	34%

II.3.2. Effect of pre-treatment on the preparation of SNC's kinetics

The kinetics of hydrolysis of different starches has been previously reported [14-17]. It is agreed that the kinetics exhibits a multi-stage hydrolysis (two or three depending on authors) with a first rapid hydrolysis of the amorphous parts of starch, a second slower one corresponding to the hydrolysis of the amorphous starch of the semi-crystalline layers and a very slow one corresponding to the hydrolysis of the crystalline part. Most recently, the kinetics of preparation of SNC was investigated in detail[10] and revealed that, using the current 5-days preparation process, SNC appeared from the first day on. Thus it supported the fact that the first 24h of the hydrolysis correspond the hydrolysis of the amorphous growth rings of starch, and that afterward, SNC are progressively "released" into the suspension. However, the semi-crystalline lamellae being harder to hydrolyze, the hydrolysis rate slows down.

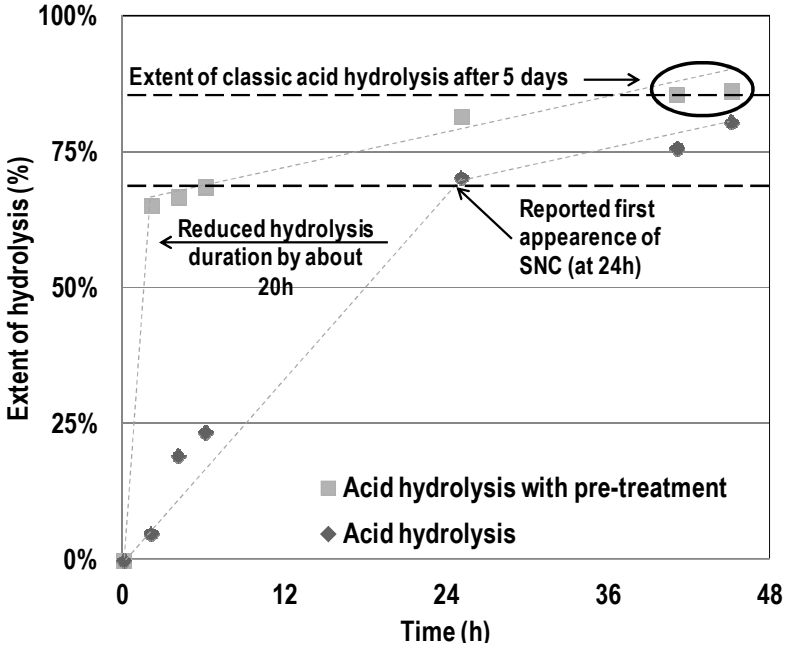

Figure 3-II.7. Kinetics of sulfuric acid hydrolysis of (♦) non-pretreated and (■) pretreated waxy maize starch.

The 5-days-acid-hydrolysis kinetics of waxy maize starch granules with (■) and without (♦) the 2h-glucoamylase pretreatment are compared in Figure 3-II.7. They both exhibit a two-stage kinetics. Although the rate of the second stage of hydrolysis is quite comparable for the pretreated and the non-pretreated starch, the rate of the first stage greatly differ. The pre-treated starch reaches the 24h extent of hydrolysis of the regular starch in only 2 to 6h (as materialized by the arrows in Figure 3-II.7). This suggests that the 2h-enzymatic pre-treatment has created efficient path-ways through the semi-crystalline granule which makes the amorphous starch more readily hydrolysable.

To confirm the postulated mechanism, AFM measurements of SNC suspensions were undertaken. They are presented in Figure 3-II.8. It can be observed that, as previously reported,[13] that some nanoparticles appear after 24h of acid hydrolysis (Figure 3-II.8.b). For the same extent of hydrolysis (about 70%), the pre-treated starch exhibits more numerous nanoparticles (Figure 3-II.8.a). However, they are larger (about 145nm) than those obtained after 24h of hydrolysis (usually between 50-100nm, here mean measurement is 68nm). Further hydrolysis allows reducing the particles size to more conventional sizes, as evidence from the micrograph of SNCs suspension obtained after 24h (Figure 3-II.8.c).

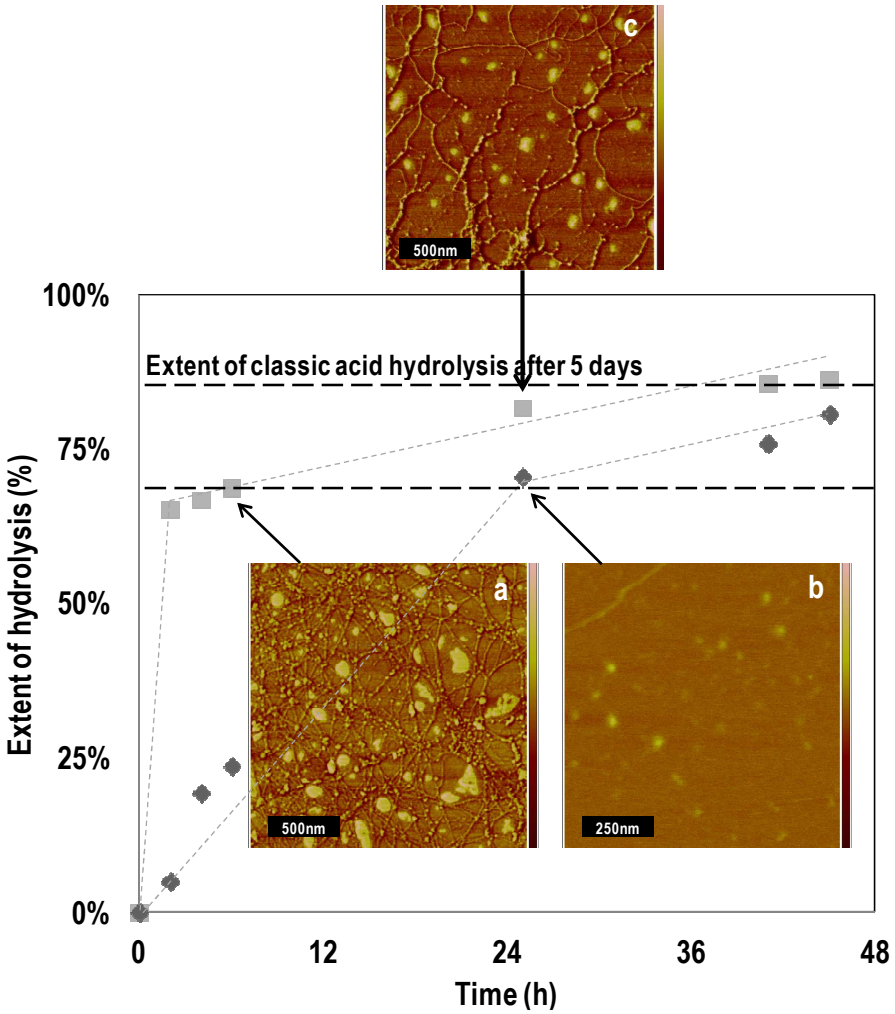

Figure 3-II.8. AFM measurement of (a) pretreated waxy maize starch after a 6h hydrolysis, (b) non-pretreated waxy maize starch after 25h and (c) pretreated starch after 25h.

First, X-ray measurements were conducted to assess the evolution of the crystallinity of pre-treated starch as a function of hydrolysis time, as presented in Figure 3-II.9. To be set free from the intensity differences due to the different amounts of material used for measurements and allow comparison, the strongest diffraction peak was attributed an intensity value of 100.

When analyzing X-ray diffractogram of starch, several methods can be considered. Most popular is the so called "two-phase method" originally developed for cellulose which assumes that relatively perfect crystalline domains (crystallites) are interspersed with amorphous regions. Thus crystallinity is calculated by subtracting the amorphous background. It underestimates crystallinity as it does not reflect the crystal-defect concept (according to which the scattering from the crystalline domains is diffuse and contributes to the amorphous background). As a consequence, a more accurate (and more time and resource-consuming) deconvolution method has recently[18] been developed for precise determination of crystallinity.

More scarcely, the peak height method developed by Segal et al.[19] and largely used for calculating cellulose's crystallinity index ($CrI=(I_{max}-I_{am})/I_{max}$), is used as a time-saving measurement for comparing the relative crystallinity of samples.

The diffractogram (Figure 3-II.9) shows a clear decrease of the amorphous background (Figure 3-II.9.a) and a consecutive increase in Segal et al.'s crystallinity Index with increasing time, suggesting a relative increase in crystallinity. This is further supported by an increase in peaks definition (Figure 3-II.9.b) with constant peak width, which results in an increase (of about 10%) in the two-phase crystallinity.

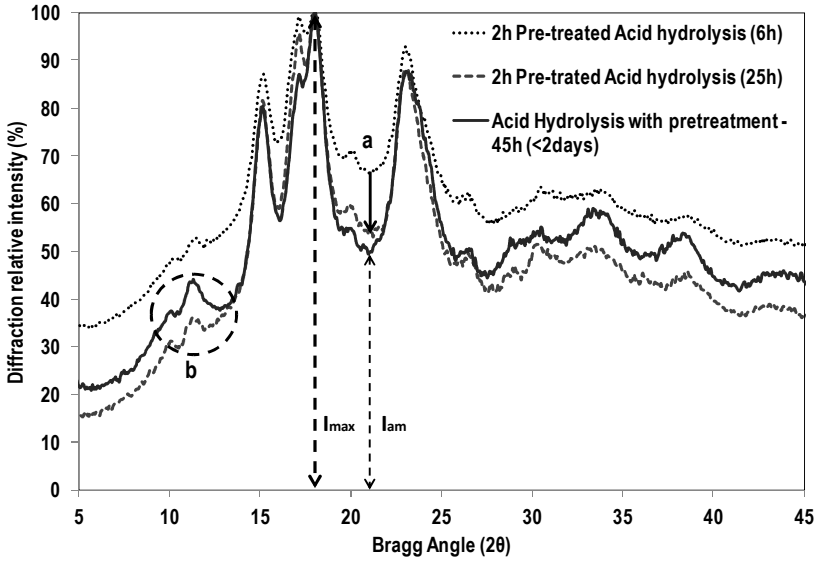

Figure 3-II.9. X-ray diffractogram of pre-treated starch for different hydrolysis time.

As a result, the crystallinity of the starch nanocrystals produced in 45h (circled in Figure 3-II.7) is compared to that of SNCs produced by a 5-days-acid hydrolysis. Figure 3-II.10 shows the diffractogram of each sample. Despite some differences at low angles, both types of SNCs show similar crystallinity index and similar peaks width. This indicates that SNCs produced in 45h present the same crystallites size and roughly the same or slightly lower crystallinity than those prepared in 120h.

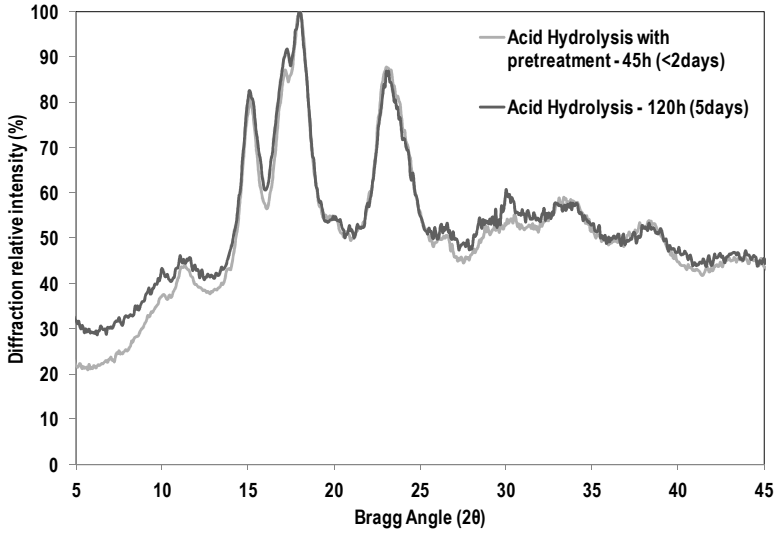

Figure 3-II.10. X-ray diffractogram of (a) pretreated waxy maize starch after a 41h hydrolysis and of (b) non-pretreated waxy maize starch after 5 days (120h).

Paper 5

Giving the previous results from kinetics, AFM and XRD, it is postulated that:

(i) First, the enzymatic pre-treatment creates porosity by hydrolyzing indifferently amorphous and crystalline starch.

(ii) As a consequence, the kinetics of the first stage of acid hydrolysis, which corresponds to the hydrolysis of the amorphous growth rings, is higher for pre-treated starch.

(iii) However, the kinetics of the second stages of hydrolysis, corresponding to the hydrolysis of the amorphous lamellae, are similar.

Thus, the study clearly shows that a 2h-glucoamylase-enzymatic pre-treatment can effectively decrease the preparation time of SNC by accelerating the hydrolysis of the amorphous growth rings. First appearance of nanoparticles occurs about 20h earlier, and regular final yield (15%) and SNC of small size are obtained after only 45h, instead of 5 days.

However, time reduction is limited by the rate of hydrolysis of the amorphous lamellae, which remains unchanged. Also, giving the hydrolyzing mechanism of the enzyme, it could be suggested that small differences observed at low diffraction angle are the reflection of some defective crystallites (due to prolonged enzymatic hydrolysis). It could also reflect a lack of acid hydrolysis duration. Thus perspectives for the optimization of the present process would consist in adjusting the duration of both the pre-treatment and the acid hydrolysis.

II.4. Conclusion

One limitation for the more widespread use and/or industrialization of starch nanocrystals (SNC) is related to its preparation time (5-days acid hydrolysis). Thus this study proposes an enzymatic pre-treatment of starch to reduce that time. It revealed that, among α- β- and gluco- amylases, the latter was most efficient for producing microporous starch while keeping intact the semi-crystalline structure of starch. With a 2 hours pre-treatment of waxy maize starch, the extent of acid hydrolysis currently reached in 24h and 120h (5days) were reached in only 6h and 45h respectively.

II.5. References

1. Le Corre, D.; Bras, J.; Dufresne, A., Starch nanoparticles: A review. *Biomacromolecules* **2010,** 11, (5), 1139-1153.

2. Angellier, H.; Choisnard, L.; Molina-Boisseau, S.; Ozil, P.; Dufresne, A., Optimization of the preparation of aqueous suspensions of waxy maize starch nanocrystals using a response surface methodology. *Biomacromolecules* **2004,** 5, 1545-1551.

3. Nitschke, M.; Bertolini, A. C.; Teixeira, M. A. V.; Garcia, C. F., Biopolymers on food technology: Production and applications of modified starches. In *Biopolymers technology*, Bertolini, A. C., Ed. Cultura Academia: São Paulo, **2007**.

4. French, D., Chemical and Physical Properties of Starch. *J. Anim Sci.* **1973,** 37, (4), 1048-1061.

5. Kim, J.-Y.; Park, D.-J.; Lim, S.-T., Fragmentation of Waxy Rice Starch Granules by Enzymatic Hydrolysis. *Cereal Chemistry* **2008,** 85, (2), 182-187.

6. Valetudie, J.-C.; Colonna, P.; Bouchet, B.; Gallant, D. J., Hydrolysis of Tropical Tuber Starches by Bacterial and Pancreatic α-Amylases. *Starch - Stärke* **1993,** 45, (8), 270-276.

7. Angellier-Coussy, H.; Putaux, J.-L.; Molina-Boisseau, S.; Dufresne, A.; Bertoft, E.; Perez, S., The molecular structure of waxy maize starch nanocrystals. *Carbohydrate Research* **2009,** 344, (12), 1558-1566.

8. Wu, Y.; Du, X.; Ge, H.; Lv, Z., Preparation of microporous starch by glucoamylase and ultrasound. *Starch - Stärke* **2011,** 63, (4), 217-225.

9. Qian, J.; Chen, X.; Ying, X.; Lv, B., Optimisation of porous starch preparation by ultrasonic pretreatment followed by enzymatic hydrolysis. *International Journal of Food Science & Technology* **2011,** 46, (1), 179-185.

10. LeCorre, D.; Bras, J.; Dufresne, A., Evidence of micro and nano-scaled particles during starch nanocrystals production and their isolation. *Biomacromolecules* **2011,** 12, (8), 3039-3046.

11. Yao, W. R.; Yao, H. Y., A new organic material for absorption - researches on porous starch (1) effect of enzyme and granular size on porous starch manufacture. *J. Chin. Cereals Oils Assoc.* **2001,** 16, 36-39.

12. Nara, S.; Komiya, T., Studies on the Relationship Between Water-satured State and Crystallinity by the Diffraction Method for Moistened Potato Starch. *Starch - Stärke* **1983,** 35, (12), 407-410.

13. LeCorre, D.; Bras, J.; Dufresne, A., Evidence of Micro- and Nanoscaled Particles during Starch Nanocrystals Preparation and Their Isolation. *Biomacromolecules* **2011,** 12, (8), 3039-3046.

14. Li, W.; Corke, H.; Beta, T., Kinetics of hydrolysis and changes in amylose content during preparation of microcrystalline starch from high-amylose maize starches. *Carbohydrate Polymers* **2007,** 69, (2), 398-405.

15. Jayakody, L.; Hoover, R., The effect of lintnerization on cereal starch granules. *Food Research International* **2002,** 35, (7), 665-680.

16. Robin, J.-P. Comportement du grain d'amidon à l'hydrolyse acide ménagée. Etude Physico-Chimique et Enzymatique de la fraction insoluble. Contribution a la connaissance de la structure de l'amylopectine. , Université Pierre et Marie Curie de Paris, Nancy, **1976**.

17. Angellier, H.; Putaux, J.-L.; Molina-Boisseau, S.; Dupeyre, D.; Dufresne, A., Starch nanocrystal fillers in an acrylic polymer matrix. *Macromolecular Symposia* **2005,** 221, (1), 95-104.

18. Lopez-Rubio, A.; Flanagan, B.M.; Gilbert, E.P.; Gidley, M.J., A novel approach for calculating starch crystallinity and its correlation with double helix content: a combined XRD and NMR study. *Biopolymers* **2008**, 89, (9), 761-768.

19. Segal, L. ; Creely, J.J. ;Martin A.E. Jr; Conrad C.M., An empirical method for estimating the degree of crystallinity of native cellulose using x-ray diffractometer. *Textile Research Journal* **1962**, 29, 786-794.

Chapter 3-III Ceramic membrane filtration for isolating starch nanocrystals

Déborah Le Corre, Julien Bras, Alain Dufresne

The International School of Paper, Print Media and Biomaterials (Pagora), Grenoble Institute of Technology, BP 65 - F-38402 Saint Martin d'Hères Cedex, France

Abstract

Starch nanocrystals (SNC) present different sizes (microscaled and nanoscaled) limiting their yield, process parameters and properties. Therefore, hydrolysate from wheat starch was filtered using a microfiltration unit equipped with ceramic membranes to assess the cross-flow membrane filtration potential of SNC suspension. Properties of feed, permeate and retentate were evaluated with dynamic light scattering, SEM, SEM-FEG and X-ray diffraction. Process parameters were also monitored. Achieved permeate flux was 306-510 $dm^3.h^{-1}.m^{-2}$ depending on membrane pore size and transmembrane pressure. Volume concentration ratio reached 13.7. Results show that microfiltration can be a promising solution to achieve separation of nanocrystals from non-fully hydrolyzed particles. No significant differences in final particles size were observed for all tested membranes. Analysis on permeate show not only that collected nanoparticles are more crystalline than feed, but also that mostly B-type particles are produced during the first day of hydrolysis. These very promising results completely change the way of thinking SNC preparation.

Keywords

Starch; Nanocrystals; Microfiltration; Membrane

Inspired from: *D. LeCorre, J. Bras, A. Dufresne, Carbohydrate Polymers* ***2011****, 86, (4), 1565-1572*

Paper 6

III.1. Introduction

These last decades an important concept has been brought up by scientists for the development of new products, i.e. the need for more efficient and less environmentally impacting materials. It has brought two scientific fields together: (i) nanotechnologies which allow the development of innovative and efficient materials, and (ii) biomaterials processing with the use of renewable raw materials for more environmentally friendly and sustainable solutions. Due to their semi-crystalline structure polysaccharides offer the opportunity to gather these two fields by producing bionanoparticles.

Starch nanocrystals (SNC) are candidates of growing interest. They are crystalline platelets resulting from the disruption of the semi-crystalline structure of starch granules by the hydrolysis of amorphous parts. Their preparation by acid hydrolysis has been optimized a few years ago[1] and very promising mechanical and barrier properties have been reported when used in nanocomposite applications[2-10]. For these reasons, SNC are being studied in details such as in a recent European Project (FlexPakRenew – FP7/2007-2013 - n° 207810) and reviews have recently been published[11, 12].

Main challenges for the development and use of SNC have only very recently been clearly identified. They are two-fold. The first one relates to the production scale. Indeed, the current protocol applies for producing small quantities of SNC (250mL) and renders a limited yield (10-15%) after a long production time (5 days). The second challenge deals with the hydrolysis of starch in relation with its onion-like structure. A very recent study[13] showed for the first time that resulting SNC suspension contains both micro and nanoparticles whatever the extent of hydrolysis. It was also proved that SNC were already present in the suspensions after only 24h hydrolysis.

An answer for overcoming these two issues would be to identify a process for extracting SNC during the hydrolysis process. First trials using differential centrifugation have been unsuccessful [13] leading to the need of investigation of a continuous extraction technique, viz. cross-flow membrane filtration. The aim is to assess the possibility of separating SNC from microparticles in a continuous flow.

Membrane separation processes driven by pressure, like microfiltration (MF) have aimed at the purification of diluted solutions with low concentration of solid and dissolved particles[14]. Ultrafiltration membranes, characterized by a mean pore size of 10^{-3} to 10^{-1} µm, find numerous applications nowadays. The starch industry for example pays great attention to the refinement of raw starch syrups after starch hydrolysis and to their wastewater treatment[15]. Also, in comparison with rotary vacuum filtration membrane processes were found more economical and more effective.[16-18] This statement led us to investigate the use of such processes to filtrate slightly bigger particles formerly known as starch hydrolysate insoluble residues and more recently identified as SNC suspension.

The idea was to check if the progressive "release" of SNC can be considered as an advantage to increase the production yield. Their continuous extraction during hydrolysis should strongly increase the quantity and the homogeneity of particles and could be a clear breakthrough in the field. To that purpose, cross-flow (tangential) filtration appeared most appropriate. Microfiltration membrane with pore size 10^{-1} to 1 µm and wheat starch, which hydrolysate has been reported to have much lower filtration rate[19], have been selected to assess the membrane filtration potential of SNC.

III.2. Materials & Methods

III.2.1. Materials

Wheat starch (Cerestar PT 20002) was kindly provided by Cargill (Krefeld, Germany). Theoretical amylose content was 28%. Sulfuric acid was purchased at 96%-99% purity from Sigma Aldrich and was used after dilution at 3.16M with distilled water.

III.2.2. Starch Nanocrystals Suspension

Wheat starch was hydrolyzed during one day, adapting the previously described optimized procedure [1] for producing SNC. Wheat starch (147g) was mixed with 1L of previously prepared diluted sulfuric acid (3M). The suspension was kept under 400 rpm mechanical stirring at 40°C, using a silicon oil bath for 5 days. The final suspension was washed by successive centrifugation *(Centrifuge 6K-15C, Sigma)* at 10,000 rpm (RCF = 16,211g) in distilled water until reaching neutral pH, and redispersed using Ultra Turrax for 5 min at 13,000 rpm to avoid aggregates. To provide sufficient amount (20L) for the pilot run, the final suspension was diluted. The final concentration was 0.5 wt %.

III.2.3. Microfiltration

A XLAB4 cross-flow pilot unit (Pall, France) was equipped with four ceramic membranes Membralox (Module T1-70) having mean pore size of 0.1, 0.2, 0.5 and 0.8 µm, as shown in Figure 3-III.1. The pilot was equipped with two parallel channels, each containing 2 membranes, the first one being submitted to higher pressure. After pre-trials performed in closed loop or recycled mode (VCF = 1) at transmembrane pressure (TMP) 60 and 100 kPa, filtration experiment was performed for the same TMPs but the permeate was collected for analysis. Cross-flow velocity was 5 $m.s^{-1}$. The pH was neutral or slightly acidic and temperature was 25°C .

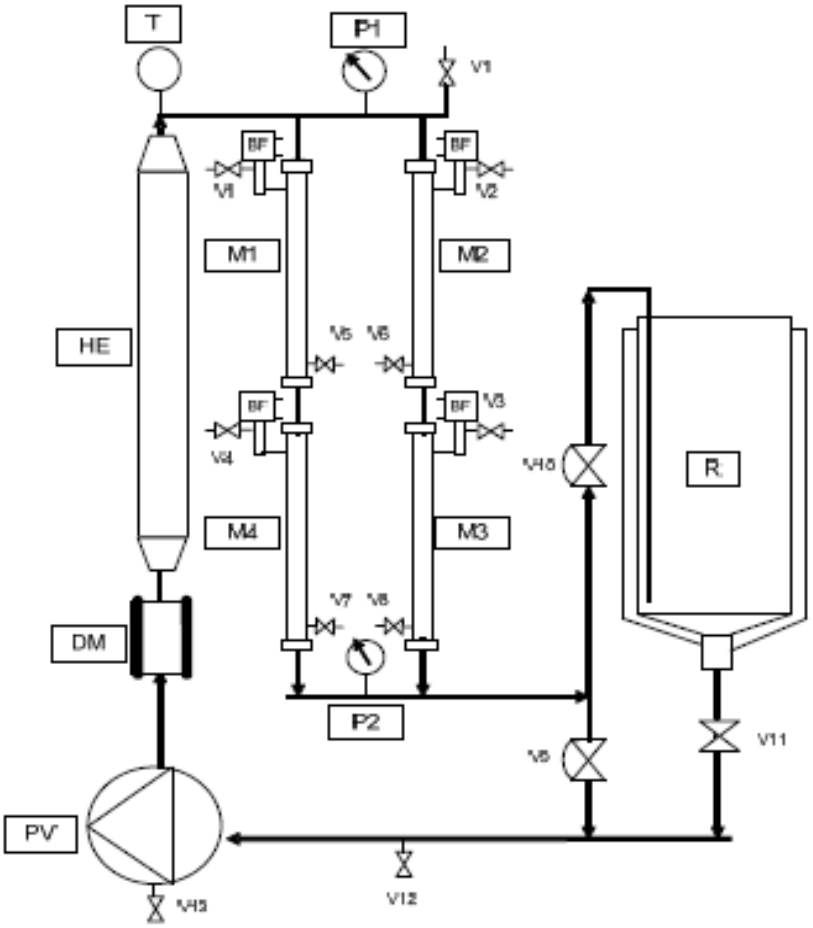

Figure 3-III.1. XLAB4 Pilot unit. M1: membrane 0.1 µm. M2: membrane 0.2 µm. M3: membrane 0.5 µm. M4: membrane 0.8 µm.

Paper 6

III.2.4. Filtration Parameters

The Volume Concentration Ratio (VCR) corresponds to the ratio of the feed volume to the volume of the retentate. It is commonly used in the industry to assess the concentration power of a filtration process. A VCR value of 1 implies that there was no concentration and hence the experiment was performed in total recycled mode [18]. In this study, VCR was assessed for the pilot containing the four membranes and not for each membrane.

The permeate flux ($J_{P,t}$) is expressed in $dm^3.h^{-1}.m^{-2}$ according to :

$$J_{P,t} = \frac{V_p}{A_f \times t} \quad (1)$$

where V_p is the volume of permeate (L), A_f is the filtration area (m^2) and t is time (h).

The reduction of permeate flux (ΔJ) is calculated from:

$$\Delta J = \frac{J_{P,0} - J_{P,t}}{J_{P,0}} \times 100 \quad (2)$$

where $J_{P,0}$ is the permeate flux at t = 0 s and $J_{P,t}$ is the permeate flux at time t.

The TransMembrane Pressure (TMP) is the pressure drop across the membrane. It is calculated according to :

$$TMP = \frac{P_f + P_r}{2} - P_p \quad (3)$$

with P_f, P_r and P_p being the feed, retentate and permeate pressure, respectively [20]. The membrane fouling model parameters, k and J_{ss}, correspond to the fouling rate and the steady state permeate flux, respectively, both expressed in $L.h^{-1}.m^{-2}$. They can be calculated by fitting experimental values to Equation:

$$J_{p,t} = J_{ss} + k.t^{-1} \quad (4)$$

Paper 6

III.2.5. Microscopies

An environmental scanning electron microscopy (ESEM) on a Quanta 200 FEI device (Everhart-Thornley Detector) was used at high voltage (10 kV) to access the morphology of native starches. Native starches were simply deposited onto carbon tape before observation.

SNC' mean size and morphology were studied using a Zeiss Ultra 55 Field Emission Gun Scanning Electron Microscope (FEG-SEM). A thin Au-Pd conductive coating (ab.1nm) was performed to reduce charge effect. The images obtained at 10 kV accelerating voltage and working distance of 8 to 10 mm lead to the best compromise in terms of SNC contrast and residual charge effect. In order to obtain the best possible resolution, the secondary electron imaging mode with the In-lens detector was used.

III.2.6. Particle Size Measurements

Particle size measurements were performed at 25°C with a commercial Zeta-sizer (Zetasizer NanoZS, Malvern, France). The particle radii were controlled by light scattering. For each measurement, the suspension was diluted to a concentration of 0.01 wt%. Then a given volume of the diluted solution was injected in the Zetasizer cell after 30 s homogenization with ultrasonic bath. The size was measured after reaching stable values.

III.2.7. X-Ray Diffraction

The wide angle X-ray diffraction analysis was performed on powders obtained from either native starch or air-dried SNC suspensions conditioned at temperate conditions (23°C, 50% RH). Measurements were then carried out at room temperature (23°C) and relative humidity (28.8%). The samples were placed in a 2.5 mm deep cell and measurements were performed with a PANanalytical, X'Pert PRO MPD diffractometer equipped with an X'celerator detector. The operating conditions for the refractometer were: Copper Kα radiation, 2θ between 4 and 44°, step size 0.067°, and counting time 90 s.

III.3. Results & Discussions

III.3.1. Filtration Process

The main objective of this experiment was to extract SNC from the hydrolysate suspensions as soon as they are produced. Figure 3-III.2 summarizes this strategy.

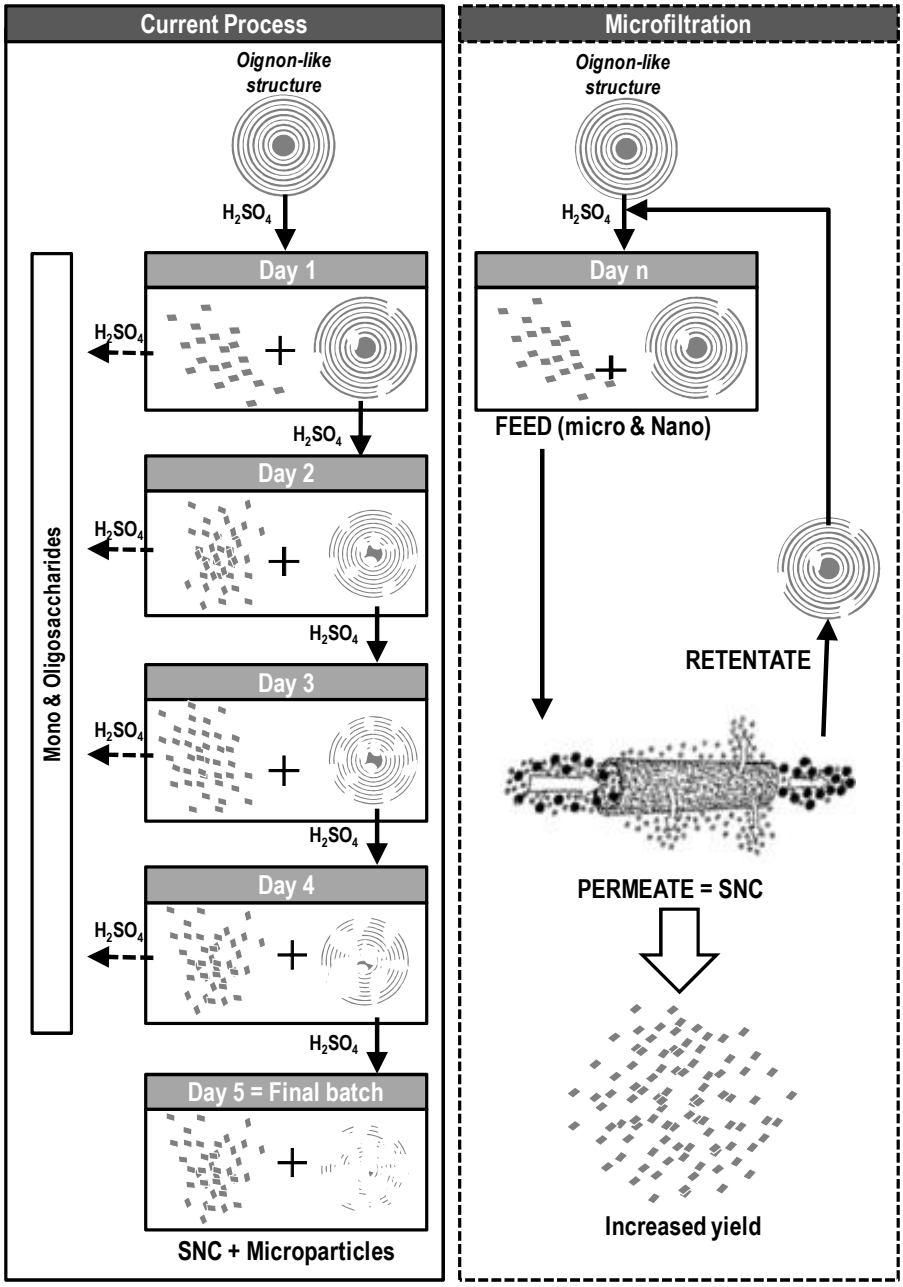

Figure 3-III.2. Schematic comparison between the current preparation process involving the progressive production of starch nanocrystals as evidenced in [21], and the proposed microfiltration process.

It is based on results from a very recent study proving the existence of SNC in the suspension after only 1 day [21]. Cross-flow microfiltration was the selected process for limiting the conversion of SNC into oligo or monosaccharides. For such an extraction to be possible, the system has to be acid-proof, hence the use of a ceramic membrane. However, the whole filtration unit, including pipes, pumps and containers should be acid-resistant as well in our conditions. Acidic conditions for the production of SNC are quite strong (3.16M H_2SO_4) compared to acidic conditions found in the industry (max. 5% HCl or 1.3M HCl). To our knowledge, no such filtration unit has been developed. Therefore, we used a regular pilot unit (Figure 3-III.1) with neutralized 1-day-hydrolyzed-starch suspension (quenched) as a proof of principle. Pre-trials were performed in recycled mode (VCR = 1) to assess the membrane behavior under different transmembrane pressure (TMP) being 60 and 100 kPa as it has been reported that for starch hydrolysate and syrups TMP higher than 103 kPa did not improve flux [16]. Recommended cross-flow velocity was also relatively high (5m.s^{-1}) as increasing cross-flow velocity is probably the easiest way to reduce fouling and maximize flux during microfiltration of corn starch hydrolysate [16].

III.3.2. Filtration Kinetics

The filtration kinetics was investigated for all four membranes during all the experiment. Experimental data are reported in Table1. No correlation was observed between decrease in permeate flux and membrane pore size due to large variations observed in Figure 3(a). However, reported permeate flux at low TMP (<100 kPa) and low temperature (25℃) are high (300-600 L.m^{-2}.h^{-1}) compared to data reported in other studies. For the filtration of corn starch hydrolysate at same cross-flow velocity (5 m.s^{-1}), reported flux were 100-180 L.m^{-2}.h^{-1} [14, 16] for TMP = 100-1000 kPa and T = 40-60℃.

Figure 3-III.3 shows the evolution of the permeate flux during filtration on membranes with different pore sizes. For all membranes, the permeate flux oscillates strongly but following a declining slope. These oscillations are possibly linked to (i) the heterogeneity of the suspension, (ii) the measurement method and/or (iii) the possible fouling that can occur during the microfiltration process. Membrane fouling is generally due to the accumulation of submicronic particles on the membrane surface and within the pores of the membrane itself. The former effect is called concentration polarization. It results from the reversible accumulation of the rejected solute in the fluid phase at the membrane-fluid interface as the solvent phase passes through the membrane.

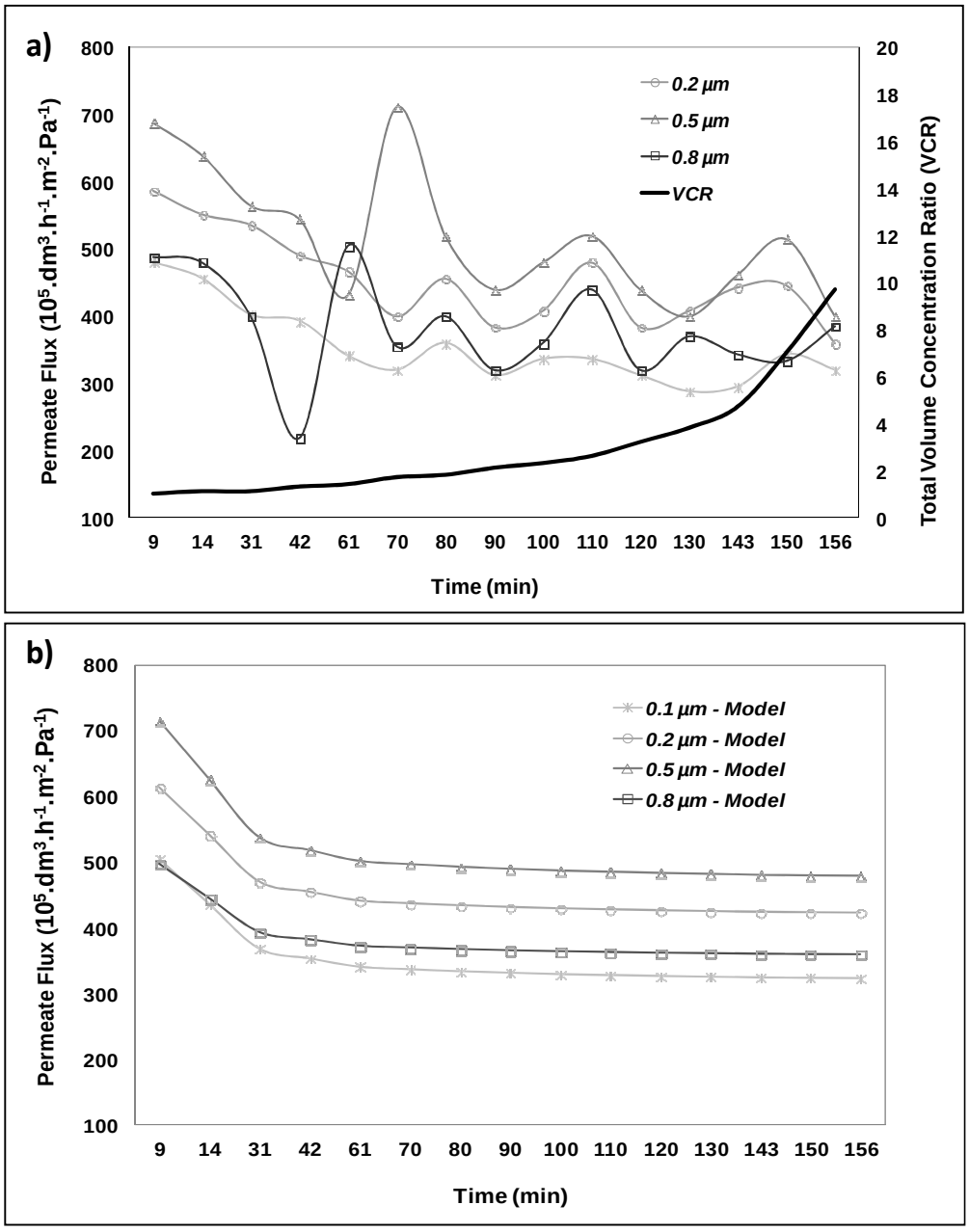

Figure 3-III.3. Evolution of the permeate flux during filtration through membranes with different pore sizes (0.1 µm, 0.2 µm, 0.5 µm, and 0.8 µm): a) actual oscillations, b) modeling with fouling parameters.

However, if steady state prevails, the solute retained will be transported back into the bulk solution through the boundary layer because of the concentration difference [22]. Internal fouling (clogging) of the pores of an asymmetric membrane, however, is very rare [23] and results in an irreversible decline in the flux with time. Concentration polarization effects can be reduced by decreasing the transmembrane pressure or lowering the feed concentration. According to Singh and Cheryan [16], the best model for describing the fouling process is given by Equation (4). The steady state flux, J_{ss}, and fouling rate, k, should be correlated with operating parameters.

Table 3-III.1. Summary of the filtration kinetics data (permeate flux) and coefficients of fouling model for microfiltration of wheat starch nanocrystals at 25°C, 5m.s^{-1}, neutral pH.

Membrane Pore Size		**0.1 µm**	**0.2 µm**	**0.5 µm**	**0.8 µm**
TMP (kPa)		100	100	60	60
Inital Permeate Flux ($dm^3.h^{-1}.m^{-2}$)	t=0h	480	587	413	293
Final Permeate Flux ($dm^3.h^{-1}.m^{-2}$)	t=2h40	320	360	240	231
Relative Reduction of Permeate Flux ΔJp (%)		**33.3%**	**38.7%**	**41.9%**	**21.2%**
Steady State Permeate Flux ($dm^3.h^{-1}.m^{-2}$)	J_{ss}	313	411	279	210
Fouling Rate ($dm^3.h^{-1}.m^{-2}$)	k	29	31	23	13
Determination Coefficient	**R^2**	**0.82**	**0.66**	**0.45**	**0.27**

Paper 6

These parameters calculated from the fouling model and reported in Table 3-III.1 allowed for drawing the declining slope as shown in Figure 3-III.3.b. It seems that the small the pore size, the higher the fouling rate (Table 3-III.1). Indeed, if the pore diameter is smaller than the largest particles, the pores will be plugged and prevent smaller particles to pass through the membrane. In this study, all membranes have pore size smaller than the largest particles. However, the smaller the membrane pore size, the more numerous the particles larger than pore size. Thus, smaller pore size membranes have a higher fouling rate. It should, nevertheless, be noted that the higher the pore size of the membrane, the lower the correlation with the fouling model as indicated by the values of the coefficient of determination R^2 reported in Table 3-III.1. It suggests that reported flux have not reached steady state and that fouling has not completely occurred. However, this gradual decrease in flux is characteristic of membrane fouling which decreases the efficiency of the filtration process. The experiment lasted over 2.5 hours and could not be extended.

Indeed, it reached maximum VCR for this pilot (13.6) before observing fouling. This was expected as the experiment was carried out on a 24h hydrolyzed starch suspension therefore containing a majority of microscopic particles for few nanometric particles. In a continuous process, retentate would be recycled back to the hydrolysis tank. Nevertheless, the loss in permeate flux was relatively moderate (20-40%).

Contrary to what was expected the filtration kinetics and fouling does not seem to be correlated to the pore size of the membrane. Strong fluctuations in flux make it difficult to appoint the best pore size for this application. Indeed, membrane 0.2 µm renders the most stable flux, while membrane 0.5 µm renders the highest flux and membrane 0.8 µm renders the smallest reduction in permeate flux. It seems that the pore size of the membrane is not a governing factor for our filtration process. Indeed, the performance of the membrane filtration and fouling mechanism depends on various factors such as the operating conditions of the system (including filtration pressure, cross-flow velocity, soluble microbial products (SMP) concentration, etc.) and the membrane characteristics (morphology, membrane pore size, zeta potential, hydrophilic affinity, etc.), but also the nature of biological polymers and bio–macromolecular characteristics (molecular weight of biopolymers, zeta potential, configuration, size distribution, etc.) [24]. These last sets of parameters probably apply to SNC suspensions. However, despite instability, microfiltration worked efficiently to isolate SNC from microparticles whichever the membrane.

III.3.3. Collected Suspensions Properties

Dynamic light scattering was used to assess differences in size among suspensions filtrated with the four different pore size ceramic membranes and between the initial suspension and the final retentate. Experimental data are collected in Table 3-III.2.

Table 3-III.2. Summary of dynamic light scattering data for feed, retentate and permeate. PdI: Polydispersity Index. % Number reflects the distribution of particles among the first and the second peak.

Sample type	Main Peak		Secondary Peak		PdI
	Mean Particle Size (nm)	% Number	Mean Particle Size (nm)	% Number	
Feed	**804** ± 205	100%			0.58 ± 0.21
Retentate	**1255** ± 318	100%			0.38 ± 0.66
Permeate 0.8µm	**51** ± 7	99% ± 0,2%	211 ± 46	1% ± 0,2%	0.77 ± 0.06
Permeate 0.5µm	**122** ± 13	13% ± 3%	480 ± 63	87% ± 3%	0.55 ± 0.05
Permeate 0.2µm	**71** ± 2	99% ± 28%	362 ± 101	1% ± 28%	0.74 ± 0.24
Permeate 0.1µm	*Not Repeatable Measurement*				

Paper 6

The high polydispersity index (PdI, ratio between width and magnitude of the size peaks) indicates a relatively broad size distribution and implies that Z-average size cannot be reported for comparison with other devices. Despite that, clear differences in size were observed between particles contained in the feed, retentate and permeate, as shown in Figure 3-III.4.a. The mean particle size for the feed suspension was estimated at 800 nm (100 number %) whereas it was much smaller for the permeate (~ 100 nm depending on membrane) and much bigger for the retentate (1255 nm) as expected. Indeed, the latter is made of particles that cannot pass through the membrane. However, higher values were expected as native wheat starch granules are 2-30 µm and are not likely to all be hydrolyzed down to 1 µm after only 1 day. An explanation could be that biggest particles undergo shear stress during fouling or precipitate to the bottom before being measured by the diffractive laser.

Finally, permeates coming from the different filtrations were compared. They all exhibited a bimodal distribution with a main peak at 50-100 nm and a secondary peak at 200-400 nm. The secondary peak was attributed to the presence of aggregates that either passed through the ceramic membrane or formed after filtration. No significant

differences were observed among permeate size obtained with membranes with different pore sizes. After 1 day hydrolysis, a membrane with pore size 0.8 µm seems enough to be efficient to discriminate granules from SNC. As it is also the membrane for which the lowest loss of permeate flux and lowest fouling was observed (Figure 3-III.1), it should be selected for future test runs. Indeed, membrane replacement accounts for about 55% of the operating costs of a ceramic membrane plant[18]. Also, potential flux improvement and further fouling reduction can be expected if cross-flow velocity is increased [16]. Thus, we recommend selecting the cheapest membrane (larger pore size) and increasing cross-flow filtration for a cost effective application of this process.

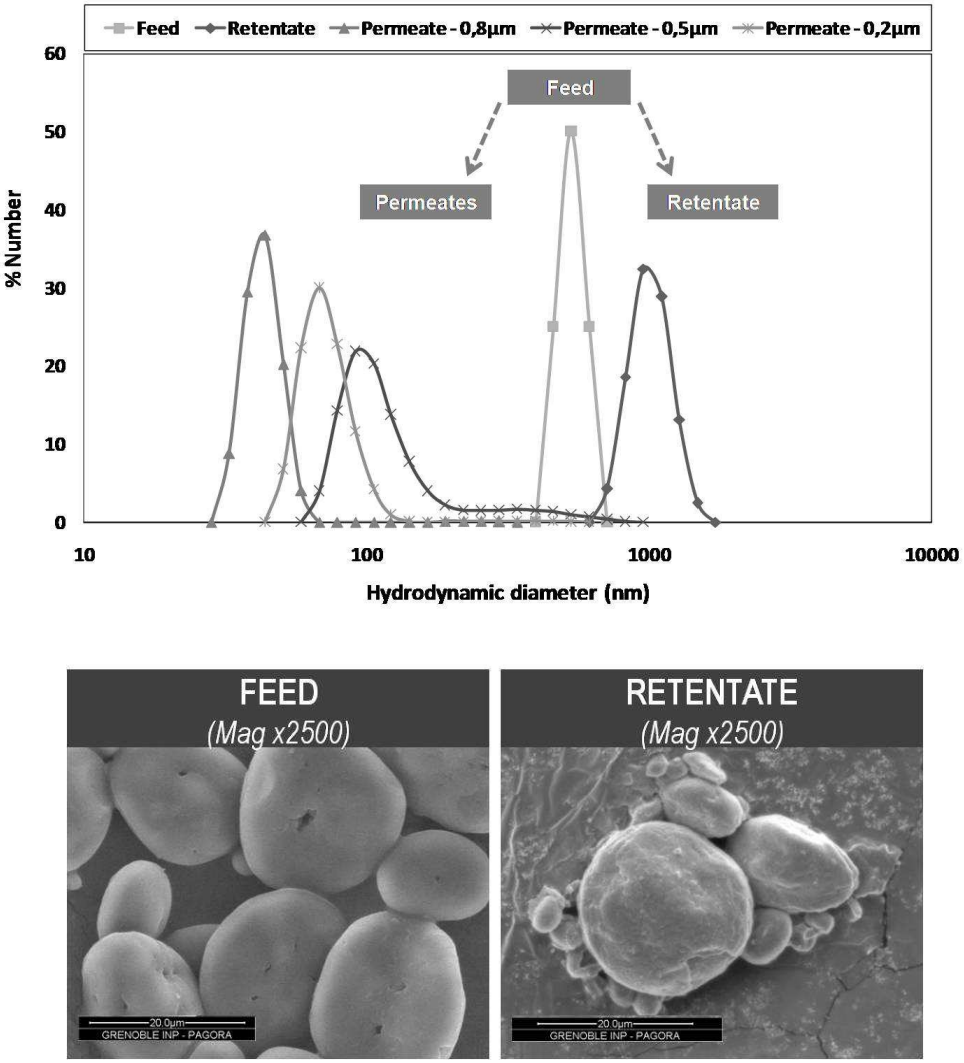

Figure 3-III.4. (a) Particle size distribution of feed, retentate and permeate suspensions determined from dynamic light scattering experiments, and (b) ESEM micrographs of 1-day-acid-hydrolysis feed suspension and retentate suspension at magnitude 2500x

SEM micrographs of the suspensions were taken to control visually the content of each suspension. As expected from wheat starch granules and giving particle size analysis, the feed suspension is made of disc-like particles and a few smaller round particles as seen in Figure 3-III.4.b. Biggest particles (granules) have also been attacked by acid as pit holes can be seen at the surface. However, SNC cannot be observed with regular ESEM at this magnitude. Figure 3-III.4.b also shows that particles from the retentate seem to have been roughly grounded. That is most likely due to the pressure applied to particles during membrane fouling, submitting them to shear stress.

FEG-SEM micrographs of the permeate show SNC of about 50 nm (Figure 3-III.5.a) and re-aggregates of particles of about 200 nm (Figure 3-III.5.b) as well as non-fully individualized nanocrytals of about 500 nm (Figure 3-III.5.c). These results confirm the dimension analysis from Table 3-III.2 and prove that cross-flow filtration is a promising solution for separating SNC from non-fully acid hydrolyzed starch granules. This is the first time that such a possibility is proposed for this application. However, it was important to prove that such a process, with the mechanical stress which may result from filtration and polarization, did not alter the structure of SNC.

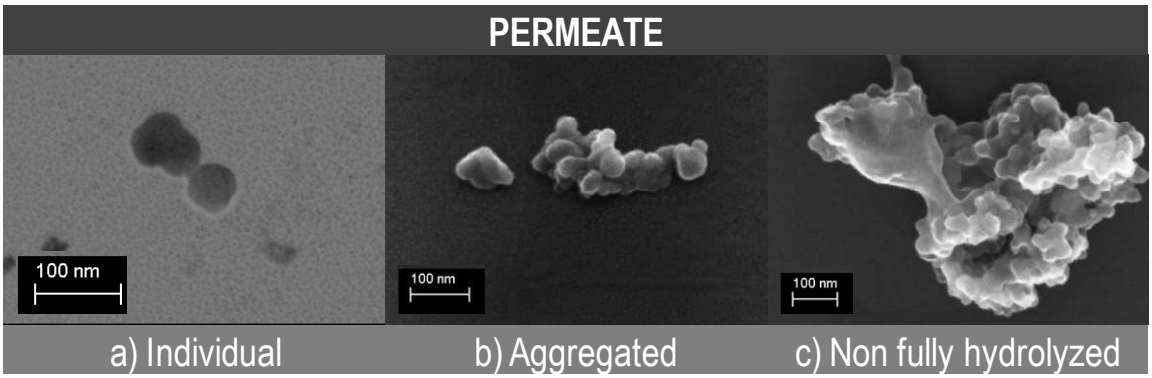

Figure 3-III.5. FEG-SEM micrographs of the 1-day-acid-hydrolysis permeate suspension: a) individual nanocrystals in transmission mode, b) re-aggregated particles in reflective mode, c) non-fully individualized particles in reflection mode

For this reason, X-Ray diffraction (XRD) measurements were used to assess the crystallinity of particles in each suspension. Figure 3-III.6 shows the X-ray diffraction patterns obtained for the feed suspension of 24-hours-hydrolyzed starch, as well as for the permeate and retentate of that same suspension after microfiltration on a 0.8 µm pore size ceramic membrane. As expected, the initially freeze-dried feed suspension rendered an A-type diffraction pattern with strong reflection peaks at 2θ values around 15° and 23° and an unresolved doublet at 17° and 18 ° as well as two weak peaks around 2θ values around 10° and 11°. Compared to the feed su spension, no significant difference was observed for the retentate. On the contrary, the diffractogram for the permeate suspension revealed two significant differences. First, sharper XRD patterns consistent with a higher level of crystallinity were observed. Calculations from this data reveal an increase of 3.5% in crystallinity from 34.6% to 38.2% for feed and permeate, respectively. Second, crystalline peaks seem to be characteristic of a B-type starch with the strongest diffraction peak at around 2θ value of 17° and a few smaller peaks at 20°, 22° and 23° and an additional peak which appeared a t about 5°.

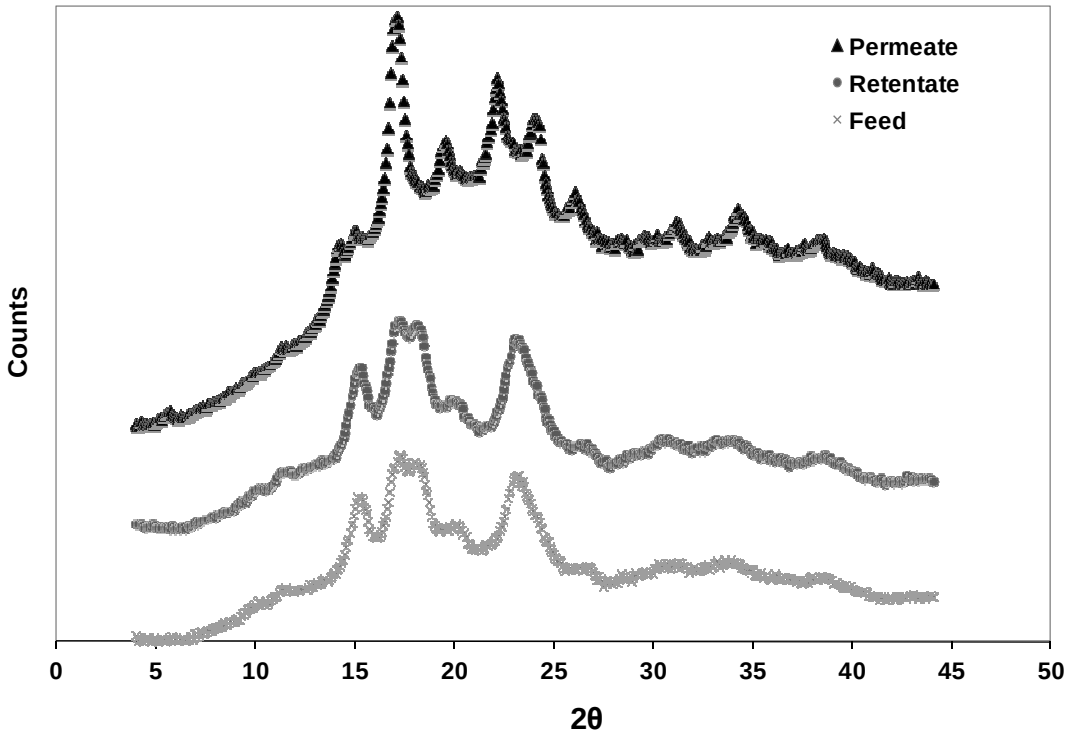

Figure 3-III.6. X-ray diffraction patterns of the feed suspension, retentate and permeate (obtained through the 0.8 µm membrane).

The first difference can be easily explained, as we believe to have collected in permeate, SNC produced after 24 hours hydrolysis. The second difference can be attributed to the fact that wheat starch granules consist of two populations, i.e. one of small (1-10 µm) spherical B-type granules and a second of bigger (15-40 µm) disc-

shaped A-type granules. As reported by Jane et al. [25], contrary to A-type starch which branch linkages might be protected in the crystalline region, B-type starch has most amylopectin branch points clustered in the amorphous region, making it more susceptible to acid hydrolysis. It is most likely that B-type crystallites are produced more quickly (i.e. after one day) than A-type ones, as granules are smaller and they can be more easily released. This observation also offers the possibility to develop a batch process by which nanocrystals with different crystalline types can be selectively isolated.

III.4. Conclusion

This study proposes, for the first time, an innovative solution against limitations of the current process for producing starch nanocrystals. Cross-flow filtration was proved to be an efficient continuous operation for separating SNC from the bulk suspension whatever the ceramic membrane pore size (0.2 µm to 0.8 µm). Such proof of principle for this strategy, offers numerous opportunities for accelerating the potential industrialization of SNC. Indeed, it could improve (i) the yield of SNC preparation, (ii) the quality and homogeneity of SNC suspensions, and (iii) the ensuing final properties of composites/materials using SNC. Also, it is an industrial process proven to be effective, economical and energy saving compared to current isolation methods (centrifugation). Contrary to frontal filtration, cross-flow filtration allowed isolation without modifying the crystalline structure of SNC (and potentially isolate one type of crystallinity), nor favoring its aggregation.

III.5. References

1. Angellier, H.; Choisnard, L.; Molina-Boisseau, S.; Ozil, P.; Dufresne, A., Optimization of the preparation of aqueous suspensions of waxy maize starch nanocrystals using a response surface methodology. *Biomacromolecules* **2004,** 5, 1545-1551.

2. Angellier, H.; Molina-Boisseau, S.; Dole, P.; Dufresne, A., Thermoplastic Starch-Waxy Maize Starch Nanocrystals Nanocomposites. *Biomacromolecules* **2006,** 7, (2), 531-539.

3. Angellier, H.; Molina-Boisseau, S.; Dufresne, A., Mechanical properties of waxy maize starch nanocrystal reinforced natural rubber. *Macromolecules* **2005,** 38, (22), 9161-9170.

4. Angellier, H.; Molina-Boisseau, S.; Dufresne, A., Waxy maize starch nanocrystals as filler in natural rubber. *Macromolecular Symposia* **2006,** 233, (1), 132-136.

5. Angellier, H.; Molina-Boisseau, S.; Lebrun, L.; Dufresne, A., Processing and Structural Properties of Waxy Maize Starch Nanocrystals Reinforced Natural Rubber. *Macromolecules* **2005,** 38, (9), 3783-3792.

6. Angellier, H.; Putaux, J.-L.; Molina-Boisseau, S.; Dupeyre, D.; Dufresne, A., Starch nanocrystal fillers in an acrylic polymer matrix. *Macromolecular Symposia* **2005,** 221, (1), 95-104.

7. Kristo, E.; Biliaderis, C. G., Physical properties of starch nanocrystal-reinforced pullulan films. *Carbohydrate Polymers* **2007,** 68, (1), 146-158.

8. Viguié, J.; Molina-Boisseau, S.; Dufresne, A., Processing and Characterization of Waxy Maize Starch Films Plasticized by Sorbitol and Reinforced with Starch Nanocrystals. *Macromolecular Bioscience* **2007,** 7, (11), 1206-1216.

9. Chen, Y.; Cao, X.; Chang, P. R.; Huneault, M. A., Comparative study on the films of poly(vinyl alcohol)/pea starch nanocrystals and poly(vinyl alcohol)/native pea starch. *Carbohydrate Polymers* **2008,** 73, (1), 8-17.

10. Chen, G.; Wei, M.; Chen, J.; Huang, J.; Dufresne, A.; Chang, P. R., Simultaneous reinforcing and toughening: New nanocomposites of waterborne polyurethane filled with low loading level of starch nanocrystals. *Polymer* **2008,** 49, (7), 1860-1870.

11. Le Corre, D.; Bras, J.; Dufresne, A., Starch nanoparticles: A review. *Biomacromolecules* **2010,** 11, (5), 1139-1153.

12. Lin, N.; Huang, J.; Chang, P. R.; Anderson, D. P.; Yu, J., Preparation, modification and application of starch nanocrystals in nanomaterials: A review. *J. Nanomater.* **2011,** 2011, 13.

13. Le Corre, D.; Bras, J.; Dufresne, A., Evidence of micro and nano-scaled particles during starch nanocrystals production and their isolation. *Biomacromolecules* **2011,** Accepted.

14. Hinkova, A.; Bohacenko, I.; Bubnik, Z.; Hrstkova, M.; Jankovska, P., Mineral membrane filtration in refinement of starch hydrolysates. *Journal of Food Engineering* **2004,** 61, (4), 521-526.

15. Pidgeon, E. F. The Application of Crossflow Membrane Filtration to Remediate Wheat Starch Processing Wastewater for Reuse. , Griffith University, **2009**.

16. Singh, N.; Cheryan, M., Fouling of a ceramic microfiltration membrane by corn starch hydrolysate. *J. Membr. Sci.* **1997,** 135, (2), 195-202.

17. Singh, N.; Cheryan, M., Membrane Technology in Corn Refining and Bioproduct-Processing. *Starch - Stärke* **1998,** 50, (1), 16-23.

18. Singh, N.; Cheryan, M., Process design and economic analysis of a ceramic membrane system for microfiltration of corn starch hydrolysate. *Journal of Food Engineering* **1998,** 38, (1), 57-67.

19. Master, A. M.; Steeneken, P. A. M., Filtration Characteristics of Maize and Wheat Starch Hydrolysates. *Cereal Chemistry* **1998,** 75, (2), 241-246.

20. Kumar, S. M.; Madhu, G. M.; Roy, S., Fouling behaviour, regeneration options and on-line control of biomass-based power plant effluents using microporous ceramic membranes. *Sep. Purif. Technol.* **2007,** 57, (1), 25-36.

21. LeCorre, D.; Bras, J.; Dufresne, A., Evidence of micro and nano-scaled particles during starch nanocrystals production and their isolation. *ACS Nano* **Submitted**.

22. Cheryan, M., *Ultrafiltration Handbook*. Technomic Publishing: Lancaster, PA, **1986**; p.

23. GmbH, M.-N., Cross-Flow filtration. http://www.microdyn-nadir.de/cms/content_details.php?page=3&id=15&lang=en, Access (April 14th, 2011).

24. Hwang, K. J.; Huang, P. S., Cross-flow microfiltration of dilute macromolecular suspension. *Sep. Purif. Technol.* **2009,** 68, 328-334.

25. Jane, J.-l.; Wong, K.-s.; McPherson, A. E., Branch-structure difference in starches of A- and B-type X-ray patterns revealed by their Naegeli dextrins. *Carbohydrate Research* **1997,** 300, (3), 219-227.

Chapter 3-IV Conclusions

In this chapter, three strategies for the optimization and scale-up of the SNCs preparation process have been proposed. They consisted respectively in: (i) studying an experimental domain with more drastic hydrolysis conditions than the current one and optimizing "2nd generation" SNCs preparation, (ii) developing a pretreatment for the granule to be more readily hydrolyzed, and (iii) assessing the potential of a continuous industrial process for isolating SNCs (2nd generation) as soon as they are produced.

Results confirmed the existence of new generation SNC and proved that SNCs can be produced in less than 5 days. On one hand, using enzymatic pre-treatment, duration can be reduced by a factor three by creating microporous starch having preferential acid diffusion pathways. On the other hand, using intensive hydrolysis conditions, duration can be very low, i.e. with SNCs observed under 15h. It was found that the yield of these new generation SNCs was very different from that of the classic suspension (i.e. quite lower) and that it evolved in an opposite direction than current SNC suspensions.

Thus, another strategy was expected and the use of microfiltration as a continuous filtration process allowed getting free from the notion of hydrolysis duration and yield. Indeed it allows extracting SNCs from the main suspension as soon as they are produced and recycling or using the macromolecular suspension.

Thus it is a great opportunity to increase the yield of 2nd generation SNC and develop a scaled-up/ industrial process. The discussion is in progress with our industrial partner and first results still confidential.

This study confirms the potential of producing at large-scale more homogeneous SNCs. As a result, in the next Chapter 4, we will suggest potential applications for SNCs and proposed explanation of achieved properties.

FIGURES

TABLES

CHAPTER 4. Use of starch nanocrystals

CHAPTER 4. SHORT SUMMARY

RESUME FRANÇAIS – FRENCH ABSTRACT

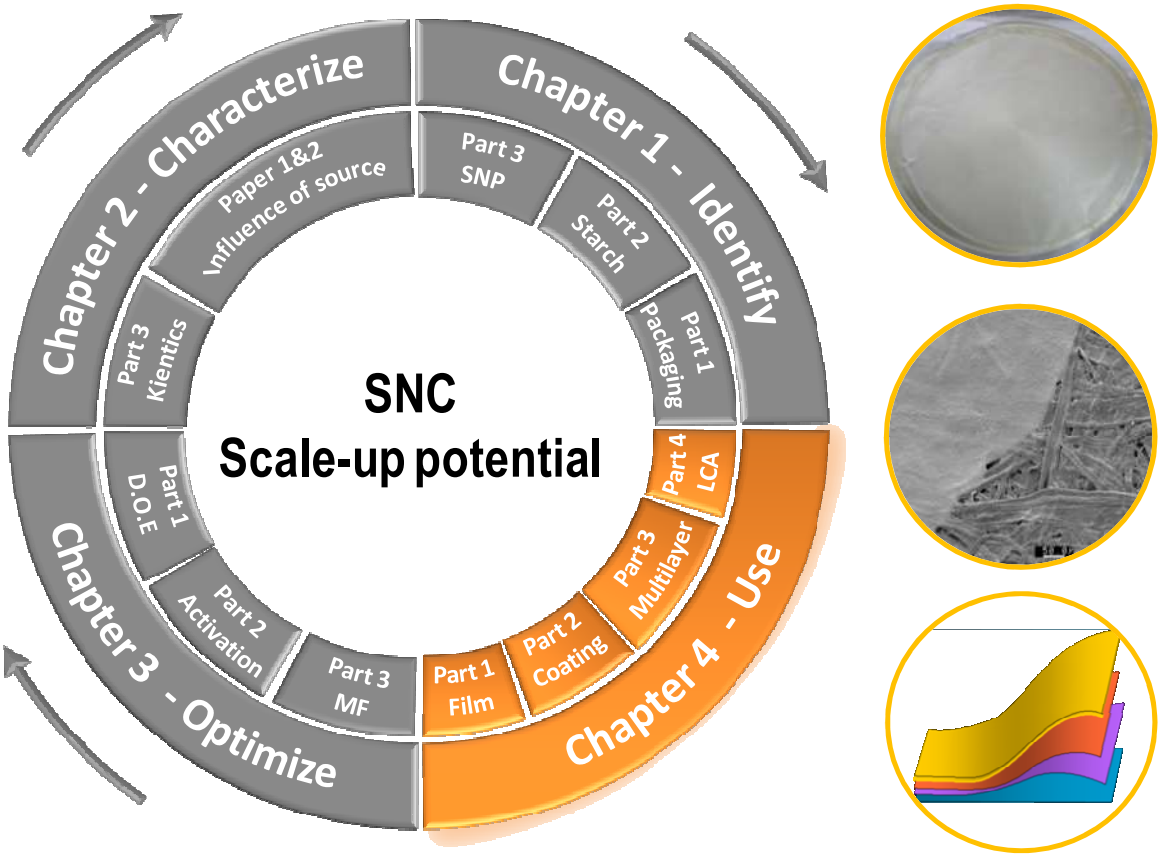

Figure 1. Représentation schématique de l'organisation du projet de thèse

Les études du chapitre précédent ont révélé que différents procédés de préparation pouvaient permettre de produire à une échelle de temps ou de rendement industriel des suspensions homogènes de SNCs.

Dans ce Chapitre 4, nous nous intéressons donc désormais aux applications industrielles que les SNCs peuvent trouver. Dans un premier temps, l'application nanocomposite (la plus publiée pour les nano-polysaccharides) a été ciblée. Elle avait pour objectif de vérifier si l'origine de l'amidon avait une influence sur les propriétés finales du matériau mis en œuvre, comme c'est le cas pour d'autres bio-nanocristaux. Puis, une application industrielle innovante a été proposée avec l'utilisation de SNCs en couchage, en tant que nano-charge d'une sauce de couchage biosourcée. Le potentiel de cette application a ensuite été étendu à une utilisation en emballage multicouches, telle que visé par le projet européen FlexPakRenew (à l'origine de cette thèse). Enfin, l'ensemble des précédentes études confirmant le potentiel des SNCs, une étude des impacts environnementaux des SNCs a été proposée.

Dans la **première partie** (Papier 6 – Soumis à *Macromolecular Material & Engineering*– Septembre 2011), nous avons donc évalué l'influence des 5 types d'amidon (du Chapitre 2) utilisés pour préparer des SNCs, sur les propriétés finales d'un nanocomposite de caoutchouc naturel chargé à 5% ou 30% en masse. Il s'agit en réalité d'évaluer l'influence sur les propriétés du nanocomposite des légères différences observées (au Chapitre 2) entre les SNCs de différentes origines.
L'étude des nanocomposites de caoutchouc naturel chargés à 30% révèle que, plus le taux d'amylose de l'amidon natif est grand, plus les propriétés de diffusion de l'eau et les propriétés mécaniques des nanocomposites sont faibles. Il est postulé que les SNCs produits à partir d'amidon riche en amylose sont moins stables/purs que les autres. Par conséquent, pour un taux de charge identique, ces derniers relargueraient lors de la mise en œuvre des chaînes d'amylose non liées qui ne participeraient pas à la formation d'un réseau diffusant ou de renfort. A 5% de renfort, pratiquement aucune différence de propriétés n'est observée entre les différents nanocomposites. Seul le gonflement au toluène nous confirme que, plus la surface spécifique des SNCs est grande, plus la formation d'un réseau percolant commence à de faibles taux de charge. Les résultats de l'étude rejoignent donc les conclusions des études précédentes. Différentes sources d'amidon peuvent être utilisées pour produire des SNCs utilisés comme nano-charges. Pour une application nanocomposite, seuls les amidons à haut taux d'amylose sont à éviter et certains critères de sélection (tel que la surface spécifique) peuvent être envisagés pour des applications précises.

Si les SNCs peuvent être utilisés comme nano-charges d'un bio-polymère, alors peut-être peuvent-ils être couchés sur un papier. La **deuxième partie** de ce chapitre (Papier 7 – Soumis à *Surface and Coatings Technology* - Aout 2011) vise donc à vérifier la compatibilité des SNCs avec un procédé de couchage papetier et à évaluer les propriétés finales des papiers en fonction du taux de charge. Par ailleurs, étant donné que nous visons des applications barrières, les SNCs de maïs cireux et de blé ont été utilisés comme recommandé par l'étude morphologique développée au chapitre 2.
Les sauces de couchages élaborées (de faible taux de matière sèche, i.e. diluée) présentaient des viscosités élevées mais industriellement viables (inférieur à 2000mPa.s au delà de $300s^{-1}$). Le caractère dilué des suspensions induit un mouillage du papier lors du procédé de couchage et un craquelage de la couche lors du séchage. En revanche, les températures de séchage mises en œuvre n'ont pas pu détériorer les SNCs. Ces derniers, lorsque introduit a 30% en masse dans la sauce de couchage, ont permis de compenser la perte de propriétés mécanique due à l'utilisation d'un biopolymère en base aqueuse, et d'améliorer (de 40%) les propriétés barrières à la vapeur d'eau du papier

couché. Des améliorations, au niveau de la matrice notamment, ainsi qu'une comparaison avec d'autres nano-charges semblent toutefois nécessaires. C'est ce qui a été réalisé dans la 3ème partie.

En effet la possibilité d'utiliser des SNCs dans un procédé de couchage ayant été vérifiée, leur utilisation en tant que composant d'un emballage multicouches, biosourcé, flexible et barrières a été envisagée. La **troisième partie** de ce chapitre présente la stratégie développée dans le cadre du projet Européen FlexPakrenew pour produire ce type d'emballage. Pour cela, deux matrices biopolymères permettant d'atteindre de plus hauts taux de matière sèche ont été utilisées: un amidon modifié et un xylane (produit issu de l'hemicellulose en bioraffinerie). A celles-ci, deux types de nano-charges plaquettaires ont été ajoutées pour augmenter la tortuosité dans ces biopolymères : des nano-argiles et des SNCs. Les performances de ces matériaux ont été étudiées en suivant trois stratégies (i) tout d'abord en couche simple sur un papier industriel, puis (ii) en multicouches (double couche) à l'échelle laboratoire, et enfin (iii) en multicouches (4 couches) à l'échelle pilote.
L'étude révèle que le mélange optimisé de nano-argiles en combinaison avec un amidon plastifié, développé par nos partenaires du projet Européen, permet d'obtenir les performances recherchées dans le cadre du projet (très bonnes propriétés barrières à la vapeur d'eau et à l'oxygène à 23°C et 50% d'humidité).
Toutefois, les résultats prouvent également que les SNCs peuvent diminuer la perméabilité à la vapeur d'eau des xylanes (d'environ 33%), et ce, plus significativement que certaines nano-argiles non optimisées. Enfin, l'utilisation des SNCs de seconde génération, en quantité plus faible (-35%), a permis d'obtenir une réduction de la perméabilité à la vapeur d'eau de 11%. Même si les SNCs n'obtiennent pas les mêmes résultats que certaines nano-argiles optimisées depuis le projet Européen Sustainpack (2003-2007), l'étude prouve pour la première fois la faisabilité du concept : « SNCs comme agents barrières en couchage » ; et ouvre ainsi la discussion à d'éventuelles améliorations. Elle confirme donc l'intérêt de produire et d'utiliser des SNCs, d'autant plus qu'ils ont l'avantage environnemental d'être d'origine renouvelable. Pour vérifier cet aspect, une étude plus complète du cycle de vie a donc été réalisée.

En effet le nombre croissant d'applications des SNCs développées ces dernières années (présentées au Chapitre 1 et développées dans ce Chapitre 4) souligne l'intérêt de produire à grande échelle des SNCs plus homogènes. Néanmoins, l'intérêt premier de ces SNCs réside dans leur caractère renouvelable et biodégradable. Ainsi, pour

présenter un intérêt environnemental incontestable, son procédé de préparation doit lui aussi présenter des impacts environnementaux limités.

Par conséquent, afin de compléter les recommandations pour l'optimisation du procédé de préparation des SNCs (développées au Chapitre 3), il nous a semblé pertinent, dans la **quatrième partie** de ce chapitre (Papier 8 - Soumis à *Starke/Starch* - Septembre 2011), (i) d'identifier, par une Analyse de Cycle de Vie (ACV) des SNCs, les étapes/procédés présentant l'impact le plus marqué; puis, (ii) de comparer les impacts environnementaux à ceux des nano-argiles (et plus précisément de montmorillonites modifiées (OMMT)), principaux concurrents des SNCs dans notre projet.
L'étude révèle que la production de SNCs requiert plus de 50% d'énergie en moins que pour les OMMTs. En revanche, contrairement aux OMMTs, les SNCs contribuent (faiblement) au réchauffement climatique (GWP) et à l'acidification des océans (AP). Néanmoins, ils présentent, contrairement aux OMMTs, l'avantage supplémentaire d'être renouvelables et biodégradables, ce qui est parfois important au niveau de l'application finale visée et dans le cadre de projets Européens.
L'ensemble des impacts étudiés suggère que l'impact environnemental des SNC est largement lié à la culture de l'amidon qui utilise de grandes surfaces au sol, de grandes quantités d'eau et des véhicules agricoles. Par conséquent, en vue d'une optimisation « durable » du procédé de préparation des SNCs, il est recommandé de développer (i) l'utilisation de cultures sauvages ou nécessitant peu d'eau ; et (ii) un procédé de transformation consommant moins d'eau et moins d'électricité que le procédé actuel.
Dans cette deuxième optique, et comme rapporté au Chapitre 3, la microfiltration semble offrir de bonnes perspectives. Enfin, une courte étude bibliographique portant sur la toxicité des OMMTs (similaire en forme au SNCs) et des nanocristaux de cellulose (similaire en composition) permet de postuler de la faible toxicité des SNCs. Toutefois, pour permettre une montée en échelle, une étude toxicologique des SNCs devra être entreprise par des laboratoires spécialisés.

Ce dernier chapitre complète donc parfaitement les précédents en proposant de nouvelles applications industrielles des SNCs, et des perspectives pour la poursuite de cette étude (orientation des SNCs en couche et toxicité). Il confirme aussi l'aspect prometteur des SNC de seconde génération, à la fois au niveau technique mais aussi au niveau environnemental.

SUMMARY - ENGLISH ABSTRACT

In Chapter 3, several optimization strategies have been developed and prove that SNCs can be: prepared in less than a day, more homogeneous and produced at higher scale. However, it has to be verified that they can be used in an industrial process and in combination with other bio-based materials.

Chapter 4 verifies that (i) different kind of SNCs can be used as filler materials; that (ii) they can be used in a coating process; and that (iii) they can be compatibilized with different biopolymers and layers, to reduce the permeability of the initial material. Also, the life cycle analysis (LCA) of SNCs produced for this application is investigated.

In the **first part** (Paper 6 submitted to *Macromolecular Material & Engineering*, September 2011), the impact of the small differences among the different SNCs (from different starches) studied in Chapter 2, on the final properties of a natural rubber-based nanocomposite are assessed. The study shows that at low loading level (5wt%) very weak differences are observed between nanocomposites. Only water diffusion through the polymer correlates with the specific surface of SNCs. At higher loading level (30wt%), it seems that the higher the amylose content of the native starch, the poorer the mechanical properties and the percolation network. It is postulated that high amylose starch SNCs might release loosely bonded amylose chains during their processing, thus performing as if the loading level was lower.

In the **second part** of this chapter (Paper 7 submitted to *Surface and Coatings Technology*, August 2011), the idea is to coat a bio-based nanocomposite on paper and thus to assess the possibility of using SNCs in coating processes. Results show that the highly diluted coating colors, exhibited increased viscosity when containing SNCs. However, they could still be considered as coating material (<2000mPa.s at shear rate higher than $300s^{-1}$); and, according to results from Chapter 2, the studied drying processes did not melt the SNCs. The mechanical testing of produced papers showed that the use of a water-based coating color induced decreased mechanical properties, due to the wetting of the paper. However, SNCs allowed compensating this loss and improving water vapor barrier.

Giving these favorable results, SNCs were considered as bio-based nano-filler material for the development of a bio-based multilayer flexible barrier packaging.

The **third part** reports the strategy implemented in the European FlexPakRenew project to develop such a packaging. Two high solid content biopolymers (modified starch and xylan) and two kinds of platelet nanofillers (nanoclays and SNCs as a renewable alternative) were investigated. The optimized combination of a mix of nanoclays with plasticized starch were most performing and allowed for reaching the project's targets in barrier properties of the multilayer (WVTR < 1g.m^{-2}.day^{-1} and OTR<10cm3.m^{-2}.day^{-1}.bar^{-1} at 23℃ and 50%RH). However, the study also reveale d that SNCs could effectively decrease the permeability of some xylan films and even more so than non optimized nanoclays. Also, it was proved that the use of more homogeneous SNCs (2nd generation SNCs), and to a lesser loading level, could further improve barrier properties of the biopolymers.

Previous studies further confirmed the industrial potential of SNCs. However, for SNCs to be fully environmentally favorable over other products, its preparation process has to have limited environmental impacts. Thus to complete our recommendations concerning the optimization and scaling-up of the SNCs' preparation process, it seemed relevant to identify most "environmentally sensitive" steps of the production process. To that intent, in the **fourth part** (Paper 8 submitted to *Starke/Starch*, September 2011), a Life Cycle Analysis (LCA) of SNCs as filler material in a multilayer packaging was performed and compared to that of its main competitor organically modified montmorillonite nanoclays (OMMT). The study revealed that the SNCs preparation process requires less energy than that of OMMT. However, their contribution to global warming and acidification was higher. Also most impacting steps were mostly related to the cultivation of starch. Thus recommendations are to limit water and energy consumption via the use of more efficient processes, such as microfiltration. The toxicity of SNC is also discussed.

This last chapter (Chapter 4) proposes a new set of applications for SNCs; as well as perspectives for the continuation of the industrialization of SNCs.

CHAPTER 4. USE OF STARCH NANOCRYSTALS

Chapter 4-I. Influence of starch nanocrystals' botanic origin on morphological and mechanical properties of natural rubber nanocomposites

Déborah LeCorre, Julien Bras, and Alain Dufresne

The International School of Paper, Print Media and Biomaterials (Pagora), Grenoble Institute of Technology, BP 65 - F-38402 Saint Martin d'Hères Cedex, France

Abstract

The structural and mechanical properties of natural rubber (NR) nanocomposites filled with starch nanocrystals (SNC) extracted from four different starch sources have been investigated. The aim of this work was to explore the influence of botanic sources on final properties of nanocomposites and SNC reinforcing capability. A general trend seems to be that the higher the amylose content of native starch granules used for preparing SNC, the lower the water uptake and reinforcing effect (except for potato starch). It is postulated that SNC prepared from higher amylose content starch might release loosely bonded amylose chains during preparation and/or soaking in water and thus prevent SNC to participate in the formation of a reinforcing network.

Keywords

Eco-composites; Nanocomposites; Nano particles ; A. Polymer-matrix composites (PMCs) ; B. Mechanical properties

Inspired from: *D. LeCorre, J. Bras, A. Dufresne, Submitted to Macromolecular Materials Engineering, 2011*

Paper 7

I.1. Introduction

Thanks to its elasticity, resilience and toughness, natural rubber (NR) is the basic constituent of many products used in the transportation, industrial and medical sectors. To tailor its mechanical properties, it is often reinforced with fillers. Most widely used fillers are carbon black, silica, and calcium carbonate[1]. The development of nano-sized particles has led to the development of nanocomposites which, compared to conventional composites, require lower filler content for achieving comparable properties without detrimental effect on impact resistance and plastic deformation. Last two decades, lamellar nanoclays reinforced NR have attracted considerable attention due to their improved mechanical and thermal stability at low loading level [2]. However, recent and growing environmental concerns have led researchers to develop renewable crystalline nanofillers from polysaccharides. Cellulose nanocrystals[3] are by far the most studied for nanocomposites applications as reported in recent reviews[4, 5]. However, there is a growing interest for developing other nanoparticles from starch[6].

Starch is a natural, renewable, and biodegradable polymer produced by many plants as a source of stored energy. Even though, a universally accepted model is still lacking for starch structure[7], the predominant model is a multi-scale structure consisting in the granule (2-100 µm), into which is found (a) alternating amorphous and semi-crystalline growth rings (120-500 nm) the latest being made of (b) amorphous and crystalline lamellae (9 nm)[8] containing (c) two glucosidic macromolecules: amylopectin and amylose (0.1-1 nm). Amylopectin is usually assumed to be the framework of the crystalline region[6].

Starch nanocrystals (SNC) result from the disruption of the semi-crystalline structure of starch granules by the hydrolysis of amorphous parts and present contrary to cellulose nanocrystals, a platelet-like morphology. Recent papers report the reinforcing effect of crab shell chitin whiskers [9], waxy maize starch nanocrystals[10, 11], and bagasse[12] or date palm tree cellulose nanocrystals[13], in a non-vulcanized NR matrix. The choice of NR matrix for the processing of such nanocomposites is appropriate because of the renewable nature of both components and because the matrix is available as aqueous dispersion (latex). Moreover, the effect of these nanocrystals can be easily compared to the one of any of the other fillers for NR published in literature[14]. Results indicate that waxy maize SNC [10] have a similar reinforcing effect than bagasse cellulose nanocrystals [12]. In addition, waxy maize SNC display higher barrier properties (due to their platelet morphology) [10] and higher biodegradability than cellulose nanocrystals[15].

Most studied SNC are produced from waxy maize starch, especially for nanocomposite applications[6], because of their high amylopectin content. Recent papers described the processing, structural[11] and mechanical[10] properties of SNC nanocomposites, as well as the reinforcing mechanism[16]. To assess the possible use of other starch sources, a recent study [17] has investigated the effect of the botanic origin and amylose content of initial starch on the final properties of ensuing starch nanocrystals. It revealed that native starch's amylose content and crystalline type are the most influencing factors on SNC's morphology, crystallinity and rheology.[17] It was shown that the higher the initial amylopectin content, the squarer the platelets. In the present paper, the swelling and mechanical properties of NR filled with SNC from four other sources have been investigated and compared to existing data for waxy maize SNC. The aim of this work was to complete our knowledge on the influence of botanic sources on the final properties of SNC and their potential in nanocomposite application.

I.2. Materials & Methods

I.2.1. Materials

Starches were kindly provided by Cargill (Krefeld, Germany) according to requirements: waxy maize starch (C☆Gel 04201, 98% amylopectin), normal maize starch (Cerestar RG 03453), amylomaize (Amylogel 03003, 65-75% amylose), potato starch (C☆Gel 30002) and wheat starch (Cerestar PT 20002). Sulfuric acid (96%-99%, Sigma Aldrich) was used after dilution at 3.16M with distilled water.

Natural Rubber (NR) was kindly provided as NR latex by Michelin (Clermont Ferrand, France) and used as matrix material. It contained spherical particles with an average diameter around 1µm and its solid content was 57.8 wt%. The density of dry NR, ρ_{NR}, was 1g.cm^{-3} and it contained more than 98% of cis-1,4-polyisoprene.

I.2.2. Starch Nanocrystals and Nanocomposite Preparation

The optimized hydrolysis process developed by Angellier et al. [18] was adapted to 1L to prepare nanocrystals from the four different starches. Briefly, 147g of starch was mixed with 1L of previously prepared diluted sulfuric acid (3.16M). The suspension was kept under 100 rpm mechanical stirring at 40°C, using a silicon bath, for 5 days. The final suspensions were washed by successive centrifugations with distilled water until reaching neutral pH and redispersed using Ultra Turrax for 5 min at 13,000 rpm to break aggregates. The obtained suspensions were filtered on a filter tissue (40 µm, ref. 03-41/31 Buisine, France). Sodium azide was added to the suspensions before storage at

4℃ to avoid microbial growth. Detailed characteriz ation of these nanocrystals is reported elsewhere[17, 19].

The SNC-NR nanocomposites were obtained by casting/evaporation at 40℃ from the mixing in various proportions of the aqueous suspensions of SNC and NR latex. Targeted loading levels were 0 wt%, 5 wt% and 30 wt%. These filler contents were chosen because they are believed to be respectively under and above the percolation threshold. The codification of the samples is reported in Table 4-I.1.

Table 4-I.1. Codification of the samples

	Origin of Starch*	SNC (wt%)	NR (wt%)
NR100	—	0	100
P21-NR95	Potato (21%)	5	95
M27-NR95	Maize (27%)	5	95
W28-NR95	Wheat (28%)	5	95
M70-NR95	Maize (70%)	5	95
P21-NR70	Potato (21%)	30	70
M27-NR70	Maize (27%)	30	70
W28-NR70	Wheat (28%)	30	70
M70-NR70	Maize (70%)	30	70

* The value into brackets corresponds to the amylose content.

I.2.3. Microscopy

An environmental scanning electron microscope (**ESEM**) on a Quanta 200 FEI device (Everhart-Thornley Detector) was used at high voltage (10 kV) to observe the fractured cross-section of the composites.

I.2.4. Water and Toluene Uptake

The kinetics of toluene and water absorption was determined for all nanocomposites. The specimens were squared films with dimensions around 10x10x0.6 mm^3. The films were assumed to be thin enough so that the diffusion was supposed to be unidirectional. First, all samples were dried in a desiccator (0%RH) for a week. After being weighted using a four-digit balance, the samples were immersed in distilled water or toluene. The samples, tested in triplicate, were removed at specific intervals and weighted. The molar water uptake (WU) as well as molar toluene uptake (TU) of each sample was calculated as follows:

$$WU/TU\ (mol\%) = Q_t\ (mol\%) = \frac{Mass\ of\ absorbed\ solvent}{Molecular\ weight\ of\ solvent \times Initial\ mass\ of\ nanocomposite}$$

$$WU/TU\ (mol\%) = = \frac{m_t - m_o}{M_w \times m_o} \times 100$$

where m_0 and m_t are the weights of the samples before and after a time t of immersion, respectively; and M_w is the molecular weight of the solvent (i.e. 18.01 g.mol^{-1} for water and 92.14 g.mol^{-1} for toluene). Reported values are the mean of triplicates. The diffusion coefficient, D, of a solvent molecule through a polymer membrane can be obtained using a Fickian's second law of diffusion [20]:

$$D = \pi\left(\frac{e \times \theta}{4Q_\infty}\right)^2$$

where e is the membrane's thickness, θ the slope of the initial linear portion of the plot of Q_t against $t^{-1/2}$ and Q_∞ is the equilibrium absorption.

The sorption coefficient, S, was calculated using:

$$S = \frac{M_\infty}{M_o} = \frac{Q_\infty}{M_w}$$

where M_∞ is the mass of solvent sorbed at equilibrium and M_o is the initial mass of the polymer film.

The permeability coefficient, P, of the solvent in the NR nanocomposite was obtained as:

$$P = D \times S$$

I.2.5. Water Vapor Permeability

Static water vapor permeability (WVP) was measured according to the cup method (ASTM Standards, 1995). Circular films (60 cm²) of NR filled with 0 wt%, 5 wt% or 30 wt% SNC were placed to hermetically cover aluminum cups containing 5g of desiccant (anhydrous $CaCl_2$). A hermetical toric joint was used to seal the cup. The whole device was weighted and placed in humidity and temperature controlled chamber (38°C, 90% RH). The cups were weighted at regular interval of time until reaching equilibrium. All the tests were performed in triplicate at atmospheric pressure (1 atm) and WVP was reported as the average of these three values:

$$WVP\,(g.m^{-1}.s^{-1}.Pa^{-1}) = \frac{\Delta m \times e}{A \times \Delta t \times \Delta P}$$

where Δm corresponds to the mass increase of the $CaCl_2$ sample, A is the area of the film, Δt is the exposure time in the chamber, e the thickness of the sample and ΔP the partial water vapor pressure difference across the film specimen corresponding to 0%-90% RH, i.e. 2,555Pa.

I.2.6. Dynamic Mechanical Analysis

Dynamical mechanical analysis (DMA) measurements were carried out for the nanocomposite films using a RSA3 (TA Instruments, USA) equipment working in tensile mode. The measurements were performed at a constant frequency of 1 Hz, strain amplitude of 0.008%, in the temperature range from −100 to 100°C, heating rate of 5°C.min $^{-1}$ and a distance between jaws of 10 mm. The width of the samples varied from 4 to 6 mm, which was measured before each analysis.

I.2.7. Tensile Tests

Tensile tests were carried out with a RSA3 (TA Instrument, USA) equipment fitted with a 100 N load cell. Measurements were performed, in triplicate, at room temperature (~25°C), with a cross head speed of 0.6 mm.min $^{-1}$ for the first 250s, then 1.5 mm.min^{-1} up to 2000s, and finally 3 mm.min^{-1} up to the break. The samples dimensions were 10x5x0.5 mm^3 and results were averaged on 4 replicates.

I.2.8. Successive Tensile Tests

Successive tensile tests were performed to characterize the damage process occurring during tensile tests. They were carried out with an Instron 4301 machine. The initial gap between pneumatic jaws was adjusted to 10 mm. At the beginning of each experiment, the sample was first stretched under a load of 0.5 N. Then, the experiment consisted in stretching the sample up to an elongation ΔL1 of 10 mm (cycle 1), then releasing the force down to 1.5 N, and stretching again the material up to ΔL2 = 2ΔL1 (cycle 2). This procedure was repeated with increasing elongation ΔLi = iΔL1 until break of the sample.

I.3. Results & Discussions

I.3.1. Structural Properties

Morphology of nanocomposite films

Scanning electron micrographs of the fractured cross-section of NR filled with 0wt%, 5 wt% and 30 wt% M27 SNC have been collected in Figure 4-I.1.

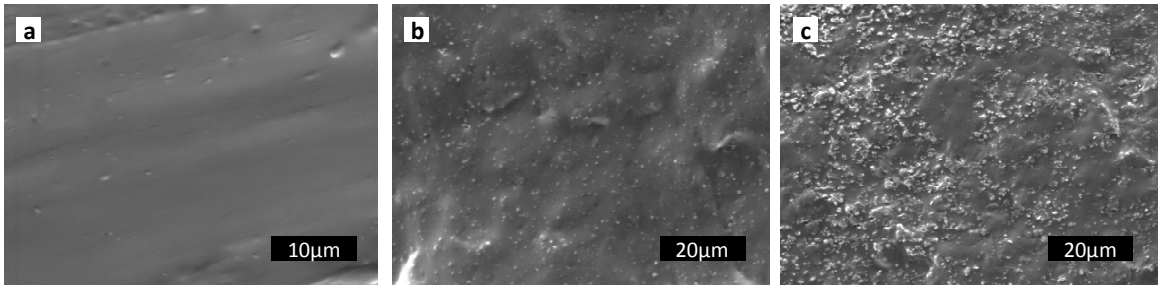

Figure 4-I.1. Scanning Electron Micrographs of the fractured cross-section of (a) NR100, (b) M27-NR95 and (c) M27-NR70.

The fractured surface of the unfilled NR matrix (Figure 4-I.1.a) is clearly smooth and uniform. By comparison, SNC and SNC concentration are easy to identify (white dots) in the filled NR composites (Figure 4-I.1.b and 1.c). Although the distribution of SNC among the matrix seems rather homogeneous, the fact that SNC can be spotted in these micrographs reveals that parts of the SNC are rather "homogeneously aggregated" throughout the matrix. A recent study[21] has proved the coexistence of both micro and nano-scaled particles among classically prepared SNC suspensions, such as the one used for this study. Thus, even though macro-scaled particles are observed, parts of SNC are also still nano-scaled and well dispersed. These observations, comparable for the films with the SNC produced from other starch sources, are in agreement with the micrographs obtained for waxy maize SNC filled NR[11]. Also, from the micrographs and from small angle light scattering performed by Angellier et al.[11], it can be considered that no particular sedimentation of SNC within the thickness of the film occurred.

Swelling/ permeation behavior

The swelling behavior of the composites was studied using two swelling media, viz. toluene which is known to be a good solvent for NR, and water which is known to be a non-solvent for NR but has a high affinity for polysaccharides. In absorption kinetic experiments, the mass of adsorbed solvent is measured as a function of time and reported as the molar mass percentage uptake as a function of time to the square root. Figure 4-I.2 displays the mean absorption kinetic of toluene (panel a) and water (panel b) for SNC/NR nanocomposites.

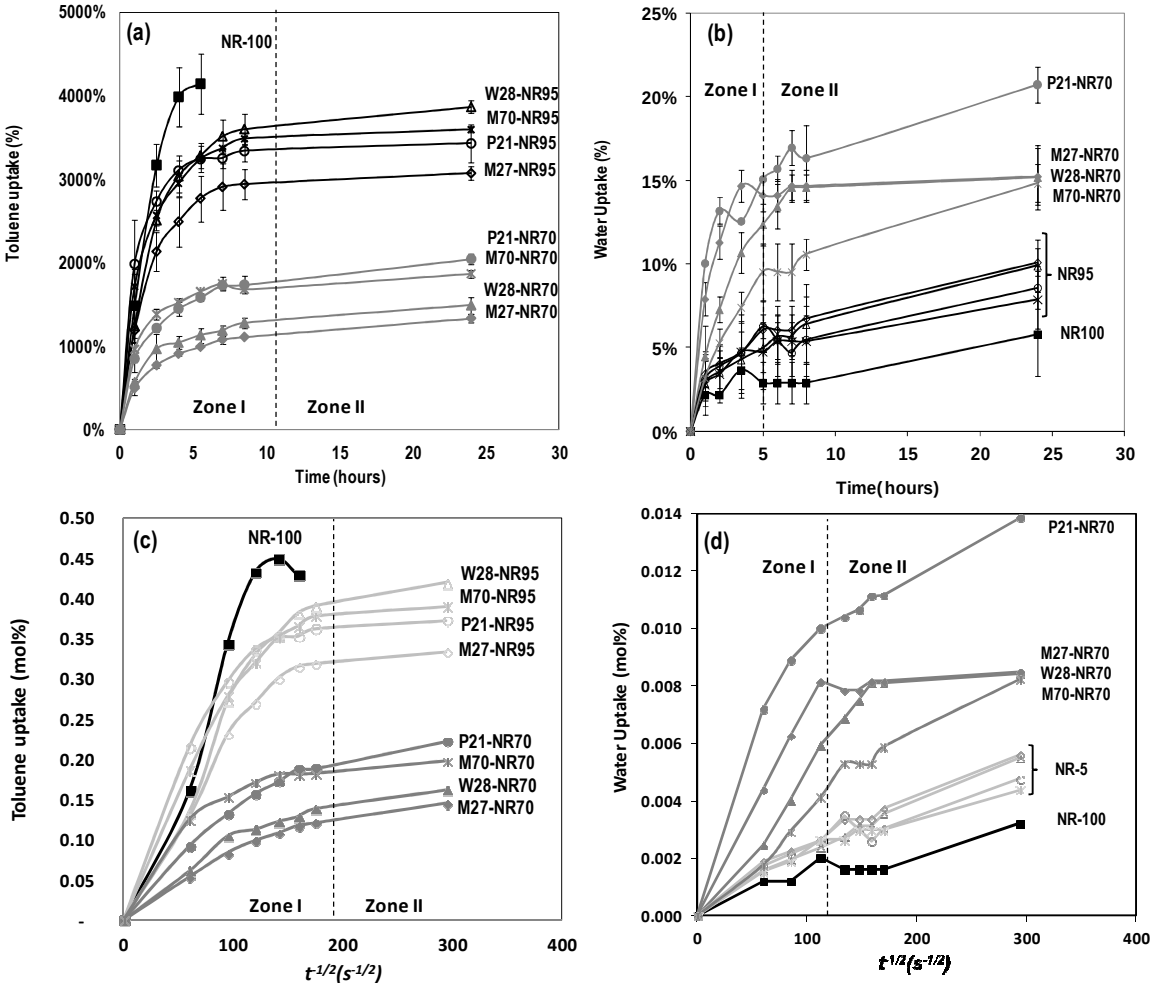

Figure 4-I.2. Evolution of (a) and (c) toluene uptake and (b) and (d) water uptake as a function of time and $t^{-1/2}.s^{-1/2}$ respectively, at room temperature for SNC-NR95 nanocomposites (empty symbol) and SNC-NR70 nanocomposites (full symbol) with SNC prepared from W21 (▲), M27 (♦), P28 (●) and M70 (ж).

Toluene. All nanocomposites absorbed toluene during the experiment. However, some films were more sensitive than others. Partial disruption of the film's integrity occurred for unfilled (NR100) or poorly loaded NR (NR95) preventing further measurements. Therefore, for the unfilled matrix, the toluene uptake at equilibrium was considered to be infinite, and measurements for SNC-NR95 nanocomposites were stopped after 24h and equilibrium was considered to be reached at this immersion time. For all nanocomposites, and as reported elsewhere[11, 13, 22], two zones can be identified: a first one (Zone I) of fast absorption kinetic for t<10h, and a second plateau-like one (Zone II) upon reaching equilibrium after 10h. The toluene uptake values at equilibrium, as well as diffusion coefficient, sorption coefficient and permeation coefficient are given in Table 4-I.2. All nanocomposites with the same SNC content show similar uptake values no matter the SNC source. No obvious correlation to starch type or initial starch amylose content was observed.

Table 4-I.2. Toluene and water sorption properties of SNC/NR nanocomposites

Medium	TOLUENE UPTAKE (TU)				WATER UPTAKE (WU)			
Sample	TU Molar % at equilib	Diffusion $D_{toluene}$ ($cm^2.s^{-1}x10^{-8}$)	Sorption S (%)	Permeation $P_{toluene}$ ($cm^2.s^{-1}x10^{-8}$)	WU Molar % at equilib	Diffusion D_{water} ($cm^2.s^{-1}x10^{-10}$)	Sorption S (%)	Permeation P_{water} ($cm^2.s^{-1}x10^{-10}$)
NR100	∞	4.2	∞	∞	0.32	0.04	6	0.24
NR-100*	∞	*40*	∞	∞	-	*0.04*	7	0.28
M1-NR95*	-	*12.8*	*3290*	*42112*	-	*0.29*	8	2.32
P21-NR95	37	1.64	3428	*5621*	0.48	0.14	9	1.26
M27-NR95	33	2.73	3071	*8383*	0.56	0.16	10	1.6
W28-NR95	42	1.35	3866	*5219*	0.55	0.14	10	1.4
M70-NR95	39	1.72	3592	*6178*	0.44	0.14	8	1.12
M1-NR70*	-	*3.4*	*1320*	*4488*	-	*5.61*	22	123.42
P21-NR70	22	1.29	2043	*2635*	1.39	3.33	25	83.25
M27-NR70	14	4.61	1332	*6140*	0.85	1.22	15	18.3
W28-NR70	16	3.17	1488	*4716*	0.84	1.15	15	17.25
M70-NR70	20	0.84	1865	*1566*	0.82	0.65	15	9.75

However, for SNC-NR95 nanocomposites, a correlation (R^2 = 0.79) between the sorption and the theoric calculated specific surface area of the different SNC, which values are reported in Table 4-I.3, was found. The higher the theoretical specific surface, the higher the toluene uptake, and the lower the diffusivity. At low filler content, particles can homogeneously disperse and effectively (i) interact with the matrix preventing the swelling of polymeric chains located at the interfacial zone and/or (ii) form a network via strong hydrogen bonds when above percolation threshold as calculated using Celzard et al.'s model[23] in Table 4-I.3. As reported for chitin[9] and cellulose nanocrystals[13], such percolation strongly modifies nanocomposite structures and properties.

Table 4-I.3. SNC specific surface area and predicted percolation threshold calculated from measured dimensions [17]

Starch type	Specific area	Percolation (wt%)			
	Calculated (m²/g)	*Celzard et al, 1996 inf*	*sup*	*Lu et Mai, 2005*	*Experimental (wt%)*
M70	325	7.1%	10.8%	13.9%	
M27	221	11.4%	17.1%	22.7%	
M1	302	11.5%	17.3%	22.9%	10%[11]
W28	465	9.1%	13.8%	17.9%	
P21	218	7.8%	11.9%	15.3%	31%[24]

For SNC-NR70 nanocomposites, no such observation can be made. This is most likely due to the aggregation phenomena at higher filler content. Indeed, as the filler content increases and thus the fraction of material able to swell (i.e. NR matrix) decreases, the toluene uptake logically decreases. However, the diffusivity of toluene through the samples remained the same suggesting that aggregation did occur (no increase in total specific area), and prevented the formation of a denser network.

Water. As for toluene experiments, all nanocomposites absorbed water during immersion, even the unfilled matrix (NR100), and all exhibit a two-stage kinetic. Zone I was reduced and plateau was reached after 5h. All films remained self standing during the experiment. Mean water uptakes of NR nanocomposites are represented in Figure 4-I.2.b.

Sorption and diffusivity values are also reported in Table 4-I.2. Roughly, the higher the hydrophilic filler content, the higher the values. However and contrary to toluene, for SNC-NR95 nanocomposites, no significant difference in uptake, sorption or diffusivity between NR nanocomposites was observed. Water uptake is in agreement with Angellier at al.'s [11] finding. For SNC-NR70 nanocomposites, all coefficients seem to decrease with increasing initial starch amylose content. This could be attributed to the presence of amorphous or less organized and less bonded amylose chains in SNC prepared from higher amylose content starch. This amorphous material does not participate to the formation of a diffusing network but participates to the water sorption explaining why similar equilibrium values are reached.

The fact that for 5 wt% SNC, water sorption does not differ among nanocomposites whereas it is correlated to the specific surface for toluene uptake suggests that in the case of toluene uptake, the second mechanism linked to the polymer

chains swelling hindrance should not be underestimated. At 30 wt% SNC filler content, a percolation network most likely exists. However, at high filler content it is suspected that: (i) poorer homogeneous distribution occurs leading to a lower specific area and thus the same toluene swelling hindrance as for 5%; and that (ii) SNC produced from higher amylose content starch might release amylose chains during soaking or preparation in water explaining diffences in water sorption kinetics.

Water Vapor Permeability

Resistance to water vapor permeation (WVP) is an essential requirement in composites for some applications such as packaging. Despite the high moisture sorption of pure polysaccharides, it has been reported that the use of cellulose nanocrystals can reduce WVP thanks to high crystallinity and induced tortuosity [25, 26]. Giving their platelet morphology, SNC are suspected, as nanoclays do, to strongly decrease WVP. WVP of studied films are reported in Figure 4-I.3. It is observed that WVP increases upon the addition of SNC. Slight differences between nanocomposites can be evidenced. Moreover, they do not correlate with initial amylose content, nor with crystalline type or botanic origin. This increase in WVP can be explained by several factors.

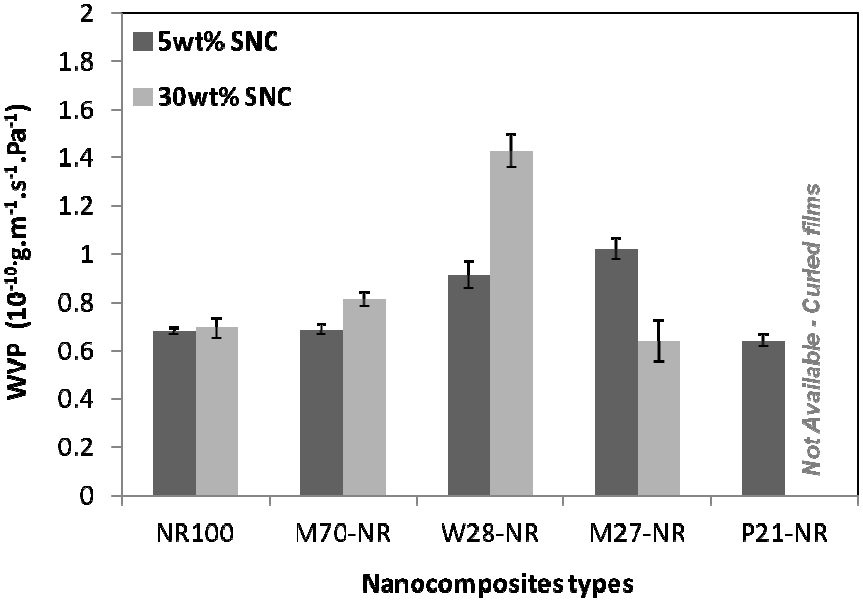

Figure 4-I.3. Water vapor permeability of SNC-NR nanocomposites.

As witnessed from WU and TU, the NR matrix is very hydrophobic and the SNC highly hydrophilic. As WVP has been measured under tropical condition (38°C, 90%RH), it is possible that the hydrophilic nature of SNC is predominant. Also, the unfilled matrix used in this study is already 10 times more impermeable to water vapor than in other studies [10, 27]. Thus the SNC might have a detrimental effect on WVP. A previous study [12] using the exact same NR matrix has also shown an increase in WVP upon the addition of cellulose nanocrystals contrary to what had been witnessed with other matrices such as PVA [25, 26]. Finally, decrease of WVP by SNC has often been reported for contents below 3 wt% [27] or higher than 30 wt% [28]. This could be explained by the fact that at very low content, SNC can effectively disperse into the matrix. At higher content (5-30 wt%) though, SNC tend to aggregate and might create defects inside the matrix. Finally at very high filler content (>30 wt%), the amount of crystalline particles is sufficiently high to lower the permeability.

I.3.2. Mechanical Properties

The potential of SNC as a reinforcing phase in the NR matrix has been evaluated from a mechanical point of view, both in the non-linear (tensile tests) and linear (DMA) range.

Tensile tests

In the non-linear range, all SNC-NR nanocomposites displayed an elasto-plastic behavior as presented in Figure 4-I.4. It is typical of amorphous rubbery materials. The stress regularly increases with the strain up to the break of the film.

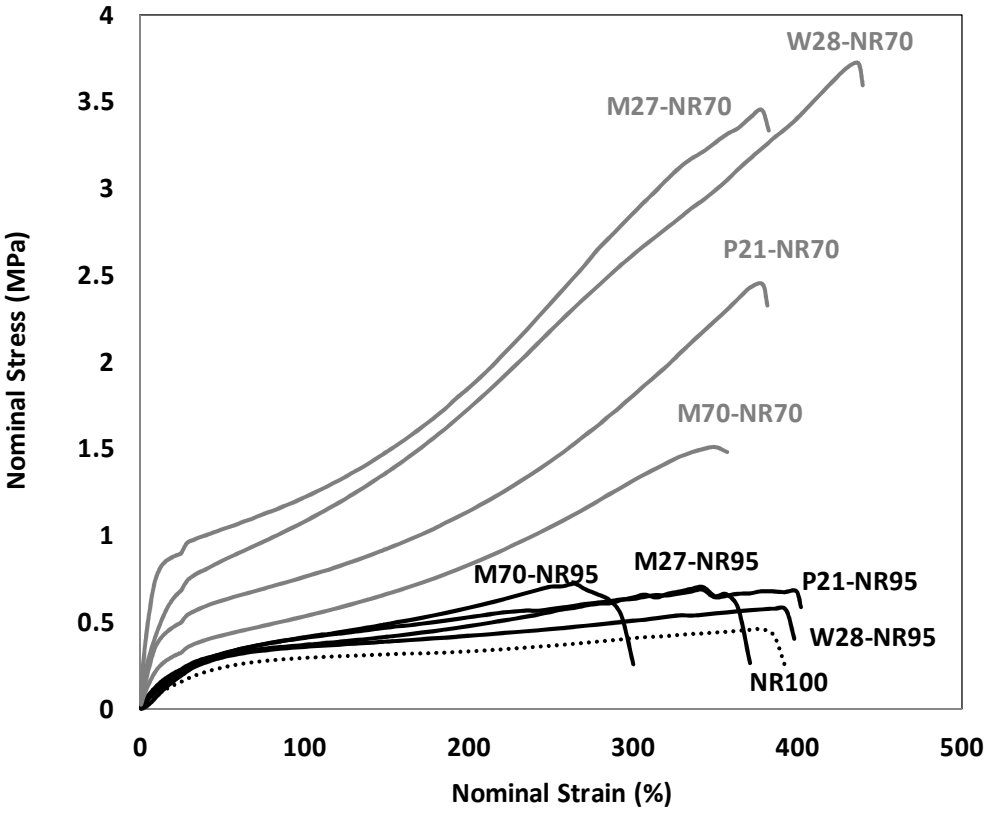

Figure 4-I.4. Typical nominal stress vs. nominal strain curves of P21, M27, W28 and M70 SNC/ NR nanocomposite films filled with 5 wt% (black curves) and 30 wt% (grey curves) SNC. Dotted curve corresponds to unfilled matrix.

Paper 7

Table 4-I.4 gathers Young's Modulus (E) and conventional modulus at 100% elongation (E_{100}), tensile strength (σ_b) and elongation at break (ε_b) for the 5 different composites at two different filler contents, viz. 5 wt% and 30 wt%. The relative data are also given in Table 4-I.4 to allow for comparison with other studies. Properties greatly evolved with increasing SNC content. For all composites, no matter which SNC's botanic origin, tensile strength and Young's modulus were improved. More unusual is the rather stable values for elongation at break which indicate that composites are reinforced without becoming brittle. Angellier et al. [10] did not reported such observation when using waxy maize SNC, although it seems that elongation at break remained relatively stable below 10 wt% SNC. On the contrary, this phenomenon was also reported for waterborne polyurethane nanocomposites filled with waxy SNC [29], suggesting it is rather linked to the matrix's properties.

Table 4-I.4. Mechanical properties of M70, M27, P21, W28 and M1 SNC/NR nanocomposites films obtained from tensile tests: tensile modulus at 100% elongation (E_{100}), tensile modulus (E), strength (σ_b) and elongation at break (ε_b) and relative tensile modulus at 100% elongation ($E_{rel,100}$), relative strength at break ($\sigma_{rel,b}$), and relative elongation at break ($\varepsilon_{rel,b}$).

Sample	E_{100} (MPa)	E (MPa)	σ_b (MPa)	ε_b(%)	$E_{rel,100}$	E_{rel}	$\sigma_{b,rel}$	$\varepsilon_{b,rel}$	Ref
NR100	0.26	0.79 ± 0.15	0.42 ± 0.03	333.78 ± 42.7	-	1.00 ± 0.38	1.00 ± 0.12	1.00 ± 0.26	Present study
M1*-NR95	-	1.60	7.20	1796.00	1.60	2.46	1.95	0.91	[10]
P21-NR95	0.42	0.91 ± 0.15	0.89 ± 0.28	427.45 ± 96.07	1.63	1.15 ± 0.35	2.11 ± 0.38	1.28 ± 0.35	Present study
M27-NR95	0.34	1.22 ± 0.10	0.93 ± 0.23	410.93 ± 65.03	1.31	1.53 ± 0.27	2.20 ± 0.31	1.23 ± 0.29	Present study
W28-NR95	0.31	0.91 ± 0.14	0.61 ± 0.05	391.05 ± 61.10	1.22	1.15 ± 0.34	1.43 ± 0.14	1.17 ± 0.28	Present study
M70-NR95	0.42	1.08 ± 0.21	0.64 ± 0.18	274.72 ± 61.23	1.63	1.35 ± 0.39	1.50 ± 0.34	0.82 ± 0.35	Present study
M1*-NR70	-	77.80	8.90	920.00	8.00	119.69	2.41	0.47	[10]
P21-NR70	0.76	4.07 ± 0.19	2.55± 0.13	392.45 ± 22.70	2.96	5.12 ± 0.23	6.03 ± 0.11	1.18 ± 0.19	Present study
M27-NR70	1.20	11.97 ± 0.41	3.60 ± 0. 25	426.76 ± 63.15	4.68	15.07 ± 0.22	8.50 ± 0.13	1.28 ± 0.28	Present study
W28-NR70	0.94	3.49 ±1.21	2.97 ± 1.10	440.68 ± 23.95	3.66	4.39 ± 0.53	7.01 ± 0.43	1.32 ± 0.18	Present study
M70-NR70	0.54	2.32 ± 0.32	1.55 ± 0.21	344.01 ± 41.81	2.11	2.92 ± 0.33	3.66 ± 0.19	1.03 ± 0.32	Present study
Bagasse CW-NR95	-	-	-	-	-	1.44	1.48	0.54	[12]
ChW-NR95	-	-	-	-	-	2.78	1.76	0.53	[9]
MMT-NR95	-	-	-	-	-	1.00	1.06	1.13	[30]
CB-NR90	-	-	-	-	-	1.41	1.16	0.66	[31]

Figure 4-I.5 represents the relative Young's Modulus E_{rel} (i.e. the ratio of Young's modulus of the composite to the one of the unfilled matrix) for each composite. Values are lower than those reported for waxy maize SNC [10]. For SNC-NR95 nanocomposites, the reinforcing effect seems to be limited and similar regardless the origin of starch. For SNC-NR70 nanocomposites, as expected, values are higher due to the network formed by the nanocrystals through more numerous hydrogen bonding (initiated from the percolation threshold).

Also, it seems that a general trend is: the greater the amylose content (and the lower the initial crystallinity) of the starch used for preparing SNC, the lower the reinforcing effect (except for potato starch), as presented in Figure 4-I.5. For example, when comparing NR composites reinforced with SNC from maize starches with decreasing amylose content (resp. 70%, 27% and 1%), the Young's modulus is multiplied respectively by 3, 15 and 100 times compared to the neat matrix. This observation supports the hypothesis of loose /less organized amylose in the matrix as described in section 3.1.1. Thus, native starch's amylose content is an important parameter to consider when preparing SNC for nanocomposite application.

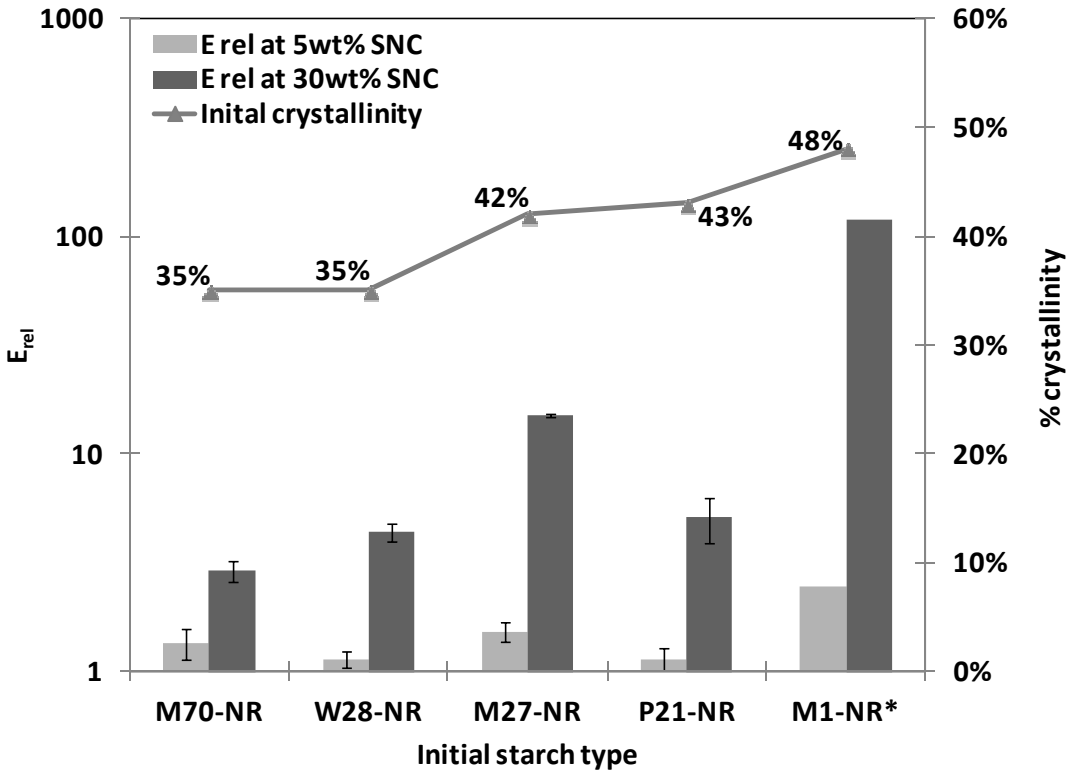

Figure 4-I.5. Relative young's modulus (Erel) for SNC-NR nanocomposites filled with SNC prepared from different starch sources with different amylose content and crystallinity index.

Dynamic mechanical analysis

In the linear range, the logarithm of the storage modulus, log(E'), and the tangent of the loss angle, tan(δ), versus the temperature was measured between -100℃ and +100℃ as presented in Figure 4-I.6.

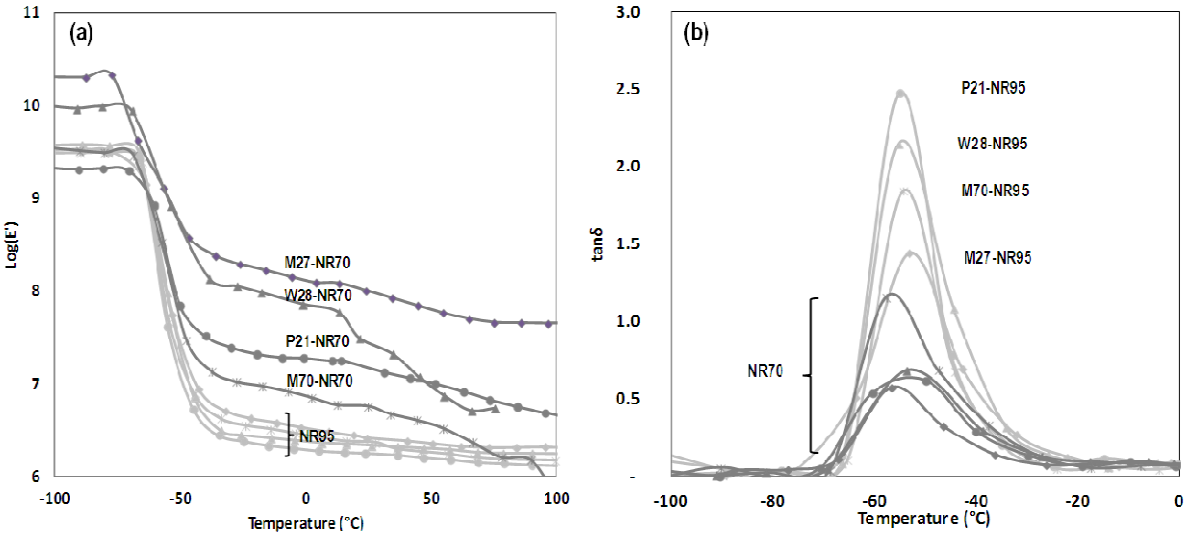

Figure 4-I.6. (a) Logarithm of the storage tensile modulus log E' and (b) tangent of the loss angle tanδ vs temperature at 1Hz for NR-based nanocomposite films reinforced with SNC prepared from W21 (▲), M27 (♦), P28 (●) and M70 (ж) -.

For SNC-NR95 nanocomposites, the curves are typical of an amorphous high molecular weight thermoplastic polymer. Below the glass transition temperature of the matrix, the polymer is in the glassy state. Then around -55℃, corresponding to T_g of the polymer and the SNC-NR95 nanocomposites (as measured by DSC - not presented here), a sharp decrease of about 3 decades is observed corresponding to the glass-rubber transition. This relaxation process results in a damping phenomenon as shown in Figure 4-I.6.b. Lastly, the modulus tends to reach a plateau corresponding to the rubbery state. As for tensile tests, the reinforcing effect of SNC is significantly higher for SNC-NR70 nanocomposites (20 times higher than for SNC-NR95). This reinforcing effect is usually ascribed to the formation of a stiff hydrogen-bonded mechanical percolation filler network [10, 14, 32]. However, it was very recently demonstrated that the behavior displayed by NR/SNC nanocomposites could not only be related to the formation of a percolating network of fillers but is actually mainly governed by filler-polymer interactions [16]. To assess this reinforcing effect, the rubbery storage moduli at 25℃ have been reported in Table 4-I.5. Also, the main α relaxation process ascribed to Tg of the matrix seems to reflect two phases. First, a rapid decrease of about 2 decades, comparable to modulus

drop of SNC-NR5 nanocomposites, and second, a slower decrease of about 1 decade before reaching the rubbery plateau most likely due to restricted molecular movement induced by the SNC network. The characteristics of the α relaxation associated with the anelastic manifestation of the glass-rubber transition of the polymer are reported in Table 4-I.5. Increasing the SNC content result in a strong decrease of its magnitude I_α as the number of mobile units participating to the relaxation process decreases.

Table 4-I.5. Rubbery storage tensile modulus estimated at 25°C (E'_{R25}) and temperature position (T_α) and magnitude (I_α) of the tanδ peak associated with the α relaxation process for SNC/NR nanocomposites films.

	E'_{R25} (Pa)	T_α(°C)	I_α
P21-NR95	1.8	-55.6	2.6
M27-NR95	2.7	-55.4	1.9
W28-NR95	2.3	-54.5	2.4
M70-NR95	2.4	-55.3	1.8
P21-NR70	23.7	-56.4	0.8
M27-NR70	32.4	-57.1	0.6
W28-NR70	49.3	-56.3	1.0
M70-NR70	5.8	-55.5	1.3

The general trend is comparable to what has been observed from tensile tests, i.e. the higher the amylose content of the starch used for preparing SNC, the lower the reinforcing effect (except for potato starch).

Successive tensile tests

Successive tensile tests were performed for all SNC-NR nanocomposites except P21-NR70 (lack of sample). Figure 4-I.7 shows the typical evolution of the stress versus strain for the unfilled matrix (NR100) and for M27-NR95 and M27-NR70. As expected, SNC brings a high reinforcement to the NR matrix especially for 30% filler content. The reinforcing effect is in the same magnitude (10^0MPa) than that measured for regular tensile tests.

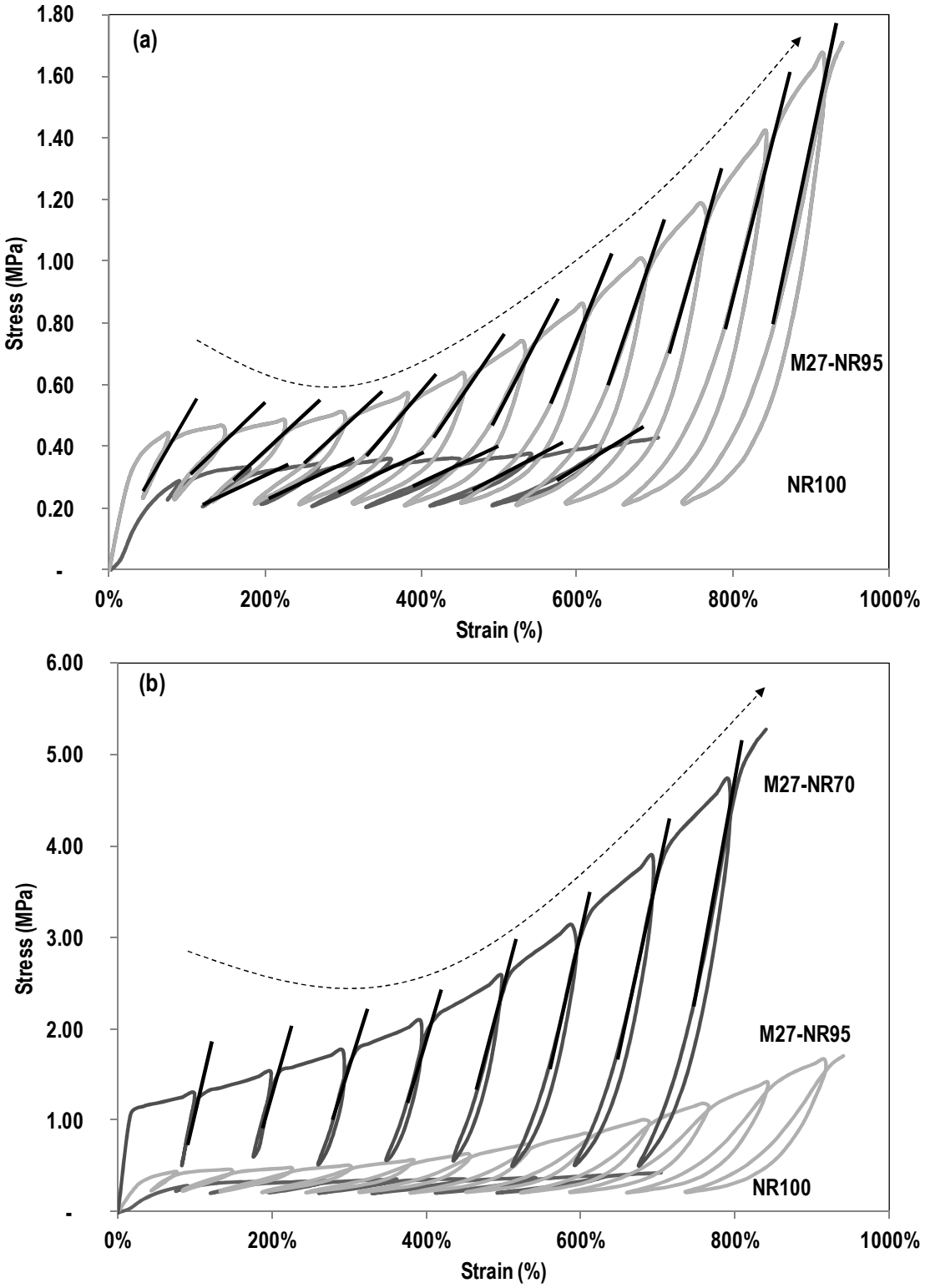

Figure 4-I.7. Evolution of stress versus strain for SNC/NR nanocomposite films during successive tensile test. Example is given for M27 SNC with NR100; NR95 and NR70:(a) allows observing the evolution of the tensile modulus for NR100 and NR95 and (b) for the NR70 nanocompositses.

Figure 4-I.7 shows that for each cycle, the elongation step and the recovery (negative elongation) differ significantly. During stretching, short macromolecular chains can diffuse within the surrounding entangled lattice but do not tangle again immediately during the recovery step because of the viscous nature of the polymer[9]. Therefore, the curves recorded during positive and negative elongation steps do not superimpose and a permanent strain remains, at the time scale of the experiment.

The mechanism involved during successive tensile tests was previously detailed for NR filled with waxy maize SNC [10], chitin [9] and cellulose whiskers [13]. For the unfilled NR matrix, the tensile modulus continuously increased during the successive tractions due to the strain-induced crystallization of NR. At low filler content (5%), the behavior of the poorly filled nanocomposite was mainly governed by that of the matrix. The tensile modulus increases from the second cycle on, as no percolation network can disrupt or limit the strain-induced-crystallization of NR. At higher filler content (above 5wt%), first the relatively high tensile modulus decreases across a few cycles (about 5) until the SNC-network was disrupted. Then the modulus stabilized, indicating the complete disruption of the network and no strain-induced crystallization of NR.

In this study, observations are somewhat comparable. The unfilled matrix exhibited stable tensile moduli over a few cycles (about 4) and then continuously increased during the successive tractions due to the strain induced crystallization. For nanocomposites filled with 5wt% and 30% wt SNC, the tensile modulus decreased over a few cycles (about 4) and then increases. This is possibly due to the presence of SNC which delayed the strain induced crystallization of the matrix. From these results, it is suggested that the SNC used in this study, were not ideally dispersed, and did not form a strong mechanical percolation network but rather a weak easily disturbed percolation network. Such a network increase Young's modulus of the nanocomposites but cannot resist successive tractions and prevent recrystallization.

Concerning the influence of SNC type, it is observed, as presented in Figure 4-I.8, that M70-NR composites show the poorest mechanical properties. For NR95, the reinforcing effect of SNC are comparable for all SNC until 300% strain after which most reinforced nanocomposites are P21-NR95 < W28-NR95 < M27-NR95. For NR70, no correlation was observed between initial starch type and successive tensile values.

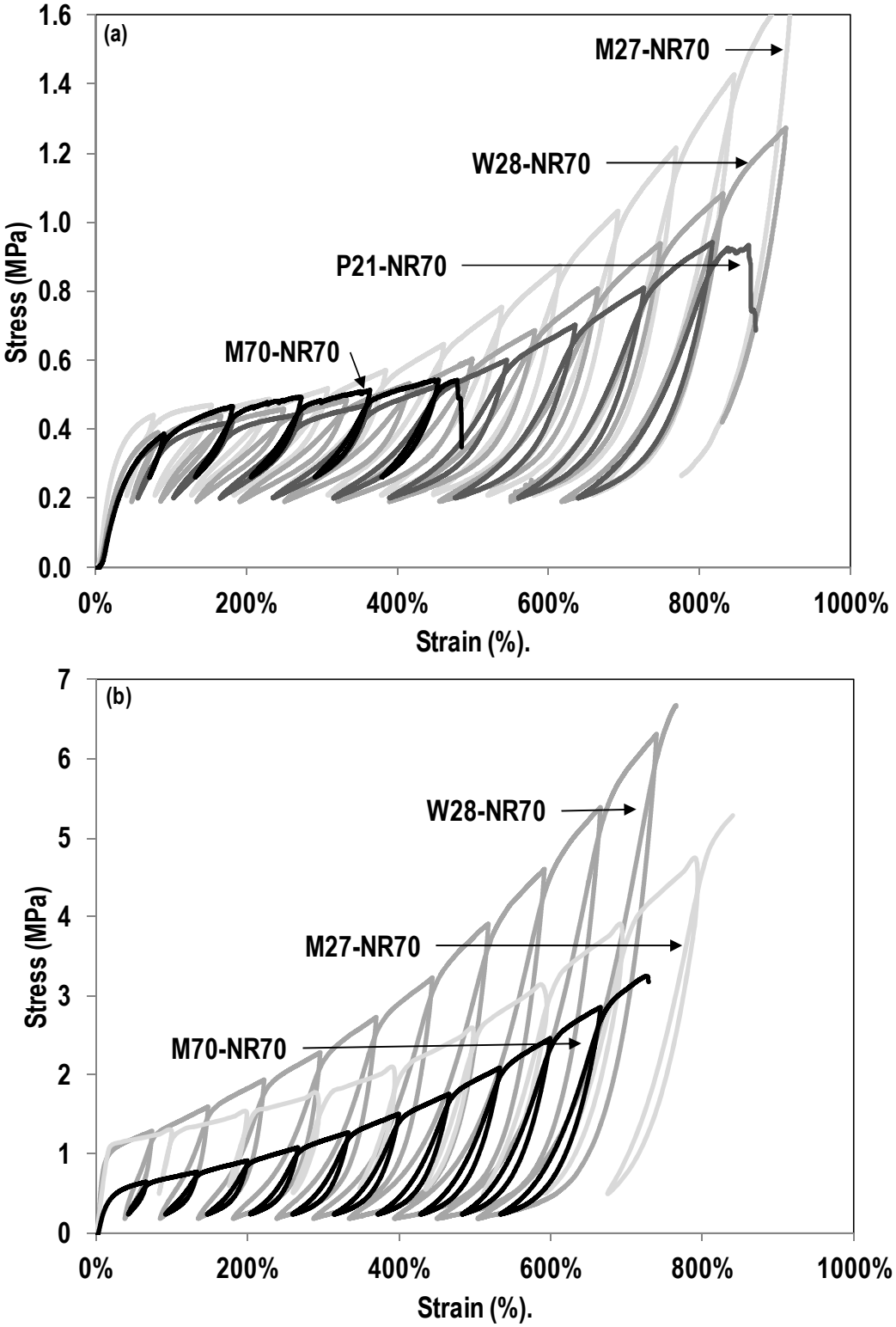

Figure 4-I.8. Evolution of stress versus strain for (a) SNC/NR95 and (b) SNC/NR70 nanocomposite films during successive tensile test.

I.4. Conclusion

Structural and mechanical properties of natural rubber (NR)-based nanocomposites reinforced with starch nanocrystals (SNC) extracted from four different botanical sources have been investigated. It reveals, from SEM and solvent uptake experiments that (i) from 5 wt% on, the gradual formation of a percolation network occurs, as shown by correlation to specific surface area; and that (ii) at 30 wt%, some SNC are “homogeneously aggregated”. Thus, when the matrix is highly hydrophobic, the SNC have a detrimental effect on water vapor permeability, especially at high filler content. Concerning the mechanical properties, at 5 wt% SNC loading, although properties are improved, no significant difference between the different nanocomposites is observed. At 30 wt% SNC though, the general trend is: the greater the amylose content of the starch used for preparing SNC, the lower the reinforcing effect (except for potato starch) keeping ductility of the material. It is postulated that SNC produced from higher amylose content starch might release loosely bonded amylose chains during preparation and/or soaking in water and thus presents fewer SNC to participate in the formation of a reinforcing and diffusing network. Thus, native starch’s amylose content is an important parameter to consider when preparing SNC for nanocomposite application.

I.5. References

1. Rezende, C. A.; Bragança, F. C.; Doi, T. R.; Lee, L.-T.; Galembeck, F.; Boué, F., Natural rubber-clay nanocomposites: Mechanical and structural properties. *Polymer* **2010,** 51, (16), 3644-3652.

2. Rooj, S.; Das, A.; Thakur, V.; Mahaling, R. N.; Bhowmick, A. K.; Heinrich, G., Preparation and properties of natural nanocomposites based on natural rubber and naturally occurring halloysite nanotubes. *Materials & Design* **2010,** 31, (4), 2151-2156.

3. Habibi, Y.; Lucia, L.; Rojas, O., Cellulose nanocrystals: chemistry, self-assembly, and applications. *Chemical Reviews* **2010,** 110, ((6)).

4. Azizi Samir, M. A. S.; Alloin, F.; Dufresne, A., Review of Recent Research into Cellulosic Whiskers, Their Properties and Their Application in Nanocomposite Field. *Biomacromolecules* **2005,** 6, (2), 612-626.

5. Siqueira, G.; Bras, J.; Dufresne, A., Cellulosic Bionanocomposites: A Review of Preparation, Properties and Applications. *Polymers* **2010,** 2, (4), 728-765.

6. Le Corre, D.; Bras, J.; Dufresne, A., Starch nanoparticles: A review. *Biomacromolecules* **2010,** 11, (5), 1139-1153.

7. Buléon, A.; Colonna, P.; Planchot, V.; Ball, S., Starch granules: structure and biosynthesis. *International Journal of Biological Macromolecules* **1998,** 23, (2), 85-112.

8. Gallant, D. J.; Bouchet, B.; Baldwin, P. M., Microscopy of starch: evidence of a new level of granule organization. *Carbohydrate Polymers* **1997,** 32, (3-4), 177-191.

9. Gopalan Nair, K.; Dufresne, A., Crab Shell Chitin Whisker Reinforced Natural Rubber Nanocomposites. 2. Mechanical Behavior. *Biomacromolecules* **2003,** 4, (3), 666-674.

10. Angellier, H.; Molina-Boisseau, S.; Dufresne, A., Mechanical properties of waxy maize starch nanocrystal reinforced natural rubber. *Macromolecules* **2005,** 38, (22), 9161-9170.

11. Angellier, H.; Molina-Boisseau, S.; Lebrun, L.; Dufresne, A., Processing and structural properties of waxy maize starch nanocrystals reinforced natural rubber. *Macromolecules* **2005,** 38, (9), 3783-3792.

12. Bras, J.; Hassan, M. L.; Bruzesse, C.; Hassan, E. A.; El-Wakil, N. A.; Dufresne, A., Mechanical, barrier, and biodegradability properties of bagasse cellulose whiskers reinforced natural rubber nanocomposites. *Industrial Crops and Products* **2010,** 32, (3), 627-633.

13. Bendahou, A.; Kaddami, H.; Dufresne, A., Investigation on the effect of cellulosic nanoparticles' morphology on the properties of natural rubber based nanocomposites. *European Polymer Journal* **2010,** 46, (4), 609-620.

14. Dufresne, A., Natural Rubber Green Nanocomposites. In *Rubber Nanocomposites: Preparation, Properties and Applications*, Thomas, S.; Stephen, R., Eds. Wiley: **2010**.

15. Kuemmerer, K.; Menz, J.; Schubert, T.; Thielemans, W., Biodegradability of organic nanoparticles in the aqueous environment. *Chemosphere* **2011,** 82, (10), 1387-1392.

16. Mélé, P.; Angellier, H.; Molina-Boisseau, S.; Dufresne, A., Reinforcing mechanisms of starch nanocrystals in a nonvulcanized natural rubber matrix. *Biomacromolecules* **2011,** 12, 1487-1493.

17. LeCorre, D.; Bras, J.; Dufresne, A., Influence of botanic origin and amylose content on the morphology of starch nanocrystals. *Journal of Nanoparticle Research* **2011,** Submitted.

18. Angellier, H.; Choisnard, L.; Molina-Boisseau, S.; Ozil, P.; Dufresne, A., Optimization of the preparation of aqueous suspensions of waxy maize starch nanocrystals using a response surface methodology. *Biomacromolecules* **2004,** 5, 1545-1551.

19. LeCorre, D.; Bras, J.; Dufresne, A., Influence of native starch's properties on starch nanocrystals thermal properties. *Carbohydrate Polymers* **2011,** Accepted.

20. Crank, J., *The mathematics of diffusion*. 2nd ed.; Clarendon Press: Oxford, **1975**; p.

21. LeCorre, D.; Bras, J.; Dufresne, A., Evidence of Micro- and Nanoscaled Particles during Starch Nanocrystals Preparation and Their Isolation. *Biomacromolecules* **2011,** 12, (8), 3039-3046.

22. Zheng, H.; Ai, F.; Chang, P. R.; Huang, J.; Dufresne, A., Structure and properties of starch nanocrystal-reinforced soy protein plastics. *Polym. Compos.* **2009,** 30, (4), 474-480.

23. Celzard, A.; McRae, E.; Deleuze, C.; Dufort, M.; Furdin, G.; Marêché, J. F., Critical concentration in percolating systems containing a high-aspect-ratio filler. *Physical Review B* **1996,** 53, (10), 6209.

24. Dufresne, A.; Cavaillé, J.-Y., Clustering and percolation effects in microcrystalline starch-reinforced thermoplastic. *Journal of Polymer Science Part B: Polymer Physics* **1998,** 36, (12), 2211-2224.

25. Garcia de Rodriguez, N. L.; Thielemans, W.; Dufresne, A., Sisal cellulose whiskers reinforced polyvinyl acetate nanocomposites. *Cellulose* **2006,** 13, (3), 261-270.

26. Paralikar, S. A.; Simonsen, J.; Lombardi, J., Poly(vinyl alcohol)/cellulose nanocrystal barrier membranes. *Journal of Membrane Science* **2008,** 320, (1-2), 248-258.

27. Garcia, N. L.; Ribba, L.; Dufresne, A.; Aranguren, M. I.; Goyanes, S., Physico-mechanical properties of biodegradable starch nanocomposites. *Macromolar Materials and Engineering* **2009,** 294, (3), 169-177.

28. Kristo, E.; Biliaderis, C. G., Physical properties of starch nanocrystal-reinforced pullulan films. *Carbohydrate Polymers* **2007,** 68, (1), 146-158.

29. Wang, Y.; Zhang, L., High-strength waterborne polyurethane reinforced with waxy maize starch nanocrystals. *J. Nanosci. Nanotechnol.* **2008,** 8, (11), 5831-5838.

30. Hrachová, J.; Komadel, P.; Chodák, I., Effect of montmorillonite modification on mechanical properties of vulcanized natural rubber composites. *Journal of Materials Science* **2008,** 43, (6), 2012-2017.

31. Arroyo, M.; López-Manchado, M. A.; Herrero, B., Organo-montmorillonite as substitute of carbon black in natural rubber compounds. *Polymer* **2003,** 44, (8), 2447-2453.

32. Dufresne, A., Polysaccharide nano crystal reinforced nanocomposites. *Canadian Journal of Chemistry* **2008,** 86, 484-494.

Chapter 4-II. All starch nanocomposite coating for barrier material

Déborah LeCorre, Alain Dufresne, Bertine Khelifi, Julien Bras

The International School of Paper, Print Media and Biomaterials (Pagora), Grenoble Institute of Technology – BP 65 – 38402 Saint Martin d'Hères Cedex – France

Abstract

Starch nanocrystals (SNC) are nano-fillers of growing interest for barrier and mechanical improvement of bio-based polymers. However, their potential use as fillers for organic coating material of industrial packaging has never been investigated. In this study, their processability in coating is assessed and the final properties of coated papers are measured. Coating colors show higher Brookfield viscosity when filled with SNC, even with the addition of water, but road coating is still possible This diluted water-based coating induces paper wetting and surface crackling issues during drying as proved by drying process analysis. However no gelatinization is observed whatever the type of drying, and SNC compensate the water induced loss of mechanical properties of the base paper and decrease the WVP up to 40% compared to the base paper.

Keywords

Starch; nanocrystals; drying; nanofiller; barrier

Inspired from: *D. LeCorre, A. Dufresne, B. Khelifi, J. Bras, Submitted to Progress in organic coatings, 2011*

Paper 8

II.1. Introduction

Nowadays, most efficient materials used for food packaging are usually undegradable[1] and fuel based, representing a serious environmental and sustainability problem. Despite an increasing number of studies[2-5], the use of bio-based materials has been limited due to their poor processing and performances such as brittleness, gas and moisture barrier. Nanofillers (defined as material exhibiting at least one dimension smaller than 100 nm[6]), have strong reinforcing effects. They have a high positive impact on mechanical properties of ensuing nanocomposites, and studies have also shown their positive impact in barrier properties[7, 8]. Thus, a solution for barrier materials consists in combining bio and nano-technologies.

Another key issue is the development of coating processes consisting in giving functionality to a material[9] by adding of a low quantity of another material.

An all-starch coating, consisting of thermoplastic starch and starch nanocrystals (SNC), is a potential candidate for this application. Indeed, starch is a natural, renewable, biodegradable polymer produced by many plants as a source of stored energy. It is one of the most abundant biomass materials in nature. It is found in plant roots, stalks, crop seeds and staple crops such as rice, corn, wheat, tapioca and potato.[1]

The predominant model for starch is a multi-scale structure consisting in the granule (2-100 µm), into which is found (a) alternating amorphous and semi-crystalline growth rings (120-500 nm) the latest being made of (b) amorphous and crystalline lamellae (9 nm)[10] containing (c) two glucosidic macromolecules: amylopectin and amylose (0.1-1 nm). Amylopectin is usually assumed to be the framework of the crystalline region. Starch nanoparticles have been reviewed recently[3] and SNC result from the disruption of the semi-crystalline structure of starch granules by the hydrolysis of amorphous parts. They exhibit a platelet-like morphology comparable to that of some clays, no matter the botanic origin of the native starch[11].

Recent studies have shown that they could be used as fillers in polymeric matrices to improve mechanical[12, 13] and barrier properties of biocomposites[14-17]. Their use for industrial packaging is now being investigated. Giving their promising platelet morphology, SNC appear to be good candidates for reducing the coating's permeability to grease, oxygen and water vapor following similar approach than non-renewable and non-degradable nanoclays[18]. However, SNC present several challenges: (i) nanoparticles tend to modify the rheological behavior of any formulation; (ii) starch tends

to gelatinize with increasing water content and temperature; and, (iii) their processing in industrial coating conditions has never been investigated.

The aim of the present study is to assess for the first time their processability in coating, and the influence of the coating formulation and drying on the final properties of a coated paper for packaging.

II.2. Materials & Methods

II.2.1. Materials

Waxy maize (WM) starch (C☆Gel 04201, 98% amylopectin) and wheat (WS) starch (Cerestar PT 20002) used to prepare SNC were kindly provided by Cargill (Krefeld, Germany). Sulfuric acid (96%-99%, Sigma Aldrich) was used after dilution at 3.16M with distilled water. A commercial acid-thinned hydroxypropylated starch (Cargill Krefeld, Germany) was used as matrix/coating medium and glycerol (99+%, Alfa Aesar, Johnson Matthey, Germany) as its plasticizer. Base paper was a 50 $g.m^{-2}$ coated on one side and non-calendered (Gerbier ,Ahlstrom Stenay, France).

II.2.2. Preparation of starch nanocrystals (SNC)

SNC from both starches were prepared separately as described elsewhere [11, 19, 20].

II.2.3. SNC characterization

SNC's morphology was characterized with a Zeiss Ultra 55 Field Emission Gun Scanning Electron Microscope (FEG-SEM). Their crystallinity was estimated by wide angle X-ray diffraction (XRD) with a PAN analytical X'Pert PRO MPD diffractometer equipped with a X'celerator detector. Differential scanning calorimetry (DSC) measurements were performed on a DSC Q100 (TA Instruments, NewCastle). Detailed results are described elsewhere [11, 21].

II.2.4. Coating color preparation

The acid-thinned hydroxypropylated starch was gelatinized under mechanical stirring. The temperature of the solution was kept at 95℃ for at least 30 min to completely gelatinize the starch granules. The opening of the flask was covered with an aluminum foil to avoid water evaporation. Starch was then cooled down to 60-65℃ and the plasticizer was added to 20 pph of the starch. The starch-glycerol mixture was kept under stirring at 60℃ for 30 min minimum. Then, th e mixture was cooled down to 40℃. In the meantime SNC the suspension was placed in an ultrasound vessel for sonication (3 times 1 min to avoid over heating), then added to the starch-glycerol mixture and dispersed by stirring for 30 min at 40℃.

To assess the influence of SNC on the properties of plasticized starch coated on paper, either 0, 5 or 30 wt % (based on dry content) of SNC was added to the plasticized starch coating color. Base coating color was made of acid-thinned hydroxypropylated starch heated at a concentration of 30 wt%, and glycerol 20 pph, so that formulations can be summarized as in Table 4-II.1.

Table 4-II.1. Formulation of glycerol-plasticized starch coating filled with 0 wt%, 5 wt% or 30 wt% starch nanocrystals (SNC).

Parts	Ref	SNC 5wt%	SNC 30wt%
Starch	100	100	100
Glycerol	20	20	20
SNC	-	6	51
Water	400	456	463

The viscosity of the three different formulations was assessed in triplicates using a Rheometer Rheolabs QC (Anton Paar, Austria) using a Couette geometry and a shear rate ramp from 0 to 1000 s^{-1} at 20℃.

II.2.5. Coating & Drying process

The coating suspensions were applied to the (non-coated) back side of the substrate using a semi-industrial rod coater (EndupapUniversal Coating Machine, L&W BK, CTP, France). It combines a classic rod coater with an in-line IR drying chamber with two lamps. With a metering bar number 5, under controlled pressure and a bar moving speed of 6.6 $m.min^{-1}$, a dry coating thickness of approximately 15 µm was obtained.

The applied coatings were dried under different conditions, including: (i) long wave IR drying system (referred to as "IR-3500W" where 3500W is the power of the lamp used for drying) , (ii) a 50°C glazing plate to simulate a contact drying cylinder (referred to as "Contact-50°C"), and (iii) ambient air drying (referred as "Ambient Air - 25°C"). All samples were touch-dry upon removal from the drying media and double coated. The monitoring of the substrate temperature was carried out with a Pico Technology thermocouple fixed onto the substrate by applying a resin (epoxy and iron) spot. The temperature was measured every second and the acquisition performed by computer connection. To calculate the power provided by the IR lamp 3500W to the paper, a copper plate sample was used as absorbing media and the following formula was used:

$$P\ (W.cm^{-2}) = \left(m\ \varepsilon\ C_p \frac{dT}{dt} \right) \frac{1}{S}$$

where m is the copper plate mass (kg), ε is the emissivity/adjustment factor, C_p is the copper heat capacity ($J.kg^{-1}.K^{-1}$), T is the temperature (K), t is the drying time (s) and S the surface of the copper plate (cm^2).

For m = 0.045 kg, ε = 0.95, C_p = 1400 J. $kg^{-1}.K^{-1}$ and S = 21x29.7 cm^2, the slope dT/dt = 2322 K.s, the power provided by IR-2500W is P = 2228.2 $W.m^{-2}$.

II.2.6. Coated paper characterization

Coated papers were characterized in terms of coating thickness, pin holes, morphology, FTIR spectroscopy and water vapor permeability. Thickness was measured using an Adamel & Lomargy (MI20, Ivry, France).

Pin holes detection was performed using colored oil. Samples of 100x40 mm^2 were taped on a cardboard sheet and the oil uniformly applied onto the sample. After 1 min, the excess oil was removed with paper tissue and the surface checked for colored dots, indicating pinholes.

Coatings surface and cross-section were analyzed with an environmental scanning electron microscope (ESEM) on a Quanta 200 FEI device by depositing samples onto a carbon tape. FTIR analysis was performed with a Mattson 5000 spectrometer, equipped with a high refractive index ZnSe crystal. Attenuated total reflectance (ATR) sampling technique was performed on paper, as samples were too opaque and thick for standard transmission method, to evidence possible molecular change in the coating.

The static water vapor permeability was measured according to the cup method (ASTM Standards, 1995) [22]. Circular coated paper samples (60 cm²) were placed to hermetically cover with a toric joint an aluminum cup containing 5g of dessiccant (anhydrous $CaCl_2$). The whole device was weighted and placed in humidity and temperature controlled chamber (23°C, 50%RH). The cups were weighted at regular interval of time until reaching equilibrium. All the tests were performed in triplicate at atmospheric pressure (1atm) and WVP was reported as the average of these three values as:

$$\mathrm{WVP}\ (\mathrm{g.m^{-1}.s^{-1}.Pa^{-1}}) = \frac{\Delta \mathrm{m.e}}{\mathrm{A}.\Delta \mathrm{t}.\Delta \mathrm{P}}$$

where Δm is the mass increase (g) of the $CaCl_2$ sample, A is the area of the paper sample, Δt is the exposure time in the chamber, e the thickness of the sample and ΔP the partial water vapor pressure difference across the film specimen corresponding to 0%-50%RH, i.e. 1426Pa.

Tensile tests were carried out with a RSA3 (TA Instrument, USA) equipment fitted with a 100N load cell. Measurements were performed, in triplicate, at room temperature (~25°C), with a cross head speed of 0.6 mm.min^{-1} for the first 250 s, then 1.5 mm.min^{-1} up to 2000 s, and finally 3 mm.min^{-1} up to the break. The samples dimensions were 10x10 mm² and results were averaged on 4 replicates.

II.3. Results & Discussions

II.3.1. SNC characterization

Two different starches were used to prepare the SNC to be used in coating color: waxy maize starch (WM) and wheat starch (WS). A previous study proves the impact of crystalline type on the morphology of SNC.[11] In this work, SNC were selected for their square-like morphology as shown in Figure 4-II.1, expecting better barrier properties. Such morphology is also close to that of nanoclays which are known to be an efficient barrier material.[23]

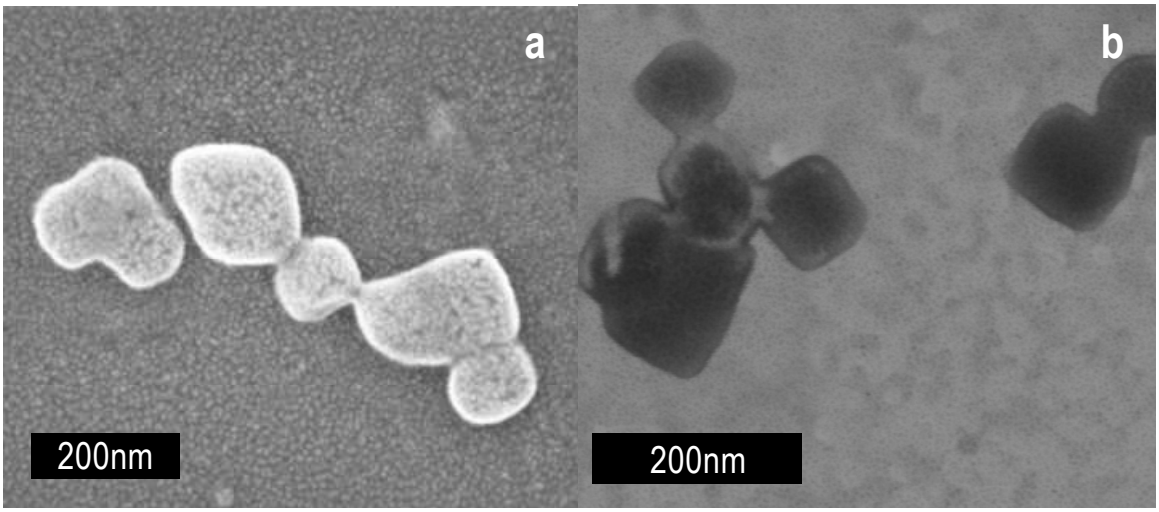

Figure 4-II.1. Field emission gun scanning electron micrographs of SNC from (a) waxy maize starch (WM SNC) and (b) wheat starch (WS SNC).

Paper 8

II.3.2. SNC & coating process

The viscosity of SNC suspensions is presented in Figure 4-II.2. As expected the addition of SNC to the coating color induced an increase in viscosity even though coating color is diluted as detailed in experimental section. However, coating was still possible as viscosity was rather close to 1000mPa.s at room temperature, especially at high shear rate, and thus could still flow. Indeed the maximum value is generally considered to be 2000mPa.s for paper coating technology. Also, SNC-filled coating color kept a shear thinning behavior.

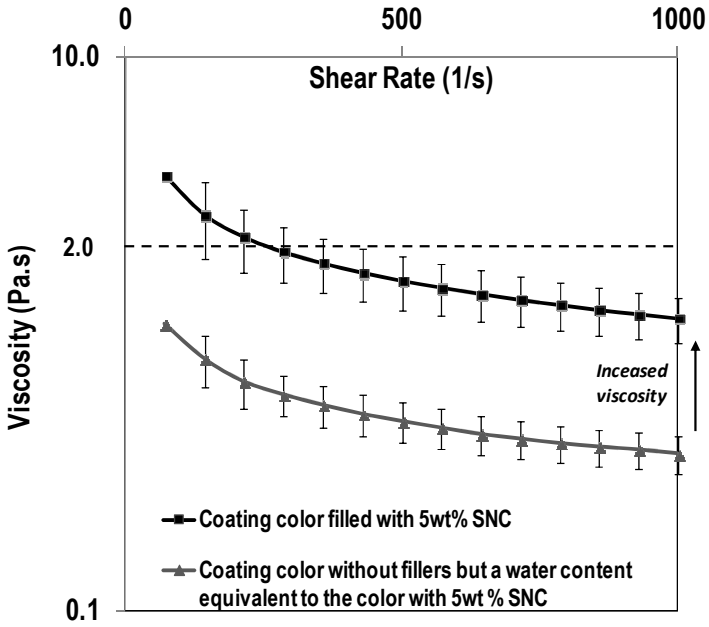

Figure 4-II.2. Viscosity of glycerol-plasticized-starch with: (▲) water (equivalent to the amount of water added when SNC are in suspension), (x) with 5% NM SNC in suspension.

After first SNC-starch coating trial, the coating's integrity was tested. Papers dried under ambient air and contact did not show any pin holes. However, IR drying was the preferred process because it is expected to dry rapidly the top layer of the coating, leaving intact the SNC. Unfortunately, papers dried with IR- 3500W for 1 to 10s showed at least pin holes or complete coating layer holes (oil penetration. test). SEM micrographs, presented in Figure 4-II.3, confirmed that IR dried papers showed cracks and blisters at the surface, and air bubbles in the cross-section. It is obvious that such defects will completely modify barrier properties and gas permeation. This is why, it was important to understand the impact of the drying technique.

First, tests were conducted to asses if SNC could be the cause of the pin-holes. Indeed, they could (i) unexpectedly gelatinize, or (ii) bring too much water to the coating color to be dried. However, the same coating without SNC was performed. Similar pin holes were obtained. SNC were therefore excluded as a cause of pin-holes defects due to gelatinization (i).

However the dilution of the coating color upon the addition of SNC (ii) can be the reason for pin holes. Thus the influence of drying has been studied in detail. This was also important for checking that SNC will not gelatinize during processing lose their crystalline structure and morphology (which are useful for barrier applications).

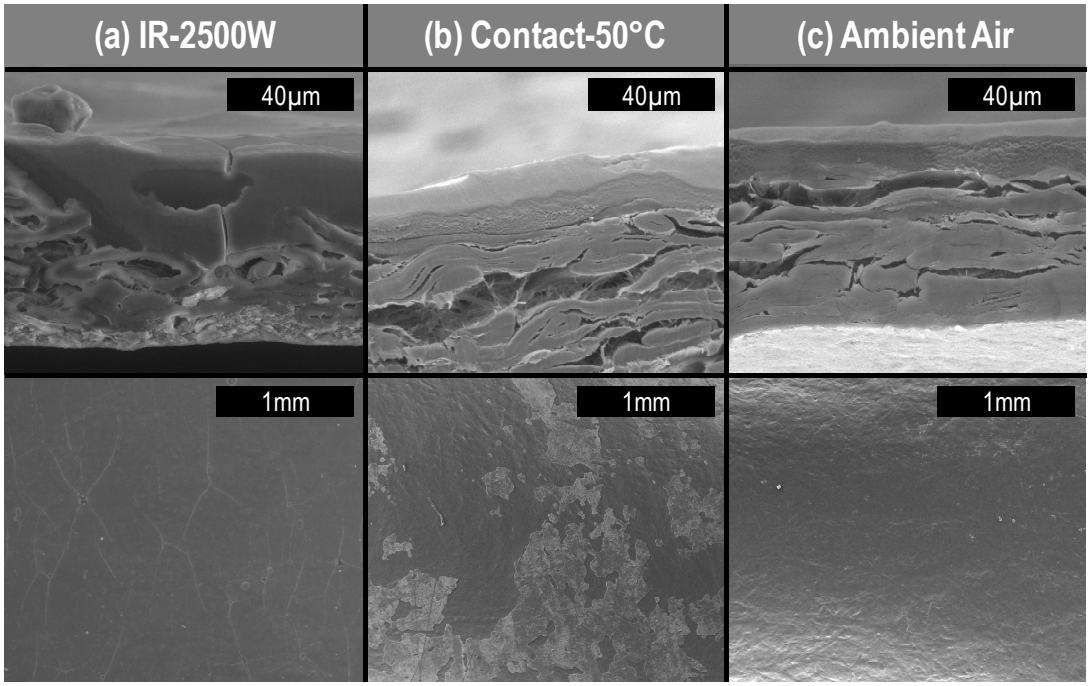

Figure 4-II.3. Scanning electron micrographs of cross-section and surface of glycerol-plasticized starch coated papers dried with (a) IR-2500W, (b) Contact-50°C and (c) Ambient Air.

II.3.3. Influence of drying

Possible explanations for the pin-hole defects induced by IR-drying could be the followings: (i) molecular changes in the coating, (ii) evaporation of the plasticizer, and/or (iii) intense vaporization, at the surface of the coating, of the water contained in the coating color.

A simple comparison of FTIR analysis (not shown) of coated paper dried with IR-3500W, Contact-50℃ and Ambient air-25℃ revealed n o significant differences, setting aside hypothesis (i).

Glycerol has a boiling point around 290℃; therefor e it is unlikely that its evaporation can cause blisters or cracks. Although the drying temperature was assessed, such high temperature could not be achieved without deterioration of the paper and starch matrix. This is not the case, eliminating hypothesis (ii).

Last hypothesis (iii) was postulated from known drying rate differences between IR drying and contact drying. Indeed IR drying is a very efficient non contact irradiation drying process which allows fast drying when containing molecules which can absorb IR radiation. In our case, the IR used was long waved, that is, usually between 3 µm and 1000 µm. It was selected because study[24] has shown that, considering the spectral characteristic of water films with thickness up to 10 µm, the spectral absorption range

from 2 to 7 µm is best suited for heating water.[24] So the water contained in the coating color absorbs the energy provided by IR. Heat is immediately conducted towards the cool ambient air, and thus the water can vaporize from the surface of the material into the air. In contact drying, the drying rate is much slower and more homogeneous in the thickness. Convective heating starts at the surface of the water pellet, and the heat is slowly conducted towards the center. However, for water to vaporize through the coating, it has to reach 100℃.

To assess (a) the temperature at which the paper is brought up during drying and (b) if SNC will gelatinize or not depending on the process, the drying kinetic of the papers for the different drying techniques has been investigated using a thermocouple (see Experimental).

As reported in a previous study,[21] whatever the starch source, SNC can be processed in a water-based media without gelatinizing at temperatures below 90℃. Thus the drying kinetics of the papers by the different drying media was recorded to check the non-gelatinization of SNC. Figure 4-II.4 shows that IR-3500W drying temperature strongly exceeds that of contact drying. Even though it seems the paper temperature never exceeds 70℃, it might be possible that higher temperature is achieved at the extreme surface of coating inducing water evaporation. Especially given (i) the explained drying mechanism of IR and (ii) the fact that no water was present on the thermocouple surface. So it seems that the high water content of the coating color could be the main reason for crackling.

In contact conditions, the heat is slowly conducted and temperature never exceeds 45℃ (Figure 4-II.4). Thus, it is obvious SNC will resist drying and won't gelatinize. So, for the rest of the study, coatings were prepared using SNC and dried with Contact-50℃.

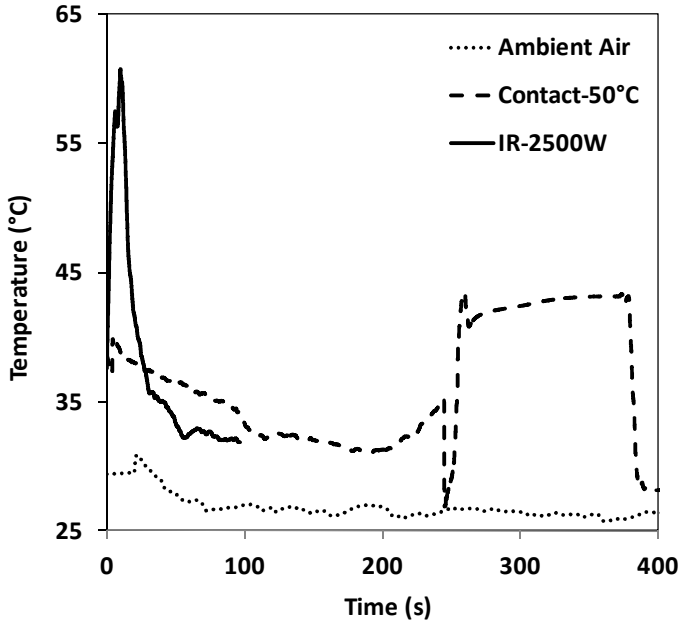

Figure 4-II.4. Temperature kinetics of glycerol-plasticized-starch coated papers dried with (…) Ambient Air, (- - -) with Contact-50°C, and (--) with IR-2500W.

II.3.4. SNC-plasticized starch coated paper properties

Water Vapor Permeability

Resistance to water vapor permeation (WVP) is an essential requirement in some applications such as packaging. Despite the high moisture sorption of pure polysaccharides, it has been reported that the use of cellulose nanocrystals can reduce WVP thanks to high crystallinity and induced tortuosity. [25, 26] Giving their crystallinity and their platelet-like morphology, SNC are suspected to contribute to the reduction of WVP. The WVP of coated papers are reported in Figure 4-II.5. Slight differences between coated papers can be evidenced. Improvement of WVP by adding SNC has already been reported for nanocomposites films with SNC contents below 3 wt% [17] or higher than 30 wt% [27]. This can be explained by the fact that at very low content, SNC can effectively disperse into the matrix. At higher contents, the amount of crystalline particles is sufficiently high to lower the permeability. The present study reveals that as for nanocomposite, the addition of SNC to the coating color renders coated papers with lower WVP than glycerol-plasticized starch-coated one. At 5 wt%, it seems that there are already enough SNC to create increased tortuosity. At 30 wt%, the decrease is more pronounced.

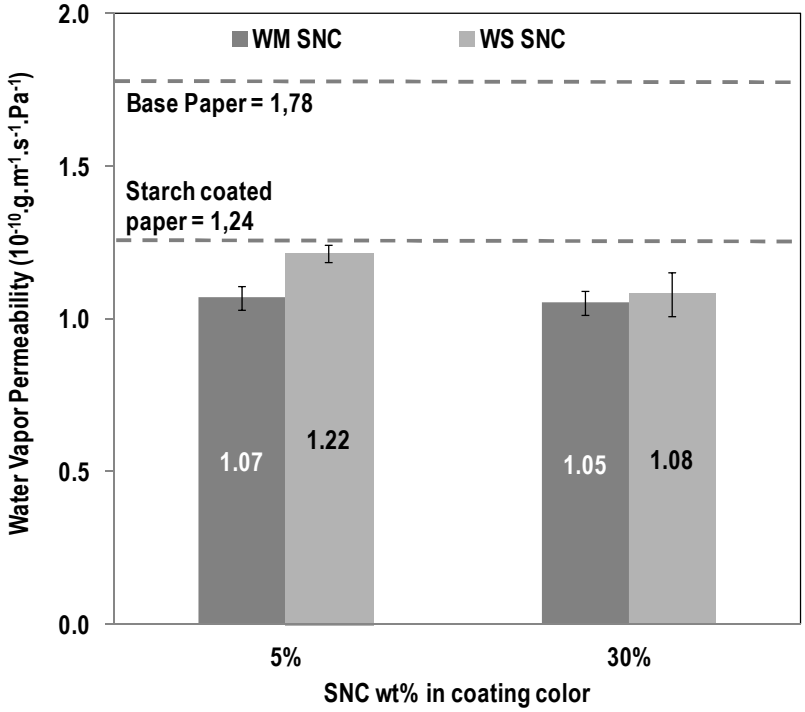

Figure 4-II.5. Water vapor permeability of papers coated with diluted coating color, WM SNC and WS SNC at 5 wt% and 30 wt%.

Paper 8

Compared to base paper, WVP decreases by up to 41%; and an improvement of 15% is achieved when comparing with starch coated paper.

Also WM SNC, which are made of amylopectin and thus theorically more crystalline than WS SNC, should allow to reach lower WVP values. It seems it seems it is not the case proving that (i) WM are not more crystalline and/or (ii) the square like morphology of WS SNC is most important.

Tensile Tests

As observed in Figure 4-II.6 and Table 4-II.2, a glycerol-plasticized starch coating is detrimental to the Young's modulus of the base paper. This is most likely due to the wetting of the paper during the coating process, which weakens the bonds of the fiber mat. Additionally, as one side of the paper is already coated and thus more closed than the other side, there are drying-induced tensions through the paper. However, the addition of SNC to the coating color can partially compensate the loss of stiffness of the papers. Similar impact was observed for the stress at break with 5 wt% SNC filling of the coating color. At 30 wt% SNC, the formation of an SNC network even increases stress at break. Indeed, it has been reported [11, 14, 27-31] that SNC are good fillers for the reinforcement of a bio-based matrix. The gain/compensation in mechanical properties is attributed to the formation of a SNC mechanical network inside the SNC-starch nanocomposite deposited onto the surface of the paper.

Table 4-II.2. Air permeability, thickness and WVP of papers coated with WM, WS and NM SNC compared to base paper and reference paper (glycerol-plasticized starch coating).

Load	Sample	Coating Thickness (µm)	$WVP_{coating}$ (10^{-10} g/m.s.Pa)	$WVP_{coated\ paper}$ (10^{-10} g/m.s.Pa)	Relative WVP Reduction	Young's Modulus (GPa)	Strengh (MPa)	Elongation at break (%)
0%	Base paper	0 ± 0.6	-	1.78 ± 0.01	0%	1.45 +/- 0.08	53.0 +/- 3.5	4.59 +/- 0.47
	S + G	34.6 ± 3.0	0.53 ± 0.00	1.24 ± 0.04	30%	1.06 +/- 0.02	49.6 +/- 5.2	5.90 +/- 0.43
5%	S + G + WS SNC	39.7 ± 1.3	0.57 ± 0.01	1.22 ± 0.03	31%	0.96 +/- 0.01	38.3 +/- 3.7	5.38 +/- 0.39
	S + G + WM SNC	29.8 ± 2.4	0.42 ± 0.02	1.07 ± 0.04	40%	1.19 +/-0.15	46.5 +/- 7.5	5.28 +/- 0.43
30%	S + G + WS SNC	24.9 ± 2.7	0.38± 0.03	1.08 ± 0.07	39%	1.26 +/- 0.14	54.0 +/- 4.6	6.06 +/- 0.29
	S + G + WM SNC	19.0 ± 1.7	0.31 ± 0.01	1.05 ± 0.04	41%	1.18 +/- 0.09	51.1 +/- 6.8	5.68 +/- 0.56

S: starch; G: glycerol; W: water

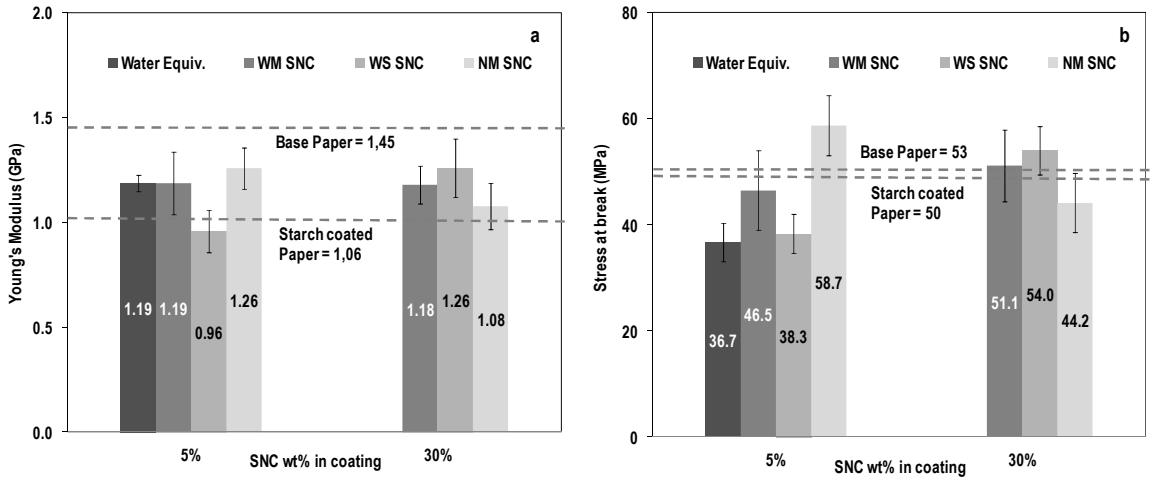

Figure 4-II.6. Mechanical properties of papers coated with diluted coating color, WM SNC and WS SNC at 5 wt% and 30 wt%, with (a) the comparison of the Young's modulus of the different papers and (b) the strength of the same paper.

Figure 4-II.7 shows that the best compromise is: the coated paper containing 30 wt% SNC. It renders (i) similar mechanical properties than base paper and higher mechanical properties than coated paper without SNC and (ii) better barrier properties (41% and 15% higher) than base paper and coated paper without SNC (respectively). This works proves that SNC are promising fillers for barrier coating if dilution is controlled.

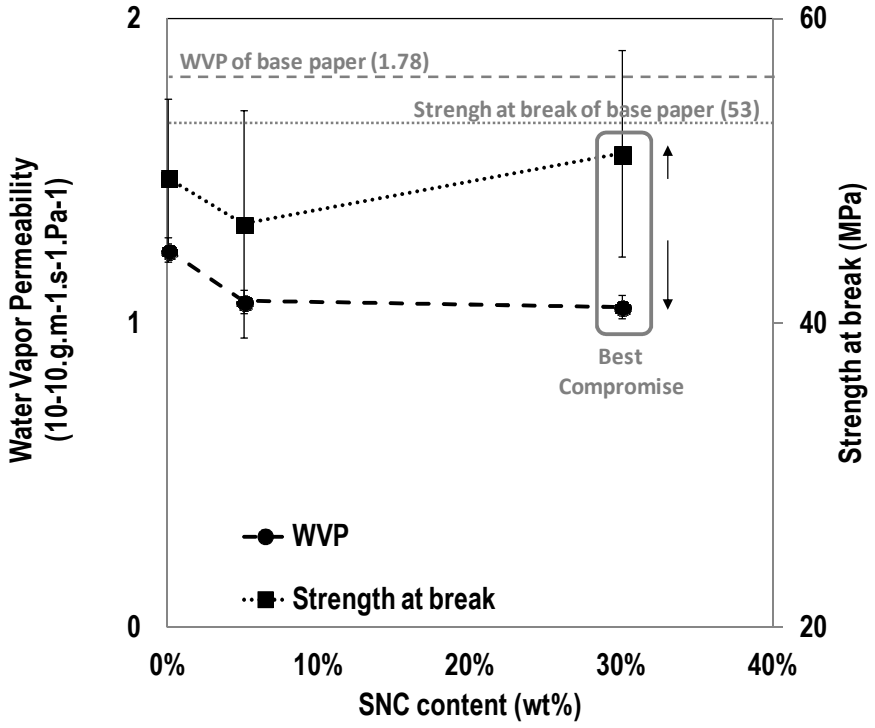

Figure 4-II.7. Water vapor permeability and strength of paper coated with 0 wt%, 5 wt% and 30 wt% WM SNC.

Paper 8

II.4. Conclusion

Starch nanocrystals (SNC) have been introduced in a starch based coating and the properties of the ensuing coating color and final paper investigated. Coating colors containing SNC showed higher viscosity but were still processable. It was shown that SNC can resist studied drying processes without gelatinizing. Crackling issues have been observed with IR drying and were due to highly diluted coating color. SNC addition to the coating color strongly decreased WVP and compensated the loss of mechanical properties due to the use of the water-based coating. Thus SNC are promising bio-nano-fillers for improving barrier properties of bio-based coated papers.

II.5. References

1. Whistler, R. L.; Paschall, E. F., *Starch: Chemistry and Technology*. New York, **1965**; p.

2. Azizi Samir, M. A. S.; Alloin, F.; Dufresne, A., Review of Recent Research into Cellulosic Whiskers, Their Properties and Their Application in Nanocomposite Field. *Biomacromolecules* **2005,** 6, (2), 612-626.

3. Le Corre, D.; Bras, J.; Dufresne, A., Starch nanoparticles: A review. *Biomacromolecules* **2010,** 11, (5), 1139-1153.

4. Siró, I.; Plackett, D., Microfibrillated cellulose and new nanocomposite materials: a review. *Cellulose* **2010,** 17, (3), 459-494.

5. Siqueira, G.; Bras, J.; Dufresne, A., Cellulosic Bionanocomposites: A Review of Preparation, Properties and Applications. *Polymers* **2010,** 2, (4), 728-765.

6. BSI - British Standards Institution, Vocabulary - Nanoparticles (PAS 71:2005). In *Publicly Available Specification*, BSI, Ed. London, **2005**.

7. Lu, C.; Mai, Y.-W., Influence of Aspect Ratio on Barrier Properties of Polymer-Clay Nanocomposites. *Physical Review Letters* **2005,** 95, (8), 088303.

8. Choudalakis, G.; Gotsis, A. D., Permeability of polymer/clay nanocomposites: A review. *European Polymer Journal* **2009,** 45, (4), 967-984.

9. Baer, D. R.; Burrows, P. E.; El-Azab, A. A., Enhancing coating functionality using nanoscience and nanotechnology. *Progress in Organic Coatings* **2003,** 47, (3-4), 342-356.

10. Buléon, A.; Colonna, P.; Planchot, V.; Ball, S., Starch granules: structure and biosynthesis. *International Journal of Biological Macromolecules* **1998,** 23, (2), 85-112.

11. LeCorre, D.; Bras, J.; Dufresne, A., Influence of botanic origin and amylose content on the morphology of starch nanocrystals. *Journal of Nanoparticle Research* **2011,** Submitted.

12. Yu, J.; Ai, F.; Dufresne, A.; Gao, S.; Huang, J.; Chang, P. R., Structure and mechanical properties of poly(lactic acid) filled with (starch nanocrystal)-graft-poly(e-caprolactone). *Macromolecular Materials and Engineering* **2008,** 293, (9), 763-770.

13. Zheng, H.; Ai, F.; Chang, P. R.; Huang, J.; Dufresne, A., Structure and properties of starch nanocrystal-reinforced soy protein plastics. *Polym. Compos.* **2009,** 30, (4), 474-480.

14. Angellier, H.; Molina-Boisseau, S.; Dufresne, A., Mechanical properties of waxy maize starch nanocrystal reinforced natural rubber. *Macromolecules* **2005,** 38, (22), 9161-9170.

15. Angellier, H.; Putaux, J.-L.; Molina-Boisseau, S.; Dupeyre, D.; Dufresne, A., Starch nanocrystal fillers in an acrylic polymer matrix. *Macromolecular Symposia* **2005,** 221, (1), 95-104.

16. García, N. L.; Ribba, L.; Dufresne, A.; Aranguren, M.; Goyanes, S., Effect of glycerol on the morphology of nanocomposites made from thermoplastic starch and starch nanocrystals. *Carbohydrate Polymers* **2011,** 84, (1), 203-210.

17. Garcia, N. L.; Ribba, L.; Dufresne, A.; Aranguren, M. I.; Goyanes, S., Physico-mechanical properties of biodegradable starch nanocomposites. *Macromolar Materials and Engineering* **2009,** 294, (3), 169-177.

18. Hohenthal, C.; Veuro, S.; Kuisma, M., D6.6: Sustainability assessment for Renewable Biopolymer Based Flexible Packaging Paper. http://www.flexpakrenew.eu/documentation.cfm, **2011,** Access

19. LeCorre, D.; Bras, J.; Dufresne, A., Evidence of micro and nano-scaled particles during starch nanocrystals production and their isolation. *Biomacromolecules* **2011,** doi: 10.1021/bm200673n.

20. LeCorre, D.; Bras, J.; Dufresne, A., Ceramic membrane filtration for isolating starch nanocrystals. *Carbohydrate Polymers* **2011,** doi:10.1016/j.carbpol.2011.06.064.

21. LeCorre, D.; Bras, J.; Dufresne, A., Influence of native starch's properties on starch nanocrystals' thermal properties. *Carbohydrate Polymers* **2011,** In Press.

22. ASTM, Standard test methods for water vapor transmission of materials - ASTM E96-95 In *ASTM book of standards*, ASTM: Philadelphia, **1995** p697-704.

23. SUSTAINPACK, *EU Framework 6 Integrated Project on New Packaging Materials.* , **June 2004 to May 2009**.

24. Dieudonné, W.; Schulze, T., Case study: Drying of water-based coatings - Efficiency leap with IR drying. Access (July 16, 2010).

25. Garcia de Rodriguez, N. L.; Thielemans, W.; Dufresne, A., Sisal cellulose whiskers reinforced polyvinyl acetate nanocomposites. *Cellulose* **2006,** 13, (3), 261-270.

26. Paralikar, S. A.; Simonsen, J.; Lombardi, J., Poly(vinyl alcohol)/cellulose nanocrystal barrier membranes. *Journal of Membrane Science* **2008,** 320, (1-2), 248-258.

27. Kristo, E.; Biliaderis, C. G., Physical properties of starch nanocrystal-reinforced pullulan films. *Carbohydrate Polymers* **2007,** 68, (1), 146-158.

28. Viguie, J.; Molina-Boisseau, S.; Dufresne, A., Processing and characterization of waxy maize starch films plasticized by sorbitol and reinforced with starch nanocrystals. *Macromol. Biosci.* **2007,** 7, (11), 1206-1216.

29. Chen, Y.; Cao, X.; Chang, P. R.; Huneault, M. A., Comparative study on the films of poly(vinyl alcohol)/pea starch nanocrystals and poly(vinyl alcohol)/native pea starch. *Carbohydrate Polymers* **2008,** 73, (1), 8-17.

30. Alexandre, M.; Dubois, P., Polymer-layered silicate nanocomposites: preparation, properties and uses of a new class of materials. *Materials Science and Engineering: R: Reports* **2000,** 28, (1-2), 1-63.

31. Angellier, H.; Molina-Boisseau, S.; Dole, P.; Dufresne, A., Thermoplastic starch-waxy maize starch nanocrystals nanocomposites. *Biomacromolecules* **2006,** 7, (2), 531-539.

Chapter 4-III. Multilayer bio-based packaging containing starch nanocrystals

Déborah LeCorre[1], Julien Bras[1], Frédéric bébien[2], Riku Talja[3], Alain Dufresne[1]

[1]*LGP2 – Laboratory of Pulp and Paper Sciences – 461, Rue de la Papeterie – BP 65 – 38402 Saint Martin d'Hères Cedex – France*

[2]*Ahlstrom Research and Services - ZI de l'Abbaye - Impasse Louis Champin - 38780 Pont-Evêque, France*

[3]*VTT - Polymers and Chemical Prouducts - P.O.Box 1000 (Tekniikantie 2) - FI-02044 VTT, Finland*

Abstract

The present study details the different steps undertaken during the European project FlexPakRenew to develop a bio-based multilayer flexible packaging material. First, it investigates at lab-scale two different bio-based polymers (starch and xylan) and two different nano-fillers (nanoclays and starch nanocrystals) for the production of the intermediate medium barrier layer. Then, lab-scale demonstrators were produced according to best results to assess process compatibility of the different layers and availability of materials. Finally, the best formulation was used to produce a pilot-scale multilayer demonstrator. Analysis of the different coatings revealed that an optimized nanoclay mix in a plasticized starch coating was the best candidate for reaching targeted WVTR and OTR, and thus was used for the pilot-scale demonstrator. However, results confirmed technical feasibility of using SNC in coatings. They also indicated that SNCs can effectively decrease the WVTR of xylan-based coating even more than some non-optimized nanoclay systems. It was also found that using more homogeneous SNC suspension (called 2nd generation SNC) required less SNC (-35%) for reaching lower WVTR (-11%).

Keywords

Starch; nanocrystals; packaging; nanofillers; barrier

III.1. Introduction

All our studies were undertaken in the framework of the European project "Flexpakrenew"[1]. The main objective of this collaborative project was to design and develop an innovative ecoefficient low-substrate flexible paper packaging from renewable resources to reduce the European's packaging industry's reliance on barrier films derived from petroleum.

Flexpakrenew is a Small and Medium-Scale focused collaborative research project (budget <5M€), financed by European Commission in the framework of the FP7 program addressing the main work program topic: NMP-2007-2.4-3 - Renewable materials for functional packaging applications. This project, coordinated by The French Pulp and Paper Research & Technical Centre (CTP), associated 10 partners (as seen in Figure 4-III.1)) from 6 European countries, namely CTP (Technical center for pulp & paper research), Ahlstrom (Speciality papers company), Cargill (Starch manufacturer), Sheffield Hallam University (Nanoclay specialists), Karlstad University (Polymer and paper converting laboratory), the IVV Fraunhofer (Technical German research centre on packaging), VTT (Finish research centre, xylan specialists), ZUT (Polish University working on biopolymers), the CERMAV (CNRS unit specialized on vegetal macromolecules) and Grenoble-INP Pagora (French engineering school and research centre on paper, converting and biomaterials).

Figure 4-III.1. FlexPakRenew's consortium

The technical challenge in this project was to develop a flexible paper, based on multilayered structure (as presented in Figure 4-III.2) with final basis weight between 50 and 90 g/m², that achieves barrier properties competitive with those of untreated plastic films (medium barrier) or treated plastic films (high barrier). The novel functional flexible packaging was developed using renewable materials and latest developments in nanotechnology, beyond state-of-the-art barrier coatings and innovative surface treatment processes. Flexible packaging for food and non food-goods were the two targets of the project. A substantial reduction in the amount of packaging going to landfill

was expected, together with considerably faster environmental degradation of the new packaging materials.[1]

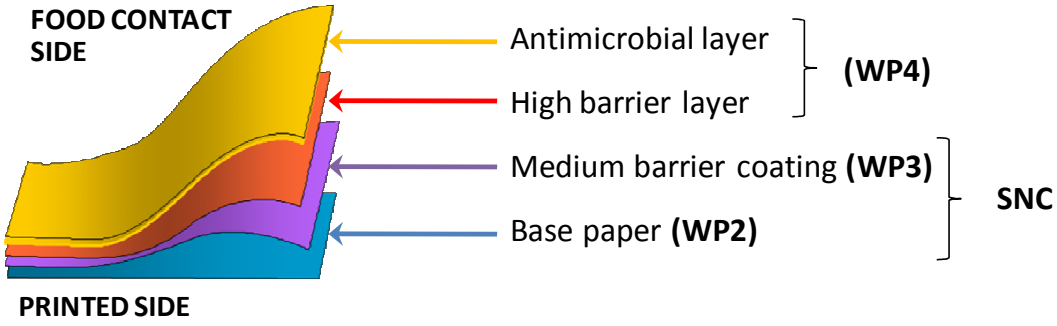

Figure 4-III.2. Structure of the multi-layer developed in the FlexPakRenew project

The project was divided in 6 work packages (WP), corresponding roughly to the different layers developed in the project. WP1 was dedicated to the coordination of the project and WP6 to the Life Cycle Analysis (LCA) of the final developed packaging. Each project partner participated in the development of 1 or 2 layers (i.e. 1 or 2 WP) in collaboration with other partners. The base paper (first layer, WP2) was developed by ARS, and primarily coated with microfibrillated cellulose (MFC) by CTP or, as alternative, with microcapsules by ZUT. The coating matrices (xylan, modified starch or polymer blends) for the medium barrier coating (second layer, WP3) were developed by other project partners (respectively VTT and KaU). ShU worked on nanoclays, as primary fillers for the coating and starch nanocrystals (SNCs) were developed at Pagora as a renewable alternative to nanoclays. Both of them were added to the coating matrices for improving barrier properties, as already presented in the previous chapter 4.III detailing monolayer coating results. Two strategies for high barrier coating (third layer, WP4) were also investigated: vacuum coating (IVV) and hydrophobic grafting (CERMAV/CTP). The anti-microbial layer (fourth layer, WP4) was developed by IVV Fraunhofer and ShU. One work package (WP5) of the project was dedicated to the production of pilot-scale demonstrator flexible barrier packaging that would combine the findings of the different partners and assess the overall performances of the packaging.

As all materials and all combinations of materials could not be tested for the pilot-scale demonstrator, a preliminary lab-scale study was designed. The present study reports main conclusions from (i) the study of the medium barrier layer, (ii) the lab-scale multi-layer demonstrators and (iii) first pilot-scaled results. It also proposes a comparison of different coating matrices, (compared to chapter 4.III), and different nanofillers.

III.2. Material & Methods

III.2.1. Materials

Base paper was a 50gsm industrial paper coated on one side and non-calendered (Gerbier, Ahlstrom Stenay, France) and is designated as “Industrial paper”. The equivalent handsheet using the industrial pulp of the previous paper has been prepared by ARS and CTP and will be designated by “Handsheet”. A commercial acid-thinned hydrophobic octenylsuccinate waxy maize starch (S), kindly provided by Cargill (Krefield, Germany) was used as matrix for coating medium, and polyethylene glycol 600 (PEG) (CARBOWAX^{TM} SENTRY^{TM}, Dow) as its plasticizer. SNC were prepared and characterized as described elsewhere[2-4]. Waxy maize (WM) starch (C☆Gel 04201, 98% amylopectin) used to prepare SNCs was kindly provided by Cargill (Krefield, Germany). Sulfuric acid (96%-99%, Sigma Aldrich France) was used after dilution at 3.16M with distilled water. Xylan from bleached birch kraft pulp (Xb) was isolated at VTT. Glycerol (G) from Sigma Aldrich was used as a potential plasticizer of xylan. Nanoclays were a mix of different nanoclays (confidential data). Polyvinyl alcohol (PVOH) was a Mowiol® from Kurraray.

III.2.2. Coating procedure

The preparation of the coating color was discussed among partners and set the same for all matrices (starch and xylan), except that xylan was plasticized with glycerol rather than PEG. Roughly, the polymer matrix was cooked under mechanical stirring. The temperature of the solution was kept at 95°C fo r at least 30 min. The opening of the flask was covered with an aluminum foil to avoid water evaporation. The polymer was then cooled down to 60-65°C and the plasticizer was added to 20 pph of the polymer. The plasticized polymer mixture was kept under stirring at 60°C for at least 30 min.

Only the type of fillers added and its preparation was different. SNCs were added in the form of a sonicated suspension (3 times 1 min to avoid over heating) to a previously cooled down (to 40°C) polymer, and left under stirring for 30min. Nanoclays were dispersed in water the day before and then added to the 60°C coating color and left under stirring for 2 hours. Formulations can be summarized as described in Table 4-III.1.

Table 4-III.1. Formulations of the coated papers

Sample Ref.	Polymer	NaC	SNC	Plasticizer	Solid content (%)
Medium barrier coatings					
S	100	-	-	-	20
S/PEG	100	-	-	20	21.9
S/Nanoclays A	100	48		-	14.7
S/PEG/NanoclaysA	100	48	-	20	16
S/PEG/SNC	100	-	48	20	20
S/PEG/SNC (F1)	100	-	51	20	20
S/PEG/SNC (F2)	100	-	31	20	20
Xb	100	-	-	-	10
Xb/SNC	100	-	47	-	12.9
Xb/G	100	-	-	20	10.7
Xb/G/SNC	100	-	47	20	14.4
Xb/G/Nanoclay B	100	47	-	20	14.4
Xb/G/Nanoclay C	100	47	-	20	14.4
Xb/G/Nanoclay D	100	47	-	20	14.4
Lab-scale multilayer					
S/PEG/SNC	100	-	48	30	20
S/PEG/Nanoclays A	100	48	-	30	15.9

The coating suspensions were applied using a semi-industrial rod coater (EndupapUniversal Coating Machine, L&W BK, CTP, France) or a bench coater (K Control Coater, RK Print Coat Instruments Ltd), with a metering bar number 5.

The drying conditions of the lab-scale handsheet-based samples were different for the starch/nanoclays and the starch/SNCs coated papers. The first sample was supported on a cardboard sheet (coated side face up) and immediately transferred to an oven and dried at 105 ℃ for 40s, and then transfer red onto a metal sheet (coating side face up) in an oven at 60ºC, anchored in place at the corners with four weights and left to dry for 4 minutes. All samples were touch-dry upon removal from the oven. The latter SNC-filled coatings were dried on a 50℃ glazing pl ate covered with Teflon® to simulate a contact drying cylinder.

III.2.3. Medium barrier coated paper

The medium barrier coated papers were produced as described in the previous section and different samples were prepared as presented in Figure 4-III.3.

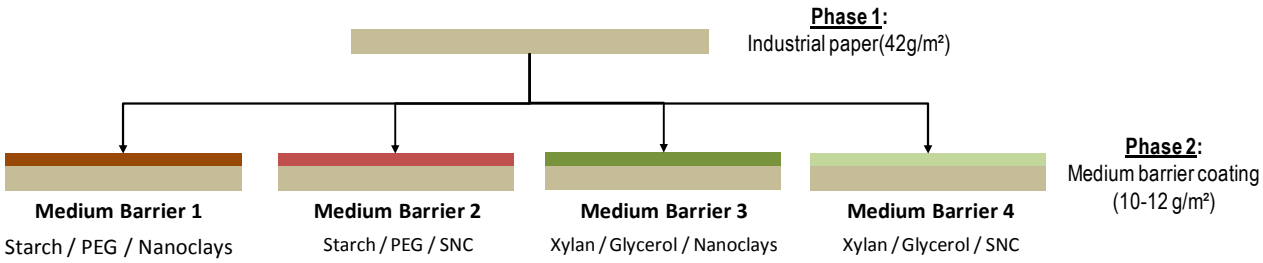

Figure 4-III.3. Schematic representation of the medium barrier coated papers

III.2.4. Multi-layer structure at lab-scale

The lab- scale demonstrator consisted in 3 phases as described in Figure 4-III.4.

Phase 1 was dedicated to producing the base-paper using industrial paper pulp on a dynamic handsheet, and spray-coating it without drying, with enzymatically pre-treated microfibrillated cellulose (first layer). Microfibrillated cellulose (MFC) is nanocellulose materials obtained by the delamination of wood fiber (with a homogeneizer). It is a semi-crystalline polymer reported to have great mechanical reinforcement[5] as well as barrier properties[6]. Phase 1 was realized by ARS (France) according to CTP's recommendations.

Phase 2 consisted in coating the medium barrier layer (second layer) on a rod coater, as detailed in previous chapter4.III. Two types of coatings (identified in WP3) and two different types of papers were prepared: 1) one with a PEG plasticized starch coating filled with nanoclays and 2) one with the PEG plasticized starch coating filled with SNC.

Phase 3 was dedicated to the: (i) PVA coating and (ii) the chromatogenic grafting.[7, 8] This phase was done at CTP (France).

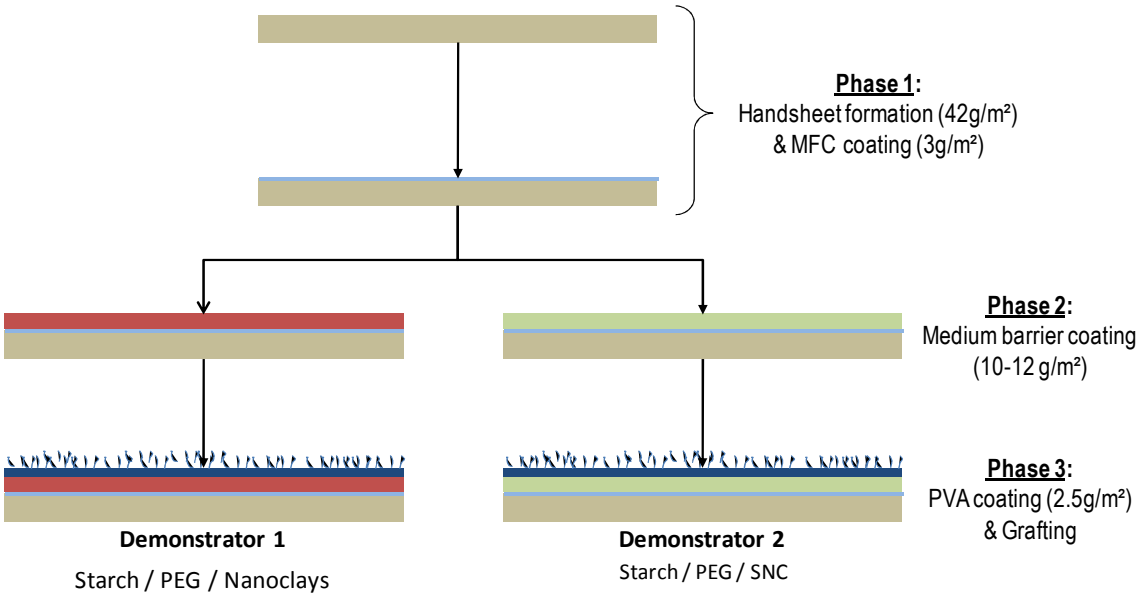

Figure 4-III.4. Schematic representation of the lab-scale demonstrators' production and final products.

III.2.5. Multilayer structure at pilot scale

Compared to the lab-scaled multilayer, the pilot-scaled multilayer comprises additional metallization and protective layers coating steps, as shown in Figure 4-III.5.

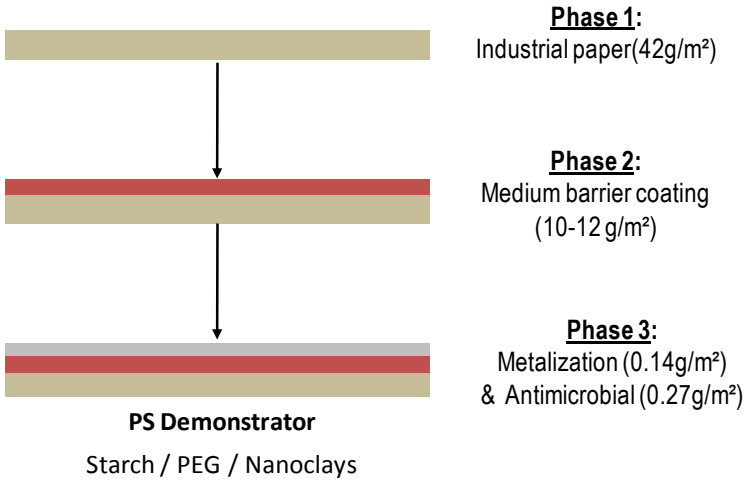

Figure 4-III.5. Pilot-scaled demonstrator multilayer structure

Detailed information on the pilot-scaled multilayer's recipes and process parameters are confidential and cannot be detailed in this chapter. Only partial results will be displayed as SNCs were not selected for pilot demonstrator. This is due to the fact that SNC's preparation process was not up-scaled, and thus SNCs were not available in large quantities. Nevertheless, authors found relevant to present some results for a better understanding of the European project's achievements.

III.2.6. Paper characterization

Thickness was measured using an Adamel & Lomargy (MI20, Ivry, France).

The **Air permeability** (ml/min) of handsheet-based samples was assessed using the Parker Print Surf (PPS). **Air permeability** measurements of industrial-paper-based samples were performed on a Bendtsen device (L&W Bendtsen Tester, Stockholm, Sweden) according to NF Q03-076. In this system, air passes through the paper sample under a constant pressure of 1.47kPa. The output value is expressed in ml/min and represents the Bendtsen permeability value.

Tensile tests were performed on an Instron extensiometer. Tensile breaking strength represents the maximum load that the paper strip can resist before breaking and is expressed as in Eq. 1. with F the mean applied strength (N) and L the width of the paper strip (m).

$$S = \frac{F}{L} \qquad \textbf{Eq}.\ 1.$$

Breaking elongation (%) corresponds to the elongation of the sample before breaking and is calculated as in Eq. 2. with l_0 (mm) the initial length of the paper sample and l (mm) the length of the sample before breaking.

$$e(\%) = \frac{l_0}{l} \qquad \textbf{Eq}.\ 2.$$

Water vapor transmission rate (WVTR in g/m².day) was measured using the cup method. Circular coated paper samples were placed to hermetically cover with a toric joint a plastic cup containing 5g of desiccant (anhydrous $CaCl_2$). The whole device was weighted and placed in humidity and temperature controlled chamber (23℃, 50%RH). The cups were weighted every hour for one day. WVTR was calculated as follow (Eq.3):

$$WVTR = slope\ of\ the\ \frac{dm}{dt}\ graph / Area\ (m^2) of\ the\ sample \qquad \textbf{Eq}.3.$$

The static **water vapor permeability** (WVP in g/m.s.Pa) was measured according to the cup method (ASTM Standards, 1995)[9]. Circular coated paper samples (60 cm²) were placed to hermetically cover with a toric joint an aluminum cup containing 5g of desiccant (anhydrous $CaCl_2$). The whole device was weighted and placed in humidity and temperature controlled chamber (23℃, 50%RH). The cups were weighted at regular interval of time until reaching equilibrium. All the tests were performed in

triplicate at atmospheric pressure (1atm) and WVP was reported as the average of these three values as (Eq.4):

$$WVP\ (g.m^{-1}.s^{-1}.Pa^{-1}) = \frac{\Delta m.e}{A.\Delta t.\Delta P} \cong WVTR\,\frac{e}{\Delta P} \qquad \textbf{Eq}.4.$$

where Δm is the mass increase (g) of the $CaCl_2$ sample, A the area of the paper sample, Δt the exposure time in the chamber, e the thickness of the sample and ΔP the partial water vapor pressure difference across the film specimen corresponding to 0%-50%RH, i.e. 1426Pa.

Oxygen permeability (when measured) was measured using an Ox-tran (Mode 2/10, Moccon, USA) at 0% RH.

III.3. Results & Discussions

III.3.1. Medium barrier coated paper

Our previous study[10] shows the positive impact of SNCs on coating barrier properties as well as some limitations linked to the crackling of the matrix during drying. This is why other bio-based polymers have been tested throughout the project.[1, 11]

Best results have been obtained with another modified starch plasticized with PEG600. It allows reaching higher solid contents and limiting the plasticizer potential evaporation. It also allowed a more effective dispersion of nanoclay as confirmed by X-ray diffraction measurements.[12]

Also, to limit competition with food resources (such as could be claimed with starch), another water soluble matrix extracted from wood biorefinery has been developed by VTT partners. A xylan-based matrix was selected for its solubility, its film forming property, its ability to be coated, its compatibility with nanofillers and its barrier properties.[13]

Finally, different nanofillers, i.e. nanoclay and SNC, were compared in coating on industrial paper for the first time, as detailed in the experimental section. Their properties were assessed for comparison of their barrier properties and for further investigation of SNC heterogeneity. Results are reported in Table 4-III.2.

Table 4-III.2. List of tested coatings on industrial papers and their properties.

Sample Ref.	Basis weight (g/m^2)	Thickness (µm)	Air Perm. (ml/min)	$WVTR_{paper}$ ($g/m^2.day$)	$WVP_{coating}$ (10^{-10} g/m.s.Pa)
Industrial paper	49.0	54.8 ± 0.5	7.5 ± 0.8	408.0 ± 20.4	-
S	71.6	67.6 ± 1.7	0.4 ± 0.2	165.8 ± 2.8	0.91 ± 0.01
S/PEG	57.4 ± 0.5	61.4 ± 1.7	4.9 ± 1.3	174.5 ± 2.6	0.87 ± 0.07
S/Nanoclay A	62.1 ±	66.2 ± 0.8	0.2 ± 0.1	68.2 ± 2.8	0.36 ± 0.04
S/PEG/Nanoclay A	63.9	64.0 ± 2.1	0.2 ± 0.1	15.9 ± 3.6	0.08 ± 0.01
S/PEG/SNC	63.9 ± 1.1	65.7 ± 7.0	6.3 ± 0.5	410.9 ± 17.4	1.18 ± 0.09
S/PEG/SNC (F1)	58.1 ± 0.6	61.4 ± 1.7	4.0 ± 1.4	458.7 ± 15.2	1.19 ± 0.09
S/PEG/SNC (F2)	60.8 ± 0.3	65.7 ± 7.0	1.3 ± 1.4	365.8 ± 4.2	0.95 ± 0.02
Xb	N.A	N.A	N.A	358.0 ± 17.9 [14]	N.A
Xb/G	N.A	N.A	N.A	337.0 ± 16.9 [14]	N.A
Xb/G/SNC	N.A	N.A	N.A	227.0 ± 11.4 [14]	N.A
Xb/G/Nanoclay B	N.A	N.A	N.A	340.0 ± 17.0 [14]	N.A
Xb/G/Nanoclay C	N.A	N.A	N.A	67.0 ± 3.4 [14]	N.A
Xb/G/Nanoclay D	N.A	N.A	N.A	102.0 ± 5.1 [14]	N.A

All papers coated with PEG-plasticized starch exhibited similar basis weight and air permeability. Indeed, they are all lower than 10ml/min i.e. under detection limit of the apparatus. This is due to the industrial base paper which has been sized and coated as it was designed for barrier packaging applications.

Concerning WVTR and WVP results, a positive impact of the starch coating (S and S/PEG) is observed. Permeability is decreased when adding nanoclay (S/NaC), especially if it has been dispersed with a plasticizer (S/PEG/NaC). This confirms some patented results obtained during a previous European project (SustainPack).

The addition of SNC to the coating color resulted, on the contrary, in a limited positive impact on WVTR compared to industrial paper, but negative impact compared to starch coated paper. This is due to the fact that the selected matrix has been optimized, explaining why we do not observe similar positive impact as in previous chapter. The hydrophilic nature of such nanofiller in high concentration (above the percolation threshold) could also be the reason for such results, as recently reported for cellulose nanofiller in HPMC (hydroxypropyl methylcellulose).[15] This could also be explained by the lower crystallinity of SNC compared to nanoclay. Oxygen permeability should give clearer information for explaining such phenomenon.

Results show that a better understanding of the SNC's homogeneity, dispersion and orientation during coating is necessary. Indeed, one can note that slightly better results are obtained when using a 2nd generation SNC (noted in F_2 in Table 4-III.2), i.e. SNC that have been fractionated/filtered (as detailed in Chapter 3), confirming our point.

It could also be noted that previous results (Table 4-III.2) were obtained for an optimum nanoclay mix whereas it has been shown recently by ShU,[12] that all nanoclays did not have equivalent barrier properties. Similar results have been observed with xylan coatings, i.e. some nanoclays gave worst WVTR results than SNC, as presented in Figure 4-III.6. More details on this material have been presented recently.[14]

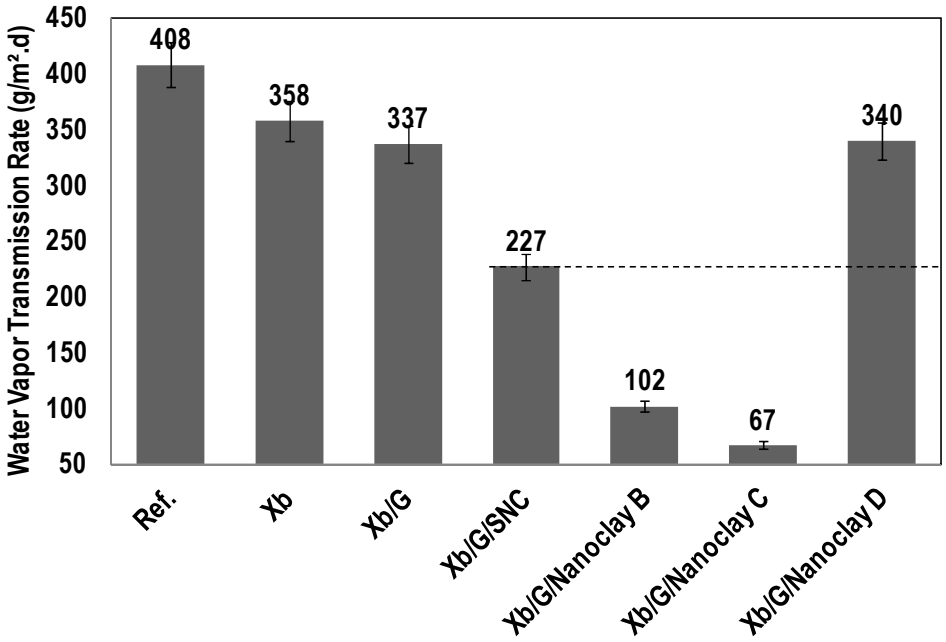

Figure 4-III.6. Water Vapor Transmission Rate of xylan-based coatings.[14]

Using xylan (as a matrix coating) did not have such a positive impact on water vapor barrier properties as starch, due to poorer film formation properties. Thus, work on xylan derivates has been undertaken (as presented recently[14]) to overcome this issue.

Nevertheless, in this study, WVTR was clearly better when adding nanofillers. Best results were obtained with nanoclays (WVTR=15g.m^{-2}.day^{-1}) but the addition of SNC reduced WVTR by 33% which was more than some nanoclays (as nanoclay D).

Thus SNCs were selected for further investigation of the lab-scale multi-layer structure. Unfortunately, due to the low availability of the xylan selected for the multi-layer and of the 2nd generation SNC, 1st generation SNC were tested in the starch matrix in the lab-scale demonstrator.

III.3.2. Lab-scale multi-layer demonstrators

The lab-scale demonstrators were produced to assess the compatibility of the different layers developed in the project (combining the findings and know-how of the different partners as detailed in experimental section); but also for checking process feasibility and properties. Figure 4-III.7 gives information about the final aspect (color, wrinkles) of the multilayer coated handsheets.

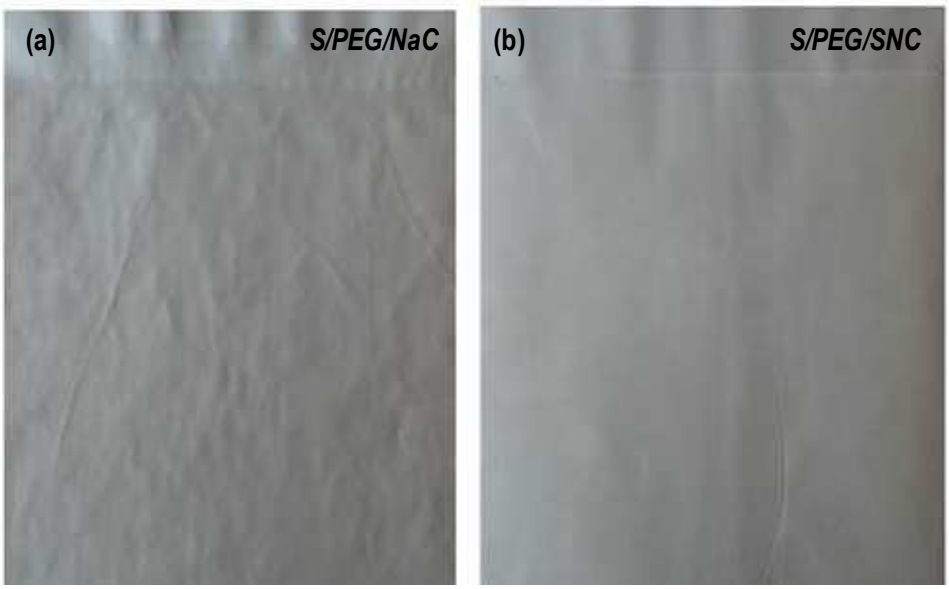

Figure 4-III.7. Photograph of the final lab-scale demonstrator. The intermediate coating is made of (a) modified starch (S), polyethylene glycol (PEG) and nanoclay (NaC); and (b) modified starch (S), polyethylene glycol (PEG) and starch nanocrystals (SNCs)

The wrinkling of the paper (a) is most likely due to the drying technique with lack of sheet tension. Demonstrator coated with modified starch and SNC as intermediate layer resulted in a non-wrinkled white paper (b). The initial coating polymer was white, did not change color during grafting and was dried under tension. On the contrary, nanoclay-filled samples rendered a “red-wine” colored paper after grafting. This was attributed to a possible reaction between the grafting reagent and nanoclay. However, this point is still under investigation by other partners. After this visual assessment, demonstrators’ mechanical and barrier properties were investigated and results are summarized in Table 4-III.3.

Table 4-III.3. List of tested papers and their properties

Sample Ref.	Perm. Air (PPS 2000)	WVTR	Tensile breaking strength (%KN/m)		Breaking elongation (%)		Aspect
	(ml/min)	(g/m².day)	MD	CD	MD	CD	
Industrial paper	771.2	691	2.7	1.5	1.7	5.2	White & Smooth
Handsheet/MFC	2738.2	484	1.26	0.66	1.09	1.77	White & Rough
S/PEG/Nanoclay A	0.9	8	2.26	0.72	1.98	1.52	Sligthly "red wine" & Wrinkles
S/PEG/SNC	44.3	115	2.22	0.51	1.64	1.12	White & No wrinkles

The air permeability of the lab-scale demonstrators was assessed, as it is a good indication that the barrier material is “closed”. For example, only a paper reaching 0ml/min can be considered for oxygen permeability tests without damaging the device. The air permeability of the demonstrator containing SNC was slightly higher than that containing nanoclay. This was attributed to the heterogeneity of the SNC suspension used for the demonstrator (1st generation SNC, F1). Indeed, it was demonstrated recently[2] that SNC suspensions contain both micro- and nano-particles contrary to nanoclay which is exfoliated/dispersed (1 day stirring) before use. Unfortunately, for all demonstrators, the air permeability remained positive. As presented in Figure 4-III.8, this can be attributed to the high air permeability of the base paper handsheet as compared to the industrial paper. Thus oxygen permeability tests were not performed for demonstrators. Also, these results explain why the second part of the study was performed on industrial paper, and why filtered SNC suspensions have been investigated.

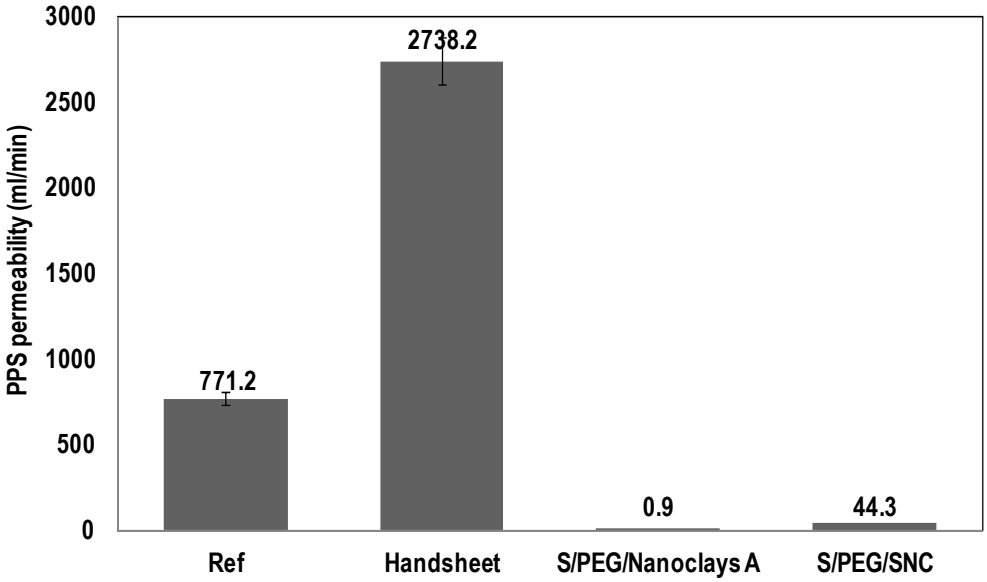

Figure 4-III.8. PPS air permeability of demonstrators and reference papers.

Water vapor transmission of the above mentioned papers was still investigated and results are presented in Figure 4-III.9.

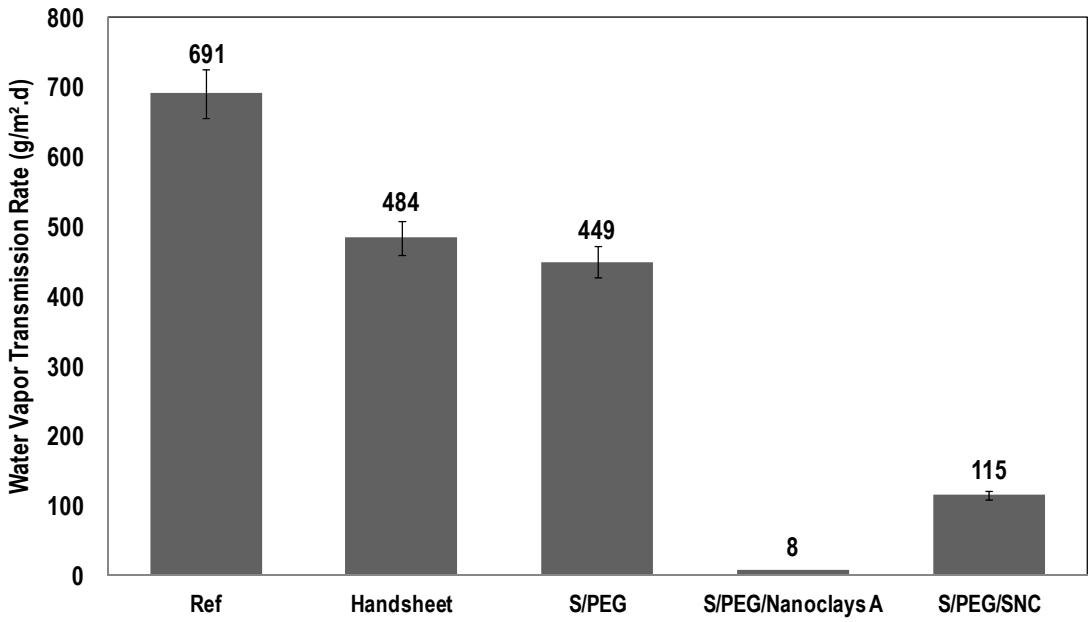

Figure 4-III.9. Water Vapor Transmission Rate (WVTR) of lab-scaled demonstrators and their references.

Although handsheets were more porous and more air permeable than the industrial paper, the coating with MFC induced, as expected, [6] a decrease in WVTR. The coating with plasticized starch further decreased WVTR by 35g/m².day. However, it is suspected to be attributable to an increase in coating thickness. The addition of nanofiller to the coating color induced a substantial decrease in WVTR. Using nanoclay was most efficient to decrease WVTR and led to a reduction of WVTR of 98%. Nevertheless, using SNC as bio-nanofiller led to a WVTR reduction of 76%, which confirm promising upscaling possibility with SNC.

Finally, the mechanical properties of the demonstrators were determined. Indeed, as reported in a previous chapter, [16] the addition of nanofillers in a polymeric matrix has a reinforcing effect. It is expected here that the nanocomposite intermediate coating would reinforce the demonstrator. As presented in Figure 4-III.10, the intermediate coating strengthens the handsheets base paper in the machine direction (MD) whereas the effect is not so pronounced in the counter machine direction (CD) of the paper. Differences among paper coated with different kinds of nanofiller were not significant. Thus from a mechanical point of view, SNC is as good a nanofiller as nanoclay.

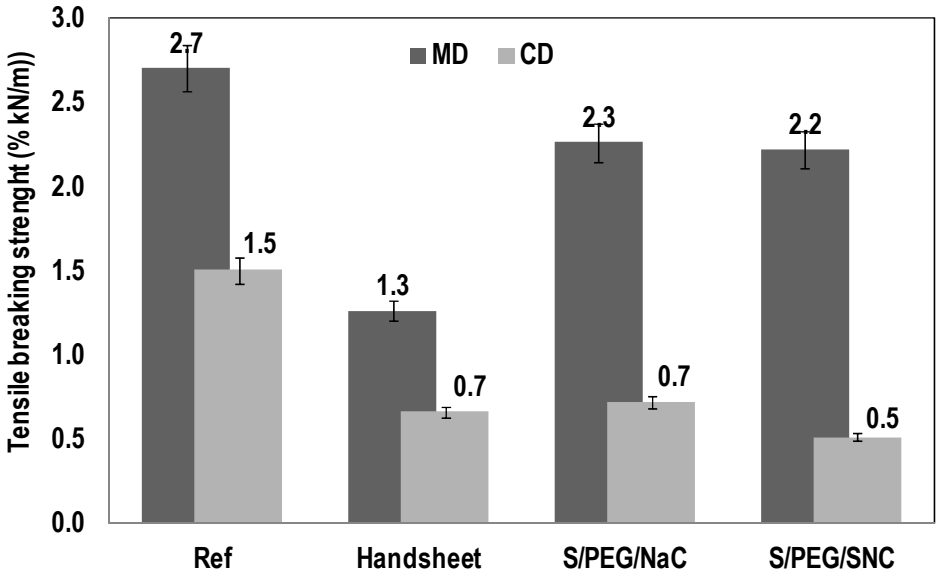

Figure 4-III.10. Tensile breaking strength of the demonstrators and their references.

This lab-scale study confirmed that the first three layers developed in the project were indeed compatible and could be considered for pilot-scale demonstrator. Despite the WVTR reduction obtained for SNC filled coating (115g.m^{-2}.day^{-1}), Nanoclay A was selected for the pilot-scale demonstrator as it reached lower WVTR (8g.m^{-2}.day^{-1}) for similar mechanical performances.

III.3.3. Pilot-scale multi-layer demonstrators

Metallization constitutes the final layer of the multilayer product developed in this study. Unfortunately, due to the roughness of the handsheets produced at lab-scale, metallization of the previous demonstrators was not possible.

Nevertheless, based on previous results (not shown in this study), pilot-scale multilayers were developed including metallization as presented in the experimental section. The nanoclay/PEG600 optimized formulation was selected for its barrier property and availability. Authors believe that when SNC preparation process will be fully optimized and scaled-up, 2nd generation SNC (F2) will allow developing equivalent pilot-scaled demonstrators.

Properties of the current pilot-scale demonstrator (not detailed here) are out-standing. For instance, WVTR reached 0.6g.m^{-2}.day^{-1} and oxygen permeability was 0.6 at 23℃ and 50%RH for the best demonstrator. Thus the targets of the FlexPakrenew project (WVTR$_{(23℃,50\%RH)}$ <1g.m^{-2}.day^{-1} and OTR$_{(23℃,50\%RH)}$ <10cm^3.m^{-2}.day^{-1}.bar^{-1})[1] were reached.

III.4. Conclusion

This study successfully details the strategy used for developing a multilayer material.

First a study of the medium barrier coating, consisting of different combinations of biopolymer (starch and xylan) filled with nanofiller (Nanoclay and SNC) was undertaken. It revealed that plasticized starch allowed reaching lower WVTR, although both SNC and nanoclay had positive impact on WVTR of xylan-based coating. Also, it was evidenced that the addition, in a lesser amount (31pph Vs. 48pph) of 2nd generation SNC (filtered) was favorable to WVTR, but this could not be produced in high enough amount. Furthermore, nanoclay allowed reaching lowest WVTR values (15g.m^{-2}.day^{-1}).

Thus the lab-scale demonstrator consisted in coating a MFC coated handsheet with a plasticized-starch coating filled with either nanoclay or 1st generation SNC, which was further coated with the coating developed in WP4. It revealed that all layers were compatible. Multilayers containing SNC and nanoclay had similar mechanical properties but the latter allowed reaching lowest WVTR (8g.m^{-2}.day^{-1}).

As a result, the plasticized-starch/nanoclay coating was selected for the production of the pilot-scale demonstrator. This demonstrator was further metalized and allowed reaching WVTR<1g.m^{-2}.day^{-1} and OTR<10cm^{3}.m^{-2}.day^{-1}.bar^{-1} which were the targets of the FlexPakRenew project.

In order to reach similar results with SNC, further work has to be done to obtain in large quantity homogeneous filtered SNC (2nd generation), as it has been shown, added to a lesser amount (-35%), they could reduce WVTR by 11% compared to 1st generation SNC. Also, their dispersion and orientation in coating should be investigated.

III.5. References

1. FlexPakRenew Public Flyer. http://www.flexpakrenew.eu/documentation.cfm, **2009,** Access (March 2009).

2. LeCorre, D.; Bras, J.; Dufresne, A., Evidence of micro and nano-scaled particles during starch nanocrystals production and their isolation. *Biomacromolecules* **2011,** 12, (8), 3039-3046.

3. LeCorre, D.; Bras, J.; Dufresne, A., Ceramic membrane filtration for isolating starch nanocrystals. *Carbohydrate Polymers* **2011,** 86, (2011), 1565-1572.

4. LeCorre, D.; Bras, J.; Dufresne, A., Influence of botanic origin and amylose content on the morphology of starch nanocrystals. *Journal of Nanoparticle Research* **2011,** Submitted.

5. Siró, I.; Plackett, D., Primary Title: Microfibrillated cellulose and new nanocomposite materials: a review. *Cellulose* **2010,** 17, (3), 459-494.

6. Syverud, K.; Stenius, P., Strength and barrier properties of MFC films. *Cellulose* **2009,** 16, (1), 75-85.

7. Berlioz, S.; Stinga, C.; Cordoret, J.-S.; Samain, D., Investigation of a novel principle of chemical grafting for modification of cellulose fibers. *Int. J. Chem. Reactor Eng.* **2008,** 6, A2.

8. Samain, D. Procédés de traitement d'un matériau solide pour le rendre hydrophobe: matériau obtenu et applications. **1998**.

9. ASTM, Standard test methods for water vapor transmission of materials - ASTM E96-95 In *ASTM book of standards*, ASTM: Philadelphia, **1995** p697-704.

10. LeCorre, D.; Bras, J.; Dufresne, A., All starch nanocomposite coating for barrier material. *Surface and Coatings Technology* **2011,** Submitted.

11. FlexPakRenew Consortium In *Innovative bio-based materials for water-based barrier coating* FlexPakRenew Workshop, Lyon Airport, May 10th 2011, **2011**.

12. Clegg, F.; Breen, C. In *Exploiting the synergies between starch, nanoclay and other additives to enhance the barrier properties of paper*, FlexPakRenew Workshop, Lyon Airport, May 10th 2011, **2011**.

13. Saxena, A.; Elder, T. J.; Ragauskas, A. J., Moisture barrier properties of xylan composite films. *Carbohydrate Polymers* **2011,** 84, (4), 1371-1377.

14. Talja, R.; Poppius-Levlin, K. In *Xylan from wood biorefinery - A novel approach*, FlexPakRenew Workshop - Innovating in fibre based flexible packaging through water based barrier coatings, anti microbial coatings, nanotechnologies and life cylce analysis., Lyon Airport, May 10th 2011, **2011**; CTP, Ed.

15. Bilbao-Sainz, C.; Bras, J.; Williams, T.; Sénechal, T.; Orts, W., HPMC reinforced with different cellulse nano-particles. *Carbohydrate Polymers* **2011,** doi:10.1016/j.carbpol.2011.06.060.

16. LeCorre, D.; Bras, J.; Dufresne, A., Influence of starch nanocrystals fillers' botanic origin on mechanical properties of natural rubber nanocomposites. *Composites Part A: Applied Science and Manufacturing* **2011,** Submitted.

Chapter 4-IV. Sustainability assessment of starch nanocrystals

Déborah LeCorre[1], Julien Bras[1], Catharina Hohenthal[2], Alain Dufresne[1]

[1]*The International School of Paper, Print Media and Biomaterials (Pagora), Grenoble Institute of Technology, BP 65 - F-38402 Saint Martin d'Hères Cedex, France*

[2] *VTT – Technical Research Center of Finland – P.O.Box 1000 – 02044 VTT, Finland*

Abstract

Fossil energy depletion and growing environmental concerns have brought up increasing interest in bio-based eco-efficient and high technology materials. Among them, starch nanocrystals (SNC) consist of crystalline nano-platelets produced from the hydrolysis of starch and mainly used as nano-fillers in polymeric matrix. New applications have brought up the need for scaling-up the SNC preparation process. However, for this new bio-based nano-material to be sustainable, its preparation and processing should have limited impacts on the environment. Thus, together with analyzing and making recommendations for the scaling-up of SNC production process, it is worth identifying "environmentally sensitive" steps using Life Cycle Analysis (LCA). To that purpose, different scenarios have been proposed and compared according to different environmental impacts. Also, a comparison to its main competitor, i.e. organically modified nanoclay (OMMT), is proposed. From a LCA point of view, SNC preparation requires less energy (GER) than OMMT extraction, but global warming (GWP) and acidification (AP) indicators were higher than for OMMT. However, SNC have the added advantages to be renewable and biodegradable contrary to OMMT which contribute to non-renewable energy and mineral depletion. Thus, used as filler, SNC have a positive impact on the end of life of the filled material. From these observations, recommendations for the scaling-up of the SNC preparation process are made and dealt mainly with the use of land and water.

Keywords

Life Cycle Analysis (LCA); Starch; Nanocrystals; Toxicology; Nanoclay

Inspired from: *D. LeCorre, J. Bras, C. Hohenthal, A. Dufresne, Submitted to Journal of polymers and the environment, 2011*

Paper 9

IV.1. Introduction

Engineered nano-scaled materials are used globally in numerous industrial applications and the list of proposed commercial applications continues to grow[1]. Indeed, these nanomaterials allow reaching outstandingly enhanced properties at very low content. Moreover, fossil depletion and growing environmental concerns have lead to the development of bio-based materials and nano-materials.

Due to their semi-crystalline structure, polysaccharides (such as cellulose) offer the opportunity to prepare bio-based nanoparticles. Indeed, since pioneer-work on polymer nanocomposites reinforced with nanoclay, at Toyota in the early 1990's, work on nanocrystalline cellulose (NCC) has exponentially increased as reviewed recently[2]. It was soon followed by investigations on chitin[3-5] and starch nanocrystals (SNC) as recently reviewed elsewhere[6]. Starch is an abundant material produced by nature and SNC are crystalline platelets resulting from the disruption of the starch granules by the hydrolysis of amorphous parts with acid. The current preparation process is lab-scaled[7] (as explained in previous chapters). Their morphology was described[8] as individualized platelets, with a thickness of 5-7 nm and equivalent diameter between 30 and 100 nm depending on the origin of starch, e.g. 40-70 nm for potato SNC[9], 30-80 nm[10] or 60-150 nm[11] for pea SNC, and 50 nm[12] or 70-100 nm[13] for waxy maize SNC. Their shape is therefore very similar to that of inorganic nanoclays. Their main and almost sole application is in nanocomposites, as SNC display (i) the same reinforcing effect than some NCC[14] (ii) higher barrier properties (due to their platelet morphology)[15, 16] and (iii) higher biodegradability than NCC and CNT (carbon nanotubes)[17]. Most recent applications, as (i) coating fillers, (ii) drug release[18, 19] and thermo-responsive materials[20] relate SNC potential for industrial development.

However, being a bio-based material is not enough to be sustainable. Their production and application processes have to have limited impacts on the environment, the society and the economy. Indeed, "sustainability" was first coined by the Brundtland Commission (formally the World Commission on Environment and Development of the United Nations in 1983), and was defined as the "social and economic advance to assure human beings a healthy and productive life, but one that did not comprise the ability of future generations to meet their own needs"[21]. More recently, Life Cycle Assessment (LCA) was standardized by the International Standardization Organization (ISO) and largely contributed in assessing environmental impacts across all stages of production, use and waste management for different materials. Up to date, no

environmental analysis of SNC has been proposed, and only very few deal with that of nanocelluloses (as developed in section I.3.5 on toxicity).

Therefore, before making recommendations for the scaling-up of SNC preparation, a LCA of the current process is expected. It would allow identifying "environmentally sensitive" steps and making recommendations for the scaling-up of the process as recently studied (previous Chapter 3).

Also, it could be considered that SNC's main competitors are organically modified nanoclays (OMMT) which present similar dimensions and morphology as SNC. OMMT are non-renewable, non-biodegradable mineral-based platelet-like nanofillers also used as reinforcing and barrier materials in polymers[22]. In the FlexPakRenew project[23], our aim was to propose a bio-based alternative to OMMT in barrier coating. Thus, SNC and OMMT available impacts are also compared in this study.

IV.2. Materials & Methods

IV.2.1. Life Cycle Analysis (LCA)

Life cycle assessment (LCA) is a standardized method for the compilation and evaluation of the inputs, outputs, and potential environmental impacts of a product system throughout its life cycle. Giving the amount of data to process, software (such as SIMAPRO 7.1 used in this study) is used for calculations. LCA methodology was standardized in 1997 by the International Standardization Organization (ISO) in their ISO-14040 [24]and distinguishes the following steps:

1. **Goal definition and scoping - Methods**. This step consists in defining (i) the functional unit to be studied, (ii) the process involved, (iii) together with the temporal and geographical scopes, as well as (iv) other products to be taken as reference for comparison.

2. **Inventory analysis (LCI) - Model.** At this stage a flow diagram is developed and computed. All inputs (such as energy and materials requirements) and outputs (such as air, water, soil emissions and other release) are identified, quantified (i.e. measured or estimated) and reported into the software.

3. **Impact assessment (LCIA) - Results.** For the environmental impact of all outputs to be assessed, a standardized method and its corresponding indicators is selected (in the standardized method data base) and applied to the collected data.

4. **Interpretation - Discussion.** The results of the LCIA (given through indicators) are discussed and compared to that of a reference product and conclusions and recommendations are made.

Impacts/Indicators definition

Here are presented the definitions of most common indicators used in the different methods used in this LCIA.

- The **Global Warming Potential (GWP)** is the potential contribution of a substance to the greenhouse effect. This value has been calculated for a number of substances over periods of 20, 100 and 500 years because it is clear that certain substances gradually decompose and will become inactive in the long run [25]. The impact of a process/product on **climate change** is calculated by multiplying each greenhouse gas (GHG) emission by a characterization factor (determined by the selected standard) and adding them together. Indeed, main GHG is water vapor but are also considered carbon dioxide (CO_2), methane, nitrous oxide (N_2O) (especially when dealing with agro-prodcuts), chlorofluorocarbons and ozone. The impact on climate change is expressed as CO_2 equivalents.

- **Energy Requirements (GER)** is the total amount of primary energy (**fossil fuel**) required for manufacturing a product.

- **Acidification** is the increase in acidity of water streams, soils or air due to human activity. It can unbalance chemical and biological ecosystems. It is mainly due to SO_2, NO_x and HCl emissions which turn into HNO_3 and H_2SO_4 by oxidation. Acid rains can reach a pH of 4-4.5 [26].

- **Eutrophication** is a natural process that occurs in aging lakes or ponds. Artificial eutrophication occurs when human activity introduces increased amounts of nutrients in the water. The body of water gradually builds up its concentration of plant nutrients such as nitrogen (N) and phosphorus (P), which speed up plant growth and eventually choke the lake of all of its animal life.

- **Ozone depletion** corresponds to the contribution of the decline of the volume of ozone in earth's stratosphere and to the ozone hole. The primary cause of ozone depletion is the presence of chlorine-containing gases (primarily CFCs and related halocarbons). In the presence of UV light, these gases dissociate, releasing chlorine atoms, which then go on to catalyze ozone destruction into O_2.

- **Ecotoxicology** has been defined as "the branch of toxicology concerned with the study of toxic effects, caused by natural or synthetic pollutants, to the constituents of ecosystems, animal (including human), vegetable and microbial, in an integral context"[27].

Other indicators have been developed depending on the method used: **Respiratory effects** (organic and inorganic) are the damages to the human health, related to respiratory problems, as a result of the dust emissions of organic and inorganic substances. A carcinogen substance is capable of causing cancer. **SMOG** (contraction of SMoke and fOG) is an air pollution produced by the photochemical reaction of sunlight with hydrocarbons and nitrogen oxides that have been released into the atmosphere, especially by automotive emissions. **Radiation** refers to the emission of radiations. **Mineral** refers to the use of mineral (non renewable) resources.

IV.2.2. Goal definition and scoping

The purpose of the LCA in the present study was (i) to investigate whether the use of SNC, produced by acid hydrolysis has environmental advantages over the use of nanoclays (OMMT), for reaching the same final properties; and (ii) to find leads for the development of a scaled-up production process.

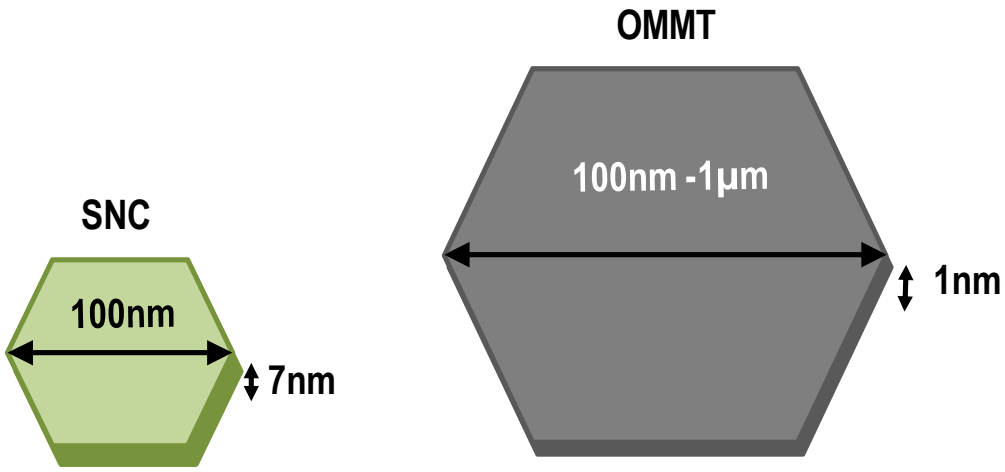

Figure 4-IV.1. Representation of SNC and OMMT.

To this end, two product systems, viz. starch nanocrystals (SNC) and nanoclays (OMMT), represented in Figure 4-IV.1, were studied and compared. Using data measured at lab-scale and the LCA data base from SIMAPRO 7.1, an impact assessment on climate change (Global Warming Potential GWP_{100}, kg $_{CO2}$eq/kg), energy requirement (Gross Energy Requirement - GER , MJ/kg) and acidification (Acidification Potential - AP, mol H+ eq/kg) is proposed. The life cycle impact assessment (LCIA) was

carried out using different methods: Eco-Indicator 99(H) was used to extract the GER, and TRACI 2V3.01 for GWP_{100} and AP assessment.

The functional unit was 1kg of SNC (size 100±50 nm) produced in 5 days in Grenoble according to the previously described protocol[7]. The function of SNC is to provide mechanical and barrier properties to the packaging it will be incorporated in.

It is assumed that energy use and emissions in nanocomposites/coating preparation are similar for both nanofillers. Thus, the LCA study does not include the converting of the products and was limited to the production and the end of life of each product (the only steps that differ).

IV.2.3. Model - Life cycle inventory data (LCI) of OMMT

The LCI for OMMT production has been assessed recently (2008) by Joshi[28] and will be considered as the reference case of this study. The OMMT production process which consists mainly in clay mining, organo-modifier production and clay processing and modification, can be modeled as in Figure 4-IV.2.

In more details, the raw clay (Ca-bentonite) is extracted and subjected to an ion exchange to replace divalent calcium ions with monovalent sodium ions. This results in an increase in the interlayer distance between the clay platelets. After separation by hydrocyclones and spray drying, another ion exchange is performed for organic modification in which sodium ions are replaced by alkyl quaternary ammonium salts. The clays are then press filtered, heat dried and grounded to reduce particle size. Figure 4-IV.2 summarizes the material requirements at intermediate production stages for the production of 1kg OMMT.

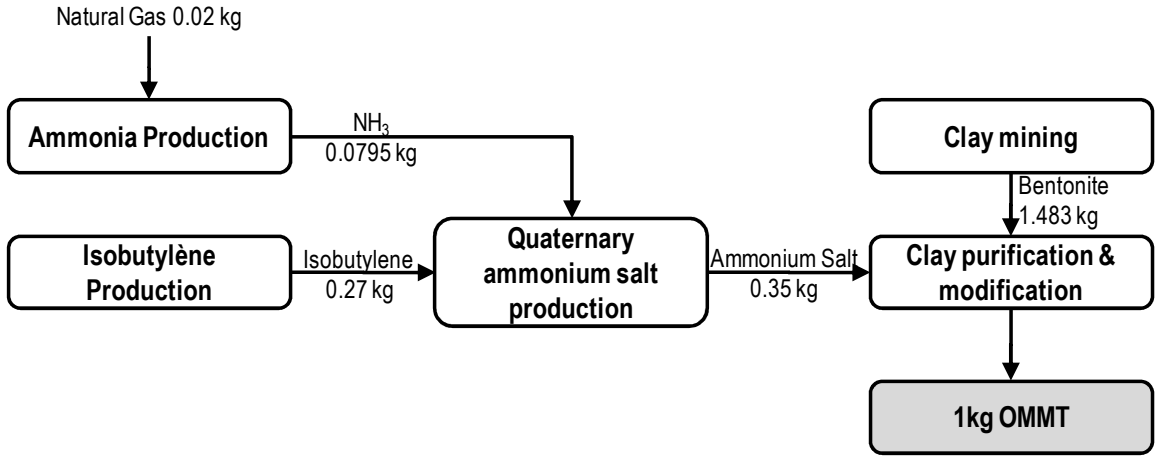

Figure 4-IV.2. Organically modified montmorillonite (OMMT) clay production process (adapted from [28]).

Paper 9

The fuel and input requirements are estimated with indirect inputs developed by Franklin Associates[29] from various industry sources and Ecobilan's DEAM™ LCA database (Ecobilan 2006):

- The mining of one megaton (Mt) of clay requires 13.6 kWh electricity, 16.2 m^3 natural gas, 6.17 kg coal, and 0.025 L residual oil.
- The estimate energy uses for the processing (i.e. separation, purification, delamination, reaction with organic modifiers, homogenization, dewatering and size reduction) of 1 Mt of OMMT is 242 kWh electricity, 111 m^3 natural gas and 0.136L distillate fuel oil.
- Ammonium salt production direct energy input estimates are 329 kwh electricity and 30.9 m^3 natural gas.
- Estimated transportation is 323 Mt-km in diesel trucks, 1,077 Mt-km in diesel railways, 28 Mt-km using barges and 5,299 Mt-km in ocean freighters. Energy and emission estimates were calculated from the Ecobilan's DEAM™ LCA database [28]. (*T-km is a payload-distance unit used in freight. It corresponds to the load of the truck (in tons) multiplied by the traveling distance (in km)*).

  Nanoclay price estimate is 4.4-10 €/kg.

IV.2.4. Model - Life cycle inventory data (LCI) of Starch Nanocrystals (SNC)

The SNC production process which consists mainly in starch production (growing and milling), starch hydrolysis and SNC washing/purification can be modeled as in Figure 4-IV.3. It summarizes material requirements at intermediate production stages for the production of 1kg SNC and were measured experimentally.

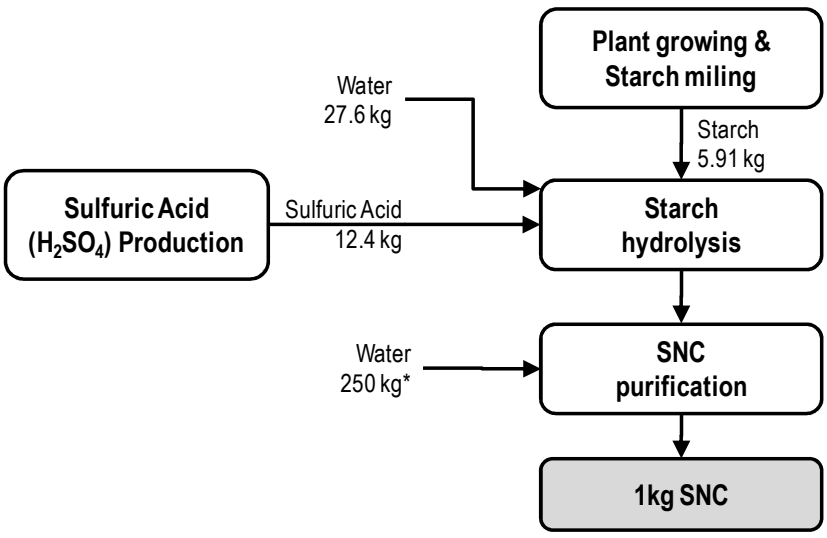

Figure 4-IV.3. Starch Nanocrystals (SNC) production process (based on experimental data). *_indicates an open circuit for water circulation which could be turned into a re-circulating circuit._

In more details, once corn is grown, starch extraction process[30] can be summarized as follow. The granule is cleaned to remove batch contaminants (such as broken corn, stones, dusts, and foreign grains); then it is steeped at 50℃ for 40-50h at acidic pH and treated with sulfur dioxide in order to eliminate the protein matrix and enable the swelling of the kernels by water absorption (water content increases from 15-45%), skin removal, germ expulsion (by milling and hydro-cyclones). Then two successive nozzle type continuous centrifugal separators remove the dissolved proteins (called gluten) from the starch milk which is then refined in a multi-step cyclone plant, the one and only step of the wet milling process where fresh water is added. Finally, the refined starch milk, having a water content of approximately 65 %, is dehydrated in peeler centrifuges to a residual water content of about 40 %.

The outputs of starch production (5.91kg) and sulfuric acid production (12.4kg) correspond to the amount of starch and acid necessary to produce 1kg of SNC. The corresponding energy inputs were estimated using the Ecobilan's TEAM^{TM} LCA database (Ecobilan 2006). They respectively accounts for 32.9% and 25.1% of the total inputs as estimated from LCA database (Ecobilan 2006).

SNC are obtained by the further processing of the starch granules. The classic and most-used SNC production process developed by Angellier et al. [7] can be described as follow. Starch granules are put together with diluted sulfuric acid and kept under constant temperature (40℃) and mechanical stirring (400 rpm) for 5 days. A condenser is used to condensate the evaporated water and to keep a constant volume.

The resulting suspension is washed by successive centrifugations in water until reaching neutral pH. Sulfuric acid hydrolyses preferentially the amorphous parts of starch rendering negatively charged (SO_3^-) crystalline nanoplatelets.

The inputs of starch hydrolysis and SNC purification were measured during a lab-scale production and correspond to:

- 552 kWh.kg^{-1} electricity and 37.7 m^3 water for SNC production
- 3.85 kWh electricity and 250 m^3 water for SNC purification as several washings by differential centrifugations in water are required.

Estimated transportation was the same as for OMMT.

IV.3. Results & Discussions

IV.3.1. Life Cycle Impact Assessment (LCIA) of SNC according to different scenarios

In order to assess possible improvement to be brought to the production process, 4 scenarios were considered.

- **Scenario 1** considers the current SNC production at lab scale.
- **Scenario 2** considers the current lab-scale production, with a decrease in water consumption of 85% (which could be achieved using close circuit and less water consuming extraction techniques).
- **Scenario 3** considers the current lab-scale production, using organic starch instead of regular starch, to assess if it has a positive environmental impact over all.
- **Scenario 4** considers that energy consumption per kg should decrease when scaling up the production process, and the use of organic starch. An estimated decrease of 50% was postulated.

Organic agriculture is an ecological production management system based on minimal use of off-farm inputs (such as synthetic fertilizers) and on management practices that restore, maintain and enhance ecological harmony.[31]

Table 4-IV.1 shows impact results computed with Eco-Indicator 99(H) for the four scenarios. This method considers three damage categories:

- Human Health (unit: DALY= Disability Adjusted Life Years, represents the degree of freedom from diseases and death)
- Ecosystem Quality (unit: PDF.m2.yr; PDF= Potentially Disappeared Fraction of plant species)
- Resources (unit: MJ surplus energy = Additional energy requirement to compensate lower future naturally occurring valuable mineral grade)

Table 4-IV.1. Impact results for SNC production according to the Eco-Indicator 99(H) method.

Impact category	Unit	Scenario 1: Current lab-scale production	Scenario 2: Reduced water consumption	Scenario 3: Use of organic starch	Scenario 4: Reduced energy requirement
Carcinogens	DALY	3.36E-05	3.32E-05	5.91E-06	5.18E-06
Resp. organics	DALY	1.42E-08	1.34E-08	1.49E-08	1.20E-08
Resp. inorganics	DALY	1.77E-05	1.68E-05	2.32E-05	2.05E-05
Climate change	DALY	2.88E-06	2.63E-06	2.19E-06	1.75E-06
Radiation	DALY	1.98E-05	1.97E-05	1.98E-05	8.25E-06
Ozone layer	DALY	2.32E-08	2.31E-08	2.31E-08	2.52E-08
Ecotoxicity	PDF*m^2yr	7.99E+00	7.61E+00	7.87E+00	5.50E+00
Acidification/ Eutrophication	PDF*m^2yr	6.09E-01	5.91E-01	1.70E+00	1.64E+00
Land use	PDF*m^2yr	5.11E+01	5.10E+01	5.87E+01	5.85E+01
Minerals	MJ surplus	1.94E+00	1.87E+00	1.92E+00	1.27E+00
Fossil fuels	MJ surplus	1.98E+01	1.89E+01	1.88E+01	1.59E+01

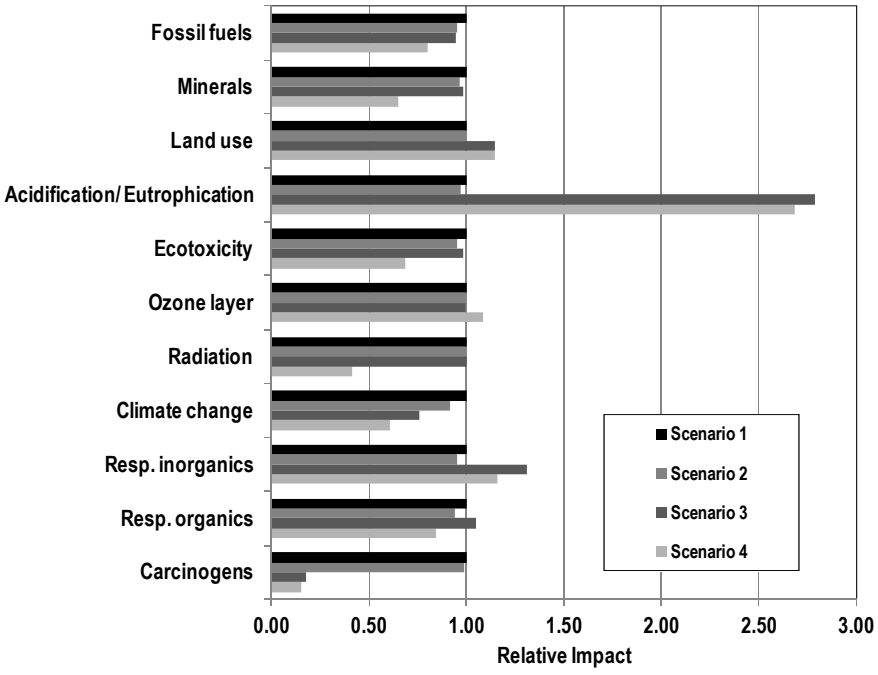

Figure 4-IV.4. Relative indicators of the impact of SNC production according to different scenarios. (using Eco-Indicators 99).

Paper 9

Figure 4-IV.4 representing *relative* impacts shows that scenarios 1 and 2 do not differ much (differences are less than -9% and mean difference is 3%). However, scenarios 3 and 4, which considers the use of organic starch, differ greatly from 1 and 2, especially for carcinogens (respectively -85% and -82%) and acidification (respectively +166% and +179%) and to a lower extent respiratory inorganic (respectively +16% and +31%), climate change (respectively -39% and -24%) and land use (+15% for both). This is mainly due to the fact that on average, organic maize yield (kg/ha) is lower than for conventional maize. Estimated yield is only 75 to 90% of the crop of conventional systems, meaning that more land must be planted in order to have an equal return. However, nitrous oxide (NO/NO_2) emissions per hectares are comparable[32] due to the use of equipments and trucks. And nitrous oxides contribute to acidification. Thus it is possible that the Ecobilan's TEAM™ LCA database reflected thess information.

Furthermore, scenario 4 is more environmentally friendly than scenario 3 as it exhibits lower radiation (-58%) and minerals (-35%). For scenario 2, a decrease in acidification was expected due to lower energy requirement. However, this cannot be observed as it combined the use of organic starch which as evidenced with scenario 4 is detrimental to acidification.

Determination of *normalized* impacts (not shown here) reveals that most impacting indicators are in order: land use > fossil fuel consumption > carcinogens. On these indicators, land use for scenarios 3 and 4 is increased by 15%, but fossil fuel energy is decreased by respectively -20% and -5% and carcinogens is decreased by respectively -85% and -82%. Overall, the cumulative impact variation is -37% for scenario 2, +116% for scenario 3 and -75% for scenario 4.

Primary conclusion is that starch cultivation has a great environmental impact over the whole SNC preparation process and that contrary to potential expectations, it was evidenced that the use of organic starch for such purpose was rather detrimental to the process' global impacts.

Thus, it seems that the development of a scale-up production process should consist in using less water (as model in scenario 2) and in using less electrical energy (as in scenario 4). This latter condition could be achieved by developing a continuous extraction process of SNC.

Table 4-IV.2 shows impact results from the TRACI 2 V3.01 method for the same four scenarios.

Table 4-IV.2. Impact results for SNC production according to TRACI 2 V3.01method.

Impact category	Unit	Scenario 1: Current lab-scale production	Scenario 2: Reduced water consumption	Scenario 3: Use of organic starch	Scenario 4: Reduced energy requirement
Global Warming	kg CO_2 eq	13.07	11.90	10.06	7.95
Acidification	H^+ moles eq	9.01	8.78	15.51	14.83
Carcinogenics	kg benzene eq	0.16	0.15	0.15	0.09
Non carcinogenics	kg toluene eq	3601.53	3215.68	3747.76	2216.99
Respiratory effects	kg eq	0.02	0.02	0.02	0.02
Eutrophication	kg N eq	0.23	0.23	0.17	0.16
Ozone depletion	Kg CFC-11 eq	0.00	0.00	0.00	0.00
Ecotoxicity	kg 2,4-D eq	80.32	33.15	115.82	61.99
Smog	kg NO_x eq	0.06	0.05	0.06	0.05

PM2.5 = particulate matter of size under 2.5µm
2,4-D = 2,4-dichlorophenoxyacetic acid used as a herbicide and pesticide

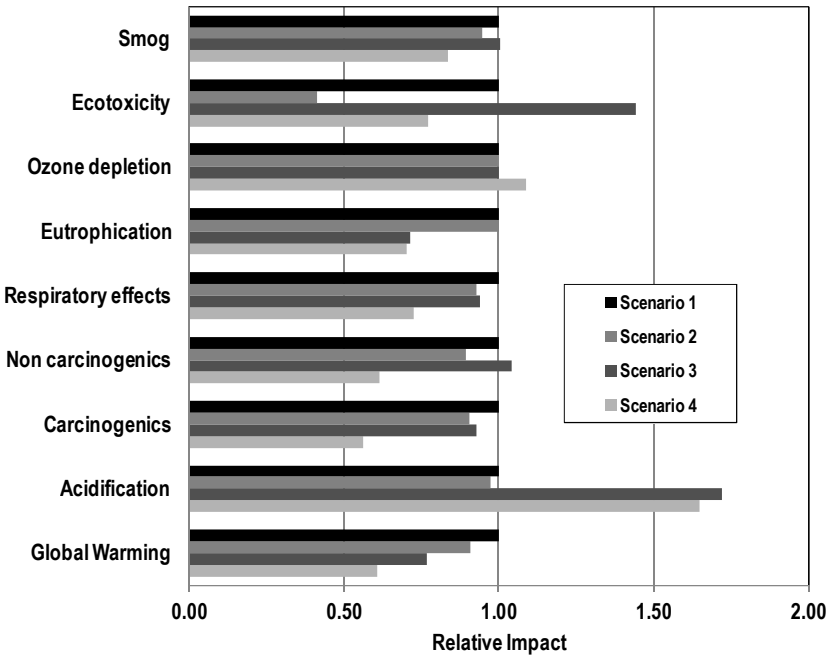

Figure 4-IV.5. Relative indicators of the impact of SNC production according to different scenarios. (using TRACI).

Paper 9

Figure 4-IV.5 displaying the *relative* impacts shows that according to the TRACI method, scenarios 1 and 2 differ more from each other than with the Eco-Indicator 99 method, with up to -59% differences in ecotoxicity and an averaged difference of -12% . Scenarios 3 and 4 also differed more from each other. However, the latter both exhibit the lowest GWP.

This is not in contradiction with high acidification levels. Indeed, as explained before, acidification is due to the use of motored equipments on larger land area for organic farming due to lower yields. Whereas, scenario 3's GWP is reduced (-23%) due to less N_20 emission, which are highly contributive GHG gas, for organic farming; and scenario 4's GWP is further decreased (-39%) by the energy saving (and thus more GHG gas emission saving) due to the scaling-up.

Overall, scenario 4 exhibited the most impact reduction with a decrease of -144% (cumulative impact variation). Scenario 2 showed a -104% impact reduction. Scenario 3's impact on the contrary increased by +56%, mostly due to increased acidification and ecotoxicity (due to the lower yield of organic farming as explained earlier).

Thus, despite different impact variation with the TRACI method, conclusions are rather similar than with the Eco-Indicator 99. Efforts should focus on saving both electrical energy and water. However, it was also evidenced that the use of organic starch for such purpose was rather detrimental to acidification whilst positive for global warming reduction.

IV.3.2. LCIA of SNC in comparison with OMMT

In Production

For comparison purposes with published LCA of OMMTs[28], Eco-Indicator 99(H) was used to extract the GER, and TRACI 2V3.01 for GWP_{100} and AP assessment. Data from the present study is compared to published ones in Table 4-IV.3. Obviously the data available for OMMT is rather advantageous.

Table 4-IV.3. GER, GWP_{100} and AP indicators for SNC (range of the four scenarios) in comparison with nanoclays.

	GER (MJ/kg)	GWP_{100} (kg.CO_2 eq /kg)	AP (H^+ eq/kg)	Ref
SNC	16-19	7.9 - 13	8.7 - 15.5	Present Study
OMMT[1]	40	1.5	-	[28]
OMMT[2]	48	2.7	0.93	[33]

[1] Quaternary ammonium salt modified

[2] Organosilane modified

As shown in Figure 4-IV.6, the production of SNC requires less than half as much energy than the production of OMMTs in all scenarios. This is due to the fact that OMMT are organically modified whereas SNC are simply hydrolyzed with a diluted acid.

However, global warming is thrice as much for SNC and acidification is almost inexistent for OMMTs production. This is due the large land use, water consumption and NO_x (which contribute drastically to GWP but not to GER) emissions of the starch cultivation.

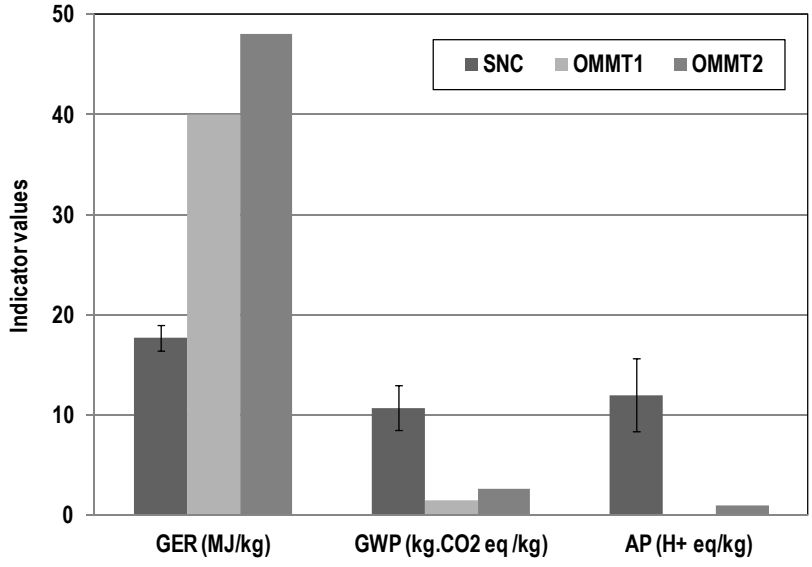

Figure 4-IV.6. Selected indicators for comparing LCA of OMMT and SNC.

Paper 9

In Use as filler material – End of life

The impact of using SNC to replace OMMT (such as done in the flexible packaging developed in FP7 European FlexPakRenew project) was assessed. The technical challenge in the project was to develop a flexible packaging based on multilayered structure (based on paper) with a total weight between 50 and 90 $g.m^{-2}$ that achieves barrier properties competitive with petroleum based plastic. The structure of the developed multilayer flexible packaging can be represented as follow (Figure 4-IV.7).

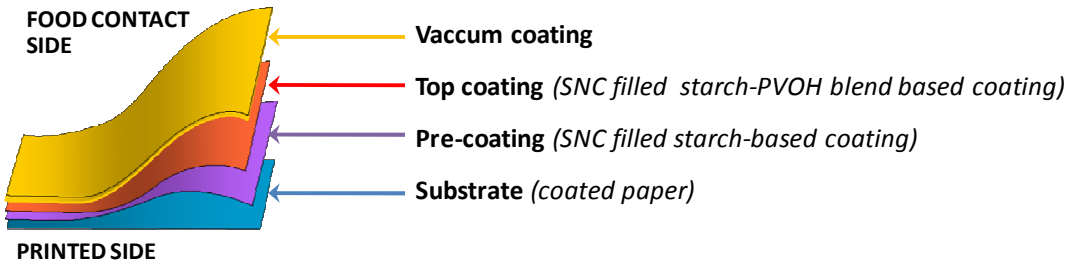

Figure 4-IV.7. Structure of the Flexible packaging developed in the FlexPakRenew project.

Giving that the same process is used for incorporating the SNC and the OMMT to the packaging, only the end of life of the two fillers has been compared. And since a potential application could be individual packaging, biodegradability could be a key property.

The share of biodegradable[34] and renewable[35] material in the coating layers was calculated in the case of OMMT and SNC and compared as presented in Figure 4-IV.8. Used in a flexible packaging with final weight 61.4 gsm, the use of SNC instead of OMMT represents an increase in biodegradable material of 17%. This also corresponds to the increase in renewable material (Figure 4-IV.9).

Paper 9

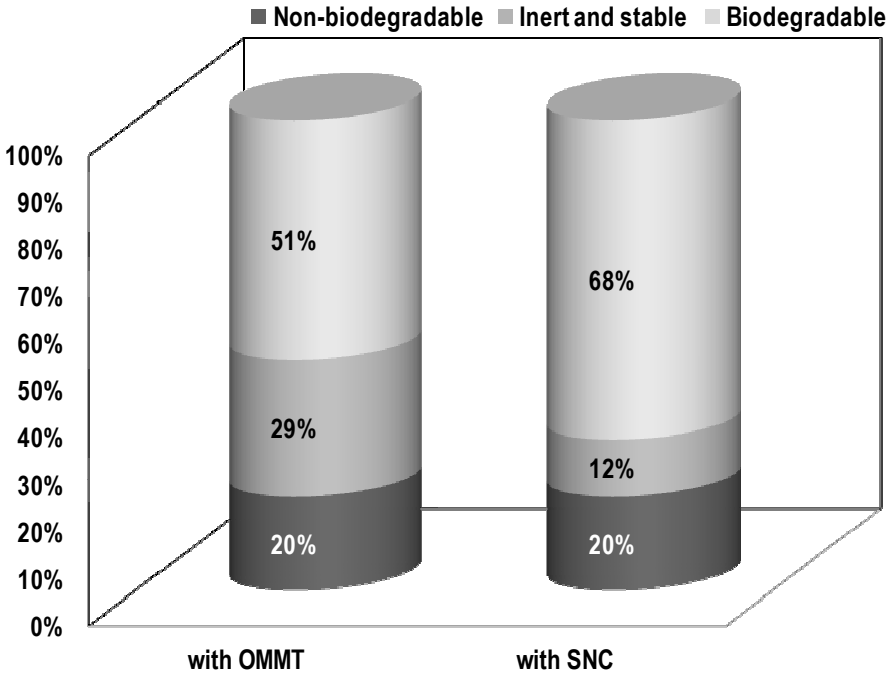

Figure 4-IV.8. Share of biodegradable material in the barrier layers (with permission from authors[34])

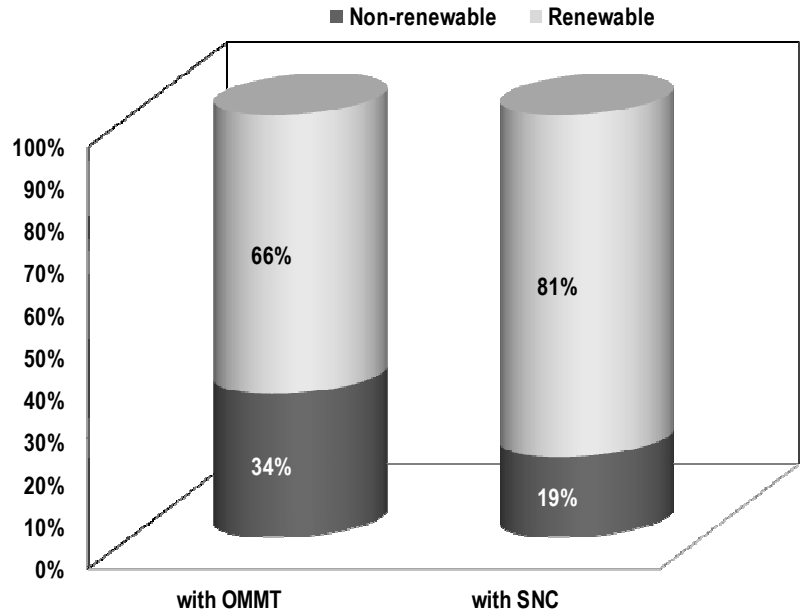

Figure 4-IV.9. Share of renewable material in the barrier layers (with permission from authors[35])

Paper 9

IV.3.3. LCIA of SNC filled packaging in comparison to other packaging

An LCA of the complete multilayer packaging has also been assessed and is presented elsewhere[34, 35] using input data from all the project partners, including that of SNC presented in this study.

The composite materials for thin and flexible packaging currently in use are based on non-renewable natural resources. The PE and PET compounds are produced from mineral oil and the barrier film is made from aluminum metal. None of these materials are biodegradable, their use has an impact on the finite natural resources and the material recycling of the composite material is challenging if not impossible from techno-economical point of view.

Another competitor for the packaging developed in the FlexPakRenew project is PLA packaging as it is marketed as a bio-plastic as it is based on renewable resources.

Thus, for the project, 2 references cases are considered (1) an industrial PE-coated paper and (2) a PLA packaging. As shown in Figure 4-IV.10, the use of renewable biodegradable materials allows reducing the packaging impact on climate change.

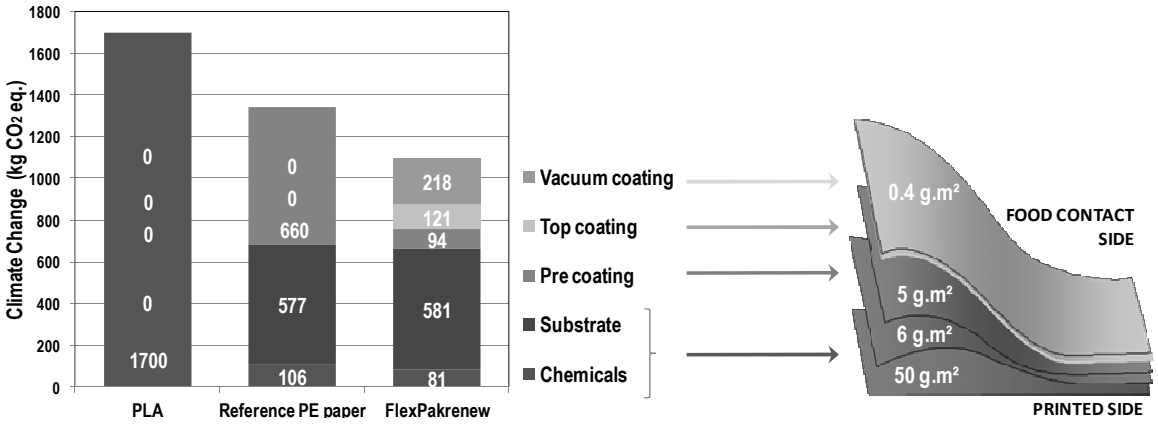

Figure 4-IV.10. Climate change for 10000m² packaging material - Adapted from [35]

Paper 9

IV.3.4. Life Cylce Interpretation

One of the main environmental goals of the European Project (FlexPakRenew) was to reduce the impact of packaging on climate change (GWP). Strong differences between SNC and OMMTs' impacts were evidenced, as displayed in Table 4-IV.3 and Figure 4-IV.10. Although reduced GER (gross energy requirement) was reached, impacts on climate change (reflected in the GWP indicator) and acidification (reflected in the AP indicator) seem to be higher for SNC. Unfortunately, data for ecotoxicity, carcinogenic impact and inorganic respiratory impact for OMMT are not available, preventing complete comparison with SNC.

The analysis of the different scenarios concluded that efforts to reduce all impacts could focus on saving both electrical energy and water consumption. Some water consumption (such as that of land watering) can hardly be lowered but water used in the SNC production process could be lowered during the scale-up.

The fact that uncertainties in life cycle inventory data of SNC production are high (they are based on estimates and laboratory data) does not, therefore, impair the robustness of the results. The real impacts of SNC production are probably even lower than estimated in this study, because the energy use in the lab- plant considered here is probably higher than the energy use in commercial-scale industrial plants. Recent study[36] has shown, as a proof of principle, that cross-flow filtration was an effective, economical and energy saving continuous operation for separating SNC from the bulk suspension compared to current isolation methods (centrifugation).

Besides the SNC/OMMT production, further impacts are related to the converting and the end-of-life of the product. In this study, the composite coating preparation (converting) was considered the same for SNC and OMMT.

When comparing the end-of-life of both materials, clear differences are revealed. OMMT are mineral-based (not renewable) and not recyclable, nor biodegradable material but are considered inactive. The mineral can be disposed of as a non toxic/inactive material in approved landfill sites in accordance with local regulations but contributes to mineral depletion. SNC on the other hand, are based on renewable resources and are biodegradable[17].

Currently, SNC barrier properties are not as high as OMMT. However, it has recently been demonstrated that better isolation / classification of SNC, thanks to an optimized production process, rendered higher barrier properties (Previous paper: Chapter 4-III). Thus, upon the optimization of the isolation process, SNC should reach

equivalent or complementary (oxygen) barrier properties as OMMT. Scaling up and production process optimization should allow reaching even lower environmental impact. Thus, for the development of bio-based biodegradable packaging, the use of SNC should be favored.

IV.3.5. SNC toxicity

Although natural nanoparticles exist in the environment it is expected that nanomaterials might enter the environment through intentional or non-intentional release during manufacturing, transport or use[37]. Controversies on the use of nanoparticles and nanotechnologies are largely driven by consumers concerns with the release of nanoparticles in the atmosphere during the manufacture, use and disposal of engineered nanomaterials, and thus its impact on the environment and on human toxicity. This is why this sustainability assessment could not be concluded without addressing the issue of SNC potential toxicity.

Commonly studied risks for humans are nanoparticles uptake through inhalation, ingestion and in some case absorption through the skin. Inhalation could cause inflammation of the respiratory system and ingestion could transport nanoparticles through the blood stream to other organs causing cardiovascular or extrapulmonary complications.

Currently, there is no study on SNC's toxicity available. However, OMMT and cellulose nanocrystals (NCC) are starting to be studied. Nevertheless, for now, knowledge about toxicological effects of these nanomaterials is limited. It is expected that toxic implications will be specific to the type of base material, its size and shape[38]. SNCs have the same platelet-shape and dimensions as non exfoliated OMMT and a chemical structure similar to that of NCC. Indeed, NCC are polysaccharide nanocrystals produced by sulfuric acid hydrolysis (presenting on its surface $–SO_3^-$ groups) just as SNCs.

In a recent study[39], it was demonstrated that nanoclays "are highly cytotoxic and as a result pose a possible risk to human health". In the cell culture medium, the nanoclays aggregated/exfoliated acted differently and this appeared to have an effect on their mechanisms of toxicity.

On the contrary first study on NCC reported low toxicity and environmental risk potential[40]. The ecotoxicological characterization involved tests with several aquatic species (e.g. Daphnia, rainbow trout and fathead minnow) and estimated thresholds of

effects for a variety of endpoints such as survival, growth and reproduction. In addition, the first round of mammalian toxicity testing has indicated no effect at the highest concentration tested. More recent communication[41] also demonstrated that cytotoxicity (intracellular toxic effect) and pro-inflammatory response for NCC were significantly lower than for MWCNT (multiwalled carbone nanotubes) and CAF (crocylodite asbestos fibers). Work on cell proliferation, DNA damages and cell death is still ongoing. Also, in the last years, the introduction NCC for drug delivery matrix tablets has become more important. In vitro tests performed on NCC-acrylic nanocomposite beads, showed that the NCC and beads produced were nontoxic[42].

As NCC do, SNC are expected to have low toxicity and environmental risk potential for several reasons:

(i) SNC have the same chemical composition as NCC and lower aspect ratio.

(ii) Starch has been part of animal's diets for thousands of year. Thus, digestive systems all contain enzymes capable of digesting SNC, i.e. hydrolyzing glucosidic bonds and rendering starch nanoelements.

(iii) SNC are produced and processed in suspension in order to limit aggregation. Indeed, during drying, SNC aggregate to form particulates of a few microns in size, thus limiting possible intake.

These arguments appear as strong advantages when compared to the polemic discussions brought up by OMMT toxicity.

IV.4. Conclusion

From a LCA point of view, SNC's production requires less energy (GER) than OMMT's extraction but global warming (GWP) and acidification (AP) indicators were higher than for OMMT. However, SNC have the added advantages to be renewable and biodegradable contrary to OMMT which contribute to non-renewable energy and mineral depletion.

From these observations, recommendations for the scaling-up of the SNC production process are made. Main concern deals with the extensive use of land and water. Thus, the scale-up industrial production process should:

(i) Be based on non-cultivated low-water consuming naturally occurring starch sources, such as amaranth and some tubers; to limit acidification and eutrophisation linked to starch cultivates.

(ii) Include less-water and energy consuming extraction and washing processes such as micro-filtration, as described in recent study[36] and previous chapter 3-III.

(iii) Reach higher yield than current process.

Also, although toxicity of SNC is expected to be limited, it should be analyzed in detail to statute on its potential advantage over other nanoparticles.

IV.5. References

1. Geraci, C. L., Nanotechnology Research at NIOSH: Supporting Safe development of the business. In *2011 TAPPI Intl Conference on Nano for Renewable Materials*, Washington, USA, **2011**.

2. Habibi, Y.; Lucia, L.; Rojas, O., Cellulose nanocrystals: chemistry, self-assembly, and applications. *Chemical Reviews* **2010,** 110, ((6)).

3. Paillet, M.; Dufresne, A., Chitin Whisker Reinforced Thermoplastic Nanocomposites. *Macromolecules* **2001,** 34, (19), 6527-6530.

4. Gopalan Nair, K.; Dufresne, A., Crab Shell Chitin Whisker Reinforced Natural Rubber Nanocomposites. 2. Mechanical Behavior. *Biomacromolecules* **2003,** 4, (3), 666-674.

5. Morin, A.; Dufresne, A., Nanocomposites of Chitin Whiskers from Riftia Tubes and Poly(caprolactone). *Macromolecules* **2002,** 35, (6), 2190-2199.

6. Le Corre, D.; Bras, J.; Dufresne, A., Starch nanoparticles: A review. *Biomacromolecules* **2010,** 11, (5), 1139-1153.

7. Angellier, H.; Choisnard, L.; Molina-Boisseau, S.; Ozil, P.; Dufresne, A., Optimization of the preparation of aqueous suspensions of waxy maize starch nanocrystals using a response surface methodology. *Biomacromolecules* **2004,** 5, 1545-1551.

8. Putaux, J. L.; Molina-Boisseau, S.; Momaur, T.; Dufresne, A., Platelet Nanocrystals Resulting from the Disruption of Waxy Maize Starch Granules by Acid Hydrolysis. *Biomacromolecules* **2003,** 4, (5), 1198-1202.

9. Chen, G.; Wei, M.; Chen, J.; Huang, J.; Dufresne, A.; Chang, P. R., Simultaneous reinforcing and toughening: New nanocomposites of waterborne polyurethane filled with low loading level of starch nanocrystals. *Polymer* **2008,** 49, (7), 1860-1870.

10. Chen, Y.; Cao, X.; Chang, P. R.; Huneault, M. A., Comparative study on the films of poly(vinyl alcohol)/pea starch nanocrystals and poly(vinyl alcohol)/native pea starch. *Carbohydrate Polymers* **2008,** 73, (1), 8-17.

11. Yu, J.; Ai, F.; Dufresne, A.; Gao, S.; Huang, J.; Chang, P. R., Structure and mechanical properties of poly(lactic acid) filled with (starch nanocrystal)-graft-poly(e-caprolactone). *Macromolecular Materials and Engineering* **2008,** 293, (9), 763-770.

12. Garcia, N. L.; Ribba, L.; Dufresne, A.; Aranguren, M. I.; Goyanes, S., Physico-mechanical properties of biodegradable starch nanocomposites. *Macromolar Materials and Engineering* **2009,** 294, (3), 169-177.

13. Namazi, H.; Dadkhah, A., Surface modification of starch nanocrystals through ring-opening polymerization of Îµ-caprolactone and investigation of their microstructures. *J. Appl. Polym. Sci.* **2008,** 110, (4), 2405-2412.

14. LeCorre, D.; Bras, J.; Dufresne, A., Influence of starch nanocrystals fillers' botanic origin on mechanical properties of natural rubber nanocomposites. *Macromolecular Materials and Engineering* **2011,** Submitted.

15. Angellier, H.; Molina-Boisseau, S.; Lebrun, L.; Dufresne, A., Processing and structural properties of waxy maize starch nanocrystals reinforced natural rubber. *Macromolecules* **2005,** 38, (9), 3783-3792.

16. Bras, J.; Hassan, M. L.; Bruzesse, C.; Hassan, E. A.; El-Wakil, N. A.; Dufresne, A., Mechanical, barrier, and biodegradability properties of bagasse cellulose whiskers reinforced natural rubber nanocomposites. *Industrial Crops and Products* **2010,** 32, (3), 627-633.

17. Kümmerer, K.; Menz, J.; Schubert, T.; Thielemans, W., Biodegradability of organic nanoparticles in the aqueous environment. *Chemosphere* **2011,** 82, (10), 1387-1392.

18. Lin, N.; Huang, J.; Chang, P. R.; Feng, L.; Yu, J., Effect of polysaccharide nanocrystals on structure, properties, and drug release kinetics of alginate-based microspheres. *Colloids and Surfaces B: Biointerfaces* **2011,** In Press, Accepted Manuscript.

19. Zhang, X.; Huang, J.; Chang, P. R.; Li, J.; Chen, Y.; Wang, D.; Yu, J.; Chen, J., Structure and properties of polysaccharide nanocrystal-doped supramolecular hydrogels based on Cyclodextrin inclusion. *Polymer* **2010,** 51, (19), 4398-4407.

20. Valodkar, M.; Thakore, S., Isocyanate crosslinked reactive starch nanoparticles for thermo-responsive conducting applications. *Carbohydrate Research* **2011,** 345, (16), 2354-2360.

21. Bruntland, G. *Our common future: The World Commission on Environment and Development*; Oxford University Press.: Oxford, **1987**.

22. Johansson, C.; Järnstrom, L.; Breen, C. Biopolymer based barrier material and method for making the same. **2010**.

23. Centre Technique du Papier (CTP), FlexPakRenew Public Flyer. http://www.flexpakrenew.eu/documentation.cfm, **2010,** Access

24. ISO 14040 *Environmental management - life cylce assessment - principles and framework.*; **1997**.

25. Goedkoop, M.; Oele, M.; Schrywer, A. d.; Vieira, M., *SimaPro database manual - Methods library*. **2008**; p.

26. Actu Environnement, Dictionnaire Encyclopedique - Definition de Acidification. **2003,** Access (16/07/2011).

27. Truhaut, R., Eco-Toxicology - Objectives, Principles and Perspectives. *Ecotoxicology and Environmental Safety* **1977,** 1, (2), 151-173.

28. Joshi, S., Can nanotechnology improve the sustainability of biobased products? The case of layered silicate biopolymer nanocomposites. *Journal of Industrial Ecology* **2008,** 12, (3), 474-489.

29. Franklin Associates, Estimates from various internal/industry sources obtained through personal communication with James Littlefield. *Chemical Engineers* **2006**, (March 15, 2006).

30. Zuckerforschung Tulln, Maize starch extraction. http://www.zuckerforschung.at/inhalt_en.php?titel=STARCH%20TECHNOLOGY&nav=nstaerkeinfo_en&con=cigsmais_en, **2009,** Access

31. Gold, M. V., What is organic production? - USDA Definition and Regulations. http://www.nal.usda.gov/afsic/pubs/ofp/ofp.shtml, **2007,** Access (September 2011).

32. Pimentel, D.; Hepperly, P.; Hanson, J.; Seidel, R.; Douds, D. *Organic and conventional farming systems: environmental and economic issues*; **2005**.

33. DeBenedetti, B.; Camino, G.; Tabuani, D.; Maffia, L.; Santarén, J.; Aguilar, E. *Comparison between eco-profiles of innovative nanoclay and traditional TBBPA flame retardants*; STRP European research program “NANOFIRE”, No. 505637, 6th Framework Program: **2006**.

34. Hohenthal, C.; Veuro, S.; Kuisma, M., D6.6: Sustainability assessment for Renewable Biopolymer Based Flexible Packaging Paper. http://www.flexpakrenew.eu/documentation.cfm, **2011,** Access

35. Hohenthal, C.; Veuro, S. In *The role of Sustainability assessment and LCA in guiding projects*, FlexPakRenew workshop, Lyon Airport, **2011**.

36. LeCorre, D.; Bras, J.; Dufresne, A., Ceramic membrane filtration for isolating starch nanocrystals. *Carbohydrate Polymers* **2011,** 86, (4), 1565-1572.

37. Vilaplana, F.; Strömberg, E.; Karlsson, S., Environmental and resource aspects of sustainable biocomposites. *Polymer Degradation and Stability* **2010,** 95, (11), 2147-2161.

38. Fleischer, T.; Grunwald, A., Making nanotechnology developments sustainable. A role for technology assessment? *Journal of Cleaner Production* **2008,** 16, (8-9), 889-898.

39. Lordan, S.; Kennedy, J.; Higginbotham, C., Cytotoxic effects induced by unmodified and organically modified nanoclays in the human hepatic HepG2 cell line. *Appl Toxicol.* **2011** 31, (1), 27-35.

40. Kovacs, T.; Naish, V.; O'Connor, B.; Blaise, C.; Gagné, F.; Hall, L.; Trudeau, V.; Martel, P., An ecotoxicological characterization of nanocrystalline cellulose (NCC). *Nanotoxicology* **2010** 4, (3), 255-270.

41. Foster, E. J.; Clift, M. J. D.; Rothen-Rutishauser, B.; Weder, C. In *Toxicology of cellulose nanowhisker based nanocomposites*, 2011 TAPPI Intl conference on Nano for Renewable Materials, Washington, **2011**.

42. Villanova, J. C. O.; Ayres, E.; Carvalho, S. M.; Patrício, P. S.; Pereira, F. V.; Oréfice, R. L., Pharmaceutical acrylic beads obtained by suspension polymerization containing cellulose nanowhiskers as excipient for drug delivery. *European Journal of Pharmaceutical Sciences* **2011,** 42, (4), 406-415.

Chapter 4-V. Conclusions

In this last chapter, the potential of SNCs in a new application, i.e. multilayer coating, has been assessed. First the influence of the botanic origin of SNCs was investigated in a monolayer nanocomposite. Then the impact of SNCs in a paper-based double coating was measured, and finally it was used in the development of a multilayer packaging.

No substantial differences were observed between nanocomposites filled with different SNC, regardless the source of starch except for those filled with high-amylose starch-based SNCs. The latter exhibited poorer properties probably because of the release of loosely bonded chains during processing.

From a more applied point of view, it was demonstrated that (i) SNCs can be used in coating processes, that (ii) they can improve barrier and mechanical properties of some bio-based polymers, and that (ii) 2nd generation SNC are indeed more efficient as barrier material.

The previous studies were completed by an environmental impact assessment of SNCs prepared for such an application. Results should be used as guidelines for the scaling-up of the preparation process and for future studies.

This last chapter proposes new industrial applications for SNCs which will require high amounts of 2nd generation SNCs. Thus, future studies should focus on the industrial scale-up of the preparation process.

Also, interesting investigations could be added to these application studies with for example: SNCs orientation in bio-based coatings, SNCs reticulation and compatibilization, or SNCs standing film for barrier.

FIGURES

TABLES

General Conclusions

General Conclusions

The main objective of this work was to assess the industrial potential of starch nanocrystals for the packaging industry. Indeed, current environmental concerns and policies among industrialists and politicians have developed interests for efficient bio-based materials, as evidenced by the financing of European projects such as the FlexPakRenew project. In the framework of this project, starch nanocrystals (SNCs) were studied as a potential bio-nano-fillers for the coating color of a multilayer barrier packaging.

SNCs combine several advantages. They are renewable, biodegradable, nano-scaled, crystalline and present platelet-like morphology favorable for seeking barrier properties. However, at the beginning of this project, they could only be produced in small amounts (250ml) at lab-scale; some of their properties were still unknown; and no perspectives of industrial-scale production and processing were proposed. This is why this study has been undertaken following four main chapters.

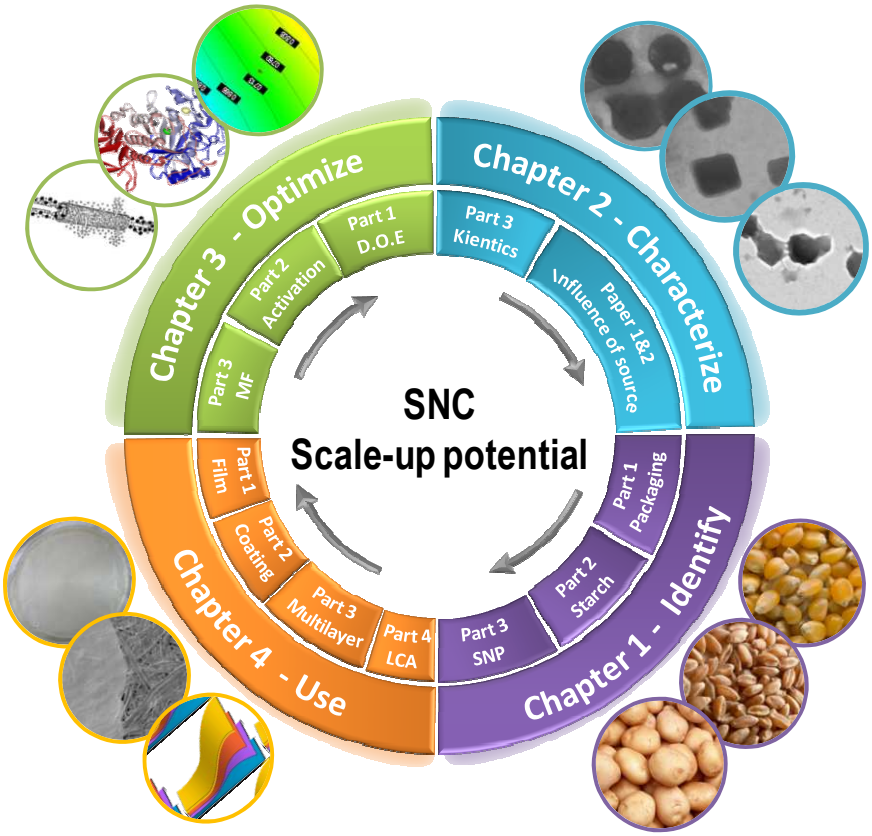

Figure 1. Schematic representation of our project and its implementation: "Project wheal"

As represented by our “project wheal”, the present research study was conducted in a progressive and structured manner with a total of 13 different parts. Our aim was to prove the potential of SNCs for scale-up while keeping in mind both the applied and the fundamental point of view.

Indeed, a detailed understanding of the material’s structure and properties was first sought for, in order to achieve the applied objectives of the European project. Also, as encouraged by the European commission and facilitated by the project dissemination consortium, we decided to have a strong dissemination policy. This led to a large number of publications and oral communications which will contribute to gaining knowledge on such a new material. These two aspects of the project are presented in Figure 2.

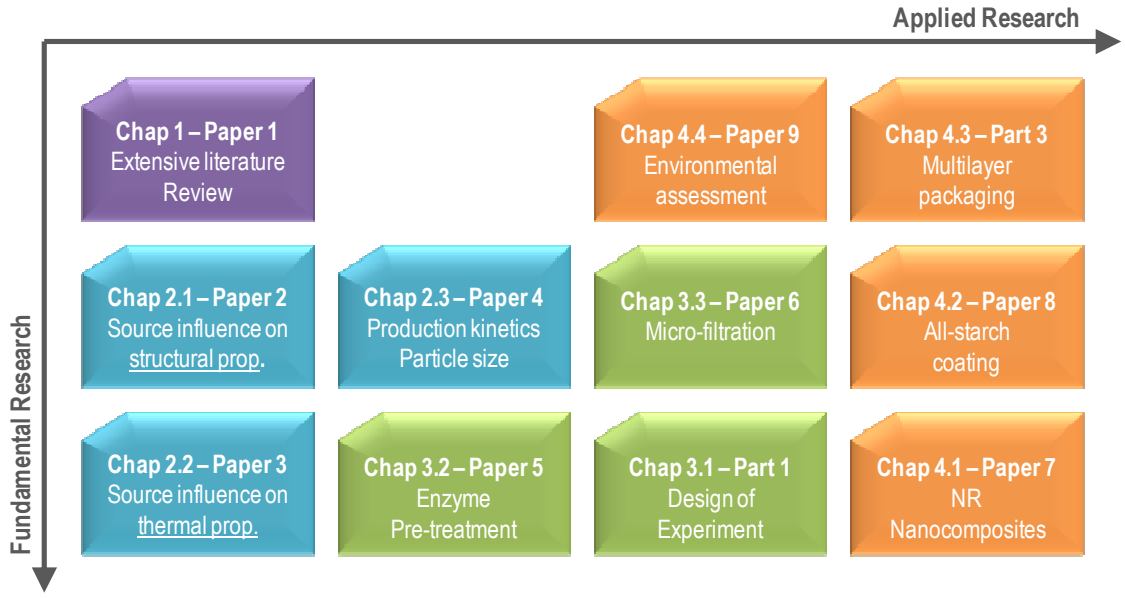

Figure 2. Organization of the different parts and/or papers of the manuscript.

This organization and this strategy have enabled us to contribute to the fields of starch nanocrystals and packaging by delivering important results and analysis.

We started this work by publishing an extensive literature review on these relatively newly (about 10 years) studied materials that are starch nanocrystals (SNCs). It was very welcomed as reflected by the unusual popularity of the article. It also allowed indentifying the challenges to overcome for better understanding and industrialization of SNC, as presented in Chapter 1. First investigations were motivated by the wish to better understand SNCs and their properties. We started by assessing if the type of starch could influence the properties of ensued SNCs. SNCs prepared from five different starch sources were investigated in terms of size, shape, crystallinity, viscosity and thermal stability.

Contrary to cellulose whiskers, little difference was found between the different SNCs allowing many raw materials to be considered as sources. Yet, slight differences (morphology, yield) were pointed out and can offer some criteria for selecting one type of native starch over another.

Then it was important to fully understand the SNCs preparation process before undertaking any optimization. The study of the kinetics of the preparation process revealed for the first time that (i) SNCs could be found in the suspension as early as 24h, and that (ii) classic SNCs suspensions are heterogeneous. These new considerations had considerable influences on the way we interpreted past results (and especially reported yields), offered promising perspectives for optimization; and led to qualifying a more homogeneous and nanoscaled new generation of SNCs.

The next step consisted in proposing three different strategies for improving the duration, the yield and/or the homogeneity of SNCs suspensions. The first one consisted in assessing if using more drastic hydrolysis conditions could allow for preparing SNCs in less than a day. A Design of Experiment was implemented to that intent. New generation SNCs were successfully prepared in less than 15h; however the actual yield of this 2nd generation SNC (and not that of the suspension) remained very low. The second strategy was focused on developing a pretreatment that could weaken the starch granule (by fragmentation or porosity). Some enzymes allowed obtaining micro-porous starch which resulted in reduced acid hydrolysis duration. Despite positive and promising results, the yield and extent of time reduction were still not fully satisfactory for industrial applications. Thus, a continuous filtration process that could fit current industrial processes was imagined. It led us to test the potential of microfiltration for isolating SNCs from the main suspension, as soon as they are prepared. This strategy was the most promising for the preparation of new generation SNCs, and offered an implementable solution for the scaling-up of the process.

The last part of the work was dedicated to qualifying the processability of SNC in our targeted application: multilayer coating. First, the influence of the type of starch used for preparing SNC was assessed in a model film. Reinforcement has been achieved almost without any influence of source, contrary to other bio-based nanocrystals. Then, the influence of adding SNCs to a bio-based coating color and on the coated papers' final properties were assessed. Results were positive in terms of water vapor barrier property. Thus, SNCs were further tested for coating in combination with two other bio-polymers as part of the strategy developed in the FlexPakRenew project for the production of a pilot-scaled multilayer packaging.

Results were compared to that obtained for an optimized nanoclays system. Although SNCs were not selected for the project, the study revealed that SNCs can effectively decrease water vapor permeability in xylan coating and compete with some non-optimized nanoclay systems. Also, the use of 2nd generation SNCs was proven more efficient. The study was completed with a rather positive environmental impact assessment of SNCs.

To summarize the contribution of this work to the field of starch nanocrystals, it can be said that

(i) it has brought important knowledge on SNCs preparation and properties,

(ii) promising solutions have been identified for the scale-up of the preparation process;

(iii) SNCs have been successfully used in an industrial process.

Evolutions of the field for the past three years have been summarized in Table 1.

As can be deduced from the number of publications, since the beginning of our project and our review, there has been an exponentially increasing interest for starch nanocrystals.

Also, SNCs used were prepared almost exclusively from waxy maize starch (and potato in the early years) whereas recently 6 other starch sources have been investigated, for which we can account for 4.

From a characterization and understanding of SNCs point of view, the field has significantly evolved. A few years ago, all evidences of SNCs were provided from TEM micrographs. In this project, we developed a number of characterization techniques using SEM equipped with a Field Emission Gun (which allows high magnification), AFM and XRD. The first technique allowed obtaining better defined images of SNCs. The second was used to compare SNCs' thicknesses with theory. The last technique effectively confirmed the gain in crystallinity of SNCs compared to native starches, due to the hydrolysis of amorphous parts. As mentioned in the manuscript, before our project, there was little understanding of the SNCs' thermal stability. Some DSC measurements had been performed for comparison with modified SNCs, but no study and qualification of the thermal properties had been proposed. Finally, SNC suspensions have also been considered from a rheological point of view. It was important to be able to assess the

gain is viscosity that they provided and thus the applications we could target, but also to be able to compare it with other nanoparticles.

From a process point of view, the preparation of SNCs had already been optimized and drastically shortened before our project. Indeed, Angellier et al. (2004) managed to take the process duration from 40 days down to 5. This might explain why, since then, no work had been undertaken to further decrease that duration. In this manuscript, we report 3 new optimization strategies and an environmental analysis to orientate future developments. Also, we propose to define a new generation of SNCs, with more homogeneous particle size.

Considering applications for SNCs, it can be evidenced that, finally, new uses are being investigated. It is important to note that currently most of them are designed either for relatively high end products (such as thermo-responsive applications and water treatment), or for large volumes markets (such as our multilayer packaging).

Table 1. Main evolutions in the field of starch nanocrystals from 2007 to 2011.

Our contribution is indicated in bold italic font.

	Before the project (2007)	After the project (2011)
Number of scientific papers	13	55 (***5***)
SNC Characterization	2 sources used: potato, waxy maize Techniques: TEM, DLS Stability in suspension	8 sources (***4***): potato, waxy maize, ***normal maize, high amylose maize, wheat, pea***, cassava, amaranth Techniques TEM, DLS, ***XRD, SEM FEG , AFM*** **Stability in suspension** ***Thermal stability*** ***Viscosity***
SNC Production	5 days SNC 1st generation (heterogeneous, size < 5µm)	***<24 hours*** ***SNC 2nd generation (filtered, size < 300nm)*** ***Environmental analysis***
Use of SNC	Composite	***Composite*** ***Paper coating – multilayer packaging*** Drug release regulator Thermo-responsive applications Water treatment

Numerous meetings and collaborations which have nourished our work were not reported here. For example, a one month exchange with Karlstad University, Sweden, allowed us to get familiar with regenerated starch nanoparticles (different from starch nanocrystals as described in the Review). The potential synergy between starch nanocrystals and nanoclays was investigated in collaboration with Sheffield University, UK. Our involvement in other work packages of the project led us to collaborate with CTP on paper machine pilot trials. Finally, we also collaborated with other partners to the production of deliverable (written reports).

Additionally, we had collaboration with the Laboratorio de Polimeros & Materiales Compositos (LP&MC) from Argentina and SNCs from pea starch were produced in the framework of collaboration with ITENE (Spain) and presented to a conference.

Obviously, a number of perspectives can be derived from the present work.

Most promising perspective would be the implementation of the proposed industrial production process for the obtaining of 2nd generation SNCs in collaboration with starch industrialists. This optimization could include an enzymatic pre-treatment before the acid hydrolysis and microfiltration. To complete the industrialization of SNC, a work on the drying of SNC should be undertaken. Indeed, economically it cannot be envisaged that SNC will be sold in suspension. To be a competitive product it has to be stored in the dry state and be redispersible at least in water. This property could be achieved by technology transfer from nanocrystalline cellulose, or by further investigating techniques developed recently. Also, the toxicity of SNC will have to be assessed by specialists.

Another interesting perspective would deal with the processing of SNCs. Indeed, for the production of 2nd generation SNCs to be profitable, several high end applications should be developed. Thus current applications need to be further studied and new applications developed. For instance, in the coating application we developed, it would be most interesting to assess the orientation of SNCs in the layer during the processing, the drying and the final step. A controlled orientation of SNCs could lead to enhanced and new properties.

We hope the present manuscript will contribute to (i) further breakthroughs in the use of this promising bio-nano-filler and (ii) attract further interests from the scientific community.

Résumé

Résumé

L'augmentation de la durée de vie d'un emballage et de son produit est une préoccupation internationale qui permettrait de limiter le gâchis alimentaire. Par ailleurs, ces dix dernières années, la demande mondiale en emballage flexible n'a cessée de croître. Etant donnée, nos habitudes de vies de plus en plus sédentaires, ce secteur devrait continuer à évoluer fortement. Pourtant cette industrie est encore, en grande majorité, basée sur des produits issus de ressources pétrolières et donc non-renouvelables.

L'épuisement constaté des ressources fossiles et les récentes prises de conscience politiques et sociétales se sont traduits par une forte demande des consommateurs pour des produits et emballages issus de ressources renouvelables, recyclables et/ou biodégradables. L'ambition du projet Européen FlexPakRenew (à l'origine de cette thèse) est de pouvoir répondre à cette demande en développant un bio-emballage innovant flexible et barrière. Dans ce cadre, une stratégie d'emballage multicouche a été suivie et différents bio-polymères, c'est à dire des polymères issus de ressources renouvelables, ont été étudiés.

Parmi ces bio-polymères, l'amidon est l'un des polysaccharides les plus utilisés en tant que biopolymère, en raison de son faible coût, de sa disponibilité mondiale et de sa production renouvelable et saisonnière. Il se trouve en effet dans les graines et racines de nombreuses plantes telles que le mais, le blé, la pomme de terre ou les pois. L'industrie des farines ou sirop d'amidon est d'ores et déjà une industrie mature.

Par ailleurs, l'amidon possède des propriétés très intéressantes. La plus exploité d'entre elles est sa capacité à gélatiniser. En effet, l'amidon, sous l'action de la température et de l'hydratation, perd toute cristallinité pour former un gel. Très utilisé dans l'alimentaire, ce gel peut être aussi plastifié pour des applications papetière ou « bioplastique ». Depuis peu, il est aussi parfois « régénéré » par réticulation, précipitation ou complexation pour former des nanoparticules d'amidon. La semi-cristallinité de l'amidon est, en revanche, beaucoup moins exploitée industriellement.

Pourtant, la structure de l'amidon consistant en une alternance de zones amorphes (i.e. non ordonnées) et de zones cristallines (i.e. ordonnées), permet de produire des bio-nanocristaux. Pour cela, les grains d'amidon subissent un traitement acide de 5 jours pendant lequel les zones amorphes sont hydrolysées et les zones cristallines de taille nanométriques (correspondant aux nano-cristaux d'amidon, notées SNCs) sont « libérées ».

Au début de notre projet, ce matériau était encore relativement peu connu puisque moins d'une vingtaine d'articles étaient parus sur le sujet. Le but de notre étude était donc d'étudier le potentiel d'utilisation de ces nanocristaux issus de l'amidon, comme substitut aux nano-charges minérales généralement utilisées dans les emballages barrières. Pour cela, de nombreuses questions restaient à résoudre. Notamment, étant donnée la variété des sources d'amidon, il fallait vérifier si tout type d'amidon pouvait indifféremment être utilisé pour produire des SNCs. Par ailleurs, étant donné le temps de préparation des SNCs (5jours), il fallait étudier la possibilité de réduire celui-ci, ou d'augmenter le rendement, pour espérer produire à grande échelle et donc en quantité suffisante des SNCs. Enfin, il fallait prouver que les SNCs pouvaient effectivement être utilisés en couchage pour une application barrière.

Pour répondre à ces questions, nous avons identifié 4 axes de travail, comme le montre la Figure 1.

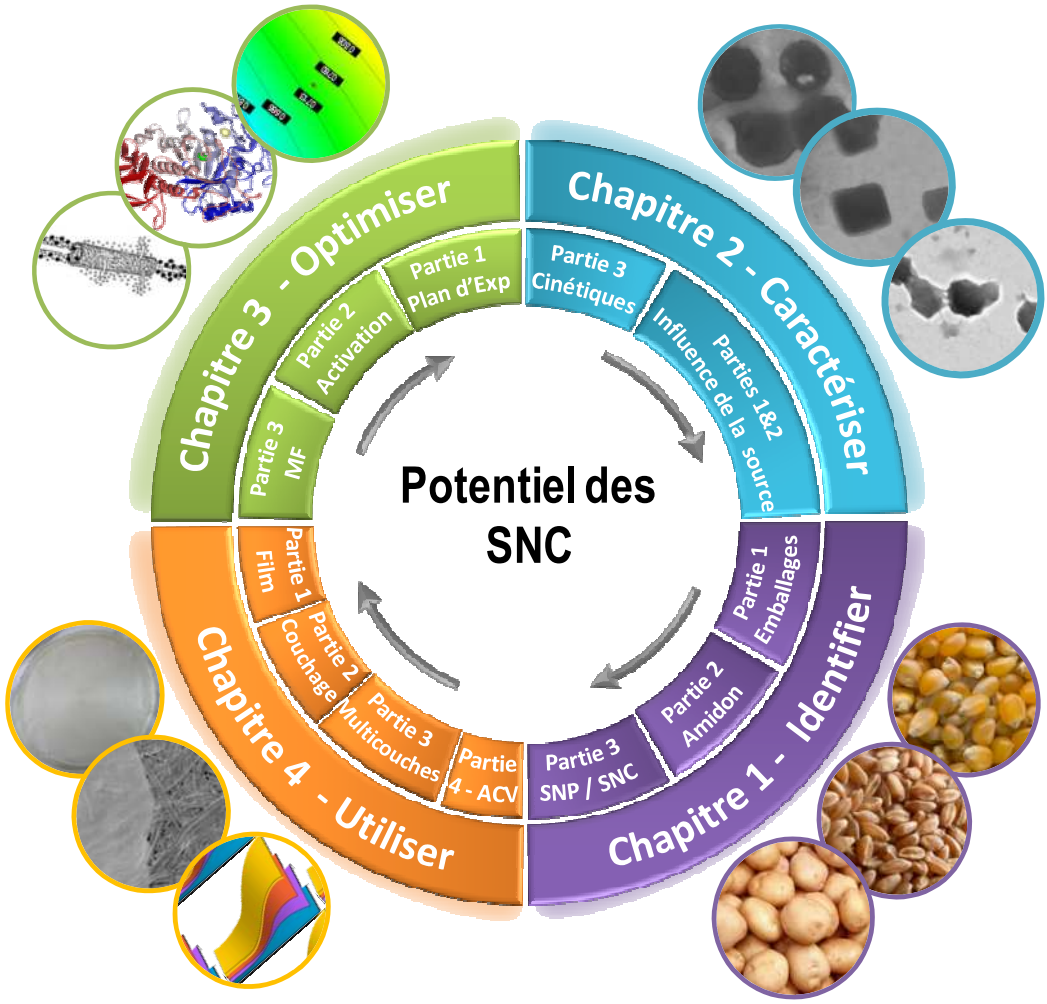

Figure 1. Représentation schématique de l'organisation du manuscrit

Le **Chapitre 1** qui introduit plus en profondeur notre thématique et fait l'état de l'art des SNCs (Partie 3 – Article 1), permet de mieux **identifier** les différents défis restant à relever pour envisager une montée en échelle du procédé de préparation des SNCs.

Le **Chapitre 2** a pour but de **caractériser** l'influence de la source d'amidon sur les propriétés structurales (Partie 1- Article 2) et thermiques (Partie 2 – Article 3); ainsi que le procédé actuel de préparation des SNCs (Partie 3 – Article 4).

Le **Chapitre 3** propose trois stratégies différentes en vue d'**optimiser** le procédé de préparation des SNCs : (i) un plan d'expérience afin de trouver les conditions optimales de préparation des SNCs en moins de 24h (Partie 1) ; (ii) un prétraitement des grains d'amidon pour diminuer la durée de l'hydrolyse acide (Partie 2 – Article 5) ; et (iii) une technique d'extraction des SNCs en continu disponible à l'échelle industrielle (Partie 3 – Article 6).

Finalement, le **Chapitre 4** évalue le potentiel d'**utilisation** des SNCs dans des applications industrielles telles qu'en film nanocomposite (Partie 1 – Article 7), en couchage (Partie 2 – Article 8) et en emballage multi-couches (Partie 3). Cette étude est complétée par une analyse du cycle de vie des SNCs pour une telle application (Partie 4 – Article 9).

Chaque chapitre est constitué de 3 articles ou parties qui rapportent des études à la fois appliquées et fondamentales, comme le montre la Figure 2.

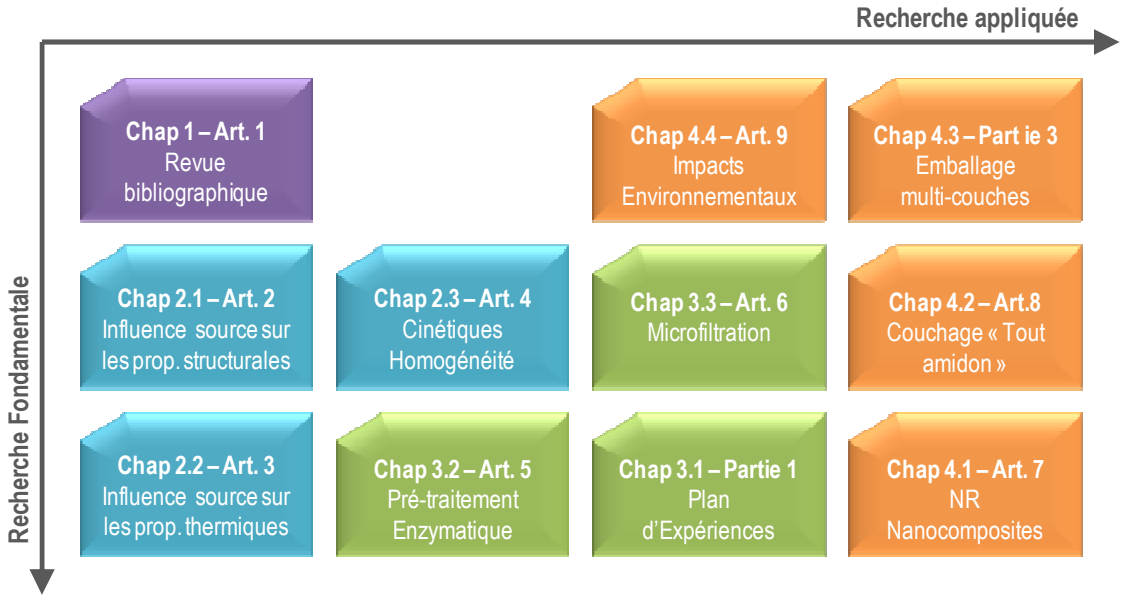

Figure 2. Représentation des différentes parties constituant ce manuscrit.

Plus en détails, le **Chapitre 1** introduit le contexte de notre projet en rappelant les bases économiques, techniques et scientifiques liées aux emballages bio-sourcés flexible et barrières. La structure (présentée Figure 3) et les propriétés de l'amidon sont détaillées pour permettre aux lecteurs de comprendre comment sont obtenues les SNCs et quelles sont les contraintes liées à ce matériau.

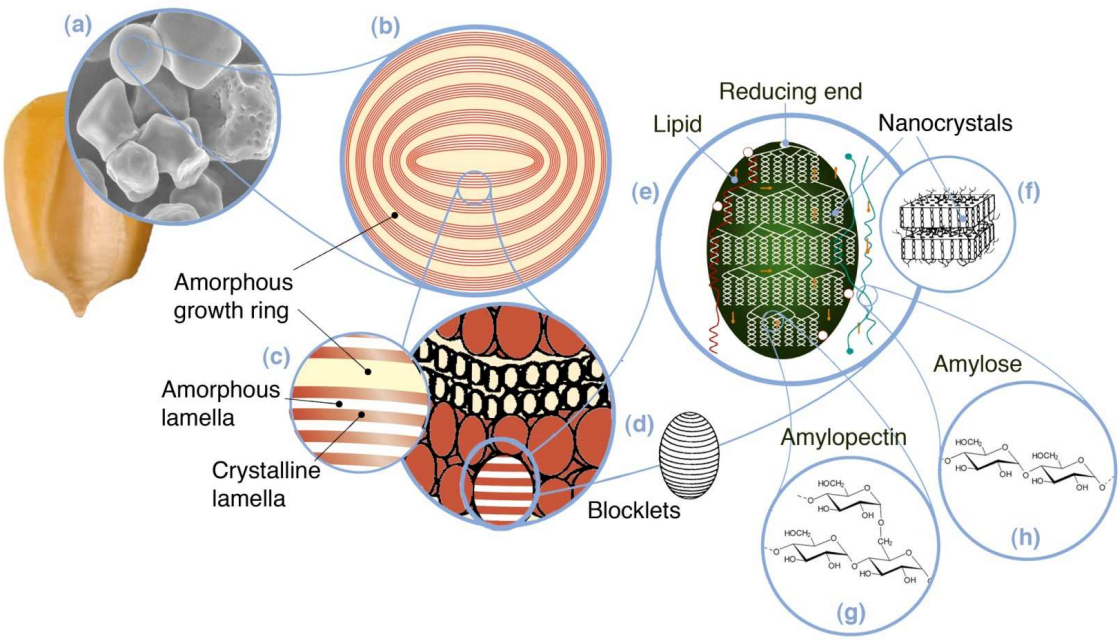

Figure 3. Structure multi-échelle de l'amidon. (a) Grain d'amidon de mais "normal" (30µm), (b) Anneaux de croissance amorphes et semi-cristallins (120-500nm), (c) Lamelles amorphes et cristallines (9nm): agrandissement des anneaux de croissance semi-cristallins:, (d) « Blocklets » (20-50nm): unité constituantes des anneaux de croissance, (e) Doubles hélices d'amylopectines formant les lamelles cristallines des « blocklets », (f) Nanocristaux: une autre représentation des lamelles cristallines appelées SNC lorsqu'elles sont « libérées » par hydrolyse acide, (g) Structure moléculaire de l'amylopectine, (h) Structure moléculaire de l'amylose (0,1-1nm).

Il s'en suit une revue détaillée (Publiée dans *Biomacromolecules*) portant sur les nanoparticules d'amidon. Elle vise à présenter les différents types de nanoparticules d'amidon (comme présenté Figure 4) ; et à décrire les procédés actuelles de caractérisation, de préparation et d'utilisation des SNCs.

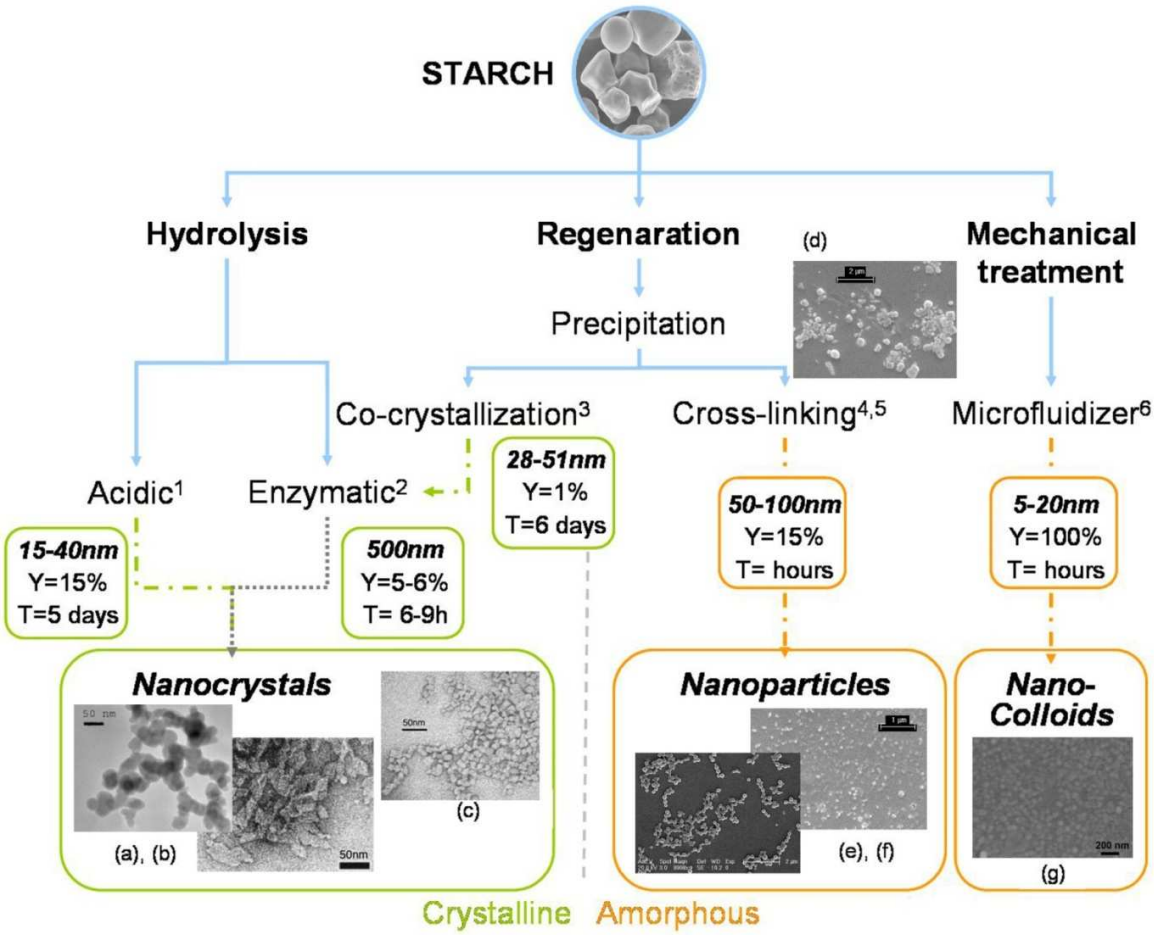

Figure 4. Different ways of producing crystalline and amorphous starch nanoparticles, hydrolysis leads to nanocrystals, whereas regeneration and mechanical treatment lead to both amorphous and crystalline particles in final batch.

1) Production de SNCs par hydrolyse acide (références regroupées dans la revue bibliographiques). (a) Micrographie MEB de SNCs de Garcia et al. – (b) Micrographie MET de SNCs de Putaux et al.

2) Tentative de production de SNCs par hydrolyse enzymatique rapporté par Kim et al. Il semble que le procédé produise des "blocklets" plutôt que des nanoparticles.

3) Préparation de nanocristaux par la formation de complexe amylose/n-butanol (Kim et Lim), complétée par une hydrolyse enzymatique. (c) Micrographie MET de SNCs après co-crystallisation et hydrolyse enzymatique.

4,5) Préparation de nanoparticles d'amidon par précipitation d'amidon gélatinisé dans un non-solvant suivie d'une réticulation. Nanoparticles (d) avant réticulation, (e) (f) après réticulation.

6) Tentative de préparation des SNCs par analogy avec les MFC (MicroFibrilles de Cellulose), i.e. par microfluidisation, par Liu et al. Après plusieurs passages des nanoparticules amorphes sont obtenues ; (g) Micrographie MET des suspensions nano-colloïdales d'amidon.

Le **Chapitre 2** étudie en détail l'influence des propriétés initiales de l'amidon (telles que l'origine botanique, le taux d'amylose ou le type cristallin) sur les propriétés des SNCs. Dans les articles 2 et 3, cinq types d'amidon couvrant trois origines botaniques différentes, trois taux d'amylose différents et deux types cristallins, ont été préparés.

Dans la première partie (Article 1 soumis à Nanoparticle Research, Juin 2011), les SNCs sont comparés en termes de taille, de morphologie, de cristallinité et de viscosité des suspensions aqueuses. L'étude révèle que, contrairement aux nanocristaux de cellulose, les différences observées sont faibles. Toutefois, selon l'application visée, des critères de sélections peuvent être trouvés. Par exemple, certains SNCs présentent une forme plaquettaire arrondie alors que d'autre sont rectangulaires (comme observé Figure 5), ce qui est plutôt favorable à une utilisation en tant que barrière.

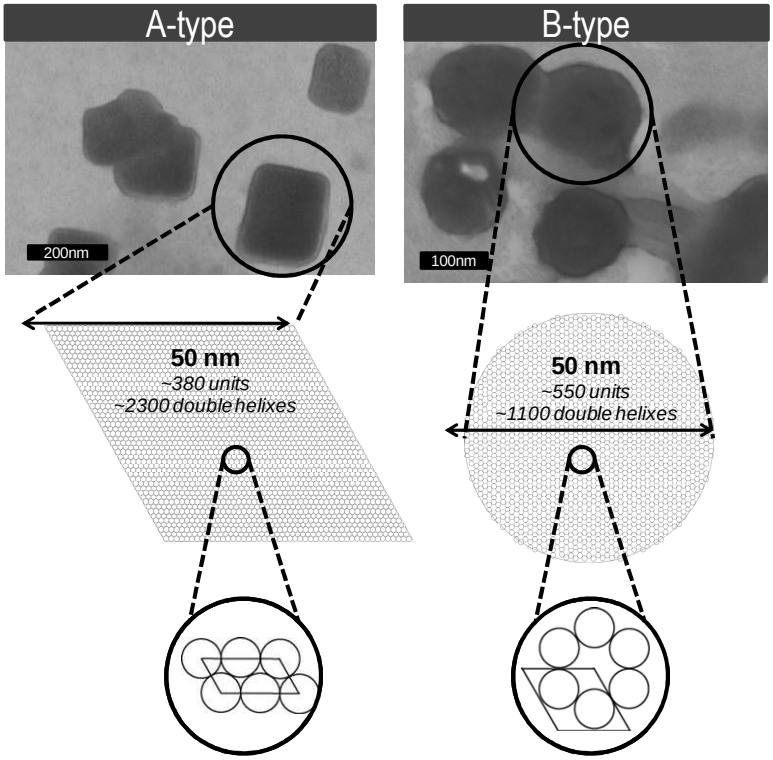

Figure 5. Nanocristaux d'amidon issues de mais cireux (A-type) et de mais à fort taux d'amylose (B-type) présentant des formes différentes, et des types cristallins différent comme le montre la représentation de l'agencement des doubles hélices d'amylopectine.

Les SNCs étant envisagés pour en faire une utilisation dans des procédés industriels (c'est-à-dire sous contraintes hygro-thermiques), la deuxième partie de ce chapitre 2 (Article 3 publié dans Carbohydrate Polymers 2011) complète l'étude précédente par l'analyse des propriétés thermiques de ces mêmes 5 différents types de SNCs.

Le but est d'évaluer (i) la stabilité thermique des SNCs pour savoir dans quel(s) type(s) de procédé(s) les SNCs peuvent être utilisés ; et (ii) l'influence de la source d'amidon utilisée sur cette stabilité thermique. Les températures maximum de mise en œuvre des SNCs sont évaluées à l'état sec à 200℃ et en suspension à 100℃. Par ailleurs, la source d'amidon utilisée semble avoir une faible influence sur les propriétés thermiques des SNCs, comme le montre la Figure 6. De plus, une étude bibliographique des propriétés thermiques de l'amidon nous permet de postuler du mécanisme de transitions thermiques des SNCs.

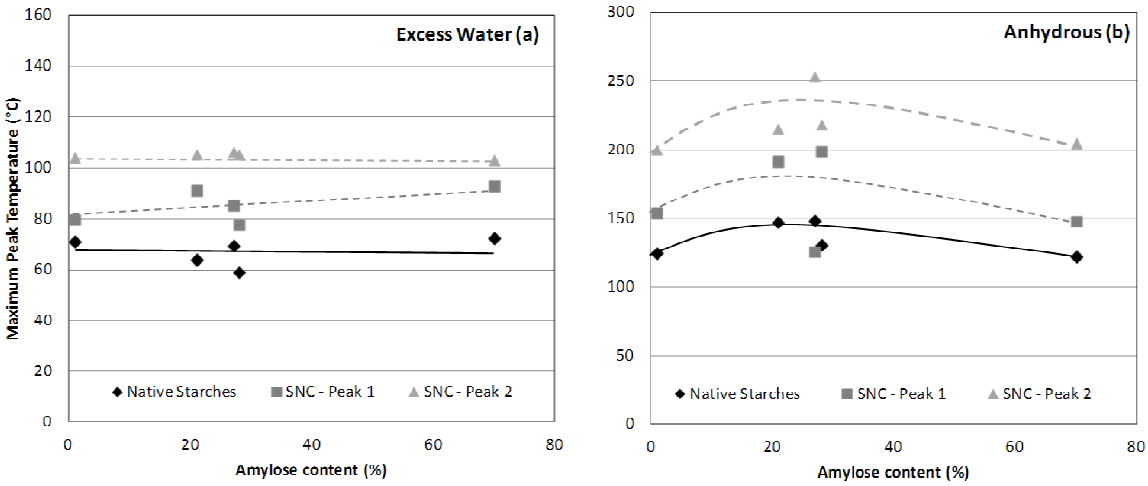

Figure 6. Evolution des pics endothermiques de l'amidon natif et des SNCs lyophilisés en fonction de leur taux d'amylose avant hydrolyse; (a) en suspension et (b) à l'état sec (conditionné à 50%HR).

La troisième partie de ce chapitre (Article 4 – publié dans *Biomacromolecules*) s'attaque à une question identifiée au cours des trois premiers articles déjà présentés : le rendement. En effet, les études antérieures (présentées au Chapitre 1) confirment que le rendement expérimental massique actuel (<15%) est inférieur à la valeur théorique de cristallinité de l'amidon (~40%). Par ailleurs, afin de viser des applications industrielles, il semblait important d'évaluer l'homogénéité et le potentiel d'homogénéisation ou de classification des suspensions produites actuellement. Pour cela, des cinétiques d'hydrolyse et une classification des suspensions par centrifugation ont été entreprises et ont révélé la présence de SNCs en suspension dès 24h, comme le montre la Figure 7. Par conséquent, l'étude souligne l'importance de mettre en place un système d'extraction des SNCs, afin d'évaluer un rendement reflétant la quantité de SNCs réellement produite ; et donne un autre éclairage à notre compréhension du procédé de préparation des SNCs. En effet, cette étude démontre que les SNCs classiquement utilisés (que nous pouvons appeler SNCs de 1ère génération) sont en réalité un mélange de micro et nanoparticules. La séparation des deux parties se traduit par la création d'une nouvelle génération de SNCs (2nd) plus petites et plus homogènes.

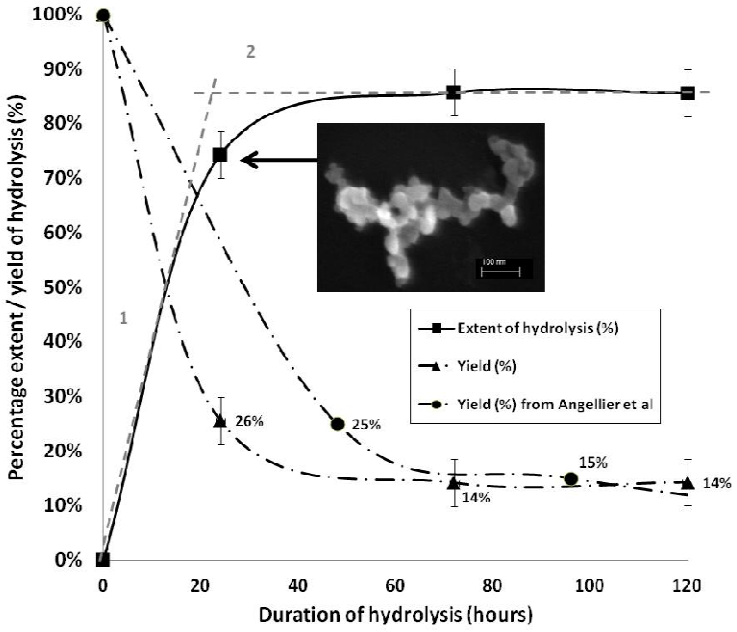

Figure 7. Cinétiques d'hydrolyses du (▪) mais cireux par de l'acide sulfurique à 3M, 40°C et 15% d'amidon et (▲) le rendement correspondant (%). (●) Cinétique de rendement de l'hydrolyse de mais cireux, dans les mêmes conditions que précédemment, tel que rapporté par Angellier et al. La micrographie SEM-FEG à 1 jour montre clairement la présence de SNCs.

Au vu des résultats positifs du Chapitre 2, il a été postulé que les SNCs pouvaient en théorie être utilisés dans des procédés industriels. Cependant, pour rendre cela possible, de plus grandes quantités, ou de plus hauts rendements en SNCs sont nécessaires.

Par conséquent, le **Chapitre 3** propose 3 nouvelles techniques d'optimisation du procédé de préparation des SNCs :

1. La recherche des paramètres optimaux de préparation en moins de 24h ;

2. Le développement d'un prétraitement de courte durée; et

3. L'utilisation d'un procédé industriel existant pour isoler les SNCs de 2nde génération en continu tout au long de leur préparation.

Dans la première partie, un plan d'expériences a été conçu afin de modéliser l'effet des principaux paramètres d'hydrolyse (concentration en acide, température, durée et concentration en amidon) sur les propriétés finales (rendement, taille, taux de charge) des SNCs obtenus en moins de 24h. Les résultats confirment que les SNCs de 2nde génération peuvent être produits en moins de 15h mais avec un rendement très faible après filtration, contrairement au rendement de la suspension (SNCs de 1ère génération), comme le montrent les Figure 8 et Figure 9.

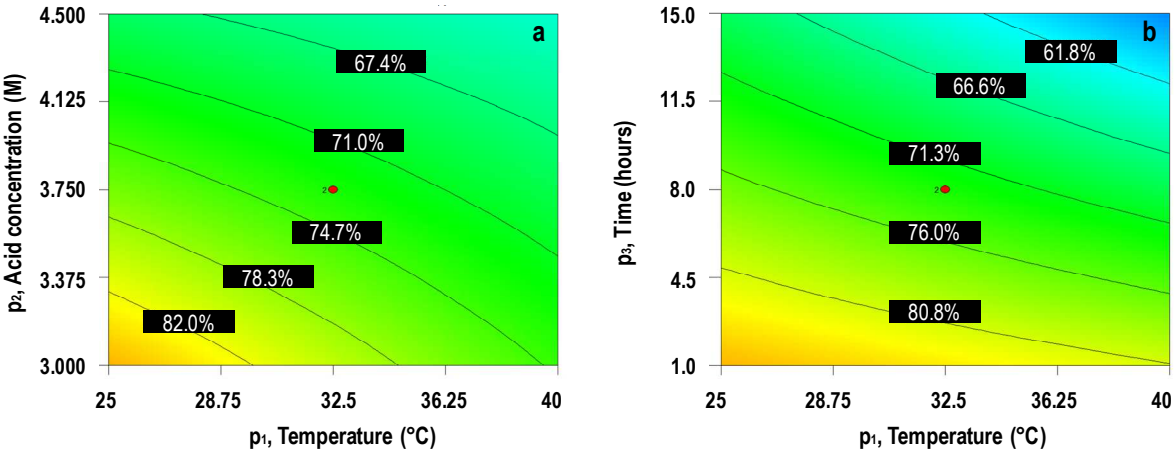

Figure 8. Surface de réponses obtenues pour le rendement de la suspension présentant la température en fonction de (a) la concentration en acide, à temps constant (8h) et concentration en amidon constante (C=27.5g/100ml) ; et en fonction (b) du temps à concentrations en acide (C=3.75M) et en amidon constantes (C=27.5g/100ml).

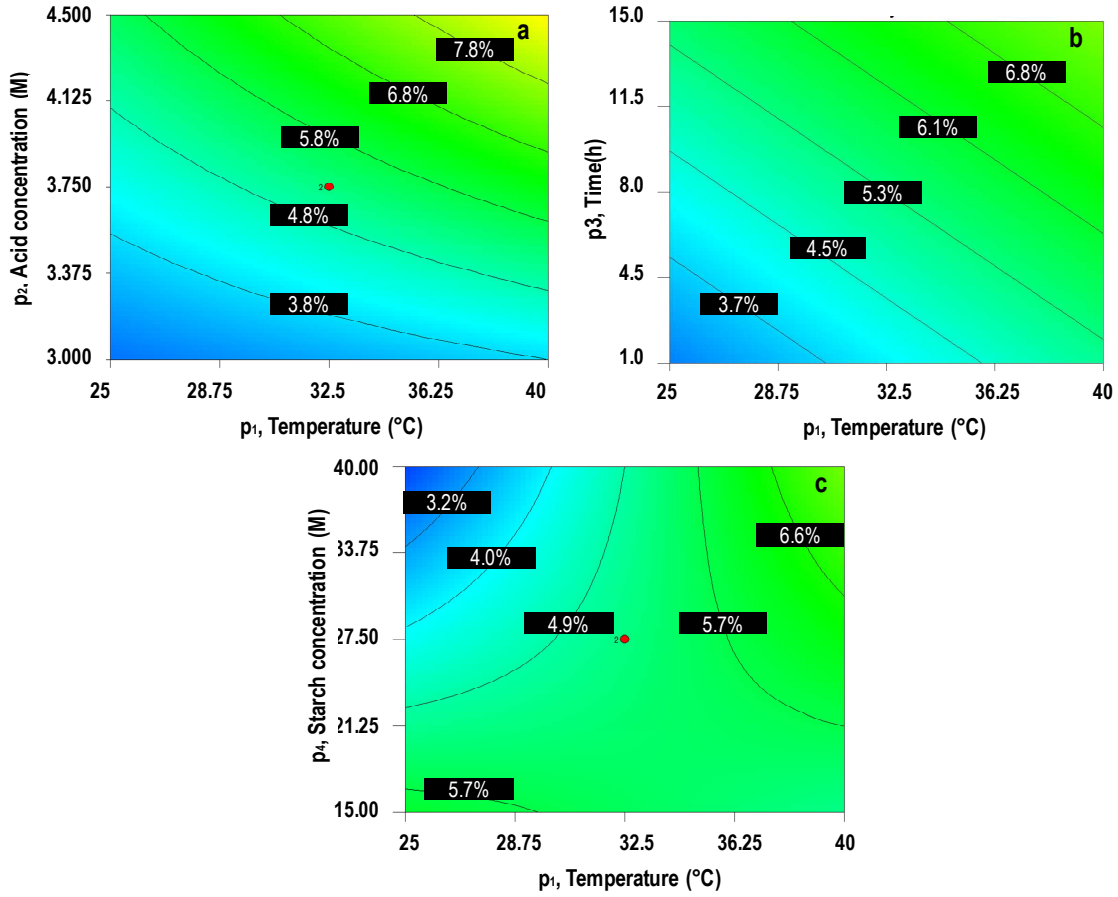

Figure 9. Surface de réponses obtenues pour le rendement en SNCs présentant la température en fonction de (a) la concentration en acide, à temps constant (8h) et concentration en amidon constante (C=27.5g/100ml) ; (b) du temps à concentrations en acide (C=3.75M) et en amidon constantes (C=27.5g/100ml) ; et (c) de la concentration en amidon à concentration en acide constante (C=3.75M) et à temps fixe (8h).

L'étude a également montré que la filtration et le taux de charge présent à la surface des SNCs préparés avec l'acide sulfurique jouent un rôle important sur l'aspect final des SNCs lyophilisés, comme le montre les Figure 10 et Figure 11.

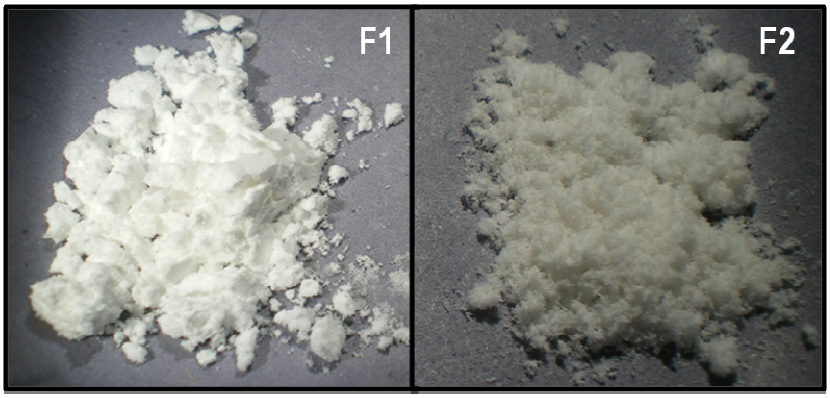

Figure 10. Photographie des suspensions de SNCs (F1) avant et (F2) après filtration à 1 µm.

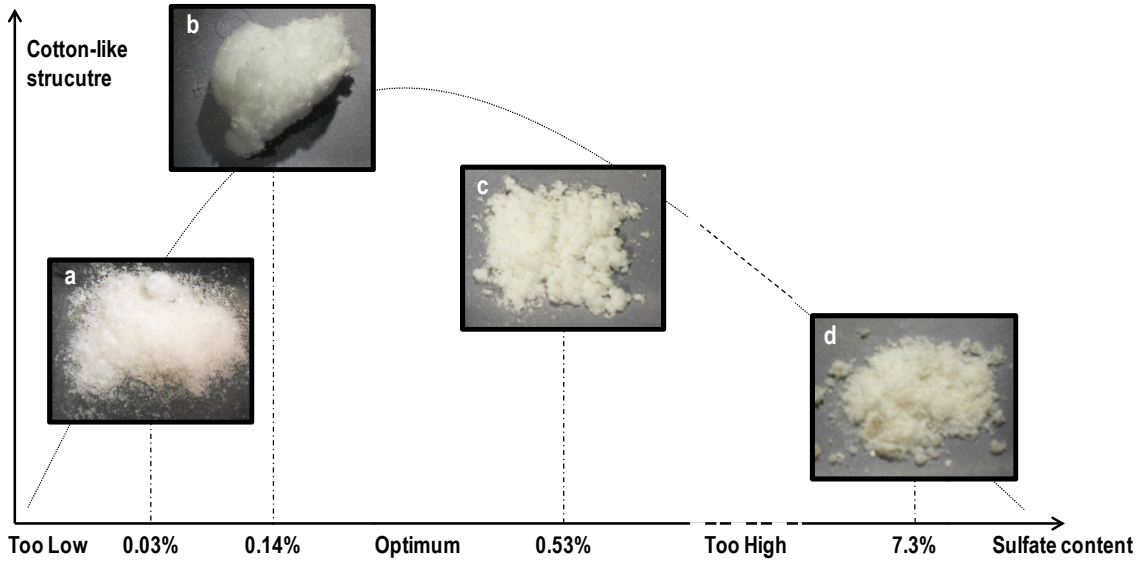

Figure 11. Evolution de l'aspect des SNCs filtrés et lyophilisés pour un taux de sulfate croissant: (a) pour une hydrolyse classique (3M) de 5 jours, (b) pour l'expérience 8 du plan, (c) pour l'expérience 3 du plan et (d) pour l'expérience 18.

Dans la seconde partie du Chapitre 3, le potentiel de prétraitement de l'amidon est évalué pour différentes enzymes. L'idée derrière cette stratégie est de créer des chemins de diffusion pour que l'acide pénètre plus facilement et de manière plus homogène les grains d'amidon. L'étude (Article 5) révèle que les glucoamylases permettent de produire un amidon microporeux et donc de réduire le temps d'hydrolyse acide, comme le montre la Figure 12. Toutefois, les rendements en SNCs filtrés c'est dire de 2nde génération restent faibles.

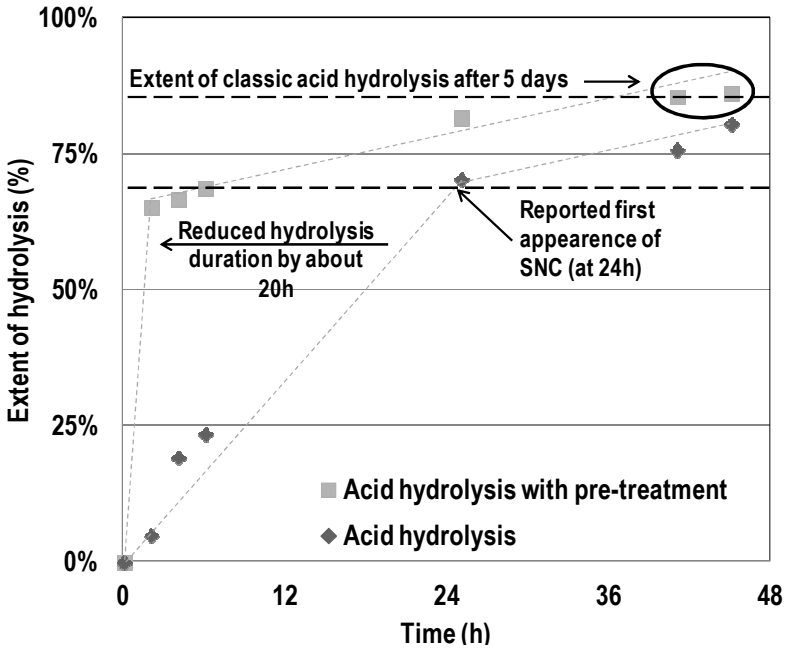

Figure 12. Cinétique d'hydrolyses acides de l'amidon de mais cireux (♦) non prétraité et (■) prétraité.

Par conséquent, la dernière stratégie de ce chapitre (Article 6, *Carbohydrate Polymers*), est basée sur des considérations plus industrielles et permet de s'affranchir des notions de durée et de rendement. Elle consiste à utiliser la microfiltration en continue. Cette dernière s'est révélée très efficace, pour isoler les SNCs de taille nanométrique au fur et à mesure de leur production et faire recirculer la suspension mère constituée de grains partiellement hydrolysés. Ce principe est schématisé sur la Figure 13 qui compare le procédé de préparation actuel, à celui proposé.

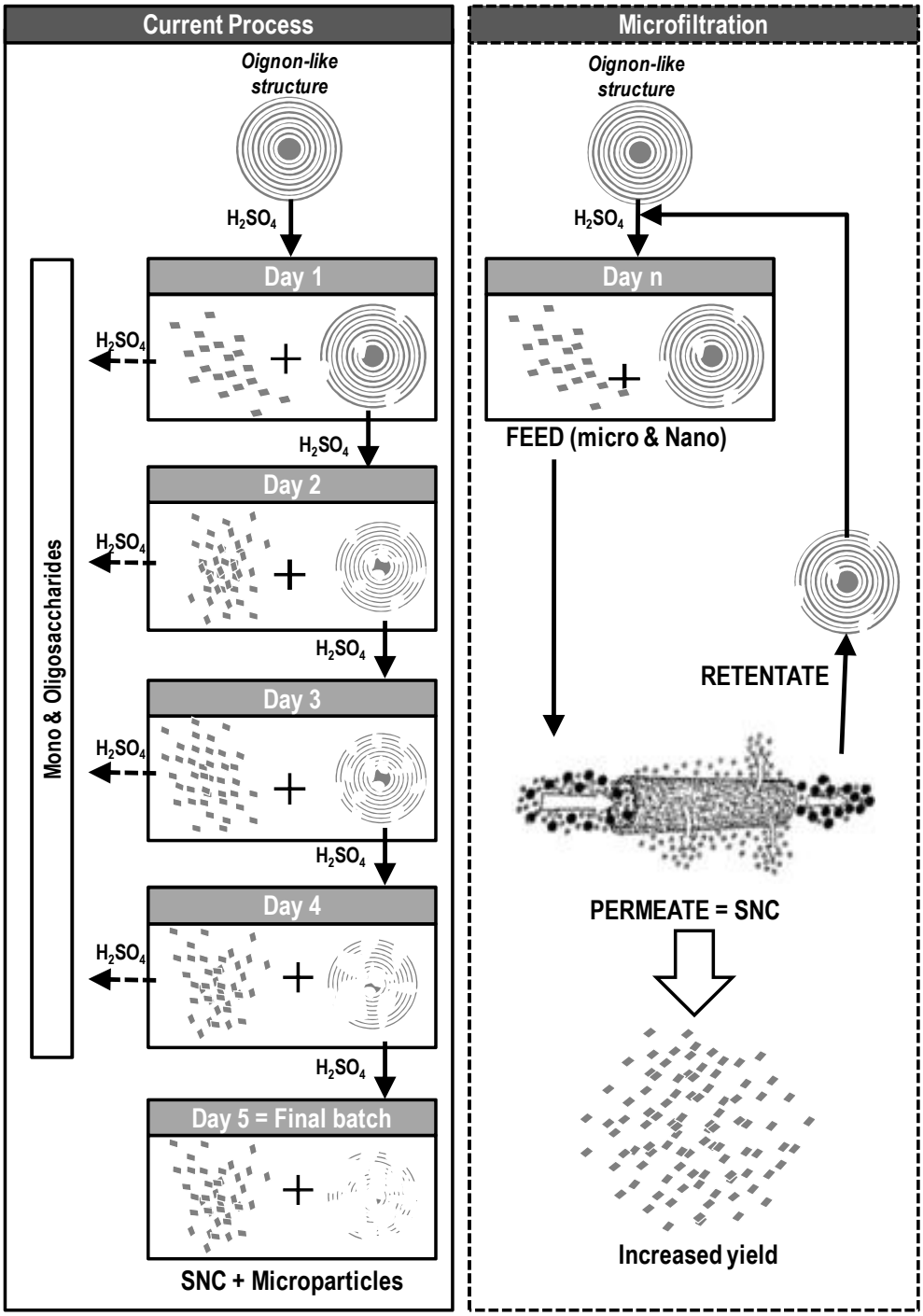

Figure 13. Représentation schématique du procédé de préparation actuel des SNCs et du procédé de microfiltration proposé.

Grâce à la compréhension des SNCs acquise aux Chapitres 1 et 2, et des possibilités d'optimisation, développées au Chapitre 3, il nous semblait pertinent de terminer ce travail par l'étude d'éventuelles applications pour les SNCs et notamment dans les emballages barrières par procédés de couchage.

Le **Chapitre 4** étudie donc le potentiel des SNCs en tant que nanocharge pour le renfort mécanique et l'effet barrière. A cette fin, les SNCs ont d'abord été étudiés dans un film modèle de biopolymère (Partie 1 – Article 7), puis en double couchage (Partie 2 – Article 8), puis dans un emballage multi-couches (Partie 3). Cette étude est complétée par une analyse du cycle de vie des SNCs en utilisation dans un tel emballage (Partie 4 - Article 9).

La partie 1 vérifie, donc plus en détail, l'influence de la source d'amidon utilisée sur les propriétés des SNCs comme charge dans un nanocomposite. L'étude confirme les résultats précédents : de faibles disparités sont observées entre les différents nanocomposites préparés. Toutefois, des différences (modérées en comparaison avec les nanocristaux de cellulose) peuvent être relevées, notamment au niveau des propriétés mécaniques comme le montre la Figure 14.

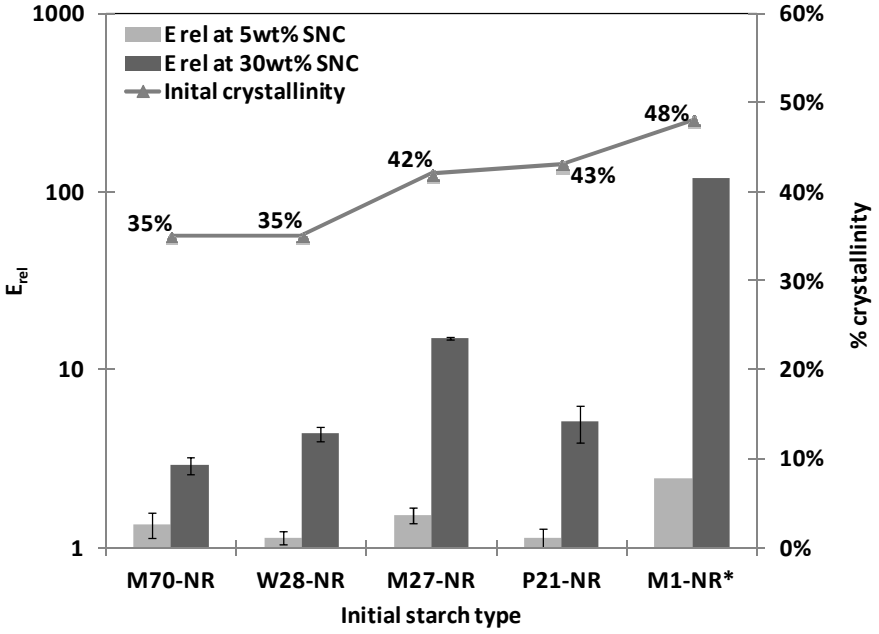

Figure 14. Module d'Young relative (Erel) des nanocomposites de caoutchouc naturel chargés avec différentes sortes de SNCs issus de : M70 – Amidon de mais a fort taux d'amylose (70%) ; W28 – amidon de blé à 28% d'amylose ; M27 – amidon de mais normal à 27% d'amylose ; P21 – amidon de pomme de terre à 21% d'amylose et M1 – Amidon de mais cireux à très faible taux d'amylopectine (<1%).

La deuxième étude de ce chapitre (Article 7, soumis à Surface and Coatings Technologies) vérifie la possibilité d'utiliser les SNCs dans un procédé de couchage, d'un point de vue rhéologique et thermique. Elle montre que les SNCs peuvent en partie compenser la perte de propriétés mécaniques due à l'utilisation de biopolymères en phase aqueuse diluée, et peuvent améliorer les propriétés barrières à la vapeur d'eau, comme le montre la Figure 15.

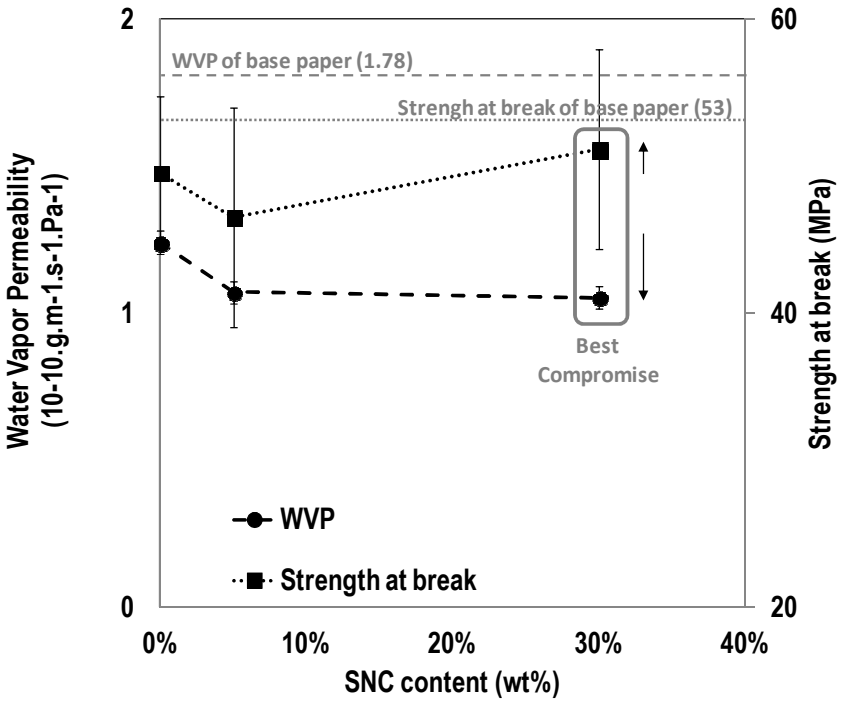

Figure 15. Perméabilité à la vapeur d'eau d'un papier industriel couché avec une sauce d'amidon plastifié et chargé à différents taux de SNC, respectivement 0%, 5% et 30% en masse.

Etant donnés ces résultats prometteurs, les SNCs ont ensuite été considérés comme une alternative renouvelable aux nanocharges minérales pour une application en emballage multicouches. Cette étude, conduite dans le cadre du projet Européen FlexPakRenew, a révélé que, dans leur stade actuel de développement, les SNCs ne pouvaient pas encore entrer en compétition avec des systèmes de nanocharges minérales optimisés depuis plusieurs années. Toutefois, l'étude révèle également que les SNCs peuvent effectivement diminuer la perméabilité à la vapeur d'eau de certains biopolymères (tel que les xylanes) et entrer en compétition avec des systèmes de nanocharges minérales de niveau de développement comparable à celui des SNCs (c.à.d. non optimisés). Par ailleurs, l'amélioration des performances des SNCs de nouvelle génération en comparaison des SNCs classiques est démontrée.

Finalement, les SNCs offrant des perspectives intéressantes, la dernière partie (Article 9 soumis à Starke/Starch, 2011) de ce dernier chapitre propose, pour l'application industrielle visée, une identification des étapes du procédé de fabrication les plus impactantes, une comparaison de leurs performances environnementales avec les nanocharges d'argile ainsi qu'une étude bibliographique sur la potentielle toxicité de ce type de nanoparticles. Celle-ci devrait permettre d'orienter les travaux futurs d'optimisation des procédés de production et d'utilisation des SNCs.

Le but de cette étude a donc été atteint puisque les différents défis identifiés au début de l'étude ont été élucidés et que :

(i) L'influence de la source d'amidon sur les SNCs et leurs propriétés a été évaluée,

(ii) Les cinétiques et rendements d'hydrolyse ont été quantifiés, et ont permis d'imaginer de nouveaux procédés de préparation des SNCs

(iii) Des solutions innovantes et applicables pour l'optimisation du procédé de préparation des SNCs de 2nde génération ont été proposées

(iv) La compatibilité des SNCs avec les procédés actuels de couchages a été démontrée, ainsi que leur impact sur les barrières

(v) Leur impact environnemental a été évalué.

Par ailleurs, il semble que ce travail présente dans son ensemble des perspectives intéressantes pour la poursuite de cette étude.
Parmi les plus prometteuses d'entre elles, nous citerons la mise en place du procédé industriel proposé pour l'obtention de SNC de 2ème génération en collaboration avec un industriel de l'amidon. Cette optimisation pourrait être complétée par un prétraitement enzymatique en amont. Pour compléter ce procédé en aval, un travail sur le séchage des SNCs devrait être entrepris. En effet, économiquement parlant, on ne peut imaginer (à moins de coût très élevés) proposer un produit en suspension. Pour être compétitifs, les SNCs doivent être vendus séchés et redispersables dans l'eau.
Une autre perspective intéressante traite de l'utilisation des SNCs. En effet, afin que les SNCs de 2ème génération soient rentables, plusieurs applications à hautes valeurs ajoutées ou de masse, doivent être développées. Pour ce faire, les applications développées récemment doivent être optimisées et l'impact sur les barrières complété. Dans l'application par couchage, il serait d'un grand intérêt de pouvoir déterminer et contrôler l'orientation des SNCs dans la couche, ou de travailler sur la compatibilisation renfort-matrice dans le cas des nanocomposites.

L'ensemble des chapitres de ce manuscrit sont donc étroitement liés. Nous espérons que l'étude, dans son ensemble, permet d'avoir une compréhension globale des SNCs, de leur préparation et de leur utilisation ; et qu'elle contribuera à de nouvelles avancées dans le domaine des nanocristaux d'origine renouvelable et suscitera l'intérêt du monde scientifique et industriel.

Abstract

The present work investigates the potential of starch nanocrystals (SNCs) for industrial scaled-up preparation and use. An extensive characterization (morphology, viscosity, thermal stability and properties in nanocomposite) of 5 different SNCs shows, contrary to nanocrystalline cellulose, the limited influence of the botanic source. The analysis of the current preparation process led to three optimization strategies, and to the definition of a new generation of SNCs with smaller dimensions and more homogeneous. A new application of SNCs is presented (multilayer packaging); and showed that SNCs can effectively reduce water vapor permeability of some biopolymers coatings. The life cycle assessment (LCA) of SNCs in this application is also proposed. This study contributes greatly to the advance of the field and offers perspectives for the industrialization of SNCs.

Keywords: Starch, Nanocrystals, Nanoparticles, Barrier, Packaging, Biopolymers, Coating, Process

Résumé

Ce travail examine la potentielle mise à l'échelle industrielle des procédés de préparation des nanocristaux d'amidon (SNCs). Une caractérisation approfondie (morphologie, viscosité, stabilité thermique et propriétés en nanocomposites) de 5 SNCs différents montre une faible influence de la source botanique, contrairement aux nanocristaux de cellulose. L'analyse du procédé de préparation actuel des SNCs a conduit à 3 nouvelles stratégies d'optimisation et à la définition d'une nouvelle génération de SNCs. Une nouvelle application des SNCs, en emballage multicouche, montre également que les SNCs peuvent être utilisés en couchage et contribuer à diminuer la perméabilité à la vapeur d'eau de certains biopolymères. Une analyse du cycle de vie des SNCs dans ce type d'application est également proposée. Cette étude contribue donc à l'avancée de cette thématique et propose des perspectives prometteuses.

Mots clefs : Amidon, Nanocristaux, Nanoparticules, Barrière, Emballage, Biopolymères, Couchage, Procédé